CONVECTIVE HEAT AND MASS TRANSFER

This book was developed by Professor S. Mostafa Ghiaasiaan during 10 years of teaching a graduate-level course on convection heat and mass transfer. The book is ideal for a graduate course dealing with theory and practice of convection heat and mass transfer. The book treats well-established theory and practice on the one hand; on the other hand, it is enriched by modern areas such as flow in microchannels and computational fluid dynamics–based design and analysis methods. The book is primarily concerned with convective heat transfer. Essentials of mass transfer are also covered. The mass transfer material and problems are presented such that they can be easily skipped, should that be preferred. The book is richly enhanced by exercises and end-of-chapter problems. Solutions are available for qualified instructors. The book includes 17 appendices providing compilations of most essential properties and mathematical information for analysis of convective heat and mass transfer processes.

Professor S. Mostafa Ghiaasiaan has been a member of the Woodruff School of Mechanical Engineering at Georgia Institute of Technology since 1991 after receiving a Ph.D. in Thermal Science from the University of California, Los Angeles, in 1983 and working in the aerospace and nuclear power industry for eight years. His industrial research and development activity was on modeling and simulation of transport processes, multiphase flow, and nuclear reactor thermal hydraulics and safety. His current research areas include nuclear reactor thermal hydraulics, particle transport, cryogenics and cryocoolers, and multiphase flow and change-of-phase heat transfer in microchannels. He has more than 150 academic publications, including 90 journal articles, on transport phenomena and multiphase flow. Among the honors he has received for his publications are the Chemical Engineering Science's Most Cited Paper for 2003–2006 Award, the National Heat Transfer Conference Best Paper Award (1999), and the Science Applications International Corporation Best Paper Award (1990 and 1988). He has been a member of American Society of Mechanical Engineers (ASME) and the American Nuclear Society for more than 20 years and was elected an ASME Fellow in 2004. Currently he is the Executive Editor of *Annals of Nuclear Energy* for Asia, Africa, and Australia. This is his second book with Cambridge University Press—the first was *Two-Phase Flow, Boiling, and Condensation, In Conventional and Miniature Systems* (2007).

Convective Heat and Mass Transfer

S. Mostafa Ghiaasiaan
Georgia Institute of Technology

CAMBRIDGE
UNIVERSITY PRESS

CAMBRIDGE UNIVERSITY PRESS
Cambridge, New York, Melbourne, Madrid, Cape Town,
Singapore, São Paulo, Delhi, Tokyo, Mexico City

Cambridge University Press
32 Avenue of the Americas, New York, NY 10013-2473, USA

www.cambridge.org
Information on this title: www.cambridge.org/9781107003507

First published 2011

Printed in the United States of America

A catalog record for this publication is available from the British Library.

Library of Congress Cataloging in Publication data

Ghiaasiaan, Seyed Mostafa, 1953–
Convective heat and mass transfer / Mostafa Ghiaasiaan.
p. cm.
Includes bibliographical references and index.
ISBN 978-1-107-00350-7 (hardback)
1. Heat – Convection. I. Title.
QC327.G48 2011
536′.25 – dc22 2011001977

ISBN 978-1-107-00350-7 Hardback

To my wife Pari Fatemeh Shafiei, and my son Saam

CONTENTS

Preface

We live in an era of unprecedented transition in science and technology education caused by the proliferation of computing power and information. Like most other science and technology fields, convective heat and mass transfer is already too vast to be covered in a semester-level course even at an outline level and is yet undergoing exponential expansion. The expansion is both quantitative and qualitative. On the quantitative side, novel and hitherto unexplored areas are now subject to investigation, not just by virtue of their intellectual challenge and our curiosity, but because of their current and potential technological applications. And on the qualitative side, massive sources of Internet-based information, powerful personal computers, and robust and flexible software and other computational tools are now easily accessible to even novice engineers and engineering students. This makes the designing of a syllabus for courses such as convection heat and mass transfer all the more challenging. Perhaps the two biggest challenges for an instructor of a graduate-level course in convection are defining a scope for the course and striking a reasonable balance between the now-classical analytic methods and the recently developing modern areas. Although the importance of modern topics and methods is evident, the coverage of these topics should not be at the expense of basics and classical methods.

This book is the outcome of more than 10 years of teaching a graduate-level course on convective heat and mass transfer. It also benefits from my more than 20 years of experience of teaching undergraduate heat transfer and other thermal fluid science courses to mechanical and nuclear engineering students. The book is designed to serve as the basis for a semester-level graduate course dealing with theory and practice of convection heat and mass transfer. My incentive in writing the book is to strike a balance between well-established theory and practice on the one hand, and modern areas such as flow in microchannels and computational fluid dynamics (CFD)–based design and analysis methods on the other. I have had much difficulty finding such a balance in the existing textbooks while teaching convection to graduate students and had to rely on my own class notes and recent issues of journals for much of the syllabi of my classes.

The book is primarily concerned with convective heat transfer. Essentials of mass transfer are also covered, although only briefly. The mass transfer material

and problems are presented such that they can be easily skipped, should that be preferred.

The book consists of 13 chapters. Chapter 1 reviews general and introductory material that is meant to refresh the student's memory about the material that he or she will need to understand the remainder of the book. Chapters 2 and 3 deal with boundary layers and the transport processes that they control. Chapter 4 discusses laminar internal flow, in considerably more detail than most similar textbooks, in recognition of the importance of laminar flow in the now-ubiquitous miniature flow passages. Chapter 5 discusses the integral method, a classical technique for the approximate solution of boundary-layer transport equations. The fundamentals of turbulence and classical models for equilibrium turbulence are discussed in Chapter 6, followed by the discussion of internal turbulent flow in Chapter 7. Chapter 8 is a short discussion of the effect of transpiration on convective transport processes, and Chapter 9 deals with analogy among heat, momentum, and mass transfer processes. Buoyancy-dominated flows are discussed in Chapters 10 and 11.

Chapter 12 is on turbulence models. These models are the bases of the now-ubiquitous CFD tools. The chapter is primarily focused on the most widely used Reynolds-averaged Navier-Stokes (RANS)–type turbulent transport models in current convective heat transfer research and analysis. The discussions are meant to show the students where these models have come from, with an emphasis on how they treat not just the fluid mechanics aspects of turbulent flow but also the transport of heat and mass. Although access to and practice with CFD tools are helpful for understanding these turbulence models, the chapter is written in a way that access to and application of CFD tools are not necessary. Only some of the problems at the end of this chapter are meant to be solved with a CFD tool. These problems, furthermore, are quite simple and mostly deal with entrance-dominated internal turbulent flows. Finally, Chapter 13 is a rather detailed discussion of flow in microchannels. The importance of flow in microchannels can hardly be overemphasized. This chapter discusses in some detail the internal gas flow situations for which significant velocity slip and temperature jump do occur.

The book also includes 17 appendices (Appendices A–Q), which provide brief compilations of some of the most essential properties and mathematical information needed for analysis of convective heat and mass transfer processes.

S. Mostafa Ghiaasiaan

Frequently Used Notation

A	Flow or surface area (m^2); atomic number
$\vec{a}$	Acceleration (m/s^2)
a	Speed of sound (m/s); one-half of the longer cross-sectional dimension (m)
a_I''	Interfacial surface area concentration (surface area per unit) mixture volume (m^{-1})
B	Blowing parameter
B_h	Mass-flux-based heat transfer driving force
$\tilde{B}_h$	Molar-flux-based heat transfer driving force
B_m	Mass-flux-based mass transfer driving force
$\tilde{B}_m$	Molar-flux-based mass transfer driving force
Bi	Biot number $= hl/k$
Br	Brinkman number $= \frac{\mu U^2}{k\lvert\Delta T\rvert}$
Bo	Buoyancy number $= \mathrm{Gr}/\mathrm{Re}^m$
b	One-half of the shorter cross-sectional dimension (m)
$\boldsymbol{C}$	Concentration ($kmol/m^3$)
C_f	Fanning friction factor (skin-friction coefficient)
C_D	Drag coefficient
C_{He}	Henry's coefficient (Pa; bars)
C_μ	Constant in the k–ε turbulence model
C_P	Constant-pressure specific heat (J/kg K)
$\tilde{\mathrm{C}}_P$	Molar-based constant-pressure specific heat (J/kmol K)
C_v	Constant-volume specific heat (J/kg K)
$\tilde{\mathrm{C}}_v$	Molar-based constant-volume specific heat (J/kmol K)
D	Tube or jet diameter (m)
D_H	Hydraulic diameter (m)
D_{ij}	Multicomponent Maxwell-Stefan diffusivities for species i and j (m^2/s)
$\mathcal{D}_{ij}$	Binary mass diffusivity for species i and j (m^2/s)
$\boldsymbol{D}_{ij}$	Multicomponent Fick's diffusivity for species i and j (m^2/s)
$\vec{\mathbf{d}}_j$	Diffusion driving force for species j (m^{-1})
E	Eddy diffusivity (m^2/s); gas molecule energy flux (W/m^2)

Ec	Eckert number $= \frac{U^2}{C_P \Delta T}$
$\boldsymbol{E}_1$, $\boldsymbol{E}$	1D and 3D turbulence energy spectrum functions based on wave number (m^3/s^2)
$\boldsymbol{E}_1^*$, $\boldsymbol{E}^*$	1D and 3D turbulence energy spectrum functions based on frequency (m^2/s)
$\boldsymbol{E_B}$	Bulk modulus of elasticity (N/m^2)
E_{ma}	Eddy diffusivity for mass transfer (m^2/s)
E_{th}	Eddy diffusivity for heat transfer (m^2/s)
$\boldsymbol{e}$	Total specific advected energy (J/kg)
$\vec{e}$	Unit vector
$\vec{F}$	Force (N)
F	Eigenfunction
$\mathcal{F}$	Dependent variable in momentum mixed-convection similarity solutions
Fo	Fourier number $= (\frac{k}{\rho C_P})\frac{t}{l^2}$
Fo_{ma}	Mass transfer Fourier number $= \mathcal{D}\frac{t}{l^2}$
Fr	Froude number $= U^2/(gD)$
f	Dependent variable in momentum similarity solutions
f	Darcy friction factor; frequency (Hz); distribution function (m^{-1} or m^{-3}); specific Helmholtz free energy (J/kg)
G	Mass flux ($kg/m^2 s$); Gibbs free energy (J); production rate of turbulent kinetic energy ($kg/m\ s^3$); filter kernel in LES method
Ga	Galileo number $= \frac{\rho_L \Delta\rho\, g\, l^3}{\mu_L^2}$
Gr_l	Grashof number $= \frac{g\beta l^3 \Delta T}{\nu^2}$
Gr_l^*	Modified Grashof number $= \frac{g\beta q'' l^4}{\nu^2 k}$
$\text{Gr}_{\text{ma},l}$	Concentration-based Grashof number $= \frac{g\beta_{\text{ma}} l^3 \Delta m_1}{\nu^2}$ or $\frac{g\beta^*_{\text{ma}} l^3 \Delta x_1}{\nu^2}$
Gz	Graetz number $= \frac{4Ul^2}{x}\left(\frac{\rho C_P}{k}\right)$
g	Specific Gibbs free energy (J/kg); gravitational constant ($= 9.807\ m/s^2$ at sea level)
$\vec{g}$	Gravitational acceleration vector (m/s^2)
H	Boundary-layer shape factor ($= \delta_1/\delta_2$); channel height (m)
He	Henry number
$\boldsymbol{h}$	Specific enthalpy (J/kg)
h	Heat transfer coefficient ($W/m^2\ K$); height (m)
h_r	Radiative heat transfer coefficient ($W/m^2\ K$)
$\boldsymbol{h}_{fg}, \boldsymbol{h}_{sf}, \boldsymbol{h}_{sg}$	Latent heats of vaporization, fusion, and sublimation (J/kg)
$\tilde{\boldsymbol{h}}_{fg}, \tilde{\boldsymbol{h}}_{sf}, \tilde{\boldsymbol{h}}_{sg}$	Molar-based latent heats of vaporization, fusion, and sublimation (J/kmol)
I_m	Modified Bessel's function of the first kind and mth order
J	Diffusive molar flux ($k\ mol/m^2\ s$)
j	Diffusive mass flux ($kg/m^2\ s$); molecular flux ($m^{-2}\ s^{-1}$)
K	Turbulence kinetic energy (J/kg)
K	Loss coefficient; incremental pressure-drop number
$\mathcal{K}$	Mass transfer coefficient ($kg/m^2\ s$)
$\tilde{\mathcal{K}}$	Molar-based mass transfer coefficient ($kmol/m^2\ s$)

k	Thermal conductivity (W/m K); wave number (m^{-1})
L	Length (m)
Le	Lewis number $= \frac{\alpha}{\mathcal{D}}$
l	Length (m)
l_c	Characteristic length (m)
l_D	Kolmogorov's microscale (m)
$l_{\text{ent,hy}}$	Hydrodynamic entrance length (m)
$l_{\text{ent,ma}}$	Mass transfer entrance length (m)
$l_{\text{ent,th}}$	Thermal (heat transfer) entrance length (m)
l_M	Turbulence mixing length (m)
$l_{\text{M, ma}}$	Turbulence mixing length for mass transfer (m)
l_{heat}	Heated length (m)
l_{th}	Turbulence mixing length for heat transfer (m)
M	Molar mass (kg/kmol)
Ma	Mach number
m	Mass fraction; dimensionless constant
$\boldsymbol{m}$	Mass (kg); mass of a single molecule (kg)
m''	Mass flux (kg/m^2s)
$\boldsymbol{N}$	Ratio between concentration-based and thermal-based Grashof numbers $= \text{Gr}_{l,\text{ma}}/Gr_l$
$\vec{N}$	Unit normal vector
N''	Molar flux (kmol/ m^2 s)
N_{Av}	Avogadro's number ($= 6.024 \times 10^{26}$ molecules/kmol)
NS	Navier-Stokes equation
Nu_l	Nusselt number $h\,l/k$
$\vec{n}$	Total mass flux (kg/m^2 s)
n	Component of the total mass flux vector (kg/m^2 s); number density (m^{-3}); dimensionless constant; polytropic exponent
$\mathcal{P}$	Property
P	Pressure (N/m^2); Legendre polynomial
Pe_l	Peclet number $= U\,l\ (\rho\,C_P/k)$
$\text{Pe}_{l,\text{ma}}$	Mass transfer Peclet number $= U\,l\,/\mathcal{D}$
Po	Poiseuille number $= \frac{2\tau_s D_H}{\mu\,U}$
Pr	Prandtl number $= \mu\,C_P/k$
P_r	Reduced pressure $= P/P_{\text{cr}}$
Pr_{tu}	Turbulent Prandtl number
p_f	Wetted perimeter (m)
p_{heat}	Heated perimeter (m)
p	Perimeter (m)
Q	Volumetric flow rate (m^3/s); dimensionless wall heat flux
$\dot{q}$	Volumetric energy generation rate (W/m^3)
q''	Heat flux (W/m^2)
R	Radius (m); gas constant (Nm/kg K)
R	Eigenfunction
Ra_l	Rayleigh number $= \frac{g\,\beta\,l^3\,\Delta T}{\nu\,\alpha}$

Ra_l^*	Modified Rayleigh number $= \frac{g\beta l^4 q''}{\nu \alpha k}$
R_c	Radius of curvature (m)
Re	Reynolds number $= \rho U l/\mu$
Re_F	Liquid film Reynolds number $= 4\Gamma_F/\mu_L$
Re_y	Reynolds number in low-Re turbulence models $= \rho K^{1/2} y/\mu$
Ri	Richardson number $= \mathrm{Gr}/\mathrm{Re}^2$
$\dot{R}_l$	Volumetric generation of species l (kmol/m^3 s)
R_u	Universal gas constant (= 8314 Nm/kmol K)
r	Distance between two molecules (Å) (Chapter 1); radial coordinate (m)
$\vec{r}$	Position vector (m)
$\dot{r}_l$	Volumetric generation rate of species l (kg/m^3 s)
$\boldsymbol{S}$	Entropy (J/K); distance defining intermittency (m)
S	Channel width (m)
Sc	Schmidt number $v/\mathcal{D}$
Sh_l	Sherwood number $= \frac{Kl}{\rho \mathcal{D}}$ or $\frac{\tilde{K} l}{\boldsymbol{C} \mathcal{D}}$
S_{ij}	Component of mean strain rate tensor (s^{-1})
St	Stanton number $= \frac{h}{\rho C_P U} = \frac{h}{\boldsymbol{C} \tilde{C}_P U} = \frac{\mathrm{Nu}_l}{\mathrm{Re}_l \mathrm{Pr}}$
$\mathrm{St}_{\mathrm{ma}}$	Mass transfer Stanton number $= \frac{\mathcal{K}}{\rho U} = \frac{\tilde{\mathcal{K}}}{\boldsymbol{C} U} = \frac{\mathrm{Sh}_l}{\mathrm{Re}_l \mathrm{Sc}}$
$\boldsymbol{s}$	Specific entropy (J/kg K)
s	Coordinate on the surface of a body of revolution (m)
T	Temperature (K)
$\mathcal{T}$	Turbulence intensity
$\vec{T}$	Unit tangent vector
t	Time (s); thickness (m)
t_c	Characteristic time (s)
$t_{c,D}$	Kolmogorov's time scale (s)
t_{res}	Residence time (s)
$\boldsymbol{U}$	Internal energy (J)
$\vec{U}$	Velocity vector (m/s)
U	Overall heat transfer coefficient (W/m^2 K); velocity (m/s)
U_τ	Friction velocity (m/s)
$\boldsymbol{u}$	Specific internal energy (J/kg)
u	Velocity in axial direction, in x direction in Cartesian coordinates, or in r direction in spherical coordinates (m/s)
u_D	Kolmogorov's velocity scale (m/s)
V	Volume (m^3)
V_d	Volume of an average dispersed phase particle (m^3)
v	Velocity in y direction in Cartesian coordinates, r direction in cylindrical and spherical coordinates, or θ direction in spherical coordinates (m/s)
$\mathbf{v}$	Specific volume (m^3/kg)
W	Work (J); width (m)
$\dot{W}$	Power (W)
We	Weber number $= \frac{\rho U^2 l}{\sigma}$

w	Velocity in z direction in Cartesian coordinates, in θ direction in cylindrical coordinates, or in φ direction in spherical coordinates (m/s); work per unit mass (W/kg)
X	Mole fraction
Y	Parameter represents the effect of fluid compressibility in turbulence models (kg/m s^3); height of a control volume (m)
y	Normal distance from the nearest wall (m)

Greek Characters

α	Thermal (energy) accommodation coefficient
$\boldsymbol{\alpha}$	Thermal diffusivity (m^2/s)
α^*	Aspect ratio
β	Wedge or cone angle (rad); coefficient of volumetric thermal expansion (1/K)
β_{ma}	Coefficient of volumetric expansion with respect to mass fraction
β^*_{ma}	Coefficient of volumetric expansion with respect to concentration $(\text{kg/m}^3)^{-1}$
$\tilde{\beta}_{\text{ma}}$	Coefficient of volumetric expansion with respect to mole fraction
Γ	Correction factor for the kinetic model for liquid-vapor interfacial mass flux; gamma function
Γ_F	Film mass flow rate per unit width (kg/m)
γ	Specific heat ration (C_P/C_v); shape factor [(Eq. 4.6.5)]
δ	Kronecker delta; gap distance (m); boundary-layer thickness (m)
δ_F	Film thickness (m)
$\delta_1,\ \delta_2,\ \delta_3, \delta_h$	Boundary-layer displacement, momentum, energy, and enthalpy thicknesses (m)
ε	Porosity; radiative emissivity; turbulent dissipation rate (W/kg)
$\tilde{\varepsilon}$	Energy representing maximum attraction between two molecules (J)
ε'	Parameter defined in Eq. (12.4.5) (W/kg)
ε_s	Surface roughness (m); a small number
ζ	Parameter defined in Eq. (3.1.26); dimensionless coordinate
η	Independent variable in similarity solution equations; dimensionless coordinate
η_c	Convective enhancement factor
θ	Nondimensional temperature; azimuthal angle (rad); angular coordinate (rad); angle of inclination with respect to the horizontal plane (rad or $^\circ$)
K	Curvature (m^{-1}); coefficient of isothermal compressibility (Pa^{-1})
κ	von Karman's constant
κ_B	Boltzmann's constant ($= 1.38 \times 10^{-23}$J/K molecule)
λ	Wavelength (m); second coefficient of viscosity $(-\frac{2}{3}\mu)$ (kg/m s); eigenvalue
λ_{mol}	Molecular mean free path (m)
μ	Viscosity (kg /m s)
ν	Kinematic viscosity (m^2/s)

ξ	Parameter defined in Eq. (3.2.41); variable
ρ	Density (kg/m^3)
σ	Normal stress (N/m^2); Prandtl number for various turbulent properties; tangential momentum accommodation coefficient
$\tilde{\sigma}$	Molecular collision diameter (Å)
σ_A	Molecular-scattering cross section (m^2)
$\sigma_c,\ \sigma_e$	Condensation and evaporation coefficients
$\dot{\sigma}'''_{\text{gen}}$	Entropy generation rate, per unit volume (J/K m^3)
τ	Molecular mean free time (s); viscous stress (N/m^2)
$\underline{\underline{\tau}}$	Stress tensor (N/m^2)
$\underline{\underline{\tau}}'$	Viscous stress tensor (N/m^2)
Φ	Dissipation function (s^{-2}); pressure strain term (W/kg)
ϕ	Velocity potential (m^2/s); pair potential energy (J); inclination angle with respect to vertical direction (rad or $^\circ$); normalized mass fraction
ϕ'	Inclination angle with respect to the horizontal plane (rad or $^\circ$)
φ	Relative humidity; nondimensional temperature for mixed convection
ψ	Stream function (m^2/s)
Ω	Specific potential energy associated with gravitation (J/kg); momentum flux of gas molecules (kg/m s)
Ω_k, Ω_D	Collision integrals for thermal conductivity and mass diffusivity
Ω_{ij}	Component of vorticity tensor (s^{-1})
ω	Humidity ratio
ϖ	Complex velocity potential (m^2/s)

Superscripts

r	Relative
$+$	Dimensionless; in wall units
$.$	Time rate
$-$	Average; in the presence of mass transfer
$-t$	Time averaged
$*$	Dimensionless or normalized; modified for velocity slip or temperature jump
$\sim$	Molar based; dimensionless

Subscripts

ad	Adiabatic
avg	Average
b	Body force
c	Center, centerline
cr	Critical
d	Dispersed phase
df	Downflow
ent	Entrance region or entrance effect

eq	Equilibrium
ev	Evaporation
ex	Exit
F	Forced convection
f	Saturated liquid
fd	Fully developed
film	Film
fr	Frictional
G	Gas phase
g	Saturated vapor; gravitational
H	Hartree's (1937) similarity solution
(H1)	Boundary conditions in which the temperature is circumferentially constant while the heat flux is axially constant
heat	Heated
hy	Hydrodynamic
I	Irreversible; gas–liquid interphase
in	Inlet
L	Liquid phase
lam	Laminar
m	Mean, bulk
ma	Mass transfer
max	Maximum
mol	Molecular
N	Natural convection
n	Sparingly soluble (noncondensable) inert species
opt	Optimized
out	Outlet
R	Reversible
rad	Radiation
ref	Reference
refl	Reflected
res	Associated with residence time
s	Wall surface; *s* surface (gas-side interphase); isentropic
sat	Saturation
(T)	Uniform wall temperature
th	Thermal
tu	Turbulent
UC	Unit cell
UHF	Uniform heat flux
UMF	Uniform mass flux
UWM	Uniform wall mass or mole fraction
UWT	Uniform wall temperature
w	Wall
x, z	Local quantity corresponding to location *x* or *z*
∞	Ambient; fully developed
$=$	Tensor

Abbreviations

CFD	Computational fluid dynamics
DDES	Delayed detached eddy simulation
DES	Detached eddy simulation
DNS	Direct numerical simulation
DSMC	Direct simulation Monte Carlo
GKT	Gas-kinetic theory
LES	Large-eddy simulation
MMFP	Molecular mean free path
ODE	Ordinary differential equation
RANS	Reynolds-averaged Navier-Stokes
RNG	Renormalized group
RSM	Reynolds stress model
SGS	Subgrid scale
UHF	Uniform heat flux
UMF	Uniform mass flux
UWM	Uniform wall mass or mole fraction
UWT	Uniform wall temperature
1D, 2D, 3D	One-, two-, and three-dimensional

1 Thermophysical and Transport Fundamentals

1.1 Conservation Principles

In this section the principles of conservation of mass, momentum, and energy, as well as the conservation of a mass species in a multicomponent mixture, are briefly discussed.

1.1.1 Lagrangian and Eulerian Frames

It is important to understand the difference and the relationship between these two frames of reference. Although the fluid conservation equations are usually solved in an Eulerian frame for convenience, the conservation principles themselves are originally Lagrangian.

In the Lagrangian description of motion, the coordinate system moves with the particle entity of interest, and we describe the flow phenomena for the moving particle or entity as a function of time. The Lagrangian method is particularly useful for the analysis of rigid bodies, but is rather inconvenient for fluids because of the relative motion of fluid particles with respect to one another. In the Eulerian method, we describe the flow phenomena at a fixed point in space, as a function of time. The Eulerian field solution for any property $\mathcal{P}$ will thus provide the dependence of $\mathcal{P}$ on time as well as on the spatial coordinates; therefore in Cartesian coordinates we will have

$$\mathcal{P} = \mathcal{P}(t, \vec{r}) = \mathcal{P}(t, x, y, z). \tag{1.1.1}$$

The relation between the changes in $\mathcal{P}$ when presented in Lagrangian and Eulerian frames is easy to derive. Suppose, for a particle in motion, $\mathcal{P}$ changes to $\mathcal{P} + d\mathcal{P}$ over the time period dt. Because in the Eulerian frame we have $\mathcal{P} = \mathcal{P}(t, x, y, z)$, then

$$d\mathcal{P} = \frac{\partial \mathcal{P}}{\partial t} dt + \frac{\partial \mathcal{P}}{\partial x} dx + \frac{\partial \mathcal{P}}{\partial y} dy + \frac{\partial \mathcal{P}}{\partial z} dz. \tag{1.1.2}$$

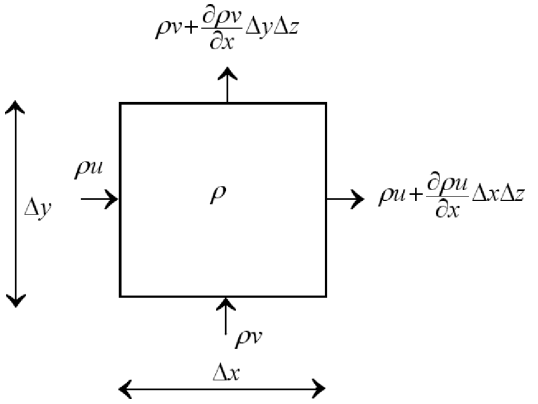

Figure 1.1. An infinitesimally small control volume.

Now, dividing through by dt, and bearing in mind that, because of the particle's motion, $dx = u\,dt$, $dy = v\,dt$, and $dz = w\,dt$, where u, v, and w are the components of the velocity vector along the x, y, and z coordinates, we get

$$\frac{d\mathcal{P}}{dt} = \frac{\partial \mathcal{P}}{\partial t} + u\frac{\partial \mathcal{P}}{\partial x} + v\frac{\partial \mathcal{P}}{\partial y} + w\frac{\partial \mathcal{P}}{\partial z}. \tag{1.1.3}$$

In shorthand,

$$\frac{d\mathcal{P}}{dt} = \frac{\partial \mathcal{P}}{\partial t} + \vec{U}\cdot\nabla\mathcal{P}. \tag{1.1.4}$$

The left-hand side of this equation is the Lagrangian frame representation of the change in $\mathcal{P}$ and is sometimes called the material derivative or the substantial derivative. It is often shown with the notation $\frac{D\mathcal{P}}{Dt}$. The relation between Lagrangian and Eulerian frames can thus be summarized as

$$\frac{D}{Dt} = \frac{\partial}{\partial t} + \vec{U}\cdot\nabla. \tag{1.1.4a}$$

1.1.2 Mass Conservation

The overall conservation of mass, without concern about individual species that may constitute a fluid mixture, is the subject of interest here. The conservation of mass species in a multicompoent mixture is discussed later in Section 1.4.

It is easier to derive the mass conservation equation first for an Eulerian frame. Consider the infinitesimally small-volume element in Cartesian coordinates shown in Fig. 1.1. The flow components in the z direction are not shown. The mass conservation principle states that mass is a conserved property. Accordingly,

$$\frac{\partial \rho}{\partial t}\Delta x\Delta y\Delta z = -\left[\frac{\partial \rho u}{\partial x} + \frac{\partial \rho v}{\partial y} + \frac{\partial \rho w}{\partial z}\right]\Delta x\Delta y\Delta z. \tag{1.1.5}$$

The right-hand side of this equation is actually the net rate of mass loss from the control volume shown in Fig. 1.1. This equation is equivalent to

$$\frac{\partial \rho}{\partial t} + \nabla\cdot\left(\rho\vec{U}\right) = 0. \tag{1.1.6}$$

It can also be written as

$$\underbrace{\frac{\partial \rho}{\partial t} + u\frac{\partial \rho}{\partial x} + v\frac{\partial \rho}{\partial y} + w\frac{\partial \rho}{\partial z}}_{\frac{D\rho}{Dt}} + \rho \nabla \cdot \vec{U} = 0, \tag{1.1.6a}$$

or, equivalently,

$$\frac{D\rho}{Dt} + \rho \nabla \cdot \vec{U} = 0. \tag{1.1.7}$$

When the fluid is incompressible, $\rho = \text{const.}$, and mass continuity leads to

$$\nabla \cdot \vec{U} = 0. \tag{1.1.8}$$

Note that, although Eqs. (1.1.6)–(1.1.8) were derived in Cartesian coordinates, they are in vector form and therefore can be recast in other curvilinear coordinates.

1.1.3 Conservation of Momentum

We derive the equation of motion for a fluid particle here by applying Newton's second law of motion. For convenience the derivations will be performed in Cartesian coordinates. However, the resulting equation of motion can then be easily recast in any orthogonal curvilinear coordinate system.

Fluid Acceleration and Forces

The starting point is Newton's second law for the fluid in the control volume $\Delta x \Delta y \Delta z$, according to which

$$\rho \left(\Delta x \Delta y \Delta z\right) \vec{a} = \vec{F}, \tag{1.1.9}$$

where $\vec{F}$ is the total external force acting on the fluid element. Now the acceleration term can be recast as

$$\vec{a} = \frac{D\vec{U}}{Dt} = \frac{\partial \vec{U}}{\partial t} + u\frac{\partial \vec{U}}{\partial x} + v\frac{\partial \vec{U}}{\partial y} + w\frac{\partial \vec{U}}{\partial z}, \tag{1.1.10}$$

where we have used the aforementioned relation between Eulerian and Lagrangian descriptions. The right-hand side of this equation is the Eulerian equivalent of its left-hand side.

The forces that act on the fluid element are of two types:

1. body forces (weight, electrical, magnetic, etc.),
2. surface forces (surface stresses).

Let us represent the totality of the body forces, per unit mass, as

$$\vec{F} = \vec{F}_b + \vec{F}_s.$$

The body force can be represented as

$$\vec{F}_b = F_{b,x}\vec{e}_x + F_{b,y}\vec{e}_y + F_{b,z}\vec{e}_z, \tag{1.1.11}$$

where $\vec{e}_x$, $\vec{e}_y$, and $\vec{e}_z$ are unit vectors for the x, y, and z coordinates, respectively.

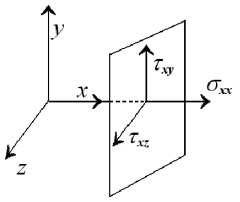

Figure 1.2. Viscous stresses in a fluid.

A viscous fluid in motion is always subject to surface forces. Let us use the convention displayed in Fig. 1.2 for showing these stresses. Thus σ_{xx} is the normal stress (normal force per unit surface area) in the x direction, and τ_{xy} is the shear stress acting in the y direction in the plane perpendicular to the x axis. For a control volume $\Delta x \Delta y \Delta z$, the force resulting from the stresses that act in the xy plane are shown in Fig. 1.3. The forces that are due to stresses in the xz and yz planes can be similarly depicted.

The stresses at any point in the flow field form a stress tensor. In Cartesian coordinates we can write

$$\begin{bmatrix} \sigma_{xx} & \tau_{xy} & \tau_{xz} \\ \tau_{yx} & \sigma_{yy} & \tau_{yz} \\ \tau_{zx} & \tau_{zy} & \sigma_{zz} \end{bmatrix}. \tag{1.1.12}$$

The stress tensor is symmetric, i.e., $\tau_{ij} = \tau_{ji}$.

The net stress force on the fluid element in Fig. 1.3 in the x direction will be

$$\Delta x \Delta y \Delta z \left[\frac{\partial \sigma_{xx}}{\partial x} + \frac{\partial \tau_{yx}}{\partial y} + \frac{\partial \tau_{zx}}{\partial z} \right]. \tag{1.1.13}$$

Combining Eqs. (1.1.9)–(1.1.13), we find that the components of the equation of motion in x, y, and z coordinates will be

$$\rho \frac{Du}{Dt} = F_{b,x} + \frac{\partial \sigma_{xx}}{\partial x} + \frac{\partial \tau_{yx}}{\partial y} + \frac{\partial \tau_{zx}}{\partial z}, \tag{1.1.14}$$

$$\rho \frac{Dv}{Dt} = F_{b,y} + \frac{\partial \tau_{xy}}{\partial x} + \frac{\partial \sigma_{yy}}{\partial y} + \frac{\partial \tau_{zy}}{\partial z}, \tag{1.1.15}$$

$$\rho \frac{Dw}{Dt} = F_{b,z} + \frac{\partial \tau_{xz}}{\partial x} + \frac{\partial \tau_{yz}}{\partial y} + \frac{\partial \sigma_{zz}}{\partial z}. \tag{1.1.16}$$

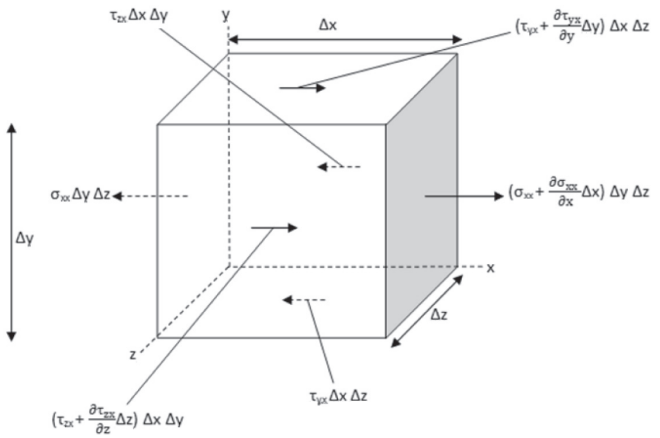

Figure 1.3. Heat conduction terms and work terms resulting from stresses in the xy plane.

In shorthand, these equations can be represented by,

$$\rho \frac{D\vec{U}}{Dt} = \vec{F}_b + \nabla \cdot \underline{\underline{\tau}}, \tag{1.1.17}$$

where $\underline{\underline{\tau}}$ is the dyadic stress tensor:

$$\underline{\underline{\tau}} = \begin{bmatrix} \sigma_{xx}\vec{e}_x\vec{e}_x & \tau_{xy}\vec{e}_x\vec{e}_y & \tau_{xz}\vec{e}_x\vec{e}_z \\ \tau_{yx}\vec{e}_y\vec{e}_x & \sigma_{yy}\vec{e}_y\vec{e}_y & \tau_{yz}\vec{e}_y\vec{e}_z \\ \tau_{zx}\vec{e}_z\vec{e}_x & \tau_{zy}\vec{e}_z\vec{e}_y & \sigma_{zz}\vec{e}_z\vec{e}_z \end{bmatrix}. \tag{1.1.18}$$

The rule for finding the divergence of a tensor is

$$\nabla \cdot \underline{\underline{\tau}} = \left[\vec{e}_i \frac{\partial}{\partial x_j}\right] \cdot \left[\tau_{jk}\vec{e}_j\vec{e}_k\right] = \frac{\partial \tau_{jk}}{\partial x_j}\vec{e}_k\,(\vec{e}_i \cdot \vec{e}_j) = \delta_{ij}\frac{\partial \tau_{jk}}{\partial x_j}\vec{e}_k, \tag{1.1.18a}$$

where subscripts i, j, and k represent the three coordinates and δ_{ij} is Kronecker's delta function. Einstein's rule for summation is used here, whereby repetition of an index in a term implies summation over that subscript. Thus $\vec{e}_i \frac{\partial}{\partial x_i}$ actually implies $\sum_{i=1}^{3} \vec{e}_i \frac{\partial}{\partial x_i}$.

Constitutive Relations for the Equation of Motion

The constitutive relation (which ties the stress tensors to the fluid strain rates and thereby to the fluid kinematics) for Newtonian fluids is

$$\sigma_{ii} = -P + \tau_{ii} = -P + 2\mu\frac{\partial u_i}{\partial x_i} + \lambda\nabla \cdot \vec{U}, \tag{1.1.19}$$

$$\tau_{ij} = \tau_{ji} = \mu\left(\frac{\partial u_i}{\partial x_j} + \frac{\partial u_j}{\partial x_i}\right), \tag{1.1.20}$$

where i and j are indices representing components of the Cartesian coordinates. The normal stress is thus made up of two components: the pressure (which is isotropic) and the viscous normal stress. Thus,

$$\sigma_{xx} = -P + \tau_{xx} = -P + 2\mu\frac{\partial u}{\partial x} + \lambda\nabla \cdot \vec{U}, \tag{1.1.21a}$$

$$\sigma_{yy} = -P + \tau_{yy} = -P + 2\mu\frac{\partial v}{\partial y} + \lambda\nabla \cdot \vec{U}, \tag{1.1.21b}$$

$$\sigma_{zz} = -P + \tau_{zz} = -P + 2\mu\frac{\partial w}{\partial z} + \lambda\nabla \cdot \vec{U}, \tag{1.1.21c}$$

$$\tau_{xy} = \tau_{yx} = \mu\left(\frac{\partial u}{\partial y} + \frac{\partial v}{\partial x}\right), \tag{1.1.21d}$$

$$\tau_{xz} = \tau_{zx} = \mu\left(\frac{\partial u}{\partial z} + \frac{\partial w}{\partial x}\right), \tag{1.1.21e}$$

$$\tau_{yz} = \tau_{zy} = \mu\left(\frac{\partial v}{\partial z} + \frac{\partial w}{\partial y}\right). \tag{1.1.21f}$$

In the preceding equations μ is the coefficient of viscosity (dynamic viscosity, in kilograms per meter times inverse seconds in SI units) and λ is the second coefficient of viscosity (coefficient of bulk viscosity). According to Stokes' assumption,

$$\lambda = -\frac{2}{3}\mu. \tag{1.1.22a}$$

This expression can be proved for monatomic gases.

Thus, in short hand, the elements of the Cartesian stress tensor can be shown as

$$\tau_{ij} = -\left(P + \frac{2}{3}\mu\frac{\partial u_k}{\partial x_k}\right)\delta_{ij} + \mu\left(\frac{\partial u_i}{\partial x_j} + \frac{\partial u_j}{\partial x_i}\right). \tag{1.1.22b}$$

The elements of the Newtonian fluid stress tensor in cylindrical and spherical coordinates can be found in Appendix A.

Equation of Motion for a Newtonian Fluid

Equation (1.1.17) can be recast as

$$\rho\frac{D\vec{U}}{Dt} = \rho\vec{g} + \nabla\cdot\underline{\underline{\tau}}. \tag{1.1.23}$$

The relationship between $\underline{\underline{\tau}}$ and the strain-rate tensor should follow the Newtonian fluid behavior described earlier. Here $\vec{g}$ is the total body force per unit mass and is identical to the gravitational acceleration when weight is the only body force present. Substitution for $\underline{\underline{\tau}}$, for Cartesian coordinates, leads to

$$\rho\frac{Du}{Dt} = \rho g_x - \frac{\partial\mathcal{P}}{\partial x} + \frac{\partial}{\partial x}\left[\mu\left(2\frac{\partial u}{\partial x} - \frac{2}{3}\nabla\cdot\vec{U}\right)\right] + \frac{\partial}{\partial y}\left[\mu\left(\frac{\partial v}{\partial x} + \frac{\partial u}{\partial y}\right)\right] + \frac{\partial}{\partial z}\left[\mu\left(\frac{\partial w}{\partial x} + \frac{\partial u}{\partial z}\right)\right], \tag{1.1.24a}$$

$$\rho\frac{Dv}{Dt} = \rho g_y - \frac{\partial\mathcal{P}}{\partial y} + \frac{\partial}{\partial x}\left[\mu\left(\frac{\partial v}{\partial x} + \frac{\partial u}{\partial y}\right)\right] + \frac{\partial}{\partial y}\left[\mu\left(2\frac{\partial v}{\partial y} - \frac{2}{3}\nabla\cdot\vec{U}\right)\right] + \frac{\partial}{\partial z}\left[\mu\left(\frac{\partial w}{\partial y} + \frac{\partial v}{\partial z}\right),\right] \tag{1.1.24b}$$

$$\rho\frac{Dw}{Dt} = \rho g_z - \frac{\partial\mathcal{P}}{\partial z} + \frac{\partial}{\partial x}\left[\mu\left(\frac{\partial w}{\partial x} + \frac{\partial u}{\partial z}\right)\right] + \frac{\partial}{\partial y}\left[\mu\left(\frac{\partial w}{\partial y} + \frac{\partial v}{\partial z}\right)\right] + \frac{\partial}{\partial z}\left[\mu\left(2\frac{\partial w}{\partial z} - \frac{2}{3}\nabla\cdot\vec{U}\right)\right]. \tag{1.1.24c}$$

For incompressible fluids we have $\nabla\cdot\vec{U} = 0$; therefore

$$\rho\frac{D\vec{U}}{Dt} = \rho\vec{g} - \nabla P + \mu\nabla^2\vec{U}. \tag{1.1.25}$$

The components of the Newtonian fluid equation of motion in cylindrical and spherical coordinates can be found in Appendix B.

1.1.4 Conservation of Energy

The conservation principle in this case is the first law of thermodynamics, which for a control volume represented by $\Delta x\Delta y\Delta z$ will be

$$\rho(\Delta x\Delta y\Delta z)\frac{D}{Dt}\left(\boldsymbol{u} + \tfrac{1}{2}U^2 - \vec{g}\cdot\vec{r}\right) = \dot{Q}_{\text{in}} - \dot{W}_{\text{out}}, \tag{1.1.26}$$

where $\dot{Q}_{\text{in}}$ is the rate of heat entering the control volume, $\dot{W}_{\text{out}}$ is the rate of work done by the control volume on its surroundings, $\boldsymbol{u}$ is the specific internal energy of

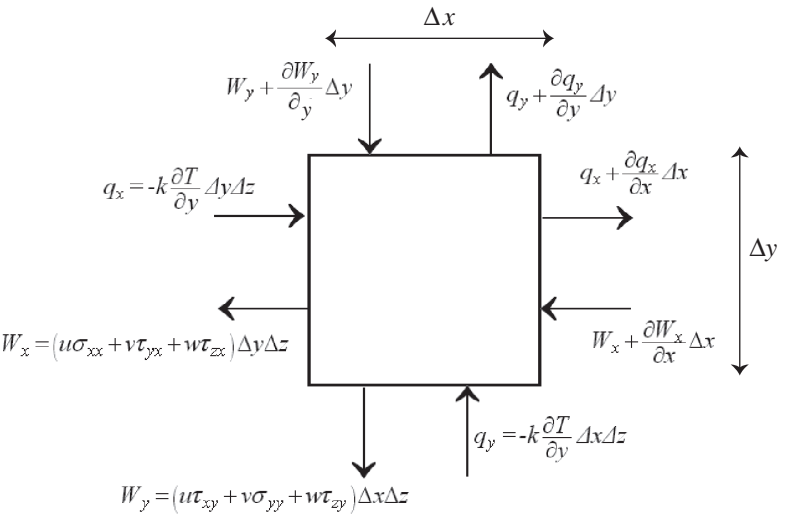

Figure 1.4. Thermal and mechanical surface energy flows in the xy plane for an infinitesimally small control volume.

the fluid, and $\vec{r}$ is the position vector. This equation accounts for both thermal and mechanical energy forms. The constitutive relation for molecular thermal energy diffusion for common materials is Fourier's law, according to which the heat flux resulting from the molecular diffusion of heat (heat conduction) is related to the local temperature gradient according to

$$\vec{q}'' = -k\nabla T. \tag{1.1.27}$$

Figure 1.4 displays the components of the thermal energy and mechanical work arriving at and leaving the control volume $\Delta x\Delta y\Delta z$ in the xy plane. In shorthand, we can write the following rates.

- Rate of accumulation of energy:

$$\rho\left(\Delta x\Delta y\Delta z\right)\frac{D}{Dt}\left(\boldsymbol{u} + \frac{1}{2}\left|\vec{U}\right|^2 - \vec{g}\cdot\vec{r}\right). \tag{1.1.28}$$

- Rate of heat added to the control volume:

$$\dot{Q}_{\text{in}} = \nabla\cdot\left(k\nabla T\right)\left(\Delta x\Delta y\Delta z\right). \tag{1.1.29}$$

- Rate of mechanical work done by the fluid element:

$$\dot{W}_{\text{out}} = -\nabla\cdot\left(\vec{U}\cdot\underline{\underline{\tau}}\right)\left(\Delta x\Delta y\Delta z\right) = -\left(\Delta x\Delta y\Delta z\right)\left\{\frac{\partial}{\partial x}\left(u\sigma_{xx} + v\tau_{yx} + w\tau_{zx}\right)\right.$$
$$\left. + \frac{\partial}{\partial y}\left(u\tau_{xy} + v\sigma_{yy} + w\tau_{zy}\right) + \frac{\partial}{\partial z}\left(u\tau_{xz} + v\tau_{yz} + w\sigma_{zz}\right)\right\}. \tag{1.1.30}$$

- Rate of body-force work done on the fluid element:

$$\left(\Delta x\Delta y\Delta z\right)\rho\vec{g}\cdot\vec{U}. \tag{1.1.31}$$

With these expressions, the first law of thermodynamics will thus lead to

$$\rho\left(\frac{D\boldsymbol{u}}{Dt}+\vec{U}\cdot\frac{D\vec{U}}{Dt}-\vec{g}\cdot\vec{U}\right)=\nabla\cdot k\nabla T+\nabla\cdot\left(\vec{U}\cdot\underline{\underline{\tau}}\right). \tag{1.1.32}$$

In Cartesian coordinates, for example, this equation expands to

$$\begin{aligned}&\rho\frac{D}{Dt}\left[\boldsymbol{u}+\tfrac{1}{2}\left(u^2+v^2+w^2\right)\right]-\rho\vec{U}\cdot\vec{g}\\&\quad=\nabla\cdot(k\nabla T)+\frac{\partial}{\partial x}\left(u\sigma_x+v\tau_{yx}+w\tau_{zx}\right)+\frac{\partial}{\partial y}\left(u\tau_{yx}+v\sigma_y+w\tau_{yz}\right)\\&\qquad+\frac{\partial}{\partial z}\left(u\tau_{zx}+v\tau_{zy}+w\sigma_z\right).\end{aligned} \tag{1.1.33}$$

The preceding equations contain mechanical and thermal energy terms, as mentioned earlier. The mechanical terms are actually redundant, however, and can be dropped from the energy conservation equation without loss of any useful information. This is because the mechanical energy terms actually do not provide any information that is not already provided by the momentum conservation equation. It should be emphasized, however, that there is nothing wrong about keeping the redundant mechanical energy terms in the energy conservation equation. In fact, these terms are sometimes kept intentionally in the energy equation for numerical stability reasons. They are dropped most of the time nevertheless.

To eliminate the redundant mechanical energy terms, consider the momentum conservation equation [Eq. (1.1.17)], which, assuming that gravitational force is the only body force, could be cast as Eq. (1.1.23). The dot product of Eq. (1.1.23) with $\vec{U}$ will provide the mechanical energy transport equation:

$$\rho\vec{U}\cdot\frac{D\vec{U}}{Dt}=\rho\vec{g}\cdot\vec{U}+\vec{U}\cdot\left(\nabla\cdot\underline{\underline{\tau}}\right). \tag{1.1.34}$$

The following identity relation can now be applied to the last term on the right-hand side of this equation,

$$\vec{U}\cdot\left(\nabla\cdot\underline{\underline{\tau}}\right)=\nabla\cdot\left(\vec{U}\cdot\underline{\underline{\tau}}\right)-\underline{\underline{\tau}}:\left(\nabla\vec{U}\right). \tag{1.1.35}$$

Now, combining Eqs. (1.1.34) and (1.1.35) and subtracting the resulting equation from Eq. (1.1.32) leads to the thermal energy equation,

$$\rho\frac{D\boldsymbol{u}}{Dt}=\nabla\cdot(k\nabla T)+\underline{\underline{\tau}}:\left(\nabla\vec{U}\right), \tag{1.1.36}$$

where the last term on the right-hand side is the viscous dissipation term. The rule for the scalar product of two Cartesian tensors is

$$\underline{\underline{a}}:\underline{\underline{b}}=[a_{ij}\vec{e}_i\vec{e}_j]:[b_{kl}\vec{e}_k\vec{e}_l]=\delta_{il}\delta_{jk}a_{ij}b_{kl}, \tag{1.1.37}$$

where Einstein's rule is used. The last term on the right-hand side of Eq. (1.1.36) thus expands to $\tau_{ij}\frac{\partial u_i}{\partial x_j}$.

The preceding derivations can be done without using tensor notation, as follows.

- In Eqs. (1.1.14), (1.1.15), and (1.1.16), replace $F_{b,x}$ with ρg_x, $F_{b,y}$ with ρg_y, and $F_{b,z}$ with ρg_z. Then multiply Eqs. (1.1.14), (1.1.15), and (1.1.16) by u, v, and w, respectively, and add up the resulting three equations to get

$$\rho \frac{D}{Dt}\left[\frac{1}{2}\left(u^2+v^2+w^2\right)\right] = u\left(\frac{\partial \sigma_{xx}}{\partial x}+\frac{\partial \tau_{yx}}{\partial y}+\frac{\partial \tau_{zx}}{\partial z}\right)+v\left(\frac{\partial \tau_{xy}}{\partial x}+\frac{\partial \sigma_{yy}}{\partial y}+\frac{\partial \tau_{zy}}{\partial z}\right) + w\left(\frac{\partial \tau_{xz}}{\partial x}+\frac{\partial \tau_{yz}}{\partial y}+\frac{\partial \sigma_{zz}}{\partial z}\right)+\rho \vec{g}\cdot\vec{U}. \tag{1.1.38}$$

  This equation is equivalent to Eq. (1.1.34).

- Subtract Eq. (1.1.38) from Eq. (1.1.33) to derive the thermal energy equation:

$$\rho \frac{D\boldsymbol{u}}{Dt} = \nabla\cdot(k\nabla T)+\sigma_{xx}\frac{\partial u}{\partial x}+\sigma_{yy}\frac{\partial v}{\partial y}+\sigma_{zz}\frac{\partial w}{\partial z}+\tau_{xy}\left(\frac{\partial u}{\partial y}+\frac{\partial v}{\partial x}\right) + \tau_{yz}\left(\frac{\partial v}{\partial z}+\frac{\partial w}{\partial y}\right)+\tau_{xz}\left(\frac{\partial u}{\partial z}+\frac{\partial w}{\partial x}\right). \tag{1.1.39}$$

  This equation is equivalent to Eq. (1.1.36).

We can further manipulate Eq. (1.1.36) and cast it in a more familiar form by noting that

$$\underline{\underline{\tau}} : \left(\nabla \vec{U}\right) = -P\left(\nabla\cdot\vec{U}\right)+\underline{\underline{\tau}}' : \left(\nabla\vec{U}\right), \tag{1.1.40}$$

where $\underline{\underline{\tau}}'$ is the viscous stress dyadic tensor whose elements for a Newtonian fluid, in Cartesian coordinates, are

$$\tau'_{ij} = \mu\left(\frac{\partial u_i}{\partial x_j}+\frac{\partial u_j}{\partial x_i}\right)+\delta_{ij}\lambda\nabla\cdot\vec{U}. \tag{1.1.41}$$

The last term on the right-hand side of Eq. (1.1.40) is the viscous dissipation term, $\mu\Phi$. The thermal energy equation then becomes

$$\rho\frac{D\boldsymbol{u}}{Dt} = \nabla\cdot(k\nabla T)-P\left(\nabla\cdot\vec{U}\right)+\mu\Phi. \tag{1.1.42}$$

Furthermore, noting that $\boldsymbol{h} = \boldsymbol{u} + P/\rho$, we can cast this equation in terms of $\boldsymbol{h}$. First, we note from Eq. (1.1.7), that

$$\nabla\cdot\vec{U} = -\frac{1}{\rho}\frac{D\rho}{Dt}. \tag{1.1.43}$$

Using this equation and the relation between $\boldsymbol{h}$ and $\boldsymbol{u}$, we can recast Eq. (1.1.42) as

$$\rho\frac{D\boldsymbol{h}}{Dt} = \nabla\cdot(k\nabla T)+\frac{DP}{Dt}+\mu\Phi. \tag{1.1.44}$$

Again, these derivations can be done without tensor notation. Starting from Eq. (1.1.39) and using the Newtonian fluid constitutive relations, namely Eqs. (1.1.21a)–(1.1.21f), we can show that

$$\sigma_{xx}\frac{\partial u}{\partial x}+\sigma_{yy}\frac{\partial v}{\partial y}+\sigma_{zz}\frac{\partial w}{\partial z}=-P\nabla\cdot\vec{U}-\frac{2}{3}\mu\left(\nabla\cdot\vec{U}\right)^2 +2\mu\left[\left(\frac{\partial u}{\partial x}\right)^2+\left(\frac{\partial v}{\partial y}\right)^2+\left(\frac{\partial w}{\partial z}\right)^2\right], \quad (1.1.45)$$

$$\tau_{xy}\left(\frac{\partial v}{\partial x}+\frac{\partial u}{\partial y}\right)=\mu\left(\frac{\partial v}{\partial x}+\frac{\partial u}{\partial y}\right)^2, \quad (1.1.46)$$

$$\tau_{yz}\left(\frac{\partial w}{\partial y}+\frac{\partial v}{\partial z}\right)=\mu\left(\frac{\partial w}{\partial y}+\frac{\partial v}{\partial z}\right)^2, \quad (1.1.47)$$

$$\tau_{zx}\left(\frac{\partial u}{\partial z}+\frac{\partial w}{\partial x}\right)=\mu\left(\frac{\partial u}{\partial z}+\frac{\partial w}{\partial x}\right)^2. \quad (1.1.48)$$

Substitution from Eqs. (1.1.45)–(1.1.48) into Eq. (1.1.39) will result in Eq. (1.1.42).

Equation (1.1.44) can be cast in terms of temperature, which is often more convenient. To do this, we note that for a pure and single-phase substance at equilibrium we have $\boldsymbol{h}=\boldsymbol{h}(T,\ P)$ and can therefore write

$$d\boldsymbol{h}=\left(\frac{\partial \boldsymbol{h}}{\partial T}\right)_P dP+\left(\frac{\partial \boldsymbol{h}}{\partial P}\right)_T dT=C_P dT+\left[v-T\left(\frac{\partial v}{\partial T}\right)_P\right]dP. \quad (1.1.49)$$

It can then easily be shown that

$$\rho\frac{D\boldsymbol{h}}{Dt}=\rho C_P\frac{DT}{Dt}+\left[1+\left(\frac{\partial \ln\rho}{\partial \ln T}\right)_P\right]\frac{DP}{Dt}. \quad (1.1.50)$$

Equation (1.1.44) can therefore be cast as

$$\rho C_P\frac{DT}{Dt}=\nabla\cdot(k\nabla T)-\left(\frac{\partial \ln\rho}{\partial \ln T}\right)_P\frac{DP}{Dt}+\mu\Phi. \quad (1.1.51)$$

For ideal gases we have $\left(\frac{\partial \ln\rho}{\partial \ln T}\right)_P=-1$. Furthermore, for fluids flowing under constant-pressure conditions or fluids that are incompressible, the second term on the right-hand side of this equation will vanish, leading to the following familiar form of the thermal energy equation:

$$\rho C_P\frac{DT}{Dt}=\nabla\cdot(k\nabla T)+\mu\Phi. \quad (1.1.52)$$

The viscous dissipation term, in Cartesian coordinates, is

$$\Phi=2\left[\left(\frac{\partial u}{\partial x}\right)^2+\left(\frac{\partial v}{\partial y}\right)^2+\left(\frac{\partial w}{\partial z}\right)^2\right]+\left(\frac{\partial v}{\partial x}+\frac{\partial u}{\partial y}\right)^2+\left(\frac{\partial w}{\partial y}+\frac{\partial v}{\partial z}\right)^2 +\left(\frac{\partial u}{\partial z}+\frac{\partial w}{\partial x}\right)^2-\tfrac{2}{3}\left(\nabla\cdot\vec{U}\right)^2. \quad (1.1.53)$$

Equation (1.1.52), expanded in polar cylindrical and spherical coordinates, can be found in Appendix C.

In the preceding derivations we did not consider diffusion processes that occur in multicomponent mixtures. The derivations were therefore for pure substances or for multicomponent mixtures in which the effects of interdiffusion of components of the fluid are neglected. In nonreacting flows the effect of the mass diffusion term is in fact usually small.

To account for the effect of diffusion that occurs in a multicomponent mixture, an additional term needs to be added to the right-hand side of Eqs. (1.1.42) and (1.1.44). Equation (1.1.44), for example, becomes,

$$\rho \frac{D\boldsymbol{h}}{Dt} = \nabla \cdot k\nabla T + \frac{DP}{Dt} + \mu\,\Phi - \nabla \cdot \sum_{l=1}^{N} \vec{j}_l\, \boldsymbol{h}_l, \tag{1.1.54}$$

where the subscript l represents species, $\vec{j}_l$ is the diffusive mass flux of species l with respect to the mixture, and N is the total number of chemical species that constitute the mixture. Equation (1.1.54) is based on the assumption that no chemical reaction takes place in the fluid mixture and neglects the diffusion–thermal effect (the Dufour effect), a second-order contributor to conduction.

The derivation of Eq. (1.1.54) is simple, and we can do this by replacing the diffusion heat flux, namely $-k\nabla T$, with

$$-k\nabla T + \sum_{l=1}^{L} \vec{j}_l \boldsymbol{h}_l. \tag{1.1.55}$$

1.2 Multicomponent Mixtures

The term mixture in this chapter refers to a mixture of two or more chemical species in the same phase. Fluids in nature are often mixtures of two or more chemical species. Multicomponent mixtures are also common in industrial applications. Ordinary dry air, for example, is a mixture of O_2, N_2, and several noble gases in small concentrations. Water vapor and CO_2 are also present in common air most of the time. Small amounts of dissolved contaminants are often unavoidable and present even in applications in which a high-purity liquid is meant to be used.

We often treat a multicomponent fluid mixture as a single fluid by proper definition of mixture properties. However, when mass transfer of one or more components of the mixture takes place, for example during evaporation or condensation of water in an air–water-vapor mixture, the composition of the mixture will be nonuniform, implying that the mixture's thermophysical properties will also be nonuniform.

1.2.1 Basic Definitions and Relations

The *concentration* or *partial density* of species l, ρ_l, is simply the in situ mass of that species in a unit mixture volume. The mixture density ρ is related to the partial densities according to

$$\rho = \sum_{l=1}^{N} \rho_l, \tag{1.2.1}$$

with the summation here and elsewhere performed on all the chemical species in the mixture. The *mass fraction* of species l is defined as

$$m_l = \frac{\rho_l}{\rho}. \tag{1.2.2}$$

The *molar concentration* of chemical species l, $\boldsymbol{C}_l$, is defined as the number of moles of that species in a unit mixture volume. The forthcoming definitions for the mixture's molar concentration and the *mole fraction* of species l will then apply:

$$\boldsymbol{C} = \sum_{l=1}^{N} \boldsymbol{C}_l, \tag{1.2.3}$$

$$X_l = \frac{\boldsymbol{C}_l}{\boldsymbol{C}}. \tag{1.2.4}$$

Clearly we must have

$$\sum_{l=1}^{N} m_l = \sum_{l=1}^{N} X_l = 1. \tag{1.2.5}$$

The following relations among mass-fraction-based and mole-fraction-based parameters can be easily derived:

$$\rho_l = M_l \boldsymbol{C}_l, \tag{1.2.6}$$

$$m_l = \frac{X_l M_l}{\sum\limits_{j=1}^{n} X_j M_j} = \frac{X_l M_l}{M}, \tag{1.2.7}$$

$$X_l = \frac{m_l / M_l}{\sum\limits_{j=1}^{N} \frac{m_j}{M_j}} = \frac{m_l M}{M_l}, \tag{1.2.8}$$

where M and M_l represent the molar masses of the mixture and the chemical-specific l, respectively, with M defined according to

$$M = \sum_{j=1}^{N} X_j M_j, \tag{1.2.9}$$

$$\frac{1}{M} = \sum_{j=1}^{N} \frac{m_j}{M_j}. \tag{1.2.10}$$

When one component, say component j, constitutes the bulk of a mixture, then

$$M \approx M_j, \tag{1.2.11}$$

$$m_l \approx \frac{X_l}{M_j} M_l. \tag{1.2.12}$$

In a gas mixture, *Dalton's law* requires that

$$P = \sum_{l=1}^{n} P_l, \tag{1.2.13}$$

where P is the mixture (total) pressure and P_l is the *partial pressure* of species l.

In a gas or liquid mixture the species that constitute the mixture are at thermal equilibrium (the same temperature). In a gas mixture that is at temperature T, at any location and any time, the forthcoming constitutive relation follows:

$$\rho_l = \rho_l\left(P_l,\ T\right). \tag{1.2.14}$$

Some or all of the components of a gas mixture may be assumed to be ideal gases, in which case, for the ideal-gas component l,

$$\rho_l = \frac{P_l}{\dfrac{R_u}{M_l}T}, \tag{1.2.15}$$

where R_u is the universal gas constant. When all the components of a gas mixture are ideal gases, then the mole fraction of species l will be related to its partial pressure according to

$$X_l = P_l / P. \tag{1.2.16}$$

EXAMPLE 1.1. The atmosphere of a laboratory during an experiment is at $T = 25\ ^\circ\text{C}$ and $P = 1.013$ bars. Measurement shows that the relative humidity in the lab is 77%. Calculate the air and water partial densities, mass fractions, and mole fractions.

SOLUTION. Let us start from the definition of relative humidity φ:

$$\varphi = P_v / P_{\text{sat}}(T).$$

Thus

$$P_v = (0.77)\,(3.14\ \text{kPa}) = 2.42\ \text{kPa}.$$

The partial density of air can be calculated by assuming air is an ideal gas at $25\ ^\circ\text{C}$ and a pressure of $P_a = P - P_v = 98.91$ kPa to be $\rho_a = 1.156\ \text{kg/m}^3$.

The water vapor is at $25\ ^\circ\text{C}$ and 2.42 kPa and is therefore superheated. Its density can be found from steam property tables to be $\rho_v = 0.0176\ \text{kg/m}^3$. Using Eqs. (1.2.1) and (1.2.2), we get $m_v = 0.015$.

EXAMPLE 1.2. A sample of pure water is brought into equilibrium with a large mixture of O_2 and N_2 gases at 1-bar pressure and 300 K temperature. The volume fractions of O_2 and N_2 in the gas mixture before it was brought into contact with the water sample were 22% and 78%, respectively. Solubility data indicate that the mole fractions of O_2 and N_2 in water for the given conditions are approximately 5.58×10^{-6} and 9.9×10^{-6}, respectively. Find the mass fractions of O_2 and N_2 in both the liquid and the gas phases. Also, calculate the molar concentrations of all the involved species in the liquid phase.

SOLUTION. Before the $O_2 + N_2$ mixture is brought in contact with water, we have

$$P_{\text{O}_2,\,\text{initial}}/P_{\text{tot}} = X_{\text{O}_2,\,G,\,\text{initial}} = 0.22,$$
$$P_{\text{N}_2,\,\text{initial}}/P_{\text{tot}} = X_{\text{N}_2,\,G,\,\text{initial}} = 0.78,$$

where $P_{\text{tot}} = 1$ bar. The gas phase, after it reaches equilibrium with water, will be a mixture of O_2, N_2, and water vapor. Because the original gas-mixture volume was large and, given that the solubilities of oxygen and nitrogen in water are very low, we can write for the equilibrium conditions

$$P_{\text{O}_2,\,\text{final}}/(P_{\text{tot}} - P_v) = X_{\text{O}_2,\,G,\,\text{initial}} = 0.22, \tag{a1}$$

$$P_{\text{N}_2,\,\text{final}}/(P_{\text{tot}} - P_v) = X_{\text{N}_2,\,G,\,\text{initial}} = 0.78. \tag{a2}$$

Now, under equilibrium,

$$X_{\text{O}_2,\,G,\,\text{final}} \approx P_{\text{O}_2,\,\text{final}}/P_{\text{tot}}, \tag{b1}$$

$$X_{\text{N}_2,\,G,\,\text{final}} \approx P_{\text{N}_2,\,\text{final}}/P_{\text{tot}}. \tag{b2}$$

We use the approximately equal signs in the previous equations because they assume that water vapor acts as an ideal gas. The vapor partial pressure will be equal to vapor saturation pressure at 300 K, namely, $P_v = 0.0354$ bar. Equations (a1) and (a2) can then be solved to get $P_{\text{O}_2,\,\text{final}} = 0.2122$ bar and $P_{\text{N}_2,\,\text{final}} = 0.7524$ bar. Approximations (b1) and (b2) then give $X_{\text{O}_2,\,G,\,\text{final}} \approx 0.2122$, $X_{\text{N}_2,\,G,\,\text{final}} \approx 0.7524$, and the mole fraction of water vapor will be

$$X_{G,v} = 1 - (X_{\text{O}_2,\,G,\,\text{final}} + X_{\text{N}_2,\,G,\,\text{final}}) \approx 0.0354.$$

To find the gas-side mass fractions, we first apply Eq. (1.2.9), and then Eq. (1.2.7):

$$M_G = 0.2122 \times 32 + 0.7524 \times 28 + 0.0354 \times 18 \Rightarrow M_G = 28.49,$$

$$m_{\text{O}_2,\,G,\,\text{final}} = \frac{X_{\text{O}_2,\,G,\,\text{final}} M_{\text{O}_2}}{M_G} = \frac{(0.2122)\,(32)}{28.49} \approx 0.238,$$

$$m_{\text{N}_2,\,G,\,\text{final}} = \frac{(0.7524)\,(28)}{28.49} \approx 0.739.$$

For the liquid side, we first get M_L, the mixture's molecular mass number from Eq. (1.2.9):

$$M_L = 5.58 \times 10^{-6} \times 32 + 9.9 \times 10^{-6} \times 28 + \left[1 - (5.58 \times 10^{-6} + 9.9 \times 10^{-6})\right] \times 18 \approx 18.$$

Therefore, from Eq. (1.2.7),

$$m_{\text{O}_2,\,L,\,\text{final}} = \frac{5.58 \times 10^{-6}}{18}(32) = 9.92 \times 10^{-6},$$

$$m_{\text{N}_2,\,L,\,\text{final}} = \frac{9.9 \times 10^{-6}}{18}(28) = 15.4 \times 10^{-6}.$$

To calculate the concentrations, we note that the liquid side is now made up of three species, all with unknown concentrations. Equation (1.2.4) should be written out for every species; Eq. (1.2.5) is also satisfied. These give four equations in terms of the four unknowns: $\boldsymbol{C}_L$, $\boldsymbol{C}_{\text{O}_2,\,L,\,\text{final}}$, $\boldsymbol{C}_{\text{N}_2,\,L,\,\text{final}}$, and $\boldsymbol{C}_{L,W}$, where $\boldsymbol{C}_L$ and $\boldsymbol{C}_{L,W}$ stand for the total molar concentrations of the liquid mixture and

the molar concentration of the water substance, respectively. This calculation, however, will clearly show that, because of the very small mole fractions (and hence small concentrations) of O_2 and N_2,

$$\boldsymbol{C}_L \approx \boldsymbol{C}_{L,\,W} = \rho_{\mathrm{L}}/\mathrm{M}_{\mathrm{L}} = \frac{996.6\ \mathrm{kg/m^3}}{18\ \mathrm{kg/kmol}} = 55.36\ \mathrm{kmol/m^3}.$$

The concentrations of O_2 and N_2 can therefore be found from Eq. (1.2.4) to be

$$\boldsymbol{C}_{\mathrm{O_2},\,L,\,\mathrm{final}} \approx 3.09 \times 10^{-4}\ \mathrm{kmol/m^3},$$
$$\boldsymbol{C}_{\mathrm{N_2},\,L,\,\mathrm{final}} \approx 5.48 \times 10^{-4}\ \mathrm{kmol/m^3}.$$

1.2.2 Thermodynamic Properties

The extensive thermodynamic properties of a single phase mixture, when represented as *per unit mass* (in which case they actually become intensive properties) can all be found from

$$\xi = \frac{1}{\rho}\sum_{l=1}^{n}\rho_l\xi_l = \sum_{l=1}^{n} m_l\xi_l, \tag{1.2.17}$$

$$\xi_l = \xi_l\left(P_l,\, T\right), \tag{1.2.18}$$

where ξ can be any mixture's specific (per unit mass) property such as ρ, $\boldsymbol{u}$, $\boldsymbol{h}$, or $\boldsymbol{s}$; and ξ_l is the same property for pure substance l. Similarly, the following expression can be used when specific properties are all defined *per unit mole*:

$$\tilde{\xi} = \frac{1}{\boldsymbol{C}}\sum_{l=1}^{n}\boldsymbol{C}_l\tilde{\xi}_l = \sum_{l=1}^{n} x_l\tilde{\xi}_l. \tag{1.2.19}$$

Let us now focus on vapor-noncondensable mixtures, which are probably the most frequently encountered fluid mixtures and are therefore very important. Vapor-noncondensable mixtures are often encountered in evaporation and condensation systems. We can discuss the properties of vapor-noncondensable mixtures by treating the noncondensable as a single species. Although the noncondensable may be composed of a number of different gaseous constituents, average properties can be defined such that the noncondensables can be treated as a single species, as is commonly done for air. The subscripts v and n in the following discussion represent the vapor and the noncondensable species, respectively.

Air–water-vapor-mixture properties are discussed in standard thermodynamic textbooks. For a mixture with pressure P_G, temperature T_G, and vapor mass fraction m_v, the relative humidity φ and humidity ratio ω are defined as

$$\varphi = \frac{P_v}{P_{\mathrm{sat}}(T_G)} \approx \frac{X_v}{X_{v,\mathrm{sat}}}, \tag{1.2.20}$$

$$\omega = \frac{m_v}{m_n} = \frac{m_v}{1 - m_v}, \tag{1.2.21}$$

where $x_{v,\text{sat}}$ is the vapor mole fraction when the mixture is saturated. The last part of Eq. (1.2.20) evidently assumes that the noncondensable and the vapor are ideal gases. A mixture is saturated when $P_v = P_{\text{sat}}(T_G)$. When $\varphi < 1$, the vapor is in a superheated state because $P_v < P_{\text{sat}}(T_G)$. In this case the thermodynamic properties and their derivatives follow the gas-mixture rules.

The vapor-noncondensable mixtures that are encountered in evaporators and condensers are usually saturated. For a saturated mixture, the following equations must be added to the other mixture rules.

$$T_G = T_{\text{sat}}(P_v), \tag{1.2.22}$$

$$\rho_v = \rho_g(T_G) = \rho_g(P_v), \tag{1.2.23}$$

$$\boldsymbol{h}_v = \boldsymbol{h}_g(T_G) = \boldsymbol{h}_g(P_v). \tag{1.2.24}$$

Using the identity $m_v = \frac{\rho_v}{\rho_n + \rho_v}$ and assuming that the noncondensable is an ideal gas, we can show that

$$\frac{P_G - P_v}{\dfrac{R_u}{M_n} T_{\text{sat}}(P_v)}(1 - m_n) - \rho_g(P_v) m_n = 0. \tag{1.2.25}$$

Equation (1.2.25) indicates that P_G, T_G, and m_v are not independent. Knowing two parameters (e.g., T_G and m_v), we can iteratively solve Eq. (1.2.25) for the third unknown parameter (e.g., the vapor partial pressure when T_G and m_v are known).

The variations of the mixture temperature and the vapor pressure are related by the Clapeyron relation:

$$\frac{dP}{dT} = \left(\frac{dP}{dT}\right)_{\text{sat}} = \frac{\boldsymbol{h}_{fg}}{T_{\text{sat}}(\boldsymbol{v}_g - \boldsymbol{v}_f)}. \tag{1.2.26}$$

Therefore

$$\frac{\partial T_G}{\partial P_v} = \frac{\partial T_{\text{sat}}(P_v)}{\partial P_v} = \frac{T_G \boldsymbol{v}_{fg}}{\boldsymbol{h}_{fg}}. \tag{1.2.27}$$

EXAMPLE 1.3. For a saturated vapor-noncondensable binary mixture, derive expressions of the forms

$$\left(\frac{\partial \rho_G}{\partial P_G}\right)_{x_n} = f(P_G, x_n),$$

$$\left(\frac{\partial \rho_G}{\partial x_n}\right)_{P_G} = f(P_G, x_n).$$

SOLUTION. Let us approximately write

$$\rho_G = \frac{P_G}{\dfrac{R_u}{M} T_G} = \frac{M P_G}{R_u T_{\text{sat}}(P_v)},$$

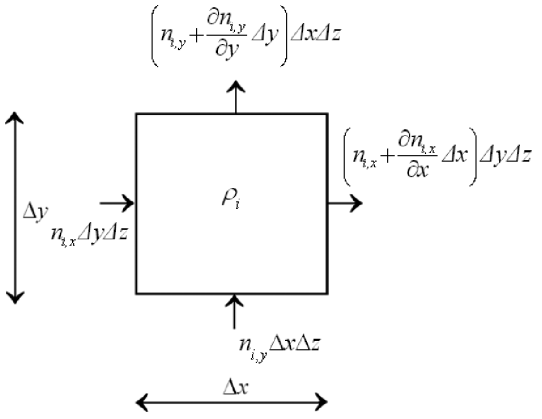

Figure 1.5. An infinitesimally small control volume for mass-species conservation.

where $M = X_n M_n + (1 - X_n)M_v$, $T_G = T_{\text{sat}}(P_v)$, and $P_v = (1 - X_n)P_G$. The argument of $T_{\text{sat}}(P_v)$ is meant to remind us that T_{sat} corresponds to $P_v = P_G(1 - X_n)$. Then

$$\left(\frac{\partial \rho_G}{\partial P_G}\right)_{X_n} = \frac{M}{R_u T_{\text{sat}}} - \frac{P_G M}{R_u T_{\text{sat}}^2}\left(\frac{\partial T_{\text{sat}}}{\partial P_G}\right).$$

Also, using the Clapeyron relation, we get

$$\frac{\partial T_{\text{sat}}}{\partial P_G} = \frac{\partial T_{\text{sat}}}{\partial P_v}\frac{\partial P_v}{\partial P_G} = \frac{\boldsymbol{v}_{fg} T_{\text{sat}}}{\boldsymbol{h}_{fg}}(1 - X_n).$$

The result will be

$$\left(\frac{\partial \rho_G}{\partial P_G}\right)_{X_n} = \frac{M}{R_u T_{\text{sat}}} - \frac{P_v \boldsymbol{v}_{fg} M}{R_u T_G \boldsymbol{h}_{fg}}.$$

It can also be proved that

$$\left(\frac{\partial \rho_G}{\partial X_n}\right)_{P_G} = \frac{P_G}{R_u T_G}(M_n - M_v) + \frac{P_G^2 \boldsymbol{v}_{fg} M}{R_u T_G \boldsymbol{h}_{fg}},$$

where $\boldsymbol{v}_{fg}$ and $\boldsymbol{h}_{fg}$ correspond to $T_{\text{sat}} = T_G$.

1.3 Fundamentals of Diffusive Mass Transfer

Often we deal with flow fields composed of mixtures of different chemical species rather than a single-component fluid. In these cases the conservation equations are more complicated because of the occurrence of mass diffusion. In a multicomponent fluid each species, in addition to its macroscopic displacement that is due to the flow (advection), also diffuses with respect to the mixture.

1.3.1 Species Mass Conservation

Consider the volume element $\Delta x \Delta y \Delta z$ in a flow field, the two-dimensional (2D) (x, y) cross section of which is shown in Fig. 1.5. We are interested in the transport of species *i.* The total mass flux of species *i* can, in general, be shown as

$$\vec{n}_i = n_{i,x}\vec{e}_x + n_{i,y}\vec{e}_y + n_{i,z}\vec{e}_z, \tag{1.3.1}$$

where $n_{i,x}$, $n_{i,y}$, and $n_{i,z}$ are components of the species mass flux along the Cartesian coordinates. Also, we define $\dot{r}_i$ as the volumetric generation rate of species i (in kilograms per cubic meter times inverse seconds in SI units). Evidently, we can apply the principle of mass conservation to species i and write

$$(\Delta x \Delta y \Delta z)\frac{\partial \rho_i}{\partial t} = -(\Delta x \Delta y \Delta z)\left[\frac{\partial n_{i,x}}{\partial x} + \frac{\partial n_{i,y}}{\partial y} + \frac{\partial n_{i,z}}{\partial z}\right] + (\Delta x \Delta y \Delta z)\,\dot{r}_i, \quad (1.3.2)$$

or, in vector form,

$$\frac{\partial \rho_i}{\partial t} + \nabla \cdot \vec{n}_i = \dot{r}_i. \quad (1.3.3)$$

It is easy to derive a similar equation in terms of molar fluxes:

$$\frac{\partial \boldsymbol{C}_i}{\partial t} + \nabla \cdot \vec{N}_i = \dot{R}_i, \quad (1.3.4)$$

where $\boldsymbol{C}_i$ (in kilomoles per cubic meter) is the concentration of species i and $\dot{R}_i$ (in kilomoles per cubic meter times inverse seconds) is its volumetric generation rate.

Summing up Eq. (1.3.3) over all the species in the mixture will lead to Eq. (1.1.6) because $\sum_i \rho_i = \rho$. Summing up Eq. (1.3.4) on all the species in the mixture, however, leads to

$$\frac{\partial \boldsymbol{C}}{\partial t} + \nabla \cdot \left(\boldsymbol{C}\vec{\tilde{U}}\right) = \sum_i \dot{R}_i. \quad (1.3.5)$$

1.3.2 Diffusive Mass Flux and Fick's Law

The mass flux of species i can be divided into two components: the advective and diffusive fluxes:

$$\vec{n}_i = \rho_i \vec{U} + \vec{j}_i = m_i\left(\rho\,\vec{U}\right) + \vec{j}_i. \quad (1.3.6)$$

In terms of the molar fluxes,

$$\vec{N}_i = \boldsymbol{C}_i\,\vec{\tilde{U}} + \vec{j}_i = X_i(\boldsymbol{C}\vec{\tilde{U}}) + \vec{J}_i. \quad (1.3.7)$$

The parameter $\vec{U}$ is the local mixture mass-average velocity, and $\vec{\tilde{U}}$ is the local mixture mole-average velocity. These are defined as

$$\vec{U} = \sum_{i=1}^{I} m_i\,\vec{U}_i = \frac{\vec{G}}{\rho} \quad (1.3.8)$$

$$\vec{\tilde{U}} = \sum_{i=1}^{I} X_i \vec{U}_i \quad (1.3.9)$$

where

$$\vec{U}_i = \frac{\vec{n}_i}{\rho_i}. \quad (1.3.10)$$

The mass-average velocity $\vec{U}$ is the mixture velocity that is used in conservation equations, including the Navier–Stokes equation. As a result, the mass-fraction-based formulation is convenient when other conservation equations are also solved.

The diffusive fluxes can thus be represented as

$$\vec{j}_i = \rho_i \left(\vec{U}_i - \vec{U} \right), \tag{1.3.11}$$

$$\vec{j}_i = \boldsymbol{C}_i \left(\vec{\tilde{U}}_i - \vec{\tilde{U}} \right). \tag{1.3.12}$$

Let us focus on the binary mixtures for now. The diffusive fluxes, according to Fick's law, can then be represented as

$$\vec{j}_1 = -\rho \mathcal{D}_{12} \nabla m_1, \tag{1.3.13}$$

$$\vec{j}_1 = -\boldsymbol{C} \mathcal{D}_{12} \nabla X_1, \tag{1.3.14}$$

where $i = 1$ or 2, representing the two species. Similar expressions can be written for the diffusive fluxes of species 2.

Fick's law thus indicates that the ordinary diffusive flux of a species in a binary mixture is proportional to the gradient of the mass fraction or concentration of that species, and diffusion takes place down the concentration gradient of a species. The parameter $\mathcal{D}_{12}$ is the binary diffusion coefficient (or mass diffusivity) of species 1 and 2.

Let us consider a quiescent binary mixture in steady state. We note that diffusion takes place even in a quiescent fluid field. Conservation of mass will then require that

$$\nabla \cdot \left(\vec{j}_1 + \vec{j}_2 \right) = 0. \tag{1.3.15}$$

We can evidently write,

$$\vec{j}_1 = -\rho \mathcal{D}_{12} \nabla m_1,$$
$$\vec{j}_2 = -\rho \mathcal{D}_{21} \nabla m_2.$$

Substituting for $\vec{j}_1$ and $\vec{j}_2$ from these expressions into Eq. (1.3.15) and noting that $m_1 + m_2 = 1$, we come to the important conclusion that

$$\mathcal{D}_{12} = \mathcal{D}_{21}. \tag{1.3.16}$$

For gas mixtures, the binary diffusion coefficients are insensitive to the magnitude of mass fractions (or concentrations). They also increase with temperature and vary inversely with pressure. For the diffusion of inert species in liquids, the mass diffusivity is sensitive to the concentration and increases with temperature.

It is important to bear in mind that Fick's law is a phenomenological model, although it is supported by the kinetic theory of gases for monatomic binary gas mixtures at moderate pressures. For values of mass diffusivities we often rely on measured and tabulated values or empirical correlations.

1.3.3 Species Mass Conservation When Fick's Law Applies

We can now combine Fick's law with the mass-species balance equations derived earlier to get, for a binary mixture,

$$\frac{\partial \rho_i}{\partial t} + \nabla \cdot \left(\rho_i \vec{U} \right) = \nabla \cdot \left(\rho \mathcal{D}_{12} \nabla m_i \right) + \dot{r}_i. \tag{1.3.17}$$

Because $\rho_i = \rho m_i$, and using Eq. (1.1.6), we can show that

$$\rho\left[\frac{\partial m_i}{\partial t} + \vec{U}\cdot\nabla m_i\right] = \nabla\cdot(\rho\mathcal{D}_{12}\nabla m_i) + \dot{r}_i. \tag{1.3.18}$$

A similar analysis in terms of molar fluxes would lead to

$$\frac{\partial \boldsymbol{C}_i}{\partial t} + \nabla\cdot\left(\boldsymbol{C}_i\vec{\tilde{U}}\right) = \nabla\cdot(\boldsymbol{C}\mathcal{D}_{12}\nabla X_i) + \dot{R}_i. \tag{1.3.19}$$

Using Eq. (1.3.5), we can cast this equation in terms of mole fractions:

$$\boldsymbol{C}\left[\frac{\partial X_1}{\partial t} + \vec{\tilde{U}}\cdot\nabla X_1\right] = \nabla\cdot(\boldsymbol{C}\mathcal{D}_{12}\nabla X_1) + X_2\dot{R}_1 - X_1\dot{R}_2 \tag{1.3.20}$$

Mass-species conservation equations in polar cylindrical and spherical coordinates can be found in Appendix D.

1.3.4 Other Types of Diffusion

Thus far we considered only one type of mass diffusion, namely the "ordinary diffusion," caused by the concentration gradient. In many processes of significance, and definitely in the processes that are of interest in this book, ordinary diffusion overwhelms other types of diffusion.

In reality, diffusion of a species with respect to the mean fluid motion in a mixture can take place because of four different mechanisms, therefore, for species l,

$$\vec{j}_l = \vec{j}_{l,m} + \vec{j}_{l,P} + \vec{j}_{l,g} + \vec{j}_{l,T}, \tag{1.3.21}$$

where, $\vec{j}_{l,m}$ is the diffusion that is due to the concentration gradient, $\vec{j}_{l,P}$ is the diffusion that is due to the pressure gradient, $\vec{j}_{l,T}$ is the diffusion caused by the temperature gradient (Soret effect), and $\vec{j}_{l,g}$ is the diffusion that is due to external forces that act unequally on various chemical species.

The thermal-diffusion flux follows the seemingly simple relation

$$\vec{j}_{l,T} = -\mathcal{D}_{l,T}\nabla\ln T, \tag{1.3.22}$$

where $\mathcal{D}_{l,T}$ is the thermal-diffusion coefficient of species i with respect to the mixture. A useful discussion of other diffusion types can be found in Bird et al. (2002).

1.3.5 Diffusion in Multicomponent Mixtures

In multicomponent mixtures (mixtures made of more than two species) the diffusion term is more complicated than Fick's law, and the diffusion of each species depends on the pair binary diffusion coefficients of that species with respect to all other components in the mixture.

Ordinary diffusion in a multicomponent mixture in many cases can be simply represented by generalizing Fick's law as [see Eq. (1.3.14)] (Cussler, 2009),

$$\vec{j}_i = -\sum_{j=1}^{n-1} D_{ij}\nabla(CX_j). \tag{1.3.23}$$

Alternatively, for a multicomponent gas at low density, the *Maxwell–Stefan equations* can be used as a good approximation (Bird et al., 2002):

$$\nabla X_i = -\sum_{j=1}^{n} \frac{1}{\boldsymbol{C}\mathcal{D}_{ij}} \left(X_j \vec{N}_i - X_j \vec{N}_j \right), \tag{1.3.24}$$

where n is the number of components in the mixture, $\mathcal{D}_{ij}$ is the binary diffusivity for species i and j, and D_{ij} is the *multicomponent Maxwell–Stefan diffusivities* for species i and j. The Maxwell–Stefan diffusivities are not all independent, and to solve Eq. (1.3.23) we need to know only $n(n-1)/2$ Maxwell–Stefan diffusivities. Likewise, to solve Eq. (1.3.24) for a mixture of n species, we need $n(n-1)/2$ binary diffusivities. Although originally derived for gas mixtures, the Maxwell–Stefan equations have been found to apply to dense gases, liquids, and polymers. For multicomponent gases at low density, $D_{ij} \approx \mathcal{D}_{ij}$. In general, however, the multicomponent Maxwell–Stefan diffusivities are strongly concentration dependent.

The diffusion processes in multicomponent mixtures are more complicated than binary mixtures because the diffusion of any specific species no longer depends on that species concentration gradient alone and can be affected by the diffusive flux of other species. We may thus encounter the following interesting situations (Bird et al., 2002):

- *reverse diffusion*, in which a species diffuses up its own concentration gradient;
- *osmotic diffusion*, in which a species diffuses even though its concentration is uniform;
- *diffusion barrier*, in which a species does not diffuse even though its concentration is nonuniform.

Fick's law thus does not apply to multicomponent fluid mixtures in general. However, Fick's law becomes accurate in a multicomponent mixture when all the pair diffusivities in the mixture are equal. Fick's law also becomes accurate when we deal with a dilute mixture of transferred species in a solvent.

Equation (1.3.23) is a special case of the *generalized Maxwell–Stefan equations*:

$$\vec{j}_i = -\mathcal{D}_{i,T} \nabla \ln T + \rho_i \sum_{j=1}^{n} \mathcal{D}_{ij} \vec{\boldsymbol{d}}_j, \tag{1.3.25}$$

where $\mathcal{D}_{i,T}$ are the *multicomponent thermal diffusivities*, and D_{ij} are the *multicomponent Fick's diffusivities*. The multicomponent Fick's diffusivities constitute a symmetric matrix ($\mathsf{D}_{ij} = \mathsf{D}_{ji}$). The parameter $\vec{\boldsymbol{d}}_j$ is the diffusion driving force for species j. The multicomponent Fick's diffusivities and the binary diffusivities are related according to

$$m_i \mathsf{D}_{ij} = \hat{D}_{ij} - \sum_{\substack{l=1 \\ l \neq i}}^{n} m_i \mathsf{D}_{il}, \tag{1.3.26}$$

$$\hat{D}_{ij} = \frac{m_i m_j}{X_i X_j} \mathcal{D}_{ij}. \tag{1.3.27}$$

The multicomponent Fick's diffusivities are also related to the multicomponent Maxwell–Stefan diffusivities. For a binary mixture, for example,

$$D_{12} = \frac{X_1 X_2}{m_1 m_2} D_{12} = -\frac{X_1 X_2}{m_2^2} D_{11} = -\frac{X_1 X_2}{m_1^2} D_{22}. \tag{1.3.28}$$

For a ternary mixture, furthermore,

$$D_{12} = \frac{X_1 X_2}{m_1 m_2} \frac{D_{12} D_{33} - D_{13} D_{23}}{D_{12} + D_{33} - D_{13} - D_{23}}. \tag{1.3.29}$$

Other entries can be easily generated by use of cyclic permutations of the indices in Eq. (1.3.29). Relations for a four-component mixture, as well as equations for calculating entries for arbitrary numbers of components can be found in Curtis and Bird (1999, 2001).

The diffusion driving-force term for an ideal-gas mixture is,

$$\boldsymbol{C} R_u T \vec{\boldsymbol{d}}_i = \nabla P_i - m_i \nabla P - \rho_i \vec{g}_i + m_i \sum_{j=1}^{n} \rho_j \vec{g}_j \tag{1.3.30}$$

where $\vec{g}_j$ is the body force (in newtons per kilogram, for example) acting on species j. When gravity is the only body force, the last two terms on the right-hand side of this equation will vanish.

The diffusive heat flux in a multicomponent mixture can also be represented as

$$\vec{q}'' = -k \nabla T + \sum_{i=1}^{n} \frac{\tilde{\boldsymbol{h}}_i}{M_i} \vec{j}_i + \sum_{i=1}^{n} \sum_{\substack{j=1 \\ j \neq 1}}^{n} \frac{\boldsymbol{C} R_u T X_i X_j}{\rho_i} \frac{\mathcal{D}_{i,T}}{D_{ij}} \left(\frac{\vec{j}_i}{\rho_i} - \frac{\vec{j}_j}{\rho_j} \right). \tag{1.3.31}$$

Detailed discussions of diffusion in multi-component mixtures can be found in Curtis and Bird (1999, 2001), Bird et al. (2002), and Cussler (2009). It is important to note that the existence of three or more species in a mixture does not always mean that Fick's law is inapplicable. In fact, Fick's law is a good approximation in many practical situations involving multicomponent mixtures. A useful discussion on this issue can be found in Cussler (2009).

1.4 Boundary and Interfacial Conditions

The differential mass, momentum, energy, and mass-species conservation equations discussed thus far evidently need boundary conditions. The boundary conditions typically occur either far away from a surface (the free-stream or ambient conditions in external flow), at the surface of a wall, or at a fluid–fluid (gas–liquid or liquid–liquid) interface.

1.4.1 General Discussion

Consider the boundary shown in Fig. 1.6, where $\vec{N}$ and $\vec{T}$ are unit normal and tangent vectors, respectively. The ambient fluid has a bulk temperature T_∞ and contains transferred species 1 at a mass fraction equal to $m_{1,\infty}$. The surface temperature is T_s, and the mass fraction of the transferred species, at the boundary but on the fluid side, is $m_{1,s}$. Let us also assume that species 1 is the only species that is

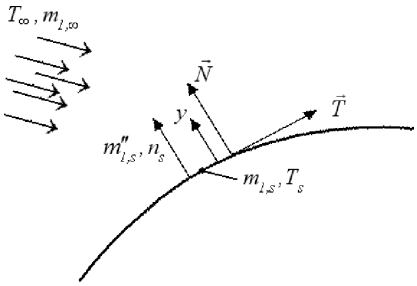

Figure 1.6. Boundary conditions for a flow field.

exchanged between the fluid and the wall surface and that the mass flux of species 1 through the boundary is very small. The boundary conditions for the conservation equations will be

$$\vec{U} \cdot \vec{T} = 0 \quad \text{(no-slip)}, \tag{1.4.1}$$

$$\rho \vec{U} \cdot \vec{N} = n_s = m''_{1,s}, \tag{1.4.2}$$

$$T = T_s \quad \text{(thermal equilibrium)}, \tag{1.4.3}$$

$$m_1 = m_{1,s}, \tag{1.4.4}$$

where n_s in the total mass flux through the boundary, which in this case is equal to $m''_{1,s}$.

Equations (1.4.1) and (1.4.3) represent, respectively, the no-slip and thermal-equilibrium boundary conditions. These boundary conditions are acceptable for the vast majority of applications, but are inadequate when rarefied gas flows are considered or when gas flow in extremely small microchannels is encountered. These applications are considered in Chapter 13.

In the absence of strong mass transfer (i.e., when $\dot{m}''_{\text{tot}} = n_s \to 0$), we define the skin-friction coefficient (the same as the Fanning friction factor in internal flow) and convective heat and mass transfer coefficients by writing

$$\mu \left.\frac{\partial u}{\partial y}\right|_{y=0} = C_f \left(\frac{1}{2}\rho U_\infty^2\right), \tag{1.4.5}$$

$$-k \left.\frac{\partial T}{\partial y}\right|_{y=0} = h\,(T_s - T_\infty)\,, \tag{1.4.6}$$

$$-\rho \mathcal{D}_{12} \left.\frac{\partial m_1}{\partial y}\right|_{y=0} = \mathcal{K}\,(m_{1,s} - m_{1,\infty})\,. \tag{1.4.7}$$

The preceding expressions show that, to find C_f, h, and $\mathcal{K}$, all we need to know is how to calculate the local profiles of velocity, temperature, and mass fraction in the fluid at the immediate vicinity of the boundary. This is not always easy, however, because of the effect of hydrodynamics on those profiles.

Thus far we considered conditions under which the total mass transfer rate at the boundary is vanishingly small. In fact, the correlations for predicting C_f, h, and $\mathcal{K}$ that can be found in the literature for numerous configurations are in general for vanishingly small boundary mass flux conditions. When a finite mass flux at the boundary occurs, not only does the transferred mass contribute to the flux of

momentum, energy, and species at the boundary, but it modifies the velocity, temperature, and concentration profiles as well. As a result C_f, h, and $\mathcal{K}$ will all be affected. A detailed discussion on the effect of boundary mass transfer (transpiration) on the transfer coefficients is provided in Chapter 8.

1.4.2 Gas–Liquid Interphase

Although the discussion of two-phase flow and change-of-phase phenomena are outside the scope of this book (for a detailed discussion see Ghiaasiaan, 2008), a brief review of the conditions at a gas–liquid interphase are necessary because such an interphase is sometimes encountered as a boundary for transport processes in a single-phase flow field.

On the molecular scale, the interphase between a liquid and its vapor is always in violent agitation. Some liquid molecules that happen to be at the interphase leave the liquid phase (i.e., they evaporate), whereas some vapor molecules collide with the interphase during their random motion and join the liquid phase (i.e., they condense). The evaporation and condensation molecular rates are equal when the liquid and the vapor phases are at equilibrium. Net evaporation takes place when the molecules leaving the surface outnumber those that are absorbed by the liquid. When net evaporation or condensation takes place, the molecular exchange at the interphase is accompanied with a thermal resistance.

1.4.3 Interfacial Temperature

Heat transfer at a gas–liquid interphase can lead to phase change. As a result, the discussion of the gas–liquid interfacial temperature inevitably involves evaporation and condensation.

For convenience of discussion, the interphase can be assumed to be separated from the gas phase by a surface [the s surface in Figs. 1.7(a) and 1.7(b)]. The temperature and the vapor partial pressure at the interphase, $P_{v,I}$, are related according to

$$T_I = T_{\text{sat}}\left(P_{v,I}\right). \tag{1.4.8}$$

The conditions that lead to Eq. (1.4.8) are established over a time period that is comparable with molecular time scales and can thus be assumed to develop instantaneously for all cases of interest to us. Assuming that the vapor is at a temperature T_v in the immediate vicinity of the s surface, the vapor molecular flux passing the s surface and colliding with the liquid surface can be estimated from the molecular effusion flux as predicted by the gas-kinetic theory, when molecules are modeled as hard spheres. If it is assumed that all vapor molecules that collide with the interphase join the liquid phase, then

$$j_{\text{cond}} = \frac{P_v}{\sqrt{2\,\pi\,\kappa_B \boldsymbol{m}_{\text{mol}}\,T_v}}, \tag{1.4.9}$$

where $\boldsymbol{m}_{\text{mol}}$ is the mass of a single molecule. This will give:

$$m''_{\text{cond}} = \boldsymbol{m}_{\text{mol}}\, j_{\text{cond}} = \frac{P_v}{\sqrt{2\pi\,\left(R_u/M_v\right)T_v}}. \tag{1.4.10}$$

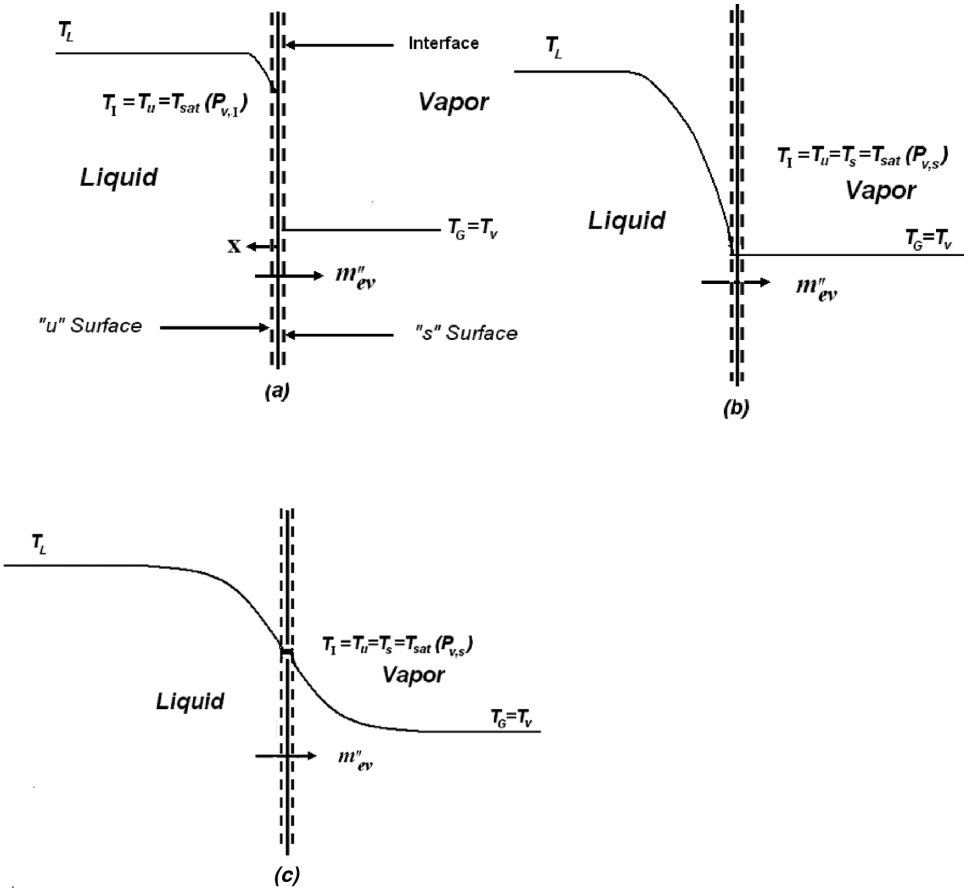

Figure 1.7. The temperature distribution near the liquid–vapor interphase: (a) early during a very fast transient evaporation, (b) quasi-steady conditions with pure vapor, (c) quasi-steady conditions with a vapor-noncondensable mixture.

The flux of molecules that leave the s surface and join the gas phase can be estimated from a similar expression in which $P_{v,I}$ and T_I are used instead of P_v and T_v, respectively. The net evaporation mass flux will then be

$$q''_s = m''_{\text{ev,net}} \boldsymbol{h}_{fg} = \boldsymbol{h}_{fg} \left[\frac{M_v}{2\pi R_u} \right]^{\frac{1}{2}} \left[\frac{P_{v,I}}{\sqrt{T_I}} - \frac{P_v}{\sqrt{T_v}} \right]. \tag{1.4.11}$$

The preceding expression is a theoretical maximum for the phase-change mass flux (the Knudsen rate). An interfacial heat transfer coefficient can also be defined according to

$$h_I = \frac{q''_s}{T_I - T_v}. \tag{1.4.12}$$

It should be noted that in common engineering calculations the interfacial thermal resistance can be comfortably neglected, and the interphase temperature profile will be similar to Fig. 1.7(b) or 1.7(c). Thermal nonequilibrium occurs at an

interphase only in extremely fast transients. In other words, *in common engineering applications it can be assumed that there is no discontinuity in the temperature, as we move from one phase to another*.

When microsystems or extremely fast transients are dealt with, however, the interfacial thermal resistance may be important. Also, the interfacial thermal resistance can be significant during the condensation of liquid metals (Rose et al., 1999).

Equation (1.4.11) is known to deviate from experimental data. It has two important shortcomings, both of which can be remedied. The first shortcoming is that it does not account for the convective flows (i.e., finite molecular mean velocities) that result from the phase change on either side of the interphase. The second shortcoming is that Eq. (1.4.11) assumes that all vapor molecules that collide with the interphase condense and none is reflected. From the predictions of the gas-kinetic theory when the gas moves with a finite mean velocity, Schrage (1953) derived

$$m''_{\text{ev,net}} = \left[\frac{M_v}{2\pi R_u}\right]^{1/2}\left[\sigma_e \frac{P_{v,I}}{\sqrt{T_I}} - \Gamma\sigma_c \frac{P_v}{\sqrt{T_v}}\right], \tag{1.4.13}$$

where Γ is a correction factor and depends on the dimensionless mean velocity of vapor molecules that cross the s surface, namely $-m''_{\text{ev,net}}/\rho_v$, normalized with the mean molecular thermal speed $\sqrt{2R_u T_v/M_v}$, defined to be positive when net condensation takes place:

$$a = -\frac{m''_{\text{ev,net}}}{\rho_v}\left(\frac{2R_u T_v}{M_v}\right)^{-1/2} \approx -\frac{m''_{\text{ev,net}}}{P_v}\sqrt{\frac{R_u T_v}{2M_v}}, \tag{1.4.14}$$

$$\Gamma = \exp\left(-a^2\right) + a\pi^{1/2}\left[1 + \operatorname{erf}(a)\right]. \tag{1.4.15}$$

The effect of mean molecular velocity needs to be considered only for vapor molecules that approach the interphase. No correction is needed for vapor molecules that leave the interphase because there is no effect of bulk motion on them. Parameters σ_e and σ_c are the evaporation and condensation coefficients, respectively, and are usually assumed to be equal, as would be required when there is thermostatic equilibrium. When $a < 10^{-3}$, as is often the case in evaporation and condensation, $\Gamma \approx 1 + a\pi^2$. Substitution into Eq. (1.4.13) and linearization then leads to

$$m''_{\text{ev,net}} = \left[\frac{M_v}{2\pi R_u}\right]^{1/2} \frac{2\sigma_e}{2-\sigma_e}\left[\frac{P_{v,I}}{\sqrt{T_I}} - \frac{P_v}{\sqrt{T_v}}\right]. \tag{1.4.16}$$

For $10^{-3} < a < 0.1$, the term $\frac{2\sigma_e}{2-\sigma_e}$ should be modified to $\frac{2\sigma_e}{2-1.046\sigma_e}$.

The magnitude of the evaporation coefficient σ_e is a subject of disagreement. For water, values in the $\sigma_e = 0.01$–1.0 range have been reported (Eames et al., 1997). Careful experiments have shown that $\sigma_e \geq 0.5$ for water (Mills and Seban, 1967), however. Some investigators have obtained $\sigma_e = 1$ (Maa, 1967; Cammenga et al., 1977) and have argued that measured smaller σ_e values by others were probably caused by experimental error.

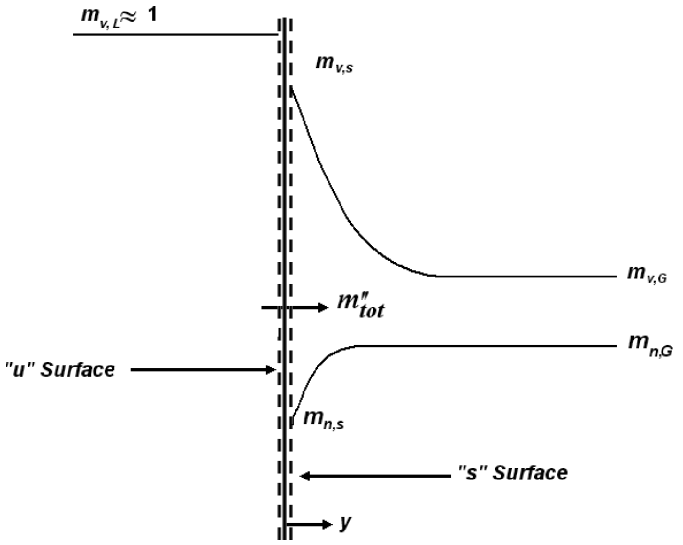

Figure 1.8. Mass fraction profiles near the liquid–vapor interphase during evaporation into a vapor-noncondensable mixture.

1.4.4 Sparingly Soluble Gases

The mass-fraction profiles for a gaseous chemical species that is insoluble in the liquid phase (a "noncondensable") during rapid evaporation are qualitatively displayed in Fig. 1.8. For convenience, once again the interphase is treated as an infinitesimally thin membrane separated from the gas and liquid phases by two parallel planes *s* and *u*, respectively. Noncondensable gases are not completely insoluble in liquids, however. For example, air is present in water at about 25 ppm by weight when water is at equilibrium with atmospheric air at room temperature. In many evaporation and condensation problems in which noncondensables are present, the effect of the noncondensable that is dissolved in the liquid phase is small, and there is no need to keep track of the mass transfer process associated with the noncondensable in the liquid phase. There are situations in which the gas released from the liquid plays an important role, however. An interesting examples is forced convection by a subcooled liquid in minichannels and microchannels (Adams et al., 1999).

The release of a sparingly soluble species in a liquid that is undergoing net phase change is displayed in Fig. 1.9, where subscript 2 represents the transferred

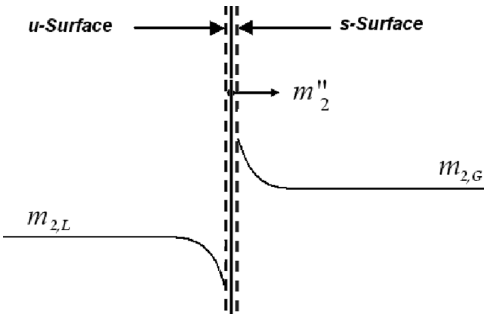

Figure 1.9. The gas–liquid interphase during evaporation and desorption of an inert species.

species. Although an analysis based on the kinetic theory of gases may be needed for the very early stages of a mass transfer transient, such analysis is rarely performed (Mills, 2001). Instead, equilibrium at the interphase with respect to the transferred species is often assumed. Unlike temperature, there is typically a significant discontinuity in the concentration (mass fraction) profiles at the liquid–gas interphase, even under equilibrium conditions. The equilibrium at the interphase with respect to a sparingly soluble inert species is governed by *Henry's Law*, according to which

$$X_{n,s} = \mathrm{He}_n X_{n,u}, \tag{1.4.17}$$

where He_n is the *Henry number* for species n and the liquid, and in general it depends on pressure and temperature. The equilibrium at the interphase can also be presented in terms of the *Henry constant*, which is defined as $C_{\mathrm{He},n} = \mathrm{He}_n P$, with P representing the total pressure. C_{He} is approximately a function of temperature only. If all the components of the gas phase are assumed to be ideal gases, then

$$C_{\mathrm{He},n} X_{n,u} = X_{n,s} P = P_{n,s}, \tag{1.4.18}$$

where $P_{n,s}$ is the partial pressure of species n at the s surface. When the bulk gas and liquid phases are at equilibrium, then

$$X_{n,L} C_{\mathrm{He},n} = X_{n,G} P = P_{n,G}, \tag{1.4.19}$$

where now all parameters represent the gas and liquid bulk conditions. Evidently C_{He} is related to the solubility of species n in the liquid. It is emphasized that the preceding linear relationships apply only to sparingly soluble gases. When the gas phase is highly soluble in the liquid, Eq. (1.4.18) should be replaced with tabulated values of a nonlinear relation of the generic form

$$P_{n,s} = P_{n,s}\left(X_{n,u},\, T_I\right). \tag{1.4.20}$$

EXAMPLE 1.4. A stagnant pool of water is originally at equilibrium with nitrogen at atmospheric pressure and 300 K temperature. A flow of oxygen is established, and as a result the surface of water is suddenly exposed to water-vapor-saturated oxygen at the same pressure and temperature. Calculate the mass transfer rate of oxygen at the surface and the concentration of oxygen 1 cm below the surface of water at 5 min after the initiation of the transient. For simplicity, assume that the gas-side mass transfer resistance is negligible.

SOLUTION. Let us first calculate the vapor partial pressure in gas phase. The oxygen is saturated with vapor; therefore

$$P_v = P_{\mathrm{sat}}|_{100\,\mathrm{K}} \approx 3540\,\mathrm{Pa},$$
$$P_{\mathrm{O}_2} = P_\infty - P_v \approx 97{,}790\ \mathrm{Pa}.$$

Because the mass transfer process is liquid-side controlled, the mass transfer resistance on the gas side is negligibly small and therefore the gas-side oxygen concentration remains uniform. Therefore

$$X_{\mathrm{O}_2,s} = X_{\mathrm{O}_2,G} = \frac{P_{\mathrm{O}_2}}{P_\infty} = \frac{97{,}790\ \mathrm{Pa}}{101{,}330\ \mathrm{Pa}} = 0.0349.$$

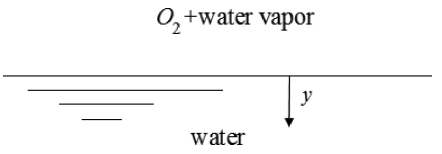

Figure 1.10. The system configuration in Example 1.4.

The concentration of oxygen at the interphase on the liquid side can now be found by applying Henry's law [see Eq. (1.4.17)]. From Appendix I,

$$C_{\mathrm{He},\mathrm{O}_2} = 45{,}000 \text{ bars} = 4.5 \times 10^9 \text{ Pa}.$$

Therefore

$$X_{\mathrm{O}_2,u} = P_{\mathrm{O}_2}/C_{\mathrm{He},\mathrm{O}_2} = (97{,}790 \text{ Pa})/\left(4.5 \times 10^9 \text{ Pa}\right) = 2.173 \times 10^{-5}.$$

Let us assume that the water pool remains stagnant and its surface remains flat. Starting from Eq. (1.3.20), the species conservation equation for oxygen will be simplified to

$$\frac{\partial X_{\mathrm{O}_2,L}}{\partial t} = \mathcal{D}_{12}\frac{\partial^2 X_{\mathrm{O}_2,L}}{\partial y^2},$$

where $\mathcal{D}_{12}$ is the oxygen–water binary mass diffusivity in the liquid. The initial and boundary conditions are

$$\begin{aligned} X_{\mathrm{O}_2,L} &= 0 \qquad \text{at } t = 0, \\ X_{\mathrm{O}_2,L} &= x_{\mathrm{O}_2,u} \quad \text{at } y = 0, \\ X_{\mathrm{O}_2,L} &= 0 \qquad \text{at } y \to \infty. \end{aligned}$$

We thus deal with diffusion in a semi-infinite medium, shown schematically in Fig. 1.10. The solution will be

$$\frac{X_{\mathrm{O}_2,L} - X_{\mathrm{O}_2,u}}{X_{\mathrm{O}_2,\infty} - X_{\mathrm{O}_2,u}} = \operatorname{erf}\left[\frac{y}{2\sqrt{\mathcal{D}_{12}t}}\right].$$

From Appendix H,

$$\mathcal{D}_{12} = 2.12 \times 10^{-5} \text{ m}^2/\text{s}.$$

The oxygen concentration at 1 cm below the surface after 5 min can now be found from

$$\frac{X_{\mathrm{O}_2,L}\big|_{5\text{ min}} - 2.173 \times 10^{-5}}{0 - 2.173 \times 10^{-5}} = \operatorname{erf}\left[\frac{0.01 \text{ m}}{2\sqrt{(2.12 \times 10^{-5} \text{ m}^2/\text{s})\,(300 \text{ s})}}\right],$$

$$X_{\mathrm{O}_2,L}\big|_{5\text{ min}} = 2.02 \times 10^{-5}.$$

We can find the oxygen molar flux at the surface after 5 min by using Eq. (1.3.14), thereby obtaining

$$J_{\mathrm{O}_2,u} = -\boldsymbol{C}_L\mathcal{D}_{12}\left.\frac{\partial X_{\mathrm{O}_2,L}}{\partial y}\right|_{y=0} = \frac{\boldsymbol{C}_L\mathcal{D}_{12}\,(X_{\mathrm{O}_2,u} - X_{\mathrm{O}_2,\infty})}{\sqrt{\pi\mathcal{D}_{12}t}}$$

$$J_{\mathrm{O}_2,u} = \frac{\left(55.36 \dfrac{\text{kmol}}{\text{m}^3}\right)(2.12 \times 10^{-5} \text{ m}^2/\text{s})(2.173 \times 10^{-5})}{\sqrt{\pi\,(2.12 \times 10^{-5} \text{ m}^2/\text{s})(300 \text{ s})}} = 1.80 \times 10^{-7} \frac{\text{kmol}}{\text{m}^2/\text{s}},$$

where for water we have used $C_L = 55.36\,\text{kmol/m}^3$. In terms of mass flux, we have

$$m''_{O_2,u} = j_{O_2,u} = J_{O_2,u} M_{O_2} = \left(1.80 \times 10^{-7}\,\frac{\text{kmol}}{\text{m}^2/\text{s}}\right)\left(32\frac{\text{kg}}{\text{kmol}}\right)$$
$$= 5.78 \times 10^{-6}\,\text{kg/m}^2/\text{s}.$$

1.4.5 Convention for Thermal and Mass Transfer Boundary Conditions

A wide variety of thermal and mass transfer boundary conditions can be encountered in practice. Standard thermal and mass transfer boundary condition types are often used in theoretical models and experiments, however. Besides being among the most widely encountered boundary conditions, these standard boundary conditions can approximate many more complicated boundary conditions that are encountered.

In this book, our discussions are limited to the following standard thermal boundary conditions:

- Uniform wall temperature, represented by UWT or (T): This boundary condition applies to all configurations. The wall in this case has a constant temperature everywhere. Condensers and evaporators are examples of this boundary condition.
- The boundary condition represented by (H1): This boundary condition applies to flow channels only. It represents conditions in which the temperature is circumferentially constant (but it may vary axially) and the heat flux is axially constant (but may vary circumferentially). Electric resistive heating, nuclear fuel rods, and counterflow heat exchangers with approximately equal fluid thermal capacity flow rates (i.e., equal $\dot{m}\,C_P$ values for the two streams), all with highly conductive wall materials, are examples.
- Uniform wall heat flux, represented by UHF or (H2): This boundary condition also applies to all configurations. The heat flux through the boundary is a constant everywhere. The examples of occurrence cited for boundary condition (H1) apply when the wall is thick and the thermal conductivity of the wall material is low.

Several other standard thermal boundary conditions can also be defined, including boundary conditions involving radiation and convection on the opposite surface of a wall. A complete table and more detailed discussion can be found in Shah and Bhatti (1987).

With regard to mass transfer, although the equivalents of all of the preceding three boundary conditions are in principle possible, only the following two important standard boundary conditions are often used:

- Uniform wall mass or mole fraction UWM: This is equivalent to the UWT boundary condition and refers to a constant mass fraction (or, equivalently, a constant mole fraction) of the transferred species everywhere on the boundary, namely,

$$m_{i,s} = \text{const.} \tag{1.4.21}$$

Or, when the mass transfer problem is formulated in terms of mole fraction,

$$X_{i,s} = \text{const.} \tag{1.4.22}$$

This is probably the most widely encountered mass transfer boundary condition. It occurs, for example, during quasi-steady evaporation from an isothermal liquid surface, during desorption of a sparingly volatile species from an isothermal liquid surface, or during sublimation of an isothermal solid material.

- Uniform wall mass flux UMF: This boundary condition is similar to the UHF just discussed with respect to thermal boundary conditions. It represents the conditions in which the mass (or molar) flux of the transferred species is a constant everywhere on the boundary. This boundary condition, for example, occurs when the transferred species is evaporated as a result of an imposed constant heat flux. When vanishingly small mass transfer rates are involved, this boundary condition in terms of mass flux can be represented as

$$m''_{i,s} = \text{const.} \tag{1.4.23}$$

In terms of molar flux,

$$N''_{i,s} = \text{const.} \tag{1.4.24}$$

1.5 Transport Properties

1.5.1 Mixture Rules

The viscosity and thermal conductivity of a gas mixture can be calculated from the following expressions (Wilke, 1950). These rules have been deduced from gas-kinetic theory (GKT) and have proved to be quite adequate (Mills, 2001):

$$\mu = \sum_{j=1}^{n} \frac{X_j \mu_j}{\sum_{i=1}^{n} X_i \phi_{ji}}, \tag{1.5.1}$$

$$k = \sum_{j=1}^{n} \frac{X_j k_j}{\sum_{i=1}^{n} X_i \phi_{ji}}, \tag{1.5.2}$$

$$\phi_{ji} = \frac{\left[1 + (\mu_j/\mu_i)^{1/2} (M_j/M_i)^{1/4}\right]^2}{\sqrt{8}\,[1 + (M_j/M_i)]^{1/2}}. \tag{1.5.3}$$

For liquid mixtures the property calculation rules are complicated and are not well established. However, for most dilute solutions of inert gases, the viscosity and thermal conductivity of the liquid are similar to the properties of pure liquid.

With respect to mass diffusivity, everywhere in this book, unless otherwise stated, we will assume that the mixture is either binary (namely, only two different species are present), or the diffusion of the transferred species takes place in

accordance with Fick's law. For example, in dealing with an air–water-vapor mixture (as it pertains to evaporation and condensation processes in air), we follow the common practice of treating dry air as a single species. Furthermore, we assume that the liquid contains only dissolved species at very low concentrations.

For the thermophysical and transport properties, including mass diffusivity, we rely primarily on experimental data. Mass diffusivities of gaseous pairs are approximately independent of their concentrations in normal pressures, but are sensitive to temperature. The mass diffusion coefficients, however, are sensitive to both concentration and temperature in liquids.

1.5.2 Transport Properties of Gases and the Gas-Kinetic Theory

The GKT provides for the estimation of the thermophysical and transport properties in gases. A simple and easy-to-read discussion of – GKT can be found in Gombosi (1994). These methods become particularly useful when empirical data are not available. The simple GKT models the gas molecules as rigid and elastic spheres (no internal degree of freedom) that influence one another only when they approach each other to within distances much smaller than their typical separation distances. Each molecule thus has a very small sphere of influence. When outside the sphere of influence of other molecules, the motion of a molecule follows the laws of classical mechanics. When two molecules collide, furthermore, their directions of motion after collision are isotropic, and, following a large number of intermolecular collisions, the orthogonal components of the molecular velocities are independent of each other. It is also assumed that the distribution function of molecules under equilibrium is isotropic. These assumptions, along with the ideal-gas law, lead to the well-known Maxwell–Boltzmann distribution, whereby the fraction of molecules with speeds in the $|\vec{U}_{\text{mol}}|$ to $|\vec{U}_{\text{mol}} + d\vec{U}_{\text{mol}}|$ range is given by $f(U_{\text{mol}})\, d\vec{U}_{\text{mol}}$, and

$$f(U_{\text{mol}}) = \left(\frac{M}{2\pi R_u T}\right)^{3/2} \exp\left(-\frac{M U_{\text{mol}}^2}{2R_u T}\right). \tag{1.5.4}$$

If the magnitude (absolute value) of velocity is of interest, the number fraction of molecules with speeds in the $|U_{\text{mol}}|$ to $|U_{\text{mol}} + dU_{\text{mol}}|$ range will be equal to $F(U_{\text{mol}})d\,U_{\text{mol}}$, where

$$F(U_{\text{mol}}) = 4\pi\, U_{\text{mol}}^2\, f(U_{\text{mol}}). \tag{1.5.5}$$

Using Eq. (1.5.5), we can find the mean molecular speed by writing

$$\langle |U_{\text{mol}}| \rangle = 4\pi \left(\frac{\beta}{\pi}\right)^{3/2} \int_0^\infty \exp\left(-\beta U_{\text{mol}}^2\right) U_{\text{mol}}^3 dU_{\text{mol}} = \sqrt{\frac{8\kappa_B T}{\pi \boldsymbol{m}_{\text{mol}}}}, \tag{1.5.6}$$

where

$$\beta = \frac{\boldsymbol{m}_{\text{mol}}}{2\,\kappa_B\, T} = \frac{M}{2\,R_u\, T}, \tag{1.5.7}$$

where $\boldsymbol{m}_{\text{mol}}$ is the mass of a single molecule and κ_B is Boltzmann's constant. (Note that $\frac{\kappa_B}{\boldsymbol{m}_{\text{mol}}} = \frac{R_u}{M}$.)

The average molecular kinetic energy can be found as

$$\langle E_{\text{kin}} \rangle = \frac{1}{2} \boldsymbol{m}_{\text{mol}} \langle U_{\text{mol}}^2 \rangle = 2\pi \left(\frac{\beta}{\pi} \right)^{3/2} \boldsymbol{m}_{\text{mol}} \int_0^\infty \exp\left(-\beta U_{\text{mol}}^2\right) U_{\text{mol}}^4 dU_{\text{mol}} = \frac{3}{2} \kappa_B T. \tag{1.5.8a}$$

This expression applies when the molecule has only three translational degrees of freedom. It thus applies to monatomic gases. When the molecule has rotational degrees of freedom as well, the right-hand side of Eq. (1.5.8a) must be increased by $\frac{1}{2}\kappa_B T$ for each rotational degree of freedom. Thus for a diatomic molecule we have

$$\langle E_{\text{kin}} \rangle = \frac{1}{2} \boldsymbol{m}_{\text{mol}} \langle U_{\text{mol}}^2 \rangle + \frac{1}{2} \kappa_B T = \frac{5}{2} \kappa_B T. \tag{1.5.8b}$$

According to the simple GKT, the gas molecules have a mean free path that follows (see Gombosi, 1994, for derivations)

$$\lambda_{\text{mol}} = \frac{1}{\sqrt{2} n \sigma_A} \approx \frac{\sqrt{2}}{2\pi} \frac{\kappa_B T}{\tilde{\sigma}^2 P}, \tag{1.5.9}$$

where σ_A is the molecular-scattering cross section and $\tilde{\sigma} \approx 2.5 \sim 6$ Å (the range of repulsive region around a molecule). A more precise expression resulting from GKT is (Eckert and Drake, 1959)

$$\lambda_{\text{mol}} = \nu \left(\frac{\pi M}{2 R_u T} \right)^{1/2}. \tag{1.5.10}$$

The molecular mean free time can then be found from

$$\tau_{\text{mol}} = \frac{\lambda_{\text{mol}}}{\langle |U_{\text{mol}}| \rangle} = \frac{1}{\sqrt{2} n \sigma_A \langle |U_{\text{mol}}| \rangle}. \tag{1.5.11}$$

Given that random molecular motions and intermolecular collisions are responsible for diffusion in fluids, expressions for μ, k, and $\mathcal{D}$ can be found based on the molecular mean free path and free time. The simplest formulas derived in this way are based on the Maxwell–Boltzmann distribution, which assumes equilibrium. We can derive more accurate formulas by taking into consideration that all diffusion phenomena actually occur as a result of nonequilibrium. The transport of the molecular energy distribution under nonequilibrium conditions is described by an integro-differential equation, known as the Boltzmann transport equation. The aforementioned Maxwell–Boltzmann distribution [Eq. (1.5.4) or (1.5.5)] is in fact the solution of the Boltzmann transport equation under equilibrium conditions. Boltzmann's equation cannot be analytically solved in its original form, but approximate solutions representing relatively slight deviations from equilibrium were derived, and these nonequilibrium solutions lead to useful formulas for the gas transport properties. One of the most well-known approximate solutions to Boltzmann's equation for near-equilibrium conditions was derived by Chapman, in 1916 and Enskog, in 1917 (Chapman and Cowling, 1970). The solution leads to widely used expressions for gas transport properties that are only briefly presented and subsequently discussed. More detailed discussions about these expressions can be found in Bird et al. (2002), Skelland (1974), and Mills (2001).

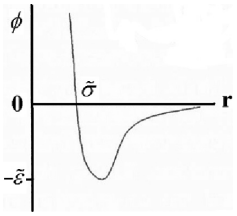

Figure 1.11. The pair potential energy distribution according to the Lennard–Jones 6–12 intermolecular potential model.

The interaction between two molecules as they approach one another can be modeled only when intermolecular forces are known. The force between two identical molecules $\vec{F}$, defined to be positive when repulsive, can be represented in terms of pair potential energy ϕ, where

$$\vec{F} = -\nabla\phi\,(r) \tag{1.5.12}$$

and r is the distance separating the two molecules. Several models have been proposed for ϕ (see Rowley, 1994, for a concise review), the most widely used among them being the empirical Lennard–Jones 6–12 model (Rowley, 1994):

$$\phi(r) = 4\tilde{\varepsilon}\left[\left(\frac{\tilde{\sigma}}{r}\right)^{12} - \left(\frac{\tilde{\sigma}}{r}\right)^{6}\right]. \tag{1.5.13}$$

Figure 1.11 depicts Eq. (1.5.19). The Lennard–Jones model, like all similar models, accounts for the fact that intermolecular forces are attractive at large distances and become repulsive when the molecules are very close to one another. The function $\phi(r)$ in the Lennard–Jones model is fully characterized by two parameters: $\tilde{\sigma}$, the collision diameter, and $\tilde{\varepsilon}$, the energy representing the maximum attraction. Values of $\tilde{\sigma}$ and $\tilde{\varepsilon}$ for some selected molecules are listed in Appendix K. The force constants for a large number of molecules can be found in Svehla (1962). When tabulated values are not known, they can be estimated by use of empirical correlations based on the molecule's properties at its critical point, liquid at normal boiling point, or the solid state at melting point (Bird et al., 2002). In terms of the substance's critical state, for example,

$$\tilde{\sigma} \approx 2.44\,(T_{\text{cr}}/P_{\text{cr}})^{1/3} \tag{1.5.14}$$

$$\tilde{\varepsilon}/\kappa_B \approx 0.77 T_{\text{cr}}, \tag{1.5.15}$$

where T_{cr} and $\tilde{\varepsilon}/\kappa_B$ are in Kelvins, P_{cr} is in atmospheres, and $\tilde{\sigma}$ calculated in this way is in angstroms. The Lennard–Jones model is used quite extensively in molecular dynamic simulations.

According to the Chapman–Enskog model, the gas viscosity can be found from

$$\mu = 2.669 \times 10^{-6}\frac{\sqrt{MT}}{\tilde{\sigma}^2\Omega_\mu} \quad \text{(kg/ms)}, \tag{1.5.16}$$

where T is in Kelvins, $\tilde{\sigma}$ is in angstroms, and Ω_μ is a collision integral for thermal conductivity or viscosity. (Collision integrals for viscosity and thermal conductivity are equal.) Appendix L contains numerical values of the collision integral for the Lennard–Jones model. For monatomic gases the Chapman–Enskog model predicts

$$k = k_{\text{trans}} = \frac{5}{2} C_v \mu = \frac{15}{4} \left(\frac{R_u}{M} \right) \mu. \tag{1.5.17}$$

For a polyatomic gas, the molecule's internal degrees of freedom contribute to the gas thermal conductivity, and

$$k = k_{\text{trans}} + 1.32 \left(C_P - \frac{5}{2} \frac{R_u}{M} \right) \mu. \tag{1.5.18}$$

The binary mass diffusivity of specifies 1 and 2 can be found from

$$\mathcal{D}_{12} = \mathcal{D}_{21} = 1.858 \times 10^{-7} \frac{\sqrt{T^3 \left(\frac{1}{M_1} + \frac{1}{M_2} \right)}}{\tilde{\sigma}_{12}^2 \Omega_D P} \quad \left(\text{m}^2/\text{s} \right), \tag{1.5.19}$$

where P is in atmospheres, Ω_D represents the collision integral for the two molecules for mass diffusivity, and

$$\tilde{\sigma}_{12} = \frac{1}{2} \left(\tilde{\sigma}_1 + \tilde{\sigma}_2 \right), \tag{1.5.20}$$

$$\tilde{\varepsilon}_{12} = \sqrt{\tilde{\varepsilon}_1 \tilde{\varepsilon}_2}. \tag{1.5.21}$$

Appendix L can be used for the calculation of collision integrals for a number of selected species (Hirschfelder et al., 1954).

EXAMPLE 1.5. Using the Chapman–Enskog model estimate the viscosity and thermal conductivity of CCl_4 vapor at 315 K temperature.

SOLUTION. We need to use Eqs. (1.5.16) and (1.5.18), respectively. From Appendix K we get,

$$\tilde{\sigma} = 5.947\,\text{Å},$$

$$\frac{\tilde{\varepsilon}}{\kappa_B} = 322.7\,\text{K}.$$

Therefore

$$\frac{\kappa_B T}{\tilde{\varepsilon}} = \frac{315\,\text{K}}{322.7\,\text{K}} = 0.976.$$

Next, we calculate the Lennard–Jones collision integral by the interpolation in Appendix L, thereby obtaining

$$\Omega_k = 1.607.$$

We can now use Eq. (1.5.16):

$$\mu = 2.669 \times 10^{-6} \frac{\sqrt{MT}}{\tilde{\sigma}^2 \Omega_k} = 2.669 \times 10^{-6} \frac{\sqrt{(153.8)\,(315)}}{(5.947)^2\,(1.607)} = 1.034 \times 10^{-5}.$$

We should now apply Eq. (1.5.17):

$$\begin{aligned} k_{\text{tran}} &= \frac{15}{4}\left(\frac{R_u}{M}\right)\mu = \frac{15}{4}\left(\frac{8314.3\,\text{J/kmol K}}{153.8\,\text{kg/kmol}}\right) 1.034 \times 10^{-5}\ \text{kg/m s} \\ &= 2.095 \times 10^{-3}\ \text{W/m K}. \end{aligned}$$

For CCl_4 vapor $C_P \approx 537$ J/kg K. We can now apply Eq. (1.5.18):

$$\begin{aligned} k &= k_{\text{trans}} + 1.32\left(C_P - \frac{5}{2}\frac{R_u}{M}\right)\mu \\ &= 2.095 \times 10^{-3}\ \text{W/m K} \\ &\quad + 1.32\left(537\ \text{J/kg K} - \frac{5}{2}\frac{8314.3\,\text{J/kmol K}}{153.8\,\text{kg/kmol}}\right)(1.034 \times 10^{-5}) \\ &\approx 7.583 \times 10^{-3}\ \text{W/m K}. \end{aligned}$$

EXAMPLE 1.6. Using the Chapman–Enskog model, estimate the binary diffusivity of CCl_4 vapor in air at 315 K temperature and 1-atm pressure.

SOLUTION. We need to apply Eq. (1.5.19). Let us use subscripts 1 and 2 to represent CCl_4 and air, respectively. From Example 1.5, therefore,

$$\begin{aligned} \tilde{\sigma}_1 &= 5.947\ \text{Å}, \\ \frac{\tilde{\varepsilon}_1}{\kappa_B} &= 322.7\ \text{K}. \end{aligned}$$

Also, from the table of Appendix K,

$$\begin{aligned} \tilde{\sigma}_2 &= 3.711\ \text{Å}, \\ \frac{\tilde{\varepsilon}_2}{\kappa_B} &= 78.6\ \text{K}. \end{aligned}$$

From Eqs. (1.5.20) and (1.5.21), respectively,

$$\begin{aligned} \tilde{\sigma}_{12} &= \frac{1}{2}(\tilde{\sigma}_1 + \tilde{\sigma}_2) = \frac{1}{2}(5.947\ \text{Å} + 3.711\ \text{Å}) = 4.829\ \text{Å}, \\ \frac{\tilde{\varepsilon}_{12}}{\kappa_B} &= \sqrt{\frac{\tilde{\varepsilon}_1}{\kappa_B}\frac{\tilde{\varepsilon}_2}{\kappa_B}} = \sqrt{(322.7\ \text{K})\,(78.6\ \text{K})} = 159.3\ \text{K}, \\ \frac{\kappa_B T}{\tilde{\varepsilon}_{12}} &= \frac{315\ \text{K}}{159.3\ \text{K}} = 1.978. \end{aligned}$$

We can now find the collision integral for mass diffusivity by interpolation in the table in Appendix L to get

$$\Omega_D = 1.079.$$

We can now substitute numbers into Eq. (1.5.19):

$$\mathcal{D}_{12} = \mathcal{D}_{21} = 1.858 \times 10^{-7} \frac{\sqrt{T^3 \left(\frac{1}{153.8} + \frac{1}{29} \right)}}{\tilde{\sigma}_{12}^2 \Omega_D P}$$

$$= 1.858 \times 10^{-7} \frac{\sqrt{(315)^3 \left(\frac{1}{153.8} + \frac{1}{29} \right)}}{(4.829)^2 (1.079)(1)} \approx 8.36 \times 10^{-6} \, \text{m}^2/\text{s}.$$

1.5.3 Diffusion of Mass in Liquids

The binary diffusivities of solutions of several nondissociated chemical species in water are given in Appendix J. The diffusion of a dilute species 1 (solute) in a liquid 2 (solvent) follows Fick's law with a diffusion coefficient that is approximately equal to the binary diffusivity $\mathcal{D}_{12}$, even when other diffusing species are also present in the liquid, provided that all diffusing species are present in very small concentrations.

Theories dealing with molecular structure and kinetics of liquids are not sufficiently advanced to provide for reasonably accurate predictions of liquid transport properties. A simple method for the estimation of the diffusivity of a dilute solution is the Stokes–Einstein expression:

$$\mathcal{D}_{12} = \frac{\kappa_B T}{3 \pi \mu_2 d_1}, \tag{1.5.22}$$

where subscripts 1 and 2 refer to the solvent and the solute, respectively, and d_1 is the diameter of a single solute molecule and can be estimated from $d_1 \approx \tilde{\sigma}$, namely, the Lennard–Jones collision diameter (Cussler, 1997). Alternatively, it can be estimated from

$$d_1 \approx \left(\frac{6}{\pi} \frac{M_1}{\rho_1 N_{\text{Av}}} \right)^{1/3}. \tag{1.5.23}$$

The Stokes–Einstein expression in fact represents the Brownian motion of spherical particles (solute molecules in this case) in a fluid, assuming creep flow (flow without slip) around the particles. It is accurate when the spherical particle is much larger than intermolecular distances. It is good for the estimation of the diffusivity when the solute molecule is approximately spherical, and is at least five times larger than the solvent molecule (Cussler, 2009).

A widely used empirical correlation for binary diffusivity of a dilute and nondissociating chemical species (species 1) in a liquid (solvent, species 2) is (Wilke and Chang, 1955)

$$\mathcal{D}_{12} = 1.17 \times 10^{-16} \frac{(\Phi_2 M_2)^{1/2} T}{\mu \tilde{V}_{b1}^{0.6}} \ (\text{m}^2/\text{s}), \tag{1.5.24}$$

where $\mathcal{D}_{12}$ is in square meters per second, $\tilde{V}_{b1}$ is the specific molar volume in cubic meters per kilomoles of species 1 as liquid at its normal boiling point; μ is the mixture liquid viscosity in kilograms per meter per second; T is the temperature in Kelvins, and Φ_2 is an association parameter for the solvent. $\Phi_2 = 2.26$ for water

Table 1.1. *Specific molar volume at boiling point for selected substances*[a]

Substance	$\tilde{V}_{b1} \times 10^3$ (m^3/kmol)	T_b (K)
Air	29.9	79
Hydrogen	14.3	21
Oxygen	25.6	90
Nitrogen	31.2	77
Ammonia	25.8	240
Hydrogen sulfide	32.9	212
Carbon monoxide	30.7	82
Carbon dioxide	34.0	195
Chlorine	48.4	239
Hydrochloric acid	30.6	188
Benzene	96.5	353
Water	18.9	373
Acetone	77.5	329
Methane	37.7	112
Propane	74.5	229
Heptane	162	372

[a] After Mills (2001).

and 1 for unassociated solvents (Mills, 2001). Values of $\tilde{V}_{b1}$ for several species are given in Table 1.1.

1.6 The Continuum Flow Regime and Size Convention for Flow Passages

With the exception of Chapter 13, where flow and heat transfer in miniature flow passages are discussed, everywhere in this book we make the following two assumptions:

1. The conservation equations discussed in Chapter 1 are applicable.
2. At an interface between a fluid and a solid there is no-slip and thermal equilibrium.

These assumptions are strictly correct if the fluid is a perfect continuum. Fluids are made of molecules, however, and at microscale are particulate. For these assumptions to be valid, the characteristic dimension of the flow field (e.g., the lateral dimension of a flow passage in internal flow or the characteristic size of a surface or an object in external flow) must be orders of magnitude longer than the length scale that characterizes the particulate (molecular) structure of the fluid. A rather detailed discussion of the fluid continuum and its breakdown is provided in Chapter 13. The following brief discussion is meant to clarify the limits of applicability of the discussions in the remainder of the book.

The length scale that characterizes the particulate nature of fluids is the intermolecular distance in liquids and the molecular mean free path in gases. The breakdown of continuum is hardly an issue for liquids for the vast majority of applications, because the intermolecular distances in liquids are extremely short, of the order of

Table 1.2. *Molecular mean free path of dry air*

T (K)	P	λ_{mol} (μm)
300	1 MPa	0.0068
300	1 bar	0.068
300	0.1 bar	0.68
300	1 kPa (0.01 bar)	6.8
600	1 MPa	0.0157
600	1 bar	0.157
600	0.1 bar	1.57
600	1 kPa (0.01 bar)	15.7

10^{-6} mm. Nevertheless, liquid flow in very small channels is different from that in conventional channels with respect to the applicability of classical theory because of the predominance of liquid–surface forces (e.g., electrostatic forces) in the former.

The molecular mean free path for gases can be estimated with the GKT, as mentioned earlier [see Eqs. (1.5.15) and (1.5.16)]. A very important dimensionless parameter that compares the molecular mean free path with the characteristic length of the flow filed is the Knudsen number:

$$\mathrm{Kn}_{l_c} = \lambda_{mol}/l_c. \tag{1.6.1}$$

Conventional fluid mechanics and heat transfer theory, in which fluids act as continua and there is no velocity slip or thermal nonequilibrium at a fluid–solid or fluid–fluid interface, applies when

$$\mathrm{Kn}_{l_c} \lesssim 0.001. \tag{1.6.2}$$

Table 1.2 displays the molecular mean free path for dry air at several pressures and two temperatures calculated with Eq. (1.5.10). As expected, λ_{mol} depends on pressure and temperature (i.e., on density) and is in the micrometer range except at very low pressures. Evidently a breakdown of continuum can occur because of the reduction of the physical size of an object or flow passage or because of the reduction of the gas density. It thus can happen in microchannels and the flow field around microscopic particles and in objects exposed to very low density (rarefied) gas. Rarefied gas flow is common for craft moving in the upper atmosphere.

PROBLEMS

Problem 1.1. Write the mass, momentum, and energy conservation equations for an incompressible, constant-property, and Newtonian fluid, for the following systems:

(a) downward flow in a vertical pipe,
(b) downward flow in the previous vertical pipe, in which the hydrodynamic entrance effects have all disappeared.
(c) Repeat part (b), this time assuming that hydrodynamic and thermal entrance effects have all disappeared.

For simplicity, assume axisymmetric flow.

Problem 1.2. A rigid and long cylindrical object is rotating around its axis at a constant rotational speed in an otherwise quiescent and infinitely large fluid. The cylinder has only rotational motion, without any translational motion. The surface temperature of the object is higher than the temperature of the ambient fluid. The motion can be assumed laminar everywhere.

(a) Write the complete mass, momentum, and energy conservation equations and their boundary conditions, assuming an incompressible, Newtonian, and constant-property fluid, in polar cylindrical coordinates.
(b) Simplify the equations for steady-state conditions.

Problem 1.3. A rigid spherical particle is moving at a constant velocity U_∞ in an otherwise quiescent and infinitely large fluid field. The particle has no rotational motion. The fluid is Newtonian and incompressible and has constant properties. The particle's surface is at a different temperature than that of the surrounding fluid.

(a) Write the complete mass, momentum, and energy conservation equations and their boundary conditions.
(b) Simplify the equations for steady-state conditions.

Problem 1.4. Using Eq. (1.1.18a) and the constitutive relations for Newtonian fluids discussed in Eqs. (1.1.19) and (1.1.20) [or, equivalently, (1.1.21a)–(1.1.21e)], formulate and expand the term $\nabla \cdot \underline{\underline{\tau}}$ in Cartesian coordinates.

Problem 1.5. Using the rule for scalar product of two tensors, show that

$$\underline{\underline{\tau}} : \left(\nabla \vec{U}\right) = \tau_{ij} \frac{\partial u_i}{\partial x_j}.$$

Expand the result in Cartesian coordinates for a Newtonian fluid.

Problem 1.6. Bernoulli's expression for an incompressible and inviscid flow along a streamline is

$$\frac{P}{\rho} + \frac{1}{2}U^2 + gz = \text{const.}$$

Derive this expression by simplifying the mechanical energy transport equation.

Also, by manipulating the energy conservation equation, prove that for incompressible and inviscid flow with negligible thermal conductivity, the following expression [strong form of Bernoulli's equation (White, 2006)] applies along a streamline:

$$\boldsymbol{u} + \frac{P}{\rho} + \frac{1}{2}U^2 + gz = \text{const.}$$

Problem 1.7. Show that for inviscid flow the fluid equation of motion reduces to

$$\rho D\,\vec{U}/D\,t = -\nabla P + \vec{F}_b.$$

Prove that for an incompressible and irrotational flow this equation will lead to

$$\rho \left\{ \left[\frac{\partial \phi}{\partial t} + \frac{1}{2}U^2 \right]_j - \left[\frac{\partial \phi}{\partial t} + \frac{1}{2}U^2 \right]_i \right\} = P_i - P_j - \rho g\,(z_j - z_i)\,,$$

where subscripts i and j refer to two arbitrary points in the flow field, and ϕ is the velocity potential whereby

$$\vec{U} = \nabla\phi.$$

Hint: For irrotational flow, $\nabla \times \vec{U} = 0$.

Problem 1.8. The annular space between two long, vertical, and coaxial cylinders is filled with an incompressible, constant-property fluid. The inner and outer radii of the annular space are R_i and R_0, respectively. The outer cylinder is rotating at a constant rotational speed of ω. The surface temperatures of the inner and outer surfaces are T_i and T_0, respectively.

Write the momentum and energy conservation equations and their boundary conditions, assuming that the flow field is laminar and viscous dissipation is not negligible. Do this by starting with the conservation equations in polar cylindrical coordinates and deleting the redundant terms. Neglect the effect of gravity.

Problem 1.9. A horizontal, infinitely large plate is initially underneath a quiescent (stagnant), infinitely large fluid that has temperature T_∞. The plate is suddenly put in motion, at $t = 0$, with a constant speed of U_0. The fluid is incompressible, and has constant properties.

(a) Starting from the momentum conservation equation, derive an expression for the velocity profile in the fluid and prove that the wall shear stress can be found from

$$\tau_s = -\mu \frac{U_0}{\sqrt{\pi \nu t}}.$$

(b) Consider the same flow field in which the lower plate is stationary, but its temperature is suddenly changed from T_∞ to T_s, at $t = 0$. Derive an expression for the temperature profile and prove that

$$q_s'' = k \frac{T_s - T_\infty}{\sqrt{\pi \alpha t}}.$$

(c) Now assume that at $t = 0$ the lower plate is put in motion with a velocity of U_0 and its temperature is simultaneously changed to T_s. Repeat parts (a) and (b).

Problem 1.10. Formally derive the mechanical energy transport equation for axisymmetric flow of an incompressible and constant property fluid in a circular-cross-section pipe. Do this by deriving the dot product of the velocity vector with the momentum conservation equation.

Problem 1.11. Repeat Problem 1.7, this time for an axisymmetric flow in spherical coordinates. (Note that in axisymmetric flow there is no dependence on $\emptyset$.)

Problem 1.12. Prove Eq. (1.1.50).

Problem 1.13. For an open system (control volume), the second law of thermodynamics requires that the rate of entropy generation always be positive. The entropy generation rate can be found from

$$\iiint_{V_{cv}} \dot{\sigma}'''_{gen} dV = \frac{d}{dt}\iiint_{V_{cv}} \rho \boldsymbol{s} dV + \iint_{A_{cv}} \rho \boldsymbol{s}(\vec{U}\cdot\vec{N})dA - \iiint_{V_{cv}} \frac{\dot{q}}{T} dV + \iint_{A_{cv}} \frac{\vec{q}''\cdot\vec{N}}{T} dA,$$

where V_{CV} and A_{CV} are the volume and surface area of the control volume, respectively, $\vec{N}$ is the unit normal vector pointing outward from the control volume, and $\dot{\sigma}'''_{gen}$ is the entropy generation rate per unit volume.

(a) Simplify this equation for a control volume that has a finite number of inlet and outlet ports through which uniform-velocity streams flow.

(b) Using the results from part (a), prove that in a flow field we must have $\dot{\sigma}'''_{gen} \geq 0$, where

$$\dot{\sigma}'''_{gen} = \rho \frac{D\boldsymbol{s}}{Dt} + \nabla \cdot \left(\frac{\vec{q}''}{T}\right) - \frac{\dot{q}}{T}.$$

Problem 1.14. Consider mixtures of water vapor and nitrogen when the mixture pressure and temperature are 100 kPa and 300 K, respectively. For relative humidity values of 0.1 and 0.75, calculate the following properties for the mixture ρ, μ, C_p, k.

Problem 1.15. Small amounts of noncondensables (usually air) usually enter the vapor in steam power plants and negatively affect the performance of the condenser. Consider saturated mixtures of steam and nitrogen for which the mixture pressure is 10 kPa. For nitrogen mole fractions of 1% and 10%, calculate the following properties for the mixture ρ, μ, C_p, k.

Mass Transfer

Problem 1.16. A bowl of water is located in a room. The water is at equilibrium with the air in the room. The room temperature and pressure are 100 kPa and 300 K, respectively. Analysis of water shows that it contains 25 ppm (by weight) of dissolved CO_2. Find the mass fraction and partial pressure of CO_2 in the air.

Problem 1.17. Using the Chapman–Enskog model, calculate the binary diffusivity for the following pairs of species at 100-kPa pressure and 300 K temperature:

(a) He–N_2
(b) CO_2–N_2
(c) HCN–Air

Problem 1.18. Using the Chapman–Enkog model, calculate the mass diffusivities of uranium Hexafluoride (UF_6) in air for the two predominant isotopes of uranium, namely ^{235}U and ^{238}U. Assume that the pressure and temperature are 0.5 bar and 300 K, respectively. Calculate the difference in diffusivities and comment on its significance.

Problem 1.19. In an experiment, a stagnant sample of water contains chlorine at a concentration of 50 ppm by weight. The local pressure and temperature are 100 kPa and 320 K, respectively. The concentration of chlorine is not uniform in the water,

and at a particular location the chlorine mass fraction gradient is 100 m^{-1}. Calculate the diffusive mass flux of chlorine at that location. Calculate the diffusive mass flux if the temperature is increased to 400 K.

Problem 1.20. In Problem 1.3, assume that the particle is made of a sparingly volatile substance, such as naphthaline. As a result of volatility, the partial pressure of the species of which the particle is made (which is the transferred species here) remains constant at the s surface. Write the species conservation equation and boundary conditions for the transferred species.

2 Boundary Layers

The conservation equations for fluids were derived in the previous chapter. Because of viscosity, the velocity boundary condition on a solid–fluid interface in common applications is no-slip. Velocity slip occurs during gas flow when the gas molecular mean free path is not negligible in comparison with the characteristic dimension of the flow passage. It is discussed in Chapter 13.

The complete solution of viscous flow conservation equations for an entire flow field, it seems, is in principle needed in order to calculate what actually takes place on the surface of an object in contact with a fluid. The complete solution of the entire flow field is impractical, however, and is fortunately unnecessary. The breakthrough simplification that made the analysis of the flow field at the vicinity of surfaces practical was introduced by Ludwig Prandtl in 1904. He suggested that any object that moves while submerged in a low-viscosity fluid will be surrounded by a thin boundary layer. The impact of the no-slip boundary condition at the surface of the object will extend only through this thin layer of fluid, and beyond it the fluid acts essentially as an inviscid fluid. In other words, outside the boundary layer the flow field does not feel the viscous effect caused by the presence of the object. It feels only the blockage caused by the presence of the object, as a result of which the streamlines in the flow field become curved around the object. Prandtl argued that this should be true for all fluids that possess small and moderate viscosity.

The boundary-layer concept is a very important tool and allows for the simplification of the analysis of virtually all transport processes in two important ways. First, it limits the domain in the flow field where the viscous and other effects of the wall must be included in the conservation equations. Second, it shows that, within the boundary layer, the conservation equations can be simplified by eliminating certain terms in those equations.

2.1 Boundary Layer on a Flat Plate

Consider the flow of a fluid parallel to a thin, flat plate, as shown in Fig. 2.1. Away from the wall the fluid has a uniform velocity profile. This is the simplest physical condition as far as the phenomenology of boundary layers is concerned and produces effects that with some variations apply to other configurations as well. For the thin plate depicted in the figure, measurements slightly above and below the

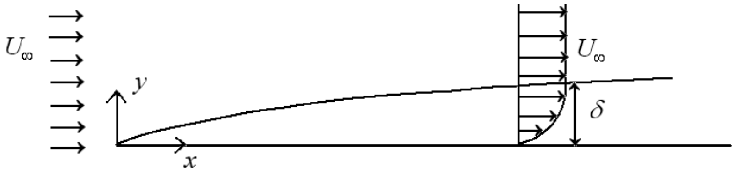

Figure 2.1. Laminar flow boundary layer on a flat plate.

plate would agree with the predictions of the inviscid flow theory. Very close to the wall, however, a nonuniform velocity profile would be noted in which, over a very thin layer of fluid of thickness δ, the fluid velocity increases from zero (at $y = 0$) to $\approx U_\infty$ (at $y = \delta$). The velocity of the fluid actually approaches U_∞ asymptotically, and δ is often defined as the normal distance from the wall where $u/U_\infty = 0.99$ or $u/U_\infty = 0.999$.

Boundary layers are not always laminar. On a flat plate, for example, for some distance from the leading edge the boundary layer remains laminar (see Fig. 2.2). Then, over a finite length (the transition zone), the flow field has characteristics of both laminar and turbulent flows. Finally, a point is reached beyond which the boundary layer is fully turbulent, where the fluid velocity at every point, with the exception of a very thin sublayer right above the surface, is characterized by sustained turbulent fluctuations.

Experiment shows that the occurrence of a laminar–turbulent boundary-layer transition depends on the Reynolds number, defined as

$$\mathrm{Re}_x = \frac{\rho U_\infty x}{\mu}. \tag{2.1.1}$$

The value of Re_x at which transition occurs depends on the surface roughness and the flow disturbances in the fluid outside the boundary layer. The transition region can occur over the range

$$2 \times 10^4 \lesssim \mathrm{Re}_x \lesssim 10^6. \tag{2.1.2}$$

For smooth surfaces the narrower range of $10^5 \lesssim \mathrm{Re}_x \lesssim 10^6$ is often mentioned. Furthermore, in engineering calculations, for simplicity, the transition region is sometimes partially incorporated into the laminar region and partially into the turbulent region, and $\mathrm{Re}_x = 5 \times 10^5$ is used.

Heat and mass transfer between a surface and a fluid also results in the development of thermal and mass transfer boundary layers. Consider the flat plate shown in Fig. 2.3, where the surface is at temperature T_s and the ambient fluid has a uniform temperature of T_∞. The thermal and concentration boundary layers that develop

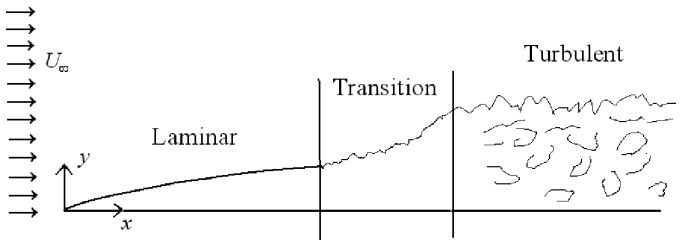

Figure 2.2. Boundary-layer flow regimes on a flat plate.

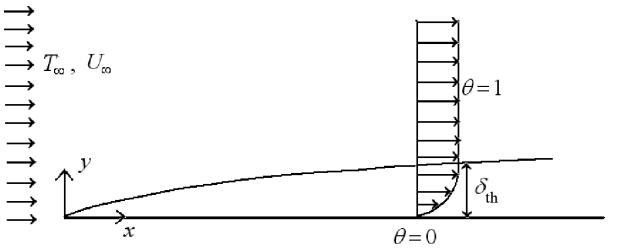

Figure 2.3. Thermal boundary layer on a flat plate.

are similar to the momentum boundary layer. Thus the thermal boundary condition at the wall ($T_s \neq T_\infty$ in this case) directly affects the fluid temperature only over a thin fluid layer, beyond which $T = T_\infty$. The temperature of the fluid approaches T_∞ asymptotically, of course, and δ_{th}, the thermal boundary-layer thickness, is often defined as

$$\theta = 0.99 \text{ or } \theta = 0.999 \text{ at } y = \delta_{th},$$

where $\theta = \frac{T-T_s}{T_\infty - T_s}$.

In the case of mass transfer (e.g., if the wall is covered with a substance undergoing slow sublimation into a gas), a similar boundary layer associated with the concentration of the transferred species is formed, as shown in Fig. 2.4. Let us use subscript 1 to refer to the transferred species. The mass fraction of the transferred species will thus be m_1. The normalized mass fraction of species 1, ϕ, is defined as

$$\phi = \frac{m_1 - m_{1,s}}{m_{1,\infty} - m_{1,s}}.$$

Thus ϕ increases from zero at the wall to 1 over a very thin layer with thickness δ_{ma}.

The following notes can be mentioned about boundary layers.

1. Velocity, thermal, and mass transfer boundary layers generally have different thicknesses ($\delta \neq \delta_{th} \neq \delta_{ma}$).
2. The thermal and mass transfer boundary layers become turbulent when the boundary layer becomes turbulent. In other words, the laminar–turbulent transition is determined primarily by the hydrodynamics.
3. The hydrodynamic resistance imposed by the surface on the fluid entirely lies in the $0 < y < \delta$ region. Likewise, resistances to heat and mass transfer entirely lie in the $0 < y < \delta_{th}$ and $0 < y < \delta_{ma}$ regions of the flow field, respectively.
4. Boundary layers are by no means limited to flat surfaces. They form on all bodies and objects. A common and familiar example is schematically displayed in Fig. 2.5.

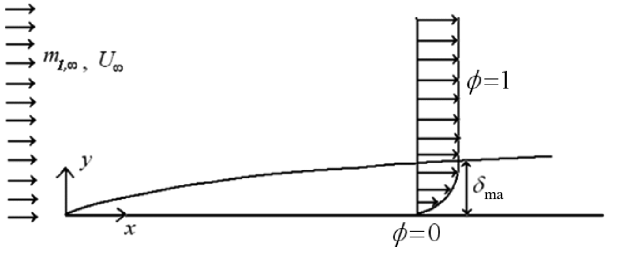

Figure 2.4. Mass transfer boundary layer on a flat plate.

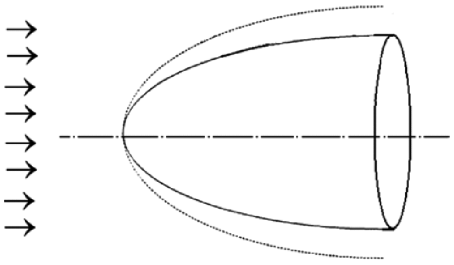

Figure 2.5. Schematic of the boundary layer on the surface of a blunt body.

Flow Field Outside the Boundary Layer

With respect to the conditions outside the boundary layer, the viscous effects are often unimportant, and because the boundary layer is typically very thin in comparison with the characteristic dimensions of the main flow, inviscid flow conservation equations can be assumed to apply for the ambient flow field by totally neglecting the boundary layer. The inviscid flow solution will provide the boundary condition for the boundary layers (i.e., the conditions at the edge of the boundary layers).

For an inviscid fluid, the Navier–Stokes equation reduces to

$$\rho \frac{D\vec{U}}{Dt} = -\nabla P - \rho \nabla \Omega, \tag{2.1.3}$$

where Ω is the specific potential energy:

$$\vec{g} = -\nabla \Omega. \tag{2.1.4}$$

Assuming steady state, we can write

$$\frac{D\vec{U}}{Dt} = \vec{U} \cdot \nabla \vec{U} = \nabla \left(\frac{1}{2} U^2 \right). \tag{2.1.5}$$

Equation (2.1.3) can be recast as

$$\nabla \left(\frac{1}{2} U^2 \right) = -\frac{1}{\rho} \nabla P - \nabla \Omega. \tag{2.1.6}$$

Along a streamline this equation reduces to

$$d \left(\frac{1}{2} U^2 \right) + \frac{dP}{\rho} + g\, dz = 0, \tag{2.1.7}$$

which is the most familiar form of Bernoulli's equation. If the flow is irrotational, furthermore,

$$\nabla \times \vec{U} = 0. \tag{2.1.8}$$

This implies that $\vec{U}$ can be expressed as the gradient of a single-valued function, i.e., the *velocity potential*:

$$\vec{U} = \nabla \phi, \tag{2.1.9a}$$

$$\nabla \cdot \vec{U} = \nabla^2 \phi = 0. \tag{2.1.9b}$$

In analyzing boundary layers, we often use a 2D flow approximation. In a 2D flow in Cartesian coordinates Eq. (2.1.8) reduces to,

$$\frac{\partial v}{\partial x} - \frac{\partial u}{\partial y} = 0 \tag{2.1.10}$$

We can define a stream function ψ according to

$$u = \partial\psi/\partial y, \tag{2.1.11}$$

$$v = -\partial\psi/\partial x. \tag{2.1.12}$$

Substitution into Eq. (2.1.10) then gives

$$\nabla^2\psi = 0. \tag{2.1.13}$$

If the flow is steady state, incompressible, and irrotational, then a solution to Eq. (2.1.9b) or (2.1.13) that satisfies Bernoulli's equation at one place will satisfy Bernoulli's equation everywhere else in the flow field.

To obtain the velocity field outside the boundary layer we thus may solve Eq. (2.1.9b) with correct boundary conditions. The overall flow field boundary conditions of course depend on the specific problem in hand.

If the viscous, body-force, and conduction terms in the energy equation are neglected, we will then have

$$\rho\frac{D}{Dt}\left(\boldsymbol{h} + \frac{1}{2}U^2\right) = \frac{\partial P}{\partial t}. \tag{2.1.14}$$

For a flow that is in steady state, this will lead to

$$\vec{U}\cdot\nabla\left(\boldsymbol{h} + \frac{1}{2}U^2\right) = 0. \tag{2.1.15}$$

This equation can be satisfied only if

$$\boldsymbol{h} + \frac{1}{2}U^2 = \text{const.} \tag{2.1.16}$$

Had we included the gravitational term (which is negligible in the great majority of problems) in the energy equation, we would have gotten

$$\boldsymbol{h} + \frac{1}{2}U^2 + gz = \text{const.} \tag{2.1.17}$$

2.2 Laminar Boundary-Layer Conservation Equations

Some of the terms in the fluid conservation equations are unimportant inside boundary layers. By dropping these terms from the conservation equations, the analysis of boundary layers becomes greatly simplified.

Consider the flow parallel to a flat plate (Fig. 2.1). As mentioned earlier, this is the simplest configuration, but provides information that is much more general. As a further simplification let us assume constant properties and incompressible flow, without body force. Also, let us assume 2D (x, y) flow. Then the conservation

equations for mass, momentum, energy and mass species (species 1 in this case) become, respectively,

$$\frac{\partial u}{\partial x} + \frac{\partial v}{\partial y} = 0, \tag{2.2.1}$$

$$u\frac{\partial u}{\partial x} + v\frac{\partial u}{\partial y} = -\frac{1}{\rho}\frac{\partial P}{\partial x} + \nu\left(\frac{\partial^2 u}{\partial x^2} + \frac{\partial^2 u}{\partial y^2}\right), \tag{2.2.2}$$

$$u\frac{\partial v}{\partial x} + v\frac{\partial v}{\partial y} = -\frac{1}{\rho}\frac{\partial P}{\partial y} + \nu\left(\frac{\partial^2 v}{\partial x^2} + \frac{\partial^2 v}{\partial y^2}\right), \tag{2.2.3}$$

$$\rho C_p\left(u\frac{\partial T}{\partial x} + v\frac{\partial T}{\partial y}\right) = k\left(\frac{\partial^2 T}{\partial x^2} + \frac{\partial^2 T}{\partial y^2}\right) + \mu\,\Phi, \tag{2.2.4}$$

$$\rho\left(u\frac{\partial m_1}{\partial x} + v\frac{\partial m_1}{\partial y}\right) = \rho\mathcal{D}_{12}\left(\frac{\partial^2 m_1}{\partial x^2} + \frac{\partial^2 m_1}{\partial y^2}\right) + \mu\,\Phi, \tag{2.2.5}$$

where, in writing Eq. (2.2.5), Fick's law is assumed to be applicable. Now, consistent with the experimental observation that $\delta \ll x$, we can perform the following order-of-magnitude analysis:

$$\frac{\partial u}{\partial x} \approx -\frac{U_\infty}{x}, \tag{2.2.6}$$

$$\frac{\partial u}{\partial y} \approx \frac{U_\infty}{\delta}, \tag{2.2.7}$$

$$\frac{\partial^2 u}{\partial x^2} \approx \frac{1}{x}\left\{\left.\frac{\partial u}{\partial x}\right|_x - \left.\frac{\partial u}{\partial x}\right|_0\right\} \approx -\frac{U_\infty}{x^2}, \tag{2.2.8}$$

$$\frac{\partial^2 u}{\partial y^2} \approx \frac{1}{\delta}\left\{\left.\frac{\partial u}{\partial y}\right|_\delta - \left.\frac{\partial u}{\partial y}\right|_0\right\} \approx \frac{1}{\delta}\left(0 - \frac{U_\infty}{\delta}\right) \tag{2.2.9}$$

$$\Rightarrow \frac{\partial^2 u}{\partial y^2} \approx -\frac{U_\infty}{\delta^2}. \tag{2.2.10}$$

Evidently, then,

$$\frac{\partial u}{\partial x} \ll \frac{\partial u}{\partial y}, \tag{2.2.11}$$

$$\frac{\partial^2 u}{\partial x^2} \ll \frac{\partial^2 u}{\partial y^2}. \tag{2.2.12}$$

The term $\frac{\partial^2 u}{\partial x^2}$ can thus be neglected in Eq. (2.2.2).

We can argue, in a similar manner, that

$$\frac{\partial T}{\partial x} \approx -\frac{T_\infty - T_s}{x}, \tag{2.2.13}$$

$$\frac{\partial T}{\partial y} \approx \frac{T_\infty - T_s}{\delta}, \tag{2.2.14}$$

$$\frac{\partial^2 T}{\partial y^2} \approx \frac{1}{\delta}\left\{\left.\frac{\partial T}{\partial y}\right|_\delta - \left.\frac{\partial T}{\partial y}\right|_0\right\} \approx \frac{T_\infty - T_s}{\delta^2}, \tag{2.2.15}$$

$$\frac{\partial^2 T}{\partial x^2} \approx \frac{1}{x}\left\{\left.\frac{\partial T}{\partial x}\right|_x - \left.\frac{\partial T}{\partial x}\right|_0\right\} \approx -\frac{T_\infty - T_s}{x^2}. \tag{2.2.16}$$

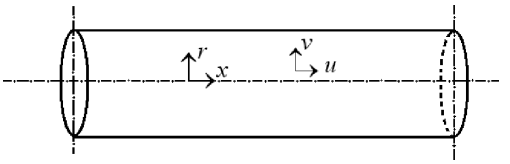

Figure 2.6. Axisymmetric flow in a tube.

Obviously, then,

$$\frac{\partial T}{\partial x} \ll \frac{\partial T}{\partial y}, \tag{2.2.17}$$

$$\frac{\partial^2 T}{\partial x^2} \ll \frac{\partial^2 T}{\partial y^2.} \tag{2.2.18}$$

Therefore the term $\frac{\partial^2 T}{\partial x^2}$ in Eq. (2.2.4) can be neglected.

A similar order-of-magnitude analysis can be performed for mass transfer [Eq. (2.2.5)], which will lead to

$$\frac{\partial m_1}{\partial x} \ll \frac{\partial m_1}{\partial y} \tag{2.2.19}$$

$$\frac{\partial^2 m_1}{\partial x^2} \ll \frac{\partial^2 m_1}{\partial y^2}. \tag{2.2.20}$$

The term $\frac{\partial^2 m_1}{\partial x^2}$ can thus be neglected in Eq. (2.2.5).

The conservation equations for the boundary layer thus reduce to

$$\frac{\partial u}{\partial x} + \frac{\partial v}{\partial y} = 0, \tag{2.2.21}$$

$$u\frac{\partial u}{\partial x} + v\frac{\partial u}{\partial y} = -\frac{1}{\rho}\frac{dP}{dx} + \nu\frac{\partial^2 u}{\partial y^2}, \tag{2.2.22}$$

$$-\frac{\partial P}{\partial y} = 0 \Rightarrow P \neq f(y), \tag{2.2.23}$$

$$\rho C_p\left(u\frac{\partial T}{\partial x} + v\frac{\partial T}{\partial y}\right) = k\frac{\partial^2 T}{\partial y^2} + \mu\left(\frac{\partial u}{\partial y}\right)^2, \tag{2.2.24}$$

$$\rho\left(u\frac{\partial m_1}{\partial x} + v\frac{\partial m_1}{\partial y}\right) = \rho\mathcal{D}_{12}\frac{\partial^2 m_1}{\partial y^2}. \tag{2.2.25}$$

A similar order-of-magnitude analysis for axisymmetric, laminar flow in a circular pipe (Fig. 2.6) will result in the following conservation equations.

For mass,

$$\frac{\partial u}{\partial x} + \frac{1}{r}\frac{\partial}{\partial r}(rv) = 0. \tag{2.2.26}$$

For momentum in the longitudinal direction,

$$u\frac{\partial u}{\partial x} + v\frac{\partial u}{\partial r} = -\frac{1}{\rho}\frac{dP}{dx} + \nu\left[\frac{1}{r}\frac{\partial}{\partial r}\left(r\frac{\partial u}{\partial r}\right)\right]. \tag{2.2.27}$$

For energy,

$$\rho C_p \left(u \frac{\partial T}{\partial x} + v \frac{\partial T}{\partial r} \right) = k \frac{1}{r} \frac{\partial}{\partial r} \left(r \frac{\partial T}{\partial r} \right) + \mu \left(\frac{\partial u}{\partial r} \right)^2 . \tag{2.2.28}$$

For mass species,

$$\rho \left(u \frac{\partial m_1}{\partial x} + v \frac{\partial m_1}{\partial r} \right) = \rho \mathcal{D}_{12} \frac{1}{r} \frac{\partial}{\partial r} \left(r \frac{\partial m_1}{\partial r} \right) . \tag{2.2.29}$$

Note that the momentum equation in the radial direction simply gives

$$\frac{\partial P}{\partial r} = 0, \quad \Rightarrow P \neq f(r).$$

2.3 Laminar Boundary-Layer Thicknesses

The order-of-magnitude analysis provides useful information about the thickness of the boundary layer as well. Starting from Eq. (2.2.22), the order of magnitude of terms on the left- and right-hand sides of the equation is

$$U_\infty \frac{U_\infty}{x}, \; v \frac{U_\infty}{\delta} \; \approx \; \nu \frac{U_\infty}{\delta^2}. \tag{2.3.1}$$

Because the orders of magnitude of terms are the same,

$$\frac{\delta}{x} \approx \mathrm{Re}_x^{-1/2}, \tag{2.3.2}$$

$$\frac{v}{U_\infty} \approx \mathrm{Re}_x^{-1/2}. \tag{2.3.3}$$

Furthermore, because boundary-layer approximations are valid only when $(\delta/x) \ll 1$, it is evident from Eq. (2.3.2) that such approximations make sense only for $\mathrm{Re}_x \gg 1$.

Now consider Eq. (2.2.24). First, consider the case in which $\delta_{\mathrm{th}} \gg \delta$, which occurs when $\mathrm{Pr} \ll 1$ [see Fig. 2.7(a)]. Neglecting the viscous dissipation term, the orders of magnitude of the terms on both sides of the equation are

$$\underbrace{u \frac{\partial T}{\partial x}}_{o\left(U_\infty \frac{\Delta T}{x}\right)} + \underbrace{v \frac{\partial T}{\partial y}}_{o\left(v \frac{\Delta T}{\delta_H}\right)} = \underbrace{\alpha \frac{\partial^2 T}{\partial y^2}}_{o\left(\alpha \frac{\Delta T}{\delta_H^2}\right)} + \frac{\mu}{\rho C_p} \left(\frac{\partial u}{\partial y} \right)^2 . \tag{2.3.4}$$

Because $v \approx U_\infty \delta / x$, the second term on the left-hand side will be small, the remainder of Eq. (2.3.4) then leads to

$$\frac{\delta_{\mathrm{th}}}{x} \approx \mathrm{Pr}^{-1/2} \mathrm{Re}_x^{-1/2}. \tag{2.3.5}$$

Combining Eqs. (2.3.2) and (2.3.4), we get,

$$\frac{\delta_{\mathrm{th}}}{\delta} \approx \mathrm{Pr}^{-1/2}. \tag{2.3.6}$$

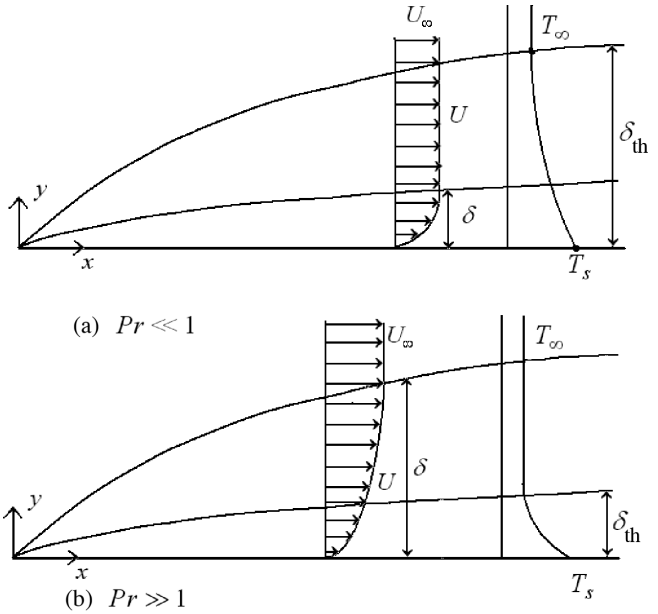

Figure 2.7. The velocity and temperature boundary layers.

Now we consider a thin thermal boundary layer, i.e., conditions in which $\delta_{\text{th}} < \delta$ [see Fig. 2.7(b)]. In this case we have,

$$u\frac{\Delta T}{x} \approx \boldsymbol{\alpha}\frac{\Delta T}{\delta_{\text{th}}^2}, \tag{2.3.7}$$

$$u \approx U_\infty \delta_{\text{th}}/\delta. \tag{2.3.8}$$

Combining these equations and using Eq. (2.3.2), we can show that

$$\frac{\delta_{\text{th}}}{\delta} \approx \text{Pr}^{-1/3}. \tag{2.3.9}$$

A similar analysis can be performed for diffusive mass transfer using Eq. (2.2.29). Let us show the thickness of the concentration boundary layer for species 1 with δ_{ma}. The parameter determining the magnitude of the ration $\delta_{\text{ma}}/\delta$ is the Schmidt number

$Sc = \nu/\mathcal{D}_{12}$. It can then be shown that

$$\frac{\delta_{\text{ma}}}{\delta} \approx \text{Sc}^{-1/2} \text{ for Sc} \ll 1, \tag{2.3.10}$$

$$\frac{\delta_{\text{ma}}}{\delta} \approx \text{Sc}^{-1/3} \text{ for Sc} > 1. \tag{2.3.11}$$

For the diffusive transport of common substances, however, Sc $\approx$ 0.2–3 for gases and Sc $\gg$ 1 for liquids.

The expressions derived thus far in this section were of course approximate. Unambiguous specification of the physical boundary-layer thicknesses is difficult. For example, an unambiguous definition of the velocity boundary-layer thickness is difficult because $u \to U_\infty$ as $y \to \infty$ asymptotically (see Fig. 2.1). We can thus

define the thickness of the boundary layer as the height above the surface where $u/U_\infty = 0.99,\ 0.999$ or even 0.9999.

The scale of the velocity boundary-layer thickness can be more adequately specified by the following precise definitions:

$$\delta_1 = \int_0^\infty \left(1 - \frac{\rho u}{\rho_\infty U_\infty}\right) dy, \tag{2.3.12}$$

$$\delta_2 = \int_0^\infty \frac{\rho u}{\rho_\infty U_\infty}\left(1 - \frac{u}{U_\infty}\right) dy, \tag{2.3.13}$$

$$\delta_3 = \int_0^\infty \frac{\rho u}{\rho_\infty U_\infty}\left(1 - \frac{u^2}{U_\infty^2}\right) dy. \tag{2.3.14}$$

It can easily be shown that $\rho_\infty U_\infty \delta_1$ is the loss in mass flow rate, per unit plate width, as a result of the presence of the boundary layer; $\rho_\infty U_\infty^2 \delta_2$ is the loss in momentum flux, per unit plate width, as a result of the presence of the boundary layer; and $\rho_\infty \frac{1}{2} U_\infty^3 \delta_3$ is the loss in kinetic energy flux, per unit plate width, as a result of the presence of the boundary layer.

The *shape factor* for a boundary layer is defined as

$$H = \frac{\delta_1}{\delta_2}. \tag{2.3.15}$$

A similar precise definition for the thermal boundary-layer thickness (called *enthalpy thickness*) is introduced later in Chapter 5.

2.4 Boundary-Layer Separation

In a region with an adverse pressure gradient (increasing pressure or decelerating flow along the main flow direction), a point may be reached where $\frac{du}{dy}|_{y=0} = 0$. This is a "point of separation," downstream of which the boundary-layer is deflected sideways from the wall, separates from the wall, and moves into the main stream.

The boundary-layer arguments and equations are not valid downstream the point of separation. A short distance behind the latter point the boundary layer becomes very thick, and in the case of blunt objects the separated boundary layer displaces the ambient potential flow from the body by a significant distance. Boundary layer separation is an important phenomenon for blunt objects because it causes the disruption of the boundary layer, its movement into the main flow, and the formation of wake flow, or transition to turbulence (see Fig. 2.8).

The separation happens only in decelerating flow. It can be understood by examining simple 2D boundary-layer equations for steady-state, incompressible flow over a flat plate (Fig. 2.1). Equation (2.2.2) then applies, according to which on the wall, where $u = v = 0$,

$$\mu \left.\frac{\partial^2 u}{\partial y^2}\right|_{y=0} = \frac{dP}{dx}. \tag{2.4.1}$$

Furthermore, because $P \neq f(y)$,

$$\left.\frac{\partial^3 u}{\partial y^3}\right|_{y=0} = 0. \tag{2.4.2}$$

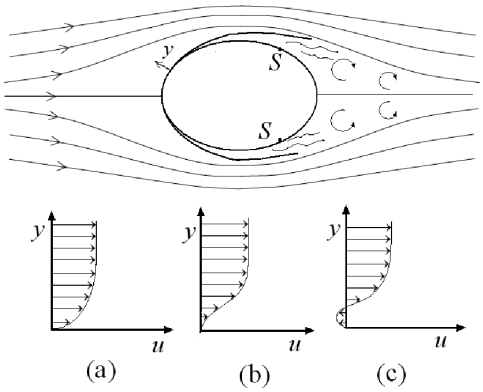

Figure 2.8. Boundary-layer separation and velocity distribution near the point of separation: (a) velocity profile upstream of separation point, (b) velocity profile at separation point, (c) velocity profile downstream of separation point.

The point $y = 0$ is thus the extremum point. It can be seen from Eq. (2.4.1) that when $dP/dx < 0$, then $\partial^2 u/\partial y^2 < 0$, and the boundary-layer velocity profile will look similar to Fig. 2.9, where $\frac{\partial u}{\partial y} > 0$ and the boundary layer remains stable.

Now, if $dP/dx > 0$ (i.e., in decelerating flow), then at $y = 0$ we $\partial^2 u/\partial y^2 > 0$. Furthermore, because $\frac{\partial^3 u}{\partial y^3}|_{y=0} = 0$, the point $y = 0$ is an extremum point for $\partial^2 u/\partial y^2$. However, at some large distance from the wall we have $\partial^2 u/\partial y^2 < 0$ in any case, and therefore there must exist a point where $\partial^2 u/\partial y^2 = 0$, i.e., an inflection point for u. The profile then will look similar to Fig. 2.10. At the point of inflection we have $\partial u/\partial y = 0$.

Thus, when the ambient potential flow is decelerating, the boundary layer always has an inflection point. Because the profile of velocity must have an inflection point when $(\frac{\partial u}{\partial y})_{y=0} = 0$ occurs, it follows that separation happens only when the flow is decelerating.

2.5 Nondimensionalization of Conservation Equations and Similitude

Consider an incompressible, binary mixture, with constant properties, without body force, and no volumetric heating or chemical reaction. Assume that Fourier's law and Fick's law apply. For this flow situation the conservation equations are as follows:

$$\text{mass, } \nabla \cdot \vec{U} = 0, \tag{2.5.1}$$

$$\text{momentum, } \rho \frac{D\vec{U}}{Dt} = -\nabla P + \mu \nabla^2 \vec{U}, \tag{2.5.2}$$

$$\text{thermal energy, } \rho C_p \frac{DT}{Dt} = k\nabla^2 T + \mu\, \Phi, \tag{2.5.3}$$

$$\text{species, } \frac{Dm_1}{Dt} = \mathcal{D}_{12} \nabla^2 m_1, \tag{2.5.4}$$

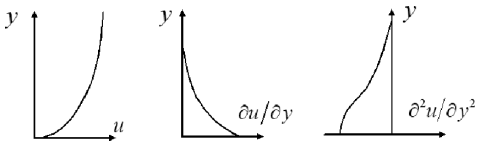

Figure 2.9. The velocity profile and its derivatives in accelerating flow.

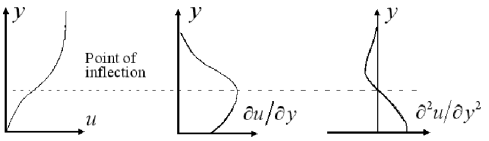

Figure 2.10. The velocity profile and its derivatives in decelerating flow.

where subscript 1 represents the transferred species. We define l as the characteristic length and U_{ref} as the characteristic velocity. We also define dimensionless parameters $x^* = x/l$, $y^* = y/l$, and $z^* = z/l$. We then have

$$\nabla^* = l\nabla, \tag{2.5.5}$$

$$\vec{U}^* = \frac{\vec{U}}{U_{\text{ref}}} \tag{2.5.6}$$

$$t^* = t\frac{U_{\text{ref}}}{L}, \tag{2.5.7}$$

$$P^* = \frac{P}{\rho U_{\text{ref}}^2}, \tag{2.5.8}$$

$$\theta = \frac{T - T_\infty}{T_s - T_\infty}, \tag{2.5.9}$$

$$\phi = \frac{m_1 - m_{1,\infty}}{m_{1,s} - m_{1,\infty}}. \tag{2.5.10}$$

The conservation equations in dimensionless form are then

$$\nabla^* \cdot \vec{U}^* = 0, \tag{2.5.11}$$

$$\frac{DU^*}{Dt^*} = -\nabla^* P^* + \frac{1}{\text{Re}_l}\nabla^{*^2} U^*, \tag{2.5.12}$$

$$\frac{D\theta}{Dt^*} = \frac{1}{\text{Re}_l \,\text{Pr}}\left(\nabla^{*^2}\theta + \text{Ec}\,\text{Pr}\,\Phi^*\right), \tag{2.5.13}$$

$$\frac{D\phi}{Dt^*} = \frac{1}{\text{Re}_l \text{Sc}}\left(\nabla^{*^2}\phi\right). \tag{2.5.14}$$

The normalization of the conservation equations thus directly leads to the derivation of several dimensionless parameters that have important physical interpretations.

$$\text{Prandtl number: Pr} = \frac{\nu}{\alpha} = \frac{\text{molecular diffusivity for momentum}}{\text{molecular diffusivity for heat}}$$

$$\text{Schmidt number: Sc} = \frac{\nu}{\mathcal{D}_{12}} = \frac{\text{molecular diffusivity for momentum}}{\text{molecular diffusivity for mass}}$$

$$\text{Eckert number: Ec} = \frac{U_{\text{ref}}^2}{C_P\,|T_s - T_\infty|} = \frac{\text{flow kinetic energy}}{\text{enthalpy difference}}$$

$$\text{Reynolds number: Re}_l = \frac{U_{\text{ref}}\,l}{\nu} = \frac{\text{inertial force}}{\text{viscous force}}.$$

Figure 2.11 displays the fluid-surface conditions. Accordingly, the boundary conditions will be as follows.

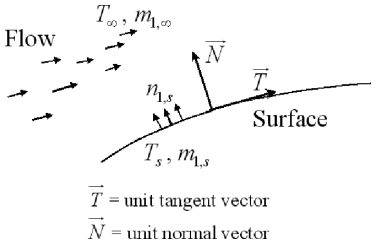

Figure 2.11. Flow boundary conditions at a surface.

At the free stream,

$$\vec{U} = \vec{U}_\infty, \tag{2.5.15}$$

$$T = T_\infty, \tag{2.5.16}$$

$$m_1 = m_{1,\infty}. \tag{2.5.17}$$

At the surface,

$$\vec{U} \cdot \vec{T} = 0, \tag{2.5.18}$$

$$\rho \vec{U} \cdot \vec{N} = n_{1,s}, \tag{2.5.19}$$

$$T = T_s, \tag{2.5.20}$$

$$m_1 = m_{1,s}. \tag{2.5.21}$$

Equation (2.5.18) represents no-slip conditions, and Eq. (2.5.20) assumes thermal equilibrium between the fluid and the wall at the surface. These equations are valid as long as the continuum assumption for the fluid is valid. Equation (2.5.19) is valid when species 1 is the only species that is transferred through the interphase.

The wall transfer rates can also be nondimensionalized. For simplicity, assume a 2D flow with y representing the normal distance from the wall. Then, for drag, we can write,

$$C_f = \frac{\tau_s}{\frac{1}{2}\rho U_{\text{ref}}^2}, \tag{2.5.22}$$

$$\tau_s = \mu \left.\frac{\partial u}{\partial y}\right|_{y=0}, \tag{2.5.23}$$

$$\Rightarrow C_f = \frac{1}{2\text{Re}_l} \left.\frac{\partial u^*}{\partial y^*}\right|_{y^*=0}. \tag{2.5.24}$$

For heat transfer, we can write,

$$-k \left.\frac{\partial T}{\partial y}\right|_{y=0} = h(T_s - T_\infty) \tag{2.5.25}$$

$$\Rightarrow \text{Nu}_l = -\left.\frac{\partial \theta}{\partial y^*}\right|_{y^*=0}, \tag{2.5.26}$$

where the Nusselt number is defined as

$$\text{Nu}_l = \frac{hl}{k}. \tag{2.5.27}$$

Likewise, for mass transfer, we have

$$-\rho \mathcal{D}_{12} \frac{\partial m_1}{\partial y}\bigg|_{y=0} = \mathcal{K}\,(m_{1,s} - m_{1,\infty}) \tag{2.5.28}$$

$$\Rightarrow \mathrm{Sh}_l = -\frac{\partial \phi}{\partial y^*}\bigg|_{y^*=0}, \tag{2.5.29}$$

where $\mathcal{K}$ is the convective mass transfer coefficient and the Sherwood number is defined as

$$\mathrm{Sh}_l = \frac{\mathcal{K} l}{\rho \mathcal{D}_{12}}. \tag{2.5.30}$$

The nondimensionalization (normalization) of the boundary-layer equations provides valuable information about conditions necessary for similitude and the functional dependencies. Consider a boundary layer that has formed as a result of a low or moderate ambient velocity. The dimensionless energy equation shows that, when $\mathrm{Ec}\,\mathrm{Pr} \ll 1$, the viscous dissipation term is insignificant and can be discarded, in which case the dimensionless thermal energy equation becomes

$$\frac{D\theta}{Dt^*} = \frac{1}{\mathrm{Re}_l\,\mathrm{Pr}} \nabla^{*2}\theta. \tag{2.5.31}$$

The dimensionless equations and boundary conditions then clearly show that, for an impermeable and stationary wall,

$$C_f = f\,(\mathrm{Re}_l,\ x^*) \tag{2.5.32}$$

$$\mathrm{Nu} = f\,(\mathrm{Re}_l,\ \mathrm{Pr}, x^*)\,, \tag{2.5.33}$$

$$\mathrm{Sh} = f\,(\mathrm{Re}_l,\ Sc, x^*)\,, \tag{2.5.34}$$

where x^* refers to the location of interest on the surface.

Furthermore, the dimensionless equations clearly show that two systems will behave similarly (i.e., the principle of similitude applies to them) when

1. they are geometrically similar, and
2. their relevant dimensionless parameters are equal.

Although the preceding arguments were made based on the examination of laminar flow equations, they apply to turbulent flow as well, even though additional dimensionless parameters (e.g., the surface relative roughness) may need to be added to the dimensionless parameters. Furthermore, the preceding derivations were based on constant properties. If this assumption is unacceptable, then the following additional dimensionless parameters will have to be introduced:

$$\mu^* = \mu/\mu_{\mathrm{ref}},$$

$$\rho^* = \rho/\rho_{\mathrm{ref}},$$

$$k^* = k/k_{\mathrm{ref}}.$$

These dimensionless parameters and their range of variations should also be maintained similarly between the model and prototype when similitude between the two systems is sought.

PROBLEMS

Problem 2.1. Prove the physical interpretations for the flat-plate boundary-layer thicknesses given in Eqs. (2.3.12)–(2.3.14).

Problem 2.2. For a laminar boundary layer with thickness δ, resulting from the flow of an incompressible fluid parallel to a flat surface, assume that the velocity profile in the boundary layer can be approximated according to

$$\frac{u}{U_\infty} = \begin{cases} 2\left(\frac{y}{\delta}\right) - 2\left(\frac{y}{\delta}\right)^3 + \left(\frac{y}{\delta}\right)^4 & \text{for } y \le \delta. \\ 1 \quad \text{for } y > \delta \end{cases}$$

Calculate the values of $\frac{\delta_1}{\delta}$, $\frac{\delta_2}{\delta}$, and $\frac{\delta_3}{\delta}$.

Find the shear stress at the wall, τ_s, as a function of μ U_∞, and δ.

Problem 2.3. Solve Problem 2.2, this time assuming that

$$\frac{u}{U_\infty} = \begin{cases} \frac{y}{\delta} & \text{for } y \le \delta \\ 1 & \text{for } y > \delta \end{cases}.$$

Also assume that the following relation applies:

$$\frac{\tau_s}{\rho U_\infty^2} = \frac{d\delta_2}{dx}.$$

Prove that

$$C_f = 0.577\ \mathrm{Re}_x^{-1/2}.$$

Problem 2.4. Consider the steady-state laminar flow of an incompressible and constant-property fluid parallel to a horizontal, infinitely large flat plate. Away from the surface the velocity of the fluid is U_∞ and its temperature is T_∞. Assume that the plate is porous and fluid with a constant velocity of v_s is sucked into the plate.

(a) Prove that the velocity profile in the direction parallel to the plate is given by $u = U_\infty[1 - \exp(-\frac{v_s}{\nu} y)]$.

(b) Assume a boundary layer can be defined, at the edge of which $u/U_\infty = 0.999$. Find the boundary-layer thickness for water and air at room temperature and atmospheric pressure.

(c) Repeat parts (a) and (b), this time assuming that the fluid is blown into the flow field through the porous plate with a constant velocity v_s.

(d) Assume that the plate is at a constant temperature T_s. Find the temperature profile in the fluid.

Problem 2.5. Consider the flow of a fluid parallel to a flat and smooth plate.

(a) Assume that the fluid is air at 100-kPa pressure, with $T_\infty = 300$ K and $U_\infty = 1$ m/s, and the plate surface is at a temperature of 350 K. Calculate the thickness of the velocity and temperature boundary layers at 1-, 10-, and 30-cm distances from the leading edge of the plate.

(b) Repeat part (a), this time assuming that the fluid is an oil with the following properties: $\mathrm{Pr} = 10$, $\rho = 753$ kg/m^3, $C_P = 2.1$ kJ/kg K, $k = 0.137$ W/m K, and $\mu = 6.6 \times 10^{-4}$ Pa s.

(c) Repeat part (a), this time assuming that the fluid is liquid sodium with $T_\infty = 400\,\text{K}$, the surface temperature is at 450 K, and $U_\infty = 2$ m/s.

Problem 2.6. Consider axisymmetric, laminar flow of an incompressible, constant-property fluid in a heated tube. Write the steady-state mass, momentum, and energy conservation equations, and nondimensionalize them, using the following definitions:

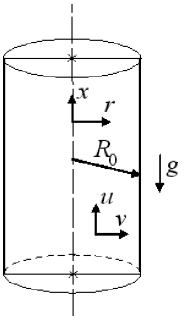

Figure P2.6.

$$u^* = \frac{u}{U_m},$$
$$v^* = \frac{v}{U_m}\text{Re}_D\text{Pr}, \quad r^* = \frac{r}{R_0},$$
$$x^* = \frac{x/R_0}{\text{Re}_D\text{Pr}},$$
$$P^* = \frac{P - P_1}{\rho U_m^2 \text{Pr}}, \quad \theta = \frac{T - T_s}{T_{\text{in}} - T_s},$$

where $\text{Re}_D = \rho U_m(2R_0)/\mu$ and U_m represents the mean velocity.

Problem 2.7. Consider steady-state, axisymmetric, and laminar flow of an incompressible, constant-property fluid in a heated tube. Perform a scaling analysis on the energy equation, and show that axial conduction in the fluid can be neglected when

$$\text{Pe} = \text{Re}_D\text{Pr} \gg 1.$$

Mass Transfer

Problem 2.8. Consider the flow of a fluid parallel to a flat and smooth plate.

(a) Assume that the fluid is air at 100-kPa pressure, with $U_\infty = 1$ m/s. The entire system is at 350 K. The surface of the plate is slightly wet, such that water vapor is transferred from the surface to the fluid. Estimate the thickness of the velocity and concentration boundary layers at 1-, 10-, and 30-cm distances from the leading edge of the plate.

(b) Repeat part (a), this time assuming that $U_\infty = 2.5$ cm/s, the fluid is water and the transferred species is chlorine.

Problem 2.9. Atmospheric air with $T_\infty = 300\,\text{K}$ and $U_\infty = 2.1$ m/s flows parallel to a flat surface. The surface temperature is 325 K. Experiments with laminar

boundary-layer flow have shown that $\mathrm{Nu}_x \sim \mathrm{Re}_x^n \mathrm{Pr}^{1/3}$. At locations where the distances from the leading edge are $x = 0.42\,\mathrm{m}$ and $x = 1.5\,\mathrm{m}$, the wall heat fluxes are measured to be $107 \frac{\mathrm{W}}{\mathrm{m}^2\,\mathrm{s}}$ and $57 \frac{\mathrm{W}}{\mathrm{m}^2\,\mathrm{s}}$, respectively. What would the evaporation mass fluxes be at these locations if, instead of a heated surface, the surface was at thermal equilibrium with air, the air was dry, and the surface was wetted with water?

Problem 2.10. Consider laminar flow of an incompressible, constant-property fluid in a tube. Assume that mass transfer takes place between the tube surface and the fluid, in which the transfer rate of the transferred species is low. Perform a scaling analysis on the mass-species conservation equation and show that axial diffusion in the fluid can be neglected when

$$\mathrm{Pe}_{\mathrm{ma}} = \mathrm{Re}_D \mathrm{Sc} \gg 1.$$

3 External Laminar Flow: Similarity Solutions for Forced Laminar Boundary Layers

The laminar boundary layers have velocity and temperature profile shapes, which remain unchanged with respect to their shape. In similarity solution methods we take advantage of this observation and attempt to define an independent variable so that with a coordinate transformation we will transform the boundary-layer equations (which are partial differential equations originally) into ordinary differential equations (ODEs). The benefit of this transformation is enormous. Similarity solutions are not possible for all flow fields and boundary conditions. However, when a similarity solution is possible, the solution can be considered exact.

In this chapter we review some important classical similarity solutions and their results. As usual, because heat or mass transfer processes are coupled to hydrodynamics, we discuss each flow configuration by first considering the hydrodynamics, followed by a discussion of heat or mass transfer.

3.1 Hydrodynamics of Flow Parallel to a Flat Plate

This is probably the simplest and most recognized similarity solution (Blasius, 1908). Consider Fig. 2.1. Assume 2D and steady-state flow of an incompressible fluid that has constant properties. Furthermore, based on the potential flow solution outside the boundary-layer, assume that $dP/dx = 0$. The boundary-layer mass and momentum conservation equations and their boundary conditions are then

$$\frac{\partial u}{\partial x} + \frac{\partial v}{\partial y} = 0, \tag{3.1.1}$$

$$u\frac{\partial u}{\partial x} + v\frac{\partial u}{\partial y} = \nu\frac{\partial^2 u}{\partial y^2}, \tag{3.1.2}$$

$$u = 0, v = 0 \text{ at } y = 0, \tag{3.1.3}$$

$$u = U_\infty \text{ at } y \to \infty. \tag{3.1.4}$$

In view of the fact that the velocity profiles at different locations along the plate are expected to be similar, let us use η as the independent variable, where

$$\eta = y\sqrt{\frac{U_\infty}{\nu x}}, \tag{3.1.5}$$

which is equivalent to assuming $\eta \sim y/\delta$, in light of Eq. (2.3.2). Thus we introduce the following coordinate transformation:

$$(x,\ y) \rightarrow (x,\ \eta)\,.$$

Recall from calculus that when we go from the coordinates (x, y) to the coordinates $(a,\ b)$, we have

$$\frac{\partial}{\partial x} = \frac{\partial a}{\partial x}\frac{\partial}{\partial a} + \frac{\partial b}{\partial x}\frac{\partial}{\partial b}, \tag{3.1.6}$$

$$\frac{\partial}{\partial y} = \frac{\partial a}{\partial y}\frac{\partial}{\partial a} + \frac{\partial b}{\partial y}\frac{\partial}{\partial b}. \tag{3.1.7}$$

Thus, in going from (x, y) to (x, η), we have

$$\frac{\partial}{\partial x} = \frac{\partial}{\partial x} + \frac{\partial \eta}{\partial x}\frac{\partial}{\partial \eta}, \tag{3.1.8}$$

$$\frac{\partial}{\partial y} = \frac{\partial \eta}{\partial y}\frac{\partial}{\partial \eta}. \tag{3.1.9}$$

Here, in writing Eq. (3.1.9) we note that $\partial y/\partial x = 0$. The left-hand side of Eqs. (3.1.8) and (3.1.9) represent the (x, y) coordinates, and their right-hand sides correspond to (x, η) coordinates.

Now assume a stream function of the form

$$\psi = \sqrt{\nu x U_\infty}\, f(\eta). \tag{3.1.10}$$

We can find the velocity components in (x, y) coordinates by writing,

$$u = \frac{\partial \psi}{\partial y} = \frac{\partial \psi}{\partial \eta}\frac{\partial \eta}{\partial y} = U_\infty f'(\eta), \tag{3.1.11}$$

$$v = -\frac{\partial \psi}{\partial x} = -\frac{\partial \psi}{\partial x} - \frac{\partial \psi}{\partial \eta}\frac{\partial \eta}{\partial x} = \frac{1}{2}\sqrt{\frac{\nu U_\infty}{x}}(\eta f' - f), \tag{3.1.12}$$

where $f' = df/d\eta$. These equations show that Eq. (3.1.10) satisfies the mass continuity equation [Eq. (3.1.1)]. Substitution into Eq. (3.1.2) leads to *Blasius*' equation:

$$f''' + \frac{1}{2}\, ff'' = 0. \tag{3.1.13}$$

The boundary conditions at $\eta = 0$ can be determined from Eqs. (3.1.3), (3.1.11), and (3.1.12), leading to

$$f(0) = 0,\ f'(0) = 0. \tag{3.1.14}$$

Furthermore, because $u \rightarrow U_\infty$ as $y \rightarrow \infty$,

$$f'(\infty) = 1. \tag{3.1.15}$$

Compared with the original boundary-layer momentum equation [Eq. (3.1.2)], the simplification we have achieved is enormous. Equation (3.1.13) is of course nonlinear. However, it is now an ODE.

The numerical solution of Eq. (3.1.13) is relatively easy. Good methods include the finite-difference solution of quasi-linearized equations or formal integration followed by iterations. To use the latter method, the following rather obvious steps can be taken. First, cast Eq. (3.1.13) as

$$\frac{f'''}{f''} = -\frac{1}{2} f. \tag{3.1.16}$$

Now apply $\int_0^\eta d\eta$ to both sides of this equation to get

$$f'' = C_1 \exp\left[-\int_0^\eta \frac{1}{2} f d\eta\right]. \tag{3.1.17}$$

Apply $\int_0^\eta d\eta$ to both sides of the preceding equation:

$$f' = C_1 \int_0^\eta \left[\exp\left(-\int_0^\eta \frac{1}{2} f d\eta\right)\right] d\eta + C_2. \tag{3.1.18}$$

We have $f'(0) = 0$; therefore $C_2 = 0$. Furthermore, from Eq. (3.1.15),

$$1 = C_1 \int_0^\infty \left[\exp\left(-\int_0^\eta \frac{1}{2} f d\eta\right)\right] d\eta \tag{3.1.18a}$$

The final result will thus be

$$f = f(0) + \frac{\displaystyle\int_0^\eta d\eta \int_0^\eta d\eta \exp\left(-\int_0^\eta \frac{1}{2} f d\eta\right)}{\displaystyle\int_0^\infty d\eta \exp\left(-\int_0^\eta \frac{1}{2} f d\eta\right)}, \tag{3.1.19}$$

$$f' = \frac{\displaystyle\int_0^\eta \exp\left(-\int_0^\eta \frac{1}{2} f d\eta\right) d\eta}{\displaystyle\int_0^\infty \exp\left(-\int_0^\eta \frac{1}{2} f d\eta\right) d\eta}, \tag{3.1.20}$$

$$f'' = \frac{\displaystyle\exp\left(-\int_0^\eta \frac{1}{2} f d\eta\right)}{\displaystyle\int_0^\infty d\eta \exp\left(-\int_0^\eta \frac{1}{2} f d\eta\right)}. \tag{3.1.21}$$

An iterative solution of these equations is easy, and can be done by the following recipe.

1. Choose a large η (e.g., $\eta_{\max} = 20$), and divide it into a number of steps, η_i.
2. Guess the distributions for f' and f [e.g., $f(\eta) = \eta,\ f'(\eta) = 1$].
3. Calculate $\exp(-\int_0^\eta \frac{1}{2} f d\eta)$, at each η_i, for all values of η between 0 and $\eta_{\max.}$
4. Calculate $\int_0^\infty \exp(-\int_0^\eta \frac{1}{2} f d\eta) d\eta$.
5. Calculate f'' at every η_i from Eq. (3.1.21).
6. Calculate f' at every η_i from Eq. (3.1.20).
7. Calculate f at every η_i from Eq. (3.1.19).
8. Using f and f' distributions, go to step 3 and repeat the procedure until convergence is achieved at every η.

Table 3.1. *The function $f(\eta)$ and its derivatives for flow parallel to a flat surface (Howarth, 1938)*

$\eta = y\left(\frac{U_\infty}{\nu x}\right)^{1/2}$	$f(\eta)$	$f'(\eta)$	$f''(\eta)$
0	0	0	0.33206
0.2	0.00664	0.06641	0.33199
0.4	0.02656	0.13277	0.33147
0.6	0.05974	0.19894	0.33008
0.8	0.10611	0.26471	0.32739
1.0	0.16557	0.32979	0.32301
1.2	0.23795	0.39378	0.31659
1.4	0.32298	0.45627	0.30787
1.6	0.42032	0.51676	0.29667
1.8	0.52952	0.57477	0.28293
2.0	0.65003	0.62977	0.26675
2.2	0.78120	0.68132	0.24835
2.6	1.07252	0.77246	0.20646
3.0	1.39682	0.84605	0.16136
3.4	1.74696	0.90177	0.11788
3.8	2.11605	0.94112	0.08013
4.2	2.49806	0.96696	0.05052
4.6	2.88826	0.98269	0.02948
5.0	3.28329	0.99155	0.01591
5.6	3.88031	0.99748	0.00543
6.2	4.47948	0.99937	0.00155
7.0	5.27926	0.99992	0.00022
8.0	6.27923	1.00000	0.00001

Values of f, f', and f'', calculated by Howarth (1938), can be found in Table 3.1 (Schlichting, 1968).

Essentially the same similarity solution can be presented in a slightly different form (Hartree, 1937). Equations (3.1.5) and (3.1.10) can be modified to

$$\eta_H = y\sqrt{\frac{U_\infty}{2\nu x}}, \tag{3.1.22}$$

$$\psi_H = \sqrt{2\nu x U_\infty}\, f_H(\eta_H). \tag{3.1.23}$$

Blasius' equation now becomes

$$f_H''' + f_H f_H'' = 0. \tag{3.1.24}$$

The function f_H' approximately follows (Jones and Watson, 1963)

$$\begin{aligned} f_H' &\approx 1 - 0.331 \int_\zeta^\infty \exp\left(-\frac{\zeta^2}{2}\right) d\zeta \\ &\approx 1 - 0.331\left(\zeta^{-1} - \zeta^{-3} + 3\zeta^{-5} \ldots\right) \exp\left(-\frac{\zeta^2}{2}\right), \end{aligned} \tag{3.1.25}$$

where

$$\zeta = \eta_H - 1.21678. \tag{3.1.26}$$

The most important result of Blasius' solution is that

$$f''(0) = 0.3321. \tag{3.1.27}$$

Now we have

$$\tau_s = \mu \left(\frac{\partial u}{\partial y} \right) \Big|_{y=0} = \mu \sqrt{U_\infty^3 / \nu x}\, f''(0). \tag{3.1.28}$$

Recall the definition of the skin-friction coefficient:

$$C_f = \frac{\tau_s}{\frac{1}{2}\rho U_\infty^2}. \tag{3.1.29}$$

We then get

$$C_f = 0.664\, \mathrm{Re}_x^{-1/2}, \tag{3.1.30}$$

The solution also shows that $f' = 0.991$ at $\eta = 5.0$. The thickness of the velocity boundary layer can thus be found from

$$\delta = 5.0x\, \mathrm{Re}_x^{-1/2}. \tag{3.1.31}$$

As a final note, an interesting shortcoming of Blasius' similarity theory should be pointed out. According to this theory, the velocity in the direction perpendicular to the wall follows Eq. (3.1.12). However, it has been shown that (Howarth, 1938; Bejan, 2004)

$$\lim_{\eta \to \infty} v = 0.86\, U_\infty\, \mathrm{Re}_x^{-1/2}, \tag{3.1.32}$$

which is clearly in disagreement with the intuitive condition of vanishing v as $\eta \to \infty$. However, Eq. (3.1.32) suggests that the condition of vanishing v is approached as $\mathrm{Re}_x \to \infty$.

3.2 Heat and Mass Transfer During Low-Velocity Laminar Flow Parallel to a Flat Plate

Heat Transfer

We now can use the known velocity profile provided by Blasius' solution, discussed in the previous section, to solve for the temperature profile in the laminar boundary layer depicted in Fig. 2.3, and from there we derive expressions for the convective heat transfer coefficient.

Consider a flat plate with a constant surface temperature. Assume a steady-state, 2D flow field with constant properties and no viscous dissipation. The thermal energy equation and its boundary conditions for the boundary layer will be

$$u \frac{\partial T}{\partial x} + v \frac{\partial T}{\partial y} = \boldsymbol{\alpha} \frac{\partial^2 T}{\partial y^2}, \tag{3.2.1}$$

$$T = T_s \quad \text{at} \quad y = 0, \tag{3.2.2}$$

$$T = T_\infty \quad \text{at} \quad y \to \infty. \tag{3.2.3}$$

We can recast these equations by using the dimensionless temperature:

$$\theta = \frac{T - T_\infty}{T_s - T_\infty}. \tag{3.2.4}$$

The result will be

$$u\frac{\partial\theta}{\partial x}+v\frac{\partial\theta}{\partial y}=\frac{\nu}{\mathrm{Pr}}\frac{\partial^2\theta}{\partial y^2}, \tag{3.2.5}$$

$$\theta=1 \quad \text{at} \quad y=0, \tag{3.2.6}$$

$$\theta=0 \quad \text{at} \quad y\to\infty. \tag{3.2.7}$$

Now let us assume that, for a given Pr, θ is a function of η, with η defined in Eq. (3.1.5). Also note that, according to Eqs. (3.1.11) and (3.1.12), we have

$$\frac{u}{U_\infty}=f'(\eta), \tag{3.2.8}$$

$$\frac{v}{U_\infty}=\frac{1}{2}\sqrt{\frac{\nu}{xU_\infty}}(\eta f'-f). \tag{3.2.9}$$

We now change the coordinates from (x, y) coordinates to (x, η). The result is

$$\theta''+\frac{1}{2}\mathrm{Pr}\,f\theta'=0, \tag{3.2.10}$$

$$\theta(0)=1, \tag{3.2.11}$$

$$\theta(\infty)=0, \tag{3.2.12}$$

where $\theta'=d\theta/d\eta$ and $\theta''=d^2\theta/d\eta^2$. We can obtain the formal solution of Eq. (3.2.10) by rewriting that equation as

$$\frac{\theta''}{\theta'}=-\frac{1}{2}\mathrm{Pr}\,f. \tag{3.2.13}$$

It can easily be shown that

$$\theta=1-\frac{\displaystyle\int_0^\eta d\eta\exp\left(-\frac{1}{2}\mathrm{Pr}\int_0^\eta d\eta f\right)}{\displaystyle\int_0^\infty d\eta\exp\left(-\frac{1}{2}\mathrm{Pr}\int_0^\eta d\eta f\right)}. \tag{3.2.14}$$

Alternatively, because $f=-2\dfrac{f'''}{f''}$, then Eq. (3.2.10) can be cast as

$$\frac{\theta''}{\theta'}=\mathrm{Pr}\left(\frac{f'''}{f''}\right). \tag{3.2.15}$$

We can then show that

$$\theta=1-\frac{\displaystyle\int_0^\eta (f'')^{\mathrm{Pr}}d\eta}{\displaystyle\int_0^\infty (f'')^{\mathrm{Pr}}d\eta}. \tag{3.2.16}$$

Evidently, knowing f'' and Pr, we can easily calculate the distribution of θ as a function of η. The solutions of Eqs. (3.2.14) [or, equivalently, Eq. (3.2.16)], are plotted in Fig. 3.1 (Eckert and Drake, 1972).

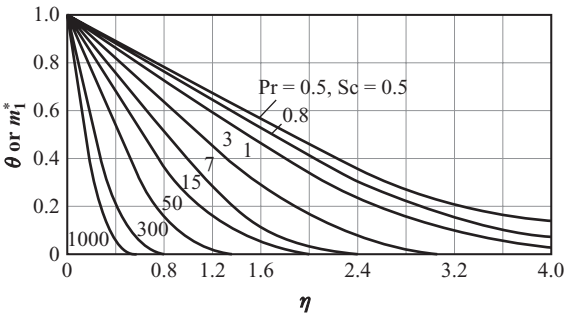

Figure 3.1. Dimensionless temperature distribution and normalized mass fraction distribution for parallel flow on a flat plate, without viscous dissipation.

We can now derive relations for Nu_x and Sh_x, i.e., the local heat and mass transfer coefficients. For heat transfer we can write

$$\mathrm{Nu}_x = \frac{h_x x}{k} = \frac{x}{k}\left(-k\left.\frac{\partial T}{\partial y}\right|_{y=0}\right) \Big/ (T_s - T_\infty)$$
$$= -\frac{x}{\sqrt{\dfrac{\nu x}{U_\infty}}}\left.\frac{d\theta}{d\eta}\right|_{\eta=0} = \mathrm{Re}_x^{1/2}(-\theta'|_{\eta=0}). \tag{3.2.17}$$

From Eq. (3.2.14),

$$\theta'|_{\eta=0} = -\frac{1}{\displaystyle\int_0^\eta \exp\left(-\frac{1}{2}\mathrm{Pr}\int_0^\eta f d\eta\right) d\eta}. \tag{3.2.18}$$

Equations (3.2.17) and (3.2.18) then give

$$\mathrm{Nu}_x = \frac{\mathrm{Re}_x^{1/2}}{\displaystyle\int_0^\infty d\eta \exp\left(-\frac{1}{2}\mathrm{Pr}\int_0^\eta f d\eta\right)}. \tag{3.2.19}$$

Mass Transfer

A similar analysis can be performed for mass transfer (see Fig. 2.4), starting from

$$u\frac{\partial m_1}{\partial x} + v\frac{\partial m_1}{\partial y} = \mathcal{D}_{12}\frac{\partial^2 m_1}{\partial y^2}, \tag{3.2.20}$$
$$m_1 = m_{1,s} \text{ at } y = 0, \tag{3.2.21}$$
$$m_1 = m_{1,\infty} \text{ at } y \to \infty, \tag{3.2.22}$$

where m_1 is the mass fraction of the transferred species. Equation (3.2.20) can be recast as

$$u\frac{\partial \phi}{\partial x} + v\frac{\partial \phi}{\partial y} = \mathcal{D}_{12}\frac{\partial^2 \phi}{\partial y^2}, \tag{3.2.23}$$

where,

$$\phi = \frac{m_1 - m_{1,\infty}}{m_{1,s} - m_{1,\infty}}, \tag{3.2.24}$$
$$\phi = 1 \text{ at } y = 0, \tag{3.2.25}$$
$$\phi = 0 \text{ at } y \to \infty. \tag{3.2.26}$$

Table 3.2. *Values of* $\mathrm{Nu}_x/\sqrt{\mathrm{Re}_x}$ *(or* $\mathrm{Sh}_x/\sqrt{\mathrm{Re}_x}$ *for various* Pr (*or* Sc) *values for flow parallel to a flat plate with* UWT *(or UWM) boundary condition*

Pr or Sc	$\mathrm{Nu}_x/\sqrt{\mathrm{Re}_x}$ or $\mathrm{Sh}_x/\sqrt{\mathrm{Re}_x}$	Pr or Sc	$\mathrm{Nu}_x/\sqrt{\mathrm{Re}_x}$ or $\mathrm{Sh}_x/\sqrt{\mathrm{Re}_x}$
0.001	0.0173	7.0	0.645
0.01	0.0516	10.0	0.730
0.1	0.140	15.0	0.835
0.5	0.259	50.	1.247
0.7	0.292	100	1.572
1.0	0.332	1000	3.387

Now, for any specific Sc, assume that $\phi = \text{func}(\eta)$ only. We can then cast the preceding equations as

$$\phi'' + \frac{1}{2}\mathrm{Sc}\ \phi' f = 0, \tag{3.2.27}$$

$$\phi = 1 \text{ at } \eta = 0, \tag{3.2.38}$$

$$\phi = 0 \text{ at } \eta \to \infty. \tag{3.2.29}$$

The formal solution will be

$$\phi(\eta) = 1 - \frac{\int_0^\eta (f'')^{\mathrm{Sc}} d\eta}{\int_0^\infty (f'')^{\mathrm{Sc}} d\eta}. \tag{3.2.30}$$

Evidently, when Pr = Sc, then the profile of θ and ϕ will be identical. The preceding analysis thus leads to

$$\mathrm{Sh}_x = \frac{\mathcal{K}x}{\rho \mathcal{D}_{12}} = \frac{\mathrm{Re}_x^{1/2}}{\int_0^\infty d\eta \exp\left(-\frac{\mathrm{Sc}}{2}\int_0^\eta d\eta f\right)}. \tag{3.2.31}$$

Correlations

Knowing Blasius' solution for the velocity profile, we can easily numerically solve Eq. (3.2.19) or (3.2.31). Clearly Nu_x will depend on Pr. Over the range $0.5 \lesssim \mathrm{Pr} \lesssim 15$ the numerical solution results can be curve fitted as

$$\mathrm{Nu}_x = 0.332\mathrm{Pr}^{1/3}\mathrm{Re}_x^{1/2}. \tag{3.2.32a}$$

Likewise, for mass transfer, Sh_x will depend on Sc, and for the range $0.5 \lesssim \mathrm{Sc} \lesssim 15$ we can write,

$$\mathrm{Sh}_x = 0.332\mathrm{Sc}^{1/3}\mathrm{Re}_x^{1/2}. \tag{3.2.32b}$$

Values of $\frac{\mathrm{Nu}_x}{\mathrm{Re}_x^{1/2}}$ as a function of Pr are given in Table 3.2. Some profiles of θ (or ϕ) were displayed earlier in Fig. 3.1.

We can easily derive the average Nusselt and Sherwood numbers by noting, for example, that

$$\langle \mathrm{Nu}_l \rangle_l = \frac{\langle h \rangle_l \, l}{k} = \int_0^l \frac{1}{x} \mathrm{Nu}_x dx.$$

We then gets

$$\langle \mathrm{Nu}_l \rangle_l = 0.664 \mathrm{Pr}^{1/3} \mathrm{Re}_l^{1/2} = 2\mathrm{Nu}_l, \tag{3.2.33a}$$

$$\langle \mathrm{Sh}_l \rangle_l = 0.664 \mathrm{Sc}^{1/3} \mathrm{Re}_l^{1/2} = 2\mathrm{Sh}_l. \tag{3.2.33b}$$

Limiting Solutions

Let us consider the conditions in which either $\mathrm{Pr} \gg 1$ or $\mathrm{Pr} \ll 1$ (and, equivalently, $\mathrm{Sc} \gg 1$ and $\mathrm{Sc} \ll 1$ for mass transfer). The general solutions represented by Eqs. (3.2.19) and (3.2.31) are of course valid for these cases. However, these solutions can be manipulated and solved analytically so that simple expressions for Nu_x and Sh_x can be derived.

Previously we showed that [see Eqs. (2.3.6) and (2.3.9)]

$$\delta_{\mathrm{th}}/\delta \approx \mathrm{Pr}^{-1/3} \ll 1 \text{ for } \mathrm{Pr} \gg 1, \tag{3.2.34}$$

$$\delta_{\mathrm{th}}/\delta \approx \mathrm{Pr}^{-1/2} \gg 1 \text{ for } \mathrm{Pr} \ll 1. \tag{3.2.35}$$

Equivalent expressions can be written for mass transfer by replacing $\delta_{\mathrm{th}}/\delta$ with $\delta_{\mathrm{ma}}/\delta$ and Pr with Sc, respectively. $\mathrm{Sc} \gg 1$ occurs in diffusive mass transfer in liquids, resulting in $\delta_{\mathrm{ma}} \ll \delta$. For gases, on the other hand, typically $\mathrm{Sc} \approx 1$, implying that $\delta_{\mathrm{ma}} \approx \delta$.

First we consider conditions in which $\mathrm{Pr} \ll 1$, which is encountered in liquid metals. For this case, because $\delta_{\mathrm{th}} \gg \delta$, the bulk of the thermal boundary layer lies outside the velocity boundary layer. We can therefore write, as an approximation,

$$f'(\eta) = \frac{u}{U_\infty} = 1, \tag{3.2.36}$$

$$f(\eta) = \eta, \tag{3.2.37}$$

$$\theta'' + \frac{1}{2}\mathrm{Pr}\ \eta\theta' = 0, \tag{3.2.38}$$

with boundary conditions

$$\theta(0) = 1,$$

$$\theta(\infty) = 0.$$

The solution of Eq. (3.2.38) leads to

$$\frac{\mathrm{Nu}_x}{\mathrm{Re}_x^{1/2}} = \frac{1}{\sqrt{\pi}} \mathrm{Pr}^{1/2}. \tag{3.2.39}$$

The derivation leading to Eq. (3.2.39) is as follows. The integration of Eq. (3.2.38) gives [see Eq. (3.2.19)]

$$\frac{\mathrm{Nu}_x}{\mathrm{Re}_x^{1/2}} = \left\{ \int_0^\infty d\eta \exp\left(-\frac{1}{2}\mathrm{Pr} \int_0^\eta \eta d\eta \right) \right\}^{-1} = \left\{ \int_0^\infty d\eta \exp\left(-\frac{1}{4}\mathrm{Pr}\eta^2 \right) \right\}^{-1}. \tag{3.2.40}$$

We define $\xi^2 = \frac{1}{4}\text{Pr}\ \eta^2$, and, from there,

$$d\eta = \frac{2}{\sqrt{\text{Pr}}} d\xi. \tag{3.2.41}$$

Equation (3.2.40) then gives

$$\frac{\text{Nu}_x}{\text{Re}_x^{1/2}} = \left\{ \frac{2}{\sqrt{\text{Pr}}} \frac{\sqrt{\pi}}{2} \text{erf}\,(\infty) \right\}^{-1} = \left\{ \frac{2}{\sqrt{\text{Pr}}} \frac{\sqrt{\pi}}{2} \right\}^{-1} = \frac{1}{\sqrt{\pi}} \text{Pr}^{1/2}, \tag{3.2.42}$$

where the error function is defined as

$$\text{erf}(x) = \frac{2}{\sqrt{\pi}} \int_0^x \exp(-\xi^2) d\xi.$$

Note that $\text{erf}\,(\infty) = 1$.

A similar analysis for mass transfer for $\text{Sc} \ll 1$ gives

$$\frac{\text{Sh}_x}{\text{Re}_x^{1/2}} = \frac{1}{\sqrt{\pi}} \text{Sc}^{1/2}. \tag{3.2.43}$$

Now, let us consider the conditions in which $\text{Pr} \gg 1$, which occur, for example, in viscous oils. We now have $\delta_{\text{th}} \ll \delta$, and the thermal boundary layer covers only a small part at the bottom of the velocity boundary layer where the dimensionless velocity profile is approximately linear. Because $f'(\eta) = \frac{u}{U_\infty}$, then $f''(\eta) = \text{const.} = f''(0)$. Thus we get

$$f(\eta) = f''(0) \frac{\eta^2}{2}. \tag{3.2.44}$$

We do not need to include a constant in the preceding integration because $f(0) = 0$ [see Eq. (3.1.14)]. Equation (3.2.19) then leads to

$$\frac{\text{Nu}_x}{\text{Re}_x^{1/2}} = 0.339 \text{Pr}^{1/3}. \tag{3.2.45}$$

Likewise, for $\text{Sc} \gg 1$, which implies that $\delta_{\text{ma}} \ll \delta$, we get

$$\frac{\text{Sh}_x}{\text{Re}_x^{1/2}} = 0.339 \text{Sc}^{1/3}. \tag{3.2.46}$$

The details of the derivation leading to Eq. (3.2.45) are as follows. Let us focus on the denominator of the right-hand side of Eq. (3.2.19), which can be written as

$$\begin{aligned} \text{I} = \int_0^\infty d\eta\ \exp\left\{ -\frac{1}{2}\text{Pr} \int_0^\eta f d\eta \right\} &= \int_0^\infty d\eta\ \exp\ \left\{ -\int_0^\eta f''(0) \frac{\eta^2}{4} \text{Pr}\, d\eta \right\} \\ &= \int_0^\infty d\eta\ \exp\left\{ -\frac{f''(0)\text{Pr}\ \eta^3}{12} \right\}. \end{aligned} \tag{3.2.47}$$

Now we define

$$\zeta = f''(0) \frac{\text{Pr}\ \eta^3}{12}. \tag{3.2.48}$$

This expression leads to

$$d\eta = \frac{1}{3} \left[\frac{12}{f''(0)\text{Pr}} \right]^{1/3} \zeta^{-2/3} d\zeta. \tag{3.2.49}$$

Equation (3.2.47) can now be cast as,

$$\mathrm{I} = \frac{1}{3}\left[\frac{12}{f''(0)\mathrm{Pr}}\right]^{1/3}\int_0^\infty \zeta^{-2/3}\exp(-\zeta)d\zeta = \frac{1}{3}\left[\frac{12}{f''(0)\mathrm{Pr}}\right]^{1/3}\Gamma\left(\frac{1}{3}\right), \quad (3.2.50)$$

where Γ represents the gamma function:

$$\Gamma(x) = \int_0^\infty \zeta^{x-1}\exp(-\zeta)\,d\zeta.$$

Furthermore, $\Gamma(1/3) \approx 2.679$. Substitution from this equation into the denominator of Eq. (3.2.19) will lead to Eq. (3.2.45).

3.3 Heat Transfer During Laminar Parallel Flow Over a Flat Plate With Viscous Dissipation

General Solution

Assuming constant properties, the thermal energy equation is now

$$u\frac{\partial T}{\partial x} + v\frac{\partial T}{\partial y} = \alpha\frac{\partial^2 T}{\partial y^2} + \frac{\nu}{C_p}\left(\frac{\partial u}{\partial y}\right)^2. \quad (3.3.1)$$

The continuity and momentum equations remain the same as Eqs. (3.1.1) and (3.1.2); therefore Blasius' solution for velocity profile will be valid.

Let us assume that the temperature is a function of η in the (x, η) coordinates. Using Blasius' similarity parameters, Eq. (3.3.1) can be cast as

$$\frac{d^2T}{d\eta^2} + \frac{\mathrm{Pr}}{2}f\frac{dT}{d\eta} = -\mathrm{Pr}\frac{U_\infty^2}{C_P}(f'')^2. \quad (3.3.2)$$

We consider two different types of boundary conditions: constant wall temperature

$$T = T_s, \text{ at } y = 0,$$

and adiabatic wall,

$$\frac{\partial T}{\partial y} = 0 \quad \text{at } y = 0.$$

In either case, we have $T = T_\infty$ at $y \to \infty$. The general solution for Eq. (3.3.2) can be written as

$$T(\eta) - T_\infty = C\theta_1(\eta) + \frac{U_\infty^2}{2C_P}\theta_2(\eta), \quad (3.3.3)$$

where

$$\theta = \frac{T - T_\infty}{T_\mathrm{s} - T_\infty}. \quad (3.3.4)$$

The function $\theta_1(\eta)$ represents the solution of the following homogeneous differential equation and boundary conditions:

$$\frac{d^2\theta_1}{d\eta^2} + \frac{1}{2}\mathrm{Pr}\,f\frac{d\theta_1}{d\eta} = 0, \quad (3.3.5)$$

$$\theta_1 = 1 \text{ at } \eta = 0, \quad (3.3.6)$$

$$\theta_1 = 0 \text{ at } \eta \to \infty. \quad (3.3.7)$$

The function $\theta_2(\eta)$ is the particular solution to the system:

$$\frac{d^2\theta_2}{d\eta^2} + \frac{1}{2}\mathrm{Pr}\, f\frac{d\theta_2}{d\eta} = -2\mathrm{Pr}\, f''^2, \tag{3.3.8}$$

$$\theta_2 = 0 \text{ at } \eta \to \infty, \tag{3.3.9}$$

$$\frac{d\theta_2}{d\eta} = 0 \text{ at } \eta = 0. \tag{3.3.10}$$

The function θ_1 has already been derived [see Eqs. (3.2.16)–(3.2.19)]. We can find the constant C in Eq. (3.3.3) by applying Eq. (3.3.6), thereby obtaining

$$C = (T_s - T_\infty) - \frac{U_\infty^2}{2C_P}\theta_2(0). \tag{3.3.11}$$

We can solve Eq. (3.3.8) by first breaking it into the following two first-order ODEs:

$$\theta_2' = \frac{d\theta_2}{d\eta}, \tag{3.3.12}$$

$$\frac{d\theta_2'}{d\eta} - \mathrm{Pr}\left(\frac{f'''}{f''}\right)\theta_2' = -2\ \mathrm{Pr}\, f''^2. \tag{3.3.13}$$

To derive this equation we use the fact that $f = -2\frac{f'''}{f''}$. The boundary condition is $\theta_2'(0) = 0$ in accordance with Eq. (3.3.10). The solution to Eq. (3.3.13) is

$$\theta_2' = -2\mathrm{Pr}\,(f'')^{\mathrm{Pr}} \int_0^\eta [f''(\xi)]^{2-\mathrm{Pr}}\, d\xi. \tag{3.3.14}$$

We can now perform one more integration and apply the boundary condition in Eq. (3.3.9) to get,

$$\theta_2 = 2\mathrm{Pr} \int_\eta^\infty d\xi\, [f''(\xi)]^{\mathrm{Pr}} \left\{ \int_0^\xi [f''(\tau)]^{2-\mathrm{Pr}} d\tau \right\}. \tag{3.3.15}$$

(Note that ξ and τ are dummy variables.) Equation (3.3.15) can easily be solved numerically. The results of the numerical solution can be curve fitted to (Schlichting, 1968),

$$\theta_2(0) = \mathrm{Pr}^{1/2} \text{ for } 0.5 < \mathrm{Pr} \lesssim 5, \tag{3.3.16}$$

$$\theta_2(0) = 1.9\ \mathrm{Pr}^{1/3} \text{ for } \mathrm{Pr} \to \infty. \tag{3.3.17}$$

Adiabatic Wall

When the wall surface is adiabatic, the homogeneous solution must be dropped because it cannot satisfy the adiabatic wall boundary condition. Thus, by setting $C = 0$, we get from Eq. (3.3.3)

$$T_{s,\mathrm{ad}} - T_\infty = \frac{U_\infty^2}{2C_P}\theta_2(0) \tag{3.3.18}$$

or

$$\frac{T_{s,\mathrm{ad}} - T_\infty}{\dfrac{U_\infty^2}{2C_P}} = r(\mathrm{Pr}), \tag{3.3.19}$$

where $r(\mathrm{Pr}) = \theta_2(0)$ is called the *recovery factor*. The surface temperature, $T_{s,\mathrm{ad}}$, is referred to as the recovery temperature. $\theta_2(0)$ can be found from Eqs. (3.3.16) or (3.3.17). Calculations also show that (White, 2006),

$$r \approx \mathrm{Pr}^{1/2} \quad \text{for } 0.1 < \mathrm{Pr} < 3, \tag{3.3.20a}$$

$$r \approx 1.905\mathrm{Pr}^{1/3} - 1.15 \quad \text{for } 3 < \mathrm{Pr}\,. \tag{3.3.20b}$$

The term $\frac{U_\infty^2}{2C_P}$ is the temperature rise in the fluid if the fluid velocity is adiabatically reduced to zero.

Although the derivations thus far have been based on the incompressible flow assumption, Eqs. (3.3.19) and (3.3.20) apply to compressible flow as well (Gebhart, 1981). For flows of ideal gases at high velocity, for example, these two equations can be combined to give

$$T_{s,\mathrm{ad}} - T_\infty = \sqrt{\mathrm{Pr}}\, T_\infty \frac{\gamma - 1}{2} Ma^2, \tag{3.3.20a}$$

where Ma represents the Mach number.

We can now obtain the boundary-layer temperature profile for an adiabatic wall by eliminating $\frac{U_\infty^2}{2C_P}$ between Eqs. (3.3.3) and (3.3.18) (note that $C = 0$), thereby obtaining

$$\frac{T(\eta) - T_\infty}{T_{s,\mathrm{ad}} - T_\infty} = \frac{1}{r\,(\mathrm{Pr})}\theta_2(\eta)\,. \tag{3.3.21}$$

Constant Wall Temperature

We can revisit the general solution, now that the solution for adiabatic wall is known. From Eq. (3.3.3),

$$C = T_s - \frac{U_\infty^2}{2C_P}\theta_2(0) - T_\infty = T_s - T_{s,\mathrm{ad}}, \tag{3.3.22}$$

where we have used Eq. (3.3.19). Equation (3.3.3) then gives

$$T(\eta) - T_\infty = (T_s - T_{s,\mathrm{ad}})\,\theta_1(\eta) + \frac{U_\infty^2}{2C_P}\theta_2(\eta). \tag{3.3.23}$$

Now,

$$q_s'' = -k\left.\frac{\partial T}{\partial y}\right|_{y=0} = k\left(\frac{U_\infty}{\nu x}\right)^{1/2}\left[-\left.\frac{d\theta_1}{d\eta}\right|_{\eta=0}\right](T_s - T_{s,\,\mathrm{ad}})\,. \tag{3.3.24}$$

This equation can be rewritten as

$$q_s'' = h_x(T_s - T_{s,\,\mathrm{ad}}), \tag{3.3.25}$$

where h_x is actually identical to the local heat transfer coefficient for laminar boundary-layer flow without viscous dissipation, discussed earlier in Section 3.2.

3.4 Hydrodynamics of Laminar Flow Past a Wedge

The steady, incompressible laminar flow past a wedge is an interesting and useful case for which a similarity solution is available.

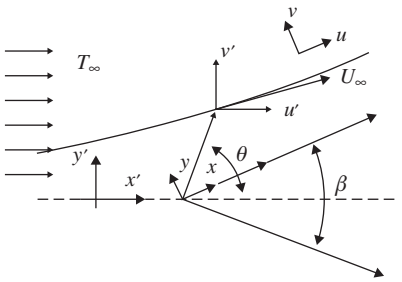

Figure 3.2. Potential flow over a wedge.

Inviscid Flow

Let us first address the flow of an inviscid fluid past a wedge. This is needed because the inviscid flow solution provides information about the velocity field outside the boundary layer.

Consider Fig. 3.2 and the $(x',\ y')$ coordinates. Recall that in 2D dimensional potential flow we have

$$\nabla^2\phi = 0 \tag{3.4.1}$$

$$\nabla^2\psi = 0, \tag{3.4.2}$$

$$u' = \frac{\partial\phi}{\partial x'} = \frac{\partial\psi}{\partial y'}, \tag{3.4.3}$$

$$v' = \frac{\partial\phi}{\partial y'} = -\frac{\partial\psi}{\partial x'}, \tag{3.4.4}$$

where ϕ and ψ are the flow potential and the stream function, respectively. We can define a complex potential ϖ as

$$\varpi = \phi + i\psi, \tag{3.4.5}$$

where $i = \sqrt{-1}$. Defining $r^* = x' + iy'$, then we obtain

$$\frac{d\varpi}{dr^*} = u' - iv' = |U|\exp(-i\theta), \tag{3.4.6}$$

where

$$|U| = \sqrt{u'^2 + v'^2}, \tag{3.4.7}$$

$$\theta = \tan^{-1}(y/x). \tag{3.4.8}$$

Now we consider the 2D inviscid and irrotational flow over the wedge, as shown in Fig. 3.2. The complex potential for the flow, in $(x',\ y')$ coordinates is (Jones and Watson, 1963)

$$\varpi = \frac{1}{m+1}U_{-1}\exp(-im\pi)\,r^{*m+1}, \tag{3.4.9}$$

where U_{-1} is the velocity at $r^* = -1$ and

$$m = \frac{\beta}{2\pi - \beta}. \tag{3.4.10}$$

Equation (3.4.9) leads to

$$u' - iv' = \frac{d\varpi}{dr^*} = U_{-1} r^m \exp[-im(\pi - \theta)]. \tag{3.4.11}$$

Thus,

$$u' = U_{-1} r^m \cos[m(\pi - \theta)], \tag{3.4.12}$$

$$v' = U_{-1} r^m \sin[m(\pi - \theta)]. \tag{3.4.13}$$

The potential flow velocity components on the surface of the wedge, where $\theta = \beta/2$, can thus be found from these equations. The fluid velocity at the surface of the wedge is then

$$|U| = \sqrt{u'^2 + v'^2} = U_{-1} x^m. \tag{3.4.14}$$

Thus for the wedge we can assume that just outside the boundary layer the fluid velocity is

$$U_\infty = C x^m. \tag{3.4.15}$$

Hydrodynamics Without Blowing or Suction

Referring to Fig. 3.2, we have (note that u and v are the velocity components along x and y, respectively)

$$\frac{\partial u}{\partial x} + \frac{\partial v}{\partial y} = 0, \tag{3.4.16}$$

$$u\frac{\partial u}{\partial x} + v\frac{\partial u}{\partial y} = -\frac{1}{\rho}\frac{dP}{dx} + \nu\frac{\partial^2 u}{\partial y^2}, \tag{3.4.17}$$

$$u = v = 0 \text{ at } y = 0, \tag{3.4.18}$$

$$u = U_\infty = C x^m \text{ as } y \to \infty. \tag{3.4.19}$$

Bernoulli's equation for the free stream gives

$$U_\infty \frac{dU_\infty}{dx} = -\frac{1}{\rho}\frac{dP}{dx}. \tag{3.4.20}$$

Equation (3.4.17) then becomes

$$u\frac{\partial u}{\partial x} + v\frac{\partial u}{\partial y} = U_\infty \frac{dU_\infty}{dx} + \nu\frac{\partial^2 u}{\partial y^2}. \tag{3.4.21}$$

For the similarity variable, let us use the same form as in Blasius' analysis, namely,

$$\eta = y\left(\frac{U_\infty}{\nu x}\right)^{1/2} = y\left(\frac{C}{\nu}\right)^{1/2} x^{\frac{m-1}{2}}. \tag{3.4.22}$$

We can similarly modify the stream function in Blasius' analysis as

$$\Psi = (\nu U_\infty x)^{1/2} f(\eta) = (\nu C x^{m+1})^{1/2} f(\eta). \tag{3.4.23}$$

Now, by switching from (x, y) to (x, η) we get

$$u = \frac{\partial \psi}{\partial y} = \frac{\partial \psi}{\partial \eta}\frac{\partial \eta}{\partial y} = U_\infty f', \tag{3.4.24}$$

$$\frac{\partial u}{\partial y} = U_\infty \left(\frac{U_\infty}{\nu x}\right)^{1/2} f'', \tag{3.4.25}$$

$$\frac{\partial^2 u}{\partial y^2} = \frac{U_\infty^2}{\nu x} f''', \tag{3.4.26}$$

$$v = -\frac{\partial \psi}{\partial x} = -\frac{\partial \psi}{\partial x} - \frac{\partial \psi}{\partial \eta}\frac{\partial \eta}{\partial x} = -U_\infty \left(\frac{U_\infty x}{\nu}\right)^{-1/2}\left(\frac{m+1}{2}\right)\left[f - \frac{1-m}{1+m}\eta f'\right]. \tag{3.4.27}$$

Note that everywhere $U_\infty = C x^m$. Substitution into Eq. (3.4.21) then gives

$$f''' + \frac{m+1}{2} f f'' + m\left[1 - f'^2\right] = 0, \tag{3.4.28}$$

$$f(0) = f'(0) = 0, \tag{3.4.29}$$

$$f'(\infty) = 1. \tag{3.4.30}$$

Equation (3.4.28) is called the *Falkner–Skan equation* (Falkner and Skan, 1931).

The wedge flow problem is sometimes presented in an equivalent but different form (Hartree, 1937). Let us define

$$\eta_H = \left(\frac{m+1}{2}\right)^{1/2}\left(\frac{U_\infty}{\nu x}\right)^{1/2} y, \tag{3.4.31}$$

$$\Psi_H = \left(\frac{2}{m+1}\right)^{1/2} (U_\infty \nu x)^{1/2} f_H(\eta_H) = \left(\frac{2C\nu}{m+1}\right)^{1/2} x^{\frac{m+1}{2}} f_H(\eta_H). \tag{3.4.32}$$

This stream function of course satisfies the continuity equation. The momentum equation [Eq. (3.4.21)] then gives

$$f_H''' + f_H f_H'' + \frac{2m}{m+1}\left(1 - f_H'^2\right) = 0, \tag{3.4.33}$$

where, according to Eq. (3.4.10),

$$\frac{\beta}{\pi} = \frac{2m}{m+1}. \tag{3.4.34}$$

This form of the solution is evidently similar to Eqs. (3.1.22)–(3.1.24), which dealt with flow parallel to a flat surface. Thus $\beta/\pi = 0$ implies flow parallel to a flat plate, and $\beta/\pi = 1$ represents stagnation flow. The boundary conditions for Eq. (3.4.33) are

$$f_H(0) = f_H'(0) = 0, \tag{3.4.35}$$

$$f_H'(\infty) = 1. \tag{3.4.36}$$

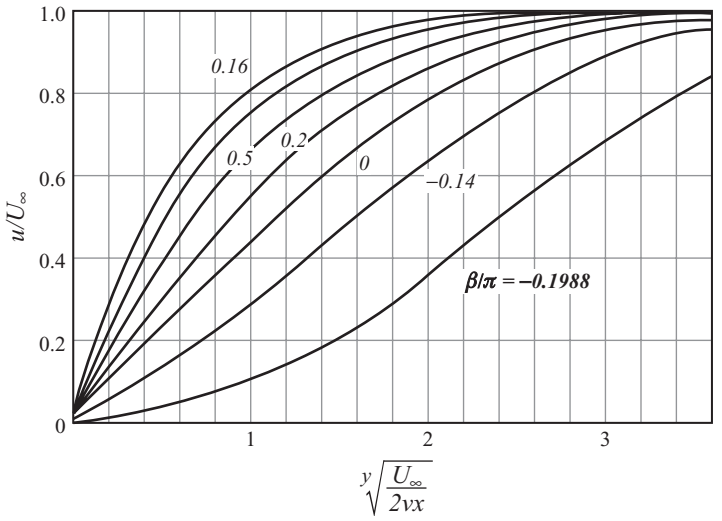

Figure 3.3. Velocity distribution for laminar flow past a wedge (after Schilichting, 1968).

Thus the Falkner–Skan solution gives

$$C_f = \frac{2\tau_s}{\rho U_\infty^2} = \frac{2\,f''(0)}{\sqrt{\mathrm{Re}_x}}. \tag{3.4.37}$$

If the analysis of Hartree (1937) is used, however, we have

$$\frac{\partial u}{\partial y} = \left(\frac{m+1}{2}\right)^{1/2} \left(\frac{U_\infty}{\nu x}\right)^{1/2} U_\infty f_H''(\eta). \tag{3.4.38}$$

As a result,

$$\tau_s = \mu \left(\frac{m+1}{2}\right)^{1/2} \left(\frac{U_\infty^3}{\nu x}\right)^{1/2} f_H''(0), \tag{3.4.39}$$

$$C_f = 2\left(\frac{m+1}{2}\right)^{1/2} \frac{f_H''(0)}{\sqrt{\mathrm{Re}_x}}. \tag{3.4.40}$$

Figure 3.3 shows the dimensionless velocity profiles for several wedge angles (Schlichting, 1968). Note that $m = 1$ represents stagnation flow and $m = 0$ corresponds to flow parallel to a flat plate. The velocity profiles do not have an inflection point for $m > 0$ (or, equivalently, for $\beta > 0$), implying that boundary-layer separation does not occur in accelerating flow. Only a slight flow deceleration can be tolerated without boundary-layer separation, however. An inflection point occurs in the velocity profile for $\beta = -0.199\pi$, indicating the occurrence of boundary-layer separation.

Hydrodynamics With Blowing or Suction Through the Wall Surface

Consider now the flow past a wedge, this time with blowing or suction through the wall surface. Equations (3.4.22)–(3.4.28) all apply. At the wall surface the no-slip boundary condition also applies; therefore

$$f'(0) = 0. \tag{3.4.41}$$

We also have,

$$f'(\infty) = 1. \tag{3.4.42}$$

With blowing or suction through the wall surface, however, $v_w \neq 0$, and from Eq. (3.4.27),

$$v_s = -Cx^m \left(\frac{Cx^{m+1}}{\nu}\right)^{-1/2} \left(\frac{m+1}{2}\right) \left[f(0) - \frac{1-m}{1+m}\eta f'(0)\right]. \tag{3.4.43}$$

Because $f'(0) = 0$, this equation leads to

$$v_s = -C^{1/2} x^{\frac{(m-1)}{2}} \nu^{1/2} \left(\frac{m+1}{2}\right) f(0). \tag{3.4.44}$$

For the similarity solution method to be possible, $f(0)$ should not depend on x; therefore

$$f(0) = \frac{-v_0}{\left[C^{1/2}\nu^{1/2}\left(\frac{m+1}{2}\right)\right]}, \tag{3.4.45}$$

which implies that

$$v_s = v_0 x^{(m-1)/2}. \tag{3.4.46}$$

For $m = 0$, which corresponds to flow parallel to a flat surface, we get

$$f(0) = -\frac{2v_0}{\sqrt{\nu U_\infty}}. \tag{3.4.47}$$

$$v_s = v_0 x^{-1/2} \tag{3.4.48}$$

3.5 Heat Transfer During Laminar Flow Past a Wedge

Heat Transfer Without Viscous Dissipation

In the discussion of the Falkner–Skan problem in the previous section, we showed that a similarity solution is possible when there is no injection or suction through the wall or when the wall injection is such that Eq. (3.4.46) applies. In this section it is shown that, when properties are constant and viscous dissipation is neglected, a similarity solution for temperature is possible only when the wall temperature varies as

$$T_s(x) - T_\infty = \Delta T_0 x^n. \tag{3.5.1}$$

Consider the flow past a wedge similar to that of Fig. 3.2. Let us start with the energy conservation equation and its boundary conditions:

$$\rho C_p \left(u\frac{\partial T}{\partial x} + v\frac{\partial T}{\partial y}\right) = k\frac{\partial^2 T}{\partial y^2}, \tag{3.5.2}$$

$$T = T_s \text{ at } y = 0, \tag{3.5.3}$$

$$\mathrm{T} \rightarrow \mathrm{T}_\infty \text{ at } y \rightarrow \infty. \tag{3.5.4}$$

Table 3.3. *Values of* $\mathrm{Nu}_x/\sqrt{\mathrm{Re}_x}$ *(or* $\mathrm{Sh}_x/\sqrt{\mathrm{Re}_x}$*) for flow past a wedge with UWT (or UWM) boundary condition*

m	Pr = 0.7 or Sc = 0.7	Pr = 0.8 or Sc = 0.8	Pr = 1.0 or Sc = 1.0	Pr = 5.0 or Sc = 5.0	Pr = 10.0 or Sc = 10.0
−0.0753	0.242	2.53	0.272	0.457	0.570
0	0.292	0.307	0.332	0.585	0.730
0.111	0.331	0.348	0.378	0.669	0.851
0.333	0.384	0.403	0.440	0.792	1.013
1.0	0.496	0.523	0.570	1.043	1.344
4.0	0.813	0.858	0.938	1.736	2.236

We define η according to Eq. (3.4.22), and we define dimensionless temperature as $\theta = \frac{T-T_\infty}{T_s-T_\infty}$, where the surface T_s follows Eq. (3.5.1). Equation (3.5.2) and its boundary conditions can then be recast as

$$\theta'' + \frac{m+1}{2}\mathrm{Pr}\, f\theta' - n\mathrm{Pr}\, f'\theta = 0, \tag{3.5.5}$$

$$\theta = 1 \text{ at } \eta = 0, \tag{3.5.6}$$

$$\theta = 0 \text{ at } \eta \to \infty. \tag{3.5.7}$$

We can find the solution for the constant wall temperature by setting $n = 0$. The wall heat flux follows:

$$q_s'' = -k\left.\frac{\partial T}{\partial y}\right|_{y=0} = -k\,(T_s - T_\infty)\,\frac{1}{x}\mathrm{Re}_x^{1/2}\theta'(0). \tag{3.5.8}$$

We thus come to the following result:

$$\mathrm{Nu}_x = -\mathrm{Re}_x^{1/2}\theta'(0). \tag{3.5.9}$$

Equation (3.5.8) also shows that $q_s'' = \text{const.}$ is obtained when

$$T_s - T_\infty = Cx^{1/2}. \tag{3.5.10}$$

Thus $n = 1/2$ actually represents a constant wall heat flux boundary condition.

Table 3.3 shows values of $\mathrm{Nu}_x/\sqrt{\mathrm{Re}_x}$ as a function of Pr for several values of m. Note that with m = 0 we have flow parallel to a flat plate.

Heat Transfer With Viscous Dissipation

We now consider laminar, steady-state, and constant-property flow past a wedge when viscous dissipation is important. The energy conservation equation and its boundary conditions are

$$u\frac{\partial T}{\partial x} + v\frac{\partial T}{\partial y} = \alpha\frac{\partial^2 T}{\partial y^2} + \frac{\nu}{C_P}\left(\frac{\partial u}{\partial y}\right)^2, \tag{3.5.11}$$

$$T = T_s \text{ at } y = 0, \tag{3.5.12}$$

$$T = T_\infty \text{ at } y \to \infty. \tag{3.5.13}$$

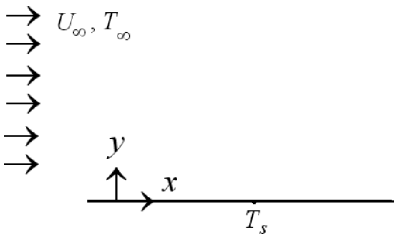

Figure 3.4. Flow parallel to a flat plate.

Let us use η as defined in Eq. (3.4.22) and the dimensionless temperature as $\theta = \frac{T-T_\infty}{T_s-T_\infty}$. The hydrodynamics of the problem are identical to the Falkner–Skan problem, and therefore Eq. (3.4.28) and its solution will apply.

Assume that the wall temperature varies according to Eq. (3.5.1). Equation (3.5.11) can then be cast as (note that $U_\infty = Cx^m$)

$$\theta'' + \frac{m+1}{2}\mathrm{Pr}\, f\theta' - n\mathrm{Pr}\, f'\theta = -\mathrm{Pr}Ex^{2m-n} f''^2, \tag{3.5.14}$$

where

$$E = \frac{C^2}{C_P}\Delta T_0. \tag{3.5.15}$$

For the similarity method to apply, the right-hand side of Eq. (3.5.14) must be independent of x, and that requires that

$$2m - n = 0. \tag{3.5.16}$$

This result implies that the surface temperature distribution depends on the wedge angle. A similarity solution is possible for $T_s = \text{const.}$ only when $m = n = 0$, which actually corresponds to a flow parallel to a flat plate.

3.6 Effects of Compressibility and Property Variations

All the similarity solutions discussed thus far dealt with incompressible, constant-property flow. These solutions can usually be corrected for the effect of temperature-dependent properties by use of semiempirical methods. These will be discussed later. It is also possible to directly include the effect of property variations in some of the theoretical derivations. The following is an example of the latter approach.

Consider steady, laminar flow parallel to a flat plate, as shown in Fig. 3.4. The conservation equations in the boundary layer are

$$\frac{\partial(\rho u)}{\partial x} + \frac{\partial(\rho v)}{\partial y} = 0, \tag{3.6.1}$$

$$\rho u\frac{\partial u}{\partial x} + \rho v\frac{\partial u}{\partial y} = \frac{\partial}{\partial y}\left(\mu\frac{\partial u}{\partial y}\right), \tag{3.6.2}$$

$$\rho C_P\left(u\frac{\partial T}{\partial x} + v\frac{\partial T}{\partial y}\right) = \frac{\partial}{\partial y}\left(k\frac{\partial T}{\partial y}\right). \tag{3.6.3}$$

The boundary conditions are as follows. At $y = 0$ we have

$$u = v = 0, \quad T = T_s.$$

At $x = 0$ and at $y \to \infty$ we have

$$u = U_\infty, \quad T = T_\infty.$$

To obtain a similarity solution, we define a stream function ψ according to

$$\frac{\rho}{\rho_\infty} u = \frac{\partial \psi}{\partial y}, \tag{3.6.4}$$

$$\frac{\rho}{\rho_\infty} v = -\frac{\partial \psi}{\partial x}, \tag{3.6.5}$$

where properties with subscript ∞ correspond to T_∞. Furthermore, we define the function $f(\eta)$ according to

$$\psi = \sqrt{\nu_\infty U_\infty x}\, f(\eta), \tag{3.6.6}$$

where η is now defined as

$$\eta = \int_0^y \frac{\rho}{\rho_\infty} \sqrt{\frac{U_\infty}{\nu_\infty x}}\, dy. \tag{3.6.7}$$

Equation (3.6.1) is satisfied. Equations (3.6.2) and (3.6.3) also transform into, respectively,

$$\frac{d}{d\eta}\left(\frac{\rho\mu}{\rho_\infty \mu_\infty} \frac{d^2 f}{d\eta^2}\right) + \frac{1}{2} f \frac{d^2 f}{d\eta^2} = 0, \tag{3.6.8}$$

$$\frac{d}{d\eta}\left(\frac{k\rho}{\rho_\infty} \frac{d\theta}{d\eta}\right) + \frac{C_P \mu_\infty}{2} f \frac{d\theta}{d\eta} = 0, \tag{3.6.9}$$

where $\theta = \frac{T - T_\infty}{T_s - T_\infty}$ and $T_s = \text{const}$. For the derivation of these equations, the transformation from coordinates (x, y) to (x, η) is carried out according to,

$$\frac{\partial}{\partial x} = \frac{\partial}{\partial x} + \left(\frac{\partial \eta}{\partial x}\right) \frac{\partial}{\partial \eta} = \frac{\partial}{\partial x} - \frac{1}{2} \frac{\eta}{x} \frac{\rho}{\rho_\infty} \frac{\partial}{\partial \eta}, \tag{3.6.10}$$

$$\frac{\partial}{\partial y} = \left(\frac{\partial \eta}{\partial y}\right) \frac{\partial}{\partial \eta} = \frac{\rho}{\rho_\infty} \sqrt{\frac{U_\infty}{\nu_\infty x}} \frac{\partial}{\partial \eta}. \tag{3.6.11}$$

Equations (3.6.8) and (3.6.9) show that a similarity solution is in principle possible. In fact, Eqs. (3.6.8) and (3.6.9) become identical to the constant-property equations when $\text{Pr} = 1$, $C_P = \text{const.}$, $\mu \sim T$, and $\rho \sim T^{-1}$. In this case relations for $\text{Nu}_{x,\infty} = \frac{h_x x}{k_\infty}$ and $C_{f,\infty} = \frac{\tau_s}{\frac{1}{2}\rho_\infty U_\infty^{1/2}}$ can be easily derived.

For most gases, however, C_P is a relatively weak function of temperature and other properties depend on temperature approximately as $k \sim T^{0.85}$, $\rho \sim T^{-1}$, and $\mu \sim T^{0.7}$.

From the results of numerical solutions of boundary-layer equations with variable properties, Kays et al. (2005) proposed the following simple method for

correcting the constant-property solution results for the effects of property variations. In general,

$$\frac{\mathrm{Nu}_x}{\mathrm{Nu}_{x,\infty}} = \left(\frac{T_s}{T_\infty}\right)^n, \tag{3.6.12}$$

$$\frac{C_f}{C_{f,\infty}} = \left(\frac{T_s}{T_\infty}\right)^m, \tag{3.6.13}$$

where Nu_∞ and $C_{f,\infty}$ are the constant-property parameters calculated from solutions in which all properties corresponded to T_∞. For air in the 600–1600 K temperature range, the recommended values of m and n are as follows.

	$T_s > T_\infty$ (heating)		$T_s < T_\infty$ (cooling)	
	m	n	m	n
$U_\infty = \text{const.}$	−0.1	−0.01	−0.05	0.0
2D stagnation point	0.4	0.1	0.30	0.07

An alternative method is to use a reference temperature for calculating properties that are to be used in the constant-property solutions. A widely accepted method for calculating the reference temperature is

$$T_{\mathrm{ref}} = T_\infty + 0.5\,(T_s - T_\infty)\,. \tag{3.6.14}$$

EXAMPLE 3.1. A Newtonian liquid with 300 K temperature flows parallel to a flat and smooth surface whose temperature is 330 K. All properties of the liquid are similar to water except that its viscosity is 20 times larger. The liquid velocity away from the surface is 80 m/s. Find the surface heat flux at a distance of 5 cm from the leading edge.

SOLUTION. We need to calculate the relevant properties of air. Let us use a reference temperature of 315 K for calculating properties and calculate the following properties of water:

$$\rho = 991.5\,\mathrm{kg/m^3}, \quad C_p = 4182\ \mathrm{J/kg\ ^\circ C}, \quad k = 0.620\ \mathrm{W/m\ K}.$$

The viscosity of the fluid is 20 times larger than that of water; therefore,

$$\mu = 1.262 \times 10^{-2}\ \mathrm{kg/m\ s};\ \mathrm{Pr} = \mu C_p/K = 85.11.$$

The viscous dissipation is likely to be significant. We should therefore use the derivations in Section 3.3. From Eqs. (3.3.20b) and (3.3.19) we get, respectively,

$$r(\mathrm{Pr}) = 1.905\mathrm{Pr}^{1/3} - 1.15 = 1.905\,(85.11)^{1/3} - 1.15 = 7.23,$$

$$T_{s,\mathrm{ad}} = T_\infty + r(\mathrm{Pr})\left[\frac{U_\infty^2}{2C_P}\right] = 300\ \mathrm{K} + (7.23)\left[\frac{(80)^2\ \mathrm{m^2}}{2\,(4182)\ \mathrm{J/kg\ K}}\right] = 305.5\ \mathrm{K}.$$

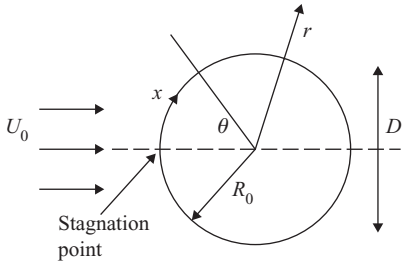

Figure 3.5. Stagnation flow on a cylinder or sphere.

The local heat transfer coefficient can be calculated from Eq. (3.2.45); therefore

$$\begin{aligned}
\mathrm{Re}_x &= \rho U_\infty x/\mu = (991.5\ \mathrm{kg/m^3})(80\ \mathrm{m/s})(0.05\ \mathrm{m})/(1.262\times 10^{-2}\ \mathrm{kg/m\ s}) \\
&= 3.142\times 10^5, \\
\mathrm{Nu}_x &= 0.339\mathrm{Pr}^{1/3}\mathrm{Re}^{1/3} = 0.339(85.11)^{1/3}(3.142\times 10^5)^{1/2} = 835.8, \\
h_x &= \mathrm{Nu}_x k/x = (835.8)(0.620\ \mathrm{W/m\ K})/(0.05\ \mathrm{m}) = 1.037\times 10^4\ \mathrm{W/m^2\ K}.
\end{aligned}$$

The local heat flux can now be calculated from Eq. (3.3.25):

$$\begin{aligned}
q_s'' &= h_x(T_s - T_{s,\mathrm{ad}}) = (1.037\times 10^4\ \mathrm{W/m^2K})\,(330\,\mathrm{K} - 302.8\,\mathrm{K}) \\
&= 2.537\times 10^5\ \mathrm{W/m^2}.
\end{aligned}$$

EXAMPLE 3.2. Derive an expression for the estimation of the convective heat transfer coefficient in laminar flow across a long cylinder with an isothermal surface in the vicinity of the stagnation line.

SOLUTION. Figure 3.5 is a schematic of the flow field and the cross section of the cylinder. The stagnation point in fact is the cross section of the stagnation line (note that the cylinder is long in the direction perpendicular to the page). Potential flow theory predicts that the velocity potential will be

$$\phi = -U_0\left(r + \frac{R_0^2}{r}\right)\cos\theta. \tag{a}$$

The tangential velocity can therefore be found from

$$u_\theta = \frac{1}{r}\frac{\partial\phi}{\partial\theta} = U_0\left(1 + \frac{R_0^2}{r^2}\right)\sin\theta. \tag{b}$$

Thus, at $r = R_0$, we have

$$u_\theta = 2U_0\sin\theta. \tag{c}$$

For points close to the stagnation line (or equivalently for $x \ll R_0$) we can write $\sin\theta \approx \theta = x/R_0$. Equation (c) then leads to

$$U_\infty = u_\theta \approx \frac{2U_0}{R_0}x. \tag{d}$$

This equation in fact depicts the fluid velocity at the outer edge of the boundary layer when the boundary-layer thickness satisfies $\delta \ll R_0$. A comparison with

Eq. (3.4.15) shows that we approximately have flow past a wedge where $C = \frac{2U_0}{R_0}$ and $m = 1$. We can thus define

$$\mathrm{Re}_x = \rho U_\infty x/\mu = \frac{x^2}{R_0^2}\mathrm{Re}_D, \tag{e}$$

$$\mathrm{Nu}_x = \frac{h_x x}{k} = \frac{x}{2R_0}\mathrm{Nu}_D, \tag{f}$$

where,

$$\mathrm{Re}_D = \rho U_0 (2R_0)/\mu,$$
$$\mathrm{Nu}_D = \frac{h_x (2R_0)}{k}.$$

Knowing the fluid Prandtl number, we can now find $\mathrm{Nu}_x/\sqrt{\mathrm{Re}_x}$ from Table 3.3. For $m = 1$ and $\mathrm{Pr} = 0.7$, for example, Table 3.3 gives

$$\frac{\mathrm{Nu}_x}{\sqrt{\mathrm{Re}_x}} = 0.496. \tag{g}$$

This will result in

$$\mathrm{Nu}_D = 0.992\mathrm{Re}_D^{1/2}. \tag{h}$$

The numerical solution of the similarity equations in this case shows (Goldstein et al., 1965, p. 632)

$$\mathrm{Nu}_D = g\,(\mathrm{Pr})\,\mathrm{Re}_D^{1/2}. \tag{i}$$

The function $g\,(\mathrm{Pr})$ has been curve fitted as

$$g\,(\mathrm{Pr}) \approx 1.14\mathrm{Pr}^{0.4}. \tag{j}$$

Expression (j) is quite accurate for $0.6 \lesssim \mathrm{Pr} \lesssim 1.1$. It overpredicts the exact solution only slightly at higher Prandtl numbers, up to $\mathrm{Pr} \lesssim 15$. For $\mathrm{Pr} = 7$ and 10, for example, Eqs. (i) and (j) result in the overprediction of Nu_D by 5% and 6.7%, respectively.

EXAMPLE 3.3. For three-dimensional (3D) stagnation flow of fluids with $\mathrm{Pr} \approx 1$ on an axisymmetric blunt body, the following correlation can be used for predicting the heat transfer coefficient in the vicinity of the stagnation point (Reshotko and Cohen, 1955),

$$\mathrm{Nu}_x = 0.76\mathrm{Re}_x^{1/2}\mathrm{Pr}^{0.4}. \tag{k}$$

Derive an expression for the heat transfer coefficient at the immediate vicinity of the stagnation point of a sphere.

SOLUTION. For the axisymetric flow of an incompressible fluid we define a *Stokes' stream function*, ψ, where $2\pi\psi$ at any point represents the volumetric flow rate of the fluid through a circle that passes through that point and has its

center located on the axis of symmetry. The potential flow past a sphere (see Fig. 3.5) leads to

$$\psi = -U_0 \left(1 - \frac{R_0^3}{r^3}\right) \frac{r^2}{2} \sin^2 \theta. \tag{l}$$

The velocities are related to Stokes' stream function according to

$$u_r = \frac{1}{r^2 \sin^2 \theta} \frac{\partial \psi}{\partial \theta}, \tag{m}$$

$$u_\theta = -\frac{1}{r \sin \theta} \frac{\partial \psi}{\partial r}. \tag{n}$$

Thus, for the outer edge of the boundary layer that forms on the surface of the sphere near the stagnation point, we have

$$U_\infty = u_\theta|_{r=R_0} = \frac{3}{2} U_0 \sin \theta \approx \frac{3}{2} U_0 \frac{x}{R_0}. \tag{o}$$

Substitution from Eq. (o) in the definition of Re_x leads

$$\mathrm{Re}_x = \rho U_\infty x/\mu = \frac{3}{4} \frac{x^2}{R_0^2} \mathrm{Re}_D. \tag{p}$$

Equation (f) in Example 3.1 can be applied. Substitution from Eq. (f) of Example 3.1 as well as Eq. (o) into Eq. (k) then leads to

$$\mathrm{Nu}_D = 1.316 \mathrm{Re}_D^{1/2} \mathrm{Pr}^{0.4}. \tag{q}$$

PROBLEMS

Problem 3.1. Consider Blasuis' solution for a boundary layer on a flat plate. Assume that the similarity function f can be approximated as

$$f'(\eta) = \sin\left(\frac{\pi}{10}\eta\right) \quad \text{for } \eta \le 5,$$
$$f'(\eta) = 1 \quad \text{for } \eta > 5.$$

(a) Examine and discuss the adequacy of the approximate function for Blasius' problem (i.e., flow paralled to a flat plate).
(b) Using the preceding approximate function, find expressions for boundary-layer displacement thickness (δ_1), momentum thickness (δ_2), and energy thickness (δ_3).

Problem 3.2. Consider the steady-state, incompressible flow of a constant-property fluid flowing parallel to a flat plate. According to Goldstein (1965), a similarity momentum equation can be obtained by using

$$\eta = \frac{y}{2} \left(\frac{U_\infty}{\nu x}\right)^{1/2},$$
$$\Psi = (U_\infty \nu x)^{1/2} f(\eta),$$
$$f'(\eta) = 2\frac{u}{U_\infty}.$$

(a) Derive the similarity momentum equation.
(b) Derive a formal closed-form solution for the equation derived in part (a).

Problem 3.3. Two parallel uniform streams of different fluids, moving horizontally in the same direction, come into contact at $x = 0$. The two streams have $U_{\infty,1}$ and $U_{\infty,2}$ free-stream velocities. The flow field remains laminar everywhere.

Formulate a similarity solution method for the problem (i.e., derive similarity differential equations and all the necessary boundary conditions for both flow fields).

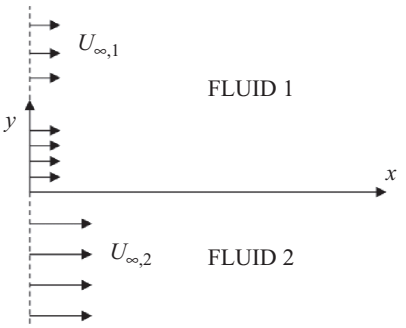

Figure P3.3.

Problem 3.4. Flow parallel to a horizontal flat plate takes place.

(a) For water at $U_\infty = 0.75$ m/s and $T_\infty = 300$ K, calculate and plot the boundary-layer thickness as a function of the distance from the leading edge, x, for $0.05 < x < 0.25$ m.
(b) Estimate and plot the thermal boundary-layer thickness δ_{th} for part (a)
(c) Repeat parts (a) and (b), this time assuming that the fluid is liquid mercury at $U_\infty = 0.25$ m/s and $T_\infty = 500$ K.

Problem 3.5. The top surface of an electronic package can be idealized as a flat horizontal surface, which is cooled by a gas with a free-stream temperature of 293 K. At the trailing edge (the downstream edge) of the plate, the Reynolds number is $\text{Re} = 1.1 \times 10^5$.

(a) Measurement shows that the temperature of the plate (which is assumed to be uniform) is 395 K. The desired temperature of the plate surface is 365 K, however. By what factor should the fluid velocity be increased to satisfy the surface temperature requirement?
(b) Assume that the fluid is atmospheric air originally flowing at a velocity of 2 m/s. What would be the maximum surface temperature if the total dissipated power was reduced to one-third of its original value, but only the downstream half of the plate was heated?

Problem 3.6. Consider the flow of an incompressible and constant-property fluid parallel to a flat surface. Assume that the wall heat flux varies according to

$$q_s'' = bx^n.$$

Prove that a similarity solution can be obtained by using Blasius' coordinate transformation and the following definition for dimensionless temperature:

$$\theta(\eta) = \frac{T - T_\infty}{\frac{2q_s'' x}{k}\mathrm{Re}_x^{-1/2}}.$$

Also, show that

$$T_s - T_\infty \sim x^{n+1/2},$$
$$\frac{\mathrm{Nu}_x}{\mathrm{Re}_x^{1/2}\mathrm{Pr}^{1/3}} = \frac{1}{2\mathrm{Pr}^{1/3}\theta(0)}.$$

Problem 3.7. Consider the flow past a wedge, similar to that of Fig. 3.2, with UWT boundary conditions.

(a) Show that when the fluid viscosity is negligibly small, the following coordinate transformation can make a similarity solution to the heat transfer problem possible:

$$(x, y) \to (x, \eta),$$
$$\eta = (m+1)^{1/2}\frac{y}{2}\left(\frac{U_\infty}{\alpha x}\right)^{1/2}.$$

(b) Prove that the solution of the similarity energy equation leads to

$$\mathrm{Nu}_x = (m+1)^{1/2}\frac{\mathrm{Re}_x^{1/2}\mathrm{Pr}^{1/2}}{\sqrt{\pi}}.$$

Problem 3.8. A flat plate that is 1 m in length is subject to a parallel flow of atmospheric air at 300 K temperature. The velocity of air is 8 m/s. At locations 0.25 and 0.6 m from the leading edge,

(a) calculate the boundary-layer thickness, u (the velocity component parallel to the plate) at $y = \delta/2$, and the wall shear stress τ_s;
(b) calculate the local skin-friction coefficient C_f.

Problem 3.9. In Problem 3.8, assuming that the surface is at 330 K,

(a) find the local heat transfer coefficient and heat flux at 0.25 and 0.6 m from the leading edge,
(b) find the temperature at $y = \delta/2$ at the locations mentioned in part (a),
(c) find the average heat transfer coefficient and total heat transfer rate for the entire plate.

Problem 3.10. A thin, flat object is exposed to air flow in the outer atmosphere where air temperature and pressure are $-50\ ^\circ$C and 7 kPa, respectively. Air flows parallel to the object at a Mach number of 0.5. The effect of radiation heat transfer can be neglected.

(a) Assuming that the plate is adiabatic, calculate the surface temperature of the plate at a distance of 4 cm from the leading edge.

(b) If the surface temperature at a distance of 4 cm from the leading edge is measured to be 25°C, find the rate and direction of heat transfer between the surface and the air at that location.

Problem 3.11. Glycerin at a temperature of 30 °C flows over a 30-cm-long flat plate at a velocity of 1 m/s. The surface of the plate is kept at a temperature of 20 °C. Find the mean heat transfer rate per unit area to the plate.

Problem 3.12. A flat plate is subject to a parallel flow of a fluid, with $U_\infty = 0.5$ m/s and $T_\infty = 400$ K. The surface temperature is 450 K. Calculate and compare the following quantities at an axial position corresponding to $x = 10$ cm when the fluid is engine oil or liquid sodium:

(a) the thickness of velocity and thermal boundary layers,
(b) the convective heat transfer coefficient and heat flux.

For properties of liquid sodium and engine oil you can use the following table:

Property	*Liquid sodium*	*Engine oil*
Density (kg/m^3)	929.1	825
Specific heat (kJ/kg K)	1.38	2.337
Kinematic viscosity (m^2/s)	7.5×10^{-7}	10.6×10^{-6}
Thermal conductivity (W/mK)	86.2	0.134

Problem 3.13. In a wind tunnel, air at 20 °C and 0.1 bar flows at a velocity of 265 m/s over a model plane wing. The wing can be idealized as a 0.1-m-long flat plate. The surface of the plate must be maintained at 55 °C. To maintain the wing at the desired temperature an electric heater is used. Calculate the electric power needed for this purpose.

Problem 3.14. Water at a temperature of 40 °C flows at a velocity of 0.2 m/s over a surface that can be modeled as a wide 100-mm-long flat plate. The entire surface of this plate is kept at a temperature of 0 °C. Plot a graph showing how the local heat flux varies along the plate. Also, plot the velocity and temperature profiles (i.e., u and T as functions of y) in the boundary layer on the plate at a distance of 60 mm from the leading edge of the plate.

Problem 3.15. Consider the steady-state, 2D flow of a compressible, variable-property fluid parallel to a flat plate [see Eqs. (3.6.1)–(3.6.3)]. Assume that $\rho\mu =$ const., and define a stream function and coordinate transformation according to,

$$\rho u = \frac{\partial \psi}{\partial y},$$
$$\rho v = -\frac{\partial \psi}{\partial x},$$
$$Y = \int_0^y \rho \, dy.$$

Show that with these definitions and transformation a similarity equation similar to Hartree's equation [Eq. (3.1.24)] can be derived.

Using the preceding results, show that

$$C_f = \sqrt{\frac{2}{\mathrm{Re}_x}} f_H''(0).$$

Problem 3.16. Water at 312 K temperature flows parallel to a flat surface at a velocity of 17 m/s. At a distance of 4 cm from the leading edge of the plate, the surface temperature is measured to be 300 K.

(a) Calculate the direction and magnitude of heat flux at the surface.
(b) Calculate the total viscous dissipation rate, per unit mass of the fluid, at the surface.
(c) Repeat parts (a) and (b), this time assuming that the surface temperature is 290 K.
(d) Repeat parts (a) and (b), this time assuming that the surface temperature is 300 K, but the fluid has a viscosity 100 times the viscosity of water and its other properties are similar to water.

Problem 3.17. Water at a temperature of 293 K flows across a 5.0-cm outer-diameter tube that has a surface temperature of 393 K. By idealizing the vicinity of the stagnation point as a flat surface that is perpendicular to the flow direction, calculate the local heat transfer coefficient and heat flux at a point that is located at 0.5-cm distance from the stagnation point in the azimuthal direction.

Problem 3.18. A spherical metal ball with a 2.5-mm diameter is in free fall in a water pool, with a terminal velocity of 1 m/s. The water temperature is 293 K, and the surface temperature of the metal ball (assumed to be uniform) is at 350 K.

(a) Calculate the heat transfer coefficient at the stagnation point of the ball.
(b) Calculate the average heat transfer coefficient between the ball surface and the water, using an appropriate correlation of your choice. You may use Appendix Q for selecting an appropriate correlation.

4 Internal Laminar Flow

Laminar flows in channels and tubes are discussed in this chapter. Internal laminar flow has numerous applications, particularly when we deal with a viscous fluid. Laminar flow is also the predominant regime in the vast majority of miniature systems and microsystems.

In this chapter the discussion is restricted to channels in which the continuum assumption is valid (see Section 1.6). The discussion of microchannels is postponed to Chapter 13. Furthermore, the classical, closed-form solutions to the laminar flow field, or empirical correlations, are emphasized. Although the numerical solution of many of these problems with computational fluid dynamics (CFD) tools is relatively easy nowadays, the convenience and the insight about the physical processes and their interrelationships that these analytical solutions provide cannot be gained from numerical simulations.

4.1 Couette and Poiseuille Flows

We start with two simple and idealized problems that can be solved analytically, leading to simple and closed-form solutions.

Couette Flow

This is the simplest, yet very important, channel flow case, which has useful implications in modeling of some difficult transport processes.

Consider the two parallel, infinitely large flat plates in Fig. 4.1 that are separated by an incompressible, constant-property fluid. Buoyancy effects are negligible, and one plate is moving at a constant velocity U with respect to the other plate. Also, the two plates are isothermal at temperatures T_1 and T_s. The mass, momentum, and energy conservation equations for the fluid will be

$$\cancel{\frac{\partial u}{\partial x}} + \cancel{\frac{\partial v}{\partial y}} = 0, \tag{4.1.1}$$

$$u\cancel{\frac{\partial u}{\partial x}} + v\cancel{\frac{\partial v}{\partial y}} = -\frac{1}{\rho}\cancel{\frac{dP}{dx}} + \nu\left(\cancel{\frac{\partial^2 u}{\partial x^2}} + \frac{\partial^2 u}{\partial y^2}\right), \tag{4.1.2}$$

$$\rho C_P\left(u\cancel{\frac{\partial T}{\partial x}} + \cancel{v}\frac{\partial T}{\partial y}\right) = k\frac{\partial^2 T}{\partial y^2} + \mu\left(\frac{\partial u}{\partial y}\right)^2. \tag{4.1.3}$$

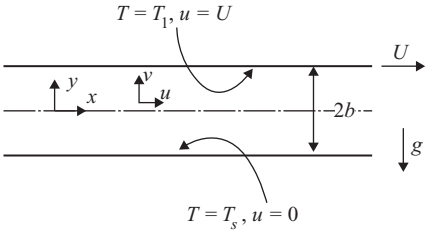

Figure 4.1. Couette flow.

As noted, all derivative terms with respect to x must vanish, in view of the infinitely large plates, including dp/dx. The mass continuity, as noted, leads to $\partial v/\partial y = 0$, which implies that v is a constant. Because $v = 0$ at $y = 0$, $v = 0$ everywhere. This flow is not pressure gradient driven; it results from the motion of the plates with respect to each other.

The momentum and energy equations thus reduce to

$$\frac{\partial^2 u}{\partial y^2} = 0, \tag{4.1.4}$$

$$k\frac{\partial^2 T}{\partial y^2} + \mu\left(\frac{\partial u}{\partial y}\right)^2 = 0. \tag{4.1.5}$$

The boundary conditions are

$$u = 0 \quad \text{at } y = -b, \tag{4.1.6a}$$

$$u = U \quad \text{at } y = b, \tag{4.1.6b}$$

$$T = T_s \quad \text{at } y = -b, \tag{4.1.6c}$$

$$T = T_1 \quad \text{at } y = b. \tag{4.1.6d}$$

The momentum equation is decoupled from the energy equation because of constant properties, and its solution gives

$$u = \frac{U}{2}\left(1 + \frac{y}{b}\right). \tag{4.1.7}$$

Now, with the velocity distribution known, the energy equation can be solved:

$$T = -\frac{\mu U^2}{4k b^2}\frac{y^2}{2} + C_1 y + C_2. \tag{4.1.8}$$

After the boundary conditions are applied, this equation becomes

$$T = \left[\frac{T_s + T_1}{2} + \frac{T_1 - T_s}{2}\frac{y}{b}\right] + \frac{\mu U^2}{8k}\left(1 - \frac{y^2}{b^2}\right). \tag{4.1.9}$$

The bracketed term on the right-hand side defines a straight line on the (T, y) coordinates, which would represent the temperature profile in the fluid if there were no motion so that pure conduction took place.

A dimensionless parameter, Brinkman's number, naturally comes from the preceding solution:

$$\mathrm{Br} = \frac{\mu U^2}{k\,|T_s - T_1|} = \mathrm{Ec}\,\mathrm{Pr}. \tag{4.1.10}$$

Other relevant dimensionless parameters are the Eckert number and the Prandtl number, $\mathrm{Pr} = \nu/\alpha$, where

$$\mathrm{Ec} = \frac{U^2}{C_p\,|T_s - T_1|}. \tag{4.1.11}$$

The viscous dissipation is important only when Br is large, and that occurs in very viscous fluids.

We can define a convection heat transfer coefficient and Nusselt number by writing

$$h = \frac{q_s''}{(T_s - T_1)}, \tag{4.1.12}$$

where

$$q_S'' = -k\left.\frac{dT}{dy}\right|_{y=-b}, \tag{4.1.13}$$

$$\mathrm{Nu}_{2b} = \frac{h(2b)}{k}. \tag{4.1.14}$$

The result will be

$$q_S'' = \frac{k}{2b}(T_s - T_1) + \frac{\mu U^2}{4b}, \tag{4.1.15}$$

$$\mathrm{Nu}_{2b} = 1 + \frac{1}{2}\mathrm{Br}. \tag{4.1.16}$$

If the top surface is used for the definitions of h and Nu, then

$$q_1'' = \frac{k}{2b}(T_s - T_1) - \frac{\mu U^2}{4b}, \tag{4.1.17}$$

$$\mathrm{Nu}_{2b} = 1 - \frac{1}{2}\mathrm{Br}. \tag{4.1.18}$$

A Fanning friction factor for the lower surface can be defined as

$$C_f = \frac{\tau_s|_{y=-b}}{\frac{1}{2}\rho U^2}, \tag{4.1.19}$$

where, from Eq. (4.1.7),

$$\tau_s|_{y=-b} = \mu\left.\frac{du}{dy}\right|_{y=-b} = \mu\frac{U}{2b}. \tag{4.1.20}$$

Equation (4.1.19) then leads to

$$C_f = \frac{2}{\mathrm{Re}_{2b}}, \tag{4.1.21}$$

where $\mathrm{Re}_{2b} = \rho U(2b)/\mu$.

Couette flow remains laminar up to $\mathrm{Re}_{2b} \approx 3000$, above which the profiles become turbulent (White, 2006).

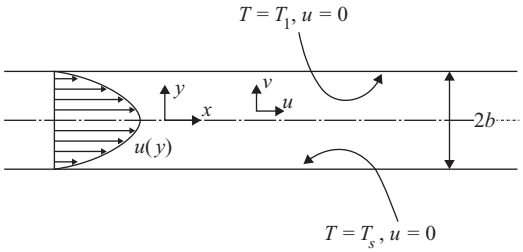

Figure 4.2. Poiseuille flow.

Poiseuille Flow

In this case we have flow between two stationary infinitely large flat plates, caused by an imposed pressure gradient, as shown in Fig. 4.2. For simplicity, assume that there is no body force along x. For an incompressible constant-property fluid in fully developed flow, Eqs. (4.1.1) and (4.1.3) and their simplifications apply. Equation (4.1.2) applies as well, except that now the pressure-gradient term on the right-hand side is no longer negligible. We thus end up with

$$v = 0, \tag{4.1.22}$$

$$\frac{d^2u}{dy^2} = \frac{1}{\mu}\frac{dP}{dx}, \tag{4.1.23}$$

$$\frac{\partial^2 T}{\partial y^2} + \frac{\mu}{k}\left(\frac{\partial u}{\partial y}\right)^2 = 0. \tag{4.1.24}$$

The boundary conditions are

$$u = 0 \quad \text{at } y = \pm b, \tag{4.1.25}$$

$$T = T_s \quad \text{at } y = -b, \tag{4.1.26}$$

$$T = T_1 \quad \text{at } y = b, \tag{4.1.27}$$

$$\frac{du}{dy} = 0 \quad \text{at } y = 0. \tag{4.1.28}$$

The hydrodynamic part of the problem leads to

$$u = \frac{3}{2}U_m\left[1 - \left(\frac{y}{b}\right)^2\right], \tag{4.1.29}$$

$$\frac{U_{\max}}{U_m} = \frac{3}{2}, \tag{4.1.30}$$

$$U_m = \frac{b^2}{3\mu}\left(-\frac{dP}{dx}\right), \tag{4.1.31}$$

where U_m and $U_{\max}$ are the mean and maximum velocities, respectively. Knowing the velocity profile from Eq. (4.1.29), we can now solve the heat transfer part, namely, Eq. (4.1.24), along with Eqs. (4.1.26) and (4.1.27). That leads to

$$T = T_s + \frac{T_1 - T_s}{2}\left(1 + \frac{y}{b}\right) + \frac{3\mu}{4k}U_m^2\left(1 - \frac{y^4}{b^4}\right). \tag{4.1.32}$$

The heat fluxes at the lower and upper boundaries can now be found from

$$q''|_{y=\pm b} = -k \left.\frac{\partial T}{\partial y}\right|_{y=\pm b}. \tag{4.1.33}$$

The magnitude and direction of the heat flow depends on the magnitude of EcPr, where the Eckert number is defined as $\mathrm{Ec} = \frac{U_m^2}{C_p|T_s - T_1|}$.

Poiseuille flow between two parallel plates remains laminar for $\mathrm{Re}_{D_H} \leq 2200$, where $\mathrm{Re}_{D_H} = \rho U_m D_H/\mu$ and $D_H = 4b$. Transition to turbulent flow occurs in the range $2200 \lesssim Re_{D_H} \lesssim 3400$, depending on the configuration of the channel entrance and the disturbance sources.

4.2 The Development of Velocity, Temperature, and Concentration Profiles

Consider the steady flow of an incompressible fluid. With respect to hydrodynamics, two laminar duct flow types are considered. The duct flow is either fully developed, in which case all flow properties except pressure are independent of the longitudinal coordinate; or it is hydrodynamically developing, in which the velocity profile varies with the longitudinal coordinate. In fully developed flow the fluid does not remember the entrance conditions, whereas in developing flow the entrance effect is present.

When the duct flow involves heat transfer with some specific wall conditions, four types of flow are considered: (1) hydrodynamically fully developed and thermally developed flow (or simply fully developed flow), in which the hydrodynamics and heat transfer processes are not affected by the entrance; (2) hydrodynamically developing and thermally developed, in which only hydrodynamic parameters are affected by the entrance; (3) hydrodynamically fully developed and thermally developing flow, in which only the heat transfer processes are affected by the entrance; and (4) simultaneously (combined) developing flow, in which the hydrodynamic and heat transfer processes are both affected by the entrance.

A similar classification can evidently be made for duct flows with mass transfer. Furthermore, these classifications are not limited to laminar flow; they apply to turbulent flow as well and are discussed in chapter 7.

4.2.1 The Development of Boundary Layers

Consider the steady flow of an incompressible fluid in an isothermal duct, depicted in Fig. 4.3(a). A boundary layer forms on the duct wall, and the thickness of the boundary layer increases along the longitudinal coordinate x. In fact, close to the inlet, where the boundary-layer thickness is much smaller than the characteristic dimension of the duct cross section, the boundary layer is essentially the same as the boundary layer on a flat plate. The growth of the boundary layer represents the spreading of the effect of fluid viscosity across the channel. As one marches along the duct, eventually the boundary layers growing on the walls merge at $x = l_{\mathrm{ent,\,hy}}$. For $x > l_{\mathrm{ent,\,hy}}$, the viscous effects spread across the duct, so that the entire flow field is in fact a boundary layer. The region $0 < x \leq l_{\mathrm{ent,\,hy}}$ is the *hydrodynamic entrance region*, and $l_{\mathrm{ent,\,hy}}$ is the hydrodynamic entrance length. In the region $0 < x \leq l_{\mathrm{ent,\,hy}}$,

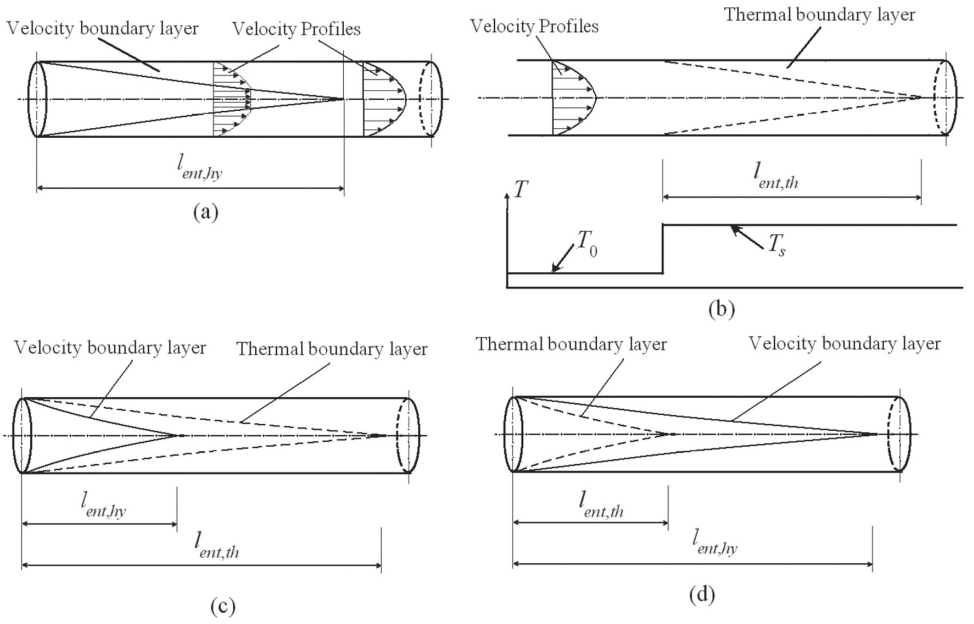

Figure 4.3. Development of velocity and thermal boundary layers in pipe flow: (a) development of the velocity boundary layer, (b) development of the thermal boundary layer in hydrodynamically fully developed flow, (c) simultaneous development of velocity and thermal boundary layers when $\Pr \gg 1$, (d) Simultaneous development of velocity and thermal boundary layers when $\Pr \ll 1$.

the flow is *hydrodynamically developing*. Beyond $l_{\text{ent, hy}}$ the flow is *hydrodynamically fully developed*.

In the hydrodynamically developing flow region the velocity profile varies with the longitudinal coordinate, i.e., $u = u(x,\ y,\ z)$. On the other hand, in the hydrodynamically developed flow region the velocity profile becomes independent of the longitudinal coordinate, namely, $u = u(y,\ z)$.

Now consider the flow field displaced in Fig. 4.3(b), where a hydrodynamically fully developed flow is underway. For $x \leq 0$, the fluid and the duct wall are at the same temperature [$T(x, y, z) = T_0$ for $x \leq 0$], and for $x > 0$ the wall temperature is T_s, where $T_s \neq T_0$. In this case, starting at $x = 0$, a thermal boundary layer forms, and its thickness grows along the duct. The behavior of the thermal boundary layer is similar to that of the thermal boundary layer on a flat plate for small values of x, and the thickness of the boundary layer represents the extent of the spreading of the thermal-diffusion effect. As we march along the duct, eventually the thermal boundary layers merge at $x = l_{\text{ent, th}}$. The region $0 < x \leq l_{\text{ent, th}}$ is the *thermal entrance region*, where hydrodynamically fully developed and *thermally developing flow* is underway. In the region $x > l_{\text{ent, th}}$, the flow field is hydrodynamically fully developed as well as thermally developed. This type of flow field is often referred to simply as fully developed flow. In this region neither the hydrodynamic nor the heat transfer processes in the flow field are affected by the duct entrance.

Now consider the conditions depicted in Figs. 4.3(c) and 4.3(d), where a fluid originally at temperature T_0 enters a duct with a wall temperature $T_s \neq T_0$. In this case velocity and temperature boundary layers both develop starting at $x = 0$. Near

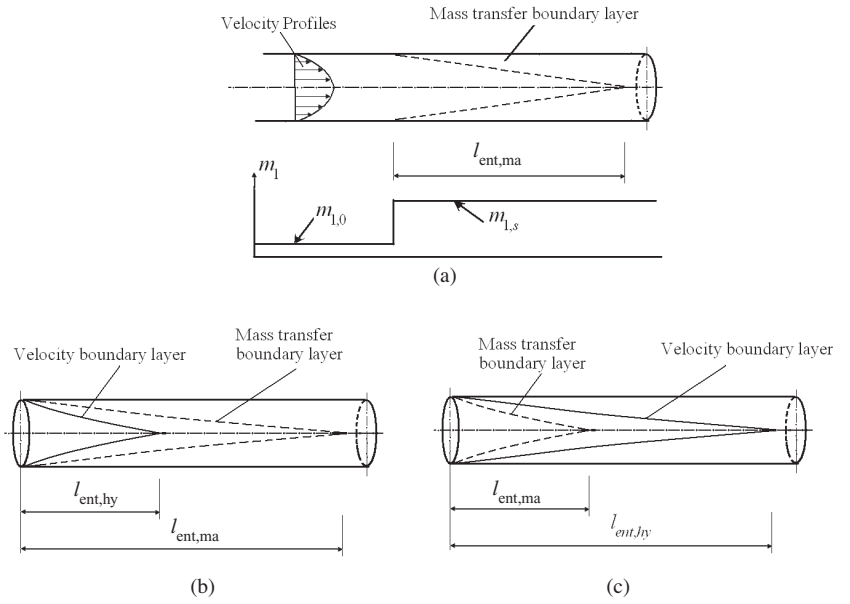

Figure 4.4. Development of velocity and mass transfer boundary layers in pipe flow: (a) development of the mass transfer boundary layer in hydrodynamically fully developed flow, (b) simultaneous development of velocity and mass transfer boundary layers when $Sc \gg 1$, (c) simultaneous development of velocity and mass transfer boundary layers when $Sc \ll 1$.

the entrance, where the thickness of either boundary layer is much smaller than the characteristic dimension of the duct cross section, the simultaneous development of the two boundary layers is similar to the development of velocity and thermal boundary layers on a flat plate. Also, similar to the case of flat plates, the ratio of the thicknesses of the boundary layers δ_{th}/δ depends on the magnitude of Pr, and $\delta_{th} \approx \delta$ for $Pr \approx 1$. When $Pr \ll 1$, for example in liquid metals, then the development of the boundary layers will resemble Fig. 4.3(d). Because of the larger thermal diffusivity, the thermal effect of the wall spreads into the flow field much faster than its viscous effect, and the thermal boundary layer is everywhere thicker than the velocity boundary layer. As a result, the thermal entrance length $l_{ent,\,th}$ will be shorter than the hydrodynamic entrance length $l_{ent,\,hy}$. An opposite situation is encountered when $Pr \gg 1$ (e.g., in viscous liquids), as in Fig. 4.3(c), where $l_{ent,\,hy} < l_{ent,\,th}$. The region represented by $x \leq (l_{ent,\,hy},\ l_{ent,\,th})$ is referred to as the *simultaneously developing flow* or the *combined entrance region*. Obviously, for $x > (l_{ent,\,hy},\ l_{ent,\,th})$ we deal with fully developed flow.

The discussion thus far considered a constant-wall-temperature boundary condition for heat transfer. Thermally developing and thermally developed flows can also occur when the boundary condition is a constant wall heat flux or a heat flux that varies as an exponential function of the longitudinal coordinate.

The preceding discussion would apply to mass transfer processes as well, when we consider the steady-state flow of an incompressible fluid in the ducts, shown in Fig. 4.4. In Fig. 4.4(a), which is similar to Fig. 4.3(b), a hydrodynamically fully developed flow is underway. The fluid initially contains a species at the mass fraction $m_{1,\,0}$,

and for $x \leq 0$ there is no mass transfer between the fluid and the wall. For $x > 0$, mass transfer takes place between the wall and the fluid driven by a constant and uniform mass fraction of species 1, $m_{1,s}$, adjacent to the wall. In this case a mass transfer boundary layer develops, which engulfs the entire duct cross section for $x > l_{\text{ent, ma}}$. In the $0 < x \leq l_{\text{ent, ma}}$ region, we deal with a hydrodynamically fully developed flow and a mass transfer developing flow. This is the mass transfer entrance region. In the $x > l_{\text{ent, ma}}$ region, we deal with developed flow with respect to hydrodynamics and mass transfer.

In Figs. 4.4(b) and 4.4(c), which are similar to Figs. 4.3(c) and 4.3(d), respectively, we deal with simultaneously developing flow or a combined entrance effect.

Mass transfer developing flow and developed flow conditions are also encountered when the mass transfer boundary condition is either a vanishingly small constant and uniform mass flux of the transport species at the wall or a vanishingly small mass flux of the transferred species that is either a constant or varies exponentially with the longitudinal coordinate. The mass flux of the transferred species needs to be small because a high mass flux would disturb and consequently affect the hydrodynamic and mass transfer boundary layers. (See the discussion in Chapter 8.)

4.2.2 Hydrodynamic Parameters of Developing Flow

The entrance length $l_{\text{ent, hy}}$ for an incompressible internal flow can be defined as the length that leads to

$$\left| \frac{U_{\max} - U_{\max,\, fd}}{U_{\max}} \right| < \varepsilon, \tag{4.2.1}$$

with $\varepsilon = 0.01$, typically. The entrance conditions obviously can affect $l_{\text{ent, hy}}$. A flat velocity profile at inlet is the most common assumption. For steady and incompressible flow, $l_{\text{ent, hy}}$ can be found by a numerical solution of the Navier–Stokes equations or other analytical methods. Useful and simple correlations are available, most of which are correlation or curve fits based on the results of model or numerical calculations.

Friction Factor Definitions

The velocity profile in the hydrodynamic entrance region of a flow passage varies along the axial direction. Pressure variation in the axial direction is thus caused by frictional loss as well as the change in the fluid momentum flux. Therefore, to avoid ambiguity, the following definitions are used. Local Fanning and Darcy friction factors are defined as

$$C_f = \frac{\tau_s}{\frac{1}{2}\rho U_m^2}, \tag{4.2.2}$$

$$f = \frac{D_H \left(-\frac{\partial P}{\partial x} \right)_{\text{fr}}}{\frac{1}{2}\rho U_m^2}. \tag{4.2.3}$$

The average friction factors, over a length l, are defined as

$$\langle C_f \rangle_l = \frac{\frac{1}{l}\int_{x=0}^{l} \tau_s(x)dx}{\frac{1}{2}\rho U_m^2} = \frac{1}{l}\int_{x=0}^{l} C_f(x)dx, \tag{4.2.4}$$

$$\langle f \rangle_l = \frac{D_H}{l}\frac{\int_{x=0}^{l}\left(-\frac{\partial P}{\partial x}\right)_{\text{fr}} dx}{\frac{1}{2}\rho U_m^2} = \frac{1}{l}\int_{x=0}^{l} f(x)\,dx. \tag{4.2.5}$$

Obviously

$$\langle C_f \rangle_l \left(\frac{1}{2}\rho U_m^2\right) = \frac{A}{p_f l}\left(P_{\text{in}} - P|_{x=l}\right)_{\text{fr}}, \tag{4.2.6}$$

$$\langle f \rangle_l \left(\frac{1}{2}\rho U_m^2\right)\frac{1}{D_H} = \frac{\left(P_{\text{in}} - P|_{x=l}\right)_{\text{fr}}}{l}, \tag{4.2.7}$$

where

$$\left(P_{\text{in}} - P|_{x=l}\right)_{\text{fr}} = \left(P_{\text{in}} - P|_{x=l}\right) + \frac{1}{A}\left[\left(\int_A \frac{1}{2}\rho u^2 dA\right)_{x=l} - \left(\int_A \frac{1}{2}\rho u^2 dA\right)_{\text{in}}\right]. \tag{4.2.8}$$

The apparent friction factors are meant to include the effect of changes in the momentum flux and are defined as

$$C_{f,\text{app},l} = \frac{\left(P_{\text{in}} - P|_{x=l}\right)A}{\frac{1}{2}\rho U_m^2 p_f l}, \tag{4.2.9}$$

$$f_{\text{app},l} = \frac{\left(P_{\text{in}} - P|_{x=l}\right)}{\frac{1}{2}\rho U_m^2\left(\frac{1}{D_H}\right)l}, \tag{4.2.10}$$

The fully developed friction factors $C_{f,fd}$ and f_{fd} are defined similarly to Eqs. (4.2.2) and (4.2.3) when they are applied to locations where the entrance effects have disappeared.

The incremental pressure-drop number is defined as

$$K(x) = 2\left(C_{f,\text{app}} - C_{f,fd}\right)\frac{p_f}{A}x. \tag{4.2.11}$$

$K(x)$ varies from zero at the inlet to a flow passage to a constant value $K(\infty)$ after fully developed conditions are reached.

Some Useful Correlations

For circular tubes, a correlation by Chen (1973) is

$$\frac{l_{\text{ent,hy}}}{D} = \frac{0.60}{0.035\text{Re}_D + 1} + 0.056\text{Re}_D. \tag{4.2.12}$$

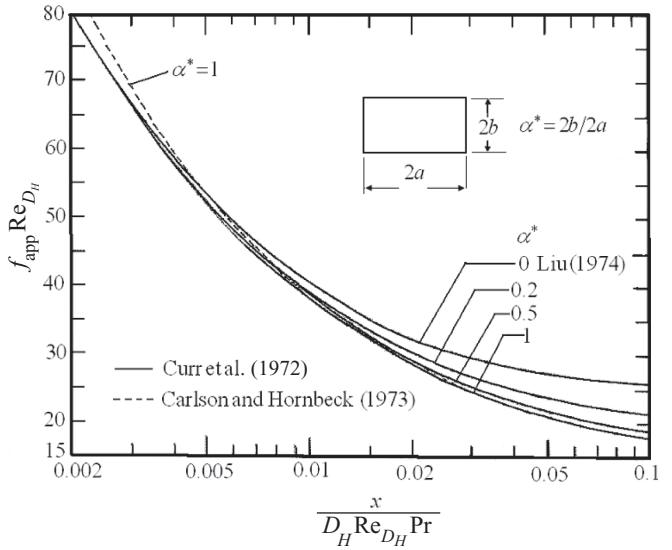

Figure 4.5. The apparent fanning friction factor for developing flow in rectangular ducts (Shah and London 1978.)

The apparent fanning friction factor, according to Shah and London (1978), can be found from

$$C_{f,\mathrm{app},x}\mathrm{Re}_D = \frac{3.44}{(x^*)^{1/2}} + \frac{\frac{1.25}{4x^*} + 16 - \frac{3.44}{(x^*)^{1/2}}}{1 + 0.00021\,(x^*)^{-2}}, \tag{4.2.13}$$

where

$$x^* = \frac{x}{D\mathrm{Re}_D.} \tag{4.2.14}$$

Equation (4.2.13) is recommended for the entire x^* range by Shah and London (1978).

For flow in a flat channel (flow between two parallel plates), Chen (1973) proposed

$$\frac{l_{\mathrm{ent,hy}}}{D_H} = 0.011\mathrm{Re}_{D_H} + \frac{0.315}{1 + 0.0175\mathrm{Re}_{D_H}}, \tag{4.2.15}$$

where $\mathrm{Re}_{D_H} = (\rho U_m D_H)/\mu$. The apparent fanning friction factor can be found from the following correlation, also proposed by Shah and London (1978):

$$C_{f,\mathrm{app}}\mathrm{Re}_{D_H} = \frac{3.44}{(x^*)^{1/2}} + \frac{24 + \frac{0.674}{4x^*} - \frac{3.44}{(x^*)^{1/2}}}{1 + 0.000029\,(x^*)^{-2}}. \tag{4.2.16}$$

For flow in rectangular ducts, the duct aspect ratio, defined as $\alpha^* = b/a$, is important. Figure 4.5 depicts the results of numerical calculation of Carlson and Hornbeck (1973) and others (Shah and London, 1978). Figure 4.6, also borrowed from Shah and London, displays $C_{f,\mathrm{app}}\mathrm{Re}_{D_H}$ for isosceles triangular ducts.

A useful, approximate correlation, based on using the square root of the channel cross-sectional area as the length scale, was derived by Muzychka and Yovanovich

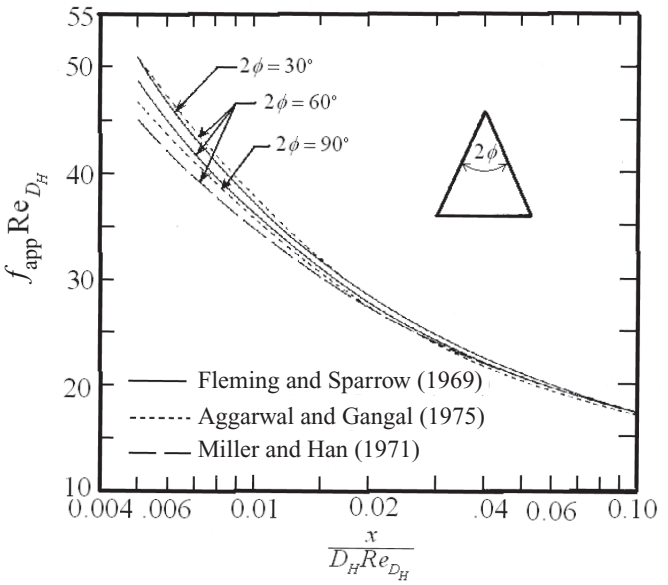

Figure 4.6. The apparent fanning friction factor for developing flow in isosceles triangular ducts (Shah and London 1978).

(2004); it predicts the apparent friction factor in the entrance region of channels with various cross-sectional geometries within ±10%. The correlation is

$$C_{f,\mathrm{app}}\mathrm{Re}_{\sqrt{A}} = \left\{ \left(\frac{12}{\sqrt{\alpha^*}\,(1+\alpha^*)\left[1 - \dfrac{192\alpha^*}{\pi^5}\tanh\left(\dfrac{\pi}{2\alpha^*}\right)\right]} \right)^2 + \left(\frac{3.44}{\sqrt{x^*}}\right)^2 \right\}^{1/2}, \tag{4.2.17}$$

where now

$$\mathrm{Re}_{\sqrt{A}} = \frac{\rho\, U_m \sqrt{A}}{\mu}, \tag{4.2.18}$$

$$x^* = \frac{x}{\sqrt{A}\,\mathrm{Re}_{\sqrt{A}}}. \tag{4.2.19}$$

The aspect ratio α^* is defined for various channel cross-sectional geometries according to Fig. 4.7. Figure 4.8 compares the prediction of an earlier version of the preceding correlation [in which the term $\left(\frac{3.44}{\sqrt{x^*}}\right)^2$ was not included] with some experimental data.

4.2.3 The Development of Temperature and Concentration Profiles

Strictly speaking, a thermal fully developed flow never occurs in channels with heat transfer. After all, the mean temperature never stops to be a function of the axial coordinate. When properties are constant, however, fully developed velocity is possible, as was explained earlier. In that case, a fully developed temperature profile

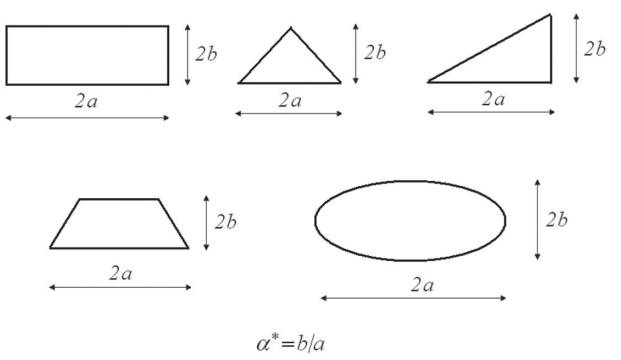

Figure 4.7. Aspect ratios for various channel cross-sectional geometries.

can also be defined based on the following definition: A fully developed temperature profile occurs when the shape of the temperature profile is independent of the longitudinal coordinate. It can be argued that a fully developed temperature profile is obtained downstream of the point where the thermal boundary layer occupies the entire flow area.

The preceding definition of thermally developed flow implies that, for any point in the cross section,

$$\frac{\partial}{\partial x}\left(\frac{T-T_s}{T_m-T_s}\right)=0, \tag{4.2.20}$$

where x is the longitudinal coordinate and T_m is the mean (mixed-cup) temperature defined as

$$T_m=\frac{1}{\dot{m}}\int_A \rho u T dA=\frac{1}{AU_m}\int_A uTdA. \tag{4.2.21}$$

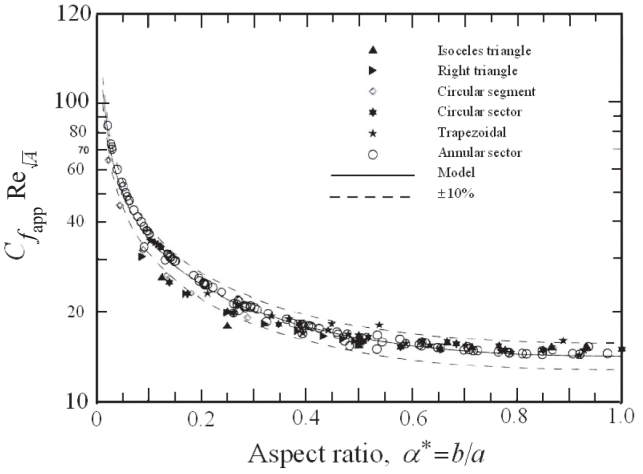

Figure 4.8. Comparison of Eq. (4.2.17) with experimental data (from Muzychka and Yovanovich, 2004).

We may ask, what boundary conditions can lead to fully developed temperature distributions? We can examine Eq. (4.2.20) by recasting it as

$$\frac{\partial T}{\partial x} = \frac{dT_s}{dx} + \frac{T - T_s}{T_m - T_s}\left(\frac{dT_m}{dx} - \frac{dT_s}{dx}\right). \tag{4.2.22}$$

For two important types of boundary conditions, the equality can be satisfied and therefore a fully developed temperature distribution will be possible.

1. $T_s = \text{const.}$: In this case, for a circular channel, for example,

$$\rho C_P u \frac{\partial T}{\partial x} = k \frac{1}{r}\frac{\partial}{\partial r}\left(r\frac{\partial T}{\partial r}\right). \tag{4.2.23}$$

   Now, using

$$\frac{\partial \mathrm{T}}{\partial x} = \frac{T - T_s}{T_m - T_s}\frac{dT_m}{dx},$$

   we get

$$\frac{1}{r}\frac{\partial}{\partial r}\left(r\frac{\partial T}{\partial r}\right) = \frac{1}{\boldsymbol{\alpha}} u \frac{T - T_s}{T_m - T_s}\frac{dT_m}{dx}, \tag{4.2.24}$$

   where $\boldsymbol{\alpha}$ is the thermal diffusivity. The solution of this equation will provide a fully developed temperature profile.

2. $q_s'' = \text{const.}$ and $h = \text{const.}$ In this case, because $q_s'' = h\,(T_s - T_m)$, then $\frac{dT}{dx} = \frac{dT_s}{dx}$ and

$$\frac{dT}{dx} = \frac{dT_s}{dx} = \frac{dT_m}{dx}. \tag{4.2.25}$$

   The energy equation then becomes

$$\frac{1}{r}\frac{\partial}{\partial r}\left(r\frac{\partial T}{\partial r}\right) = \frac{u(r)}{\boldsymbol{\alpha}}\frac{dT_m}{dx}. \tag{4.2.26}$$

The previous two boundary conditions are actually special cases of a more general class of problems with exponentially varying wall heat fluxes (Sparrow and Patankar, 1977). Our interest, however, is with the aforementioned two boundary conditions.

The uniform wall temperature (isothermal) boundary condition is represented by the subscript UWT. The subscript UHF refers to a uniform wall heat flux (isoflux) boundary condition. Furthermore, the subscript **H1** represents conditions in which the wall heat flux is axially constant and the temperature profile is circumferentially constant. The latter boundary condition is rather unlikely to occur in many practical applications. Nevertheless, it can easily be imposed in numerical simulations and was investigated rather extensively in the past.

The equivalent diffusive mass transfer problem is now discussed. Consider diffusive mass transfer between the wall of a pipe and its fluid, assuming that the mass flux at the wall surface is vanishingly small and that the diffusion of the transferred species represented by the subscript 1 is governed by Fick's law. Fully developed

mass fraction profile can then be assumed when the shape of the mass-fraction profile does not change with the longitudinal coordinate, and that requires

$$\frac{\partial}{\partial x}\left(\frac{m_1 - m_{1,s}}{m_{1,m} - m_{1,s}}\right) = 0. \tag{4.2.27}$$

Following the steps taken for temperature, we note that a fully developed mass-fraction distribution will be possible for two important boundary conditions:

1. $m_{1,s} = \text{const.}$, in which case we get

$$\frac{1}{r}\frac{\partial}{\partial r}\left(r\frac{\partial m_1}{\partial r}\right) = \frac{1}{\mathcal{D}_{12}} u \frac{m_1 - m_{1,s}}{m_{1,m} - m_{1,s}} \frac{dm_{1,m}}{dx}, \tag{4.2.28}$$

   where

2. $m''_{1,s} = \text{const.}$ and $\mathcal{K} = \text{const.}$, where $\mathcal{K}$ is the mass transfer coefficient between the wall and the fluid, so that

$$m''_{1,s} = \mathcal{K}\left(m_{1,s} - m_{1,m}\right). \tag{4.2.29}$$

   In this case we will have

$$\frac{dm_1}{dx} = \frac{dm_{1,s}}{dx} = \frac{dm_{1,m}}{dx}. \tag{4.2.30}$$

   The mass-species conservation equation then becomes

$$\frac{1}{r}\frac{\partial}{\partial r}\left(r\frac{\partial m_1}{\partial r}\right) = \frac{u(r)}{\mathcal{D}_{12}} \frac{dm_{1,m}}{dx}. \tag{4.2.31}$$

   The uniform mass fraction or concentration boundary condition is designated with the subscript UWM. The uniform and constant wall mass flux (isoflux) boundary condition is designated by UMF.

4.3 Hydrodynamics of Fully Developed Flow

Recall that this type of flow occurs in the steady, incompressible, constant-property flow in a uniform cross-section channel. Only pressure changes along the longitudinal coordinate x and other properties remain independent of x.

Circular Pipes: The Hagen–Poiseuille Flow

This refers to a fully developed, laminar flow in a circular duct, originally solved by Hagen in 1839 and by Poiseuille in 1840. The momentum conservation equation for the longitudinal direction (x) is

$$-\frac{1}{\mu}\frac{dP}{dx} + \frac{1}{r}\frac{\partial}{\partial r}\left(r\frac{\partial u}{\partial r}\right) = 0, \tag{4.3.1}$$

where x and r are the axial and radial coordinates, respectively. The boundary conditions are

$$\frac{\partial u}{\partial r} = 0 \quad \text{at } r = 0,$$
$$u = 0 \quad \text{at } r = R_0.$$

The solution of Eq. (4.3.1) is

$$u = \frac{R_0^2}{4\mu}\left(-\frac{dP}{dx}\right)\left[1-\left(\frac{r}{R_0}\right)^2\right]. \tag{4.3.2}$$

This can be used to derived the following useful relations:

$$u(r) = 2U_m\left[1-\left(\frac{r}{R_0}\right)^2\right], \tag{4.3.3}$$

$$U_m = \frac{R_0^2}{8\mu}\left(-\frac{dP}{dx}\right), \tag{4.3.4}$$

$$\dot{m} = \rho\frac{\pi R_0^4}{8\mu}\left(-\frac{dP}{dx}\right). \tag{4.3.5}$$

Also, given the definition of the Darcy friction factor,

$$\left(-\frac{dP}{dx}\right) = \frac{f}{D}\frac{1}{2}\rho U_m^2, \tag{4.3.6}$$

we can easily prove that

$$f = 64/\mathrm{Re}_D. \tag{4.3.7}$$

The Fanning friction factor (the skin-friction coefficient), C_f, is defined according to

$$\tau_s = C_f\frac{1}{2}\rho U_m^2. \tag{4.3.8}$$

This leads to

$$C_f = f/4 = 16/\mathrm{Re}_D, \tag{4.3.9}$$

where,

$$\mathrm{Re}_D = \rho U_m D_D/\mu. \tag{4.3.10}$$

Solutions for the Poiseuille flow in ducts with rectangular, triangular, elliptical, trapezoidal, and many other geometric cross sections are available. The solutions for five widely encountered cross-sectional configurations, shown in Fig. 4.9, are given. More solutions can be found in Shah and Bhatti (1987) and White (2006).

Flat Channels

$$u(x,y) = \frac{1}{2\mu}\left(-\frac{dP}{dx}\right)\left(b^2-y^2\right), \tag{4.3.11}$$

$$U_m = \frac{1}{3\mu}\left(-\frac{dP}{dx}\right)b^2, \tag{4.3.12}$$

$$C_f\mathrm{Re}_{D_H} = 24. \tag{4.3.13}$$

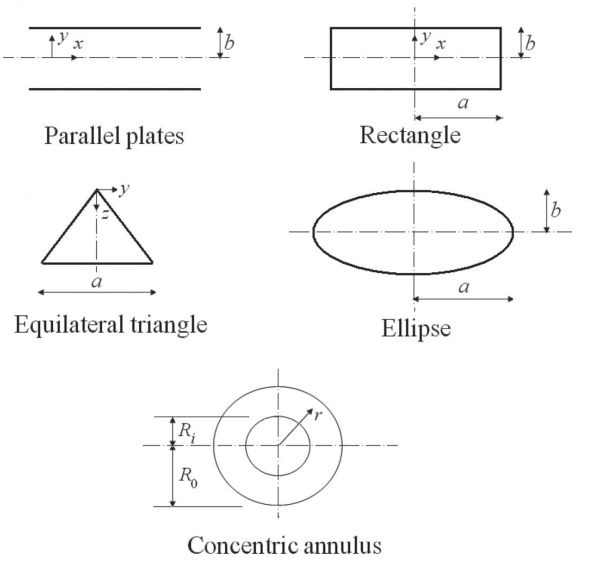

Figure 4.9. Some channel cross-section geometries.

Rectangular Ducts

$$u(y,z) = \frac{16a^2}{\pi^3\mu}\left(-\frac{dP}{dx}\right)\sum_{j=1,3,5,\ldots}^{\infty}(-1)^{\frac{j-1}{2}}\left[1-\frac{\cosh\left(\frac{j\pi y}{2a}\right)}{\cosh\left(\frac{j\pi b}{2a}\right)}\right]\cos\left(\frac{j\pi z}{2a},\right) \tag{4.3.14}$$

$$U_m = \frac{a^2}{3\mu}\left(-\frac{dP}{dx}\right)\left[1-\frac{192}{\pi^5}\left(\frac{a}{b}\right)\sum_{j=1,3,5,\ldots}^{\infty}\frac{1}{j^5}\tanh\left(\frac{j\pi b}{2a}\right)\right], \tag{4.3.15}$$

$$C_f\mathrm{Re}_{D_H} = \frac{24}{\left(1+\frac{1}{\alpha^*}\right)^2\left[1-\frac{192}{\pi^5\alpha^*}\sum_{j=1,3,5,\ldots}^{\infty}\frac{1}{j^5}\tanh\left(\frac{j\pi\alpha^*}{2}\right)\right]}. \tag{4.3.16}$$

A curve fit to the predictions of the preceding expression is

$$C_f\mathrm{Re}_{D_H} \approx 24[1-1.3553\alpha^*+1.9467\alpha^{*2}-1.7012\alpha^{*3}+0.9564\alpha^{*4}-0.2537\alpha^{*5}], \tag{4.3.17}$$

where $\alpha^* = b/a$ ($\alpha^* \le 1$). Equation (4.3.17), developed by Shah and Bhatti (1987), deviates from the original value by less than 0.05%.

Equilateral Triangular Ducts

$$u(y,z) = \left(-\frac{1}{\mu}\frac{dP}{dx}\right)\frac{1}{2\sqrt{3}a}\left(z-\frac{\sqrt{3}}{2}a\right)\left(3y^2-z^2\right), \tag{4.3.18}$$

$$U_m = \frac{a^2}{80\mu}\left(-\frac{dP}{dx}\right), \tag{4.3.19}$$

$$C_{\mathrm{f}}\mathrm{Re}_{D_H} = \frac{40}{3}, \tag{4.3.20}$$

$$D_H = \frac{a}{\sqrt{3}}, \tag{4.3.21}$$

$$\dot{m} = \frac{\sqrt{3}}{320}\rho\frac{a^4}{\mu}\left(-\frac{dP}{dx}\right). \tag{4.3.22}$$

Ellipse

$$u(y,z) = \frac{1}{2\mu}\left(-\frac{dP}{dx}\right)\left(\frac{a^2b^2}{a^2+b^2}\right)\left(1-\frac{y^2}{a^2}-\frac{z^2}{b^2}\right), \tag{4.3.23}$$

$$U_m = \frac{b^2}{1+\alpha^{*2}}\frac{1}{4\mu}\left(-\frac{dP}{dx}\right), \tag{4.3.24}$$

$$\alpha^* = b/a \quad (\alpha^* \le 1), \tag{4.3.25}$$

$$C_f\mathrm{Re}_{D_H} = 2\left(1+\alpha^{*2}\right)\left[\frac{\pi}{E(\xi)}\right]^2, \tag{4.3.26}$$

$$\mathrm{A} = \pi ab, \tag{4.3.27}$$

$$D_H = \frac{\pi b}{E(\xi)}, \tag{4.3.28}$$

where

$$\xi = 1-\alpha^{*2} \tag{4.3.29}$$

and $E(\xi)$ is the Complete elliptic integral of the second kind:

$$\begin{aligned} E(\xi) &= \int_0^{\frac{\pi}{2}}\sqrt{1-\xi^2\sin^2\theta}\,d\theta \\ &= \frac{\pi}{2}\left\{1-\left(\frac{1}{2}\right)^2\xi^2-\left(\frac{1\times3}{2\times4}\right)^2\frac{\xi^4}{3}-\left(\frac{1\times3\times5}{2\times4\times6}\right)^2\frac{\xi^6}{5}\cdots\right\}. \end{aligned} \tag{4.3.30}$$

Concentric Circular Annulus

$$u(r) = \left[R_0^2-r^2+\left(R_0^2-R_i^2\right)\frac{\ln(r/R_0)}{\ln(R_0/R_i)}\right]\left(-\frac{1}{4\mu}\frac{dP}{dx}\right), \tag{4.3.31}$$

$$U_m = \frac{1}{8\mu}\left(-\frac{dP}{dx}\right)\left[R_0^2+R_i^2-\frac{\left(R_0^2-R_i^2\right)}{\ln(R_0/R_i)}\right], \tag{4.3.32}$$

$$C_f\mathrm{Re}_{D_H} = \frac{16(R_0-R_i)^2}{R_0^2+R_i^2-\dfrac{R_0^2-R_i^2}{\ln(R_0/R_i)}}, \tag{4.3.33}$$

$$D_H = 2\left(R_0-R_i\right), \tag{4.3.34}$$

$$r_{\max} = \left\{\left[R_0^2-R_i^2\right]/\left[2\ln\left(R_0/R_i\right)\right]\right\}^{1/2}, \tag{4.3.35}$$

where $r_{\max}$ is radius where maximum velocity occurs.

4.4 Fully Developed Hydrodynamics and Developed Temperature or Concentration Distributions

In this section we discuss analytical solutions for two widely encountered boundary conditions: constant wall temperature and constant wall heat flux. The equivalent mass transfer solutions, wherever such solutions are relevant, are also briefly discussed.

4.4.1 Circular Tube

Uniform Heat Flux Boundary Conditions

Starting from Eq. (4.2.26), and using the fully developed velocity profile, we have

$$\frac{k}{r}\frac{\partial}{\partial r}\left(r\frac{\partial T}{\partial r}\right) = 2\rho C_p U_m \left(1 - \frac{r^2}{R_0^2}\right)\frac{dT_m}{dx}. \tag{4.4.1}$$

An energy balance on the flow channel gives

$$\rho C_p U_m \frac{dT_m}{dx} = \frac{2}{R_0} q_s''. \tag{4.4.2}$$

Equation (4.4.1) can be cast as

$$\frac{\partial}{\partial r}\left(r\frac{\partial T}{\partial r}\right) = \frac{2}{\alpha} U_m r \left(1 - \frac{r^2}{R_0^2}\right)\frac{dT_m}{dx}. \tag{4.4.3}$$

Now we can perform the following operations to this equation:

1. Apply $\int_0^r dr$, noting that $\frac{\partial T}{\partial r}|_{r=0} = 0$.
2. Divide through by r.
3. Apply $\int_r^{R_0} dr$, noting that $T = T_s$ at $r = R_0$.
4. Eliminate dT_m/dx in favor of q_s'', using Eq. (4.4.2).

The result is

$$T_s - T = \frac{2U_m R_0^2}{\alpha}\frac{dT_m}{dx}\left[\frac{3}{16} + \frac{1}{16}\left(\frac{r}{R_0}\right)^4 - \frac{1}{4}\left(\frac{r}{R_0}\right)^2\right]. \tag{4.4.4}$$

Now we can actually obtain a relation for T_m by writing

$$T_s - T_m = \frac{1}{\pi R_0^2 U_m}\int_0^{r_0} u(r)(T_s - T)2\pi r\, dr. \tag{4.4.5a}$$

This will give

$$T_s - T_m = \frac{11}{48}\frac{U_m}{\alpha} R_0^2 \frac{dT_m}{dx}. \tag{4.4.5b}$$

Now, eliminating dT_m/dx from this equation by using Eq. (4.4.2) and noting that $q_s'' = h(T_s - T_m)$, we get

$$\mathrm{Nu}_{D,\mathrm{UHF}} = hD/k = \frac{48}{11} \approx 4.364. \tag{4.4.6}$$

The equivalent mass transfer problem represents a pipe flow in which a vanishingly small and constant mass flux $m''_{1,s}$ of the transferred species 1 flows through the pipe wall. The solution of the problem is

$$\mathrm{Sh}_{D,\mathrm{UMF}} = \frac{\mathcal{K}D}{\rho\mathcal{D}_{12}} \approx 4.364. \tag{4.4.7}$$

The temperature distribution can also be presented in terms of the inlet temperature. By subtracting Eq. (4.4.5b) from Eq. (4.4.4) and using Eq. (4.4.2), we get

$$T - T_m = \frac{2q''_s R_0}{k}\left[\frac{1}{2}\left(\frac{r}{R_0}\right)^2 - \frac{1}{8}\left(\frac{r}{R_0}\right)^4 - \frac{7}{48}\right]. \tag{4.4.8a}$$

The integration of Eq. (4.4.2) leads to

$$T_m - T_{\mathrm{in}} = \frac{2q''_s x}{\rho C_P U_m R_0} = \frac{4q''_s \boldsymbol{\alpha}\, x}{k\, U_m D^2}. \tag{4.4.8b}$$

Subtracting Eq. (4.4.8a) from Eq. (4.4.8b) leads to

$$\frac{T - T_{\mathrm{in}}}{q''_s D/k} = \frac{4x}{DPe} + \left[\frac{1}{2}\left(\frac{r}{R_0}\right)^2 - \frac{1}{8}\left(\frac{r}{R_0}\right)^4 - \frac{7}{48}\right], \tag{4.4.8c}$$

where $\mathrm{Pe} = U_m D/\boldsymbol{\alpha}$ is the Peclet number.

The aforementioned analytical solution can be modified to include the effects of volumetric energy generation (caused, for example, by radioactive decay) and viscous dissipation. The result will be (Tyagi, 1966; Shah and London, 1978)

$$\mathrm{Nu}_{D,\mathrm{UHF}} = \frac{48}{11}\frac{1}{1 + \frac{3}{44}q^*_v + \frac{48}{11}\mathrm{Br}'}, \tag{4.4.9}$$

where Br' is the constant wall heat flux Brinkman number, defined as

$$\mathrm{Br}' = \frac{\mu\, U_m^2}{q''_s D}, \tag{4.4.10}$$

$$q^*_v = \dot{q}_v D/q''_s. \tag{4.4.11}$$

The temperature profile in this case is

$$\begin{aligned} T_s - T = \frac{U_m}{8R_0^2\boldsymbol{\alpha}}\frac{dT_m}{dx}\left(r^2 - R_0^2\right)\left\{\left(r^2 - 3R_0^2 - 16R_0^2 C_5\right)\right. \\ \left. + C_6\left[r^2 - 3R_0^2 - 2\left(r^2 - R_0^2\right)\right]\right\}, \end{aligned} \tag{4.4.12}$$

$$T_s - T_m = \frac{11}{48}\frac{U_m}{\boldsymbol{\alpha}}R_0^2\frac{dT_m}{dx}\left(1 + \frac{64}{11}C_5 + \frac{5}{11}C_6\right), \tag{4.4.13}$$

where

$$C_5 = -\frac{q^*_v}{8\left[q^*_v + 4\left(1 + 8\mathrm{Br}'\right)\right]}, \tag{4.4.14}$$

$$C_6 = -\frac{32\,\mathrm{Br}'}{q^*_v + 4\left(1 + 8\mathrm{Br}'\right)}. \tag{4.4.15}$$

Uniform Wall Temperature Boundary Conditions

We now consider the isothermal wall conditions (for heat transfer) and equivalently the constant wall mass fraction or concentration (for mass transfer).

First we consider heat transfer. In this case, by substituting from the fully developed velocity profile into Eq. (4.2.26), we get

$$\frac{1}{r}\frac{\partial}{\partial r}\left(r\frac{\partial T}{\partial r}\right) = \frac{2}{\alpha}U_m\left(1-\frac{r^2}{R_0^2}\right)\frac{T-T_s}{T_m-T_s}\frac{dT_m}{dx}. \tag{4.4.16}$$

This problem was solved by Bhatti and reported by Shah and Bhatti (1987). Accordingly, the solution is

$$\frac{T-T_s}{T_m-T_s} = \sum_{n=0}^{\infty} C_{2n}\left(\frac{r}{R_0}\right)^{2n}, \tag{4.4.17}$$

$$C_0 = 1, \tag{4.4.18}$$

$$C_2 = -\frac{\lambda_0^2}{2^2} \tag{4.4.19}$$

$$\vdots$$

$$C_{2n} = \frac{\lambda_0^2}{(2n)^2}\left(C_{2n-4} - C_{2n-2}\right), \tag{4.4.20}$$

$$\lambda_0 = 2.70436442. \tag{4.4.21}$$

The series in Eq. (4.4.17) rapidly converges, and for all practical purposes 10 terms in the series are sufficient. It can also be shown that

$$\mathrm{Nu}_{D,\mathrm{UWT}} = \frac{\lambda_0^2}{2} = 3.6568. \tag{4.4.22}$$

When $x^* = \frac{x}{D\mathrm{Re}\,\mathrm{Pr}} > 0.0335$, the temperature profile asymptotically reaches

$$\frac{T_m-T_s}{T_{\mathrm{in}}-T_s} = 0.81905\exp\left(-2\lambda_0^2 x^*\right). \tag{4.4.23}$$

The equivalent mass transfer problem represents a pipe flow in which the mass fraction of a transferred species, represented by the subscript 1, at the wall surface is a constant $m_{1,s}$. It is further assumed that the mass flux at the wall surface is vanishingly small. We then can show that (Problem 4.31)

$$\mathrm{Sh}_{D,\mathrm{UWM}} = \frac{\mathcal{K}D}{\rho\mathcal{D}_{12}} = 3.6568. \tag{4.4.24}$$

The aforementioned solution assumes that axial heat conduction (or, equivalently, axial diffusion of mass species 1) in the fluid is negligible. This is a common assumption that is in principle valid when $\mathrm{Pe}\to\infty$, where $\mathrm{Pe} = \mathrm{Re}_D\mathrm{Pr}$ is the Peclet number. The assumption of negligible axial conduction in the fluid becomes invalid in low-flow conditions for fluids with very low Prandtl numbers, e.g., liquid metals.

The effect of fluid axial conduction in creep flow was studied by several authors in the past (see Shah and London, 1978). Michelsen and Villadsen (1974) derived,

$$\mathrm{Nu}_{D,\mathrm{UWT}} = \begin{cases} 3.6568\left(1+\dfrac{1.227}{\mathrm{Pe}^2}+\cdots\right) & \text{for } \mathrm{Pe}>5 \quad (4.4.25) \\ 4.1807\left(1-0.0439\mathrm{Pe}+\cdots\right) & \text{for } \mathrm{Pe}<1.5 \quad (4.4.26) \end{cases}.$$

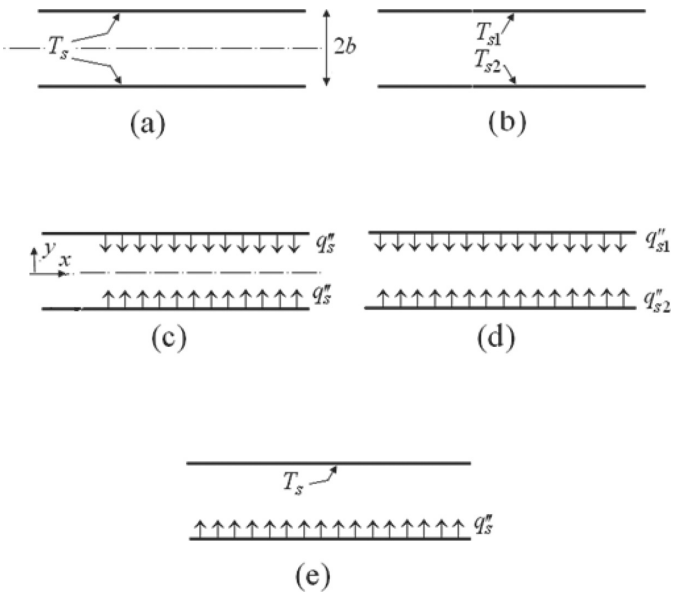

Figure 4.10. Various wall boundary conditions for flat channels.

Regarding the equivalent mass transfer problem, we note that, for $\mathrm{Pe}_{\mathrm{ma}} \to \infty$, the axial diffusion of the transferred species has no effect, where the mass transfer Peclet number is defined as $\mathrm{Pe}_{\mathrm{ma}} = \mathrm{Re}_D \mathrm{Sc}$. For the diffusion of inert gases in liquids, Sc is large, typically several hundred, and the conditions in which $\mathrm{Pe}_{\mathrm{ma}}$ is small enough to render the axial diffusion significant are rather rare. Nevertheless, when small $\mathrm{Pe}_{\mathrm{ma}}$ is encountered, we can use

$$\mathrm{Sh}_{D,\mathrm{UWM}} = \begin{cases} 3.6568\left(1 + \dfrac{1.227}{\mathrm{Pe}_{\mathrm{ma}}^2} + \cdots\right) & \text{for } \mathrm{Pe}_{\mathrm{ma}} > 5 \quad (4.4.27) \\ 4.1807\left(1 - 0.0439\mathrm{Pe}_{\mathrm{ma}} + \cdots\right) & \text{for } \mathrm{Pe}_{\mathrm{ma}} < 1.5 \quad (4.4.28) \end{cases}$$

4.4.2 Flat Channel

Fully developed flow between two parallel plates is the simplest channel flow, and analytical solutions to the thermally developed conditions for this geometry are relatively straightforward. Simple analytical solutions for various boundary conditions are available. Some important boundary condition combinations are shown in Fig. 4.10.

First consider uniform wall heat flux on both walls [Fig. 4.10(c)], i.e., the UHF boundary condition. Neglecting viscous dissipation, the energy equation is

$$\frac{3}{2}U_m\left[1 - \left(\frac{y}{b}\right)^2\right]\frac{\partial T_m}{\partial x} = \alpha\frac{\partial^2 T}{\partial y^2}, \tag{4.4.29}$$

where the boundary conditions are

$$\frac{\partial T}{\partial y} = 0 \quad \text{at } y = 0, \tag{4.4.30}$$

$$k\frac{\partial T}{\partial y} = q_s'' \quad \text{at } y = b. \tag{4.4.31}$$

Let us nondimensionalize these equations by using $\eta = y/b$ and

$$\theta = \frac{T - T_{\text{ref}}}{\frac{q_s'' D_H}{k}}, \tag{4.4.32}$$

$$x^* = \frac{x}{D_H \text{Re}_{D_H} \text{Pr}}. \tag{4.4.33}$$

The results are

$$\frac{\partial^2 \theta}{\partial \eta^2} = \frac{3}{32}\left(1 - \eta^2\right), \tag{4.4.34}$$

$$\frac{\partial \theta}{\partial \eta} = 0 \quad \text{at } \eta = 0, \tag{4.4.35}$$

$$\frac{\partial \theta}{\partial \eta} = \frac{1}{4} \quad \text{at } \eta = 1. \tag{4.4.36}$$

An energy balance on the flow channel gives

$$\frac{dT}{dx} = \frac{dT_m}{dx} = \frac{q_s''}{\rho C_P U_m b}. \tag{4.4.37}$$

This is equivalent to

$$\frac{d\theta}{dx^*} = \frac{d\theta_m}{dx^*} = 4. \tag{4.4.38}$$

The solution to the preceding system is

$$\theta = \frac{3}{16}\eta^2 - \frac{1}{32}\eta^4 - \frac{39}{1120} + 4x^*. \tag{4.4.39}$$

Thus, for the UHF boundary conditions [Fig. 4.10(c)] it can be shown that

$$T(y) = T_s - \frac{3}{2}\frac{q''}{bk}\left(\frac{5}{12}b^2 - \frac{y^2}{2} + \frac{y^4}{12b^2}\right), \tag{4.4.40}$$

$$T_m = T_s - \frac{17}{140}\frac{q_s'' D_H}{k}, \tag{4.4.41}$$

$$\text{Nu}_{D_H} = (hD_H)/k = 140/17. \tag{4.4.42}$$

The preceding equations are for no volumetric energy generation or viscous dissipation. With the latter effects included, Eq. (4.4.42) should be replaced with (Tyagi, 1966; Shah and London, 1978)

$$\text{Nu}_{D_H} = \frac{140}{17}\left[\frac{1}{1 + \frac{3}{68}q_v^* + \frac{108}{17}\text{Br}'}\right], \tag{4.4.43}$$

where q_v^* and Br' are defined as

$$q_v^* = \dot{q}_v D_H / q_s'', \tag{4.4.44}$$

$$\text{Br}' = \frac{\mu\, U_m^2}{q_s'' D_H}. \tag{4.4.45}$$

The mean fluid temperature will then vary according to

$$\dot{m}\, C_P \frac{d\, T_m}{dt} = 2q_s'' + 2\, b\dot{q}_v + \frac{96\mu\, U_m^2 b}{D_H^2}. \tag{4.4.46}$$

When the surfaces are subject to two different but uniform heat fluxes [Fig. 4.10(d)],

$$\mathrm{Nu}_{D_H,1} = \frac{140}{26 - 9\dfrac{q_{s2}''}{q_{s1}''}}, \tag{4.4.47}$$

$$\mathrm{Nu}_{D_H,2} = \frac{140}{26 - 9\dfrac{q_{s1}''}{q_{s2}''}}. \tag{4.4.48}$$

These equations indicate that $\mathrm{Nu}_{D_H,2} = \infty$ when $\frac{q_{s1}''}{q_{s2}''} = \frac{26}{9}$, which implies that in this case

$$T_{s2} = T_m.$$

When temperature is specified at one surface and heat flux on the other surface [Fig. 4.10(e)], then

$$\mathrm{Nu}_{D_H,T} = 4, \tag{4.4.49}$$

$$\mathrm{Nu}_{D_H,q''} = 4, \tag{4.4.50}$$

where the subscripts T and q'' refer to the surfaces with constant temperature and heat flux, respectively. When $q_s'' = 0$ (i.e., adiabatic condition at one of the wall surfaces), then

$$\mathrm{Nu}_{D_H,T} = 4.8608, \tag{4.4.51}$$

$$\mathrm{Nu}_{D_H,q''} = 0. \tag{4.4.52}$$

Equation (4.4.52) obviously corresponds to the adiabatic wall condition.

For a uniform wall temperature on both wall surfaces [Fig. 4.10(a)], which corresponds to UWT boundary conditions, it can be shown that

$$\mathrm{Nu}_{D_H,\mathrm{UWT}} = 7.5407. \tag{4.4.53}$$

The derivation of Eq. (4.4.53) does not consider axial conduction in the fluid, which is justifiable when $\mathrm{Pe} \gg 1$. As mentioned before, axial conduction in the fluid can be important at very low Pe, in particular in creep flow. The following asymptotic expressions, which are due to Pahor and Strand (1961), include the effect of axial conduction (Shah and London, 1978):

$$\mathrm{Nu}_{D,\mathrm{UWT}} = \begin{cases} 7.540\left(1 + \dfrac{3.79}{\mathrm{Pe}^2} + \cdots\right) & \text{for } \mathrm{Pe} \gg 5 \quad (4.4.54) \\ 8.118\,(1 - 0.031\mathrm{Pe} + \cdots) & \text{for } \mathrm{Pe} \ll 1 \quad (4.4.55) \end{cases}.$$

For the conditions displayed in Fig. 4.10(b), $\mathrm{Nu}_{D_H} = 4$ for either of the two surfaces, as long as axial conduction and viscous dissipation are ignored. When viscous

dissipation is considered, then, according to Cheng and Wu (1976) (Shah and London, 1978),

$$\mathrm{Nu}_{D_H,1} = \frac{4\,(1-6\mathrm{Br})}{1-\dfrac{48}{35}\mathrm{Br}}, \tag{4.4.56}$$

$$\mathrm{Nu}_{D_H,2} = \frac{4\,(1+6\mathrm{Br})}{1+\dfrac{48}{35}\mathrm{Br}}, \tag{4.4.57}$$

where subscripts 1 and 2 refer to surfaces with temperatures T_{s1} and T_{s2} and $T_{s1} > T_{s2}$ is assumed. The Brinkman number is defined as

$$\mathrm{Br} = \frac{2\mu\, U_m^2}{k\left(\dfrac{T_{s1}+T_{s2}}{2} - T_m\right)}. \tag{4.4.58}$$

4.4.3 Rectangular Channel

For a rectangular channel with sharp corners, when a constant heat flux q_s'' is imposed over the entire perimeter, the predictions of an analytical solution to the problem can be approximated within ±0.03% by the following correlation (Shah and London, 1978):

$$\mathrm{Nu}_{D_H,\mathrm{UHF}} = 8.235\left(1 - 2.0421\alpha^* + 3.0853\alpha^{*2} - 2.4765\alpha^{*3} + 1.0578\alpha^{*4} - 0.1861\alpha^{*5}\right). \tag{4.4.59}$$

Several other combinations of the boundary conditions are possible and are discussed in Shah and London (1978). For a prescribed uniform temperature at all four walls, i.e., the UWT boundary conditions, the following correlation approximates the numerical solution results within ±0.1% (Shah and Bhatti, 1987):

$$\mathrm{Nu}_{D_H,\mathrm{UWT}} = 7.541\left(1 - 2.61\alpha^* + 4.97\alpha^{*2} - 5.119\alpha^{*3} + 2.702\alpha^{*4} - 0.548\alpha^{*5}\right). \tag{4.4.60}$$

4.4.4 Triangular Channel

For an equilateral triangular channel with sharp corners, subject to the **(H1)** boundary conditions (i.e., axially constant wall heat flux and azimuthally constant wall temperature),

$$\mathrm{Nu}_{D_H,(\mathrm{H1})} = 28/9. \tag{4.4.61}$$

When volumetric energy generation and viscous dissipation are considered (Tyagi, 1966; Shah and London, 1978),

$$\mathrm{Nu}_{D_H,(\mathrm{H1})} = \frac{28}{9}\left[\frac{1}{1+\dfrac{1}{12}q_v^* + \dfrac{40}{11}\mathrm{Br}'}\right]. \tag{4.4.62}$$

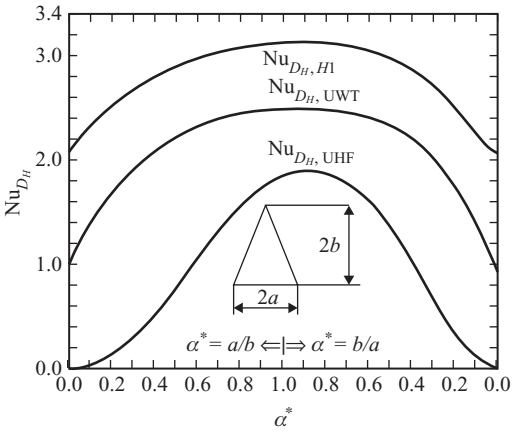

Figure 4.11. Nusselt numbers in isosceles triangular channels. $Nu_{D_H,(H1)}$ represents circumferentially constant wall temperature and axially constant wall heat flux (from Shah and London, 1978).

In the latter case, the fluid mean temperature varies according to

$$\dot{m}C_P \frac{dT_m}{dx} = 3aq_s'' + \frac{\sqrt{3}}{4}a^2\dot{q}_v + 20\sqrt{3}\mu U_m^2. \tag{4.4.63}$$

Furthermore, for an equilateral triangle,

$$\mathrm{Nu}_{D_H,\mathrm{UHF}} = 1.892, \tag{4.4.64}$$

$$\mathrm{Nu}_{D_H,\mathrm{UWT}} = 2.47. \tag{4.4.65}$$

Figure 4.11 displays Nusselt numbers for uniformly heated, as well as uniform wall temperature, isosceles rectangular channels.

Other combinations of boundary conditions are possible and are discussed in Shah and London (1978) and Shah and Bhatti (1987).

4.4.5 Concentric Annular Duct

The fully developed hydrodynamic aspects were discussed earlier in Section 4.3. With regard to heat transfer, a multitude of conditions may be considered, depending on whether the boundary conditions are a constant wall heat flux or a constant wall temperature on either or both of the channel walls. Because the energy equation is linear and homogenous, the superposition principle can be applied such that, for any permutation of the aforementioned boundary conditions, the solution can be presented in terms of the superposition of a few "fundamental" solutions. We subsequently discuss the case of hydrodynamically and thermally developed flow with constant-temperature or constant-heat-flux boundary conditions on both walls.

We define $r^* = R_i/R_0$ and assume that

$$T = T_i \quad \text{at } r = R_i,$$

$$T = T_0 \quad \text{at } r = R_0.$$

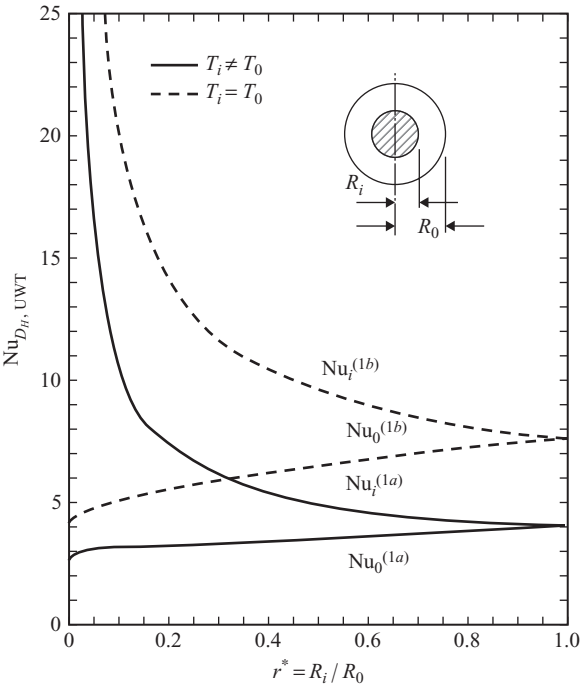

Figure 4.12. Fully developed Nusselt numbers for constant wall temperatures in concentric annuli (after Shah and Bhatti, 1987).

Also, we define

$$\mathrm{Nu}_i^{(1a)} = h_i D_H / k \quad \text{when} \quad T_i \neq T_0 \neq T_{\mathrm{in}}, \tag{4.4.66}$$

$$\mathrm{Nu}_0^{(1a)} = h_0 D_H / k \quad \text{when} \quad T_i \neq T_0 \neq T_{\mathrm{in}}, \tag{4.4.67}$$

$$\mathrm{Nu}_i^{(1b)} = h_i D_H / k \quad \text{when} \quad T_i = T_0 \neq T_{\mathrm{in}}, \tag{4.4.68}$$

$$\mathrm{Nu}_0^{(1b)} = h_0 D_H / k \quad \text{when} \quad T_i = T_0 \neq T_{\mathrm{in}}. \tag{4.4.69}$$

The values of these Nusselt numbers are plotted in Fig. 4.12 as functions of r^*. For the case $T_i{=}T_0{=}T_s$, namely the UWT boundary conditions,

$$\mathrm{Nu}_{D_H,\,\mathrm{UWT}} = \frac{\mathrm{Nu}_0^{(1b)} + \left(\dfrac{R_i}{R_0}\right)\mathrm{Nu}_i^{(1b)}}{1 + \left(\dfrac{R_i}{R_0}\right)} \tag{4.4.70}$$

Now we consider constant heat fluxes on both walls. We define

$$\mathrm{Nu}_{ii} = h_i D_H / k \quad \text{when} \quad q_i'' \neq 0, \quad q_0'' = 0, \tag{4.4.71}$$

$$\mathrm{Nu}_{00} = h_0 D_H / k \quad \text{when} \quad q_i'' = 0, \quad q_0'' \neq 0, \tag{4.4.72}$$

$$\mathrm{Nu}_i = h_i D_H / k \quad \text{when} \quad q_i'' \neq 0, \quad q_0'' \neq 0, \tag{4.4.73}$$

$$\mathrm{Nu}_0 = h_0 D_H / k \quad \text{when} \quad q_i'' \neq 0, \quad q_0'' \neq 0. \tag{4.4.74}$$

Table 4.1. *Fundamental solutions and influence coefficients for thermally developed flow in concentric annular ducts (after Lundberg et al., 1963, and Kays and Perkins, 1972)*

R_i/R_0	Nu_{ii}	Nu_{00}	θ_i^*	θ_0^*
0	∞	4.365	∞	0
0.05	17.81	4.792	2.18	0.0294
0.1	11.91	4.834	1.383	0.0562
0.2	8.499	4.883	0.905	0.1041
0.4	6.583	4.979	0.603	0.1823
0.6	5.912	5.099	0.473	0.2455
0.8	5.58	5.24	0.401	0.299
1	5.385	5.385	0.346	0.346

The solutions for Nu_{ii} and Nu_{00} as functions of r^* were obtained (Lundberg et al., 1963; Reynolds et al., 1963) and are tabulated extensively in heat transfer hand books (Shah and Bhatti, 1987; Ebadian and Dong, 1998). Table 4.1 is a brief summary. Knowing Nu_{ii} and Nu_{00}, we can now find Nu_i and Nu_0 by superposition:

$$\mathrm{Nu}_i = \frac{\mathrm{Nu}_{ii}}{1 - \left(q_0''/q_i''\right)\theta_i^*}, \tag{4.4.75}$$

$$\mathrm{Nu}_0 = \frac{\mathrm{Nu}_{00}}{1 - \left(q_i''/q_0''\right)\theta_0^*}, \tag{4.4.76}$$

where θ_i^* and θ_0^* are "influence coefficients"; their values are also tabulated in Table 4.1 (Kays and Perkins, 1972). These equations lead to the following expression for the temperature difference between the inner and outer surfaces:

$$T_i - T_0 = \frac{D_H}{k}\left[q_i''\left(\frac{1}{\mathrm{Nu}_{ii}} + \frac{\theta_0^*}{\mathrm{Nu}_{00}}\right) - q_0''\left(\frac{1}{\mathrm{Nu}_{00}} + \frac{\theta_i^*}{\mathrm{Nu}_{ii}}\right)\right]. \tag{4.4.77}$$

Note that in the preceding equations the heat flux is positive when it flows into the fluid. The heat flux ratio q_i''/q_0'' can be either positive or negative.

For the simpler UWT and UHF boundary conditions, Shah and Bhatti (1987) developed the following useful curve fits to the numerical calculation results. We define

$$r^* = R_i/R_0.$$

For $0 \le r^* \le 0.02$,

$$\mathrm{Nu}_{D_H,\mathrm{UWT}} = 3.657 + 98.95r^*, \tag{4.4.78}$$

$$\mathrm{Nu}_{D_H,\mathrm{UHF}} = 4.364 + 100.95r^*. \tag{4.4.79}$$

For $0.02 \le r^* \le 1$,

$$\mathrm{Nu}_{D_H,\mathrm{UWT}} = 5.3302\left(1 + 3.2904r^* - 12.0075r^{*2} + 18.8298r^{*3} - 9.6980r^{*4}\right), \tag{4.4.80}$$

$$\mathrm{Nu}_{D_H,\mathrm{UHF}} = 6.2066\left(1 + 2.3108r^* - 7.7553r^{*2} + 13.2851r^{*3} - 10.5987r^{*4} + 2.6178r^{*5} + 0.468r^{*6}\right). \tag{4.4.81}$$

Now we assume a constant-temperature condition on one wall and a constant heat flux on the other, namely,

$$T = T_1 \quad \text{at } r = R_1,$$
$$q_s'' = q_2'' \quad \text{at } r = R_2,$$

where R_1 or R_2 could be either the shorter or longer radii. In this case,

$$\mathrm{Nu}_i = \mathrm{Nu}_i^{(1a)}, \tag{4.4.82}$$
$$\mathrm{Nu}_0 = \mathrm{Nu}_0^{(1a)}. \tag{4.4.83}$$

The functions $\mathrm{Nu}_i^{(1a)}$ and $\mathrm{Nu}_0^{(1a)}$ are depicted in Fig. 4.12.

4.5 Fully Developed Hydrodynamics, Thermal or Concentration Entrance Regions

We may now focus on fully developed hydrodynamics and developing temperature and concentration profiles, with the boundary conditions either a uniform wall temperature, or equivalently for mass transfer, a uniform mass fraction of the transferred species adjacent to the wall. The case of constant wall heat flux is dealt with in Section 4.7.

The idealization of fully developed hydrodynamics is a good approximation even for combined thermal and hydrodynamic entrance problems in which $\mathrm{Pr} \gg 1$, e.g., for viscous liquids, because in this case the velocity boundary layer develops much faster than the thermal boundary layer. When $\mathrm{Pr} \leq 1$, e.g., for gases, however, this idealization can lead to considerable error for combined entrance problems.

A similar argument can be made for combined hydrodynamic and mass transfer channel flows. Thus, for $\mathrm{Sc} \gg 1$, which applies to the vast majority of problems dealing with mass transfer in liquids, the forthcoming solutions are good approximations to combined entrance problems. For diffusive mass transfer in gases, however, $\mathrm{Sc} \approx 1$, and the approximation will be poor.

4.5.1 Circular Duct With Uniform Wall Temperature Boundary Conditions

We now consider the development of the temperature profile in a circular channel with fully developed hydrodynamics, subject to a sudden change in the channel wall temperature, as shown in Fig. 4.13. This is the well-known Graetz's problem, a classical subject in heat transfer and applied mathematics that has been investigated extensively. Qualitatively, we expect the temperature profiles to develop as shown in Fig. 4.14. The development of mass fraction profiles in the mass transfer version of Graetz's problem would be similar.

The energy equation is

$$u\frac{dT}{dx} = \frac{\alpha}{r}\frac{\partial}{\partial r}\left(r\frac{\partial T}{\partial r}\right). \tag{4.5.1}$$

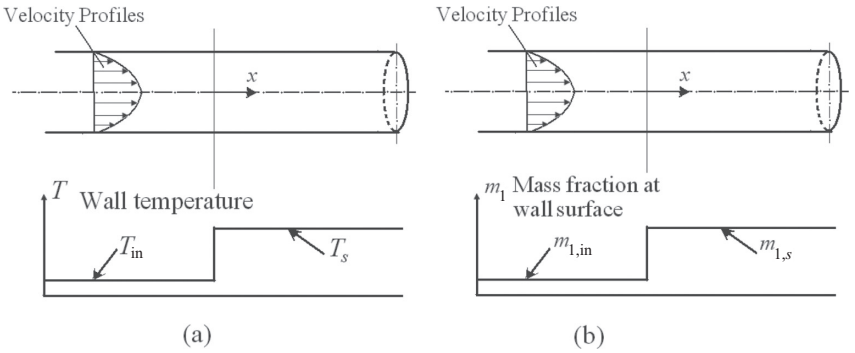

Figure 4.13. Graetz's problem: (a) heat transfer, (b) mass transfer.

The velocity profile follows Eq. (4.3.3). The boundary conditions for Eq. (4.5.1) are

$$T = T_{\text{in}} \quad \text{at } x = 0, \tag{4.5.2a}$$

$$\frac{\partial T}{\partial r} = 0 \quad \text{at } r = 0, \tag{4.5.2b}$$

$$T = T_s \quad \text{at } r = R_0 \text{ and } x > 0. \tag{4.5.2c}$$

Let us nondimensionalize the equations by using

$$\theta = \frac{T - T_s}{T_{\text{in}} - T_s}, \tag{4.5.3}$$

$$r^* = \frac{r}{R_0}, \tag{4.5.4}$$

$$x^* = \frac{x}{R_0 \text{Re}_D \,\text{Pr}}, \tag{4.5.5}$$

$$\text{Re}_D = \frac{2U_m R_0}{\nu}. \tag{4.5.6}$$

We then get

$$\frac{\partial \theta}{\partial x^*} = \frac{2}{r^* f(r^*)} \frac{\partial}{\partial r^*} \left(r^* \frac{\partial \theta}{\partial r^*} \right), \tag{4.5.7}$$

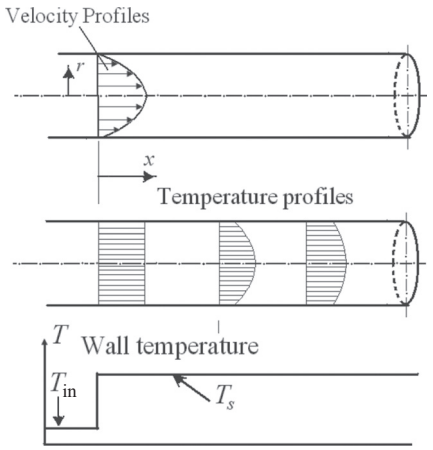

Figure 4.14. The development of fluid temperature profiles in Graetz's problem.

where

$$f(r^*) = \frac{u(r^*)}{U_m}. \tag{4.5.8}$$

For laminar flow we have

$$f(r^*) = 2\left(1 - r^{*2}\right). \tag{4.5.9}$$

The boundary conditions are

$$\theta = 1 \text{ at } x^* \leq 0, \tag{4.5.10}$$

$$\theta = 0 \text{ at } r^* = 1 \text{ and } x^* > 0, \tag{4.5.11}$$

$$\frac{\partial \theta}{\partial r^*} = 0 \text{ at } r^* = 0. \tag{4.5.12}$$

This is a linear and homogenous partial differential equation and can be solved by the method of separation of variables. We assume

$$\theta(r^*, x^*) = R(r^*)F(x^*). \tag{4.5.13}$$

Substitution into Eq. (4.5.7) and separation of the variables then leads to

$$\frac{F'}{F} = \frac{2\left(r^* R'' + R'\right)}{r^* f(r^*) R}. \tag{4.5.14}$$

The only way this equation and its boundary conditions can be satisfied is for both sides to be equal to a negative quantity, $-\lambda^2$. The x^*-dependent differential equation gives

$$F = C \exp\left(-\lambda^2 x^*\right). \tag{4.5.15}$$

The r^* – dependent differential equation is now

$$\left(r^* R_n'\right)' + \frac{1}{2}\lambda_n^2 \left[r^* f(r^*)\right] R_n = 0. \tag{4.5.16}$$

This equation, along with the boundary conditions in Eqs. (4.5.11) and (4.5.12), represent a Sturm–Liouville boundary value problem (see Appendix 4A). The general solution to Eq. (4.5.7) will then be

$$\theta = \sum_{n=0}^{\infty} C_n R_n(r^*) \exp\left(-\lambda_n^2 x^*\right), \tag{4.5.17}$$

where

$$C_n = \frac{\int_0^1 r^* f(r^*) R_n dr^*}{\int_0^1 r^* f(r^*) R_n^2 dr^*}. \tag{4.5.18}$$

The eigenvalues λ_n and the eigenfunctions R_n represent the solutions of Eq. (4.5.16).

Table 4.2. *Eigenvalues and constants for Graetz's problem (Bhatti and Shah, 1987)*

n	λ_n	C_n
0	2.70436	1.47643
1	6.67903	−0.80612
2	10.67338	0.58876
3	14.67107	−0.47585
4	18.66987	0.40502
5	22.66914	−0.35575
6	26.66866	0.31917
7	30.66832	−0.29074
8	34.66807	0.26789
9	38.66788	−0.24906
10	42.66773	0.23322

The functions R_n, with a weighting function $r^*(1 - r^{*2})$ are orthogonal in the $r^* = 0$–1 interval, such that (Skelland, 1974)

$$\int_0^1 R_j\,(r^*)\,[(1/2)\,r^*\,f\,(r^*)]\,dr^* = -\frac{1}{\lambda_j^2}\left(\frac{dR_j}{dr^*}\right)_{r^*=1}, \quad j \neq k, \tag{4.5.19}$$

$$\int_0^1 R_j\,(r^*)\,R_k\,(r^*)\,[(1/2)\,r^*\,f\,(r^*)]\,dr^* = \begin{cases} 0 \\ \dfrac{1}{2\lambda_j}\left[\dfrac{dR_j}{dr^*}\left(\dfrac{dR}{d\lambda}\right)_j\right]_{r^*=1}, \end{cases} \quad j = k\ . \tag{4.5.20}$$

We thus derive

$$C_n = -\frac{2}{\lambda_n\left(\dfrac{dR}{d\lambda}\right)_{n,\,r^*=1}}. \tag{4.5.21}$$

The first 11 eigenvalues and constants C_n for Graetz's problem are shown in Table 4.2, borrowed from Bhatti and Shah (1987). Table 4.3 depicts the values of the eigenfunctions R_n. For $n > 2$ one can use (Sellars et al., 1956)

$$\lambda_n \approx 4n + \frac{8}{3}, \tag{4.5.22}$$

$$C_n \approx \frac{(-1)^n(2.8461)}{\lambda_n^{2/3}}, \tag{4.5.23}$$

$$-C_n R_n'(1) = \frac{2.0256}{\lambda_n^{1/3}}. \tag{4.5.24}$$

One can then show that the average dimensionless temperature follows:

$$\theta_m = 2\int_0^1 \theta(r^*)r^* f(r^*)dr^* = 8\sum_0^\infty \frac{G_n}{\lambda_n^2}\exp\left(-\lambda_n^2 x^*\right) \tag{4.5.25}$$

Table 4.3. *Values of the eigenfunction $R_n(r^*)$ for Graetz's Problem (Brown, 1960; Larkin, 1961)*

n	$r^* = 0.2$	$r^* = 0.4$	$r^* = 0.5$	$r^* = 0.6$	$r^* = 0.8$
0	0.92889	0.73809	0.61460	0.48130	0.22426
1	0.60470	−0.10959	−0.34214	−0.43218	−0.28449
2	0.15247	−0.39208	−0.14234	0.16968	0.30272
3	−0.23303	0.06793	0.31507	0.11417	−0.29224
4	−0.40260	0.29907	−0.07973	−0.25523	0.25918
5	−0.32121	−0.04766	−0.20532	0.19750	−0.20893
6	−0.07613	−0.25168	0.19395	−0.01391	0.14716
7	0.17716	0.03452	0.05514	−0.15368	−0.07985
8	0.29974	0.22174	−0.20502	0.19303	0.01298
9	0.23915	−0.02483	0.08126	−0.09176	0.04787
10	0.04829	−0.20058	0.13289	−0.06474	−0.09797

where

$$G_n = -\frac{1}{2} C_n \left.\frac{dR_n}{dr^*}\right|_{r^*=1} = \frac{2.0256}{2\lambda_n^{1/3}}. \tag{4.5.26}$$

Also, using

$$\mathrm{Nu}_{D,\mathrm{UWT}}(x^*) = \frac{2R_0 \left(k \dfrac{\partial T}{\partial r}\right)_{r=R_0}}{k(T_s - T_m)},$$

One can show that

$$\mathrm{Nu}_{D,\mathrm{UWT}}(x^*) = \frac{\displaystyle\sum_{n=0}^{\infty} G_n \exp\left(-\lambda_n^2 x^*\right)}{2\displaystyle\sum_{n=0}^{\infty} \frac{G_n}{\lambda_n^2} \exp\left(-\lambda_n^2 x^*\right)}. \tag{4.5.27}$$

It can also be shown that

$$\langle \mathrm{Nu}_{D,\mathrm{UWT}} \rangle_{x^*} = -\frac{\ln \theta_m(x^*)}{2x^*}. \tag{4.5.28}$$

Thermally-developed flow occurs when $\mathrm{Nu}_{D,\mathrm{UWT}}(x^*)$ asymptotically approaches a constant. Calculations show that thermally-developed flow occurs when $x^* > 0.1$. Only the first term in the series will be significant for this large value of x^*, and we will have

$$\mathrm{Nu}_{D,\mathrm{UWT}}(x^*) = \mathrm{Nu}_{D,\mathrm{UWT}}(\infty) = \frac{1}{2}\lambda_0^2 = 3.657. \tag{4.5.29}$$

This expression is of course identical to the result obtained with fully-developed velocity and temperature profiles. Thus, the thermal entrance length will then be,

$$\frac{l_{\mathrm{ent,th}}}{D} \approx 0.05 \mathrm{Re}_D \mathrm{Pr}. \tag{4.5.30}$$

Lévêque Solution

The infinite series solution to Graetz's problem converges fast for large x^* values, thus requiring few terms. For very small values of x^*, however, the convergence is slow, and a multitude of terms would be necessary. For $x^* < 10^{-4}$, we can derive a simple solution very close to the inlet where the thermal (or mass transfer) boundary layer is very thin by assuming that the velocity profile across the thermal boundary layer (or concentration boundary layer) is linear. The solution that is derived this way is useful for fluids with $\mathrm{Pr} \gg 1$, for which the thermal boundary layer remains thin over a long distance from inlet. The solution will be even more useful for mass transfer in liquids, where Sc is typically quite large.

Starting from Eq. (4.5.1), and given that we are interested in the near wall zone where $\frac{r}{R_0} \ll 1$, we can write

$$u\frac{\partial T}{\partial x} \approx \boldsymbol{\alpha}\frac{\partial^2 T}{\partial y^2}, \tag{4.5.31}$$

where y is the distance from the wall. Furthermore,

$$u = 2\,U_m\left[1 - \left(\frac{r}{R_0}\right)^2\right] \approx B_v\,y, \tag{4.5.32}$$

where $B_v = 4U_m/R_0$ is the velocity gradient near the wall. The energy equation then reduces to

$$B_v y\frac{\partial T}{\partial x} = \boldsymbol{\alpha}\frac{\partial^2 T}{\partial y^2}. \tag{4.5.33}$$

We assume $\theta = \frac{T-T_m}{T_s-T_m} = \theta\,(\eta)$, where

$$\eta = \frac{y}{C}x^{-1/3}, \tag{4.5.34}$$

$$C = \left[\frac{9\boldsymbol{\alpha}}{B_v}\right]^{1/3}. \tag{4.5.35}$$

Equation (4.5.33) then reduces to

$$\theta'' + 3\eta^2\theta' = 0. \tag{4.5.36}$$

The boundary conditions are

$$\theta = 1 \quad \text{at } \eta = 0, \tag{4.5.37}$$

$$\theta = 0 \quad \text{at } \eta = \infty. \tag{4.5.38}$$

The solution to the preceding equation is

$$\theta = 1 - \frac{\displaystyle\int_0^{\eta} \exp(-\eta'^3)d\eta'}{\displaystyle\int_0^{\infty} \exp(-\eta'^3)d\eta'}. \tag{4.5.39}$$

It can easily be shown that

$$\int_0^{\infty} \exp(-\eta'^3)d\eta' = \frac{1}{3}\Gamma\left(\frac{1}{3}\right), \tag{4.5.40}$$

where Γ is the gamma function:

$$\Gamma(\xi) = \int_0^\theta t^{\xi-1}\exp(-t)dt, \tag{4.5.41}$$

We thus get

$$\theta = 1 - \frac{1}{\frac{1}{3}\Gamma\left(\frac{1}{3}\right)}\int_0^\eta \exp(-\eta'^3)d\eta' = 1 - 1.119\int_0^\eta \exp(-\eta'^3)d\eta'. \tag{4.5.42}$$

This leads to

$$\mathrm{Nu}_{D,\,\mathrm{UWT}}(x) = \frac{q_s''(2R_0)}{k(T_s - T_m)} \approx \frac{q_s''(2R_0)}{k(T_s - T_{\mathrm{in}})} = 1.077\left(\frac{2R_0}{x}\right)^{1/3}(\mathrm{Re}_D\,\mathrm{Pr})^{1/3}. \tag{4.5.43}$$

Mass Transfer

The mass transfer equivalent of Graetz's problem is schematically shown in Fig. 4.13(b), where laminar and hydrodynamically fully developed flow is underway and the diffusive transport of species 1 is assumed to be governed by Fick's law. Up to the axial location $x = 0$, the mass fraction of the transferred species 1 is uniform and equal to $m_{1,\mathrm{in}}$. The wall boundary condition is changed to a constant mass fraction for the transferred species at the wall. The transport equation for species 1 is then

$$u\frac{\partial m_1}{\partial x} = \frac{\mathcal{D}_{12}}{r}\frac{\partial}{\partial r}\left(r\frac{\partial m_1}{\partial r}\right), \tag{4.5.44}$$

where, at $x = 0$, $m_1 = m_{1,\mathrm{in}}$, at $r = 0$, at $r = R_0$, and for $x > 0$, $m_1 = m_{1,\mathrm{s}}$:

$$\begin{aligned} m_1 &= m_{1,in} \quad \text{at } x = 0,\\ \partial m_1/\partial r &= 0 \quad \text{at } r = 0,\\ m_1 &= m_{1,s} \quad \text{at } r = R_0 \text{ and for } x > 0. \end{aligned}$$

Now we define $\phi = \frac{m_1 - m_{1,s}}{m_{1,\mathrm{in}} - m_{1,s}}$. Also, we define dimensionless coordinates as $r^* = \frac{r}{R_0}$ and $x^* = \frac{x}{R_0 \mathrm{Re}_D \mathrm{Sc}} = \frac{x}{R_0 \mathrm{Pe}_{\mathrm{ma}}}$, where the mass transfer Peclet number is defined as $\mathrm{Pe}_{\mathrm{ma}} = \mathrm{ReSc}$. The species mass conservation equation and its boundary conditions are then identical to Eqs. (4.5.7)–(4.5.12) if everywhere θ is replaced with ϕ.

The solution then leads to

$$\mathrm{Sh}_{D,\,\mathrm{UWM}}(x^*) = \frac{\mathcal{K}(2R_0)}{\rho\mathcal{D}_{12}} = \frac{\sum_{n=0}^{\infty} G_n \exp\left(-\lambda_n^2 x^*\right)}{2\sum_{n=0}^{\infty}\frac{G_n}{\lambda_n^2}\exp\left(-\lambda_n^2 x^*\right)}, \tag{4.5.45}$$

where

$$m_{1,\,s}'' = \mathcal{K}(m_{1,\,s} - m_{1,\,m}).$$

It is emphasized that the preceding expression is valid when the total mass flux through the wall surface is vanishingly small.

Similar to the heat transfer case, only the first term in the series is important for $x^* > 0.1$, whereby

$$\mathrm{Sh}_{D,\,\mathrm{UWM}}(x^*) = \mathrm{Sh}_{D,\,\mathrm{UWM}}(\infty) = \frac{1}{2}\lambda_0^2 = 3.657. \tag{4.5.46}$$

The mass transfer entrance length then corresponds to $x^* = 0.1$, leading to

$$l_{\mathrm{ent,ma}} \approx 0.05 \mathrm{Re}_D Sc. \tag{4.5.47}$$

The equivalent Lévêque's problem for mass transfer applies to the conditions shown in Fig. 4.13(b) for very small values of x^*. Assuming low mass transfer conditions and an incompressible, constant-property mixture, the transport equation for the transferred species 1 will be

$$B_v y \frac{\partial m_1}{\partial x} = \mathcal{D}_{12} \frac{\partial^2 m_1}{\partial y^2}. \tag{4.5.48}$$

We now define $\phi = \frac{m_1 - m_{1,m}}{m_{1,s} - m_{1,m}} = \phi(\eta')$, where η' is found from Eq. (4.5.34), but C is replaced with C', where

$$C' = \left[\frac{9\mathcal{D}_{12}}{B_v}\right]^{1/3}. \tag{4.5.49}$$

The dimensionless form of Eq. (4.5.48) and its boundary conditions are then the same as Eqs. (4.5.36)–(4.5.38), when everywhere θ is replaced with ϕ. The solution of these equations then gives

$$\begin{aligned}\mathrm{Sh}_{D,\,\mathrm{UWM}}(x) &= \frac{m''_{1,s}(2R_0)}{\rho\mathcal{D}_{12}(m_{1,s} - m_{1,m})} \approx \frac{m''_{1,s}(2R_0)}{\rho\mathcal{D}_{12}(m_{1,s} - m_{1,\mathrm{in}})} \\ &= 1.077\left(\frac{2R_0}{x}\right)^{1/3}(\mathrm{Re}_D \mathrm{Sc})^{1/3}.\end{aligned} \tag{4.5.50}$$

4.5.2 Circular Duct With Arbitrary Wall Temperature Distribution in the Axial Direction

Graetz's solution provides us with the fluid temperature response (and thereby wall heat transfer coefficient or Nusselt number) to a step change in wall temperature. In view of the fact that the thermal energy conservation equation for constant-property fluids, in the absence of dissipation, is linear and homogeneous, Graetz's solution can be used to calculate the response to any arbitrary wall temperature distribution and even to a finite number of step changes in the wall temperature (Tribus and Klein, 1953; Sellars et al., 1956). This can be done by using the superposition principle.

Consider the displayed system in Fig. 4.15. Let us assume a step change, from T_{in} to T_s, taking place in a wall temperature at location ξ^*. According to Graetz's solution, the fluid temperature at point (x^*, r^*) will be

$$\frac{T(x, y) - T_s}{T_{\mathrm{in}} - T_s} = \theta(y^*, r^*), \;\; y^* = x^* - \xi^*, \tag{4.5.51}$$

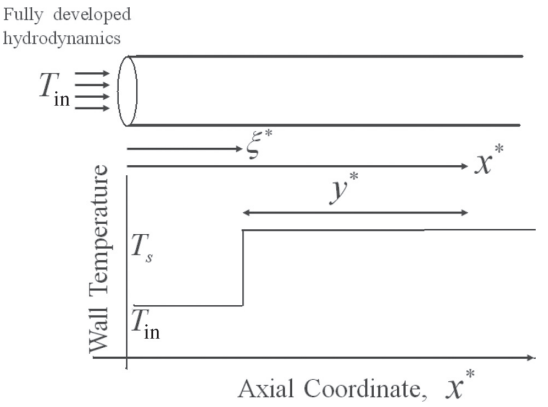

Figure 4.15. Wall temperature step change in a hydrodynamically fully developed pipe flow.

where θ is Graetz's solution [see Eq. (4.5.17)]:

$$\theta = \sum_{n=0}^{\infty} C_n R_n(r^*) \exp\left(-\lambda_n^2 y^*\right). \tag{4.5.52}$$

If the step change at ξ^*, instead of being $T_s - T_{in}$, is only an infinitesimal amount $d(T_s - T_{in})$, Eq. (4.5.51) gives, for the point (x^*, r^*),

$$dT = [1 - \theta(x^* - \xi^*, r^*)]\, dT_s. \tag{4.5.53}$$

This is the change in the temperature of the fluid at (x^*, r^*), resulting from an infinitesimal change in wall temperature by dT_s at location ξ^*. If, instead of dT_s, we had ΔT_s, we would get

$$\Delta T = [1 - \theta(x^* - \xi^*, r^*)]\, \Delta T_s. \tag{4.5.54}$$

Now, by using superposition, we can find the response of $T(x^*, r^*)$ to any arbitrary distribution of wall temperature by applying $\int_{\xi^*=0}^{x^*}$ to both sides of Eq. (4.5.53), noting that $T = T_{in}$ at $\xi^* = 0$:

$$T - T_{in} = \int_0^{x^*} [1 - \theta(x^* - \xi^*, r^*)] \left(\frac{dT_s}{d\xi^*}\right) d\xi^* + \sum_{i=1}^{N} [1 - \theta(x^* - \xi_i^*, r^*)] \Delta T_{s,i}, \tag{4.5.55}$$

where N is the number of finite wall temperature step changes. Thus $dT_s/d\xi^*$ is the slope of the arbitrary wall temperature distribution.

Having found the fluid temperature distribution, we can now calculate the wall heat flux q_s'' at x^* from

$$q_s''(x^*) = \left(\frac{k}{R_0}\right)\left(\frac{\partial T}{\partial r^*}\right)_{r^*=1}. \tag{4.5.56}$$

We now solve this along with Eq. (4.5.55), bearing in mind that

$$\left(\frac{\partial \theta}{\partial r^*}\right)_{r^*=1} = \sum_{n=0}^{\infty} C_n \left(\frac{\partial R_n}{\partial r^*}\right)_{r^*=1} \exp\left(-\lambda_n^2 x^*\right) = -2 \sum_{n=0}^{\infty} G_n \exp\left(-\lambda_n^2 x^*\right), \tag{4.5.57}$$

where values of $G_n = -\frac{1}{2} C_n \left(\frac{\partial R_n}{\partial r^*}\right)_{r^*=1}$ were tabulated earlier. We then can show that, for an arbitrary wall temperature T_s profile with N finite step changes in the

wall temperature,

$$q_s''(x^*) = -\left(\frac{k}{R_0}\right)\left\{\int_0^{x^*}\left[-2\sum_{n=0}^{\infty} G_n \exp\left[-\lambda_n^2(x^* - \xi^*)\right]\right]\left(\frac{dT_s}{d\xi^*}\right)d\xi^* - 2\sum_{i=1}^{N}\Delta T_{s,i}\sum_{n=0}^{\infty} G_n \exp\left[-\lambda_n^2(x^* - \xi_i^*)\right]\right\}. \tag{4.5.58}$$

Note that Eqs. (4.5.55) and (4.5.58) are quite general. For the simple case of only one finite jump in T_s occurring at $x^* = \xi^* = 0$, followed by a continuous T_w profile, we have

$$q_s''(x^*) = \left(-\frac{k}{R_0}\right)\left\{\int_0^{x^*}\left[-2\sum_{n=0}^{\infty} G_n \exp\left[-\lambda_n^2(x^* - \xi^*)\right]\right]\left(\frac{dT_s}{dx^*}\right)d\xi^* - 2\left(T_s - T_{\text{in}}\right)_{x^*=0}\sum_{n=0}^{\infty} G_n \exp\left(-\lambda_n^2 x^*\right)\right\}. \tag{4.5.59}$$

For a linear wall temperature distribution, $dT_s/d\xi^*$ can be replaced with a constant. Using these equations, we can get a formula for the Nusselt number at x^*. First, let us perform an overall energy balance to get T_m at x^*:

$$\pi R_0^2 \rho\, U_m\left(T_m - T_{\text{in}}\right) = 2\pi R_0 \int_0^x q_s''\, dx. \tag{4.5.60}$$

With T_m found, we can then find the heat transfer coefficient from

$$h|_{x^*} = \left(\frac{q_s''}{T_s - T_m}\right)_{x^*}. \tag{4.5.61}$$

The equivalent mass transfer problem can be easily developed, whereby the local mass fractions of a transferred species *i,* as well as the wall mass flux of that species in response to an arbitrary longitudinal distribution of the mass fraction of the transferred species at the fluid–wall interface, can be found (see Problem 4.33).

4.5.3 Circular Duct With Uniform Wall Heat Flux

Let us first consider the case of constant wall heat flux, namely, the UHF boundary condition. The problem is a modification of Graetz's problem, often referred to as the *extended Graetz problem*, in which, referring to Fig. 4.14, the boundary condition now represents a constant heat flux for $x \geq 0$.

Let us define the dimensionless temperature as

$$\theta = \frac{T - T_{\text{in}}}{\left(\frac{2q_s'' R_0}{k}\right)}. \tag{4.5.62}$$

The energy equation is the same as Eq. (4.5.7), where $r^* = \frac{r}{R_0}$, $x^* = \frac{x}{R_0 \text{Re}_D \,\text{Pr}}$, and $f(r^*) = 2(1 - r^{*2})$ for laminar flow. The boundary conditions, however, are now, $\theta(0, r^*) = 0$,

$$\partial\theta\left(x^*, 1\right)/\partial r^* = 1/2 \text{ and } \frac{\partial\theta}{\partial r^*}\left(x^*, 0\right) = 0.$$

Let us use the superposition principle and cast the solution as

$$\theta = \theta_1 + \theta_2, \tag{4.5.63}$$

where θ_1 represents the thermally developed solution to the problem and θ_2 is the entrance region solution. For θ_1 we have

$$\frac{\partial \theta_1}{\partial x^*} = \frac{2}{r^* f(r^*)} \frac{\partial}{\partial r^*} \left(r^* \frac{\partial \theta_1}{\partial r^*} \right), \tag{4.5.64}$$

with boundary conditions

$$\begin{aligned} \theta_1(0, r^*) &= 0, \\ \frac{\partial \theta_1 (x^*, r^*)}{\partial r^*} &= \frac{1}{2} \quad \text{at } r^* = 1, \\ \frac{\partial \theta_1 (x^*, r^*)}{\partial r^*} &= 0 \quad \text{at } r^* = 0. \end{aligned}$$

The thermally developed part has already been solved, and the solution [Eq. (4.4.8c)] can be cast in terms of the dimensionless parameters here as

$$\theta_1 = 2x^* + \left[\frac{1}{2} r^{*2} - \frac{1}{8} r^{*4} - \frac{7}{48} \right]. \tag{4.5.65}$$

For the entrance region part we can write

$$\frac{\partial \theta_2}{\partial x^*} = \frac{2}{r^* f(r^*)} \frac{\partial}{\partial r^*} \left(r^* \frac{\partial \theta_2}{\partial r^*} \right). \tag{4.5.66}$$

The separation-of-variables technique can be applied, which leads to Eqs. (4.5.13)–(4.5.16). The boundary conditions for Eq. (4.5.66) are

$$\frac{\partial \theta_2 (x^*, r^*)}{\partial r^*} = 0 \quad \text{at } r^* = 1, \tag{4.5.67}$$

$$\frac{\partial \theta_2 (x^*, r^*)}{\partial r^*} = 0 \quad \text{at } r^* = 0, \tag{4.5.68}$$

$$\theta_2 (0, r^*) = - \left[\frac{1}{2} r^{*2} - \frac{1}{8} r^{*4} - \frac{7}{48} \right]. \tag{4.5.69}$$

Note that the last boundary condition is required because $\theta_1(0, r^*) + \theta_2(0, r^*) = 0$. Siegel et al. (1958) solved this eigenvalue problem to get

$$\theta = \frac{T - T_{\text{in}}}{\left(\dfrac{2q_s'' R_0}{k} \right)} = 2x^* + \frac{1}{2} r^{*2} - \frac{1}{8} r^{*4} - \frac{7}{48} + \frac{1}{2} \sum_{n=1}^{\infty} C_n R_n(r^*) \exp(-2\beta_n^2 x^*), \tag{4.5.70}$$

with β_n, R_n, and C_n representing the eigenvalues, eigenfunctions, and constants. Values of these for $n = 1, 2, \ldots, 20$ can be found in Table 4.4 (Hsu, 1965). Obviously,

$$\theta_m = \frac{T_m - T_{\text{in}}}{\left(\dfrac{2q_s'' R_0}{k} \right)} = 2x^*. \tag{4.5.71}$$

Table 4.4. *The eigenvalues and constants for Eq. (4.5.70)*

n	C_n	β_n^2	$R_n(1)$
1	0.4034832	25.67961	−0.4925166
2	−0.1751099	83.86175	0.3955085
3	0.1055917	174.16674	−0.3458737
4	−0.0732824	296.5363	0.31404646
5	0.05503648	540.9472	−0.2912514
6	−0.04348435	637.38735	0.2738069
7	0.03559508	855.84953	−0.2598529
8	−0.02990845	1106.32903	0.2483319
9	0.0256401	1388.8226	−0.2385902
10	−0.02233368	1703.3278	0.2301990
11	0.01970692	2049.8430	−0.2228628
12	−0.01757646	2438.3668	0.2163703
13	0.01581844	2838.8981	−0.2105659
14	−0.01434637	3281.4362	0.2053319
15	0.01309817	3755.9803	−0.200577

Siegel et al. (1958) also derived

$$\mathrm{Nu}_{D,\mathrm{UHF}}(x^*) = \left(\frac{1}{\theta_s - \theta_m}\right) = \left[\frac{11}{48} + \frac{1}{2}\sum_{n=1}^{\infty} C_n R_n(1) \exp\left(-2\beta_n^2 x^*\right)\right]^{-1}. \quad (4.5.72)$$

Algebraic correlations that predict the preceding results and the results from the Lévêque analysis (for x^* very small) with very good approximation are provided by Shah and London (1978). Accordingly,

$$\mathrm{Nu}_{D,\mathrm{UHF}}(x^*) = 1.302\left(\frac{x^*}{2}\right)^{-1/3} - 1 \text{ for } \left(\frac{x^*}{2}\right) < 5 \times 10^{-5}, \quad (4.5.73)$$

$$\mathrm{Nu}_{D,\mathrm{UHF}}(x^*) = 1.302\left(\frac{x^*}{2}\right)^{-1/3} - 0.5 \text{ for } 5 \times 10^{-5} \le \left(\frac{x^*}{2}\right) \le 1.5 \times 10^{-3}, \quad (4.5.74)$$

$$\mathrm{Nu}_{D,\mathrm{UHF}}(x^*) = 4.364 + 8.68\left(10^3 \frac{x^*}{2}\right)^{-0.506} \exp\left(-\frac{41x^*}{2}\right) \text{ for } \left(\frac{x^*}{2}\right) > 1.5 \times 10^{-3}. \quad (4.5.75)$$

These correlations are accurate to within ± 1% (Shah and Bhatti, 1987).

In the equivalent mass transfer problem, a constant and small mass flux of an inert transferred species 1 takes place at the wall at $x > 0$. The species transport equation will be similar to Eq. (4.5.44), with the following boundary conditions:

$$\partial m_1/\partial r = 0 \text{ at } r = 0 \text{ and } x > 0,$$
$$\rho \mathcal{D}_{12} \frac{\partial m_1}{\partial r} = m''_{1,s} \text{ at } r = R_0.$$

A normalized mass fraction is then defined as

$$\phi = \frac{m_1 - m_{1,\mathrm{in}}}{\dfrac{m''_{1,s} D}{\rho \mathcal{D}_{12}}}. \quad (4.5.76)$$

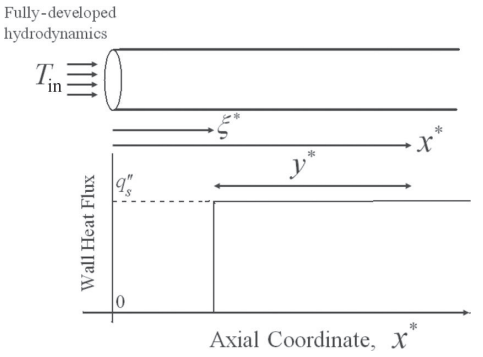

Figure 4.16. Wall heat flux step change in a hydrodynamically fully developed flow.

The coordinates are also nondimensionalized as $r^* = \frac{r}{R_0}$ and $x^* = \frac{x}{R_0 \mathrm{Re}_D \mathrm{Sc}} = \frac{x}{R_0 \mathrm{Pe}_{\mathrm{ma}}}$, where the mass transfer Peclet number is defined as $Pe_{\mathrm{ma}} = \mathrm{ReSc}$. The dimensionless mass-species conservation equation and its boundary conditions are then

$$\begin{aligned} \frac{\partial \phi}{\partial x^*} &= \frac{2}{r^* f(r^*)} \frac{\partial}{\partial r^*}\left(r^* \frac{\partial \phi}{\partial r^*}\right), \\ \phi\,(0, r^*) &= 0 \\ \frac{\partial \phi\,(x^*,\, r^*)}{\partial r^*} &= 0 \quad \text{at } r^* = 0, \\ \frac{\partial \phi\,(x^*,\, r^*)}{\partial r^*} &= \frac{1}{2} \quad \text{at } r^* = 1. \end{aligned} \tag{4.5.77}$$

The solution then leads to

$$\phi_m = \frac{m_{1,m} - m_{1,\mathrm{in}}}{\left(\dfrac{m_{1,s}'' D}{\rho \mathcal{D}_{12}}\right)} = 2x^*, \tag{4.5.78}$$

$$\mathrm{Sh}_{D,\mathrm{UMF}}(x^*) = \left[\frac{11}{48} + \frac{1}{2}\sum_{n=1}^{\infty} C_n R_n(1) \exp\left(-2\beta_n^2 x^*\right)\right]^{-1}. \tag{4.5.79}$$

Equations (4.5.73)–(4.5.75) are all applicable when everywhere $\mathrm{Nu}_{D,\mathrm{UHF}}(x^*)$ is replaced with $\mathrm{Sh}_{D,\mathrm{UMF}}(x^*)$ and it is borne in mind that x^* is now defined as $x^* = \frac{x}{R_0 \mathrm{Pe}_{\mathrm{ma}}}$.

4.5.4 Circular Duct With Arbitrary Wall Heat Flux Distribution in the Axial Coordinate

We now discuss the case of an arbitrary wall heat flux distribution. Again, utilizing the linear and homogeneous nature of the thermal energy equation, we can use superposition.

From Eq. (4.5.70), the response of fluid temperature at (x^*, r^*) to a finite step in wall heat flux from zero to q_s'' taking place at ξ^* (see Fig. 4.16) is

$$(T - T_{\mathrm{in}})_{x^*, r^*} = \frac{2r_0}{k}\, q_s''\big|_{\xi^*}\, \theta(x^* - \xi^*, r^*), \tag{4.5.80}$$

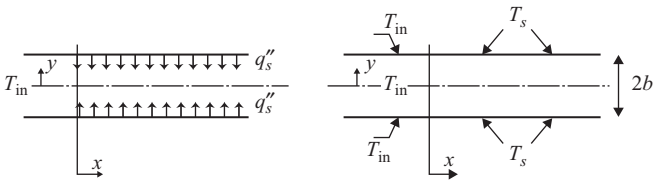

(a) UHF (b) UWT

Figure 4.17. Thermally developing flow in a flat channel.

where $\theta^*(x^* - \xi^*, r^*)$ is the right-hand side of Eq. (4.5.70) when x^* is replaced with $x^* - \xi^*$ everywhere in that equation. The response to an infinitesimally small heat flux, dq_s'', is

$$dT = \frac{2R_0}{k}\, dq_s''\big|_{\xi^*}\, \theta(x^* - \xi^*, r^*). \tag{4.5.81}$$

Thus, by applying $\int_{\xi^*=0}^{x^*}$ to both sides, we get

$$(T - T_{\text{in}})\big|_{x^*,r^*} = \frac{2R_0}{k}\int_0^{x^*} \theta(x^* - \xi^*, r^*)\frac{dq_s''}{d\xi^*}d\xi^* + \frac{2R_0}{k}\sum_{i=1}^{N} \Delta q_{s,i}''\theta(x^* - \xi_i^*, r^*). \tag{4.5.82}$$

Using Eq. (4.5.82), we can find the wall temperature and $\text{Nu}_{D,\text{UHF}}(x^*)$ for any arbitrary distribution that is piecewise continuous.

4.5.5 Flat Channel With Uniform Heat Flux Boundary Conditions

We now consider the problem displayed in Fig. 4.17(a).

We define the dimensionless temperature as

$$\theta = \frac{T - T_{\text{in}}}{\dfrac{q_s'' D_H}{k}}. \tag{4.5.83}$$

The energy equation can then be cast as

$$\frac{3}{32}\left(1 - \eta^2\right)\frac{\partial\theta}{\partial x^*} = \frac{\partial^2\theta}{\partial\eta^2}, \tag{4.5.84}$$

where $\eta = y/b$ and $x^* = \frac{x}{D_H \text{Re}_{D_H}\text{Pr}}$. The boundary conditions are

$$\theta = 0 \quad \text{at } x^* = 0, \tag{4.5.85}$$

$$\frac{\partial\theta}{\partial\eta} = 0 \quad \text{at } \eta = 0, \tag{4.5.86}$$

$$\frac{\partial\theta}{\partial\eta} = \frac{1}{4} \quad \text{at } \eta = 1. \tag{4.5.87}$$

We proceed by writing

$$\theta = \theta_1 + \theta_2, \tag{4.5.88}$$

where θ_1 is the solution to the thermally developed problem and θ_2 is the remainder of the solution. The thermally developed part has already been solved in Section 4.4

Table 4.5. *Eigenvalues and constants for the thermally developing flow in a flat channel with UHF boundary conditions (Sparrow et al., 1963)*

n	C_n	λ_n	$R_n(1)$
1	0.17503	4.287224	−1.2697
2	−0.051727	8.30372	1.4022
3	0.025053	12.3106	−1.4916
4	−0.014924	16.3145	1.5601
5	0.0099692	20.3171	−1.6161
6	−0.0072637	24.3189	1.6638
7	0.0054147	28.3203	−1.7054
8	−0.0042475	32.3214	1.7425
9	0.0034280	36.3223	−1.7760
10	−0.0028294	40.3231	1.8066

[Eqs. (4.4.29)–(4.4.39)], where T_{ref} should be replaced with T_{in}. From Eq. (4.4.39) we can thus write

$$\theta_1 = 4x^* + \frac{3}{16}\eta^2 - \frac{1}{32}\eta^4 - \frac{39}{1120}, \tag{4.5.89}$$

$$\theta_m = 4x^*. \tag{4.5.90}$$

The remainder of the solution, θ_2, must now satisfy

$$\frac{3}{32}\left(1-\eta^2\right)\frac{\partial\theta_2}{\partial x^*} = \frac{\partial^2\theta_2}{\partial\eta^2}, \tag{4.5.91}$$

$$\frac{\partial\theta_2}{\partial\eta} = 0 \quad \text{at } \eta = 0, \tag{4.5.92}$$

$$\frac{\partial\theta_2}{\partial\eta} = 0 \quad \text{at } \eta = 1, \tag{4.5.93}$$

$$\theta_2 = -\left[\frac{3}{16}\eta^2 - \frac{1}{32}\eta^4 - \frac{39}{1120}\right] \quad \text{at } x^* = 0. \tag{4.5.94}$$

This is a Sturm–Liouville boundary value problem and can be solved by the separation-of-variables techniques. Details of the solution can be found in Cess and Shaffer (1959) and Sparrow et al. (1963). The outcome of the solution is

$$\theta = 4x^* + \frac{3}{16}\eta^2 - \frac{1}{32}\eta^4 - \frac{39}{1120} + \frac{1}{4}\sum_{n=1}^{\infty} C_n R_n(\eta)\exp\left(-\frac{32}{3}\lambda_n^2 x^*\right), \tag{4.5.95}$$

$$\text{Nu}_{D_H,\,\text{UHF}}(x^*) = \left[\frac{17}{140} + \frac{1}{4}\sum_{n=1}^{\infty} C_n R_n(1)\exp\left(-\frac{32}{3}\lambda_n^2 x^*\right)\right]^{-1}, \tag{4.5.96}$$

where λ_n and $(R_n(\eta)$ are the eigenvalues and eigenfunctions; they are listed in Table 4.5 (Sparrow et al., 1963). For higher-order eigenvalues, eigenfunctions, and

C_n, Cess and Shaffer (1959) derived the following asymptotic relations:

$$\lambda_n \approx 4n + \frac{1}{3}, \tag{4.5.97}$$

$$R_n(1) = (-1)^n (0.97103)\,\lambda_n^{1/6}, \tag{4.5.98}$$

$$C_n \approx (-1)^{n+1} (2.4727)\,\lambda_n^{-11/6}. \tag{4.5.99}$$

The solution of the preceding equations shows that the thermal entrance length, defined based on $\mathrm{Nu}_{D_H,\mathrm{UHF}}(x^*)$ approaching the thermally developed value of 140/17 within 5%, is

$$\frac{l_{\mathrm{ent,th,UHF}}}{D_H} \approx 0.0115439 \mathrm{Re}_{D_H} \mathrm{Pr}. \tag{4.5.100}$$

For thermally developed conditions, furthermore, $\mathrm{Nu}_{D_H,fd} = 140/17 \approx 8.235$.

Shah developed the following correlations that reproduce the results of the exact analytical solution within better than ±1% (Shah and London, 1978):

$$\mathrm{Nu}_{D_H,\mathrm{UHF}}(x^*) = \begin{cases} 1.490\,(x^*)^{-1/3} \quad \text{for } x^* \le 0.0002 & (4.5.101) \\ 1.490\,(x^*)^{-1/3} - 0.4 \ \text{ for } 0.0002 < x^* \le 0.001 & (4.5.102) \\ 8.235 + 8.68\left(10^3 x^*\right)^{-0.506} \exp(-164x^*) \ \text{ for } x^* > 0.001 & (4.5.103) \end{cases}, \tag{4.5.102}$$

$$\left\langle \mathrm{Nu}_{D_H,\mathrm{UHF}} \right\rangle_x = \begin{cases} 2.236\,(x^*)^{-1/3} \quad \text{for } x^* \le 0.001 & (4.5.104) \\ 2.236\,(x^*)^{-1/3} + 0.9 \ \text{ for } 0.001 < x^* \le 0.01. & (4.5.105) \\ 8.235 + 0.0364/x^* \ \text{ for } x^* > 0.01 & (4.5.106) \end{cases}$$

The equivalent mass transfer problem leads to Eqs. (4.5.95) and (4.5.96) for the mass-fraction distribution and mass transfer coefficient, respectively, provided that θ is replaced with ϕ, T is replaced with m_1, and $\mathrm{Nu}_{D_H,\mathrm{UHF}}(x^*)$ is replaced with $\mathrm{Sh}_{D_H,\mathrm{UMF}}(x^*)$, where now

$$x^* = \frac{x}{D_H \mathrm{Re}_{D_H} \mathrm{Sc}}, \quad \phi = \frac{m - m_{1,\mathrm{in}}}{\left(\dfrac{m''_{1,s} D_H}{\rho \mathcal{D}_{12}}\right)}, \quad \mathrm{Sh}_x = \frac{m''_{1,s} D_H}{\rho \mathcal{D}_{12} (m_{1,s} - m_{1,m})}$$

The aforementioned discussion about the eigenvalues and eigenfunctions all apply. The mass transfer entrance length will also follow:

$$\frac{l_{\mathrm{ent,ma,UMF}}}{D_H} \approx 0.0115 \mathrm{Re}_{D_H} \mathrm{Sc}. \tag{4.5.107}$$

Equations (4.5.101)–(4.5.106) are all applicable when everywhere Nu is replaced with Sh.

4.5.6 Flat Channel With Uniform Wall Temperature Boundary Conditions

Consider the case of UWT boundary conditions [see Fig. 4.17(b)]. We deal here with Graetz's problem in a 2D channel. We define $\theta = \frac{T - T_s}{T_{\mathrm{in}} - T_s}$. The energy equation will be the same as Eq. (4.5.91) with the following boundary conditions:

$$\theta = 0 \quad \text{at } \eta = 1, \tag{4.5.108}$$

$$\frac{\partial \theta}{\partial \eta} = 0 \quad \text{at } \eta = 1, \tag{4.5.109}$$

$$\theta = 1 \quad \text{at } x^* = 0, \tag{4.5.110}$$

where $\eta = y/b$, $x^* = \frac{x}{D_H \mathrm{Re}_{D_H} \mathrm{Pr}}$, and $\mathrm{Re}_{D_H} = \rho U_m D_H/\mu$. The system represented by these equations can be solved by the separation-of-variables technique, and that leads to

$$\theta = \sum_{n=1}^{\infty} C_n R_n(\eta) \exp\left(-\frac{32}{3}\lambda_n^2 x^*\right), \tag{4.5.111}$$

where λ_n and $R_n(\eta)$ are the eigenvalues and eigenfunctions associated with

$$\frac{d^2 R_n}{d\eta^2} + \lambda_n^2 \left(1-\eta^2\right) R_n = 0, \tag{4.5.112}$$

$$R_n(1) = 0, \tag{4.5.113}$$

$$\left.\frac{dR_n}{d\eta}\right|_{\eta=1} = 0. \tag{4.5.114}$$

The constants C_n are found from

$$C_n = \left[\int_0^1 R_n \left(1-\eta^2\right) d\eta \Big/ \int_0^1 R_n^2 \left(1-\eta^2\right) d\eta\right]. \tag{4.5.115}$$

The local wall heat flux can then be found from

$$\frac{q_s'' D_H}{k\left(T_{\mathrm{in}} - T_s\right)} = 4\sum_{n=1}^{\infty} C_n R_n'(1) \exp\left(-\frac{32}{3}\lambda_n^2 x^*\right). \tag{4.5.116}$$

It can also be shown that

$$\theta_m = 3\sum_{n=1}^{\infty} \frac{G_n}{\lambda_n^2} \exp\left(-\frac{32}{3}\lambda_n^2 x^*\right), \tag{4.5.117}$$

$$\mathrm{Nu}_{D_H,\mathrm{UWT}}(x^*) = \frac{q_s'' D_H}{k(T_s - T_{\mathrm{m}})} = \frac{8}{3}\frac{\sum_{n=1}^{\infty} G_n \exp\left(-\frac{32}{3}\lambda_n^2 x^*\right)}{\sum_{n=1}^{\infty} \frac{G_n}{\lambda_n^2} \exp\left(-\frac{32}{3}\lambda_n^2 x^*\right)}, \tag{4.5.118}$$

$$\left\langle \mathrm{Nu}_{D_H} \right\rangle_x = \frac{1}{4x^*} \ln\left(\frac{1}{\theta_m\left(x^*\right)}\right), \tag{4.5.119}$$

where

$$G_n = -(C_n/2) R_n'(1). \tag{4.5.120}$$

Table 4.6 displays the first 10 eigenvalues and their corresponding constants (Sparrow et al., 1963). For the remainder of eigenvalues, Sellars et al. (1956) derived

$$\lambda_n \approx 4n + \frac{5}{3}, \tag{4.5.121}$$

$$C_n \approx (-1)^n (2.28)\, \lambda_n^{-7/6}, \tag{4.5.122}$$

$$-C_n R_n'(1) = 2.025 \lambda_n^{-1/3}. \tag{4.5.123}$$

The preceding solution indicates that

$$\frac{l_{\mathrm{ent,th,UWT}}}{D_H} \approx 0.00797 \mathrm{Re}_{D_H} \mathrm{Pr}. \tag{4.5.124}$$

Table 4.6. *Eigenvalues and constants for the thermally developing flow in a flat channel with UWT boundary conditions (Sparrow et al., 1963)*

n	C_n	λ_n	$R_n'(1)$
1	1.200830	1.6816	−1.4292
2	−0.29916	5.6699	3.8071
3	0.160826	9.6682	−5.9202
4	−0.107437	13.6677	7.8925
5	0.079646	17.6674	−9.7709
6	−0.062776	21.6672	11.5798
7	0.051519	25.6671	−13.3339
8	0.043511	29.6670	15.0430
9	0.037542	33.6670	−16.7141
10	0.032933	37.6669	18.3525

In the thermally developed conditions we have $\mathrm{Nu}_{D_H} = 7.541$.

The preceding series solutions are not convenient for very small x^* (e.g., $x^* \leq 10^{-3}$), in which a large number of terms in the series are needed. For $x^* \ll 1$, however, we note that the thermal boundary layer is extremely thin, and the local velocity distribution in the thermal boundary layer is approximately a linear function of the distance from the wall. Lévêque's solution method, described earlier, can then be applied, and that leads to

$$\theta = \frac{T - T_s}{T_{\text{in}} - T_s} = \frac{1}{\Gamma\left(\frac{4}{3}\right)} \int_0^X \exp\left(-x'^3\right) dx', \tag{4.5.125}$$

where

$$X = \frac{1 - \left(\frac{y}{b}\right)}{2(6x^*)^{1/3}}. \tag{4.5.126}$$

$$\mathrm{Nu}_{D_H,\mathrm{UWT}}(x^*) = \frac{2}{\Gamma(4/3)\,(6x^*)^{1/3}}. \tag{4.5.127}$$

The following correlations approximate the aforementioned exact solutions within better than ±3% (Shah and London, 1978).

$$\mathrm{Nu}_{D_H,\mathrm{UWT}}(x^*) = \begin{cases} 1.233\,(x^*)^{-1/3} + 0.4 \quad \text{for } x^* \leq 0.001 & , \quad (4.5.128) \\ 7.541 + 6.874(10^3 x^*)^{-0.488} \exp(-245x^*) \quad \text{for } x^* > 0.001 & (4.5.129) \end{cases}$$

$$\left\langle \mathrm{Nu}_{D_H,\mathrm{UWT}} \right\rangle_x = \begin{cases} 1.849\,(x^*)^{-1/3} \quad \text{for } x^* \leq 0.0005 & (4.5.130) \\ 1.849\,(x^*)^{-1/3} + 0.6 \quad \text{for } 0.0005 < x^* \leq 0.006, & (4.5.131) \\ 7.541 + \dfrac{0.0235}{x^*} \quad \text{for } x^* > 0.006 & (4.5.132) \end{cases}$$

where $\mathrm{Nu}_{D_H,\mathrm{UWT}}(x^*)$ is the local Nusselt number and $\langle \mathrm{Nu}_{D_H,\mathrm{UWT}} \rangle_x$ is the average Nusselt numbers over the length x.

Table 4.7. *Local Nusselt number in rectangular ducts for fully developed hydrodynamics and thermally developing flow with UWT boundary conditions*

$1/x^*$	$\alpha^* = 1$	$\alpha^* = 0.5$	$\alpha^* = 0.2$	$\alpha^* = 1/6$
0	2.975	3.39	4.92	5.22
10	2.86	3.43	4.94	5.24
20	3.08	3.54	5.04	5.34
30	3.24	3.70	5.31	5.41
60	3.78	4.16	5.40	5.64
80	4.10	4.46	5.62	5.86
100	4.35	4.72	5.83	6.07
140	4.85	5.15	6.26	6.47
180	5.24	5.54	6.63	6.86

In the equivalent mass transfer problem we deal with the solution of

$$\frac{3}{32}\left(1-\eta^2\right)\frac{\partial \phi}{\partial x^*} = \frac{\partial^2 \phi}{\partial \eta^2}, \tag{4.5.133}$$

with the following boundary conditions:

$$\begin{aligned} \phi &= 0 \quad \text{at } \eta = 1, \\ \frac{\partial \phi}{\partial \eta} &= 0 \quad \text{at } \eta = 1, \\ \phi &= 1 \quad \text{at } x^* = 0, \end{aligned}$$

where $x^* = \frac{x}{D_H \mathrm{Re}_{D_H} \mathrm{Sc}}$ and $\phi = \frac{m_1 - m_{1,s}}{m_{1,\mathrm{in}} - m_{1,s}}$. The aforementioned derivations and correlations, including Eqs. (4.5.127)–(4.5.132), are then all applicable when everywhere Nu is replaced with Sh.

4.5.7 Rectangular Channel

The solutions for rectangular channels depend on the duct cross-section aspect ratio. Table 4.7 displays the solution results of Wibulswan (1966) for the UWT boundary condition.

For a square channel subject to axially uniform heat flux and peripherally uniform temperature (i.e., the **H1** boundary conditions), the following correlation was proposed by Perkins et al. (1973) (Shah and London, 1978):

$$\mathrm{Nu}_{D_H,\text{H1}}(x^*) = \frac{1}{0.277 - 0.152\exp\left(-38.6x^*\right)}. \tag{4.5.134}$$

Useful information about developing flow in these and other channel geometries can be found in Shah and London (1978) and Shah and Bhatti (1987).

4.6 Combined Entrance Region

We now consider the simultaneous development of velocity and thermal (or concentration) boundary layers in a laminar internal flow.

The relevance of the solutions and correlations discussed in Section 4.5 depends on the magnitude of Pr for heat transfer and Sc for mass transfer, because these parameters determine the relative pace of the development of the boundary layers. When $Pr \gg 1$ (or when $Sc \gg 1$ for mass transfer), the velocity boundary layer develops much faster than the thermal (or concentration) boundary layer [see Fig. 4.3(c) or 4.4(b)]. In these cases we can assume, as an approximation, that the flow is hydrodynamically fully developed everywhere. The solutions and correlations discussed in Section 4.5 can then be applied. For the limit of $\mathrm{Pr} \to \infty$ (or $\mathrm{Sc} \to \infty$ for mass transfer) the solutions of the previous section are precisely applicable.

The solutions and correlations of the previous section can lead to considerable error when $\mathrm{Pr} \lesssim 1$ (or when $\mathrm{Sc} \lesssim 1$ for mass transfer), however. With $\mathrm{Pr} \simeq 1$ the velocity and thermal boundary layers develop at the same pace, and with $\mathrm{Pr} < 1$ the thermal boundary layer in fact develops slower than the velocity boundary layer.

For circular tubes, Churchill and Ozoe (1973a, 1973b) derived the following correlations for the local Nusselt numbers, which are applicable for $0.1 \leq \mathrm{Pr} \leq 1000$:

$$\frac{\mathrm{Nu}_{D,\,\mathrm{UHF}}(x^*) + 1.0}{5.364\left[1 + (\mathrm{Gz}/55)^{10/9}\right]^{3/10}} = \left\{1 + \left(\frac{\mathrm{Gz}/28.8}{\left[1 + (\mathrm{Pr}/0.0207)^{2/3}\right]^{1/2}\left[1 + (\mathrm{Gz}/55)^{10/9}\right]^{3/5}}\right)^{5/3}\right\}^{3/10}, \quad (4.6.1)$$

$$\frac{\mathrm{Nu}_{D,\,\mathrm{UWT}}(x^*) + 1.7}{5.357\left[1 + (\mathrm{Gz}/97)^{8/9}\right]^{3/8}} = \left\{1 + \left(\frac{\mathrm{Gz}/71}{\left[1 + (\mathrm{Pr}/0.0468)^{2/3}\right]^{1/2}\left[1 + (\mathrm{Gz}/97)^{8/9}\right]^{3/4}}\right)^{4/3}\right\}^{3/8}, \quad (4.6.2)$$

where $\mathrm{Gz} = \frac{\pi}{4x^*}$ is the Graetz number, $x^* = \frac{x}{D\,\mathrm{Re}_D\,\mathrm{Pr}}$, and the length scale for the Nusselt numbers is the tube diameter.

For flow in flat channels (flow between two flat plates), Stephan (1959) derived the following correlation as a curve fit to some numerical calculations:

$$\left\langle \mathrm{Nu}_{D,UWT} \right\rangle_x = 7.55 + \frac{0.024\,(x^*)^{-1.14}}{1 + 0.0358\,\mathrm{Pr}^{0.17}\,(x^*)^{-0.64}}. \quad (4.6.3)$$

By differentiating the preceding equation with respect to x^*, the local Nusselt number can be represented as (Shah and Bhatti, 1987)

$$\mathrm{Nu}_{D_H,\mathrm{UWT}}(x^*) = 7.55 + \frac{0.024\,(x^*)^{-1.14}\left[0.0179\,\mathrm{Pr}^{0.17}\,(x^*)^{-0.64} - 0.14\right]}{\left[1 + 0.0358\,\mathrm{Pr}^{0.17}\,(x^*)^{-0.64}\right]^2}. \quad (4.6.4)$$

Muzychka and Yovanovich (2004) noted that, by using the square root of the flow cross-sectional area, $\sqrt{A}$, as the length scale, a correlation applicable to several cross-sectional geometries, for UWT and UHF both, could be developed.

Table 4.8. *Parameters for the correlation of Muzychka and Yovanovich (2004)*

Boundary Condition		
UWT	$C_1 = 3.24,\ C_3 = 0.409$	$f(\mathrm{Pr}) = \dfrac{0.564}{\left[1 + \left(1.644\,\mathrm{Pr}^{1/6}\right)^{9/2}\right]^{2/9}}$
UHF	$C_1 = 3.86,\ C_3 = 0.501$	$f(\mathrm{Pr}) = \dfrac{0.886}{\left[1 + \left(1.909\,\mathrm{Pr}^{1/6}\right)^{9/2}\right]^{2/9}}$
Nusselt Number Type		
Local	$C_2 = 1,\ C_4 = 1$	
Average	$C_2 = \dfrac{3}{2},\quad C_4 = 2$	

(They used a similar argument and approach for hydrodynamically fully developed and thermally developing flow, which was discussed earlier.) They thus proposed

$$\mathrm{Nu}_{\sqrt{A}} = \left[\left[\frac{C_4\, f(\mathrm{Pr})}{\sqrt{x^*}}\right]^m + \left\{\left[C_2 C_3 \left(\frac{C_f \mathrm{Re}_{\sqrt{A}}}{x^*}\right)^{1/3}\right]^5 + \left[C_1 \left(\frac{C_f \mathrm{Re}_{\sqrt{A}}}{8\sqrt{\pi}(\alpha^*)^\gamma}\right)\right]^5\right\}^{m/5}\right]^{1/m}, \tag{4.6.5}$$

where the *blending parameter m* is found from

$$m = 2.27 + 1.65\ \mathrm{Pr}^{1/3}. \tag{4.6.6}$$

The parameters used in Eq. (4.6.5) are summarized in Table 4.8. The parameter γ, called the shape factor, varies in the $-3/10$ to $1/10$ range. For rectangle and ellipsoid channel cross sections, $\gamma = 1/10$. For rhombus, isosceles, and right triangles, $\gamma = -3/10$. In comparison with exact solutions, the preceding correlation results in errors typically smaller than 25%. We can easily write the mass transfer equivalent of these correlations by applying the analogy between heat and mass transfer. We do this by everywhere replacing Nu with Sh and Pr with Sc. It is important to remember, however, that the following conditions must be met for the analogy to work: Mass transfer rates should be small, and Pr and Sc must have similar magnitudes.

4.7 Effect of Fluid Property Variations

Accounting for the dependence of fluid properties on temperature in numerical analysis is relatively straightforward, even though it often adds considerably to the computational cost.

For engineering calculations, however, the common practice has been to utilize the constant-property solutions when such solutions are available, but to correct their predictions for property-variation effects by use of one of the following two methods:

1. Use a reference temperature and find the properties at that temperature.
2. Use a property ratio-correction function for adjusting the results of the constant property analytical solutions.

From the latter approach, Kays et al. (2005) recommend the following. For liquids, use

$$\frac{C_f}{C_{f,m}} = \left(\frac{\mu_s}{\mu_m}\right)^m, \tag{4.7.1}$$

$$\frac{\mathrm{Nu}}{\mathrm{Nu}_m} = \left(\frac{\mu_s}{\mu_m}\right)^n, \tag{4.7.2}$$

where μ_s and μ_m represent the fluid viscosity at T_s and T_m, respectively; Nu_m is the constant-property Nusselt number based on properties that are all found at T_m; and for liquids

$$\begin{aligned} m &= 0.5 \quad \text{for cooling} \quad (\mu_s > \mu_m), \\ m &= 0.58 \quad \text{for heating} \quad (\mu_s < \mu_m), \\ n &= -0.14. \end{aligned}$$

For gases, Equations (4.7.1) and (4.7.2) are used, this time with

$$\begin{aligned} n &= 0, \\ m &= 1. \end{aligned}$$

EXAMPLE 4.1. A flat channel with $b = 2.5$ mm and a heated length of $l = 1.30$ m is subjected to a constant wall heat flux over a part of its length. A Newtonian liquid ($\rho = 753$ kg/m^3, $C_P = 2.09$ kJ/kg K, $k = 0.137$ W/m K, and $\mu = 6.61 \times 10^{-4}$ N s/m^2) flows through the duct with a mass flow rate of 0.25 kg/s per meter of channel width. The average fluid temperatures at inlet and exit of the heated segment are 20 C and 80 C, respectively.

(a) Assume that at the entrance to the heated section the fluid velocity and temperature profiles are both uniform. Determine the heat transfer coefficient and wall surface temperature at the exit of the heated section.

(b) Now assume that at the entrance to the heated section the flow is hydrodynamically fully developed but has a uniform temperature. Calculate the wall surface temperature at 8 mm downstream from the entrance to the heated section.

SOLUTION. First, let us find the heat flux by performing an energy balance on the heated channel:

$$\begin{aligned} q_s'' &= \frac{\dot{m} C_P \left(T_{m,\mathrm{exit}} - T_{\mathrm{in}}\right)}{2l} = \frac{(0.25\,\mathrm{kg/s\ m})\,(2090\,\mathrm{J/kg\ ^\circ C})\,(80-20)^\circ\mathrm{C}}{2\,(1.3\ \mathrm{m})} \\ &= 12{,}058\,\mathrm{W/m^2}. \end{aligned}$$

Next, we calculate the Prandtl number and mean velocity and from there the Reynolds number:

$$\mathrm{Pr} = \mu C_P / k = \frac{(6.61 \times 10^{-4}\ \mathrm{kg/m\ s})(2090\,\mathrm{J/kg\ ^\circ C})}{0.137\,\mathrm{W/m\ ^\circ C}} = 10.08,$$

$$U_m = \frac{\dot{m}}{2\rho b} = \frac{(0.25\ \mathrm{kg/s\ m})}{2(753\ \mathrm{kg/m^3})(2.5 \times 10^{-3}\ \mathrm{m})} = 0.0664\,\mathrm{m/s},$$

$$\mathrm{Re}_{D_H} = \frac{\rho U_m D_H}{\mu} = \frac{\left(753\ \mathrm{kg/m^3}\right)(0.0664\ \mathrm{m/s})\left(4 \times 2.5 \times 10^{-3}\ \mathrm{m}\right)}{6.61 \times 10^{-4}\ \mathrm{kg/m\ s}} = 756.4.$$

The flow is clearly laminar.

Part (a). We can also estimate the entrance length from Eq. (4.5.100) to determine whether using a thermally developed flow correlation would be appropriate. Equation (4.5.100) is actually for the thermal entrance length when the flow is hydrodynamically fully developed, but here we are interested in a rough estimate:

$$l_{\text{ent,th,UHF}} \approx 0.0115 \text{Re}_{D_H} \text{Pr}\, D_H = 0.0115 \times 756.4 \times 10.08 \times (4 \times 2.5 \times 10^{-3}\ \text{m}) = 0.8805\ \text{m}.$$

Because $l > l_{\text{ent,th,UHF}}$, the application of a thermally developed correlation is justifiable. Therefore, from Eq. (4.5.96),

$$\text{Nu}_{D_H} = 140/17 \approx 8.235$$
$$h_{\text{exit}} = \text{Nu}_{D_H} k/D_H = 8.235(0.137\ \text{W/m}\,^\circ\text{C})/(4 \times 2.5 \times 10^{-3}\ \text{m}) = 112.8\ \text{W/m}^2\,^\circ\text{C}.$$

We can now find the surface temperature at the exit by writing

$$T_{s,\text{exit}} = T_{m,\text{exit}} + q_s''/h_{\text{exit}} = 80\,^\circ\text{C} + \frac{12,058\ \text{W/m}^2}{112.8\ \text{W/m}^2\,^\circ\text{C}} = 186.8\,^\circ\text{C}.$$

Part (b). We can use the curve fits in Eqs. (4.5.101)–(4.5.106), whichever is applicable. Therefore,

$$x^* = \frac{x}{D_H \text{Re}_{D_H} \text{Pr}} = \frac{0.008\ \text{m}}{(4 \times 2.5 \times 10^{-3}\ \text{m})\,(378.2)\,(10.08)} = 0.000105,$$
$$\text{Nu}_{D_H,\text{UHF}}(x^*) = 1.490\,(x^*)^{-1/3} - 0.4 = 1.490\,(0.000105)^{-1/3} - 0.4 = 31.2,$$
$$h = \text{Nu}_{D_H,\text{UHF}}(x^*) k/D_H = 31.2 \times (0.137\ \text{W/m}\,^\circ\text{C})/(4 \times 2.5 \times 10^{-3}\ \text{m}) = 427.4\ \text{W/m}^2\,^\circ\text{C},$$
$$T_m = T_{\text{in}} + \frac{2q_s'' x}{\dot{m} C_p} = 20 + \frac{2(12,058\ \text{W/m}^2)\,(0.008\ \text{m})}{(0.25\ \text{kg/s m})\,(2090\ \text{J/kg}\,^\circ\text{C})} = 20.4\,^\circ\text{C},$$
$$T_s = T_m + q_s''/h = 20.4\,^\circ\text{C} + \frac{12,058\ \text{W/m}^2}{427.4\ \text{W/m}^2\,^\circ\text{C}} = 48.6\,^\circ\text{C}.$$

EXAMPLE 4.2. Atmospheric air at a temperature of 300 K flows through a short pipe segment. The diameter of the pipe segment is 5 cm, and its length is 2.0 cm. The air Reynolds number defined based on the pipe diameter is 1000. The pipe segment's surface temperature is 400 K.

(a) Calculate the heat transfer coefficient halfway through the pipe segment by approximating the flow on the pipe surface as the flow on a flat plate.
(b) Assume that the pipe segment is actually a segment of a long pipe. The segment is preceded by a long adiabatic segment in which hydrodynamic fully developed conditions are obtained by air before it enters the segment whose wall surface temperature is 400 K. Calculate the heat transfer coefficient halfway through the pipe segment by using Lévêque's solution.

SOLUTION. First, let us find properties of air at $T_\infty = 300\,\text{K}$:

$$\rho = 1.177\,\text{kg/m}^3,\ C_P = 1005\,\text{J/kgK},\ k = 0.02565\,\text{W/m K},$$
$$\mu = 1.857 \times 10^{-5}\ \text{kg/m s},\ \text{Pr} = 0.7276.$$

Part (a). We can use Eq. (3.2.32a) for calculating the local Nusselt number. First we need the mean velocity, which we can use as U_∞ in the aforementioned correlation:

$$U_\infty = U_m = \mathrm{Re}_D \frac{\mu}{\rho D} = (1000)\frac{1.857 \times 10^{-5}\ \text{kg/m s}}{(1.177\ \text{kg/m}^3)(0.05\ \text{m})} = 0.3157\ \text{m/s}.$$

Then,

$$\begin{aligned}
\mathrm{Re}_x &= \rho U_\infty x/\mu = (1.177\ \text{kg/m}^3)(0.3157\ \text{m/s})(0.01\ \text{m})/1.857 \times 10^{-5}\ \text{kg/m s} \\
&= 200, \\
\mathrm{Nu_x} &= 0.332\mathrm{Pr}^{1/3}\,\mathrm{Re}_x^{1/2} = (0.332)\,(0.7276)^{1/3}\,(200)^{1/2} = 4.22, \\
h_x &= \mathrm{Nu}_x \frac{k}{x} = 4.22\frac{0.02565\ \text{W/m K}}{0.01\ \text{m}} = 10.82\ \text{W/m}^2\ \text{K}.
\end{aligned}$$

Part (b). We now use Eq. (4.5.43) to get

$$\begin{aligned}
\mathrm{Nu}_{D,\,\mathrm{UWT}}(x) &\approx 1.077\left(\frac{2R_0}{x}\right)^{1/3}(\mathrm{Re}_D\,\mathrm{Pr})^{1/3} \\
&= 1.077\left(\frac{0.05\ \text{m}}{0.01\ \text{m}}\right)^{1/3}(1000 \times 0.7276)^{1/3} = 16.56, \\
h_{x,\mathrm{Leveq}} &= \mathrm{Nu}_{D,\,\mathrm{UWT}}(x)\frac{k}{D} = 16.56\frac{0.02565\ \text{W/m K}}{0.05\ \text{m}} \approx 8.5\ \text{W/m}^2\ \text{K}.
\end{aligned}$$

EXAMPLE 4.3. In an experiment, mercury at a local mean (bulk) temperature of 30 °C flows through a horizontal pipe whose diameter is 1 cm with a mass flow rate of 0.02 kg/s. The wall surface temperature is constant at 70 °C. The flow can be assumed to be thermally developed. Calculate the heat transfer coefficient by assuming negligible axial conduction in mercury. Repeat the solution, this time accounting for the effect of axial conduction.

SOLUTION. First, let us use properties of saturated liquid mercury at 50 °C:

$$\begin{aligned}
&\rho = 13{,}506\ \text{kg/m}^3;\ C_P = 139\ \text{J/kg K},\ k = 9.4\ \text{W/m K}; \\
&\nu = 0.104 \times 10^{-6}\ \text{m}^2/\text{s};\ \mathrm{Pr} = 0.021.
\end{aligned}$$

We can now calculate the mean velocity, and from there the Reynolds number:

$$\begin{aligned}
U_m &= \frac{\dot{m}}{\rho\frac{\pi}{4}D^2} = \frac{0.02\ \text{kg/s}}{(13{,}506\ \text{kg/m}^3)\frac{\pi}{4}(0.01\ \text{m}^2)} = 0.01885\ \text{m/s}, \\
\mathrm{Re}_D &= U_\infty D/\nu = (0.01885\ \text{m/s})(0.01\text{m})/0.104 \times 10^{-6}\ \text{m}^2/\text{s} = 1813, \\
\mathrm{Pe} &= \mathrm{Re}_D\,\mathrm{Pr} = (1{,}813)(0.021) = 38.07.
\end{aligned}$$

Neglecting the effect of axial conduction in the fluid and assuming thermally developed flow, we have,

$$h = (3.6568)\,(9.4\ \text{W/m K})/(0.01\ \text{m}) = 3437\ \text{W/m}^2\ \text{K}.$$

We now repeat the calculation of the heat transfer coefficient by accounting for the effect of axial conduction in the fluid. From Eq. (4.4.25),

$$\mathrm{Nu}_{D,\mathrm{UWT}} \approx 3.6568\left(1+\frac{1.227}{\mathrm{Pe}^2}\right) = 3.6568\left[1+\frac{1.227}{(38.07)^2}\right] = 3.66$$
$$\Rightarrow h \approx 3440\ \mathrm{W/m^2\ K}.$$

The effect of axial conduction in the fluid on the heat transfer coefficient is evidently negligibly small.

Appendix 4A: The Sturm–Liouville Boundary-Value Problems

Consider the following differential equation and boundary conditions on the interval $a \le x \le b$:

$$\frac{d}{dx}\left[p(x)\frac{d\phi}{dx}\right] + [q(x) + \lambda s(x)]\phi = 0, \tag{4A.1}$$
$$a_1\phi(a) + a_2\phi'(a) = 0, \tag{4A.2}$$
$$b_1\phi(b) + b_2\phi'(b) = 0, \tag{4A.3}$$

where $p(x)$, $p'(x)$, $q(x)$, and $s(x)$ are real and continuous for $a \le x \le b$; $p(x) > 0$; and a_1, a_2, b_1, and b_2 are all constants. According to the Sturm–Liouville theorem, the differential equation has nontrivial solutions only for certain, real values of λ_n (the eigenvalues) for $n = 1,\ 2,\ 3, \ldots, \infty$. The solutions (eigenfunctions) $\phi_n(x)$ and $\phi_m(x)$ are orthonormal to each other with respect to the weighting function $s(x)$ if $m \ne n$, so that,

$$\int_a^b s(x)\,\phi_m(x)\,\phi_n(x) = 0 \quad \text{when } m \ne n. \tag{4A.4}$$

The complete solution to the differential equation will be

$$y(x) = \sum_{n=1}^{\infty} C_n\phi_n(x), \tag{4A.5}$$

where

$$C_n = \frac{\int_a^b s(x)\ y(x)\,\phi_n(x)\,dx}{\int_a^b s(x)\ [\phi_n(x)]^2\,dx}. \tag{4A.6}$$

If the eigenvalues are numbered in order, i.e., $\lambda_1^2 < \lambda_2^2 < \lambda_3^2, \ldots$, then $\phi_n(x)$, the eigenfunction corresponding to λ_n, will have $n-1$ zeros in the $a < x < b$ interval.

PROBLEMS

Problem 4.1. In a journal bearing, the diameter of the shaft is 12 cm and the diameter of the sleeve is 12.04 cm. The bearing is lubricated by an oil with the following properties:

$\mathrm{Pr} = 10;\ \rho = 753\ \mathrm{kg/m^3};\ C_P = 2.1\ \mathrm{kJ/kg\ K};\ \mathrm{k} = 0.137\ \mathrm{W/m\ K};\ \mu = 6.6 \times 10^{-4}\ \mathrm{Pa\ s}.$

For a shaft rotational speed of 1100 RPM (revolutions per minute), with no load, measurements show that the temperature drop across the lubricant oil layer is 18 °C, and the sleeve surface temperature is 20 °C. For these operating conditions,

(a) calculate the shaft torque,
(b) find the total viscous dissipation rate and the total heat transfer rate through the journal bearing.

Problem 4.2. Consider laminar and thermally developed flow of a constant-property fluid in a channel with UHF boundary condition. By performing a scaling analysis, show that Nu_{D_H} must be of the order of 1.

Problem 4.3. Consider Problem 1.8. Solve the conservation equations for the described boundary conditions and derive expressions for the velocity and temperature profiles.

Problem 4.4. Two infinitely large parallel plates form a flat channel whose axial coordinate makes an angle of ϕ with respect to the vertical plane (see Fig. P4.4). A liquid flows through the channel. The pressure gradient in the flow direction is negligible and the flow is caused by the gravitational effect.

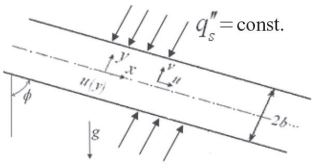

Figure P4.4.

(a) Assuming steady and laminar flow, derive expressions for the velocity profile and the total mass flow rate per unit width of the flat channel.
(b) Assuming UHF boundary conditions, derive an expression for the wall heat transfer coefficient.
(c) Assume that the liquid is water at room temperature and atmospheric pressure, $\phi = 60^\circ$, and $b = 1.5$ mm. Calculate the total mass flow rate per unit depth, in kilograms per meter per seconds and the wall heat transfer coefficient in watts per square meter times per Centigrade, and the axial gradient of the mean liquid temperature.

Problem 4.5. Consider a thermally developed laminar flow of an incompressible and constant-property fluid in a flat channel with UHF boundary conditions. Assume slug flow, i.e., a flat velocity profile across the channel ($u = U$ everywhere). Prove that

$$\mathrm{Nu}_{D_H} = 12.$$

Problem 4.6 Consider a fully developed laminar flow of an incompressible and constant-property fluid in a flat channel. One of the walls is adiabatic whereas the other wall is subject to a constant heat flux (see Fig. P4.6). Derive an expression for the Nusselt number.

Hint: Thermally developed flow requires that

$$\frac{dT}{dx} = \frac{dT_{s,1}}{dx} = \frac{dT_{s,2}}{dx},$$

where $T_{s,1}$ and $T_{s,2}$ are the channel surface temperatures.

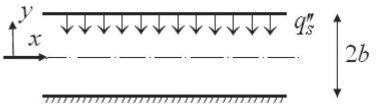

Figure P4.6.

Problem 4.7. A fluid flows in a laminar regime through a circular channel, a concentric annulus with an inner-to-outer radii ratio of 0.5, or a rectangular channel with a cross-section aspect ratio of 2. The channels have equal cross-sectional areas so that the fluid velocity is the same in all of them. Assume steady, thermally developed flow in all of the channels.

(a) Determine the ratios of the friction factor–perimeter products for the three channels. (Use the circular channel as the reference.)
(b) Determine the ratios of the heat transfer coefficient–perimeter products for the three channels.

Problem 4.8. A fluid flows in a laminar regime through either a circular or an equilateral triangular cross-sectional channel. The two channels have equal cross-sectional areas, so that the average fluid velocity is the same. Assume thermally developed flow.

(a) Determine the ratio of the friction factor–surface area product of the two.
(b) Determine the ratio of the heat transfer coefficient–surface area product of the two.

Problem 4.9. Consider a thermally developed laminar flow of an incompressible and constant-property fluid in a circular cross-section pipe with UHF boundary conditions. Assume slug flow, i.e., a flat velocity profile across the channel ($u = U$ everywhere). Prove that

$$\mathrm{Nu}_{D_H,\mathrm{UHF}} = 8.$$

Repeat the solution, this time assuming UWT boundary conditions, and prove that

$$\mathrm{Nu}_{D_H,\mathrm{UWT}} = 5.75.$$

Problem 4.10. For an axisymmetric, steady-state, and fully-developed flow of an incompressible, constant-property fluid in a circular pipe, when viscous dissipation is important, show that the thermal energy equation becomes

$$\rho C_P \left(u \frac{\partial T}{\partial z} + v \frac{\partial T}{\partial r} \right) = \frac{k}{r} \frac{\partial}{\partial r} \left(r \frac{\partial T}{\partial r} \right) + \mu \left(\frac{\partial u}{\partial r} \right)^2 .$$

Now consider a long and fully insulated pipe, with an inlet temperature of T_{in}. Derive an expression for the temperature profile far away from the pipe where the flow is thermally developed.

Problem 4.11. Prove Eq. (4.4.40).

Problem 4.12. Prove Eq. (4.5.43).

Problem 4.13. Consider a thermally developing flow in an initially hydrodynamically fully developed flow in a circular tube with 4-cm diameter.

(a) For Re = 500 and 1000, estimate the thermal entrance length for air, water, glycerin, and mercury, all at 300 K. Assuming constant wall surface temperature, calculate the heat transfer coefficients for all the fluids once thermally developed flow is reached.
(b) Repeat part (a), this time assuming that the tube is 1.5 mm in diameter.

Problem 4.14. Oil flows through a 10-mm-diameter tube with a Reynolds number of 1000 and an inlet temperature of 50 °C. The flow is hydrodynamically fully developed. Over a segment of the tube a wall heat flux of 1.0 kW/m^2 is imposed. Calculate the heat transfer coefficient and wall temperature at the following distances from the point where heating is initiated: 1, 10, and 25 cm. Assume that the oil has a density of 890 kg/m^3, a specific heat of 1.9 kJ/kg K, a viscosity of 0.1 kg/ms, and a thermal conductivity of 0.15 W/m K.

Problem 4.15. A tube with 2-cm inner diameter and 1.0-m length, has a uniform wall temperature. Water at 300 K, with fully developed velocity, enters the tube with a mean velocity of 0.05 m/s. The mean water exit temperature is 350 K.

(a) Find the surface temperature by using a thermally developed flow correlation.
(b) If the boundary condition was constant heat flux, what would be the required heat flux?
(c) For part (b), calculate the heat transfer coefficient and wall temperature at the middle of the tube.

Problem 4.16. An organic fluid that is initially at a temperature of 10 °C is heated to an exit mean temperature of 50 °C by passing it through a heated pipe with 12-mm diameter and 2-m length. The flow is hydrodynamically fully developed before it enters the heated segment. The mass flow rate of the fluid is 0.1 kg/s. The properties of the fluid are as follows:

$$\mathrm{Pr} = 10,\ \rho = 800\ \mathrm{kg/m^3},\ k = 0.12\ \mathrm{W/m\ K},\ \mu = 0.008\ \mathrm{kg/m\ s}.$$

(a) Calculate the local Nusselt number and heat transfer coefficient at 1 and 10 cm downstream from the location where heating is initiated.
(b) Assuming thermally developed flow everywhere, calculate and plot the mean fluid temperature with distance along the pipe.

Problem 4.17. A circular duct with an inner diameter of 6.35 mm and a heated length of 122 cm is subjected to a constant wall heat flux over part of its length. A Newtonian liquid ($\rho = 753$ kg/m^3, $C_P = 2.09$ kJ/kg K, $k = 0.137$ W/m K, $\mu = 6.61 \times 10^{-4}$ N s/m^2) flows through the duct with a mass flow rate of 1.26×10^{-3} kg/s. The average fluid temperatures at the inlet and the exit of the heated segment are 20 and 75.5 °C, respectively.

(a) Assume that at the entrance to the heated section the fluid velocity and temperature profiles are both flat (i.e., temperature and velocity are uniformly distributed). Determine the wall surface temperature at the exit of the heated section.
(b) Now assume that at the entrance to the heated section the flow is hydrodynamically fully developed, but has a uniform temperature. Calculate the

wall surface temperature 1.0 cm downstream from the entrance to the heated section.

Problem 4.18. Water at atmospheric pressure flows in a circular tube with a diameter of 3 mm. The water temperature at inlet is 224 K. The surface temperature is 350 K.

(a) Find the mean fluid temperature at a location 0.01 m downstream from the inlet.
(b) Can thermally developed conditions be assumed at the location in part (a)?
(c) Assuming thermally developed flow at the preceding location, calculate the local heat transfer coefficient.
(d) According to Michelsen and Villasden (1974), the effect of axial conduction in the fluid can be estimated from Eqs. (4.4.25) and (4.4.26). Estimate the effect of fluid axial conduction on the heat transfer coefficient.

Problem 4.19. Atmospheric air at a temperature of 300 K flows through a short pipe segment as shown in Fig. P4.19. The diameter of the pipe segment is 5 cm, and its length is 2.5 cm. The air mean velocity is 0.06 m/s. The pipe segment's surface temperature is 450 K.

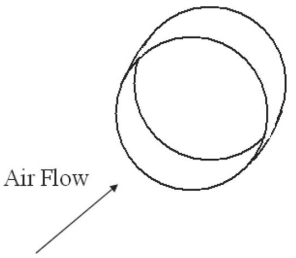

Figure P4.19.

Calculate the average heat transfer coefficient in two ways: (a) by approximating the flow on the pipe surface as the flow on a flat plate, and (b) by using the correlation of Hausen (1983):

$$\langle \mathrm{Nu}_{D_H} \rangle = 3.66 + \frac{0.0668 \mathrm{Re}_{D_H} \mathrm{Pr} \dfrac{D}{l}}{1 + 0.045 \left[\mathrm{Re}_{D_H} \mathrm{Pr} \dfrac{D}{l} \right]^{0.66}} \left(\frac{\mu_m}{\mu_s} \right)^{0.14}.$$

Compare and discuss the results.

Problem 4.20. In an experiment, liquid sodium flows upward through a vertical, uniformly heated tube with 4-*mm* inside diameter and 35-cm length. The pressure and temperature at the inlet are 2 bars and 150 °C, respectively. The heat flux is 15,000 W/m^2.

(a) In a test, the average inlet velocity is 0.147 m/s. Estimate the heat transfer coefficient and wall surface temperature at 10 cm from the inlet and at the exit.
(b) In choosing the thermally developed Nusselt number correlation, is it reasonable to neglect the effect of axial conduction in the fluid?

Problem 4.21. Consider Graetz's problem, discussed in Section 4.5. Assume plug flow regime, i.e., a uniform velocity distribution. The resulting problem is sometimes

referred to as the simplified Graetz problem. Using the separation of variables technique, derive an analytical solution for the temperature profile as a function of axial and radial coordinates.

Problem 4.22. Apply Lévêque's solution method to the thermal entrance problem in a flat channel with UWT boundary condition and thereby prove Eqs. (4.5.125) and (4.5.127).

Problem 4.23. In an experiment, liquid sodium flows upward through a vertical, uniformly heated annulus whose inner and outer diameters are 4.1 and 5.5 mm, respectively, and with a length of 60 cm. The pressure and temperature at the inlet are 3 bars and 140 °C, respectively. The heat flux, which is imposed uniformly on all surfaces, is 9000 W/m^2.

(a) In a test, the average inlet velocity is 0.22 m/s. Estimate the heat transfer coefficient and wall surface temperature 5 cm from the inlet, in the middle, and at the exit of the annular channel.
(b) In choosing the thermally developed Nusselt number correlation, is it reasonable to neglect the effect of axial conduction in the fluid?

Problem 4.24. Liquid sodium flows upward through a vertical tube with 6-mm inside diameter and a length of 115 cm. The pressure and temperature at the inlet are 2 bars and 100 °C, respectively. The wall surface temperature is constant at 400 °C. The sodium velocity at the inlet is 0.27 m/s.

(a) Estimate the mean sodium temperature 1 cm from the inlet and at the exit, assuming that the axial conduction in the flowing sodium is negligible.
(b) Calculate the heat transfer coefficient in the two locations of the tube in two ways: first, by neglecting axial conduction in sodium, and second, by considering the effect of axial conduction in the flowing sodium.

Problem 4.25. In Problem 4.19, assume that the pipe segment is actually a segment of a long pipe. The segment is preceded by a long adiabatic segment in which hydrodynamic fully developed conditions are obtained by air before it enters the segment whose wall surface temperature is 450 K. Calculate the average heat transfer coefficient by using the Lévêque solution and the correlation of Hausen (1983). Discuss the result.

Problem 4.26. Consider the entrance-region steady-state and laminar flow of an incompressible liquid ($\rho = 1000\,\text{kg/m}^3$, $\mu = 10^{-3}$ Pa s) into a smooth square duct with 2-mm hydraulic diameter. For $\text{Re}_{D_H} = 2000$, calculate the local apparent Fanning friction factor by using the correlation of Muzychka and Yovanovich (2004), Eq. (4.2.17). Plot $C_{f,\text{app},x}\text{Re}_{D_H}$ as a function of x^*, using the correlation of Muzychka and Yovanovich, and compare the results with the tabulated results of Shah and London (1978). Selected tabulated results of Shah and London are as follows:

$\frac{x}{D_H\text{Re}_{D_H}}$	$C_{f,\text{app},x}\text{Re}_{D_H}$	$\frac{x}{D_H\text{Re}_{D_H}}$	$C_{f,\text{app},x}\text{Re}_{D_H}$
0.001	111.0	0.010	38.0
0.002	80.2	0.015	32.1
0.004	57.6	0.020	28.6
0.006	47.6	0.040	22.4
0.008	41.8	0.10	17.8

Problem 4.27. A circular pipe with 1-mm diameter carries a hydrodynamic fully developed flow. The fluid properties are as follows: $\rho = 1000$ kg/m^3, $\mu = 0.001$ kg/m s, $C_P = 1.0$ kJ/kg K.

The fluid temperature is uniform at 300 K. Starting at a location designated with axial coordinate $x = 0$, a uniform wall temperature of 350 K is imposed.

Assuming $\mathrm{Re}_D = 100$, for $\mathrm{Pe} = 60$ and $\mathrm{Pe} = 10{,}000$, calculate and tabulate the mean temperature T_m and the local Nusselt number $\mathrm{Nu}_{D,x}$ as a functions of x for $x^* \leq 0.07$. Plot $\mathrm{Nu}_{D,x}$ and $\theta_m = \frac{T_m - T_s}{T_{\mathrm{in}} - T_s}$ as a functions of $x^* = \frac{x}{R_0 \mathrm{Re}_D \mathrm{Pr}}$ for both cases.

Problem 4.28. A circular pipe with 1-mm diameter carries a hydrodynamic fully developed flow. The fluid properties are as follows: $\rho = 1000$ kg/m^3, $\mu = 0.001$ kg/m s, $C_P = 1.0$ kJ/kg K. The fluid inlet temperature is uniform at 300 K and $\mathrm{Re}_D = 100$. Starting at a location designated with axial coordinate $x = 0$ a uniform wall heat flux is imposed on the flow.

(a) For $\mathrm{Pe} = 60$ and a heat flux of 2.08×10^5 W/m^2, and for 5 mm $< x <$ 2.5 cm, calculate and tabulate the local Nusselt number $\mathrm{Nu}_{D,x}$ as a function of x. Plot $\mathrm{Nu}_{D,x}$ as a function of $x^* = \frac{x}{R_0 \mathrm{Re}_D \mathrm{Pr}}$.

(b) Repeat part (a), this time assuming a heat flux of 1250 W/m^2 and $\mathrm{Pe} = 10{,}000$.

Problem 4.29. A flat channel with 1-mm hydraulic diameter carries a hydrodynamic fully developed flow. The fluid properties are as follows: $\rho = 1000$ kg/m^3, $\mu = 0.001$ kg/m s, $C_P = 1.0$ kJ/kg K.

The fluid temperature is uniform at 300 K. Starting at a location designated with axial coordinate $x = 0$, a uniform wall temperature of 350 K is imposed.

Assuming $\mathrm{Re}_{D_H} = 100$, for $\mathrm{Pe} = 60$ and $\mathrm{Pe} = 10{,}000$, calculate and tabulate the mean temperature T_m and the local Nusselt number $\mathrm{Nu}_{D,x}$ as functions of x for $x^* \leq 0.1$. Plot $\mathrm{Nu}_{D_H,x}$ and $\theta_m = \frac{T_m - T_s}{T_{\mathrm{in}} - T_s}$ as functions of $\frac{2x}{D_H \mathrm{Re}_{D_H} \mathrm{Pr}}$ for both cases. Using the calculated results, determine the thermal entrance lengths.

Problem 4.30. A volumetrically heated plate that is 10 cm wide, 10 cm tall, and 5 mm in thickness is sandwiched between two insulating layers, each 5 mm thick. The plate is to be cooled by air flow through parallel microchannels. The air flow is caused by a fan that causes the pressure at the inlet to the microchannels to be 100 Pa larger than the pressure at the exhaust end of the channels. The channels exhaust into atmospheric air. The inlet air is at 298 K temperature. Based on design considerations, the porosity of the plate is not to exceed 25%. The plate is made of a high-thermal-conductivity material and can be assumed to remain isothermal at 363 K.

Assuming uniform-size, parallel cylindrical micorchannels with hydraulic diameters in the 50-μm to 1-mm range, calculate the maximum thermal load that can be disposed by the cooling air. Based on these calculations, determine the optimum coolant channel diameter. For simplicity, you may use heat transfer coefficients representing thermally developed flow.

Mass Transfer

Problem 4.31. Prove that Eq. (4.4.7) applies for fully developed flow in a circular tube with UWM boundary condition when mass transfer rates are low. Prove this by systematic derivations similar to the derivations in Subsection 4.4.1.

Problem 4.32. Prove that Eq. (4.4.24) applies for fully developed flow in a circular tube with UWM boundary condition when mass transfer rates are low. Prove this by systematic derivations similar to the derivations in Subsection 4.4.1. Also, write the equivalent of Eq. (4.4.23) for mass transfer.

Problem 4.33. By systematically following the derivations in Subsection 4.5.2, derive the mass transfer equivalents of Eqs. (4.5.58) and (4.5.59).

Problem 4.34. Pure water at atmospheric pressure and 300 K temperature flows in a circular tube with a diameter of 3 mm with 2 cm/s mean velocity. The tube wall is made of a substance that is sparingly soluble in water. The dissolution of the wall material (the transferred species) takes place such that the mass fraction of the transferred species at the wall surface remains constant at 5×10^{-4}. The mass transfer properties of the transferred species are assumed to be similar to those of CO_2.

(a) Can we assume developed canditions with respect to mass transfer at 0.1 m and 0.5 m downstream from the inlet?
(b) Assuming developed flow conditions at 0.5 m downstream from the inlet, calculate the local mass transfer coefficient.
(c) Estimate the effect of axial mass diffusion in the fluid on the mass transfer coefficient in part (b).

Problem 4.35. A segment of a tube with 2-cm inner diameter and a length of 10.00 m has its inner surface covered by a chemical that dissolves in water and releases CO_2, resulting in a constant CO_2 mass fraction at the wall surface. Pure water with fully developed velocity enters the tube segment with a mean velocity of 0.04 m/s. The mean mass fraction of CO_2 in water at the exit from the tube segment is 5×10^{-4}. The entire system is at 300 K temperature.

(a) Find the mass fraction of CO_2 at the surface by using an appropriate mass transfer correlation. Note that you should search a standard heat transfer textbook, find an empirical correlation that accounts for the entrance effect, and develop its equivalent mass transfer version.
(b) If the boundary condition was a constant heat flux, what would be the required CO_2 mass flux at the surface?
(c) For part (b), calculate the mass transfer coefficient and the mass fraction of CO_2 at the wall in the middle of the tube.

Problem 4.36. Consider a steady-state slug flow (i.e., flow with uniform velocity equal to U) of an incompressible and constant-property fluid in a flat channel (see Fig. P4.36). The system is isothermal. Assume that the walls of the channel contain a slightly soluble substance, so that downstream from location $x = 0$, a species designated by subscript 1 diffuses into the fluid. The boundary condition downstream the location where $x = 0$ is thus UWM (i.e., $m_1 = m_{1,s}$ at surface for $x \geq 0$), whereas upstream from that location the concentration of the transferred species is uniform

and equal to $m_{1,\text{in}}$ ($m_1 = m_{1,\text{in}}$ for $x \leq 0$ and all y). Assume that the diffusion of the transferred species in the fluid follows Fick's law.

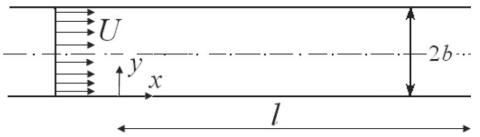

Figure P4.36.

(a) Derive the relevant conservation equations and simplify them for the given system.

(b) Prove that, for $\sqrt{\mathcal{D}_{12} l / U} \ll b$, where b is defined in Fig. P4.36, the local and average mass transfer coefficients can be found from

$$\mathcal{K}_x = \frac{\rho \mathcal{D}_{12}}{\sqrt{\pi \mathcal{D}_{12} x / U}},$$
$$\langle \mathcal{K} \rangle_l = \frac{2\rho \mathcal{D}_{12}}{\sqrt{\pi \mathcal{D}_{12} l / U}}.$$

Problem 4.37. Atmospheric air at a temperature of 300 K flows through the short pipe segment described in Problem 4.19. The diameter of the pipe segment is 5 cm and its length is 1.5 cm. The air Reynolds number defined based on the pipe diameter is 1500. The pipe segment's surface is covered by a layer of naphthalene. Calculate the average mass transfer coefficient in two ways: (a) by approximating the flow on the pipe surface as the flow on a flat plate, and (b) by using the following arrangement, for mass transfer, of the correlation of Hausen (1983) (see Appendix Q):

$$\langle \text{Sh}_{D_H} \rangle = 3.66 + \frac{0.0668 \text{Re}_{D_H} \text{Sc} \dfrac{D}{l}}{1 + 0.045 \left[\text{Re}_{D_H} \text{Sc} \dfrac{D}{l} \right]^{0.66}}.$$

Compare and discuss the results.

For naphthalene vapor in air under atmospheric pressure, Sc = 2.35 at 300 K (Cho et al., 1992; Mills, 2001). Furthermore, the vapor pressure of naphthalene can be estimated from (Mills, 2001)

$$P_v(T) = 3.631 \times 10^{13} \exp(-8586/T),$$

where T is in Kelvins and P_v is in pascals.

Problem 4.38. Based on an asymptotic interpolation technique, Awad (2010) derived the forthcoming expressions for hydrodynamically fully-developed flow and thermally developing flow in a flat channel with UWT boundary conditions,

$$\text{Nu}_{D_H,\text{UWT}}(x^*) = \left\{ \left[1.233 (x^*)^{-1/3} + 0.4 \right]^6 + (7.541)^6 \right\}^{1/6}$$
$$\langle \text{Nu}_{D_H,\text{UWT}} \rangle_x = \left\{ \left[1.849 (x^*)^{-1/3} \right]^{3.5} + (7.541)^{3.5} \right\}^{1/3.5}$$

1. Repeat the solution of Problem 4.29 using the preceding expressions.
2. Write and discuss the equivalent mass transfer expressions.

Problem 4.39. Based on an asymptotic interpolation technique, Awad (2010) derived the forthcoming expressions for hydrodynamically fully-developed flow and thermally developing flow in a flat channel with UHF boundary conditions,

$$\mathrm{Nu}_{D_H,\mathrm{UHF}}(x^*) = \left\{\left[1.490(x^*)^{-1/3}\right]^{4.5} + (8.235)^{4.5}\right\}^{1/4.5}$$
$$\langle \mathrm{Nu}_{D_H,\mathrm{UHF}}\rangle_x = \left\{\left[2.236(x^*)^{-1/3}\right]^{3.5} + (8.235)^{3.5}\right\}^{1/3.5}.$$

(a) For the flow conditions of Problem 4.29, assume that the channel boundary condition is UHF with $q_s'' = 100\ \mathrm{W/m^2}$. Assuming $\mathrm{Re}_{D_H} = 100$, for $\mathrm{Pe} = 60$ and $\mathrm{Pe} = 10{,}000$, calculate and tabulate the mean temperature T_m, and local Nusselt number, $\mathrm{Nu}_{D,x}$, as a function of x, for $x^* \leq 0.1$. Plot $\mathrm{Nu}_{D_H,x}$ and $\theta_m = \frac{T_m - T_s}{T_{\mathrm{in}} - T_s}$ as a function of $\frac{2x}{D_h \mathrm{Re}_{D_H} \mathrm{Pr}}$ for both cases. Using the calculated results determine the thermal entrance lengths.

(b) Write and discuss the equivalent mass transfer expressions.

5 Integral Methods

An integral method is a powerful and flexible technique for the approximate solution of boundary-layer problems. It is based on the integration of the boundary-layer conservation equations over the boundary-layer thickness and the assumption of approximate and well-defined velocity, temperature, and mass-fraction profiles in the boundary layer. In this way, the partial differential conservation equations are replaced with ODEs in which the dependent variable is the boundary-layer thickness. The solution of the ODE derived in this way then provides the thickness of the boundary layer. Knowing the boundary-layer thickness, along with the aforementioned approximate velocity and temperature profiles, we can then easily find the transport rates through the boundary layer. The integral technique is quite flexible and, unlike the similarity solution method, can be applied to relatively complicated flow configurations.

5.1 Integral Momentum Equations

Let us first consider the velocity boundary layer on a flat plate that is subject to the steady and uniform parallel flow of a fluid, as shown in Fig. 5.1. We define a control volume composed of a slice of the flow field that has a thickness dx and height Y. We choose Y to be large enough so that it will be larger than the boundary-layer thickness throughout the range of interest. The inflow and outflow parameters relevant to momentum and energy are also depicted in Fig. 5.1.

We can start from the steady-state mass conservation:

$$\frac{\partial \rho u}{\partial x} + \frac{\partial \rho v}{\partial y} = 0. \tag{5.1.1}$$

We now apply $\int_0^Y$ to both sides of this equation to get

$$\rho v|_Y = (\rho v)_s - \frac{d}{dx}\int_0^Y \rho u dy. \tag{5.1.2}$$

We can derive the integral momentum equation in the x direction by directly performing a momentum balance on the depicted control volume:

$$\frac{d}{dx}\int_0^Y \rho u^2 dy + (\rho v)_Y U_\infty = -\mu_s \left.\frac{\partial u}{\partial y}\right|_{y=0} - Y\frac{dP}{dx}. \tag{5.1.3}$$

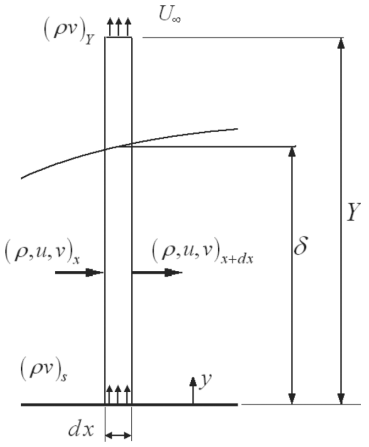

Figure 5.1. The definitions for the integral analysis of the boundary layer on a flat surface.

We note that, from Bernoulli's equation,

$$-\frac{dP}{dx} = \rho_\infty U_\infty \frac{dU_\infty}{dx}. \tag{5.1.4}$$

Therefore,

$$Y\frac{dP}{dx} = -\rho_\infty \frac{dU_\infty}{dx}\int_0^Y U_\infty dy. \tag{5.1.5}$$

Substituting for $Y\frac{dP}{dx}$ from Eq. (5.1.5) and substituting for $(\rho v)_Y$ from Eq. (5.1.2), we find that Eq. (5.1.3) becomes

$$\frac{d}{dx}\int_0^Y \rho u^2 dy - U_\infty \frac{d}{dx}\int_0^Y \rho u\, dy - \rho_\infty \frac{dU_\infty}{dx}\int_0^Y U_\infty dy = -(\rho v)_s U_\infty - \mu_s \left.\frac{\partial u}{\partial y}\right|_{y=0}. \tag{5.1.6}$$

The second and third terms on the left-hand side of this equation add up to give

$$-\frac{d}{dx}\left\{U_\infty \int_0^Y \rho u\, dy\right\} - \frac{dU_\infty}{dx}\int_0^Y (\rho_\infty U_\infty - \rho u)\, dy. \tag{5.1.7}$$

The integral momentum equation for the boundary layer then becomes

$$\frac{d}{dx}\int_0^Y \left(\rho u^2 - \rho U_\infty u\right) dy - \frac{dU_\infty}{dx}\int_0^Y (\rho_\infty U_\infty - \rho u)\, dy = -(\rho v)_s U_\infty - \mu_s \left.\frac{\partial u}{\partial y}\right|_{y=0}. \tag{5.1.8}$$

We can further manipulate this equation by noting that

$$\frac{dU_\infty}{dx}\int_0^Y (\rho_\infty U_\infty - \rho u)\, dy = \frac{dU_\infty}{dx}\int_0^Y \rho_\infty U_\infty \left(1 - \frac{\rho u}{\rho_\infty U_\infty}\right) dy. \tag{5.1.9}$$

Recalling the definitions of the displacement and momentum boundary-layer thicknesses [Eqs. (2.3.12) and (2.3.13), respectively], we can then cast Eq. (5.1.8) as

$$\frac{d}{dx}\left(\rho_\infty U_\infty^2 \delta_2\right) + \rho_\infty U_\infty \frac{dU_\infty}{dx}\delta_1 = \tau_s + (\rho v)_s U_\infty, \tag{5.1.10}$$

where $\tau_s = \mu \frac{\partial u}{\partial y}|_{y=0}$. Equation (5.1.10) is the integral momentum equation for steady, parallel flow past a flat plate.

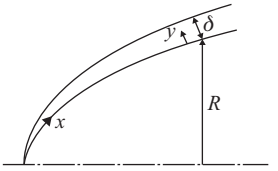

Figure 5.2. Boundary layer for flow past an axisymmetric blunt body.

Up to this point, no approximation has been introduced into the equations. Approximation is introduced only when we make an assumption regarding the velocity profile in the boundary layer.

An important application of the integral method is the flow over an axisymmetric object (Fig. 5.2). For this case, assuming $R \gg \delta$ everywhere, we can show that (see Problem 5.1),

$$\frac{1}{R}\frac{d}{dx}\left\{R\int_0^\delta \left(\rho u^2 - \rho U_\infty u\right) dy\right\} - \frac{dU_\infty}{dx}\int_0^\delta \left(\rho_\infty U_\infty - \rho u\right) dy = -(\rho v)_s\, U_\infty - \mu_s \left.\frac{\partial u}{\partial y}\right|_{y=0}. \tag{5.1.11}$$

Equation (5.1.11) can also be recast as,

$$\frac{\tau_s + (\rho v)_s\, U_\infty}{\rho_\infty U_\infty^2} = \frac{d\delta_2}{dx} + \delta_2\left[\left(2 + \frac{\delta_1}{\delta_2}\right)\frac{1}{U_\infty}\frac{dU_\infty}{dx} + \frac{1}{\rho_\infty}\frac{d\rho_\infty}{dx} + \frac{1}{R}\frac{dR}{dx}\right]. \tag{5.1.12}$$

This equation of course reduces to flow parallel to a flat plate when $R \to \infty$.

We now apply the integral momentum method to two important problems.

5.2 Solutions to the Integral Momentum Equation

5.2.1 Laminar Flow of an Incompressible Fluid Parallel to a Flat Plate without Wall Injection

Consider the flow field shown in Fig. 5.3. For this system $\frac{dU_\infty}{dx} = 0$ and Eq. (5.1.10) gives

$$\frac{\tau_s}{\rho U_\infty^2} = \frac{d\delta_2}{dx}. \tag{5.2.1}$$

For the velocity profile in the boundary layer at any fixed location along the plate, let us assume a third-order polynomial:

$$u = a + by + cy^2 + dy^3. \tag{5.2.2}$$

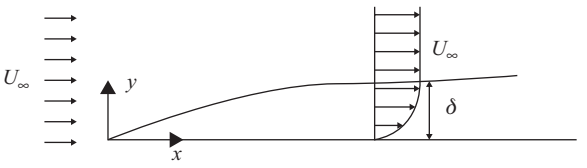

Figure 5.3. Boundary layer for flow parallel to a flat plate.

The assumed profile has four unknown coefficients, and therefore we need four boundary conditions. The velocity profile must satisfy

$$u = U_\infty \quad \text{at } y = \delta, \tag{5.2.3}$$

$$u = 0 \quad \text{at } y = 0, \tag{5.2.4}$$

$$\frac{\partial u}{\partial y} = 0 \quad \text{at } y = \delta, \tag{5.2.5}$$

$$\frac{\partial^2 u}{\partial y^2} = 0 \quad \text{at } y = 0. \tag{5.2.6}$$

The last boundary condition is the result of the fact that the momentum equation must be applicable at $y = 0$, namely,

$$\underbrace{u}_{0}\frac{\partial u}{\partial x} + \underbrace{v}_{0}\frac{\partial u}{\partial y} = -\frac{1}{\rho}\underbrace{\frac{dp}{dx}}_{0} + \nu\frac{\partial^2 u}{\partial y^2}. \tag{5.2.7}$$

With the preceding conditions, the velocity profile will be

$$\frac{u}{U_\infty} = \begin{cases} \frac{3}{2}\eta - \frac{1}{2}\eta^3 & \text{for } \eta \le 1 \\ 1 & \text{for } \eta > 1 \end{cases}, \tag{5.2.8}$$

where $\eta = y/\delta$.

Next, having an approximate velocity profile, we can find the displacement (δ_1) and momentum boundary-layer (δ_2) thicknesses. First we note that

$$\delta_1 = \int_0^Y \left(1 - \frac{\rho u}{\rho_\infty U_\infty}\right) dy = \int_0^\delta \left(1 - \frac{\rho u}{\rho_\infty U_\infty}\right) dy, \tag{5.2.9}$$

$$\delta_2 = \int_0^Y \frac{\rho u}{\rho_\infty U_\infty}\left(1 - \frac{u}{U_\infty}\right) dy = \int_0^\delta \frac{\rho u}{\rho_\infty U_\infty}\left(1 - \frac{u}{U_\infty}\right) dy. \tag{5.2.10}$$

We were able to replace the upper limits of these integrals with δ because for $y > \delta$ the integrands in both equations are equal to zero. Now, using the velocity profile of Eq. (5.2.8), and noting that the fluid is incompressible, we get

$$\delta_1 = \delta \int_0^1 \left(1 - \frac{u}{U_\infty}\right) d\eta = \frac{3}{8}\delta, \tag{5.2.11}$$

$$\delta_2 = \delta \int_0^1 \frac{u}{U_\infty}\left(1 - \frac{u}{U_\infty}\right) d\eta = \frac{39}{280}\delta. \tag{5.2.12}$$

We can now find the shear stress at the wall by writing

$$\tau_s = \mu \left.\frac{\partial u}{\partial y}\right|_{y=0} = \frac{\mu}{\delta}\left.\frac{\partial u}{\partial \eta}\right|_{\eta=0} = \frac{3\mu U_\infty}{2\delta}. \tag{5.2.13}$$

Therefore Eq. (5.2.1) can be recast as

$$\delta\, d\delta = \frac{140}{13}\frac{\nu}{U_\infty} dx. \tag{5.2.14}$$

Table 5.1. *Predictions of the integral method for steady-state, incompressible flow parallel to a flat plate (after Schlichting, 1968)*

Velocity profile $\frac{u}{U_\infty} = F(\eta)$	$\frac{\delta_2}{\delta}$	$F'(0)$	$H = \frac{\delta_1}{\delta_2}$	$C_f \mathrm{Re}_x^{1/2}$
$F(\eta) = \eta$	$\frac{1}{6}$	1.0	3.0	0.577
$F(\eta) = \frac{3}{2}\eta - \frac{1}{2}\eta^3$	$\frac{39}{280}$	$\frac{3}{2}$	2.7	0.646
$F(\eta) = 2\eta - 2\eta^3 + \eta^4$	$\frac{37}{315}$	2.0	2.55	0.686
$F(\eta) = \sin(\pi/2\eta)$	$\frac{(4-\pi)}{2\pi}$	$\frac{\pi}{2}$	2.66	0.655
Exact (similarity)	–	–	2.59	0.664

This simple ODE can now be solved with the boundary condition $\delta = 0$ at $x = 0$, to get

$$\delta = \sqrt{\frac{280\nu x}{13U_\infty}} \approx 4.64 x \mathrm{Re}_x^{-1/2}. \tag{5.2.15}$$

At this point we know the boundary-layer thickness and its velocity profile. Clearly then, we know all the hydrodynamics aspects of the boundary layer. (Of course, we know these things approximately.) For example, we can substitute for δ from this equation into Eq. (5.2.13) to get

$$C_f = \frac{\tau_s}{\frac{1}{2}\rho U_\infty^2} = 0.646 \mathrm{Re}_x^{-1/2}. \tag{5.2.16}$$

This expression does well when it is compared with experimental data.

To better understand the strength of the integral technique, the method's predictions for several other assumed velocity profiles are depicted in Table 5.1. They show that even with a simple and unrealistic linear velocity profile the discrepancy between the result of the integral method and the exact solution is relatively small.

For laminar flow parallel to a flat surface, the method of analysis can be depicted in the following generic form. Suppose the assumed velocity profile is

$$\frac{u}{U_\infty} = F(\eta). \tag{5.2.17}$$

This velocity distribution must of course satisfy the key boundary conditions, such as those in Eqs. (5.2.3)–(5.2.6). It can then be shown that (Schlichting, 1968)

$$\delta(x) = \sqrt{2F'(0)/c_1}\, x \mathrm{Re}_x^{-1/2}, \tag{5.2.18}$$

$$C_f = \sqrt{2F'(0)\, c_1}\, \mathrm{Re}_x^{-1/2}, \tag{5.2.19}$$

$$\delta_1 = c_2 \delta, \tag{5.2.20}$$

$$\delta_2 = c_1 \delta, \tag{5.2.21}$$

where

$$c_1 = \int_0^1 F(\eta)\,[1 - F(\eta)]\,d\eta, \tag{5.2.22}$$

$$c_2 = \int_0^1 [1 - F(\eta)]\,d\eta. \tag{5.2.23}$$

5.2.2 Turbulent Flow of an Incompressible Fluid Parallel to a Flat Plate without Wall Injection

A detailed discussion of turbulence is presented in Chapter 6. It will be shown that in turbulent boundary layers the velocity and temperature distributions, when they are cast in proper dimensionless forms, follow universal profiles. These profiles are significantly different than the velocity and temperature profiles in laminar boundary layers. Nevertheless, as subsequently shown in the following text, the integral method can be applied to turbulent boundary layers as well, so long as the aforementioned turbulent velocity (and temperature) profiles are approximated by properly selected functions.

Equation (5.1.11) was derived without any particular assumption about the flow regime. It thus applies to laminar or turbulent flow. For incompressible flow, this equation reduces to

$$\frac{d}{dx}\left(U_\infty^2 \delta_2\right) + U_\infty \frac{dU_\infty}{dx}\delta_1 = \frac{\tau_s + (\rho v)_s\, U_\infty}{\rho}, \tag{5.2.24}$$

where,

$$\delta_1 = \int_0^Y \left(1 - \frac{u}{U_\infty}\right) dy, \tag{5.2.25}$$

$$\delta_2 = \int_0^Y \frac{u}{U_\infty}\left(1 - \frac{u}{U_\infty}\right) dy. \tag{5.2.26}$$

The turbulent pipe flow data have shown that, in most of the turbulent boundary layer, excluding a very thin layer at the immediate vicinity of the wall, the "1/7 power-law" velocity distribution applies, whereby $u \sim y^{1/7}$. Therefore a good choice for the velocity profile in the boundary layer would be

$$u/U_\infty = (y/\delta)^{1/7}. \tag{5.2.27}$$

Thus, defining $\eta = y/\delta$, we have

$$\frac{\delta_1}{\delta} = \int_0^1 \left(1 - \eta^{1/7}\right) d\eta = \frac{1}{8}, \tag{5.2.28}$$

$$\frac{\delta_2}{\delta} = \int_0^1 \eta^{1/7}\left(1 - \eta^{1/7}\right) d\eta = \frac{7}{72}. \tag{5.2.29}$$

Substitution of these equations into Eq. (5.2.24) then leads to the ODE with δ as its unknown.

Let us now consider the case in which $U_\infty = \text{const.}$, with no material injection at the wall ($v_s = 0$). Equation (5.2.24) then gives

$$\frac{7}{72} U_\infty^2 \frac{d\delta}{dx} = \frac{\tau_s}{\rho}. \tag{5.2.30}$$

If Eq. (5.2.27) was actually accurate all through the boundary layer, then we could use it for finding the wall shear stress from $\tau_s = \mu \frac{\partial u}{\partial y}|_{y=0}$. This, along with Eq. (5.2.27), would then close Eq. (5.2.30) and δ would be predicted. This approach will lead to a result that does not match with the experimental data, however, because Eq. (5.2.27) is inaccurate very near the wall, where the velocity profile actually follows the universal law-of-the-wall profile (to be discussed in Section 6.5). [Note that Eq. (5.2.27) predicts that $\frac{\partial u}{\partial y}|_{y\to 0} \to \infty$, which is unphysical.]

To close Eq. (5.2.30), we thus should use a reasonable approximation to the law-of-the-wall velocity profile. An approximation to the logarithmic law-of-the-wall velocity distribution that applies up to at least $y^+ = 1500$ is

$$u^+ = 8.75 y^{+1/7}, \tag{5.2.31}$$

where,

$$u^+ = \frac{u}{U_\tau}, \tag{5.2.32}$$

$$y^+ = \frac{y U_\tau}{\nu}, \tag{5.2.33}$$

$$U_\tau = \sqrt{\tau_s/\rho}. \tag{5.2.34}$$

Applying Eq. (5.2.31) to the edge of the boundary layer, where $y = \delta$ and $u = U_\infty$, leads to

$$\frac{U_\infty}{\sqrt{\tau_s/\rho}} = 8.75 \left(\frac{\delta \sqrt{\tau_s/\rho}}{\nu} \right)^{1/7}. \tag{5.2.35}$$

We must now eliminate τ_s from Eq. (5.2.30) by using Eq. (5.2.35). This will give a differential equation with δ as its dependent variable. The solution of the differential equation with the condition $\delta = 0$ at $x = 0$ will then result in

$$\frac{\delta}{x} = 0.036 \left(\frac{72}{7} \right) \mathrm{Re}_x^{-0.2}, \tag{5.2.36}$$

$$\frac{\delta_2}{x} = 0.036 \, \mathrm{Re}_x^{-0.2}. \tag{5.2.37}$$

We can now introduce δ from Eq. (5.2.36) into Eq. (5.2.35) and apply $C_f = \frac{\tau_s}{\frac{1}{2}\rho U_\infty^2}$ to get

$$C_f = 0.0574 \, \mathrm{Re}_x^{-0.2}. \tag{5.2.38}$$

Equation (5.2.38) is accurate up to Re_x of several million. For $\mathrm{Re}_x \geq 10^6$, Eq. (5.2.31) becomes inaccurate. The empirical correlation of Schultz-Grunow (1941) can then be used, whereby, for $\mathrm{Re}_x \geq 5 \times 10^5$,

$$C_f = 0.37 \left(\log_{10} \mathrm{Re}_x \right)^{-2.584}. \tag{5.2.39}$$

5.2.3 Turbulent Flow of an Incompressible Fluid Over a Body of Revolution

This is a case in which the integral method provides a simple and useful solution for the friction factor.

Consider Fig. 5.2. Equation (5.1.12) can be rewritten as

$$\frac{\tau_s + (\rho v)_s U_\infty}{\rho_\infty U_\infty^2} = \frac{d\delta_2}{dx} + \delta_2 \left[(2+H) \frac{1}{U_\infty} \frac{dU_\infty}{dx} + \frac{1}{\rho_\infty} \frac{d\rho_\infty}{dx} + \frac{1}{R} \frac{dR}{dx} \right], \quad (5.2.40)$$

where H is the shape factor, defined as $H = \delta_1/\delta_2$ [see Eq. (2.3.15)].

Assume incompressible and steady-state flow, and note that $\frac{dU_\infty}{dx}$ should be found by use of potential flow theory. Assuming $R \gg \delta$ everywhere, Eq. (5.2.25) and (5.2.26) will apply for $Y > \delta$ and $Y \ll R$. We also assume that the flow is accelerating ($dP/dx < 0$ or $dU_\infty/dx > 0$) so that the approximation represented by Eq. (5.2.31) applies. Applying Eq. (5.2.31) to the edge of the boundary layer, once again we get Eq. (5.2.35). Furthermore, by assuming that the 1/7-power-law velocity profile applies, we find that Eqs. (5.2.27)–(5.2.29) apply, leading to

$$H = \frac{72}{56}. \quad (5.2.41)$$

Now, using Eq. (5.2.29) for eliminating δ in Eq. (5.2.35) in favor of δ_2, we get

$$\tau_s = 0.0125 \rho U_\infty^2 \left(\frac{\delta_2 U_\infty}{\nu} \right)^{-1/4}. \quad (5.2.42)$$

We can now substitute for τ_s from this equation and substitute for H from Eq. (2.3.15) into Eq. (5.2.40), obtaining,

$$0.0125 \rho U_\infty^2 \left(\frac{\delta_2 U_\infty}{\nu} \right)^{-1/4} = \frac{d\delta_2}{dx} + 3.29 \frac{\delta_2}{U_\infty} \frac{dU_\infty}{dx} + \frac{\delta_2}{R} \frac{dR}{dx}. \quad (5.2.43)$$

This equation can be rewritten as

$$0.0125 U_\infty^{-1/4} \nu^{1/4} = \delta_2^{1/4} \frac{d\delta_2}{dx} + 3.29 \delta_2^{5/4} \frac{1}{U_\infty} \frac{dU_\infty}{dx} + \frac{\delta_2^{5/4}}{R} \frac{dR}{dx}. \quad (5.2.44)$$

The right-hand side of this equation can be recast as

$$\frac{\frac{d}{dx} \left[R^{5/4} U_\infty^{5/4(3.29)} \delta_2^{5/4} \right]}{\frac{5}{4} R^{5/4} U_\infty^{5/4(3.29)} \delta_2^{5/4}}. \quad (5.2.45)$$

As a result, we get

$$\frac{d}{dx} \left[R^{5/4} U_\infty^{4.11} \delta_2^{5/4} \right] = \left(1.56 \times 10^{-2} \right) R^{5/4} U_\infty^{3.86} \nu^{1/4}. \quad (5.2.46)$$

The good thing about this equation is that its right-hand side does not depend on δ_2. Assuming that at $x = 0$, at least one of R, x, or δ_2 is equal to zero, then we can integrate the two sides of this equation from $x = 0$ to an arbitrary x, leading to,

$$\delta_2 = \frac{0.036 \nu^{0.2}}{R U_\infty^{3.29}} \left\{ \int_0^x R^{5/4} U_\infty^{3.86} dx \right\}^{4/5}. \quad (5.2.47)$$

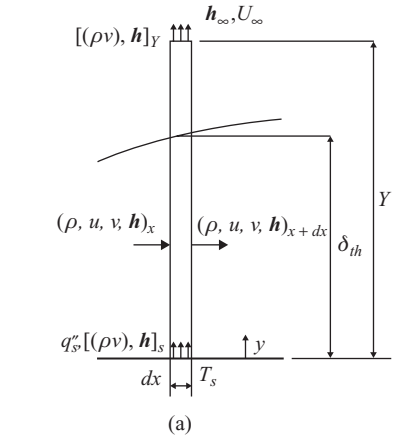

Figure 5.4. Thermal boundary layers (a) on a flat surface, (b) on an axisymmetric blunt body.

Note that this equation is based on the assumption that the boundary layer is turbulent right from the leading edge of the surface and is therefore a good approximation when x is large. If not, the analysis must be repeated, accounting for the initial segment of the surface where a laminar boundary layer occurs.

5.3 Energy Integral Equation

We now apply the integral method to the energy equation.

Consider Fig. 5.4. We assume a 2D flow and define Y as the constant thickness of a layer of fluid adjacent to the surface, chosen such that it is everywhere larger than the velocity or thermal boundary-layer thickness. By applying the first law of thermodynamics to the control volume depicted in Fig. 5.4(a), we can write

$$\int_0^Y \rho u \mathbf{h}^* dy\Big|_x + q''_s dx + (\rho v \mathbf{h}^*)_s dx = \int_0^Y \rho u \mathbf{h}^* dy\Big|_{x+dx} + (\rho v)_Y h^*_\infty dx, \qquad (5.3.1)$$

where $\mathbf{h}^* = \mathbf{h} + \frac{1}{2}|\vec{U}|^2$ is the stagnation enthalpy. Mass conservation requires that $\partial \rho u/\partial x + \partial \rho v/\partial y = 0$.

Now we apply $\int_0^Y dy$ to both sides of this equation to get

$$\int_0^Y \frac{\partial \rho u}{\partial x} dy + (\rho v)\big|_Y - (\rho v)\big|_s = 0. \qquad (5.3.2)$$

This gives

$$(\rho v)_Y \mathbf{h}^*_\infty = (\rho v)_s \mathbf{h}^*_\infty - \frac{d}{dx}\int_0^Y \rho u \mathbf{h}^*_\infty dy + \frac{d\mathbf{h}^*_\infty}{dx}\int_0^Y \rho u dy. \qquad (5.3.3)$$

Substitution into Eq. (5.3.1) then gives

$$q_s'' + (\rho v \mathbf{h}^*)_s = \frac{d}{dx}\int_0^Y \rho u \mathbf{h}^* dy + (\rho v)_s \mathbf{h}_\infty^* - \frac{d}{dx}\int_0^Y \rho u \mathbf{h}_\infty^* dy + \frac{d\mathbf{h}_\infty^*}{dx}\int_0^Y \rho u dy. \tag{5.3.4}$$

When $\frac{d\mathbf{h}_\infty^*}{dx} = 0$ (a good assumption, even in accelerating or decelerating flows), we get

$$q_s'' = \frac{d}{dx}\int_0^Y (\mathbf{h}^* - \mathbf{h}_\infty^*)\,\rho u dy - (\rho v)_s\,(\mathbf{h}_s^* - \mathbf{h}_\infty^*)\,. \tag{5.3.5}$$

For a boundary layer developing on the inside or outside surface of a body of revolution [Fig. 5.4(b)], Eq. (5.3.5) becomes

$$q_s'' = \frac{1}{R}\frac{d}{dx}\left[R\int_0^Y dy \rho u(\mathbf{h}^* - \mathbf{h}_\infty^*)\right] - (\rho v)_s(\mathbf{h}_s^* - \mathbf{h}_\infty^*). \tag{5.3.6}$$

Similar to the integral momentum equations, we can define an enthalpy boundary layer thickness Δ_2 as

$$\Delta_2 = \int_0^\infty \frac{\rho u(\mathbf{h}^* - \mathbf{h}_\infty^*)}{\rho_\infty U_\infty(\mathbf{h}_s^* - \mathbf{h}_\infty^*)} dy. \tag{5.3.7}$$

Equation (5.3.6) can then be recast as

$$\frac{q_s''}{\rho_\infty U_\infty(\mathbf{h}_s^* - \mathbf{h}_\infty^*)} + \frac{(\rho v)_s}{\rho_\infty U_\infty} = \frac{d\Delta_2}{dx} + \Delta_2\left[\frac{1}{U_\infty}\frac{dU_\infty}{dx} + \frac{1}{\rho_\infty}\frac{d\rho_\infty}{dx} + \frac{1}{R}\frac{dR}{dx} + \frac{1}{(\mathbf{h}_s^* - \mathbf{h}_\infty^*)}\frac{d(\mathbf{h}_s^* - \mathbf{h}_\infty^*)}{dx}\right]. \tag{5.3.8}$$

Obviously this equation reduces to that for a flat plate when $R \to \infty$.

The preceding derivations considered total energy (thermal + mechanical). We can apply the integral method to the thermal energy, bearing in mind that the viscous dissipation term should in general be included (see Problem 5.4). For low-velocity situations the viscous dissipation term in the thermal energy equation can often be neglected, and changes in kinetic energy are small. Then, assuming that the flow is incompressible, we can write $\mathbf{h}^* \approx C_p(T - T_{\text{ref}})$, and that results in

$$\Delta_2 = \int_0^\infty \frac{u}{U_\infty}\left(\frac{T - T_\infty}{T_s - T_\infty}\right) dy, \tag{5.3.9}$$

$$\frac{q_s''}{\rho_\infty U_\infty C_p(T_s - T_\infty)} = \frac{d\Delta_2}{dx} + \Delta_2\left[\frac{1}{U_\infty}\frac{dU_\infty}{dx} + \frac{1}{\rho_\infty}\frac{d\rho_\infty}{dx} + \frac{1}{R}\frac{dR}{dx} + \frac{1}{T_s - T_\infty}\frac{d(T_s - T_\infty)}{dx}\right]. \tag{5.3.10}$$

Equation (5.3.10) can be further simplified for flow over a flat surface with constants U_∞, ρ, and T_s (UWT boundary condition) with no wall injection, to get

$$\frac{q_s''}{\rho U_\infty C_p(T_s - T_\infty)} = \frac{d\Delta_2}{dx}. \tag{5.3.11}$$

Figure 5.5. Velocity and thermal boundary layers for parallel flow on a flat plate.

Or, in terms of the heat transfer coefficient,

$$\frac{h}{\rho U_\infty C_p} = \mathrm{St} = \frac{d\Delta_2}{dx}. \tag{5.3.12}$$

It is worth noting that the derivations up to this point are all precise within their underlying assumptions. Approximations that are characteristic of the integral method come into the picture once we insert assumed velocity and temperature profiles in the integral boundary-layer equations.

5.4 Solutions to the Energy Integral Equation

5.4.1 Parallel Flow Past a Flat Surface

This is the simplest application of the integral method for heat transfer. The system of interest is displayed in Fig. 5.5. Assume that the flow is steady state, the fluid is incompressible and has constant properties. Also, assume that there is no blowing or suction through the wall. We deal with the formation and growth of thermal and velocity boundary layers, starting from the same point. When thermal and velocity boundary layers start from the same physical or virtual point, they are referred to as *equilibrium boundary layers.*

Consider a laminar boundary layer with UWT surface conditions and no mass transfer through the surface. The hydrodynamics of the problem has already been solved. For the thermal boundary layer, assume $v_s = 0$ and dU_∞/dx. The boundary-layer momentum equation has already been solved [see Eq. (5.2.15)]. For the thermal boundary layer, given that $dU_\infty/dx = 0$, Eq. (5.3.11) applies.

Let us use a third-order polynomial for the temperature profile:

$$T = a + bT + cT^2 + dT^3. \tag{5.4.1}$$

To apply the boundary conditions that this distribution needs to satisfy, we start from the lowest-order boundary conditions and proceed. Thus we write

$$T = T_s \quad \text{at } y = 0, \tag{5.4.2a}$$

$$T = T_\infty \quad \text{at } y = \delta_{\mathrm{th}}, \tag{5.4.2b}$$

$$\frac{\partial T}{\partial y} = 0 \quad \text{at } y = \delta_{\mathrm{th}}, \tag{5.4.2c}$$

$$\frac{\partial^2 T}{\partial y^2} = 0 \quad \text{at } y = 0. \tag{5.4.2d}$$

We derive the last boundary condition by examining the energy equation at $y = 0$, whereby,

$$u\frac{\partial T}{\partial x} + v\frac{\partial T}{\partial y} = \alpha\frac{\partial^2 T}{\partial y^2}.$$

Because $u = v = 0$ at $y = 0$, then $\partial^2 T/\partial y^2 = 0$ at $y = 0$. Equation (5.4.1) leads to

$$\frac{T - T_\infty}{T_s - T_\infty} = 1 - \frac{3}{2}\left(\frac{y}{\delta_{\text{th}}}\right) + \frac{1}{2}\left(\frac{y}{\delta_{\text{th}}}\right)^3. \tag{5.4.3}$$

For the velocity boundary layer we can use Eq. (5.2.8). Let us assume that $\delta_{\text{th}} < \delta$ everywhere, which will be true for $\text{Pr} > 1$. Substitution into the definition of Δ_2 gives

$$\begin{aligned}\Delta_2 &= \int_0^Y \frac{u}{U_\infty}\left(\frac{T - T_\infty}{T_s - T_\infty}\right) dy \\ &= \delta_{\text{th}} \int_0^1 \left[\frac{3}{2}\frac{\delta_{\text{th}}}{\delta}\left(\frac{y}{\delta_{\text{th}}}\right) - \frac{1}{2}\left(\frac{\delta_{\text{th}}}{\delta}\right)^3\left(\frac{y}{\delta_{\text{th}}}\right)^3\right]\left[1 - \frac{3}{2}\left(\frac{y}{\delta_{\text{th}}}\right) + \frac{1}{2}\left(\frac{y}{\delta_{\text{th}}}\right)^3\right] d\left(\frac{y}{\delta_{\text{th}}}\right).\end{aligned} \tag{5.4.4}$$

Note that there is no need to integrate beyond δ_{th} because for $y > \delta_{\text{th}}$ we have $\frac{T - T_\infty}{T_s - T_\infty} = 0$. Now, for convenience define $r = \delta_{\text{th}}/\delta$. Then Eq. (5.4.4) can be recast as

$$\Delta_2 = r\delta \int_0^1 \left[\frac{3}{2}r\eta - \frac{1}{2}r^3\eta^3\right]\left[1 - \frac{3}{2}\eta + \frac{1}{2}\eta^3\right] d\eta. \tag{5.4.5}$$

This integral gives

$$\Delta_2 = 3\delta(r^2/20 - r^4/280). \tag{5.4.6}$$

With $r < 1$, the second term in the parentheses is much smaller than the first term and can therefore be neglected. This equation then leads to

$$\frac{d\Delta_2}{dx} \approx \frac{3\delta}{10} r \frac{dr}{dx} + \frac{3}{20} r^2 \frac{d\delta}{dx}. \tag{5.4.7}$$

Next, let us get $d\Delta_2/dx$ from Eq. (5.3.11) by writing

$$\frac{d\Delta_2}{dx} = \frac{1}{\rho U_\infty C_p (T_s - T_\infty)}\left(-k \left.\frac{\partial T}{\partial y}\right|_{y=0}\right) = \frac{3}{2}\frac{\boldsymbol{\alpha}}{U_\infty \delta_{\text{th}}} = \frac{3\boldsymbol{\alpha}}{2U_\infty r\delta}, \tag{5.4.8}$$

where $\frac{\partial T}{\partial y}|_{y=0}$ was found from Eq. (5.4.3). Combining Eqs. (5.4.7) and (5.4.8), we have, after some simple manipulations,

$$2\delta^2 r^2 \frac{dr}{dx} + r^3 \delta \frac{d\delta}{dx} = 10\frac{\boldsymbol{\alpha}}{U_\infty}. \tag{5.4.9}$$

We can substitute for δ from Eq. (5.2.15) to get

$$r^3 + 4r^2 x \frac{dr}{dx} = \frac{13}{14}\frac{1}{\text{Pr}}. \tag{5.4.10}$$

Let us define $R = r^3$. Equation (5.4.10) can then be cast as

$$R + \frac{4}{3} x \frac{dR}{dx} = \frac{13}{14\text{Pr}}. \tag{5.4.11}$$

The general solution to this equation is

$$R = Cx^{-3/4} + \frac{13}{14\text{Pr}}. \tag{5.4.12}$$

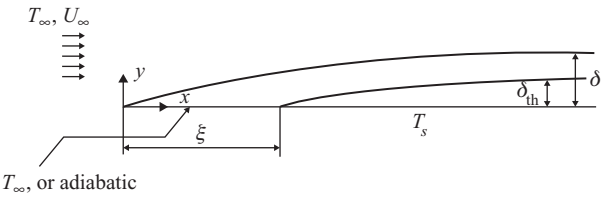

Figure 5.6. A flat surface with an adiabatic starting segment.

The first term on the right-hand side of this equation is the solution to the homogeneous differential equation we obtain by equating the left-hand side of Eq. (5.4.11) with zero and the second term on the right-hand side of the equation is a particular solution to Eq. (5.4.11).

We can now apply the boundary condition $r = 0$ at $x = 0$ to Eq. (5.4.12), which can be satisfied only if $C = 0$, and therefore

$$r = \left(\frac{13}{14\text{Pr}}\right)^{1/3}. \tag{5.4.13}$$

The definition of the local Nusselt number gives

$$\text{Nu}_x = \frac{h_x x}{k} = \frac{x}{k}\frac{q_s''}{T_s - T_\infty} = \frac{x}{k}\frac{-k}{T_s - T_\infty}\left.\frac{\partial T}{\partial y}\right|_{y=0}. \tag{5.4.14}$$

Using Eq. (5.4.3), we find that this equation gives

$$\text{Nu}_x = \frac{3}{2}\frac{x}{r\delta}. \tag{5.4.15}$$

Substituting for δ and r from Eqs. (5.2.15) and (5.4.13), respectively, then leads to

$$\text{Nu}_x = 0.3317\text{Re}_x^{1/2}\text{Pr}^{1/3}. \tag{5.4.16}$$

The discussion thus far was limited to a laminar boundary layer. A similar analysis can be easily performed for turbulent flow, provided that (a) the dimensionless velocity and temperature profiles are approximated by functions that are appropriate for turbulent boundary layers, and (b) it is borne in mind that very close to the wall the approximate profiles for velocity and temperature should be abandoned and instead near-wall turbulent profile characteristics be used. A good example will be discussed shortly, in which heat transfer on a flat plate that includes an adiabatic segment is addressed.

5.4.2 Parallel Flow Past a Flat Surface With an Adiabatic Segment

This is an important example for the application of the integral method. It is particularly useful because it is the starting point for the solution of the heat transfer problems for nonisothermal surfaces (see Fig. 5.6).

Laminar Boundary Layer

Consider laminar flow with UWT boundary condition. A careful review of the previous section will show that the derivations up to Eq. (5.4.12) are valid, provided that $r < 1$ everywhere. (Note that now it is not necessary to have $\text{Pr} > 1$ in order for the condition $r < 1$ to be met. The latter condition will be met as long as the

thermal boundary layer does not grow to become thicker than the velocity boundary layer.) The boundary condition for Eq. (5.4.12), however, is now $r = 0$ *at* $x = \xi$. Application of this condition to Eq. (5.4.12) leads to

$$C = -\frac{13}{14\mathrm{Pr}}\xi^{3/4}. \tag{5.4.17}$$

We then get

$$r = \left(\frac{13}{14\mathrm{Pr}}\right)^{1/3}\left[1 - \left(\frac{\xi}{x}\right)^{3/4}\right]^{1/3}. \tag{5.4.18}$$

Using Eq. (5.4.15), we finally get

$$\mathrm{Nu}_x = \mathrm{Nu}_{x0}\left[1 - \left(\frac{\xi}{x}\right)^{3/4}\right]^{-1/3}, \tag{5.4.19}$$

where

$$\mathrm{Nu}_{x0} = 0.3317\,\mathrm{Re}_x^{1/2}\mathrm{Pr}^{1/3}. \tag{5.4.20}$$

Nu_{x0} represents the local Nusselt number (i.e., Nu_x) at the limit of $\xi = 0$, namely, when there is no adiabatic wall segment.

Let us now discuss UHF boundary conditions. In this case, an integral analysis leads to (Hanna and Myers, 1962)

$$\mathrm{Nu}_x = \mathrm{Nu}_{x0}\left[1 - \frac{\xi}{x}\right]^{-1/3}, \tag{5.4.21}$$

$$Nu_{x0} = 0.418\,\mathrm{Re}_x^{1/2}\mathrm{Pr}^{1/3}, \tag{5.4.22}$$

where $\mathrm{Nu}_x = \frac{q_s'' x}{(T_s - T_\infty)k}$. The constant in the preceding equation has been derived to be 0.453 by Kays et al. (2005).

Note that when UHF boundary conditions are dealt with, we are interested in knowing the surface temperature. Equations (5.4.21) and (5.4.22), with 0.418 as the constant, thus lead to

$$(T_s - T_\infty) = \frac{q_s'' x}{0.418\mathrm{Re}_x^{1/2}\mathrm{Pr}^{1/3}k\left[1 - \frac{\xi}{x}\right]^{-1/3}}. \tag{5.4.23}$$

Turbulent Boundary Layer

A similar analysis, this time for a turbulent boundary layer, can be performed. The general approach is the same as for laminar boundary layers, with two differences. First, the assumed dimensionless velocity and temperature profiles should be compatible with turbulent boundary layers. Second, we must bear in mind that the simple profiles that are assumed for velocity and temperature will not be accurate very close to the wall where the laws of the wall will determine the local shapes of these profiles. In this respect, the situation will be similar to what we discussed in Section 5.1, where we applied Eq. (5.2.31).

Let us consider UWT conditions and make the following assumptions:

1. The velocity profile in the boundary layer, except very close to the wall, follows the 1/7-power distribution,

$$\left(\frac{u}{U_\infty}\right) = \left(\frac{y}{\delta}\right)^{1/7}. \tag{5.4.24}$$

2. Except at very close distances from the wall, the temperature distribution also follows the 1/7-power distribution,

$$\left(\frac{T - T_\infty}{T_s - T_\infty}\right) = 1 - \left(\frac{y}{\delta_{th}}\right)^{1/7}. \tag{5.4.25}$$

3. Everywhere we have $\delta_{\text{th}} \leq \delta$.

We also note that Eqs. (5.2.36) and (5.2.37) apply. An analysis using the integral method then gives (Burmeister, 1993)

$$\frac{q_s''}{\rho C_P (T_s - T_\infty)} = \text{St}_x = \frac{C_f}{2}\left[1 - \left(\frac{\xi}{x}\right)^{9/10}\right]^{-1/9}, \tag{5.4.26}$$

where $\text{St}_x = \frac{\text{Nu}_x}{\text{Re}_x \text{Pr}}$. However, to expand the applicability of this expression to situations in which $\text{Pr} \neq 1$, we replace St_x with $\text{St}_x \text{Pr}^{0.4}$. In doing this, we actually apply an important analogy between heat and momentum transport (the Chilton–Colburn analogy), discussed in Chapter 9. Furthermore, we substitute for C_f from Eq. (5.2.38) to finally get

$$\text{St}_x \text{Pr}^{0.4} = \frac{\text{Nu}_x}{\text{Re}_x \text{Pr}^{0.6}} = \left.\frac{\text{Nu}_x}{\text{Re}_x \text{Pr}^{0.6}}\right|_{\xi=0}\left[1 - \left(\frac{\xi}{x}\right)^{9/10}\right]^{-1/9}, \tag{5.4.27}$$

where,

$$\left.\frac{\text{Nu}_x}{\text{Re}_x \text{Pr}^{0.6}}\right|_{\xi=0} = 0.0287 \text{Re}_x^{-0.2}. \tag{5.4.28}$$

5.4.3 Parallel Flow Past a Flat Surface With Arbitrary Wall Surface Temperature or Heat Flux

For this case, the thermal energy equation when properties are constant and there is no viscous dissipation is

$$\rho C_P \frac{DT}{Dt} = k \nabla^2 T. \tag{5.4.29}$$

This is a linear and homogeneous partial differential equation, and therefore the superposition principle can be applied to its solutions. This will allow us to deduce the solution to any arbitrary wall temperature distribution if the solution to a step change in the wall temperature followed by a constant wall temperature is known.

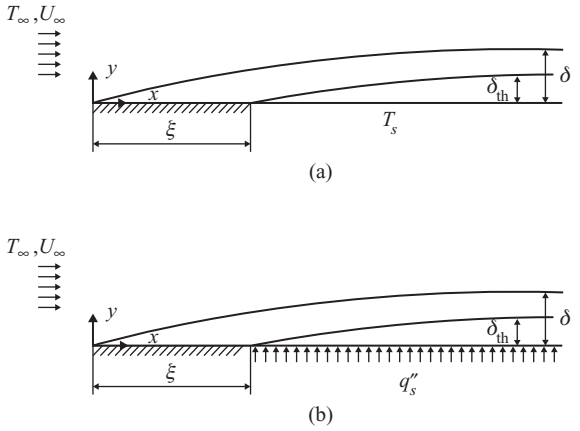

Figure 5.7. Boundary layers on a flat surface with an adiabatic starting segment and a step change in surface temperature or heat flux: (a) constant wall temperature, (b) constant wall heat flux.

Laminar Boundary Layer

Let us first address the case of a known wall temperature distribution. Consider the problem displayed in Fig. 5.7(a), where the wall has undergone a temperature step change from T_∞ to T_s at $\xi = 0$. Then

$$T = T_\infty \quad \text{at } y = 0 \quad \text{and} \quad x < \xi, \tag{5.4.30}$$

$$T = T_s \quad \text{at } y = 0 \quad \text{and} \quad x \geq \xi. \tag{5.4.31}$$

Let us show the solution to the energy equation for the preceding step change in the wall temperature as

$$\frac{T - T_\infty}{T_s - T_\infty} = \theta(x, \xi, y). \tag{5.4.32}$$

If, instead of $(T_s - T_\infty)$, only a temperature jump of dT_s had occurred at the wall, we would get

$$d\,(T - T_\infty) = dT_s \theta(x, \xi, y). \tag{5.4.33}$$

Now, to find the temperature at point (x, y) as a result of an arbitrary T_s distribution, we can use the principle of superposition and write

$$T(x, y) - T_\infty = \int_0^x \theta(x, \xi, y) \frac{dT_s}{d\xi} d\xi + \sum_{i=1}^{N} \Delta T_{s,i} \theta(x, \xi_i, y), \tag{5.4.34}$$

where $\Delta T_{s,i}$ represent finite jumps in wall temperature occurring at ξ_i locations and dT_s is the infinitesimal wall temperature variation at location ξ.

Furthermore, we can get the heat flux and local Nusselt number by noting that

$$q''_x = -k \left.\frac{\partial T}{\partial y}\right|_{y=0} = -k \left[\int_0^x \left.\frac{\partial \theta(x, \xi, y)}{\partial y}\right|_{y=0} \frac{dT_s}{d\xi} d\xi + \sum_{i=1}^{N} \left.\frac{\partial \theta(x, \xi_i, y)}{\partial y}\right|_{y=0} \Delta T_{s,i} \right]. \tag{5.4.35}$$

Now, because $\theta = \frac{T - T_\infty}{T_s - T_\infty}$,

$$-k \left.\frac{\partial \theta}{\partial y}\right|_{y=0} = -\frac{k}{(T_s - T_\infty)} \left.\frac{\partial T}{\partial y}\right|_{y=0} = h. \tag{5.4.36}$$

Thus Eq. (5.4.35) actually means

$$q_s'' = \int_0^x h(\xi, x)\frac{dT_s}{d\xi}d\xi + \sum_{i=1}^{\infty} h(\xi_i, x)\Delta T_{s,i}. \tag{5.4.37}$$

Note that $h(\xi, x)$ is the heat transfer coefficient at location x resulting from a wall temperature jump at location ξ and can therefore be found from Eqs. (5.4.19) and (5.4.20) for a laminar boundary layer.

Now let us address the case of an arbitrary wall heat flux distribution. The outline of an analysis can be found in Kays et al. (2005). Accordingly, the wall temperature at location x, resulting from an arbitrary wall heat flux distribution, can be found from

$$T_s(x) - T_\infty = \frac{0.623}{k}\mathrm{Re}_x^{-1/2}\mathrm{Pr}^{-1/3}\int_{\xi=0}^{x}\left[1 - \left(\frac{\xi}{x}\right)^{3/4}\right]^{-2/3} q_s''(\xi)d\xi. \tag{5.4.38}$$

For $q_s'' = \text{const.}$, this equation leads to

$$\mathrm{Nu}_x = \frac{q_s''}{T_s(x) - T_\infty}\frac{x}{k} = 0.453\,\mathrm{Re}_x^{1/2}\mathrm{Pr}^{1/3}. \tag{5.4.39}$$

Turbulent Boundary Layer

The essential elements of the analysis just presented are the same for turbulent boundary layers. Equation (5.4.37) applies for an arbitrary wall temperature distribution, provided that the heat transfer coefficient $h(\xi, x)$ is found from a turbulent boundary-layer correlation, for example Eqs. (5.4.27) and (5.4.28). For an arbitrary wall heat flux distribution, by use of the 1/7-power velocity and temperature distributions in the boundary layer, the method leads to (Kays et al., 2005)

$$T_s(x) - T_\infty = \frac{3.42}{k}\mathrm{Re}_x^{-0.8}\mathrm{Pr}^{-0.6}\int_{\xi=0}^{x}\left[1 - \left(\frac{\xi}{x}\right)^{9/10}\right]^{-8/9} q_s''(\xi)d\xi. \tag{5.4.40}$$

For, $q_s''(\xi) = \text{const.}$, this leads to

$$\mathrm{Nu}_x = 0.030\,\mathrm{Re}_x^{0.8}\mathrm{Pr}^{0.6}. \tag{5.4.41}$$

5.5 Approximate Solutions for Flow Over Axisymmetric Bodies

For flow and heat transfer over bodies of arbitrary shape numerical methods are often needed. CFD tools are indeed convenient for such analyses. Simple, analytical solutions are available for a few cases, however, that can provide useful fast and approximate solutions. These approximate solutions are based on the integral energy equation without an attempt to include the momentum equation in the analysis.

For laminar flow of a constant-property fluid over an axisymmetric body with UWT surface conditions, an analysis based on the hypothesis that the thickness of any boundary layer depends only on local parameters and that the functional

Table 5.2. *Constants in Eq. (5.5.1) (from Kays et al., 2005)*

Pr	C_1	C_2	C_3
0.7	0.418	0.435	1.87
0.8	0.384	0.450	1.90
1.0	0.332	0.475	1.95
5.0	0.117	0.595	2.19
10.0	0.073	0.685	2.37

dependence of the boundary-layer thickness on local parameters is similar to the functional dependence in wedge flow leads to (Kays et al., 2005)

$$\mathrm{St}_x = \frac{C_1 \mu^{1/2} R \left(\rho_\infty U_\infty\right)^{C_2}}{\left[\int_0^x \left(\rho_\infty U_\infty\right)^{C_3} R^2 dx\right]^{1/2}}, \tag{5.5.1}$$

where the coordinate x and the radius R are defined in Fig. 5.8. The constants C_1, C_2, and C_3 depend on the Prandtl number, as listed in Table 5.2. Note that ρ_∞ and U_∞ are not constants. The velocity U_∞, in particular, will depend on x, even for a incompressible flow, and can be found from the solution of potential flow.

An approximate solution for turbulent flow of a constant-property fluid over an axisymmetric body, when $T_\infty = \text{const.}$, but with arbitrarily varying T_s and U_∞, leads to (Kays et al., 2005)

$$\mathrm{St}_x = 0.0287 \mathrm{Pr}^{-0.4} \frac{R^{0.25} \left(T_s - T_\infty\right)^{0.25} \mu^{0.2}}{\left[\int_0^x \rho_\infty U_\infty \left(T_s - T_\infty\right)^{1.25} R^{1.25} dx\right]^{0.2}}, \tag{5.5.2}$$

where $x = 0$ corresponds to the virtual origin of the thermal boundary layer. This expression applies when gradients of pressure and surface temperature are moderate. It is derived based on the hypothesis that the heat transfer coefficient depends on local parameters only and assuming that viscous dissipation is negligible.

EXAMPLE 5.1. An incompressible and constant-property fluid flows parallel to a flat plate whose surface temperature varies, as shown in Fig. 5.9. Derive an analytical expression that can be used for calculating the convective heat transfer coefficient for points where $x > l_1 + l_2$, assuming that the boundary layer remains laminar.

SOLUTION. The wall temperature profile is shown in Fig. 5.9. Note that $\Delta T_{s,1}$ and $\Delta T_{s,l_2}$ are positive, but $\Delta T_{s,2}$ is negative.

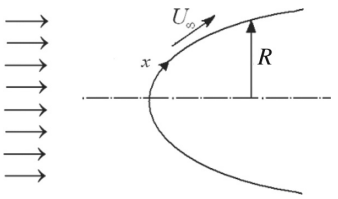

Figure 5.8. Flow past an axisymmetric body.

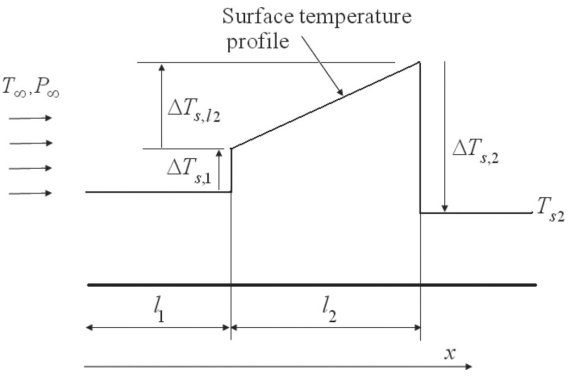

Figure 5.9. The system described in Example 5.1.

We can find the heat transfer coefficient at location x by writing

$$h(x) = \frac{q_s''(x)}{T_s(x) - T_\infty},$$

where $q_s''(x)$ is to be found from Eq. (5.4.37).

To evaluate the first term on the right-hand side of Eq. (5.4.37), we note that

$$\frac{dT_s}{d\xi} = 0 \quad \text{for} \quad \xi < l_1,$$
$$\frac{dT_s}{d\xi} = \frac{\Delta T_{s,l_2}}{l_2} \quad \text{for} \quad l_1 < \xi < l_1 + l_2,$$
$$\frac{dT_s}{d\xi} = 0 \quad \text{for} \quad l_1 + l_2 < \xi.$$

Furthermore, from Eqs. (5.4.19) and (5.4.20) we can write

$$h(\xi, x) = \frac{k}{x}\mathrm{Nu}_{x0}\left[1 - \left(\frac{\xi}{x}\right)^{3/4}\right]^{-1/3}$$
$$= \frac{k}{x}\left(0.3317\mathrm{Re}_x^{1/2}\mathrm{Pr}^{1/3}\right)\left[1 - \left(\frac{\xi}{x}\right)^{3/4}\right]^{-1/3}.$$

We therefore get, for $x \geq l_1 + l_2$,

$$\int_{\xi=0}^{x} h(\xi, x)\frac{dT_s}{d\xi}d\xi = \int_{\xi=l_1}^{l_1+l_2} \frac{k}{x}\left(0.3317\mathrm{Re}_x^{1/2}\mathrm{Pr}^{1/3}\right)\left[1 - \left(\frac{\xi}{x}\right)^{3/4}\right]^{-1/3}\frac{\Delta T_{s,l_2}}{l_2}d\xi.$$

Let us now address the second term on the right-hand side of Eq. (5.4.37). We note that there are two abrupt temperature jumps: one at $x = l_1$ (or $\xi = l_1$) and one at $x = l_1 + l_2$ (or $\xi = l_1 + l_2$). We therefore have

$$\sum_{i=1}^{\infty} h(\xi_i, x)\Delta T_{s,i} = \frac{k}{x}\left(0.3317\mathrm{Re}_x^{1/2}\mathrm{Pr}^{1/3}\right)\left[1 - \left(\frac{l_1}{x}\right)^{3/4}\right]^{-1/3}\Delta T_{s,1}$$
$$+ \frac{k}{x}\left(0.3317\mathrm{Re}_x^{1/2}\mathrm{Pr}^{1/3}\right)\left[1 - \left(\frac{l_1 + l_2}{x}\right)^{3/4}\right]^{-1/3}\Delta T_{s,2}.$$

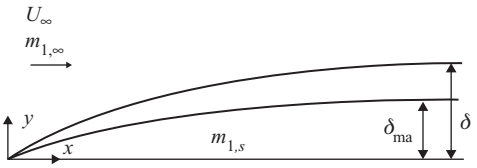

Figure 5.10. Velocity and mass transfer boundary layers for parallel flow on a flat plate.

The heat transfer coefficient at a location where $x > l_1 + l_2$ can therefore be found from

$$h(x) = \frac{0.3317k\mathrm{Pr}^{1/3}}{T_{s2} - T_\infty}\frac{\mathrm{Re}_x^{1/2}}{x}\left\{\int_{\xi=l_1}^{l_1+l_2}\left[1-\left(\frac{\xi}{x}\right)^{3/4}\right]^{-1/3}\frac{\Delta T_{s,l_2}}{l_2}d\xi\right.$$
$$\left.+\left[1-\left(\frac{l_1}{x}\right)^{3/4}\right]^{-1/3}\Delta T_{s,1}+\left[1-\left(\frac{l_1+l_2}{x}\right)^{3/4}\right]^{-1/3}\Delta T_{s,2}\right\}.$$

EXAMPLE 5.2. Perform the mass transfer equivalent of the derivations discussed in Subsections 5.4.1 and 5.4.2.

SOLUTION. First consider the system shown in Fig. 5.10, which is the mass transfer equivalent of Fig. 5.5. Let us use subscript 1 to represent the transferred species. The mass fractions of the transferred species at the surface and in the ambient flow are $m_{1,s}$ and $m_{1,\infty}$, respectively. We also assume that we deal with low mass transfer rates.

An analysis similar to that of Section 5.3 can be performed to derive

$$n_{1,s} = \frac{d}{dx}\int_0^Y (m_1 - m_{1,\infty})\rho u dy - (\rho v)_s(m_{1,s} - m_{1,\infty}), \tag{a}$$

where $n_{1,s}$ is the total mass flux of species 1 at the surface (i.e., at $y = 0$). We can define a modified mass transfer boundary layer thickness Δ_{ma} according to

$$\Delta_{ma} = \int_0^\infty \frac{\rho u(m_1 - m_{1,\infty})}{\rho_\infty U_\infty(m_{1,s} - m_{1,\infty})}dy. \tag{b}$$

For an incompressible fluid and assuming that only species 1 is transferred between the surface and the fluid (which implies that $n_{1,s} = m''_{1,s}$), we then get

$$\frac{m''_{1,s}}{\rho U_\infty(m_{1,s} - m_{1,\infty})} = \frac{d\Delta_{ma}}{dx}. \tag{c}$$

We now consider laminar flow, assuming a mass fraction distribution in the mass transfer boundary layer as

$$\frac{m_1 - m_{1,\infty}}{m_{1,s} - m_{1,\infty}} = 1 - \frac{3}{2}\left(\frac{y}{\delta_{ma}}\right) + \frac{1}{2}\left(\frac{y}{\delta_{ma}}\right)^3. \tag{d}$$

Steps similar to those in Section 5.4 can now be followed, assuming that $\delta_{ma} < \delta$, which would be valid for $\mathrm{Sc} > 1$. The analysis leads to

$$\mathrm{Sh}_x = 0.3317\mathrm{Re}_x^{1/2}\mathrm{Sc}^{1/3}, \tag{e}$$

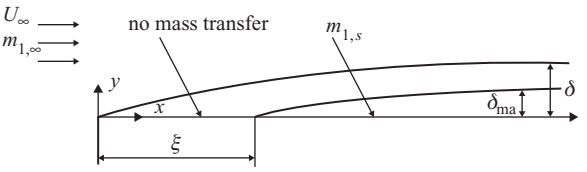

Figure 5.11. A flat surface with UMF surface conditions preceded by a segment with no mass transfer.

where

$$\mathrm{Sh}_x = \frac{\mathcal{K}_x x}{\rho \mathcal{D}_{12}} = \frac{m''_{1,s} x}{\rho \mathcal{D}_{12} (m_{1,s} - m_{1,\infty})}. \tag{f}$$

This equation is similar to Eq. (5.4.16), and we could in fact derive it from that equation by considering the similarity between heat and mass transfer processes.

We now consider the system shown in Fig. 5.11. Assuming that $\delta_{\mathrm{ma}} < \delta$ is satisfied, an analysis similar to that of Section 5.4 for laminar flow would then lead to

$$\mathrm{Sh}_x = \mathrm{Sh}_{x0} \left[1 - \left(\frac{\xi}{x} \right)^{3/4} \right]^{-1/3}, \tag{g}$$

where Sh_{x0} is to be calculated from Eq. (e). Equations (e) and (g) are obviously similar to Eqs. (5.4.20) and (5.4.19), respectively.

For a turbulent boundary layer, again an analysis similar to the one described in Section 5.4 would lead to [see Eqs. (5.4.27) and (5.4.28)]

$$\frac{\mathrm{Sh}_x}{\mathrm{Re}_x \, \mathrm{Sc}^{0.6}} = \left. \frac{\mathrm{Sh}_x}{\mathrm{Re}_x \, \mathrm{Sc}^{0.6}} \right|_{\xi=0} \left[1 - \left(\frac{\xi}{x} \right)^{9/10} \right]^{-1/9}, \tag{h}$$

where

$$\left. \frac{\mathrm{Sh}_x}{\mathrm{Re}_x \mathrm{Sc}^{0.6}} \right|_{\xi=0} = 0.0287 \mathrm{Re}_x^{-0.2}. \tag{i}$$

EXAMPLE 5.3. Dry air at 300 K temperature and 1-bar pressure flows parallel to a flat surface at a velocity of 1.5 m/s. The flat surface is everywhere at 300 K temperature. The surface is dry up to a distance of 12 cm downstream from the leading edge of the surface, but is maintained wet with water beyond that point. Calculate the evaporation rate at a distance of 18 cm from the leading edge, assuming that the surface temperature is maintained at 300 K everywhere. Also, calculate the rate and direction of heat transfer that is needed to maintain the surface at 300 K.

SOLUTION. Figure 5.11 is a good depiction of the system. Let us first calculate properties. For simplicity we use properties of pure air, all at 300 K temperature and 1-bar pressure. This approximation is reasonable, because the mass fraction of water vapor will be small:

$$\rho = 1.161 \, \mathrm{kg/m^3}, \; C_P = 1005 \, \mathrm{J/kg\,K}, \; k = 0.0256 \, \mathrm{W/m\,K},$$
$$\nu = 1.6 \times 10^{-5} \, \mathrm{m^2/s}, \; \mathrm{Pr} = 0.728.$$

The binary mass diffusivity of air–water vapor can be found from Appendix H:

$$\mathcal{D}_{12} = 2.6 \times 10^{-5}\,\mathrm{m^2/s},$$
$$Sc = \frac{\nu}{\mathcal{D}_{12}} = \frac{1.6 \times 10^{-5}\,\mathrm{m^2/s}}{2.6 \times 10^{-5}\,\mathrm{m^2/s}} = 0.651.$$

Next we see if the boundary layer remains laminar over the distance of interest:

$$\mathrm{Re}_x = U_\infty x/\nu = (1.5\,\mathrm{m/s})(0.18\,\mathrm{m})/(1.6 \times 10^{-5}\,\mathrm{m^2/s}) = 16{,}882.$$

The boundary layer will be laminar. We can therefore use Eqs. (e) and (g) of the previous example.

$$\mathrm{Sh}_{x,0} = 0.3317\mathrm{Re}_x^{1/2}\mathrm{Sc}^{1/3} = 0.3317\,(16{,}882)^{1/2}\,(0.615)^{1/3} = 36.65,$$
$$\mathrm{Sh}_x = Sh_{x0}\left[1 - (\xi/x)^{3/4}\right]^{-1/3} = (36.65)\left[1 - (0.12/0.18)^{3/4}\right]^{-1/3} = 57.27.$$

The mass transfer coefficient can now be found from the definition of Sh_x:

$$\mathrm{Sh}_x = \frac{\mathcal{K}_x x}{\rho\mathcal{D}_{12}} \Rightarrow \mathcal{K}_x = \mathrm{Sh}_x \frac{\rho\mathcal{D}_{12}}{x}$$
$$= (57.27)\,\frac{(1.161\,\mathrm{kg/m^3})\left(2.6 \times 10^{-5}\,\mathrm{m^2/s}\right)}{(0.18\,\mathrm{m})} = 9.61 \times 10^{-3}\,\mathrm{kg/s},$$

where we use subscripts 1 and 2 to refer to water vapor and air, respectively. To calculate the mass transfer rate, we need the water-vapor mass fractions in air, both at the surface and at the far field. Because the air is dry, then $m_{1,\infty} = 0$. We can find the air mole fraction of water vapor at the surface by writing

$$X_{1,s} = \frac{P_{1,s}}{P} = \frac{P_{\mathrm{sat}}\,(T_s)}{P} = \frac{3536\,\mathrm{Pa}}{10^5\,\mathrm{Pa}} = 0.0354,$$
$$m_{1,s} = \frac{X_{1,s}M_1}{X_{1,s}M_1 + (1 - X_{1,s})\,M_2}$$
$$= \frac{(0.0354)\,(18\,\mathrm{kg/kmol})}{(0.0354)\,(18\,\mathrm{kg/kmol}) + (1 - 0.0354)\,(29\,\mathrm{kg/kmol})} = 0.0222.$$

Note that, to write the last equation, we used Eqs. (1.2.5) and (1.2.7). The evaporation mass flux can now be calculated:

$$m_1'' = \mathcal{K}_x\,(m_{1,s} - m_{1,\infty}) = (9.61 \times 10^{-3}\,\mathrm{kg/m^2\,s})\,(0.0222 - 0)$$
$$= 2.137 \times 10^{-4}\,\mathrm{kg/m^2\,s}.$$

To find the heat transfer rate, we note that, because the surface and the flow field are at the same temperature, there will be no sensible heat transfer between the surface and the fluid. The energy flow at the vicinity of the interface will then be similar to that shown in Fig. 5.12. An energy balance for the interface then leads to

$$m_1''\boldsymbol{h}_f + q'' = m_1''\boldsymbol{h}_g,$$

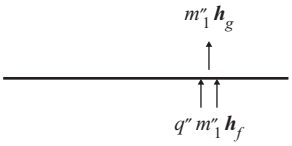

Figure 5.12. The energy flows at the vicinity of the surface in Example 5.3.

where $\boldsymbol{h}_f$ and $\boldsymbol{h}_g$ represent specific enthalpies of saturated liquid water and steam at 300 K. We therefore get

$$q'' = m''_1 \boldsymbol{h}_{fg} = (2.137 \times 10^{-4}\,\text{kg/m}^2\,\text{s})(2.437 \times 10^6\,\text{J/kg}) = 520.8\,\text{W/m}^2.$$

Thus, to maintain the surface at 300 K, the surface actually has to be heated to make up for the latent heat that leaves the wet surface because of evaporation.

PROBLEMS

Problem 5.1. Prove Eq. (5.1.11).

Problem 5.2. Consider the steady-state and laminar flow of an incompressible and constant-property fluid parallel to a flat plate (Fig. 5.3). Assume a fourth-order polynomial velocity profile of the form

$$u = a + by + cy^2 + dy^3 + ey^4.$$

Using an analysis similar to that of Subsection 5.2.1, show that

$$\delta = \sqrt{\frac{1260}{37}} x \text{Re}_x^{-1/2}.$$

Problem 5.3. Consider the laminar flow of an incompressible, non-Newtonian fluid parallel to a flat surface, where the following constitutive relation applies:

$$\tau_{xy} = K\left(\frac{\partial u}{\partial y}\right)^n,$$

where coordinates x and y are defined as in Fig. 5.3. Assuming a velocity profile similar to Eq. (5.2.8), derive an expression of the form $\frac{\delta}{x} = f(\text{Re}_x, n)$, where the Reynolds number is defined as

$$\text{Re}_x = \frac{\rho x^n U_\infty^{(2-n)}}{K},$$

$$\frac{\delta}{x} = c(n)\,\text{Re}_x^{-\frac{1}{n+1}},$$

$$c(n) = \left[7.18\left(\frac{3}{2}\right)^n (n+1)\right]^{\frac{1}{n+1}}.$$

Problem 5.4. Consider the flow of a viscous fluid parallel to a flat surface.

(a) Show that the thermal energy equation reduces to

$$\rho\left(u\frac{\partial \boldsymbol{h}}{\partial x} + v\frac{\partial \boldsymbol{h}}{\partial y}\right) = u\frac{dP}{dx} + \mu\left(\frac{\partial u}{\partial y}\right)^2 + \frac{\partial}{\partial y}\left(\frac{\mu}{\text{Pr}}\frac{\partial \boldsymbol{h}}{\partial y}\right).$$

(b) By applying integration over the thickness of the thermal boundary layer to all the terms in this equation, derive a differential equation in terms of the boundary-layer enthalpy thickness defined as

$$\delta_{\boldsymbol{h}} = \int_{y=0}^{\infty} \frac{\rho u}{\rho_\infty U_\infty} \left(\frac{\boldsymbol{h}}{\boldsymbol{h}_\infty} - 1 \right) dy.$$

Problem 5.5. Consider the laminar flow of an incompressible, constant-property fluid parallel to a flat plate. The surface is at a constant temperature T_s (Fig. 5.5). Assume that the velocity and the temperature profiles are both linear. Apply the integral method and derive an expression for Nu_x.

Problem 5.6. Consider the laminar flow of an incompressible, constant-property fluid flow parallel to a flat plate. Assume that $\mathrm{Pr} > 1$ and that the surface temperature varies according to,

$$T_s(x) = T_\infty + Cx^{1/2}.$$

Apply the integral method, with Eq. (5.2.8) representing the velocity profile, and assume that the temperature profile follows a third-order parabola. Prove that

$$\mathrm{Nu}_x = 0.417 \mathrm{Pr}^{1/3} \mathrm{Re}_x^{1/2}.$$

Problem 5.7. Consider the system described in Problem 5.2. Assume that the plate surface is heated, with a UWT surface condition. Also, assume that the thermal boundary layer is smaller than the velocity boundary layer ($\delta_{\mathrm{th}}/\delta \leq 1$) everywhere. Assume a fourth-order temperature profile in the boundary layer, namely,

$$T = A + BT + CT^2 + DT^3 + ET^4.$$

Perform an analysis similar to that of Subsection 5.4.1, and derive a polynomial expression of the form $f(\delta_{\mathrm{th}}/\delta) = 0$.

Problem 5.8. In Problem 5.5 assume that the plate is adiabatic for $0 \leq x \leq \xi$. Assume that the velocity and temperature profiles in the velocity and thermal boundary layers, respectively, are both linear. Prove that

$$\mathrm{Nu}_x = 0.289 \mathrm{Pr}^{1/3} \mathrm{Re}_x^{1/2} \left[1 - \left(\frac{\xi}{x} \right)^{3/4} \right]^{-1/3}.$$

Problem 5.9. Consider the flow field in Fig. 5.6 and assume that the boundary layer is laminar. Assume that the plate is adiabatic for $0 \leq x < \xi$ and there is a constant wall heat flux of q_s'' for $x \geq \xi$. Use the velocity profile in Eq. (5.2.8), and for the temperature profile in the thermal boundary layer assume that

$$\frac{T - T_\infty}{\dfrac{q_s'' \delta_{\mathrm{th}}}{3k}} = 2 - 3 \left(\frac{y}{\delta_{\mathrm{th}}} \right) + \left(\frac{y}{\delta_{\mathrm{th}}} \right)^3.$$

Apply the integral method, and derive expressions for $T_s - T_\infty$ and Nu_x.

Problem 5.10. Atmospheric air at a temperature of 300 K flows parallel to a smooth and flat surface with a velocity of $U_\infty = 3$ m/s. The surface temperature of the plate varies with distance from the leading edge x according to,

$$T_s = 300 + 30\left(\frac{x}{l_1}\right)^{0.7}, \quad l_1 = 0.2 \text{ m},$$

where T_s is in Kelvins. Derive an analytical expression that can be used for calculating the convective heat transfer coefficient up to the point at which the surface temperature reaches 350 K.

Problem 5.11. Atmospheric air at a temperature of 300 K flows parallel to a flat surface with a velocity of $U_\infty = 5$ m/s. At a location x_0, where $\text{Re}_{x0} = 5 \times 10^6$, the plate surface is heated, and the heat flux varies according to

$$q_s'' = q_{s0}''\sqrt{x - x_0},$$

where x is the distance from the leading edge of the plate and $q_{s0}'' = 200$ W/m^2. The surface is adiabatic at locations where $x < x_0$.

Calculate the surface temperature at $x - x_0 = 0.1$ m.

Problem 5.12. Atmospheric air at a temperature of 20 °C flows parallel to a smooth and flat surface with a velocity of $U_\infty = 2$ m/s. The surface temperature of the plate varies with distance from the leading edge x according to

$$\begin{aligned} T_s &= 20\,^\circ\text{C} \quad \text{for} \quad 0 \le x < l_1, \\ T_s &= 40\,^\circ\text{C} + (20\,^\circ\text{C})\,\frac{x - l_1}{l_2} \quad \text{for} \quad l_1 \le x < l_1 + l_2, \\ T_s &= 20\,^\circ\text{C} \quad \text{for} \quad l_1 + l_2 \le x, \end{aligned}$$

where,

$$\begin{aligned} l_1 &= 10 \text{ cm}, \\ l_2 &= 10 \text{ cm}. \end{aligned}$$

Calculate the convective heat transfer coefficient at $x = 25$ cm.

Mass Transfer

Problem 5.13. Consider mass transfer for the flat surface shown in Fig. P5.13. Assume that the mass fraction of the inert transferred species 1 at the surface is a constant $m_{1,s}$ and that Fick's law applies.

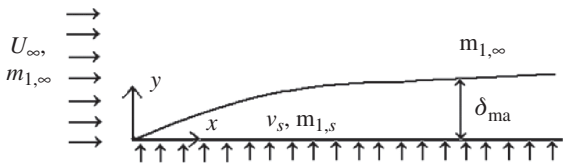

Figure P5.13

Prove the following relation:

$$\frac{d}{dx}\int_0^{\delta_{ma}} (m_{1,\infty} - m_1)\, u dy = \mathcal{D}_{12}\left.\frac{\partial m_1}{\partial y}\right|_{y=0} + v_s\,(m_{1,\infty} - m_{1,s})\,.$$

Problem 5.14. Consider the flow of air with 60% relative humidity and 80-m/s velocity parallel to a flat plate whose surface temperature is at 4 °C. The air temperature is 20 °C. At the location 15 cm downstream from the leading edge, does condensation take place? If so, estimate the condensation rate and discuss the causes of inaccuracy in your solution

6 Fundamentals of Turbulence and External Turbulent Flow

Laminar flow in low-viscosity fluids is relatively rare in nature and industry. Turbulent flow is among the most complicated and intriguing natural phenomena and is not well understood, despite more than a century of study. Nevertheless, out of necessity, investigators developed simple models that can be used for engineering design and analysis.

Turbulent flows at relatively high Reynolds numbers (fully turbulent flows) are characterized by extremely irregular fluctuations in velocity, temperature, pressure, and other properties. At each point the velocity and other properties fluctuate around a mean value.

Turbulent flows are characterized by eddies and vortices. Chunks of fluid covering a wide size range move randomly around with respect to the mean flow. Fluid particles move on irregular paths, and the result is very effective mixing. Even the smallest eddies are typically orders of magnitude larger than the molecular mean free path (MMFP) (in gases) and the intermolecular distances. Within the small eddies, molecular (laminar) transport processes take place, but the interaction among eddies often dominates the overall transport processes and make molecular transport effects unimportant.

With respect to analysis, the Navier–Stokes equations discussed earlier in principle can be applied to turbulent flow as well. However, to obtain a meaningful solution, these equations must be solved in such a way that the largest and smallest eddies in the flow field are resolved. This approach [direct numerical simulation (DNS)] is extremely computational intensive, and it is possible at this time only for simple flow configurations and low Reynolds numbers. Simpler, semiempirical analysis methods are used in practice instead. An encouraging observation in this respect is that, despite their extremely random behavior, the turbulent fluctuations and their resulting motions actually often follow statistical patterns.

6.1 Laminar–Turbulent Transition and the Phenomenology of Turbulence

The exact nature of all the processes that lead to transition from laminar to turbulent flow are not fully understood. Transition in pipes was discovered by Reynolds in 1883, who showed that such a transition occurred in the $\mathrm{Re_D} = 2000$–13000 range.

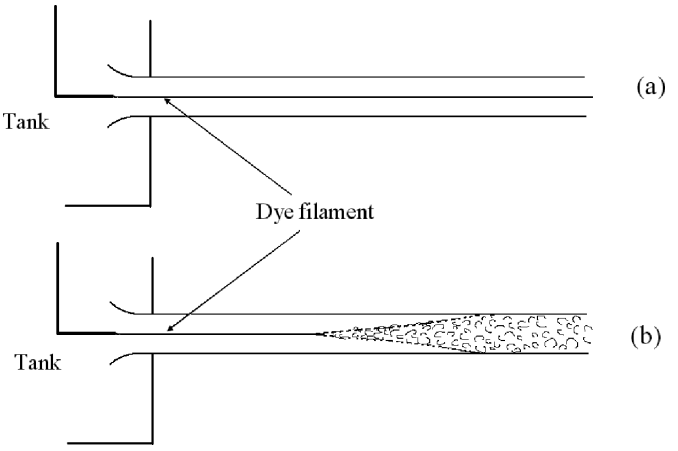

Figure 6.1. The pipe flow dye experiment of Reynolds (1883): (a) laminar flow, (b) turbulent flow.

The qualitative transition process is as shown in Fig. 6.1. Important observations are these:

1. Transition takes place away from the entrance, with the actual transition point approaching the entrance as Re is increased.
2. There is a finite region in which transition to turbulence is completed beyond which equilibrium, fully developed turbulent flow is encountered, where there is a balance between the rates of production and decay of turbulence.
3. In the region where transition is underway the flow is intermittent. At any point in the flow field, over time, laminar and turbulent flow characteristics can intermittently be observed.

The transition process in boundary layers over flat surfaces or blunt bodies has somewhat similar characteristics. Laminar–turbulent flow transition takes place over a finite length in which the flow behavior is intermittent. Figure 6.2 shows the flow past a smooth flat surface without external disturbance. Accordingly, as we move downstream from the leading edge:

1. a stable laminar boundary layer occurs near the leading edge,
2. unstable, 2D waves take place farther downstream,
3. the 2D waves lead to 3D spanwise hairpin eddies,
4. at locations of high shear, vortex breakdown leads to 3D fluctuations,
5. turbulent spots are formed, and
6. the turbulent spots coalesce, leading to fully turbulent flow.

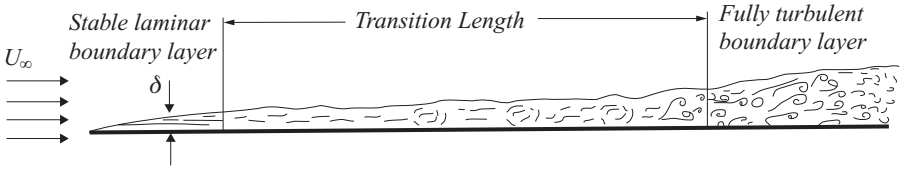

Figure 6.2. Schematic of boundary layer for flow parallel to a smooth and flat plate. (From White, 2006.)

The turbulent spots develop randomly in the flow field. Spanwise 3D vortices are formed in turbulent spots, which can have hairpin structures with their heads lifted with respect to the main flow by about 45°. The hairpin vortices eventually result in bursts. The turbulent spots are thus the source of turbulent bursts, as a result of which chunks of slow-moving fluid move from the bottom of the boundary layer and are mixed with the faster-moving fluid, causing turbulence. The ejected fluid at each burst is of course replaced with fluid coming from the bulk flow. Thus the processes near the wall, including turbulent spots and bursts, are responsible for the turbulent kinetic energy generation.

For flow parallel to a flat plate, the laminar–turbulent transition takes place over the range $\mathrm{Re}_x = 3 \times 10^5$–$2.8 \times 10^6$, depending on a number of parameters, including the surface roughness, level of turbulence in the ambient flow, and the nature of other flow disturbances. The higher limit represents a smooth surface with low main flow turbulence intensity. The following parameters cause the transition to take place at a lower Reynolds number: adverse pressure gradient, free-stream turbulence, and wall roughness.

The structure of the boundary layer in fully turbulent flow is similar in internal and external flows. The boundary layer itself can be divided into an *inner layer* and an *outer layer*. This is because, as mentioned earlier, a turbulent boundary layer is made of two rather distinct layers: the inner layer and the outer layer. In the inner layer, which typically represents 10%–20% of the thickness of the boundary layer, the fluid behavior is dominated by the shear stress at the wall. In the outer layer, on the other hand, the flow behavior is determined by the turbulent eddies and the effect of the wall is only through the retardation of the velocity. The inner layer itself can be divided into three sublayers, the most important of which are a very thin viscous sublayer adjacent to the wall and a fully turbulent sublayer (also referred to as the overlap layer) in which the effect of viscosity is unimportant. The viscous and fully turbulent layers are separated by a buffer-layer. The behavior of the viscous layer is very similar to laminar boundary layers (except for its occasional penetration by turbulent eddies) and is dominated by fluid viscosity. The transport processes are thus governed by laminar (molecular) processes. The viscous sublayer has an approximately constant mean thickness in fully developed flow, although the thickness continually changes over time.

As mentioned earlier, despite the complexity of turbulence and the lack of sufficient physical understanding of its mechanisms, numerous models and empirical correlations have been developed for engineering analysis. Generally speaking, turbulence models can be divided into three groups:

1. Statistical methods. In this approach, statistical properties of fluctuations, and their properties and correlations, are studied.
2. Semiempirical methods. Here, turbulent properties such as mean velocity and temperature, wall heat transfer, and friction, etc., are of interest.
3. Methods that attempt to resolve eddies. These methods are based on the resolution of the turbulent eddies so that their behavior can be predicted mechanistically. DNS and large-eddy simulation (LES) are the most important among these methods. In DNS, all important eddies whose behavior has an impact on the flow and transport processes are resolved. In LES, however, only large

eddies whose behavior is case specific are resolved, and the small eddies whose behavior tends to be universal are modeled.

In this chapter we are primarily interested in the second group of models, which include the majority of current techniques in engineering. We also briefly review the third group of models. These methods are computationally expensive and at this time are used in research only.

6.2 Fluctuations and Time (Ensemble) Averaging

Turbulence fluctuations make the analysis of turbulent flow based on local and instantaneous Navier–Stokes equations extremely time consuming, even with fast computers. We can derive useful and tractable equations by performing averaging, which essentially filters out the fluctuations. Although information about the fluctuations is lost as a result of averaging, the influence of these fluctuations on the important transport phenomena can be incorporated back into the averaged conservation equations by proper modeling. This leads to the appearance of new terms in the averaged equations. Some important definitions need to be mentioned and discussed before averaged equations are discussed.

Strictly speaking, turbulent flows can never be in steady state because of the fluctuations. As a result we use the term *stationary* to refer to a system whose behavior remains unchanged with time from a statistical viewpoint.

In an *isotropic* turbulent field, the statistically averaged properties are invariant under the rotation of the coordinate system or under reflection with respect to a coordinate plane. Thus, in an isotropic turbulent field, the statistical features of the flow field have no preference for any particular direction.

A turbulent flow field is *homogeneous* if the turbulent fluctuations have the same structure everywhere.

Because in steady state (i.e., in stationary state) each flow property can be presented as a mean value plus a superimposed random fluctuation, we can write for any property

$$\phi = \overline{\phi} + \phi', \tag{6.2.1}$$

where,

$$\overline{\phi} = \frac{1}{t_0}\int_{t-t_0/2}^{t+t_0/2} \phi dt. \tag{6.2.2}$$

Because the fluctuations are random, furthermore,

$$\overline{\phi'} = 0. \tag{6.2.3}$$

These definitions are not limited to stationary conditions, however. Equation (6.2.2), which is based on time averaging, can be replaced with *ensemble averaging* when a transient process is of interest. Ensemble averaging means averaging of a property that has been measured in a large number of experiments, in every case at the same location and at the same time with respect to the beginning of the experiment.

Although the average of fluctuations of any property is equal to zero, the averages of products of fluctuations are in general finite.

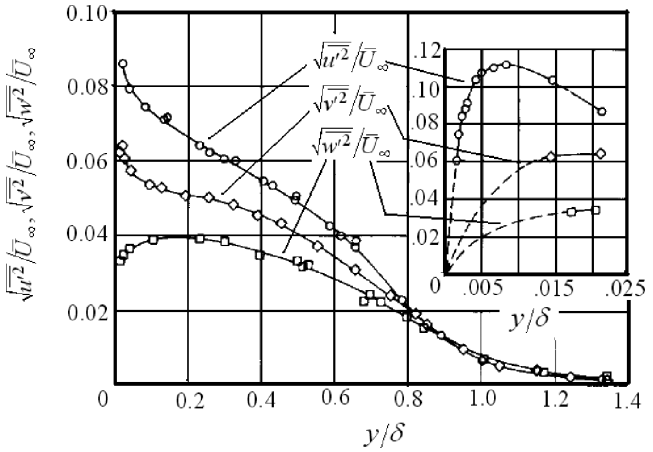

Figure 6.3. Turbulence fluctuations of velocity in parallel flow over a flat plate (Klebanoff, 1955).

The following quantity is called the *turbulence intensity* or *turbulence level*:

$$T = \frac{\sqrt{\frac{1}{3}\left(\overline{u'^2} + \overline{v'^2} + \overline{w'^2}\right)}}{\left|\vec{U}\right|}. \tag{6.2.4}$$

For an isotropic turbulent flow this reduces to

$$T = \frac{\sqrt{\overline{u'^2}}}{|\vec{U}|}. \tag{6.2.5}$$

An idea about the magnitude of these fluctuations can be obtained from Fig. 6.3, which shows the magnitude of fluctuations for the boundary layer on a flat plate at $\mathrm{Re}_x \approx 4.2 \times 10^6$, where u' is in the main flow direction, v' is in the direction vertical to the surface, and w' is in the spanwise direction.

6.3 Reynolds Averaging of Conservation Equations

For simplicity, let us focus on a low-speed, constant-property flow. The local and instantaneous values of the fluctuating properties can be written as

$$u = \overline{u} + u', \tag{6.3.1a}$$
$$v = \overline{v} + v', \tag{6.3.1b}$$
$$w = \overline{w} + w', \tag{6.3.1c}$$
$$P = \overline{P} + P', \tag{6.3.1d}$$
$$T = \overline{T} + T', \tag{6.3.1e}$$
$$m_1 = \overline{m}_1 + m_1', \tag{6.3.1f}$$
$$\rho = \overline{\rho} + \rho' \approx \overline{\rho}. \tag{6.3.1g}$$

The last expression, namely $\rho \approx \overline{\rho}$, is an important approximation that was proposed by Boussinesq. In Eq. (6.3.1f) m_1 is the mass fraction of the transferred species 1.

We would like to apply time averaging to the conservation equations after local and instantaneous terms in these equations have all been replaced with the right-hand sides of the preceding expressions. In performing this averaging, we would note that if f and g are two such properties, namely,

$$f = \overline{f} + f',$$
$$g = \overline{g} + g',$$

then the following apply:

$$\overline{f'} = \overline{g'} = \overline{f'\overline{f}} = \overline{g'\overline{f}} = 0, \tag{6.3.2}$$

$$\overline{\overline{f}} = \overline{f}, \tag{6.3.3}$$

$$\overline{f\overline{g}} = \overline{f}\,\overline{g}, \tag{6.3.4}$$

$$\overline{fg} = \overline{f}\,\overline{g} + \overline{f'g'}, \tag{6.3.5}$$

$$\left(\overline{\frac{\partial f}{\partial s}}\right) = \frac{\partial \overline{f}}{\partial s}, \tag{6.3.6}$$

$$\left(\overline{\int f ds}\right) = \int \overline{f} ds. \tag{6.3.7}$$

Now let us consider the mass, momentum, thermal energy, and mass-species conservation equations in Cartesian coordinates. Using Einstein's rule, we find these equations in local and instantaneous forms:

- mass,

$$\frac{\partial \rho}{\partial t} + \frac{\partial}{\partial x_j}(\rho u_j) = 0; \tag{6.3.8}$$

- momentum in i coordinates,

$$\frac{\partial}{\partial t}(\rho u_i) + \frac{\partial}{\partial x_j}(\rho u_i u_j) = -\frac{\partial P}{\partial x_i} + \frac{\partial \tau_{ij}}{\partial x_j} + \rho g_i, \tag{6.3.9}$$

  where

$$\tau_{ij} = \mu\left(\frac{\partial u_i}{\partial x_j} + \frac{\partial u_j}{\partial x_i}\right); \tag{6.3.10}$$

- thermal energy,

$$\frac{\partial}{\partial t}(\rho C_p T) + \frac{\partial}{\partial x_j}(\rho C_p u_j T) = -\frac{\partial q_j''}{\partial x_j} + \mu\Phi, \tag{6.3.11}$$

  where

$$q_j'' = -k\frac{\partial T}{\partial x_j}, \tag{6.3.12}$$

$$\mu\Phi = \frac{\mu}{2}\left(\frac{\partial u_i}{\partial x_j} + \frac{\partial u_j}{\partial x_i}\right)^2; \tag{6.3.13}$$

- species,

$$\frac{\partial}{\partial t}(\rho m_1) + \frac{\partial}{\partial x_j}(\rho m_1 u_j) = -\frac{\partial}{\partial x_j} j_{1,x_j}, \tag{6.3.14}$$

where

$$j_{1,j} = -\rho \mathcal{D}_{12} \frac{\partial m_1}{\partial x_j}, \tag{6.3.15}$$

where $\mathcal{D}_{12}$ is the mass diffusivity of species 1 with respect to the mixture. We have thus assumed that Fourier's law and Fick's law govern the molecular diffusion of heat and mass, respectively. The preceding equations are local and instantaneous. Now, substituting from Eqs. (6.3.1a) $\sim$ (6.3.1g) in the preceding equations and performing averaging on all the terms in each equation, we get

$$\frac{\partial \rho}{\partial t} + \frac{\partial}{\partial x_j}(\rho \overline{u}_j) = 0, \tag{6.3.16}$$

$$\frac{\partial}{\partial t}(\rho \overline{u}_i) + \frac{\partial}{\partial x_j}(\rho \overline{u}_i \overline{u}_j) = -\frac{\partial \overline{P}}{\partial x_i} + \frac{\partial}{\partial x_j}\left(\overline{\tau}_{ij} - \rho \overline{u_i' u_j'}\right) + \rho g_i, \tag{6.3.17}$$

$$\frac{\partial}{\partial t}\left(\rho C_p \overline{T}\right) + \frac{\partial}{\partial x_j}\left(\rho C_p \overline{u}_j \overline{T}\right) = -\frac{\partial}{\partial x_j}\left(\overline{q}_j + \rho C_p \overline{u_j' T'}\right) + \mu \overline{\Phi}, \tag{6.3.18}$$

$$\frac{\partial}{\partial t}(\rho \overline{m}_1) + \frac{\partial}{\partial x_j}(\rho \overline{m}_1 \overline{u}_j) = -\frac{\partial}{\partial x_j}\left(\overline{j}_{1,j} + \rho \overline{u_j' m_1'}\right), \tag{6.3.19}$$

$$\mu \overline{\Phi} = \frac{\mu}{2} \overline{\left(\frac{\partial \overline{u}_i}{\partial x_j} + \frac{\partial u_i'}{\partial x_j} + \frac{\partial \overline{u}_j}{\partial x_i} + \frac{\partial u_j'}{\partial x_i}\right)^2}. \tag{6.3.20}$$

These are the Reynolds-average conservation equations, which are complicated because of the presence of terms such as $\overline{u_i' u_j'}$ and $\overline{u_i' \phi'}$, where ϕ' is the fluctuation of any scalar transported property.

We can now see that all the flux terms have a laminar and a turbulent component. For example,

$$\tau_{ij} = \rho \left[\nu \left(\frac{\partial \overline{u}_i}{\partial x_j} + \frac{\partial \overline{u}_j}{\partial x_i} \right) - \overline{u_i' u_j'} \right], \tag{6.3.21}$$

$$q_j'' = \rho C_P \left(-\alpha \frac{\partial \overline{T}}{\partial x_j} + \overline{u_j' T'} \right), \tag{6.3.22}$$

$$j_{1,j} = \rho \left(-\mathcal{D}_{12} \frac{\partial \overline{m}_1}{\partial x_j} + \overline{u_j' m_1'} \right). \tag{6.3.23}$$

The *Reynolds stress* is defined as

$$\tau_{ij,tu} = -\rho \overline{u_i' u_j'}. \tag{6.3.24}$$

6.4 Eddy Viscosity and Eddy Diffusivity

The idea for eddy diffusivity is originally due to Boussinesq, who in 1877 suggested that the cross correlation of fluctuation velocities was proportional to the mean velocity gradient, with the proportionality coefficient representing the turbulent viscosity (White, 2006). Accordingly,

$$-\rho \overline{u_i' u_j'} = \rho E_{ij} \left(\frac{\partial \overline{u}_j}{\partial x_i} + \frac{\partial \overline{u}_i}{\partial x_j} \right), \tag{6.4.1}$$

where E_{ij} are the elements of an eddy diffusivity tensor, a second-order tensor. If we assume that turbulence is isotropic, the eddy diffusivity will be a scalar, whereby

$$-\rho\overline{u_i'u_j'} = \rho\, E\left(\frac{\partial\overline{u}_i}{\partial x_j} + \frac{\partial\overline{u}_j}{\partial x_i}\right) - \frac{2}{3}\delta_{ij}\rho K, \tag{6.4.2}$$

where the turbulent kinetic energy is defined as,

$$K = \frac{1}{2}\overline{u_i'u_i'}. \tag{6.4.3}$$

The term $-\frac{2}{3}\delta_{ij}K$ is added to the right-hand side of Eq. (6.4.2) to avoid unphysical predictions; otherwise the equation would predict zero turbulence kinetic energy for an incompressible fluid! Using Eqs. (6.4.2) and (6.3.21) will give

$$\tau_{ij} = \rho(\nu + E)\left(\frac{\partial\overline{u}_i}{\partial x_j} + \frac{\partial\overline{u}_j}{\partial x_i}\right) - \frac{2}{3}\delta_{ij}\rho K. \tag{6.4.4}$$

We can similarly define heat and mass transfer eddy diffusivities. Recall that for molecular diffusion we define the Prandtl and Schmidt numbers as

$$\mathrm{Pr} = \frac{\nu}{\alpha},$$
$$\mathrm{Sc} = \frac{\nu}{\mathcal{D}_{12}}.$$

We can likewise define the *turbulent Prandtl number* and *turbulent Schmidt number* as

$$\mathrm{Pr}_{\mathrm{tu}} = \frac{E}{E_{\mathrm{th}}}, \tag{6.4.5}$$

$$\mathrm{Sc}_{\mathrm{tu}} = \frac{E}{E_{\mathrm{ma}}}. \tag{6.4.6}$$

As a result, we can write

$$\rho\overline{u_j'T'} = -\rho E_{\mathrm{th}}\frac{\partial\overline{T}}{\partial x_j} = -\rho\frac{E}{\mathrm{Pr}_{\mathrm{tu}}}\frac{\partial\overline{T}}{\partial x_j}, \tag{6.4.7}$$

$$\rho\overline{u_j'm_1'} = -\rho E_{\mathrm{ma}}\frac{\partial\overline{m}_1}{\partial x_j} = -\rho\frac{E}{\mathrm{Sc}_{\mathrm{tu}}}\frac{\partial\overline{m}_1}{\partial x_j}, \tag{6.4.8}$$

$$q_j'' = -\rho C_p(\alpha + E_{\mathrm{th}})\frac{\partial\overline{T}}{\partial x_j} = -\rho\, C_p\left(\frac{\nu}{\mathrm{Pr}} + \frac{E}{\mathrm{Pr}_{\mathrm{tu}}}\right)\frac{\partial\overline{T}}{\partial x_j}, \tag{6.4.9}$$

$$j_{1,j} = -\rho\,(\mathcal{D}_{12} + E_{\mathrm{ma}})\,\frac{\partial\overline{m}_1}{\partial x_j} = -\rho\left(\frac{\nu}{\mathrm{Sc}} + \frac{E}{\mathrm{Sc}_{\mathrm{tu}}}\right)\frac{\partial\overline{m}_1}{\partial x_j}. \tag{6.4.10}$$

The momentum, thermal energy, and mass-species equations will now look a lot like the laminar forms of the same equations. The parameters that we need to quantify somehow are E, $\mathrm{Pr}_{\mathrm{tu}}$, and $\mathrm{Sc}_{\mathrm{tu}}$. The following points must be noted in this respect:

1. The fact that turbulence was assumed to be locally isotropic does not mean that E is a constant. The assumption implies that the variations of E are not very sharp and E does not depend on direction locally.

2. Because the transport processes of momentum, energy, and species by turbulent eddies are physically similar, we would expect that $\mathrm{Pr_{tu}} \approx 1$ and $\mathrm{Sc_{tu}} \approx 1$. This is indeed the case and in practice for common fluids $\mathrm{Pr_{tu}} \approx \mathrm{Sc_{th}} \lesssim 1$. (Fluids with $\mathrm{Pr} \ll 1$ are an exception.)

The 2D boundary-layer equations for an incompressible fluid, in Cartesian coordinates, now become,

$$\frac{\partial \rho}{\partial t} + \frac{\partial (\rho \overline{u})}{\partial x} + \frac{\partial (\rho \overline{v})}{\partial y} = 0, \tag{6.4.11}$$

$$\frac{\partial \overline{u}}{\partial t} + \overline{u}\frac{\partial \overline{u}}{\partial x} + \overline{v}\frac{\partial \overline{u}}{\partial y} = -\frac{1}{\rho}\frac{\partial \overline{P}}{\partial x} + \frac{\partial}{\partial y}\left[(\nu + E)\frac{\partial \overline{u}}{\partial y}\right], \tag{6.4.12}$$

$$\frac{\partial \overline{T}}{\partial t} + \overline{u}\frac{\partial \overline{T}}{\partial x} + \overline{v}\frac{\partial \overline{T}}{\partial y} = \frac{\partial}{\partial y}\left[\left(\frac{\nu}{\mathrm{Pr}} + \frac{E}{\mathrm{Pr_{tu}}}\right)\frac{\partial \overline{T}}{\partial y}\right] + \frac{\mu \overline{\Phi}}{\rho C_p}, \tag{6.4.13}$$

$$\mu \overline{\Phi} = \frac{\partial \overline{u}}{\partial y}\left(\mu \frac{\partial \overline{u}}{\partial y} - \rho \overline{u'v'}\right) = \rho(\nu + E)\left(\frac{\partial \overline{u}}{\partial y}\right)^2, \tag{6.4.14}$$

$$\frac{\partial \overline{m}_1}{\partial t} + \overline{u}\frac{\partial \overline{m}_1}{\partial x} + \overline{v}\frac{\partial \overline{m}_1}{\partial y} = \frac{\partial}{\partial y}\left[\left(\frac{\nu}{\mathrm{Sc}} + \frac{E}{\mathrm{Sc_{tu}}}\right)\frac{\partial \overline{m}_1}{\partial y}\right]. \tag{6.4.15}$$

6.5 Universal Velocity Profiles

Useful and concise discussions of the observations that have led to the proposition of universal velocity profiles and the characteristics of the universal velocity profiles can be found in White (2006) and Cebeci and Cousteix (2005).

Velocity and temperature profiles in fully developed turbulent boundary layers have peculiar and interesting characteristics that are very useful. The characteristics of these profiles helped us develop models and develop the concepts of a heat–momentum–mass transfer analogy.

Let us consider a boundary-layer flow in which the flow parameters do not vary strongly with the main flow direction (unlike, for example, the flow field near a flow separation point). We have seen that in laminar boundary layers a single dimensionless parameter [e.g., η in Eq. (3.1.5) in Blasius' analysis] can be used to represent the dimensionless velocity (as well as temperature and concentration) in the entire boundary layer. No single dimensionless parameter can be used to develop a velocity profile for the entire turbulent boundary layer, however. This is because, as mentioned earlier, a turbulent boundary layer is made of two rather distinct layers: the inner layer and the outer layer. In the inner layer, which typically represents 10%–20% of the thickness of the boundary layer, the mean velocity profile is strongly influenced by viscosity and the shear stress at the wall, whereas the effect of the conditions of the outer part of the boundary layer on the velocity profile is negligibly small. In the outer layer, on the other hand, the flow behavior is determined by the turbulent eddies, the viscosity has little effect, and the effect of wall is only through the retardation of the velocity. The velocity profiles in the two layers smoothly merge in the *overlap layer.* Because the velocity profile in the inner and

overlap layers are independent of the flow conditions in the outer layer and beyond, they are essentially the same for internal and external flows.

The universal velocity profiles, subsequently described in some detail, apply to the inner and overlap layers.

Smooth Surfaces

For flow parallel to a smooth and flat surface, it has been found that the mean (i.e., the time- or ensemble-averaged) velocity profile can be divided into three sublayers. The extent of these sublayers, and expressions representing their velocity distributions, are as follows:

1. the viscous sublayer ($y^+ < 5$),

$$u^+ = y^+; \tag{6.5.1}$$

2. the buffer layer ($5 < y^+ < 30$),

$$u^+ = 5.0 \ln y^+ - 3.05; \tag{6.5.2}$$

3. the fully turbulent (overlap) zone ($y^+ > 30$),

$$u^+ = \frac{1}{\kappa} \ln y^+ + B, \tag{6.5.3}$$

where the dimensionless velocity and normal distance from the wall are defined, respectively, as

$$u^+ = \frac{\overline{u}}{U_\tau}, \tag{6.5.4}$$

$$y^+ = y \frac{U_\tau}{\nu}. \tag{6.5.5}$$

The term overlap refers to the merging of the inner and outer zones of the boundary layers. In the viscous sublayer, viscous effects are dominant and the flow field is predominantly laminar. In the fully turbulent zone, turbulent eddies dominate all transport processes, and viscous effects are typically negligible. In the buffer zone, viscous (molecular) diffusion and turbulent effects are both important. The parameter k (Karman's constant) and B are universal constants, and according to Nikuradse they have the following values:

$$\kappa = 0.4,$$

$$B = 5.5.$$

The preceding equations predict velocity profiles on smooth surfaces very well. Equation (6.5.3), in particular, is good for up to $y^+ \approx 400$, and after that it tends to underpredict u^+.

It should be emphasized that Eqs. (6.5.1)–(6.5.3) apply to a boundary-layer flow in which the flow parameters do not vary strongly with the main flow direction. The ideal situation would be when $U_\infty = \text{const.}$ for the boundary layer. However, Eq. (6.5.3) has been found to predict experimental data with moderate positive and negative pressure gradients in the flow direction, even though such pressure gradients modify the velocity profile in the wake zone of the boundary layer.

Equations (6.5.1)–(6.5.3) are not the only way we can depict the universal velocity profile. As an example, the following composite expression, proposed by Spalding (1961), was found to provide excellent agreement with all three sublayers:

$$y^+ = u^+ + \exp(-\kappa B)\left[\exp(\kappa u^+) - 1 - \kappa u^+ - \frac{(\kappa u^+)^2}{2} - \frac{(\kappa u^+)^3}{6}\right]. \quad (6.5.6)$$

Effect of Surface Roughness

The preceding universal velocity profile is for smooth surfaces. Experiments show that, for flow past a rough surface, a logarithmic velocity profile does occur and Eq. (6.5.3) is satisfied. The constant B needs to be modified, however. Its magnitude depends on the roughness height ε_s and it decreases with increasing ε_s. Equation (6.5.3) can be cast for a rough surface as

$$u^+ = \frac{1}{\kappa}\ln y^+ + B - \Delta B\left(\varepsilon_s^+\right), \quad (6.5.7)$$

where $\varepsilon_s^+ = \varepsilon_s \frac{U_\tau}{v}$. Experiments furthermore have lead to the following important observations:

- For $\varepsilon_s^+ < 5$, surface roughness has no effect on the logarithmic velocity profile, and the surface is called *hydraulically smooth* (or simply *smooth*).
- For $\varepsilon_s^+ \gtrsim 70$, the effect of surface roughness is so strong that it makes the contribution of viscosity negligible. The surface is then referred to as *fully rough*.
- For $5 \lesssim \varepsilon_s^+ \lesssim 70$, we deal with the transition conditions and surface roughness and viscosity are both important.

For a flat, fully rough surface, it turns out that

$$(B - \Delta B) = \frac{1}{\kappa}\ln\left(\frac{32.6}{\varepsilon_s^+}\right). \quad (6.5.8)$$

When $y^+ > \varepsilon_s^+$, Eqs. (6.5.7) and (6.5.8) simply lead to

$$u^+ = \frac{1}{\kappa}\ln\left(\frac{y}{\varepsilon_s}\right) + 8.5. \quad (6.5.9)$$

This is a further indication of the insignificance of the viscosity effect for fully rough surfaces.

For flat surfaces with $\frac{\varepsilon_x}{x} > \frac{\mathrm{Re}_x}{1000}$, using Eq. (6.5.9), we can derive (White, 2006),

$$C_f \approx \left[1.4 + 3.7\log_{10}(x/\varepsilon_s)\right]^{-2}. \quad (6.5.10)$$

The following empirical correlations, developed by Schlichting (1968), are used more often:

$$C_f = \left[2.87 + 1.58\log_{10}\left(\frac{x}{\varepsilon_s}\right)\right]^{-2.5}, \quad (6.5.11)$$

$$\langle C_f\rangle_l = \frac{1}{l}\int_0^l C_f dx \approx \left[1.89 + 1.62\log_{10}\left(\frac{l}{\varepsilon_s}\right)\right]^{-2.5}. \quad (6.5.12)$$

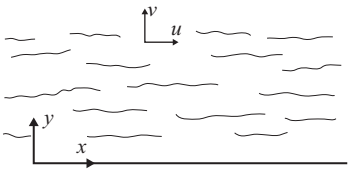

Figure 6.4. A 2D boundary-layer flow field.

6.6 The Mixing-Length Hypothesis and Eddy Diffusivity Models

Prandtl's mixing-length hypothesis (Prandtl, 1925) is one of the earliest and simplest models for equilibrium turbulence.

The simple kinetic theory of gases predicts that,

$$\mu = \frac{1}{3}\rho\lambda_{\text{mol}}\left\langle|U_{\text{mol}}|\right\rangle, \tag{6.6.1a}$$

where λ_{mol} is the MMFP and $\langle|U_{\text{mol}}|\rangle$ is the mean speed of molecules. A more accurate expression, based on the Chapman and Enskog approximate solution of the Boltzmann's transport equation (Chapman and Cowling, 1970), is (Eckert and Drake, 1959)

$$\mu = 0.499\rho\lambda_{\text{mol}}\left\langle|U_{\text{mol}}|\right\rangle. \tag{6.6.1b}$$

Equation (6.6.1b) is actually what leads to Eq. (1.5.10).

Now we consider the 2D boundary-layer flow in Fig. 6.4, and assume that x is the coordinate along the direction of the main flow and u is the fluid velocity in that direction. In analogy with Eq. (6.6.1a) or (6.6.1b), Prandtl assumed that

$$\mu_{\text{tu}} = \frac{\tau_{\text{tu}}}{\dfrac{\partial\overline{u}}{\partial y}} = \rho l_M U_{\text{tu}}, \tag{6.6.2}$$

where l_M is the mixing length, namely the length a typical eddy must travel before it loses its identity, and U_{tu} is the turbulent velocity, i.e., the velocity of an eddy with respect to the local mean flow.

Equation (6.6.2) has two unknowns. We can get rid of one of the unknowns by assuming that

$$U_{\text{tu}} = l_M\left|\frac{\partial\overline{u}}{\partial y}\right|. \tag{6.6.3}$$

The consequence is that

$$\tau_{\text{tu}} = \rho l_M^2\left|\frac{\partial\overline{u}}{\partial y}\right|\frac{\partial\overline{u}}{\partial y}. \tag{6.6.4}$$

An implicit assumption leading to this model is that fluctuations in the y direction are proportional to those in x direction, such that

$$-v' \approx u' \approx l_M\left|\frac{\partial\overline{u}}{\partial y}\right|. \tag{6.6.5}$$

Then,

$$-\overline{u'v'} = E\left(\frac{\partial\overline{u}}{\partial y}\right) = l_M^2\left(\frac{\partial\overline{u}}{\partial y}\right)^2. \tag{6.6.6}$$

Thus the mixing-length hypothesis leads to

$$E = l_M^2 \left| \frac{\partial \overline{u}}{\partial y} \right|. \tag{6.6.7}$$

We must now determine l_M, which can evidently vary from place to place. We can use the universal velocity profile for this purpose.

In the viscous sublayer, obviously, $l_M = 0$ and $E = 0$, which is consistent with $u^+ = y^+$. In the overlap (fully turbulent) zone, the only meaningful length scale is the normal distance from the wall, y. Therefore, for $35 < y^+ \lesssim 400$,

$$l_M = \kappa y. \tag{6.6.8}$$

We can obtain confirmation for this equation by noting that, in the boundary layer, very near the wall, we have $\tau \approx \tau_s$. Thus τ can be considered to be constant. This is because, as $y \to 0$, the x-momentum equation gives

$$\underbrace{\overline{u}}_{0} \frac{\overline{\partial u}}{\partial x} + \underbrace{\overline{v}}_{0} \frac{\partial \overline{u}}{\partial y} = -\frac{1}{\rho} \underbrace{\frac{\partial \overline{p}}{\partial x}}_{0} + \frac{1}{\rho} \frac{\partial \tau}{\partial y}. \tag{6.6.9}$$

Proceeding with $\tau \approx \tau_s$ and noting that $\mu \ll E$ in the fully turbulent zone, we can then write for the fully turbulent zone

$$\tau_s \approx \rho E \frac{\partial \overline{u}}{\partial y}. \tag{6.6.10}$$

Now, using $l_M = \kappa y$ gives

$$\frac{\partial u^+}{\partial y^+} = \frac{1}{\kappa y^+}. \tag{6.6.11}$$

The solution of this ODE then leads to Eq. (6.5.3).

In the outer layer of a turbulent boundary layer ($y^+ \gtrsim 400$), it appears that $l_M \sim$ const. For $y/\delta \lesssim a/\kappa$, Escudier (1966) suggested (Launder and Spalding, 1972)

$$\frac{l_M}{\delta} = \kappa \frac{y}{\delta}, \tag{6.6.12}$$

where δ is the boundary-layer thickness (say, $\delta_{0.99}$) and $a \approx 0.09$.

The preceding discussion left out the viscous and buffer sublayers. A better assessment of l_M in a turbulent boundary layer actually shows that (White, 2006),

$$l_M \sim y^2, \quad \text{viscous sublayer}, \tag{6.6.13}$$

$$l_M \sim y, \quad \text{overlap zone}, \tag{6.6.14}$$

$$l_M \approx \text{const.}, \quad \text{outer layer}. \tag{6.6.15}$$

Relation Between Mixing Length and Eddy Diffusivity

A composite model for l_M or the eddy diffusivity would obviously be very useful. (Composite means a single expression or group of expressions that covers all three sublayers of a turbulent boundary layer.) Many such models have been proposed; some of the most widely used are as follows.

Van Driest (1956) proposed,

$$l_M = \kappa y \left[1 - \exp\left(-\frac{y^+}{A} \right) \right], \tag{6.6.16}$$

where $A = 26$ for a smooth and flat surface. This expression evidently includes a damping factor that accounts for the damping effect of the wall on the turbulent eddies. The constant A depends on the conditions, including the pressure gradient, surface roughness, and the presence or otherwise of blowing or suction through the wall.

Note that, by knowing l_M, we can find E. The approach is as follows. In the boundary layer on a flat surface, as mentioned earlier, the shear stress τ_{yx} is approximately constant and equal to τ_s; therefore

$$\tau_s = \rho\left(E + \nu\right)\frac{d\overline{u}}{dy}. \tag{6.6.17}$$

This is equivalent to

$$U_\tau^2 = \left(\nu + E\right)\frac{d\overline{u}}{dy} = \left(\nu + l_M^2\left|\frac{d\overline{u}}{dy}\right|\right)\frac{d\overline{u}}{dy}. \tag{6.6.18}$$

This equation in dimensionless form gives

$$\left(1 + l_M^{+2}\left|\frac{du^+}{dy^+}\right|\right)\frac{du^+}{dy^+} = 1. \tag{6.6.19}$$

This equation can be recast as

$$\left(\frac{dy^+}{du^+}\right)^2 - \frac{dy^+}{du^+} - l_M^{+2} = 0. \tag{6.6.20}$$

This quadratic equation can now be solved for $\frac{dy^+}{du^+}$ to get

$$\left(\frac{dy^+}{du^+}\right) = \frac{1}{2} + \frac{1}{2}\left(1 + 4l_M^{+2}\right)^{1/2}. \tag{6.6.21}$$

Now, because we have $\rho\left(E + \nu\right)\frac{d\overline{u}}{dy} = \tau_s$, we can write

$$\frac{E + \nu}{\nu} = \frac{dy^+}{du^+}. \tag{6.6.22}$$

The preceding two equations then give

$$\frac{E}{\nu} = -\frac{1}{2} + \frac{1}{2}\left(1 + 4l_M^{+2}\right)^{1/2}. \tag{6.6.23}$$

Thus, if we use van Driest's model, the eddy diffusivity will follow:

$$\frac{E}{\nu} = -\frac{1}{2} + \frac{1}{2}\left\{1 + 4\kappa^2 y^{+2}\left[1 - \exp\left(\frac{-y^+}{A}\right)\right]^2\right\}^{1/2}, \quad A = 26. \tag{6.6.24}$$

Note that, by knowing E, we can integrate the following equation, which we derive by manipulating Eq. (6.6.22):

$$u^+\left(y^+\right) = \int_0^{y^+}\frac{dy^+}{\frac{E}{\nu} + 1}. \tag{6.6.25}$$

This equation is in fact another form of the law of the wall.

The following correlation is a very good representation of the turbulent core in fully turbulent flow in a smooth pipe with $\mathrm{Re}_D \gtrsim 10^5$ (Nikuradse, 1932; Schlichting, 1968):

$$\frac{l_M}{R_0} = 0.14 - 0.08\left(\frac{r}{R_0}\right)^2 - 0.06\left(\frac{r}{R_0}\right)^4. \tag{6.6.26a}$$

This correlation is not accurate very close to the wall. We can remedy this deficiency by multiplying the right-hand side of Eq. (6.6.26a) by van Driest's damping factor, which is defined as

$$\left[1 - \exp\left(-\frac{y^+}{26}\right)\right]. \tag{6.6.26b}$$

Mixing Length for Scalar Quantities

The derivation of Eq. (6.6.7), as noted, was based on the assumption that axial and lateral fluid velocity fluctuations are proportional and that, for the direction parallel to the wall, $u' \approx l_M|\frac{\partial \overline{u}}{\partial y}|$. These assumptions lead us to

$$\tau_{xy} = -\rho\overline{u'v'} = \rho E\left(\frac{\partial \overline{u}}{\partial y}\right) = \rho l_M^2\left|\frac{\partial \overline{u}}{\partial y}\right|\left(\frac{\partial \overline{u}}{\partial y}\right). \tag{6.6.27}$$

Let us now consider the transport of the scalar quantity ϕ for which the turbulent diffusion flux is [see Eq. (6.3.22) or (6.3.23)]

$$j_{\phi,y,tu} = \rho\overline{v'\phi'}. \tag{6.6.28}$$

We can proceed by making the following assumptions:

1. The fluid lumps that transport the quantity ϕ have to move l_ϕ in the direction perpendicular to the main flow before they lose their identities.
2. The fluctuations in the direction of the main flow and the direction perpendicular to the main flow are proportional in terms of their magnitudes.

With these assumptions we can write

$$\phi' \approx l_\phi \frac{\partial \overline{\phi}}{\partial y}. \tag{6.6.29}$$

Using this equation and the fact that $v' \approx -l_M|\frac{\partial \overline{u}}{\partial y}|$, we find that Eq. (6.6.28) gives (Launder and Spalding, 1972)

$$j_{\phi,y,\mathrm{tu}} = -\rho l_M l_\phi\left|\frac{\partial \overline{u}}{\partial y}\right|\frac{\partial \overline{\phi}}{\partial y}. \tag{6.6.30}$$

This implies that

$$E_\phi = l_M l_\phi\left|\frac{\partial \overline{u}}{\partial y}\right|. \tag{6.6.31}$$

Thus, for heat transfer and for the diffusive transfer of the transferred species [species 1 in Eq. (6.3.23)], we have

$$E_{\text{th}} = l_M l_{\text{th}} \left| \frac{\partial \overline{u}}{\partial y} \right|, \tag{6.6.32}$$

$$E_{\text{ma}} = l_M l_{\text{ma}} \left| \frac{\partial \overline{u}}{\partial y} \right|. \tag{6.6.33}$$

We can now assign the following physical interpretations to turbulent Prandtl and Schmidt numbers:

$$\text{Pr}_{\phi,\text{tu}} = \frac{E}{E_\phi} = \frac{l_M}{l_\phi}, \tag{6.6.34}$$

$$\text{Pr}_{\text{tu}} = \frac{E}{E_{\text{th}}} = \frac{l_M}{l_{\text{th}}}, \tag{6.6.35}$$

$$\text{Sc}_{\text{tu}} = \frac{E}{E_{\text{ma}}} = \frac{l_M}{l_{\text{ma}}}. \tag{6.6.36}$$

A somewhat different interpretation was made by Hinze (1975), who wrote, based on the aforementioned two assumptions,

$$\phi' \approx l_\phi \frac{\partial \overline{\phi}}{\partial y}, \tag{6.6.37}$$

$$v' \approx -l_\phi \frac{\partial \overline{u}}{\partial y}. \tag{6.6.38}$$

As a result, combining the constant with l_ϕ, Hinze derived

$$j_{\phi,y,\text{tu}} = -\rho l_\phi^2 \left| \frac{\partial \overline{u}}{\partial y} \right| \frac{\partial \overline{\phi}}{\partial y}, \tag{6.6.39}$$

$$E_\phi = l_\phi^2 \left| \frac{\partial \overline{u}}{\partial y} \right|. \tag{6.6.40}$$

Thus, according to Hinze's interpretation,

$$\text{Pr}_{\text{tu}} = \left(\frac{l_M}{l_{\text{th}}} \right)^2, \tag{6.6.41}$$

$$\text{Sc}_{\text{tu}} = \left(\frac{l_M}{l_{\text{ma}}} \right)^2. \tag{6.6.42}$$

6.7 Temperature and Concentration Laws of the Wall

Temperature Law of the Wall

Consider 2D flow over a flat surface, without blowing or suction, with an isothermal surface. Assume that the flow is fully turbulent. The boundary-layer thermal energy equation will then be (see Fig. 6.5)

$$\rho C_p \left(\overline{u} \frac{\partial \overline{T}}{\partial x} + \overline{v} \frac{\partial \overline{T}}{\partial y} \right) = -\frac{\partial q''_y}{\partial y} + \tau_{yx} \frac{\partial \overline{u}}{\partial y}, \tag{6.7.1}$$

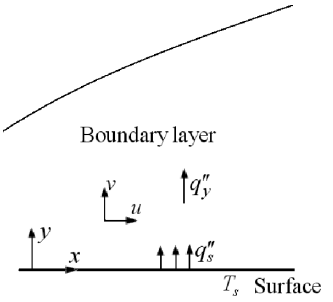

Figure 6.5. Heat transfer in a boundary layer.

where τ_{yx} is the local shear stress and

$$\frac{\partial q''_y}{\partial y} \approx -\rho C_p v_s \frac{\partial \overline{T}}{\partial y}. \tag{6.7.2}$$

We can apply the Taylor expansion to this equation and keep only one term in the expansion series to get

$$q''_y \approx q''_s - \rho C_p v_s \left(\overline{T} - T_s\right). \tag{6.7.3}$$

For an impermeable wall we have $v_s = 0$, and therefore

$$q''_y \approx q''_s = -\rho C_p \left(\alpha + E_{\text{th}}\right) \frac{\partial \overline{T}}{\partial y} = -\rho C_p \left(\frac{\nu}{\text{Pr}} + \frac{E}{\text{Pr}_{\text{tu}}}\right) \frac{\partial \overline{T}}{\partial y}. \tag{6.7.4}$$

This equation can be recast as

$$T^+ = \frac{T_s - \overline{T}}{\dfrac{q''_s}{\rho C_p U_\tau}} = \int_0^{y^+} \frac{dy^+}{\dfrac{1}{\text{Pr}} + \dfrac{E}{(\nu \text{Pr}_{\text{tu}})}}. \tag{6.7.5}$$

Equation (6.7.5) can now be integrated by appropriate correlations for the eddy diffusivity in order to derive the *temperature law of the wall*, a concept originally suggested by von Karman (1939). We also note that from Eq. (6.6.22) that

$$\frac{E}{\nu} = \left(\frac{du^+}{dy^+}\right)^{-1} - 1. \tag{6.7.6}$$

Very close to the wall, in the viscous sublayer where $y^+ < 5$, we note that $\frac{1}{\text{Pr}} + \frac{E}{\nu \text{Pr}_{\text{tu}}} \approx \frac{1}{\text{Pr}}$. This is acceptable unless $\text{Pr} \gg 1$ (viscous oils, for example). We then get

$$T^+ = \text{Pr} y^+ \text{for } y^+ < 5. \tag{6.7.6}$$

In the buffer zone, $5 < y^+ < 30$; using Eq. (6.5.2), (6.7.6), and (6.7.5), we get

$$T^+ = 5\text{Pr} + \int_5^{y^+} \frac{dy^+}{\dfrac{y^+}{5\text{Pr}_{\text{tu}}} + \left(\dfrac{1}{\text{Pr}} - \dfrac{1}{\text{Pr}_{\text{tu}}}\right)}. \tag{6.7.7}$$

This, for $\kappa = 0.4$, leads to

$$T^+ = 5\left\{\text{Pr} + \text{Pr}_{\text{tu}} \ln\left[1 + \frac{\text{Pr}}{\text{Pr}_{\text{tu}}}\left(\frac{y^+}{5} - 1\right)\right]\right\}. \tag{6.7.8}$$

According to a numerical curve fit of Eq. (6.7.5), Kader (1981) derived the following improved expression for the buffer zone:

$$T^+ = \frac{\mathrm{Pr_{th}}}{\kappa} \ln y^+ + A\,(\mathrm{Pr})\,, \tag{6.7.9}$$

where,

$$A \approx \left(3.85\mathrm{Pr}^{1/3} - 1.3\right)^2 + 2.12 \ln (\mathrm{Pr})\,. \tag{6.7.10}$$

Finally, for the fully turbulent zone, $y^+ > 30$, we have $\frac{1}{\mathrm{Pr}} + \frac{E}{\nu \mathrm{Pr_{tu}}} \approx \frac{E}{\nu \mathrm{Pr_{tu}}}$. This approximation would be acceptable unless $\mathrm{Pr} \ll 1$. The approximation thus does not apply to liquid metals, for example, for which the $1/\mathrm{Pr}$ term must be kept in the derivations. From Eq. (6.5.3), then

$$\begin{aligned} \frac{du^+}{dy^+} &= \frac{1}{\kappa y^+}, \\ \Rightarrow \frac{E}{\nu} &= \kappa y^+. \end{aligned} \tag{6.7.11}$$

Equation (6.7.5) then gives

$$T^+ = 5\left\{\mathrm{Pr} + \mathrm{Pr_{tu}} \ln\left[1 + 5\frac{\mathrm{Pr}}{\mathrm{Pr_{tu}}}\right]\right\} + \int_{30}^{y^+} \frac{\mathrm{Pr_{tu}} dy^+}{\kappa y^+}.$$

This gives

$$T^+ = 5\mathrm{Pr_{tu}}\left\{\frac{\mathrm{Pr}}{\mathrm{Pr_{tu}}} + \ln\left[1 + 5\frac{\mathrm{Pr}}{\mathrm{Pr_{tu}}}\right] + \frac{1}{5\kappa} \ln\left(\frac{y^+}{30}\right)\right\}. \tag{6.7.12}$$

Note that we can easily show that

$$\mathrm{St} = \frac{q_s''}{\rho C_P U_\infty (T_s - T_\infty)} = \frac{1}{U_\infty^+ T_\infty^+}, \tag{6.7.13}$$

$$U_\infty^+ = \frac{U_\infty}{\sqrt{\tau_s/\rho}} = \frac{1}{\sqrt{\frac{C_f}{2}}} = \frac{1}{\sqrt{\frac{f}{8}}}. \tag{6.7.14}$$

Thus, by combining these two equations, we get

$$T_\infty^+ = \frac{\sqrt{C_f/2}}{\mathrm{St}}. \tag{6.7.15}$$

This relation gives us a good tool for obtaining a relation between St and C_f based on the universal velocity and temperature profiles. This issue is discussed in Chapter 9.

It should be emphasized that the preceding temperature profiles are not applicable when significant adverse or favorable pressure gradients are present in the flow direction. This is unlike the logarithmic velocity law of the wall, which applies even when moderate pressure gradients are present.

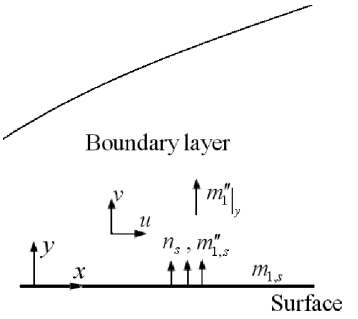

Figure 6.6. Mass transfer in a boundary layer.

Concentration Law of the Wall

Consider the following two conditions:

1. Species 1 is the only transferred species at the wall, and its mass flux is very small, i.e.,

$$m_{1,s}'' \approx 0. \tag{6.7.16}$$

2. If the mass flux through the wall includes other species in addition to the transferred species of interest, we have a vanishingly small total mass flux (representing all the transferred species) through the wall, i.e.,

$$n_s \approx 0. \tag{6.7.17}$$

In these cases, assuming that Fick's law applies, we can write (see Fig. 6.6)

$$m_{1,s}'' = -\rho \mathcal{D}_{12} \left. \frac{\partial \overline{m}_1}{\partial y} \right|_{y=0}. \tag{6.7.18}$$

In the turbulent boundary layer near the wall, similar to our treatment of the thermal boundary layer, we can write

$$m_1'' = -\rho \left(\frac{\nu}{\mathrm{Sc}} + \frac{E}{\mathrm{Sc_{tu}}} \right) \left. \frac{\partial \overline{m}_1}{\partial y} \right|_{y=0} \approx \text{const.} = m_{1,s}''. \tag{6.7.19}$$

Now we define

$$m_1^+ = \frac{m_{1,s} - m_1}{\dfrac{m_{1,s}''}{\rho U_\tau}}. \tag{6.7.20}$$

We can then write

$$m_1^+ = \int_0^{y^+} \frac{dy^+}{\dfrac{1}{\mathrm{Sc}} + \dfrac{E}{\nu \mathrm{Sc_{tu}}}}. \tag{6.7.21}$$

We can now derive the mass-fraction law of the wall by integrating this equation following essentially the same steps as those for temperature. Thus, excluding conditions in which $\mathrm{Sc} \gg 1$ or $\mathrm{Sc} \ll 1$, we get the following expressions:

- viscous sublayer ($y^+ < 5$), assuming that $\frac{E}{\nu \mathrm{Sc_{tu}}} \ll \frac{1}{\mathrm{Sc}}$,

$$m_1^+ = \mathrm{Sc} y^+; \tag{6.7.22}$$

- buffer zone ($5 < y^+ < 30$),

$$m_1^+ = 5\left\{\mathrm{Sc} + \mathrm{Sc_{tu}} \ln\left[1 + \frac{\mathrm{Sc}}{\mathrm{Sc_{tu}}}\left(\frac{y^+}{5} - 1\right)\right]\right\}; \tag{6.7.23}$$

- fully turbulent zone, assuming that $\frac{E}{\nu \mathrm{Sc_{tu}}} \gg \frac{1}{\mathrm{Sc}}$,

$$m_1^+ = 5\mathrm{Sc_{tu}}\left\{\frac{\mathrm{Sc}}{\mathrm{Sc_{tu}}} + \ln\left[1 + 5\frac{\mathrm{Sc}}{\mathrm{Sc_{tu}}}\right] + \frac{1}{5\kappa}\ln\left(\frac{y^+}{30}\right)\right\}. \tag{6.7.24}$$

The conditions in which these relations are applicable are met, for example, for the binary diffusion of gaseous species for which typically Sc is of the order of 1. For dilute solutions in liquids, however, Sc is typically large. For dilute solutions of common chemical species in water, for example, Sc is typically of the order of 10^2–10^3.

6.8 Kolmogorov Theory of the Small Turbulence Scales

Kolmogorov's theory of isotropic turbulence, proposed in early 1940s, provides a powerful and useful framework for modeling the behavior of turbulent eddies that are much smaller than the largest-eddy scales in a highly turbulent flow field. An important application of this theory is the behavior of particles of one fluid phase dispersed in another. Particles of one phase entrained in a highly turbulent flow of another phase (e.g., microbubbles in a turbulent liquid flow) are common in many two-phase flow systems. Examples include agitated mixing vessels and floatation devices. Turbulence determines the behavior of particles by causing particle dispersion, particle–particle collision, particle–wall impact, and coalescence and breakup when particles are fluidic.

A turbulent flow field is *isotropic* when the statistical characteristics of the turbulent fluctuations remain invariant with respect to any arbitrary rotation or reflection of the coordinate system. A turbulent flow is called *homogeneous* when the statistical distributions of the turbulent fluctuations are the same everywhere in the flow field. In isotropic turbulence, clearly, $\overline{u_1'^2} = \overline{u_2'^2} = \overline{u_3'^2}$, where subscripts 1, 2, and 3 represent the 3D orthogonal coordinates. Isotropic turbulence is evidently an idealized condition, although near-isotropy is observed in some systems, for example, in certain parts of a baffled agitated mixing vessel. However, in practice a *locally isotropic* flow field can be assumed in many instances, even in flows such as the flow in pipes, by excluding regions that are in the proximity of walls (Schlichting, 1968).

Highly turbulent flow fields are characterized by random and irregular fluctuations of velocity (as well as other properties) at each point. These velocity fluctuations are superimposed on the base flow and are characterized by turbulent eddies. Eddies can be thought of as vortices that move randomly around and are responsible for velocity variation with respect to the mean flow. The size of an eddy represents the magnitude of its physical size. It can also be defined as the distance over which the velocity difference between the eddy and the mean flow changes appreciably (or the distance over which the eddy loses its identity).

The largest eddies are typically of the order of the turbulence-generating feature in the system. These eddies are too large to be affected by viscosity, and their kinetic energy cannot be dissipated. They produce smaller eddies, however,

and transfer their energy to them. The smaller eddies in turn generate yet smaller eddies, and this cascading process proceeds until energy is transferred to eddies small enough to be controlled by viscosity. Energy dissipation (or viscous dissipation, i.e., irreversible transformation of the mechanical flow energy to heat) then takes place.

A turbulent flow whose statistical characteristics do not change with time is called *stationary*. (We do not use the term steady state here because of the existence of time fluctuations.) A turbulent flow is in *equilibrium* when the rate of kinetic energy transferred to eddies of any certain size is equal to the rate of energy dissipation by those eddies, plus the kinetic energy lost by those eddies to smaller eddies. Conditions close to equilibrium can (and often do) exist under nonstationary situations when the rate of kinetic energy transfer through eddies of a certain size is much larger than their rate of transient energy storage or depletion.

The distribution of energy among eddies of all sizes can be better understood by use of the *energy spectrum* of the velocity fluctuations and by noting that as eddies become smaller the frequency of velocity fluctuations that they represent becomes larger. Suppose we are interested in the streamwise turbulence fluctuations at a particular point. We can write

$$\int_0^\infty \boldsymbol{E}_1(k_1, t)dk_1 = \overline{u_1'^2}, \tag{6.8.1}$$

where $\boldsymbol{E}_1(k_1, t)$ is the one-dimensional (1D) energy spectrum function for velocity fluctuation u_1' in terms of the wave numbers k_1. The wave number is related to frequency according to $k_1 = 2\pi f/\overline{U}_1$, where f represents frequency. Instead of Eq. (6.8.1), We could write

$$\int_0^\infty \boldsymbol{E}_1^*(f, t)df = \overline{u_1'^2}, \tag{6.8.2}$$

$$\boldsymbol{E}_1^*(f, t) = \boldsymbol{E}_1(k_1, t)\frac{d\,k_1}{df} = \frac{2\pi}{\overline{U}_1}\boldsymbol{E}_1(k_1, t), \tag{6.8.3}$$

where $\overline{U}_1$ is the mean streamwise velocity and $\boldsymbol{E}_1^*(f, t)$ is the 1D energy spectrum function of velocity fluctuation u_1' in terms of frequency f. For an isotropic 3D flow field, we can write (Hinze, 1975)

$$\int_0^\infty \boldsymbol{E}(k, t)dk = \frac{3}{2}\overline{u'^2}, \tag{6.8.4}$$

where $\boldsymbol{E}(k, t)$ is the 3D energy spectrum function and k is the radius vector in the 3D wave-number space. The qualitative distribution of the 3D spectrum for isotropic turbulence is depicted in Fig. 6.7 (Pope, 2000; Mathieu and Scott, 2000). The spectrum shows the existence of several important eddy size ranges. The largest eddies, which undergo little change as they move, occur at the lowest-frequency range. The energy containing eddies, named so because they account for most of the kinetic energy in the flow field, occur next. Eddies in the *universal equilibrium range* occur next, and are called so because they have *universal* characteristics that do not depend on the specific flow configuration. These eddies do not remember how they were generated and are not aware of the overall characteristics of the flow field. As a result, they behave the same way, whether they are behind a turbulence

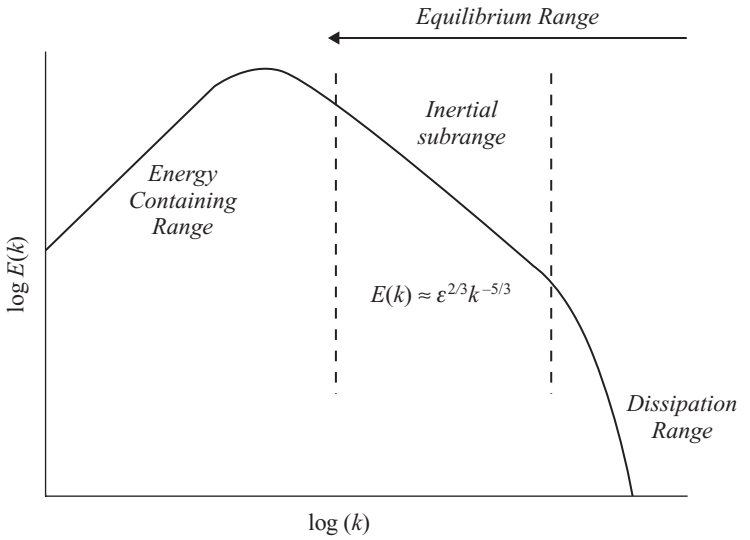

Figure 6.7. Schematic of the 3D energy spectrum in isotropic turbulence.

generating grid in a wind tunnel or in a floatation device. These eddies follow local isotropy, except very close to the solid surfaces.

The universal equilibrium range itself includes two important eddy size ranges: the *dissipation range* and the *inertial size range.* In the *dissipation range* the eddies are small enough to be viscous. Their behavior can be affected by only their size, fluid density, viscosity, and the turbulence dissipation rate (energy dissipation per unit mass), ε. (The dissipation rate actually represents the local intensity of turbulence.) A simple dimensional analysis using these properties leads to the *Kolmogorov microscale*:

$$l_D = \left(\nu^3/\varepsilon\right)^{1/4}. \tag{6.8.5}$$

Likewise, we can derive the following expressions for Kolmogorov's velocity and time scales:

$$u_D = (\nu\varepsilon)^{1/4}, \tag{6.8.6}$$

$$t_{c,D} = (\nu/\varepsilon)^{1/2}. \tag{6.8.7}$$

Eddies with dimensions less that about $10\,l_D$ have laminar flow characteristics. Thus, when two points in the flow field are separated by a distance $\Delta r < 10\,l_D$, they are likely to be within a laminar vortex. In that case, the variation of fluctuation velocities over a distance of Δr can be represented by (Schulze, 1984)

$$\sqrt{\overline{\Delta u'^2}} = 0.26\sqrt{\frac{\varepsilon}{\nu}}\,\Delta r. \tag{6.8.8}$$

The *inertial size range* refers to eddies with characteristic dimensions from about $20\,l_D$ to about $0.05\,\Lambda$, where Λ represents the turbulence macroscale. The macroscale of turbulence represents approximately the characteristic size of the largest vortices or eddies that occur in the flow field. The inertial eddies are too large

to be affected by viscosity, and their behavior is determined by inertia. Because little energy dissipation occurs in this range the flux of energy cascading through the spectrum is approximately the same for wave numbers in the inertial range and is equal to the total turbulent energy dissipation rate ε. The behavior of inertial eddies can thus be influenced by only their size, the fluid density, and turbulent dissipation. The variation of fluctuation velocities across Δr, when Δr is within the inertial size range, can then be represented by (Schulze, 1984)

$$\sqrt{\overline{\Delta u'^2}} = (1.38)\,\varepsilon^{1/3}\,(\Delta r)^{1/3}. \tag{6.8.9}$$

An important characteristic of the inertial zone is that, in that eddy scale range,

$$\boldsymbol{E}(k) = C\varepsilon^{2/3}k^{-5/3}, \tag{6.8.10}$$

where the coefficient C is the universal constant. The preceding relation is referred to as *Kolmogorov's power law*. The validity of this expression was confirmed experimentally. According to Batchelor (1970), $C = 1.7$. The constant C in practice varies slightly and has a recommended value of approximately 1.5.

There is some doubt about the validity of the assumption that the inertial range is controlled by ε only, and therefore about the universality of a constant C, in part because of the intermittency in turbulent fluctuations. Nevertheless, Eq. (6.8.10) with $C \approx 1.5$ is found to apply to a wide variety of flows, even those with mean velocity gradients. A detailed and useful discussion of Kolmogorov's theory can be found in Mathieu and Scott (2000). Equation (6.8.10) provides a simple method for ascertaining the existence of an inertial eddy size range in a complex turbulent flow field.

Bubbles, readily deformable particles, and their aggregates when they are suspended in highly turbulent liquids, often have dimensions within the eddy scales of the inertial range. Their characteristics and behavior can thus be assumed to result from interaction with inertial eddies (Coulaloglou and Tavralides, 1977; Narsimhan et al., 1979; Schulze, 1984; Tobin et al., 1990).

The size of a dispersed fluid particle in a turbulent flow field is determined by the combined effects of breakup and coalescence processes. In dilute suspensions for which breakup is the dominant factor, the maximum size of the dispersed particles can be represented by a critical Weber number, defined as

$$\mathrm{We}_{\mathrm{cr}} = \frac{\rho_c \overline{\Delta u'^2} d_d}{\sigma}, \tag{6.8.11}$$

where subscripts c and d represent the continuous and dispersed phases, respectively, and $\overline{\Delta u'^2}$ represents the magnitude of velocity fluctuations across the particle (i.e., over a distance of $\Delta r \approx d_d$, where d_d is the diameter of the dispersed phase particles). For particles that fall within the size range of viscous eddies, therefore, Eqs. (6.8.8) and (6.8.11) result in

$$d_{d,\max} \approx \left(\frac{\nu\sigma}{\rho_c\varepsilon}\right)^{1/3} \mathrm{We}_{\mathrm{cr}}{}^{1/3}. \tag{6.8.12}$$

For particles that fall in the inertial eddy size range in a locally isotropic turbulent field, Eqs. (6.8.9) and (6.8.11) indicate that the maximum equilibrium particle diameter should follow:

$$d_{d,\max} \approx \left(\frac{\sigma}{\rho_c}\right)^{3/5} \mathrm{We}_{\mathrm{cr}}{}^{3/5}\, \varepsilon^{-2/5}. \tag{6.8.13}$$

The right-hand side of this equation also provides the order of magnitude of the particle Sauter mean diameter, $d_{d,32}$. In a pioneering study of the hydrodynamics of dispersions, Hinze (1955) noted that 95% of particles in an earlier investigation were smaller than

$$d_{d,\max} = 0.725 \left(\frac{\sigma}{\rho_c}\right)^{3/5} \varepsilon^{-2/5}. \tag{6.8.14}$$

The validity of Eq. (6.8.13) has been experimentally demonstrated (Narsimhan et al., 1979; Tobin et al., 1990; Tsouris and Tavlarides, 1994; Bose et al., 1997).

6.9 Flow Past Blunt Bodies

Flows across blunt bodies are accompanied by the formation and growth of boundary layers. Depending on the blunt-body characteristic size and flow properties, however, complex boundary-layer flow regime transitions can occur that result in a strongly nonuniform skin-friction coefficient and heat transfer coefficient. We can better understand the complexity of these phenomena by reviewing the cross flow on a single cylinder, which is probably the simplest of blunt bodies. The phenomena observed here, at least qualitatively, are representative of other blunt bodies as well.

Figure 6.8 displays and describes the various hydrodynamic flow regimes in cross flow on a cylinder with a smooth surface (Lienhard, 1966; Lienhard and Lienhard, 2005). An excellent description and demonstration of the hydrodynamic flow regimes can be found in Coutanceau and Defaye (1991). Velocity and thermal boundary layers form on the surface, starting at the vicinity of the stagnation point, and grow with distance from the stagnation point. The flow field remains attached, laminar, and fore–aft symmetric only at extremely low Reynolds numbers ($\mathrm{Re}_D \lesssim 0.1$). The flow remains laminar and attached everywhere on the cylinder surface, but the flow field becomes fore–aft asymmetrical only in the range $0.1 < \mathrm{Re}_D \lesssim 4.5$). With increasing Re_D, the flow field becomes more disordered. The boundary layers that form on the surface of the cylinder remain laminar everywhere for $\mathrm{Re}_D \lesssim 3 \times 10^5$, and transition to turbulence occurs somewhere on the surface in the $3 \times 10^5 \lesssim \mathrm{Re}_D \lesssim 3.5 \times 10^6$ range. In turbulent flow, the boundary layers over some part of the cylinder will of course remain laminar. The occurrence of boundary-layer separation further complicates the flow field around the cylinder. Boundary-layer separation was discussed in Section 2.4. Boundary-layer separation occurs at $\theta \approx 80^\circ$, where θ is the azimuthal angle ($\theta = 0$ for the stagnation point). In the turbulent regime, however, $\theta \approx 140^\circ$.

The outcome of the aforementioned processes is a very nonuniform heat transfer coefficient on the cylinder. Figure 6.9 displays the measured heat transfer

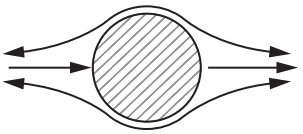

$\text{Re}_D < 5$ Regime of unseparated flow.

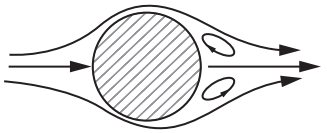

$5 \text{ to } 15 \leq \text{Re}_D < 40$ A fixed pair of Föpple vortices in the wake

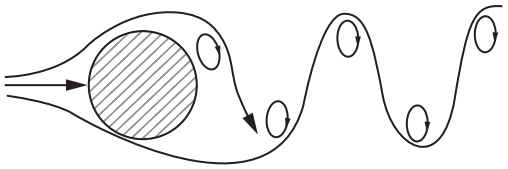

$40 \leq \text{Re}_D < 90$ and $90 \leq \text{Re}_D < 150$

Two regimes in which vortex street is laminar:

Periodicity governed in low-Re_D range by wake instabability.

Periodicity governed in high-Re_D range by vortex shedding.

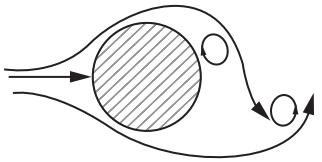

$150 \leq \text{Re}_D < 300$ Transition range to turbulence in vortex.

$300 \leq \text{Re}_D \lesssim 3 \times 10^5$ Vortex street is fully turbulent, and the flow field is increasingly 3-dimensional.

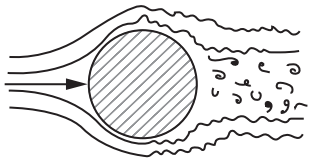

$3 \times 10^5 \lesssim \text{Re}_D < 3.5 \times 10^6$

Laminar boundary layer has undergone turbulent transition. The wake is narrower and disorganized. No vortex street is apparent.

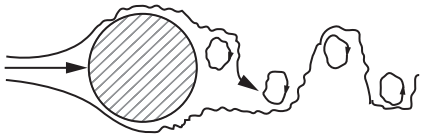

$3.5 \times 10^6 \leq \text{Re}_D < \infty$ | ?)

Reestablishment of the turbulent vortex street that was evident in $300 \leq \text{Re}_D \lesssim 3 \times 10^5$. This time the boundary layer is turbulent and the wake is thinner.`

Figure 6.8. Regimes of flow across circular cylinders (from Lienhard and Lienhard, 2005).

coefficients for air flow across a cylinder (Giedt, 1949). A similar nonuniformity in local heat transfer coefficients can be observed in flow over other blunt bodies.

In most engineering applications, however, we are interested in the circumferentially averaged heat transfer coefficients. Reliable empirical correlations are available for cylinders, spheres, and many other regular geometric configurations, some of which can be found in Table Q.1 in Appendix Q.

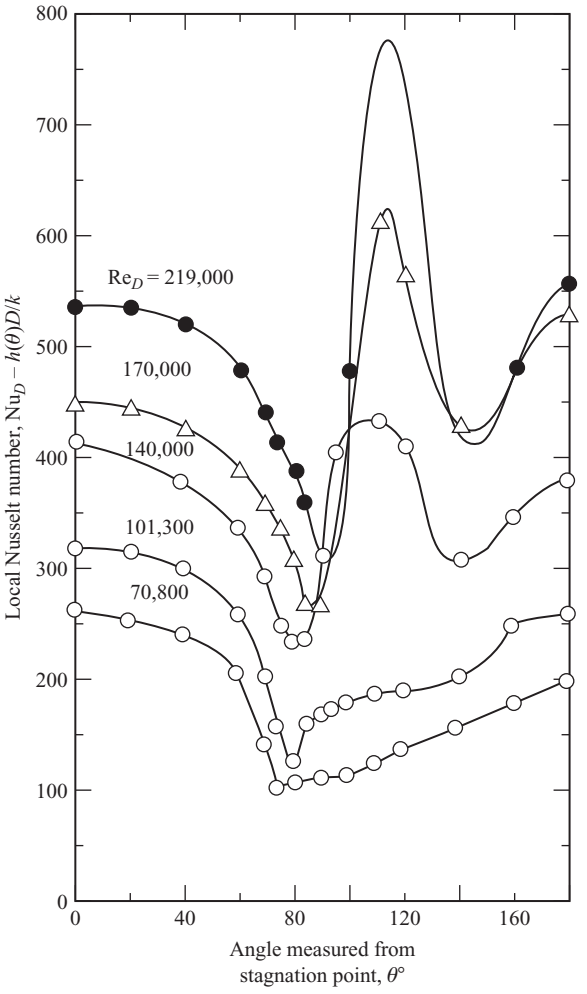

Figure 6.9. Local heat transfer coefficients for atmospheric air flow across a circular cylinder (Giedt, 1949).

EXAMPLE 6.1. Water flows through a flat channel with a hydraulic diameter of 5 cm. At a location where the flow field is fully developed, the water mean temperature is 40 °C. The tube wall surface temperature is $T_s = 70$ °C every where. The Reynolds number defined based on the hydraulic diameter is 2×10^4. Using the velocity and temperature laws of the wall, calculate the mean (time-average) velocity and temperature at $y = 0.5$ mm, where y is the normal distance from the wall. The heat transfer coefficient is 1300 w/m^2 K. For wall friction, you may use the correlation of Dean (1978):

$$C_f = 0.0868\ \mathrm{Re}_{D_H}^{-0.25}.$$

SOLUTION. First, let us calculate properties at the reference temperature of

$$T_f = \frac{1}{2}(T_s + T_m) = 55\ ^\circ\mathrm{C}.$$

The results will be

$$\rho = 985.7\,\mathrm{kg/m^3},\ C_P = 4182\,\mathrm{J/kg\ ^\circ C},\ k = 0.636\,\mathrm{W/m\,K},$$
$$\nu = 5.12 \times 10^{-7}\,\mathrm{m^2/s},\ \mathrm{Pr} = 3.31.$$

Next we calculate the mean and friction velocities:

$$U_m = \mathrm{Re}_{\mathrm{D}_H} \nu / \mathrm{D}_H = (2 \times 10^4)(5.12 \times 10^{-7}\,\mathrm{m^2/s})/(0.05\,\mathrm{m}) = 0.205\,\mathrm{m/s},$$

$$C_f = \frac{0.0868}{\mathrm{Re}_{\mathrm{D}_H}^{0.25}} = \frac{0.0868}{(2 \times 10^4)^{0.25}} = 0.0073,$$

$$\tau_s = C_f \frac{1}{2} \rho U_m^2 = (0.0073)\,\frac{1}{2}\left(985.7\,\mathrm{kg/m^3}\right)\,(0.205\,\mathrm{m/s})^2 = 0.1506\,\mathrm{N/m^2},$$

$$U_\tau = \sqrt{\tau_s/\rho} = \sqrt{(0.1506\,\mathrm{N/m^2})/(985.7\,\mathrm{kg/m^3})} = 0.01236\,\mathrm{m/s}.$$

Let us now find the local time-average velocity at $y = 0.5\,\mathrm{mm}$:

$$y^+ = y U_\tau / \nu = \left(0.5 \times 10^{-3}\mathrm{m}\right)(0.01236\,\mathrm{m/s})/\left(5.12 \times 10^{-7}\mathrm{m^2/s}\right) = 12.08.$$

The point of interest is obviously in the buffer sublayer, and therefore

$$u^+ = 5\,\ln y^+ - 3.05 = 5\,\ln(12.08) - 3.05 = 9.409,$$
$$u = u^+ U_\tau = (9.409)\,(0.01236\,\mathrm{m/s}) = 0.1163\,\mathrm{m/s}.$$

We next calculate the local mean temperature. First we need to calculate the wall heat flux, as follows. From the correlation of Dittus and Boelter (1930) (see Table Q.3 in Appendix Q),

$$\begin{aligned} h = \mathrm{Nu}_{\mathrm{D}_H} \frac{k}{\mathrm{D}_H} &= \left[0.023 \mathrm{Re}_D^{0.8} \mathrm{Pr}^{0.4}\right] \frac{k}{\mathrm{D}_H} \\ &= \left[(0.023)\left(2 \times 10^4\right)^{0.8} (3.31)^{0.4}\right] \frac{0.636\,\mathrm{W/m\,^\circ C}}{(0.05\,\mathrm{m})} \\ &= 1304\,\mathrm{W/m^2\,^\circ C}. \end{aligned}$$

We can now calculate the wall heat flux:

$$q_s'' = h\,(T_s - T_m) = \left(1304\,\mathrm{W/m^2\,^\circ C}\right)(70 - 40)^\circ\,\mathrm{C} = 3.911 \times 10^4\,\mathrm{W/m^2}.$$

We then assume that $\mathrm{Pr_{tu}} = 1$ and proceed by writing

$$\begin{aligned} T^+ &= 5\left\{\mathrm{Pr} + \mathrm{Pr_{tu}} \ln\left[1 + \frac{\mathrm{Pr}}{\mathrm{Pr_{tu}}}\left(\frac{y^+}{5} - 1\right)\right]\right\} \\ &= 5\left\{3.31 + (1)\ln\left[1 + \frac{3.31}{1}\left(\frac{12.08}{5} - 1\right)\right]\right\} = 25.27, \end{aligned}$$

$$\frac{T_s - T}{\dfrac{q_s''}{\rho C_P U_\tau}} = T^+$$

$$\Rightarrow T = T_s - \frac{q_s''}{\rho C_P U_\tau} T^+$$

$$= 70\,^\circ\mathrm{C} - \frac{3.911 \times 10^4\,\mathrm{W/m^2}}{(985.7\,\mathrm{kg/m^3})\,(4182\,\mathrm{J/kg\,^\circ C})\,(0.01236\,\mathrm{m/s})}\,(25.27)$$

$$= 50.6\,^\circ\mathrm{C}.$$

EXAMPLE 6.2. A dilute suspension of cyclohexane in distilled water at a temperature of 25 °C flows in a smooth pipe with 5.25-cm inner diameter. The mean velocity is 2.5 m/s. Estimate the size of the cyclohexane particles in the pipe. The two phases are assumed to be mutually saturated, whereby $\rho_c = 997\ \mathrm{kg/m^3}$,

$\mu_c = 0.894 \times 10^{-3}\ \frac{\text{kg}}{\text{ms}}$, and $\rho_d = 761\,\text{kg/m}^3$, where subscripts c and d represent the continuous and dispersed phases, respectively. For the distilled-water–cyclohexane mixture, when the two phases are mutually saturated, the interfacial tension is $\sigma = 0.0462$ N/m.

SOLUTION. We can use Eq. (6.8.14), provided that we can estimate the turbulent dissipation rate in the pipe. We can estimate the latter from

$$\overline{\varepsilon} \approx \frac{1}{\rho_c} U_m \left|(\nabla P)_{\text{fr}}\right|.$$

To find the frictional pressure gradient, let us write

$$Re_D = \rho_c U_m D/\mu_c \approx 1.46 \times 10^5,$$
$$f = 0.316\text{Re}_D^{-0.25} \approx 0.0162,$$
$$\left|(\nabla P)_{\text{fr}}\right| = f\frac{1}{\text{D}}\frac{1}{2}\rho_c U_m^2 \approx 959\,\text{N/m}^3.$$

The dissipation rate will then be

$$\overline{\varepsilon} \approx 2.4\ \text{W/kg}.$$

Eq. (6.8.14) then gives

$$d_{\max} \approx 1.28 \times 10^{-3}\,\text{m} = 1.28\ \text{mm}.$$

EXAMPLE 6.3. Consider the steady, fully developed, turbulent flow of water in a horizontal pipe, with $\text{Re}_D = 4.0 \times 10^4$. The water temperature is 25 °C.

(a) Calculate the maximum wall roughness size for hydraulically smooth conditions for a tube with D = 25 mm. Also estimate the Kolmogorov microscale and the lower limit of the size range of inertial eddies in the turbulent core of the tube.
(b) Repeat part (a) for a tube with D = 0.8 mm.

For both cases, for estimating the size of Kolmogorov's eddies, assume a hydraulically smooth wall and assume that conventional friction-factor correlations apply.

SOLUTION. (a) The properties are

$$\rho = 997.1\,\text{kg/m}^3, \quad \mu = 8.94 \times 10^{-4}\,\text{m/kg s}.$$

Using $\text{Re}_D = \rho U_m D/\mu$, we find $U_m = 1.435$ m/s. We can then calculate the friction factor f from Blasius' correlation, and use it for the calculation of the absolute value of the pressure gradient. The results will be

$$f = 0.316\text{Re}^{-0.25} \approx 0.0223,$$
$$\left|(\nabla P)_{\text{fr}}\right| = f\frac{1}{\text{D}}\frac{1}{2}\rho U_m^2 \approx 916\,\text{N/m}^3.$$

The mean dissipation rate $\overline{\varepsilon}$ can be found from

$$\overline{\varepsilon} \approx \frac{1}{\rho} U_m \left|(\nabla P)_{\text{fr}}\right|.$$

The results will be $\overline{\varepsilon} \approx 1.317$ W/kg. The Kolmogorov microscale can now be calculated from Eq. (6.8.5), where $\nu = \mu/\rho = 8.96 \times 10^{-7}$ m^2/s and $\overline{\varepsilon} = 1.317$ W/kg are used. The result will be

$$l_D \approx 2.7 \times 10^{-5}\,\text{m} = 27\,\mu\text{m}.$$

The size range of viscous eddies will therefore be $l \leq 10\, l_D \approx 270\,\mu$m. The lower limit of the size range of inertial eddies will be $l \approx 20\, l_D \approx 0.54$ mm. It is to be noted that these calculations are approximate and the viscous dissipation rate is not uniform in a turbulent pipe.

(b) For the tube with $D = 0.8$ mm, the calculations lead to

$$\left|(\nabla P)_{\text{fr}}\right| \approx 2.8 \times 10^7\ \text{N/m}^3$$
$$\overline{\varepsilon} \approx 1.26 \times 10^6\ \text{W/kg},$$
$$l_D \approx 8.7 \times 10^{-7}\,\text{m} = 0.87\,\mu\text{m}.$$

The size range of viscous eddies will thus be $l \lesssim 8.7\ \mu$m, and the lower limit of the inertial eddy size will be approximately only 17 μm.

PROBLEMS

Problem 6.1. Perform calculations for the range $0 < y^+ < 300$ and compare the predictions of the expression proposed by Spalding (1961) [Eq. (6.5.6)] with the predictions of Eqs. (6.5.1)–(6.5.3).

Problem 6.2. In a flat channel with rough walls, away from the immediate vicinity of the walls, the velocity profile conforms to

$$\frac{\overline{u}}{U_m} = c(y/b)^{1/10},$$

where y is the distance from the wall and the distance between the walls is equal to $2b$.

(a) Find an expression for the eddy diffusivity distribution in the channel.
(b) Repeat part (a), this time assuming that the channel is circular and the velocity profile away from the immediate vicinity of the wall conforms to

$$\frac{\overline{u}}{U_m} = c(y/R)^{1/10}.$$

where R is the pipe radius.
(c) Why is the immediate vicinity of the wall excluded from the previous velocity profiles?

Problem 6.3. Water flows through a flat channel with a hydraulic diameter of 22 mm. The flow Reynolds number is 4.5×10^4. Assume fully developed flow.

(a) Assuming a smooth wall surface, calculate the wall shear stress.
(b) Estimate the thicknesses of the viscous and buffer layers.
(c) Assume heat transfer takes place in the channel and the boundary condition is UWT with $T_s = 90\,^\circ$C. At a location where the water mean temperature

is 60 °C, calculate the heat flux at the wall and estimate the liquid temperature at $y = 20\,\mu$m, 65 μm, and 1 mm, where y is the normal distance from the wall.

For friction-factor and heat transfer coefficients, for simplicity, use circular channel correlations with appropriate application of the hydraulic diameter.

Problem 6.4. An alternative to the expression for the buffer-zone velocity profile is (Levich, 1962)

$$u^+ = 10\,\tan^{-1}\left(0.1y^+\right) + 1.2 \quad \text{for } 5 < y^+ < 30.$$

Using this expression, repeat the analysis in Section 6.7 and derive equations similar to Martinelli's temperature law of the wall.

Problem 6.5. Water at room temperature flows through a 5-cm-diameter smooth tube at $\mathrm{Re}_D = 20000$.

(a) Calculate C_f, U_{m}^+, and R^+.
(b) Using van Driest's expression for mixing length, calculate the eddy diffusivity E at $y^+ = 10$ and $y^+ = R^+/3$, where y is the distance from the wall.

Problem 6.6. The eddy diffusivity model of Deissler (1953) for fully turbulent flow in a circular tube is

$$\frac{E}{\nu} = n^2u^+y^+\left[1 - \exp\left(-n^2u^+y^+\right)\right] \quad \text{for } y^+ < 26.$$

Prandtl proposed the following expression for eddy diffusivity in the turbulent core of a pipe:

$$\frac{E}{\nu} = \left[\frac{y^+\left(1 - \dfrac{y^+}{R_0^+}\right)}{2.5} - 1\right].$$

Consider water at 1-bar pressure and 300 K temperature flowing in a smooth-wall pipe whose diameter is 7.5 cm at a Reynolds number of 2.5×10^4. Using the previous eddy diffusivity models (in which Prandtl's expression is used for $y^+ > 26$), calculate and plot E/ν as a function of r/R, using the preceding expressions and using the eddy diffusivity model of van Driest for flow past a flat surface [Eq. 6.6.24)]. Find the dimensionless distance from the wall (y/R) for which the flat surface eddy diffusivity model deviates significantly from the preceding expressions.

Problem 6.7. For a flow of room-temperature water in a 2-mm-diameter tube, calculate the thicknesses of the viscous and buffer sublayers for $\mathrm{Re}_D = 8 \times 10^3$, 1.5×10^4 , and 1.5×10^5.

Problem 6.8. Water at a temperature of 70 °C flows at a velocity of 0.15 m/s over a surface that can be modeled as a wide 150-mm-long flat plate. The entire surface of this plate is kept at a temperature of 0 °C. Plot a graph showing how the local heat flux varies along the plate. Also, plot the velocity and temperature profiles (i.e., $\overline{u}$ and $\overline{T}$ as functions of y) in the boundary layer on the plate at a distance of 85 mm from the leading edge of the plate.

Problem 6.9. On a fully-rough surface, the roughness elements make the viscous sublayer insignificant. Show that the velocity profile in Eq. (6.5.8) can be derived by assuming the following expression for the mixing length.

$$l_m^+ = \kappa(y^+ + 0.031\,\varepsilon_s^+)$$

Using Eq. (6.5.7) and (6.5.8), derive an expression for Fanning friction factor in terms of the boundary layer thickness δ.

7 Internal Turbulent Flow

7.1 General Remarks

Near-wall phenomena in internal turbulent flow has much in common with external turbulent flow, and the discussions of property fluctuations and near-wall phenomena in the previous chapter all apply to internal flow as well. The confined nature of the flow field, however, implies that, unlike external flow in which the free-stream conditions are not affected by what happens at the wall, the transport phenomena at the wall do affect the mean flow properties.

Consider fully developed internal flow in a smooth pipe, shown in Fig. 7.1. Similar to external flow, the entire flow field in the pipe can be divided into three zones: the viscous sublayer, the buffer zone, and the turbulent core. The mean thickness of the viscous sublayer is equal to $y^+ = 5$, where $y^+ = yU_\tau/\nu$ is the distance from the wall in wall units and the buffer zone extends to $y^+ = 30$. Close to the wall, where the effect of wall curvature is small and the fluid is not aware that the overall flow field is actually confined, the universal velocity profile presented in Eqs. (6.5.1)–(6.5.3) apply. Only when we approach the centerline does Eq. (6.5.3) deviate from measurements. Similar observations can be made about noncircular ducts.

Laminar–Turbulent Flow Transition

Similar to external flow for a steady, incompressible flow in a duct, there are three major flow regimes; laminar, transition, and fully turbulent. Transition from laminar to turbulent flow is a crucial regime change and is sensitive to duct geometry, surface roughness, and the strength of disturbances in the fluid. The most important parameter affecting the transition is the Reynolds number that is defined based on the cross-section characteristic dimension. Surface roughness and disturbances all cause the transition to occur at a lower Re (or flow rate). In well-controlled and essentially disturbance-free experiments with smooth circular pipes, laminar flow has been maintained up to $\mathrm{Re}_D \approx 10^5$. In practice, however, the transition occurs at a much lower Re. Laminar flow is known to persist for $\mathrm{Re}_D \leq \mathrm{Re}_{D,\mathrm{cr}} \approx 2300$, irrespective of the disturbances. In practice, it is often assumed that laminar flow persists for $\mathrm{Re}_D \leq 2100$, the transition flow regime occurs for $2100 < \mathrm{Re}_D < 10^4$, and the flow regime is fully turbulent for $\mathrm{Re}_D > 10^4$. One important reason for the choice of $\mathrm{Re}_D = 2100$ for the lower end of the transition regime is to make sure

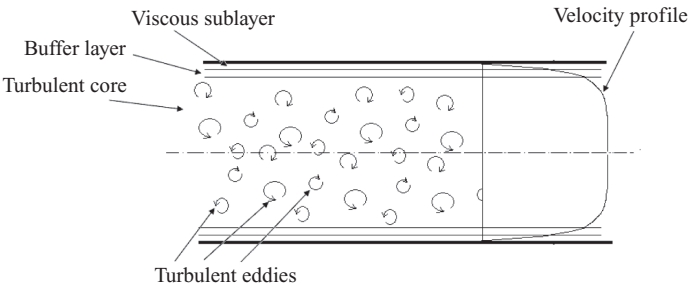

Figure 7.1. Fully developed turbulent velocity profile in a smooth circular duct.

that the interpolation correlations for the transition regime smoothly merge with the laminar flow correlation. In the transition regime, similar to the discussion in the previous chapter, the flow field is intermittent. At any location the flow behaves intermittently as turbulent or laminar in time; and if we freeze the flow field at an instant and examine the instantaneous behavior in the channel, we would note that some parts of the flow field are turbulent whereas others are laminar.

For noncircular channels, the conditions leading to flow regime transition out of laminar flow can be represented by a critical Reynolds number. Using the well-accepted transition criteria for circular pipes by replacing $\mathrm{Re}_{D,\mathrm{cr}}$ with $\mathrm{Re}_{D_H,\mathrm{cr}}$ has been recommended (Schlichting, 1968) for rectangular, triangular, and annular ducts, where D_H is the hydraulic diameter. This approach will provide only an estimate of the conditions that lead to the disruption of laminar flow in noncircular channels. For flow between parallel plates, for example, the transition is affected by the channel entrance and the existing disturbances and can occur in the $\mathrm{Re}_{D_H,\mathrm{cr}} \approx 2200$–$3200$ regime (Beavers et al., 1971).

The surface roughness effect on the flow field is similar to what was explained in Section 6.5. For $\varepsilon_s^+ \leq 5$, the roughness is submerged in the viscous sublayer. The duct is hydraulically smooth, the surface roughness has virtually no effect, and $C_f = f(\mathrm{Re}_{D_H})$. When $\varepsilon_s^+ > 70$ the duct surface is fully rough, the effect of roughness on wall shear stress is overwhelming, and $C_f = f(\varepsilon_s^+)$. A transition regime is encountered for $5 < \varepsilon_s^+ \leq 70$, where $C_f = f(\mathrm{Re}_{D_H}, \varepsilon_s^+)$.

The surface roughness affects the wall–fluid heat and mass transfer by increasing the total interfacial area and, more important, by causing local mixing of the fluid. The surface roughness thus increases the local friction factor as well as the heat and mass transfer coefficients. An empirical correlation for the effect of roughness on local heat transfer, which is due to Norris (1970), for example, suggests that

$$\mathrm{Nu}_{D_H}/\mathrm{Nu}_{D_H,\mathrm{smooth}} = \min\left[(C_f/C_{f,\mathrm{smooth}})^n, (4)^n\right], \tag{7.1.1}$$

$$n = 0.68\,\mathrm{Pr}^{0.215} \quad \text{for } \mathrm{Pr} < 6, \tag{7.1.2}$$

$$n = 1 \quad \text{for } \mathrm{Pr} > 6. \tag{7.1.3}$$

Equation (7.1.3) gives a conservative estimate of the effect of surface roughness. The heat transfer enhancement caused by surface roughness is higher for fluids with large Pr, because for these fluids $\delta > \delta_{\mathrm{th}}$, where δ and δ_{th} are the hydrodynamic and thermal boundary-layer thicknesses, respectively; therefore the thermal resistance

is confined to a thin fluid layer near the wall where the effect of surface roughness is strong.

Using the analogy between heat and mass transfer, the enhancement caused by surface roughness on mass transfer when the mass flux is vanishingly small can be obtained from the preceding expressions by replacing everywhere Nu_{D_H} with Sh_{D_H} and Pr with Sc.

Boundary Condition and Development of Temperature and Concentration Profiles

The heat and mass transfer boundary conditions discussed in Subsection 1.4.5 obviously apply to turbulent flow as well. However, for fluids with $\mathrm{Pr} \lesssim 0.5$ (for heat transfer) or $\mathrm{Sc} \lesssim 0.5$ (for mass transfer), there is no need to analyze each boundary condition separately, and the same correlations apply to all the depicted boundary conditions. The reason is that, for fluids that have high Pr, the temperature profile is approximately flat a very small distance from the wall, and consequently the boundary condition has little effect on the behavior of the bulk fluid. For fluids with $\mathrm{Pr} \ll 0.5$, such as liquid metals, however, the temperature profile is relatively round and as a result empirical correlations will depend on the boundary-condition types.

The development of velocity, temperature, and concentration boundary layers in turbulent duct flow is qualitatively similar to that of laminar flow. A velocity boundary layer forms and grows with increasing distance from inlet until it completely engulfs the entire cross section, and we can define the hydrodynamic entrance length as the length at which the boundary layers merge. The hydrodynamic entrance length in turbulent flow is shorter than laminar flow, however, and strongly depends on the entrance conditions, the intensity of disturbances, and surface roughness. Idealized analysis is possible with simplifying assumptions, for example by assuming a flat inlet velocity profile, a smooth surface, and a power-law velocity profile in the developing boundary layer (see Subsection 7.2.1). In practice, a multitude of hard-to-control parameters affect the entrance length, including the inlet geometry, inlet flow turbulence intensity, wall surface roughness, and other disturbances. As a result, a widely used estimation for circular and noncircular ducts is

$$\frac{l_{\mathrm{ent,hy}}}{D_H} \approx 10. \tag{7.1.4}$$

For fluids with $\mathrm{Pr} \approx 1$ (or $\mathrm{Sc} \approx 1$ for mass transfer) in which the velocity and temperature (or concentration) profiles develop at the same pace,

$$\frac{l_{\mathrm{ent,th}}}{D_H} \approx 10, \tag{7.1.5}$$

$$\frac{l_{\mathrm{ent,ma}}}{D_H} \approx 10. \tag{7.1.6}$$

Idealized analytical solutions, however, indicate that $\frac{l_{\mathrm{ent,th}}}{D_H}$ depends on Pr, and it monotonically increases with decreasing Pr. Likewise $\frac{l_{\mathrm{ent,ma}}}{D_H}$ depends on Sc, and monotonically increases with decreasing Sc.

7.2 Hydrodynamics of Turbulent Duct Flow

7.2.1 Circular Duct

Entrance Region

Idealized analysis is possible with simplifying assumptions, for example, by assuming a flat inlet velocity profile, smooth surface and power-law velocity profile in the developing boundary layer. Zhi-qing (1982), for example, assumed that in turbulent flow the velocity profile in the developing boundary layer followed the 1/7th-power law, so that

$$\frac{\overline{u}(r)}{U_{\max}} = \begin{cases} (y/\delta)^{1/7} & \text{for } 0 \le y \le \delta \\ 1 & \text{for } y > \delta \end{cases}. \tag{7.2.1}$$

Using the integral method for boundary-layer analysis, furthermore, Zhi-qing derived

$$\frac{x/D}{\mathrm{Re}_D^{1/4}} = 1.4039\left(\frac{\delta}{R_0}\right)^{5/4}\left[1 + 0.1577\left(\frac{\delta}{R_0}\right) - 0.1793\left(\frac{\delta}{R_0}\right)^2 - 0.0168\left(\frac{\delta}{R_0}\right)^3 + 0.0064\left(\frac{\delta}{R_0}\right)^4\right]. \tag{7.2.2}$$

The hydrodynamic entrance length can be found by use of $\delta = R_0$ in the preceding equation, which leads to

$$\frac{l_{\mathrm{ent,hy}}}{D} = 1.3590\mathrm{Re}_D^{0.25}. \tag{7.2.3}$$

The analysis provides the following useful results:

$$C_{f,\mathrm{app},x}\mathrm{Re}_D^{0.25} = \frac{(U_{\max}/U_m)^2 - 1}{4x/\left(D\,\mathrm{Re}_D^{0.25}\right)}, \tag{7.2.4}$$

where, from Eq. (7.2.1),

$$\frac{U_m}{U_{\max}} = 1 - \frac{1}{4}\left(\frac{\delta}{R_0}\right) + \frac{1}{15}\left(\frac{\delta}{R_0}\right)^2. \tag{7.2.5}$$

Fully Developed Flow

Except very near the wall, where the velocity profile resembles the universal velocity profile for flat surfaces, the velocity distribution in a smooth pipe can be approximately represented by a power law (Nikuradse, 1932),

$$\frac{\overline{u}}{U_{\max}} = \left(\frac{y}{R_0}\right)^{1/n}, \tag{7.2.6}$$

which leads to

$$\frac{U_m}{U_{\max}} = \frac{2n^2}{(n+1)(2n+1)}. \tag{7.2.7}$$

The parameter n is not a constant, however, and increases with Re_D, as shown in Table 7.1. The power-law distribution does not apply very close to the wall.

Table 7.1. *Values of constant n in Eqs. (7.2.6) and (7.2.7) (Nikuradse, 1932)*

Re_D	4000	2.3×10^4	1.1×10^5	1.1×10^6	2.0×10^6	3.2×10^6
n	6	6.6	7	8.8	10	10

The *velocity defect law* (Prandtl, 1933), which applies to the turbulent core in the pipe (i.e., outside the viscous sublayer and the buffer zone), is

$$\frac{U_{\max} - \overline{u}}{U_\tau} = 2.5 \ln \frac{R_0}{y}. \tag{7.2.8}$$

An accurate empirical fit is due to Wang (1946):

$$\frac{U_{\max} - \overline{u}}{U_\tau} = 2.5 \left[\ln \frac{1 + \sqrt{1 - \dfrac{y}{R_0}}}{1 - \sqrt{1 - \dfrac{y}{R_0}}} - 2 \tan^{-1} \sqrt{1 - \frac{y}{R_0}} \right.$$
$$\left. - 0.572 \ln \frac{2.53 - \dfrac{y}{R_0} + 1.75\sqrt{1 - \dfrac{y}{R_0}}}{2.53 - \dfrac{y}{R_0} - 1.75\sqrt{1 - \dfrac{y}{R_0}}} + 1.143 \tan^{-1} \frac{1.75\sqrt{1 - \dfrac{y}{R_0}}}{0.53 + \dfrac{y}{R_0}} \right]. \tag{7.2.9}$$

Application of Eddy Diffusivity Models

The concept of an eddy diffusivity model was discussed earlier in Section 6.6, which can be utilized for the derivation of the velocity profile.

For fully developed flow a force balance on the fluid element shown in Fig. 7.2 indicates that

$$\frac{\tau_{rx}}{r} = \frac{1}{2}\left(-\frac{dP}{dx} + \rho g_x\right) = \text{const.} \tag{7.2.10}$$

Thus, at any radius r,

$$\tau_{rx} = \frac{r}{R_0}\tau_s. \tag{7.2.11}$$

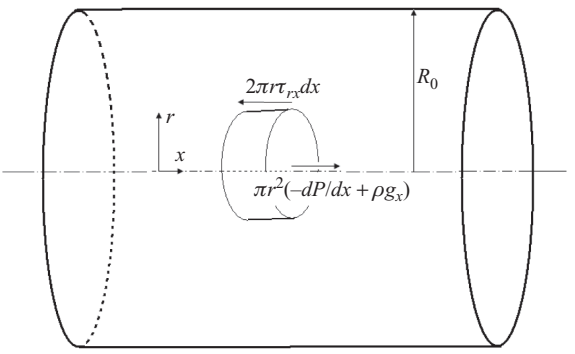

Figure 7.2. Forces on a fluid slice in a fully developed duct flow.

This leads to

$$\rho\left(\nu + E\right)\frac{d\overline{u}}{dr} = \frac{r}{R_0}\tau_s. \tag{7.2.12}$$

We can nondimensionalize and integrate the resulting differential equation to get

$$u^+ = \frac{1}{R_0^+}\int_{r^+}^{R_0^+}\frac{r^+dr^+}{\dfrac{E}{\nu}+1} = \frac{1}{R_0^+}\int_0^{y^+}\frac{\left(R_0^+ - y^+\right)dy^+}{\dfrac{E}{\nu}+1}, \tag{7.2.13}$$

where quantities representing length with the superscript + are in wall units, and $u^+ = \overline{u}/U_\tau$. The dimensionless velocities are thus all time or ensemble averaged. The preceding equation can be used for deriving the following expression for average velocity:

$$U_m^+ = \frac{2}{R_0^{+2}}\int_0^{R^+} u^+\left(R_0^+ - y^+\right)dy^+ = \frac{2}{R_0^{+2}}\int_0^{R_0^+} u^+ r^+\,dy^+. \tag{7.2.14}$$

Using $\tau_s = C_f\frac{1}{2}\rho U_m^2$, we can easily show that

$$U_m^+ = \sqrt{\frac{2}{C_f}} = \sqrt{\frac{8}{f}}. \tag{7.2.15}$$

The preceding two equations result in

$$f = \frac{8R_0^{+2}}{\mathrm{Re}_D}\left\{\int_0^{R_0^+}\left[\int_{r^+}^{R_0^+}\frac{r^+dr^+}{\dfrac{E}{\nu}+1}\right]r^+dr^+\right\}^{-1}. \tag{7.2.16}$$

It can also be easily shown that

$$U_m^+ = \mathrm{Re}_D/\left(2R_0^+\right), \tag{7.2.17}$$

where, of course, $\mathrm{Re}_D = \rho U_m D/\mu$.

Integration of Eq. (7.2.13) along with a suitable eddy diffusivity model will provide the velocity profile in the tube. The application of Eq. (7.2.16), furthermore, would lead to a friction factor. Some widely used eddy diffusivity expressions for smooth, circular tubes are subsequently discussed.

The eddy diffusivity model of von Karman (1939) is based on the separate expressions for the viscous sublayer, the buffer sublayer, and the turbulent core:

$$\frac{E}{\nu} = 0 \quad \text{for } y^+ < 5, \tag{7.2.18}$$

$$\frac{E}{\nu} = \frac{y^+}{5} - 1 \quad \text{for } 5 < y^+ < 30, \tag{7.2.19a}$$

$$\frac{E}{\nu} = \frac{y^+\left(1 - \dfrac{y^+}{R_0^+}\right)}{2.5} - 1 \quad \text{for } y^+ > 30. \tag{7.2.19b}$$

The eddy diffusivity model of Reichardt (1951) is a composite expression that applies for all y^+:

$$\frac{E}{\nu} = \kappa\left[y^+ - y_n^+ \tanh\left(\frac{y^+}{y_n^+}\right)\right] \quad \text{for } y^+ \le 50, \tag{7.2.20a}$$

$$\frac{E}{\nu} = \frac{\kappa}{3}y^+\left[0.5 + \left(\frac{r^+}{R_0^+}\right)^2\right]\left(1 + \frac{r^+}{R_0^+}\right) \quad \text{for } y^+ > 50, \tag{7.2.20b}$$

where $y_n^+ = 11$. The velocity profile will be

$$u^+ = 2.5\ln(1 + 0.4y^+) + 7.8\left[1 - \exp(-y^+/11) - \left(y^+/11\right)\exp\left(-0.33y^+\right)\right], \tag{7.2.21}$$

The eddy diffusivity model of Deissler (1953, 1955) is

$$\frac{E}{\nu} = n^2u^+y^+\left[1 - \exp\left(-n^2u^+y^+\right)\right] \quad \text{for } y^+ < 26 \tag{7.2.22}$$

$$E = \kappa^2\frac{(du/dy)^3}{\left(d^2u/dy^2\right)^2} \quad \text{for } y^+ > 26, \tag{7.2.23}$$

where $n = 0.124$. This model leads to the following velocity profile:

$$u^+ = \int_0^{y^+}\frac{dy^+}{1 + n^2u^+y^+\left[1 - \exp(-n^2u^+y^+)\right]}, \quad n = 0.124 \quad \text{for } 0 \le y^+ \le 26, \tag{7.2.24}$$

$$u^+ = 2.78\ln y^+ + 3.8 \quad \text{for } y^+ \ge 26. \tag{7.2.25}$$

The eddy diffusivity model of van Driest (1956), given earlier in Eq. (6.6.24), leads to

$$u^+ = \int_0^{y^+}\frac{2dy^+}{1 + \left\{1 + 0.64y^{+2}\left[1 - \exp(-y^+/26)\right]^2\right\}^{1/2}}, \tag{7.2.26}$$

which applies for all y^+.

The velocity profile in the turbulent core of a rough pipe follows the aforementioned power law [Eq. (7.2.6)] with $n = 4$–5. It also follows the velocity defect law, indicating that the turbulent characteristics of the core are independent of the wall conditions. The fully developed velocity profile in a fully rough pipe follows:

$$u^+ = 2.5\ln\frac{y^+}{\varepsilon_s^+} + 8.5, \tag{7.2.27}$$

where $\varepsilon_s^+ = \varepsilon_s U_\tau/\nu$.

Turbulence Model of Churchill

Consider the flow field shown in Fig. 6.4, where a fully developed 1D turbulent flow in x direction is under way. We can write

$$\tau_{xy} = \mu\frac{d\overline{u}}{dy} - \rho\overline{u'v'}. \tag{7.2.28}$$

Using Eq. (7.2.11) and nondimensionalizing, we find that this equation leads to (Churchill, 1997a),

$$\left(1-\frac{y^+}{R_0^+}\right)\left[1-\overline{(u'v')}^{++}\right]=\frac{du^+}{dy^+}, \tag{7.2.29}$$

where

$$\overline{(u'v')}^{++}=\left(-\rho\overline{u'v'}\right)/\tau_{xy}. \tag{7.2.30}$$

The quantity $\overline{(u'v')}^{++}$ represents the fraction of shear stress (or, equivalently, the rate of momentum transfer in the y direction) that is due to turbulence fluctuations. The velocity profile can now be found from

$$u^+=\int_0^{y^+}\left(1-\frac{y^+}{R_0^+}\right)\left[1-\overline{(u'v')}^{++}\right]dy^+. \tag{7.2.31}$$

It can also be easily shown that

$$\left(\frac{2}{C_f}\right)^{1/2}=U_m^+=-\frac{2}{R_0^+}\int_0^1 u^+\left(1-\frac{y^+}{R_0^+}\right)dy^+. \tag{7.2.32}$$

For fully developed turbulent flow in a circular pipe, a useful algebraic expression for $\overline{(u'v')}^{++}$ is (Churchill, 2000)

$$\overline{(u'v')}^{++}=\left\{\left[0.7\times10^{-3}y^{+3}\right]^{-8/7}+\left|\exp\left(-\frac{1}{0.436y^+}\right)-\frac{1}{0.436R_0^+}\left(1+\frac{6.95y^+}{R_0^+}\right)\right|^{-8/7}\right\}^{-7/8} \tag{7.2.33}$$

This expression predicts a $\overline{(u'v')}^{++}\to0.7\times10^{-3}y^{+3}$, as $y^+\to0$, which is consistent with the DNS results of Rutledge and Sleicher (1993). The term within the absolute-value signs is equivalent to the semilogarithmic distribution of the overlap zone in the $30<y^+<0.1R_0^+$ range, and leads to the expected asymptote $u^+\to u_{\mathrm{CL}}^+$ as $y^+\to R_0^+$. The range of validity of this correlation is at least $y^+<300$, which represents the upper limit of y^+ for which the semilogarithmic velocity profile is accurate.

For the range $150<R_0^+<50{,}000$, Yu et al. (2001) curve fitted the precisely computed values of U_m^+ with the following simple correlation, which predicted the precisely computed results within only 0.02%:

$$U_m^+=3.2-\frac{227}{R_0^+}+\left(\frac{50}{R_0^+}\right)^2+\frac{1}{0.436}\ln\left(R_0^+\right). \tag{7.2.34}$$

Yu et al. also developed the following correlation, which is valid for $R_0^+>500$:

$$U_c^+=7.52+\frac{1}{0.436}\ln\left(R_0^+\right). \tag{7.2.35}$$

where U_c is the centerline velocity.

Wall Friction

As mentioned earlier, the law of the wall discussed in Section 6.5 is a reasonable approximation for the velocity profile inside a fully turbulent pipe. Prandtl assumed

that Eq. (6.5.3), with the well-accepted constants $\kappa = 0.4$ and $B = 5.5$ could be used for the velocity profile in the entire pipe cross section, because the viscous and buffer sublayers are typically very thin. Substitution of the latter velocity distribution into Eq. (7.2.14) then leads to (White, 2006)

$$U_m^+ = \left(\frac{1}{\kappa}\ln R_0^+ + B - \frac{3}{2\kappa}\right). \tag{7.2.36}$$

Combining this equation with Eq. (7.2.15) and a slight adjustment of coefficients to make up for the fact that the analysis thus far has neglected the viscous and buffer sublayers, then led to

$$\frac{1}{\sqrt{C_f}} = 1.7272\ln\left(\mathrm{Re}_D\sqrt{C_f}\right) - 0.395. \tag{7.2.37}$$

Blasius' correlation (1913) is a simple and widely used correlation that is consistent with the 1/7–power approximate velocity profile:

$$C_f = 0.079\mathrm{Re}_D^{-1/4}. \tag{7.2.38}$$

The preceding correlation results from using the following velocity profile in Eq. (7.2.14), and applying Eq. (7.2.15):

$$u^+ = 8.74y^{+1/7}. \tag{7.2.39}$$

Blasius' correlation is valid for $\mathrm{Re}_D \lesssim 10^5$.

For a fully rough tube the same integration can be carried out, using Eq. (6.5.9) for the velocity profile, and that leads to (White, 2006)

$$\frac{1}{\sqrt{f}} = 2.0\log_{10}\left[\frac{\mathrm{Re}_D\sqrt{f}}{1 + 0.1\left(\frac{\varepsilon_s}{D}\right)\mathrm{Re}_D\sqrt{f}}\right] - 0.8. \tag{7.2.40}$$

The correlation of Colebrook (1939) is among the most widely used and is valid for the entire $5 \le \varepsilon_s^+ \le 70$ range:

$$\frac{1}{\sqrt{f}} = -2.0\log_{10}\left[\frac{\varepsilon_s/D}{3.7} + \frac{2.51}{\mathrm{Re}_D\sqrt{f}}\right]. \tag{7.2.41}$$

A correlation that predicts the friction factor within ±2% in comparison with the correlation of Colebrook and is explicit in terms of f, is (Haaland, 1983)

$$\frac{1}{\sqrt{f}} = -1.8\log_{10}\left[\left(\frac{\varepsilon_s/D}{3.7}\right)^{1.11} + \frac{6.9}{\mathrm{Re}_D}\right]. \tag{7.2.42}$$

Transition Flow

The transition flow regime in a smooth pipe is often defined as the range $2300 \le \mathrm{Re}_D < 4000$, even though the upper limit of the range is not well defined. The correlations for pressure drop or heat or mass transfer in the transition regime are often based on interpolation between well-established correlations for laminar and fully turbulent flow regimes.

For friction in a fully developed flow in a smooth pipe, a correlation proposed by Hrycak and Andrushkiw (1974) for the range $2100 < \mathrm{Re}_D < 4500$ is

$$C_f = -3.20 \times 10^{-3} + 7.125 \times 10^{-6}\mathrm{Re}_D - 9.70 \times 10^{-10}\mathrm{Re}_D^2. \tag{7.2.43}$$

A widely used correlation for flow in rough walled pipes for the laminar and turbulent flow regimes is the correlation of Churchill (1977a):

$$C_f = 2\left[\left(\frac{C_1}{\mathrm{Re}_D}\right)^{12} + \frac{1}{(A+B)^{3/2}}\right]^{1/12}, \tag{7.2.44}$$

where

$$A = \left\{\frac{1}{\sqrt{C_t}}\ln\left[\frac{1}{\left(\frac{7}{\mathrm{Re}_D}\right)^{0.9} + 0.27\frac{\varepsilon_s}{D}}\right]\right\}^{16} \tag{7.2.45}$$

$$B = \left(\frac{37{,}530}{\mathrm{Re}_D}\right)^{16}, \tag{7.2.46}$$

For circular channels, $C_1 = 8$ and $\frac{1}{\sqrt{C_t}} = 2.457$.

7.2.2 Noncircular Ducts

For noncircular channels that do not have sharp corners, the hydrodynamic entrance length and the friction factor can be estimated by use of circular pipe correlations with the channel hydraulic diameter. For triangular, rectangular, and annular channels, experimental data have shown that this approximation does well. When very sharp corners are present, as in triangular passages with one or two small angles, the laminar sublayer may partially fill the sharp corners.

For estimating the turbulent friction factor in noncircular channels, we may also use the concept of effective diameter, defined such that the fully developed laminar flow correlation for circular channels would apply to noncircular channels as well (Jones, 1976; Jones and Leung, 1981; White, 2006):

$$D_{\mathrm{eff}} = D_H \frac{16}{(C_f \mathrm{Re}_{D_H})_{\mathrm{lam}}}. \tag{7.2.47}$$

Some useful correlations for specific channel geometries are subsequently provided.

Flat Channels

The laminar–turbulent transition takes place in the $2200 < \mathrm{Re}_{D_H} < 3400$ range. Hrycak and Andrushkiw (1974) recommended the following correlation for the $2300 < \mathrm{Re}_{D_H} < 4000$ range (Ebadian and Dong, 1998):

$$C_f = -2.56 \times 10^{-3} + 4.085 \times 10^{-6}\mathrm{Re}_{D_H} - 5.5 \times 10^{-10}\mathrm{Re}_{D_H}^2. \tag{7.2.48}$$

For fully developed flow, for the $5000 < \mathrm{Re}_{D_H} < 3 \times 10^4$ range, Beavers et al. (1971) proposed

$$C_f = 0.1268\mathrm{Re}_{D_H}^{-0.3}, \tag{7.2.49}$$

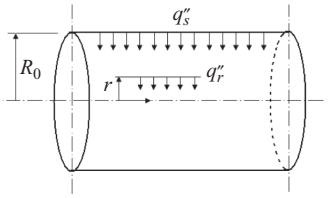

Figure 7.3. Flow in a pipe with UHF boundary conditions.

and for the $1.2 \times 10^4 < \mathrm{Re}_{D_H} < 1.2 \times 10^6$ range, Dean (1978) proposed

$$C_f = 0.0868 \mathrm{Re}_{D_H}^{-0.25}. \tag{7.2.50}$$

For fully developed turbulent flow, the following velocity defect law was proposed by Goldstein (1937):

$$\frac{U_{\max} - \overline{u}}{U_\tau} = -3.39 \left[\ln\left(1 - \sqrt{\frac{y}{b}}\right) + \sqrt{\frac{y}{b}} \right] - 0.172, \tag{7.2.51}$$

where y is the normal distance from the duct axis and b is the half-distance between the two walls (see Fig. 4.9).

Rectangular Ducts

For rectangular ducts, Jones (1976) derived an expression for turbulent-flow-equivalent diameter, which can be approximated as (Ebadian and Dong, 1998)

$$D_{\text{eff}} = \frac{2}{3} D_H + \frac{11}{24} \alpha^* \left(2 - \alpha^*\right), \tag{7.2.52}$$

where α^* is the aspect ratio of the cross section. We can apply correlations based on smooth, circular ducts to rectangular ducts by using this expression.

More detailed information about flow in noncircular channels can be found in Bhatti and Shah (1987) and Ebadian and Dong (1998).

7.3 Heat Transfer: Fully Developed Flow

7.3.1 Universal Temperature Profile in a Circular Duct

Consider an incompressible, constant-property fluid flowing in a circular duct with UHF boundary conditions (see Fig. 7.3). The flow field is thermally developed. Neglecting the viscous dissipation, the energy conservation equation will be

$$\overline{u} \frac{\partial \overline{T}}{\partial x} \approx U_m \frac{\partial \overline{T}}{\partial x} = \frac{1}{r} \frac{\partial}{\partial r} \left[r \left(\alpha + E_{\text{th}}\right) \frac{\partial \overline{T}}{\partial r} \right]. \tag{7.3.1}$$

We have used $\overline{u} \approx U_m$, because in a turbulent pipe flow the velocity profile is approximately flat, except for a thin layer next to the wall.

Because $\frac{\partial \overline{T}}{\partial x} = \frac{\partial \overline{T}_m}{\partial x}$ in a thermally developed pipe flow with UHF boundary conditions, an overall energy balance on the pipe gives

$$U_m \rho C_P \frac{\partial \overline{T}}{\partial x} = \frac{2 q''_s}{R_0}. \tag{7.3.2}$$

Equation (7.3.1) can be cast as

$$\rho C_P \overline{u} \frac{\partial \overline{T}}{\partial x} = \rho C_P U_m \frac{\partial \overline{T}}{\partial x} = \frac{1}{r} \frac{\partial}{\partial r} \left(r q_r'' \right), \tag{7.3.3}$$

where $q_r'' = k \frac{\partial \overline{T}}{\partial r}$ is the local heat flux in the radial direction, defined to be positive in the inward direction. From Eqs. (7.3.2) and (7.3.3) we get

$$\frac{\partial}{\partial r} \left(r q_r'' \right) = \frac{2 q_s'' r}{R_0}. \tag{7.3.4}$$

This leads to

$$q_r'' = q_s'' \left(1 - \frac{y}{R_0} \right). \tag{7.3.5}$$

We can also write

$$(\alpha + E_{\text{th}}) \frac{\partial \overline{T}}{\partial r} = \frac{q_r''}{\rho C_P}. \tag{7.3.6}$$

Equations (7.3.5) and (7.3.6) then lead to

$$\left(\frac{\nu}{\text{Pr}} + \frac{E}{\text{Pr}_{\text{tu}}} \right) \frac{\partial \overline{T}}{\partial r} = \frac{q_s''}{\rho C_P} \left(1 - \frac{y}{R_0} \right). \tag{7.3.7}$$

We also note that, in a fully developed pipe flow,

$$\frac{\tau}{r} = \frac{\tau_s}{R_0}, \tag{7.3.8}$$

$$(\nu + E) \frac{\partial \overline{u}}{\partial y} = \frac{\tau_s}{\rho} \left(1 - \frac{y}{R_0} \right). \tag{7.3.9}$$

Using Eqs. (7.3.7) and (7.3.9), along with the turbulent law-of-the-wall velocity distribution, we can derive a universal temperature profile for pipe flow for $\text{Pr} \gtrsim 0.1$ (Martinelli, 1947), as follows.

First, let us nondimensionalize Eq. (7.3.7) by defining

$$T^+ = \frac{T_s - \overline{T}}{\dfrac{q_s''}{\rho C_P U_\tau}}. \tag{7.3.10}$$

Equation (7.3.7) then leads to

$$T^+ = \int_0^{y^+} \frac{\left(1 - \dfrac{y^+}{R_0^+} \right) dy^+}{\dfrac{1}{\text{Pr}} + \dfrac{E}{(\nu \text{Pr}_{\text{tu}})}}. \tag{7.3.11}$$

Equation (7.3.9), furthermore, will give

$$\left(1 + \frac{E}{\nu} \right) \frac{\partial u^+}{\partial y^+} = 1 - \frac{y^+}{R_0^+}.$$

In the viscous sublayer ($y^+ < 5$) where we have $\frac{1}{\mathrm{Pr}} \gg \frac{E}{(\nu \mathrm{Pr_{tu}})}$ and $1 - \frac{y^+}{R_0^+} \approx 1$, we get

$$T^+ = \mathrm{Pr} y^+. \tag{7.3.12}$$

In the buffer zone ($5 < y^+ < 30$), where molecular and turbulent diffusivities are both important, we get from Eqs. (6.5.2) and (7.3.9)

$$E = \frac{1 - \dfrac{y^+}{R_0^+}}{\dfrac{du^+}{dy^+}} - \nu = \frac{1 - \dfrac{y^+}{R_0^+}}{\dfrac{5}{y^+}} - \nu. \tag{7.3.13}$$

Equation (7.3.11) then gives

$$T^+ = 5\left\{Pr + \mathrm{Pr_{tu}} \ln\left[1 + \frac{\mathrm{Pr}}{\mathrm{Pr_{tu}}}\left(\frac{y^+}{5} - 1\right)\right]\right\}. \tag{7.3.14}$$

Finally, in the fully turbulent core, where $E \gg \nu$, Eq. (6.5.3) gives

$$\frac{\partial u^+}{\partial y^+} = \frac{1}{\kappa y^+}.$$

Equation (7.3.9) then leads to

$$E + \nu \approx E \approx \nu\kappa \left(1 - \frac{y^+}{R_0^+}\right) y^+. \tag{7.3.15}$$

Substituting into Eq. (7.3.11) and neglecting the term $1/\mathrm{Pr}$ in the latter equation, we get

$$T^+ - T^+|_{y^+=30} = \int_{30}^{y^+} \frac{\mathrm{Pr_{tu}} dy^+}{\kappa y^+} = \frac{\mathrm{Pr_{tu}}}{\kappa} \ln \frac{y^+}{30} = \frac{\mathrm{Pr_{tu}}}{\kappa} \ln\left[\frac{y}{60R_0}\sqrt{\frac{C_f}{2}}\mathrm{Re}_D\right], \tag{7.3.16}$$

where $T^+|_{y^+=30}$ is to be found by use of $y^+ = 30$ in Eq. (7.3.14). In deriving this equation we used

$$U_\tau = U_m\sqrt{\frac{C_f}{2}}. \tag{7.3.17}$$

We can now obtain the dimensionless temperature difference between the wall and the tube centerline by using $y^+ = R_0^+$ in Eq. (7.3.16):

$$T_c^+ = \frac{T_s - \overline{T}_c}{\dfrac{q_s''}{\rho C_P U_\tau}} = 5\mathrm{Pr_{tu}}\left\{\frac{\mathrm{Pr}}{\mathrm{Pr_{tu}}} + \ln\left[1 + 5\frac{\mathrm{Pr}}{\mathrm{Pr_{tu}}}\right] + \frac{1}{5\kappa}\ln\left[\frac{\mathrm{Re}_D}{60}\sqrt{\frac{C_f}{2}}\right]\right\}. \tag{7.3.18}$$

When $\mathrm{Pr} \ll 1$, which occurs in liquid metals, the thermal diffusivity is too large to be neglected anywhere in the pipe. Equations (7.3.12) and (7.3.14) apply. However, in the turbulent core the approximation of Eq. (7.3.15) no longer applies. We should find the temperature profile in the turbulent core ($y^+ > 30$) by applying Eq. (7.3.11), without neglecting $1/\mathrm{Pr}$ in the denominator on the right-hand side.

The integration leads to (Martinelli, 1947)

$$T^+ - T^+\big|_{y^+=y_2^+} = \frac{1}{2\kappa}\ln\left[\frac{5\Lambda + \frac{y^+}{R_0^+}\left(1-\frac{y^+}{R_0^+}\right)}{5\Lambda + \frac{y_2^+}{R_0^+}\left(1-\frac{y_2^+}{R_0^+}\right)}\right] + \frac{1}{2\kappa\sqrt{1+20\Lambda}}\ln\left\{\left[\frac{\left(2\frac{y^+}{R_0^+}-1\right)+\sqrt{1+20\Lambda}}{\left(2\frac{y^+}{R_0^+}-1\right)-\sqrt{1+20\Lambda}}\right]\left[\frac{\left(\frac{2y_2^+}{R_0^+}-1\right)-\sqrt{1+20\Lambda}}{\left(\frac{2y_2^+}{R_0^+}-1\right)+\sqrt{1+20\Lambda}}\right]\right\}, \tag{7.3.19}$$

where y_2^+ is the distance from the wall to the edge of the buffer zone (typically $y_2^+ \approx 30$), and

$$\Lambda = \frac{\mathrm{Pr_{tu}}}{\mathrm{Re}_D \mathrm{Pr}\sqrt{\frac{C_f}{2}}}. \tag{7.3.19a}$$

7.3.2 Application of Eddy Diffusivity Models for Circular Ducts

Equation (7.3.1) can be nondimensionalized and rewritten as

$$\frac{2U_\tau T^*}{R_0 U_m}\overline{u} = \frac{1}{r}\frac{\partial}{\partial r}\left[r\left(\alpha + E_{\mathrm{th}}\right)\frac{\partial \overline{T}}{\partial r}\right], \tag{7.3.20}$$

where

$$T^* = q_s''/(\rho C_p U_\tau). \tag{7.3.21}$$

The boundary conditions for this second-order ODE are

$$\text{at } r = 0, \quad \frac{\partial \overline{T}}{\partial y} = 0; \tag{7.3.22}$$

$$\text{at } r = R_0 \quad -k\frac{\partial \overline{T}}{\partial y} = k\frac{\partial \overline{T}}{\partial r} = q_s''. \tag{7.3.23}$$

We can now apply two integrations to the right-hand side of this equation. The first integration, between the centerline and an arbitrary r, gives

$$(R_0 - y)\left(\alpha + E_{\mathrm{th}}\right)\frac{\partial \overline{T}}{\partial y} = -\frac{2U_\tau T^*}{R_0 U_m}\int_y^R \overline{u}\,(R_0 - y)\,dy. \tag{7.3.24}$$

The second integration, this time between the wall and an arbitrary r, leads to

$$\overline{T} = T_s - \frac{2U_\tau T^*}{R_0 U_m}\int_0^y dy' \frac{1}{(R_0 - y')\left(\alpha + E_{\mathrm{th}}\right)}\int_{y'}^{R_0} dy''\overline{u}\,(R_0 - y''). \tag{7.3.25}$$

where y' and y'' are dummy variables. We can now get T_m from

$$U_m\left(T_m - T_s\right) = \frac{2}{R_0^2}\int_0^{R_0}\overline{u}\left(\overline{T} - T_s\right)r\,dr = -\frac{2}{R_0^2}\int_0^{R_0}\overline{u}\left(\overline{T} - T_s\right)(R_0 - y)\,dy. \tag{7.3.26}$$

Substituting from Eq. (7.3.25) into this equation, we get

$$T_m^+ = \frac{4}{{R_0}^{+3}\left(U_m^+\right)^2}\int_0^{R_0^+}\left(R_0^+ - y^+\right)u^+ dy^+ \times \int_0^{y^+}\frac{1}{\left(R_0^+ - y^{+\prime}\right)\left(\frac{E_{\text{th}}}{\nu}+\frac{1}{\text{Pr}}\right)}dy^{+\prime}\int_{y^{+\prime}}^{R_0^+}\left(R_0^+ - y^{+\prime\prime}\right)u^+ dy^{+\prime\prime}. \quad (7.3.27)$$

In dimensionless form, this equation gives

$$T_m^+ = \frac{4}{R_0^{+3}\left(U_m^+\right)^2}\int_0^{R_0^+}\left(R_0^+ - y^+\right)u^+ dy^+ \times \int_0^{y^+} dy^{+\prime}\frac{1}{\left(R_0^+ - y^{+\prime}\right)\left(\frac{E_{\text{th}}}{\nu}+\frac{1}{\text{Pr}}\right)}\int_{y^{+\prime}}^{R_0^+} dy^{+\prime\prime}u^+\left(R_0^+ - y^{+\prime\prime}\right), \quad (7.3.28)$$

where $T^+ = (T_s - \overline{T})\rho C_P \frac{U_\tau}{q_s''}$.

There is the following relationship between T_m^+ and St [note the similarity to Eq. (6.7.13)]:

$$\text{St} = \frac{q_s''}{\rho C_P U_m\left(T_s - T_m\right)} = \frac{1}{U_m^+ T_m^+}. \quad (7.3.29)$$

Thus, by using an appropriate model for E and an appropriate value for Pr_{tu}, we can find not only a "universal" dimensionless temperature profile, but also a relation for St.

Also, from Eq. (7.3.9) we can derive

$$u^+ = \frac{1}{R_0^+}\int_0^{y^+}\frac{\left(R_0^+ - y^+\right)dy^+}{\frac{E}{\nu}+1}. \quad (7.3.30)$$

Furthermore,

$$U_m^+ = \frac{2}{R_0^{+2}}\int_0^{R_0^+} u^+\left(R_0^+ - y^+\right)dy^+, \quad (7.3.31)$$

$$\text{Re}_D = \frac{2U_m R_0}{\nu} = 4\int_0^{R_0^+} u^+ dy^+ - \frac{4}{R_0^+}\int_{y^{+\prime}}^{R_0^+} u^+ y^+ dy^+. \quad (7.3.32)$$

The simultaneous solution of Eqs. (7.3.28) and (7.3.30), using an adequate eddy diffusivity model and a correct value for Pr_{tu}, would in principle provide us with correlations in the following generic forms:

$$\text{St} = f\left(\text{Re}_D,\ \text{Pr}\right),$$
$$\text{Nu}_D = \text{Re}_D\text{PrSt} = f\left(\text{Re}_D,\ \text{Pr}\right).$$

The following is a straightforward recipe for performing parametric calculations:

1. Choose a value for R_0^+.
2. From Eq. (7.3.30) obtain the profile for u^+.

3. Find U_m^+ from Eq. (7.3.31) and find Re_D from Eq. (7.3.32).
4. Find T_m^+ from Eq. (7.3.28).
5. Find St from Eq. (7.3.29).

Extensive parametric calculations were carried out by Petukhov (1970), who assumed $\mathrm{Pr}_{\mathrm{tu}} = 1$ and used the eddy diffusivity model of Reichardt (1951) [see Eqs. (7.2.20a) and (7.2.20b)]. Petukhov curve fitted the results of his parametric calculations for the range $10^4 \leq \mathrm{Re}_D \leq 5 \times 10^6$ and $0.5 \leq \mathrm{Pr} \leq 2000$, and derived the following widely used correlation:

$$\mathrm{Nu}_D = \frac{\left(\frac{f}{8}\right)\mathrm{Re}_D\mathrm{Pr}}{K_1(f) + K_2(\mathrm{Pr})\left(\frac{f}{8}\right)^{1/2}\left(\mathrm{Pr}^{2/3} - 1\right)}, \tag{7.3.33}$$

where,

$$K_1(f) = 1 + 3.4f, \tag{7.3.34}$$

$$K_2(\mathrm{Pr}) = 11.7 + 1.8\mathrm{Pr}^{1/3}. \tag{7.3.35}$$

Petukhov also suggested the following expression for the friction factor:

$$f = (1.82\log_{10}\mathrm{Re}_D - 1.64)^{-2}. \tag{7.3.36}$$

The preceding correction is for constant properties. To account for property variations with temperature for liquids, Petukhov suggested

$$\frac{\mathrm{Nu}_D}{\mathrm{Nu}_{D,m}} = \left(\frac{\mu_m}{\mu_s}\right)^n, \tag{7.3.37}$$

where subscripts m and s represent mean and surface temperatures, respectively. For heating the fluid, $n = 0.11$, and for cooling, $n = 0.25$. Also, when the fluid is heated,

$$\frac{C_f}{C_{fm}} = \frac{1}{6}\left(7 - \frac{\mu_m}{\mu_s}\right), \tag{7.3.38}$$

and for cooling the fluid,

$$\frac{C_f}{C_{fm}} = \left(\frac{\mu_s}{\mu_m}\right)^{0.24}. \tag{7.3.39}$$

For liquids for which viscosity varies with temperature but specific heat and thermal conductivity are approximately constant, Petukhov recommended Eq. (7.3.37) for the range $0.08 \leq \mu_s/\mu_m \leq 40$.

For gases, we can use Eq. (7.3.37) with $n = -0.25$ when the fluid is being heated and $n = 0$ when the fluid is cooled, and

$$\frac{C_f}{C_{fm}} = \left(\frac{T_s}{T_m}\right)^{-0.1}. \tag{7.3.40}$$

One of the most accurate correlations for turbulent pipe flow is the following empirical correlation, which was proposed by Gnielinski (1976) for the parameter range $2300 < \mathrm{Re}_D < 5 \times 10^6$ and $0.5 < \mathrm{Pr} < 2300$:

$$\mathrm{Nu}_D = \frac{(\mathrm{Re}_D - 1000)\,\mathrm{Pr}\dfrac{C_f}{2}}{1.0 + 12.7\sqrt{\dfrac{C_f}{2}}\left(\mathrm{Pr}^{2/3} - 1\right)}. \tag{7.3.41}$$

7.3.3 Noncircular Ducts

The hydrodynamics of fully developed turbulent flow in noncircular ducts was discussed earlier in Subsection 7.2.2. For heat and mass transfer, the circular duct correlations, when used by replacing diameter with hydraulic diameter, can provide good approximations for the heat and mass transfer coefficients for flow in flat channels and in annular and rectangular channels, as long as sharp-angled corners are not present. More accurate methods are available for regular and widely encountered cross-section geometries, however.

For fully developed flow in flat channels (flow between two parallel plates), it was found that the circular-channel correlations can be applied, provided that the hydraulic diameter is used in the circular-duct correlations. Also, for fluids with $\mathrm{Pr} \gtrsim 0.7$ and $\mathrm{Re}_{D_H} \gtrsim 10^5$, there is virtually no difference between heat transfer coefficients representing UWT and UHF boundary conditions.

For flow in rectangular ducts, we can use the circular-duct correlations by replacing the channel diameter with the hydraulic diameter as an approximation. However, we can obtain a better approximation by using the effective diameter depicted in Eq. (7.2.47).

7.4 Heat Transfer: Fully Developed Hydrodynamics, Thermal Entrance Region

7.4.1 Circular Duct With Uniform Wall Temperature or Concentration

Consider the conditions shown in Fig. 4.15, where now a fully developed turbulent pipe flow is exposed to UWT boundary conditions at $x \geq 0$. Figure 4.15 and its discussion were related to Graetz's problem for laminar flow. We are now dealing with the turbulent Graetz problem. Equations (4.5.1)–(4.5.13) will all apply if we make the following two modifications:

1. Replace Eq. (4.5.7) with

$$\frac{\partial\theta}{\partial x^*} = \frac{2}{r^* f(r^*)}\frac{\partial}{\partial r^*}\left[\left(1 + \frac{\mathrm{Pr}}{\mathrm{Pr}_{\mathrm{tu}}}\frac{E(r^*)}{\nu}\right) r^*\frac{\partial\theta}{\partial r^*}\right]. \tag{7.4.1}$$

2. Replace Eq. (4.5.9) with an appropriate turbulent velocity profile.

Table 7.2. *Selected eigenvalues and constants for the turbulent Graetz problem for small Prandtl numbers (Notter and Sleicher, 1972)*

Pr	Re_D	λ_0^2	λ_1^2	λ_2^2	C_0	C_1	C_2	G_0	G_1	G_2
0.1	10,000	18.66	113.6	296.0	1.468	0.774	0.540	1.928	1.235	0.965
	20,000	27.12	171.6	450.7	1.444	0.728	0.499	2.89	1.701	1.304
	50,000	48.05	327.5	876.1	1.398	0.644	0.431	5.34	2.65	1.959
	100,000	77.13	564.7	1534	1.361	0.577	0.378	8.79	3.77	2.71
	200,000	127.4	1007	2777	1.325	0.515	0.332	14.79	5.46	3.84
	500,000	253.6	2226	6239	1.284	0.444	0.280	29.9	9.16	6.27
0.72	10,000	64.38	646.8	1870	1.239	0.369	0.227	7.596	1.829	1.217
	20,000	109.0	1119	3240	1.231	0.352	0.208	13.06	2.95	1.784
	50,000	219.0	2350	6808	1.220	0.333	0.193	26.6	5.63	3.32
	100,000	375.9	4183	12,130	1.21	0.319	0.185	45.8	9.25	5.48
	200,000	651.2	7539	21,940	1.200	0.302	0.177	79.6	15.05	9.10
	500,000	1357	16,630	48,540	1.19	0.282	0.165	166.0	28.9	17.5

Substitution of Eq. (4.5.13) into Eq. (7.4.1) then gives,

$$\frac{F'}{F} = \frac{2}{r^* f(r^*)} \frac{\dfrac{d}{dr^*}\left\{\left[1 + \dfrac{\mathrm{Pr}}{\mathrm{Pr_{tu}}}\dfrac{E(r^*)}{\nu}\right] r^* \dfrac{\partial R}{\partial r^*}\right\}}{R} = -\lambda^2. \tag{7.4.2}$$

Thus Eq. (4.5.15) will be applicable, and Eq. (4.5.16) will be replaced with

$$\frac{d}{dr^*}\left\{\left[1 + \frac{\mathrm{Pr}}{\mathrm{Pr_{tu}}}\frac{E(r^*)}{\nu}\right] r^* \frac{\partial R_n}{\partial r^*}\right\} + \frac{\lambda_n^2}{2} r^* f(r^*) R_n = 0. \tag{7.4.3}$$

The boundary conditions for this equation are

$$R_n'(0) = 0,$$
$$R_n(1) = 0.$$

Equations (4.5.17)–(4.5.21) will all formally apply, bearing in mind that the eigenvalues and eigenfunctions are now solutions to Eq. (7.4.3). Equations (4.5.25)–(4.5.29) will all apply as well bearing in mind that λ_0 has a different value now. To solve Eq. (7.4.3) for eigenvalues and eigenfunctions, an eddy diffusivity model as well as a correlation for $\mathrm{Pr_{tu}}$ are of course needed.

The turbulent Graetz problem was solved in the past (Latzko, 1921; Notter and Sleicher, 1971a, 1971b, 1972). Notter and Sleicher (1971a, 1972), for example, derived empirical expressions for $E(\mathrm{r}^*)$ and $\mathrm{Pr_{tu}}$ and used them in the numerical solution of the aforementioned equations for the range $0 < \mathrm{Pr} < 10^4$. Some examples of their calculation results are summarized in Tables 7.2 and 7.3, where the function G_n is defined similarly to Eq. (4.5.26):

$$G_n = -\frac{C_n R_n'(1)}{2}.$$

Asymptotic values for the eigenvalues and constants, to be used for the calculation of λ_n, C_n, and G_n for n larger than those given in Tables 7.2 and 7.3, can be found

Table 7.3. *Selected eigenvalues and constants for the turbulent Graetz problem for large Prandtl numbers (Notter and Sleicher, 1972)*

Pr	Re_D	λ_0^2	C_0	G_0
8	10^4	176.6	1.056	21.6
	2×10^4	313.5	1.056	38.7
	5×10^4	685.6	1.054	85.4
	10^5	1232	1.054	154.0
	2×10^5	2271	1.054	284.0
	5×10^5	5020	1.052	625.0
	10^6	9369	1.052	1170
20	10^4	247.9	1.033	30.3
	2×10^4	448.2	1.033	55.4
	5×10^4	990.6	1.032	124.0
	10^5	1799	1.032	225.0
	2×10^5	3346	1.032	418.0
	5×10^5	7509	1.031	936.0
	10^6	14,090	1.031	1760
50	10^4	348.0	1.019	42.6
	2×10^4	631.1	1.019	78.1
	5×10^4	1393	1.018	174.0
	10^5	2570	1.018	321.0
	2×10^5	4778	1.018	598.0
	5×10^5	10,800	1.018	1350
	10^6	20,420	1.018	2550

from the following expressions:

$$\lambda_n = \left(n + \frac{2}{3}\right) \Big/ G, \tag{7.4.4}$$

$$C_n = \frac{0.897\,(-1)^n H^{1/6}}{G\sqrt{2g_0}\lambda_n^{2/3}} \left\{ \frac{1}{1 + \dfrac{1}{(G\lambda_n)^2}\left[\dfrac{c}{2\pi}\left(\ln(G\lambda_n\pi) - \dfrac{2}{3}\right) + \dfrac{1}{6\pi^2}\right]} \right\}, \tag{7.4.5}$$

$$G_n = \frac{0.201}{G}\left[\frac{(\mathrm{Re}_D f/32)}{\lambda_n}\right]^{1/3} \left\{1 - \frac{1}{(G\lambda_n)^2}\left[\frac{c}{2\pi}\left(\ln(G\lambda_n\pi) - 1\right) + \frac{7}{36\pi^2}\right]\right\}, \tag{7.4.6}$$

where parameter H is defined as

$$H = \mathrm{Re}_D f/32. \tag{7.4.7}$$

The parameters G, g_0, and c are all functions of Re_D and Pr, and typical values for them are given in Table 7.4 (Notter and Sleicher, 1972).

7.4.2 Circular Duct With Uniform Wall Heat Flux

The *turbulent extended Graetz problem*, in which the boundary condition for the duct is the UHF for $x \geq 0$, was also solved by several authors (Sparrow et al., 1957;

Table 7.4. *Values of parameters* G, g_0, *and* c

Pr = 0.1				Pr = 0.72			
Re_D	G	g_0	c	Re_D	G	g_0	c
10,000	0.154	2.51	7.0	10,000	0.0609	19.1	15
20,000	0.125	3.98	9.0	20,000	0.0456	33.9	15
50,000	0.0891	8.16	11	50,000	0.0311	72.7	11
100,000	0.0671	14.8	13	100,000	0.0232	131	7.8
200,000	0.0497	27.6	14	200,000	0.0172	238	3.9
500,000	0.0331	63.7	15				

Notter and Sleicher, 1971b; Weigand et al., 2001). Defining the dimensionless temperature according to Eq. (4.5.62), the energy equation represented by Eq. (4.5.1) can be cast as Eq. (7.4.1) with the following boundary conditions:

$$\theta\,(0,\, r^*) = 0,$$
$$\frac{\partial\theta}{\partial r^*}\,(x^*,\, 1) = \frac{1}{2},$$
$$\frac{\partial\theta}{\partial r^*}\,(x^*,\, 0) = 0,$$

where, again, $r^* = \frac{r}{R_0}$ and $x^* = \frac{x}{R_0 \mathrm{Re}_D \,\mathrm{Pr}}$. As we did in Subsection 4.5.3 for laminar flow, we can assume that

$$\theta = \theta_1 + \theta_2, \tag{7.4.8}$$

where θ_1 is the solution to the thermally developed problem and θ_2 represents the entrance-region solution. The differential equations governing θ_1 and θ_2 will be similar to Eqs. (7.4.1) when θ is replaced once with θ_1 and once with θ_2. The fully developed developed solution can then be cast as

$$\theta_1\,(x^*,\, r^*) = 2x^* + \tilde{H}\,(r^*)\,. \tag{7.4.9}$$

The first term on the right-hand side represents the axial variation of the mean fluid temperature. Substitution of this equation into the aforementioned differential equation for θ_1 will then lead to

$$\frac{d}{dr^*}\left\{\left[1 + \frac{\mathrm{Pr}}{\mathrm{Pr}_{\mathrm{tu}}}\frac{E(r^*)}{\nu}\right] r^* \frac{d\tilde{H}\,(r^*)}{dr^*}\right\} - r^* f\,(r^*) = 0. \tag{7.4.10}$$

The boundary conditions for this equation are

$$\frac{d\tilde{H}}{dr^*}\,(1) = \frac{1}{2},$$
$$\frac{d\tilde{H}}{dr^*}\,(0) = 0.$$

Table 7.5. *Selected eigenvalues and constants for the turbulent extended Graetz problem (Notter and Sleicher, 1972)*

Pr	Re_D	$\bar{\lambda}_1^2$	$\bar{\lambda}_2^2$	$\bar{\lambda}_3^2$	$-\bar{G}_1$	$-\bar{G}_2$	$-\bar{G}_3$
0.1	10,000	69.52	224.9	463.0	0.737	0.0286	0.0165
	50,000	219.6	695.9	1421	0.0250	0.0109	0.00667
	100,000	396.9	1247	2531	0.0143	0.00663	0.00427
	500,000	1718	5341	10,750	0.00344	0.00176	0.00122
0.72	10,000	519.2	1624	3202	0.0123	0.00738	0.00653
	50,000	1952	6154	12,480	0.00296	0.00147	0.00106
	100,000	3510	11,030	22,340	0.00164	0.00081	0.00056
	500,000	14,310	44,690	89,830	0.000405	0.00020	–

Equation (7.4.10) is a Sturm–Liouville problem and was solved (Sparrow et al., 1957). The solution leads to (Notter and Sleicher, 1971b; 1972)

$$\mathrm{Nu}_{D,\mathrm{UHF},fd} = \frac{1}{16\sum_{0}^{\infty} G_n \lambda_n^{-4}}, \tag{7.4.11}$$

where G_n and λ_n are the same as those for the UWT solution. This series solution converges very rapidly, and for $\mathrm{Pr} \gtrsim 1$ only the first term in the series is sufficient.

The entrance-effect part of the problem can be solved by the separation-of-variables technique, and that leads to

$$\theta_2(x^*, r^*) = \sum_{n=1}^{\infty} \bar{C}_n \bar{R}_n(r^*) \exp\left(-\bar{\lambda}_n^2 x^*\right), \tag{7.4.12}$$

where the differential equation leading to the eigenfunctions and eigenvalues is identical to Eq. (7.4.3), with the following boundary conditions:

$$\bar{R}_n'(1) = 0,$$
$$\bar{R}_n(0) = 0.$$

The constant $\bar{C}_n$ can be found from (Notter and Sleicher, 1971b)

$$\bar{C}_n = \frac{2}{\bar{\lambda}_n \dfrac{\partial \bar{R}_n'}{\partial \bar{\lambda}_n}(1)}. \tag{7.4.13}$$

The analysis leads to the following expression for the entry-region Nusslet number (Notter and Sleicher, 1972):

$$\mathrm{Nu}_{D,\mathrm{UHF}}(x^*) = \frac{2}{\dfrac{2}{\mathrm{Nu}_{D,\mathrm{UHF},fd}} + \sum_{n=1}^{\infty} \bar{G}_n \exp\left(-\bar{\lambda}_n^2 x^*\right)}. \tag{7.4.14}$$

Table 7.5 provides some numerical values of the eigenvalues and the constants $\bar{G}_n$. For n larger than the values in Table 7.5, $\bar{\lambda}_n$ and $\bar{G}_n$ can be found from the following

asymptotic relations:

$$\bar{\lambda}_n = \frac{1}{\mathsf{G}} \left\{ n + \frac{1}{3} - \frac{0.189 G^{2/3}}{H^{1/3} \left(n + \frac{1}{3} \right)^{2/3}} \right\}, \tag{7.4.15a}$$

$$\overline{\mathsf{G}}_n = \frac{0.762}{G H^{1/3} \bar{\lambda}_n^{5/3}} \frac{\left[1 + \dfrac{0.343}{H^{1/3} \bar{\lambda}_n^{2/3}} \right]}{\left[1 - \dfrac{0.343}{H^{1/3} \bar{\lambda}_n^{2/3}} \right]}. \tag{7.4.15b}$$

The parameters G and H are the same as those for UWT case.

Calculations, furthermore, show that

$$\mathrm{Nu}_{D,\mathrm{UHF}}(x^*) \approx \mathrm{Nu}_{D,\mathrm{UWT}}(x^*) \quad \text{for } \mathrm{Pr} \gtrsim 0.72. \tag{7.4.16}$$

Therefore, for fluids with large Prandtl numbers $\mathrm{Nu}_{D,\mathrm{UHF}}(x^*)$ can be found by use of the method for finding $\mathrm{Nu}_{D,\mathrm{UWT}}(x^*)$ described earlier.

7.4.3 Some Useful Correlations for Circular Ducts

As noted earlier, reliable correlations for the eddy diffusivity and the turbulent Prandtl number are needed for the solution of the turbulent Graetz problem. This is particularly important for liquid metals, for which $\mathrm{Pr}_{\mathrm{tu}}$ deviates significantly from unity. Weigand et al. (1997) proposed the following correlation, to be used for all values of Pr:

$$\mathrm{Pr}_{\mathrm{tu}} = \left\{ \frac{1}{2\mathrm{Pr}_{\mathrm{tu,fd}}} + C\,\mathrm{Pe}_{\mathrm{tu}} \sqrt{\frac{1}{\mathrm{Pr}_{\mathrm{tu,fd}}}} - (C\,\mathrm{Pe}_{\mathrm{tu}})^2 \left[1 - \exp\left(- \frac{1}{C\,\mathrm{Pe}_{\mathrm{tu}} \sqrt{\mathrm{Pr}_{\mathrm{tu,fd}}}} \right) \right] \right\}^{-1}, \tag{7.4.17}$$

where,

$$\mathrm{Pe}_{\mathrm{tu}} = \frac{E}{\nu} \mathrm{Pr}, \tag{7.4.18}$$

$$C = 0.3, \tag{7.4.19}$$

$$\mathrm{Pr}_{\mathrm{tu},\,fd} = 0.85 + \frac{100}{\mathrm{PrRe}_D^{0.888}}. \tag{7.4.20}$$

Equation (7.4.20) was derived earlier by Jischa and Rieke (1979), with the numerator of the second term on the right-hand side being 182.4 rather than 100.

By using the preceding expressions for $\mathrm{Pr}_{\mathrm{tu}}$ and Eqs (6.6.26a) and (6.6.26b) for calculating the eddy diffusivity, Weigand et al. (2001) solved the extended Graetz problem for a smooth pipe with piecewise constant wall heat flux.

Calculations have shown that the local Nusselt numbers for UWT and UHF for turbulent pipe flow are approximately the same for $\mathrm{Pr} > 0.2$. For these conditions the average Nusselt number for the thermally developing flow for either boundary

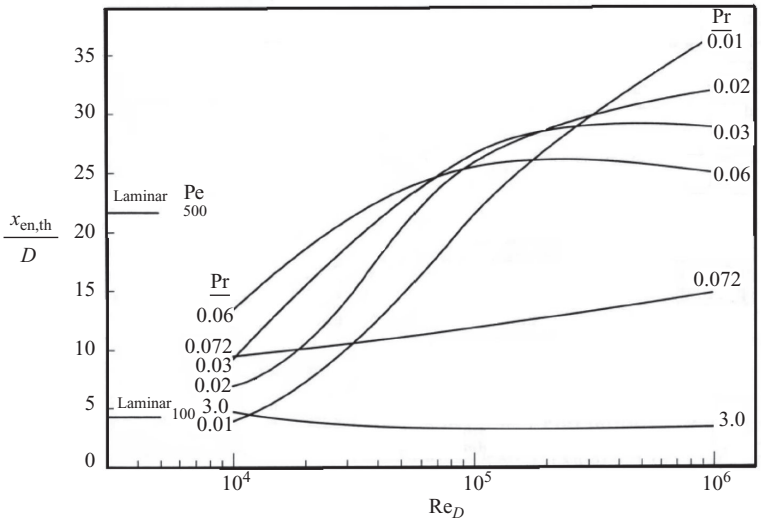

Figure 7.4. The entrance length in a pipe with UHF boundary conditions (Notter and Sleicher, 1972).

condition can be estimated from the following empirical correlation of Al-Arabi (1982), for $x/D > 3$ and $5000 < \mathrm{Re}_D < 10^5$:

$$\frac{\langle \mathrm{Nu}_D \rangle_x}{\mathrm{Nu}_{D,fd}} = 1 + \frac{CD}{x}, \tag{7.4.21}$$

where C is to be found from

$$\frac{C\,\mathrm{Pr}^{1/6}}{(x/D)^{0.1}} = 0.68 + \frac{3000}{\mathrm{Re}_D^{0.81}}, \tag{7.4.22}$$

where $\mathrm{Nu}_{D,fd}$ is the thermally developed Nusselt number.

For liquid metals ($\mathrm{Pr} < 0.03$), Chen and Chiou (1981) developed the following correlation. For $x/D > 2$ and $\mathrm{Pe} > 500$,

$$\frac{\mathrm{Nu}_{D,\mathrm{UHF}}(x)}{\mathrm{Nu}_{D,\mathrm{UHF},fd}} = \frac{\mathrm{Nu}_{D,\mathrm{UWT}}(x)}{\mathrm{Nu}_{D,\mathrm{UWT},fd}} = 1 + \frac{2.4}{x/D} - \frac{1}{(x/D)^2} \tag{7.4.23}$$

For $l/D > 2$ and $\mathrm{Pe} > 500$,

$$\frac{\langle \mathrm{Nu}_D \rangle_{l,\mathrm{UHF}}}{\mathrm{Nu}_{D,\mathrm{UHF},fd}} = \frac{\langle \mathrm{Nu}_D \rangle_{l,\mathrm{UWT}}}{\mathrm{Nu}_{D,\mathrm{UWT},fd}} = 1 + \frac{7}{l/D} + \frac{2.8}{l/D} \ln\left(\frac{l/D}{10}\right), \tag{7.4.24}$$

where

$$\mathrm{Nu}_{D,\mathrm{UHF},fd} = 5.6 + 0.0165\mathrm{Re}_D^{0.85}\mathrm{Pr}^{0.86}, \tag{7.4.25}$$

$$\mathrm{Nu}_{D,\mathrm{UWT},fd} = 4.5 + 0.0156\mathrm{Re}_D^{0.85}\mathrm{Pr}^{0.86}. \tag{7.4.26}$$

Figure 7.4 displays the thermal entrance length for the UHF boundary conditions, defined as the distance to the location at which the local Nusselt number is larger than the fully developed Nusselt number only by 5% (Notter and Sleicher, 1972). The thermal entrance lengths for the UWT boundary condition are slightly shorter

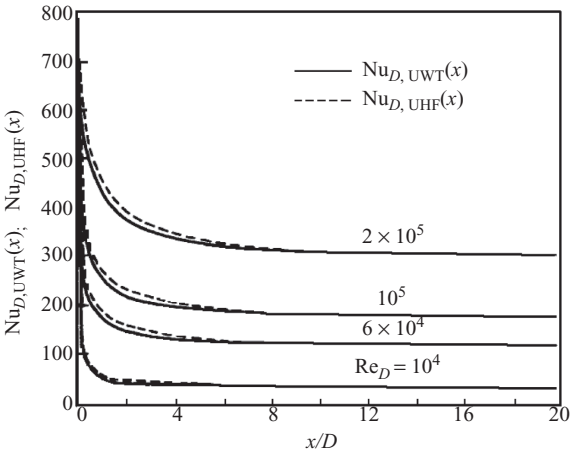

Figure 7.5. Variations of local Nusselt numbers for gas flow in a circular duct for Pr = 0.7 (after Deissler, 1953).

than the thermal entrance lengths for UHF boundary conditions. Furthermore, the thermal entrance length is sensitive to Pr as well as to Re.

7.4.4 Noncircular Ducts

Thermally developing flow in ducts with various cross-sectional geometries have been investigated in the past. Good reviews can be found in Bhatti and Shah (1987) and Ebadian and Dong (1998). Channel cross-section configurations for which detailed studies were reported include flat ducts (flow between parallel plates), rectangular, trapezoidal, triangular, annular, and several others. A variety of boundary conditions are plausible for these geometries, because each side of the channel can be subject to constant wall temperature, constant heat flux, or adiabatic conditions.

It is important to remember that it is relatively straightforward to simulate developing flow in flow passages of various cross-section shapes by use of CFD codes. The most widely applied turbulent models that are used in CFD codes are discussed in Chapter 12.

7.5 Combined Entrance Region

Figure 7.5 displays the calculation results of Deissler (1953) that were obtained with air (Pr = 0.7) for a circular pipe. These calculations were based on the assumption of uniform temperature and velocity distributions at inlet. The entrance length increases with increasing Re_D, and it increases with decreasing Pr. For $\mathrm{Pr} \geq 0.7$, an entrance length of about $8D$ is observed for $\mathrm{Re}_D \approx 2 \times 10^5$. Furthermore, there is little difference between the local Nusselt numbers and between the entrance lengths for the UWT and UHF boundary conditions.

Experiments have shown that the duct inlet configuration has a significant effect on the local Nusselt number as well as the entrance length in simultaneously developing flow (Boelter et al., 1948; Mills, 1962). For air flow, Boelter et al. measured the $\mathrm{Nu}_{D,\mathrm{UWT}}(x)/\mathrm{Nu}_{D,\mathrm{UWT},fd}$ as a function of x/D for several entrance configurations. Mills (1962) made similar measurements for the $\mathrm{Nu}_{D,\mathrm{UHF}}(x)/\mathrm{Nu}_{D,\mathrm{UHF}fd}$ ratio.

Table 7.6. *Values of constants C and n in Eq. (7.5.1) for flow in the entrance region of a circular pipe for* Pr = 0.7 *(Shah and Bhatti, 1987)*

Entrance configuration	C	n
Long calming section	0.9756	0.760
Sharp (square) entrance	2.4254	0.676
180° round bend	0.9759	0.700
90° round bend	1.0517	0.629
90° elbow	2.0152	0.614

From Mills' measurements, Bhatti and Shah (1987) developed the following empirical correlation for estimating the mean Nusselt number in the entrance region of circular pipes with UWT and UHF conditions for Pr = 0.7:

$$\frac{\langle \mathrm{Nu}_D \rangle_l}{\mathrm{Nu}_{D,fd}} = 1 + \frac{C}{(l/D)^n}, \tag{7.5.1}$$

where n and C depend on the duct inlet conditions, as shown in Table 7.6. The equation is meant to apply to both UWT and UHF boundary conditions.

For $9000 \leq \mathrm{Re}_D \leq 8.8 \times 10^4$, based on experimental data dealing with circular ducts with square-inlet conditions, Molki and Sparrow (1986) developed the following correlations for Pr = 2.5:

$$C = 23.99\mathrm{Re}_D^{-0.230}, \tag{7.5.2}$$

$$n = 0.815 - 2.08 \times 10^{-6}\mathrm{Re}_D. \tag{7.5.3}$$

For liquid metals (Pr < 0.03) flowing in a smooth pipe with uniform inlet velocity, Chen and Chiou (1981) developed the following empirical correlations, which are valid for $2 \leq l/D \leq 3.5$ and Pe > 500:

$$\frac{\mathrm{Nu}_D(x)}{\mathrm{Nu}_{D,fd}} = 0.88 + \frac{2.4}{x/D} - \frac{1.25}{(x/D)^2} - E, \tag{7.5.4}$$

$$\frac{\langle \mathrm{Nu}_D \rangle_l}{\mathrm{Nu}_{D,fd}} = 1 + \frac{5}{l/D} + \frac{1.86}{l/D} \ln\left(\frac{l/D}{10}\right) - F \tag{7.5.5}$$

where, for UWT conditions,

$$E = \frac{40 - (x/D)}{190} \tag{7.5.6}$$

$$F = 0.09. \tag{7.5.7}$$

For UHF conditions, furthermore,

$$E = F = 0. \tag{7.5.8}$$

Equations (7.5.4) and (7.5.5) apply for both UWT and UHF boundary conditions. With UWT, $\mathrm{Nu}_{D,fd}$ is calculated from Eq. (7.4.25). Likewise, with UHF, $\mathrm{Nu}_{D,fd}$ is found from Eq. (7.4.26).

EXAMPLE 7.1. Consider fully developed turbulent flow of water at a mean temperature of 35 °C in a smooth tube with a diameter of 4.5 cm. The wall temperature is 60 °C. The mean velocity is 1.6 m/s. Estimate the fluid time-averaged velocity, temperature, and turbulent thermal conductivity at a normal distance from the wall equal to 0.4 mm, using expressions borrowed from flow over a flat surface.

SOLUTION. First, we find the properties at the mean temperature (35 °C).

$$\rho = 994\,\text{kg/m}^3,\ C_P = 4183\,\text{J/kg °C},\ k = 0.6107\,\text{W/m K},$$
$$\mu = 7.2 \times 10^{-4}\,\text{kg/m s},\ \text{Pr} = 4.93.$$

We also calculate the thermal conductivity at the film temperature,

$$T_{\text{film}} = \frac{1}{2}(T_s + T_m) = 47.5\,^\circ\text{C}$$

and the viscosity at the surface temperature 60 °C, leading to

$$k_{\text{film}} = 0.6275\,\text{W/m K},\ \mu_s = 4.67 \times 10^{-4}\ \text{kg/m s}.$$

Let us calculate the Reynolds number:

$$\begin{aligned}\text{Re}_D &= \rho U_m D/\mu = \left(\rho = 994\,\text{kg/m}^3\right)(1.6\,\text{m/s})\,(0.045\,\text{m})/(7.2 \times 10^{-4}\,\text{kg/m s}) \\ &= 9.94 \times 10^4.\end{aligned}$$

The flow is clearly turbulent. We now calculate the wall shear stress by taking the following steps:

$$\begin{aligned}f_m &= \left[1.82\log\left(\text{Re}_D\right) - 1.62\right]^{-2} = \left[1.82\log\left(9.94 \times 10^4\right) - 1.62\right]^{-2} \\ &= 0.0179 \quad \text{[from Eq. (7.3.36)]}, \\ f &= f_m \frac{1}{6}\left[7 - \frac{\mu}{\mu_s}\right] = (0.0179)\,\frac{1}{6}\left[7 - \frac{7.2 \times 10^{-4}\,\text{kg/m s}}{4.67 \times 10^{-4}\,\text{kg/m s}}\right] \\ &= 0.0163 \quad \text{[from Eq. (7.3.38)]}, \\ \text{Nu}_{D,m} &= \frac{\left[\text{Re}_D - 1000\right]\text{Pr}\,\dfrac{f_m}{8}}{1 + 12.7\sqrt{\dfrac{f_m}{8}}\left[\text{Pr}^{2/3} - 1\right]} = \frac{\left[9.94 \times 10^4 - 1000\right](4.93)\,\dfrac{0.0179}{8}}{1 + 12.7\sqrt{\dfrac{0.0179}{8}}\left[(4.93)^{2/3} - 1\right]} \\ &= 473.2 \quad \text{[from Eq. (7.3.41)]}, \\ \text{Nu}_D &= \text{Nu}_{D,m}\,(\mu/\mu_s)^{0.11} = (473.2)\left(\frac{7.2 \times 10^{-4}\,\text{kg/m s}}{4.67 \times 10^{-4}\,\text{kg/m s}}\right)^{0.11} \\ &= 496.3 \quad \text{[from Eq. (7.3.37)]}.\end{aligned}$$

We can now calculate the shear stress and heat flux at the wall by taking the following steps:

$$\tau_s = \frac{f}{8}\rho U_m^2 = (0.0163)\,\frac{1}{8}\left(994\,\text{kg/m}^3\right)\,(1.6\,\text{m/s})^2 = 5.177\,\text{N/m}^2,$$
$$U_\tau = \sqrt{\tau_s/\rho} = \sqrt{(5.177\,\text{N/m}^2)\,/\,(994\,\text{kg/m}^3)} = 0.0722\,\text{m/s},$$

$$h = \mathrm{Nu}_D \frac{k_{\text{film}}}{D} = (496.3)\,\frac{0.6275\,\text{W/m K}}{0.045\,\text{m}} = 6921\,\text{W/m}^2\,\text{K},$$
$$q_s'' = h\,(T_s - T_m) = 6921\,\text{W/m}^2\,\text{K}\;(60-35)\;K = 1.73\times 10^5\,\text{W/m}^2.$$

We now find the velocity and temperature at $y = 0.4\,\text{mm}$ as follows, where properties at T_m are used for simplicity and $\mathrm{Pr}_{\text{tu}} = 1$ is assumed:

$$y^+ = y\rho U_\tau/\mu = \left(0.4\times 10^{-3}\,\text{m}\right)\left(994\,\text{kg/m}^3\right)\left(0.0722\,\text{m/s}\right)/7.2\times 10^{-4}\,\text{kg/m s}$$
$$= 39.9,$$
$$u^+ = \frac{1}{\kappa}\ln\left(y^+\right) + 5.5 = \frac{1}{0.4}\ln(39.9) + 5.5 = 14.71,$$
$$u = u^+ U_\tau = (14.71)\,(0.0722\,\text{m/s}) = 1.062\,\text{m/s},$$
$$T^+ = 5\mathrm{Pr}_{\text{tu}}\left\{\frac{\mathrm{Pr}}{\mathrm{Pr}_{\text{tu}}} + \ln\left[1 + 5\frac{\mathrm{Pr}}{\mathrm{Pr}_{\text{tu}}}\right] + \frac{1}{5\kappa}\ln\left(\frac{y^+}{30}\right)\right\}$$
$$= 5\,(1)\left\{\frac{4.93}{(1)} + \ln\left[1 + 5\frac{4.93}{(1)}\right] + \frac{1}{5\,(0.4)}\ln\left(\frac{39.9}{30}\right)\right\} = 41.6,$$
$$\frac{T_s - T}{\dfrac{q_s''}{\rho C_P U_\tau}} = T^+$$
$$\Rightarrow T = T_s - \frac{q_s''}{\rho C_P U_\tau}T^+$$
$$= 60\,^\circ\text{C} - \frac{1.73\times 10^5\,\text{W/m}^2}{(994\,\text{kg/m}^3)\,(4183\,\text{J/kg}\,^\circ\text{C})\,(0.0722\,\text{ms})}\,(41.6)$$
$$= 36.02\,^\circ\text{C}.$$

To find the turbulent thermal conductivity, we need to calculate the local eddy diffusivity. We can use the eddy diffusivity model of Reichhardt, Eq. (7.2.20a):

$$E = \frac{\mu}{\rho}\kappa\left[y^+ - y_n^+\tanh\left(\frac{y^+}{y_n^+}\right)\right]$$
$$= \frac{7.2\times 10^{-4}\,\text{kg/m s}}{(994\,\text{kg/m}^3)}\,(0.4)\left[39.9 - (11)\tanh\left(\frac{39.9}{11}\right)\right]$$
$$= 8.37\times 10^{-6}\,\text{m}^2/\text{s},$$
$$E_{\text{th}} = \frac{E}{\mathrm{Pr}_{\text{tu}}} = E = 8.37\times 10^{-6}\,\text{m}^2/\text{s},$$
$$k_{\text{tu}} = \rho\, C_P E_{\text{th}} = \left(994\ \text{kg/m}^3\right)\left(4183\,\text{J/kg}\,^\circ\text{C}\right)\left(8.37\times 10^{-6}\,\text{m}^2/\text{s}\right) = 34.8\,\text{W/m K}.$$

It can be observed that k_{tu} is almost 55 times larger than k_{film}.

EXAMPLE 7.2. A Fully developed flow of water is under way in a smooth pipe that is 5 cm in inner diameter, with a mean velocity of 2.1 m/s. The wall surface temperature is 350 K. At a location where the bulk temperature is 300 K, find the shear stress τ_{rx}, the eddy diffusivity, and turbulent thermal conductivity at 2-cm radial distance from the centerline. Assume that the turbulent Prandtl number is equal to one.

SOLUTION. The problem deals with fully developed water flow in a smooth tube with UWT boundary conditions. It is similar to Example 7.1, and therefore the following calculations are performed.

First, we find the properties at the mean temperature (35 °C):

$$\rho = 996.6\,\text{kg/m}^3,\ C_P = 4183\,\text{J/kg °C},\ k = 0.598\,\text{W/m K},$$
$$\mu = 8.54 \times 10^{-4}\,\text{kg/m s},\ \text{Pr} = 5.98.$$

We also calculate the thermal conductivity at the film temperature,

$$T_{\text{film}} = \frac{1}{2}(T_s + T_m) = 325\,\text{K},$$

and the viscosity at the surface temperature, 60 °C, leading to

$$k_{\text{film}} = 0.6326\,\text{W/m K},\ \mu_s = 3.7 \times 10^{-4}\,\text{kg/m s}.$$

Let us calculate the Reynolds number:

$$\begin{aligned}\text{Re}_D &= \rho U_m D/\mu = \left(996.6\,\text{kg/m}^3\right)(2.1\,\text{m/s})(0.05\,\text{m}) \,/\, \left(8.54 \times 10^{-4}\,\text{kg/m s}\right)\\ &= 1.225 \times 10^5.\end{aligned}$$

The flow is clearly turbulent. We now calculate the wall shear stress by taking the following step:

$$\begin{aligned}f_m &= \left[1.82\log\left(\text{Re}_D\right) - 1.62\right]^{-2} = \left[1.82\log\left(1.225 \times 10^5\right) - 1.62\right]^{-2}\\ &= 0.0171 \quad \text{[from Eq. (7.3.36)]},\\ f &= f_m \frac{1}{6}\left[7 - \frac{\mu}{\mu_s}\right] = (0.0171)\frac{1}{6}\left[7 - \frac{8.54 \times 10^{-4}\,\text{kg/m s}}{3.69 \times 10^{-4}\,\text{kg/m s}}\right]\\ &= 0.01337 \quad \text{[from Eq. (7.3.38)]},\\ \text{Nu}_{D,m} &= \frac{\left[\text{Re}_D - 1{,}000\right]\text{Pr}\,\frac{f_m}{8}}{1 + 12.7\sqrt{\frac{f_m}{8}}\left[\text{Pr}^{2/3} - 1\right]} = \frac{\left[1.225 \times 10^5 - 1000\right](4.93)\,\frac{0.0171}{8}}{1 + 12.7\sqrt{\frac{0.0171}{8}}\left[(5.98)^{2/3} - 1\right]}\\ &= 554.1 \quad \text{[from Eq. (7.3.41)]},\\ \text{Nu}_D &= \text{Nu}_{D,m}\left(\mu/\mu_s\right)^{0.11} = (554.1)\left(\frac{8.54 \times 10^{-4}\,\text{kg/m s}}{3.69 \times 10^{-4}\,\text{kg/m s}}\right)^{0.11}\\ &= 607.7 \quad \text{[from Eq. (7.3.37)]}.\end{aligned}$$

We can now calculate the shear stress and heat flux at wall by taking the following steps:

$$\begin{aligned}\tau_s &= \frac{f}{8}\rho U_m^2 = (0.0171)\frac{1}{8}\left(996.6\,\text{kg/m}^3\right)(2.1\,\text{m/s})^2 = 7.35\,\text{N/m}^2,\\ U_\tau &= \sqrt{\tau_s/\rho} = \sqrt{(7.35\,\text{N/m}^2)(996.6\,\text{kg/m}^3)} = 0.0859\,\text{m/s},\\ h &= \text{Nu}_D\frac{k_{\text{film}}}{D} = (607.7)\frac{0.6326\,\text{W/m K}}{0.05\,\text{m}} = 7,690\,\text{W/m}^2\,\text{K},\\ q_s'' &= h\left(T_s - T_m\right) = 7690\,\text{W/m}^2\,\text{K}\,(350 - 300)\,\text{K} = 3.844 \times 10^5\,\text{W/m}^2.\end{aligned}$$

We can find the local shear stress τ_{rx} by writing

$$\tau_{rx} = \frac{r}{(D/2)}\tau_s = \frac{2\,\text{cm}}{(5\,\text{cm}/2)}\left(7.348\,\text{N/m}^2\right) = 5.88\,\text{N/m}^2.$$

Now, to find the local eddy diffusivity and turbulent thermal conductivity, we write

$$y = \frac{D}{2} - r = \frac{0.05\,\text{m}}{2} - 0.02\,\text{m} = 0.005\,\text{m},$$
$$\nu = \mu/\rho = \left(8.54 \times 10^{-4}\,\text{kg/m s}\right) / \left(996.6\,\text{kg/m}^3\right) = 8.57 \times 10^{-7}\,\text{m}^2/\text{s},$$
$$y^+ = yU_\tau/\nu = \left(0.5 \times 10^{-3}\text{m}\right)(0.0859\,\text{m/s}) / \left(8.57 \times 10^{-7}\,\text{m}^2/\text{s}\right) = 500.9.$$

We estimate the eddy diffusivity from the eddy diffusivity model of von Karman (1939), Eq. (7.2.19b):

$$E = \nu\left[\frac{y^+\left(1 - \dfrac{y^+}{R_0^+}\right)}{2.5} - 1\right] = \nu\left[\frac{y^+\left(1 - \dfrac{y}{\dfrac{D}{2}}\right)}{2.5} - 1\right]$$
$$= \left(8.57 \times 10^{-7}\text{m}^2/\text{s}\right)\left[\frac{(500.9)\left(1 - \dfrac{0.005\,\text{m}}{0.025\,\text{m}}\right)}{2.5} - 1\right]$$
$$= 1.365 \times 10^{-4}\,\text{m}^2/\text{s}.$$

We can now calculate the turbulent thermal conductivity:

$$k_{\text{tu}} = \rho\, C_P E_{\text{th}} = \rho\, C_P \frac{E}{\text{Pr}_{\text{tu}}}$$
$$= \left(996.6\,\text{kg/m}^3\right)(4183\,\text{J/kg}\,^\circ\text{C})\,\frac{1.365 \times 10^{-4}\,\text{m}^2/\text{s}}{1} = 569.1\,\text{W/m}\,^\circ\text{C}.$$

We can realize the significance of the contribution of turbulence to diffusion by noting that

$$E/\nu \approx 159,$$
$$k_{\text{tu}}/k_{\text{film}} \approx 900.$$

EXAMPLE 7.3. Consider a hydrodynamically fully developed flow of a viscous oil in a 7.5-cm-diameter pipe, where the oil temperature is uniform at 300 K and the wall is adiabatic. The flow rate of the oil is such that $\text{Re}_D = 10^4$. At a location designated with $x = 0$, a wall heat flux of 2 kW/m^2 is imposed. Using the analytical solution of Notter and Sleicher (1972), find the Nusselt number

and calculate the wall temperature at $x = 80$ cm. Compare the fully developed Nusselt number with a widely used empirical correlation.
The following thermophysical properties can be assumed for the oil:

$$\rho = 750\,\text{kg/m}^3,\ C_P = 2.2\ \text{kJ/kg K},\ k = 0.14\ \text{W/m K},\ \mu = 1.28 \times 10^{-3}\ \text{Pa s}.$$

SOLUTION. First, let us calculate the mean velocity and the mass flow rate:

$$U_m = \frac{\mu}{\rho D}\text{Re}_D = \left(10^4\right)\frac{\left(1.28 \times 10^{-3}\,\text{kg/m s}\right)}{\left(750\,\text{kg/m}^3\right)(0.075\,\text{m})} = 0.2276\,\text{m/s},$$

$$\dot{m} = \rho U_m \pi \frac{D^2}{4} = \left(750\,\text{kg/m}^3\right)(0.2276\,\text{m/s})\,\pi\frac{(0.075\,\text{m})^2}{4} = 0.754\,\text{kg/s}.$$

We can now calculate the mean temperature at the location where $x = 80$ cm by a simple energy balance:

$$\dot{m}C_P\left[T_m(x) - T_{\text{in}}\right] = \pi D x q_s''$$

$$\Rightarrow T_m(x) = T_{\text{in}} + \frac{\pi D x q_s''}{\dot{m}C_P}$$

$$= 300\,\text{K} + \frac{\pi\,(0.075\,\text{m})\,(0.8\,\text{m})\left(2 \times 10^3\,\text{W/m}^2\right)}{(0.754\,\text{kg/s})\,(2200\,\text{J/kg K})} = 300.2\,\text{K}.$$

The flow is clearly turbulent. Because $\text{Pr} > 1$, the solution for UWT and UHF boundary conditions are essentially the same. We can therefore use Table 7.3 along with Eqs. (4.5.25)–(4.5.29). Therefore

$$\text{Pr} = \mu C_P/k = \left(1.28 \times 10^{-3}\,\text{kg/m s}\right)(2,200\,\text{J/kg K})/(0.14\,\text{W/m K}) = 20.11$$

$$x^* = \frac{x}{(D/2)\,\text{Re}_D\,\text{Pr}} = \frac{(0.8\,\text{m})}{(0.075\,\text{m}/2)\,(10^4)\,(20.11)} = 1.06 \times 10^{-4},$$

$$\lambda_0^2 = 247.9,$$

$$C_0 = 1.033,$$

$$G_0 = 30.3.$$

Because $x/D = (0.8\,\text{m})/(0.075\,\text{m}) = 10.67 \gtrsim 10$, thermally developed flow can be assumed. Then, according to Eq. (4.5.29),

$$\text{Nu}_D(x) = \frac{\lambda_0^2}{2} = \frac{247.9}{2} = 123.9,$$

$$h_x = \text{Nu}_D(x)\frac{k}{D} = (123.9)\frac{(0.14\,\text{W/m K})}{0.075\,\text{m}} = 231.4\,\text{W/m}^2\,\text{K}.$$

Note that the conditions necessary for the validity of the thermally developed flow assumption is different in turbulent and laminar flow. In laminar flow, the validity of the assumption requires that $x^* > 0.1$, whereas in turbulent flow $x/\text{D} \gtrsim 10$ is considered sufficient.

The local surface wall temperature can now be calculated as

$$T_s(x) = T_m(x) + \frac{q_s''}{h_x} = 300.2\,\text{K} + \frac{\left(2 \times 10^3\,\text{W/m}^2\right)}{231.4\,\text{W/m}^2\,\text{K}} = 308.9\,\text{K}.$$

We can compare the predicted Nusselt number with a few empirical correlations. From Eq. (7.3.36) we get

$$f = 0.0314.$$

The correlation of Gnielinski (1976) [Eq. (7.3.41)] will then give

$$\mathrm{Nu}_D(x)\big|_{\text{Gnielinski}} = 116.8.$$

Application of the correlation of Petukhov (1970) [Eqs. (7.3.33)–(7.3.35)] gives,

$$K_1(f) = 1.107$$
$$K_2(f) = 12.36,$$
$$\mathrm{Nu}_D(x)\big|_{\text{Petukhov}} = 130.4.$$

Finally, the correlation of Dittus and Boelter (1930) [see Table Q.3 in Appendix Q] gives

$$\mathrm{Nu}_D(x)\big|_{D-B} = 121.1.$$

PROBLEMS

Problem 7.1. Consider turbulent entrance flow in a flat channel, and assume that the velocity distribution is as follows:

$$\frac{\overline{u}(y')}{U_{\max}} = \begin{cases} (y'/\delta)^{1/7} & \text{for } 0 \le y' \le \delta \\ 1 & \text{for } y' > \delta \end{cases}, \tag{a}$$

where y' is the normal distance from the wall.

(a) Prove that at any location along the channel the velocity on the centerline is related to the inlet velocity according to

$$U_C = \frac{U_{\text{in}} b}{b - \frac{\delta}{8}}. \tag{b}$$

(b) Using Eq. (5.1.10) where U_∞ is replaced with U_C and assuming that Eq. (5.2.31) can be applied to the edge of the boundary layer where $y' = \delta$, prove that

$$\frac{d}{d\tilde{x}} \frac{7\tilde{\delta}}{72\left(1 - \frac{\tilde{\delta}}{2}\right)^2} + \frac{\tilde{\delta}}{8\left(1 - \frac{\tilde{\delta}}{2}\right)} \frac{d}{d\tilde{x}} \frac{1}{\left(1 - \frac{\tilde{\delta}}{2}\right)} = \frac{1}{\tilde{\delta}^{1/4}\left[8.75\left(1 - \frac{\tilde{\delta}}{2}\right)\right]^{7/4}}, \tag{c}$$

where

$$\tilde{x} = \frac{x}{D_H \mathrm{Re}_{D_H}^{1/4}}, D_H = 4b, \tilde{\delta} = \frac{\delta}{D_H}. \tag{d}$$

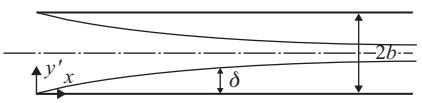

Figure P7.1.

Discuss the relevance of this analysis to the analysis of Zhi-Qing (Subsection 7.2.1).

Problem 7.2. Using the methodology of Problem 7.1, prove that

$$\Delta P_M = \frac{1}{2}\rho U_{\text{in}}^2 \left[\frac{1 - 8\tilde{\delta}/9}{\left(1 - \tilde{\delta}/2\right)^2} - 1 \right],$$
$$\tau_s = \frac{1}{2}\rho U_{\text{in}}^2 \frac{2}{\text{Re}_{D_H}^{1/4}} \frac{1}{\tilde{\delta}^{1/4}\left[8.75\left(1 - \tilde{\delta}/2\right)\right]^{7/4}},$$

where ΔP_M is the pressure drop that is due to the change in the velocity distribution in the channel and τ_s is the local wall shear stress.

Problem 7.3. Water at room temperature flows through a smooth pipe with an inner diameter of 10 cm. The flow is fully developed, and $\text{Re}_D = 1.5 \times 10^5$.

(a) Calculate the eddy diffusivity and shear stress τ_{rz} at distances 3 mm and 1 cm from the wall.
(b) Find the effective thermal conductivity $(k + k_{\text{tu}})$ at the locations specified in part (a).
(c) Repeat parts (a) and (b), this time using the eddy diffusivity model of Reichardt (1951).
(d) Repeat parts (a)–(c), this time assuming that the tube wall is rough so that $\varepsilon_s/D = 0.01$.

Explain all your assumptions.

Problem 7.4. A 1.4-m-long tube with an inner diameter of 1.25 cm is subject to a uniform wall heat flux of 2.43×10^4 W/m^2. The tube is cooled by an organic oil, with an inlet temperature of 0 °C. Calculate the wall inner surface temperature at the exit for the following two oil mass flow rates:

(a) 0.11 kg/s,
(b) 1.26 kg/2.

The oil average properties are
$\text{Pr} = 10$, $\rho = 753$ kg/m^3, $C_P = 2.1$ kJ/kg K, $k = 0.137$ W/mK, $\mu = 6.6 \times 10^{-4}$ Pa s.

Problem 7.5. Water flows in a tube that has an inner diameter of 2.54 cm and is 2.5 m long. The tube wall temperature is constant at 100 °C, and the water inlet temperature is 15 °C. The water mean velocity at the inlet is 4.6 m/s.

1. Calculate the average water temperature at tube exit, using Gnielinski's correlation by
   (a) assuming constant fluid properties,
   (b) accounting for property variations that are due to temperature change.
2. Repeat the calculations of part 1, assuming that the tube has a roughness value of approximately 4.6×10^{-2} mm.

Problem 7.6. In light of the results of Problem 7.1, we can assume that fully developed flow is achieved when $\delta = b$. Using a numerical solution method of your choice, solve Eq. (c) in Problem 7.1 and obtain the hydrodynamic entrance length for several values of Re_{D_H} in the range of 5×10^3–10^5. Compare your results with

the predictions of the following expression:

$$\frac{l_{\text{ent,hy}}}{D_H} = 0.79\text{Re}_{D_H}^{0.25}. \tag{e}$$

Problem 7.7. Consider a fully developed turbulent flow of atmospheric water at a mean temperature of 25 °C in a smooth tube with a diameter of 3.5 cm. The wall temperature is 50 °C. The flow Reynolds number is 2×10^5.

(a) Find the heat flux at the wall using an empirical correlation of your choice.
(b) Estimate the fluid time-averaged velocity and temperature at normal distances from the wall equal to 25 μm and 0.5 mm from the wall.
(c) Estimate the turbulent thermal conductivity at the locations in part (b)

Problem 7.8. Water, at a temperature of 10 °C, flows in a hydraulically smooth tube that has an inner diameter of 5 cm, with a mean velocity of 1.05 m/s. At location A, where the flow is hydrodynamically fully developed, a wall heat flux of 2×10^5 W/m^2 is imposed on the tube.

(a) Find the location of point B, where the fluid mean temperature reaches 30 °C. Is the flow thermally developed at that location?
(b) Assuming that the flow at location B is thermally developed, find the local heat transfer coefficient, wall friction factor, and wall temperature, using appropriate constant-property correlations.
(c) Calculate the eddy diffusivity and the mixing length at location B at a distance of 1 mm from the wall.
(d) Calculate the mean (i.e., time-averaged) fluid temperature at location B at 1-mm distance from the wall.
(e) Improve the results in part (b) for the effect of temperature on properties.

For simplicity, assume that water is incompressible. Also, for part (d), use the universal temperature profile for a flat surface as an approximation.

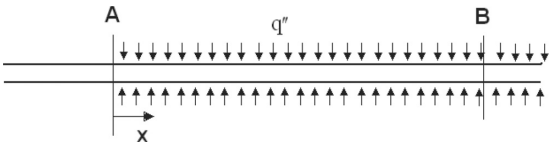

Figure P7.8.

Problem 7.9. The fuel rods in an experimental nuclear reactor are arranged in a rectangular pattern, as shown in the figure. The fuel-rod diameter is 1.14 cm, and

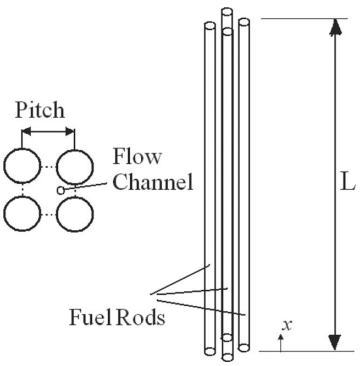

Figure P7.9.

the pitch is pitch = 1.65 cm. The rod bundle is 3.66 m tall. Assume that the core operates at 6.9 MPa and that the water temperature at the inlet is 544 K. Heat flux on the fuel-rod surface is uniform and equal to 6.31×10^4 W/m^2. The flow is assumed to be 1D, and the mass flow rate through a unit cell is 0.15 kg/s. Estimate the fuel-rod surface temperature at x = 10-cm, x =25 cm, and 50-cm locations.

Problem 7.10. Based on the derivations in Section 7.3 and the recipe described following Eq. (7.3.32), write a computer code that can calculate the fully developed Nusselt number for turbulent flow of an incompressible and constant-property fluid in a smooth circular tube. Use the expression of Reichardt (1951) [see Eqs. (7.2.20a) and (7.2.20b)] for eddy diffusivity and assume that $\mathrm{Pr}_{\mathrm{tu}} = 1$.

Apply the developed computer code to calculate and plot the Nusselt number as a function of the Reynolds number for the flow of room-temperature water (mean temperature equal to 20 °C) in a tube with 1-mm inner diameter for the range Re_D = 5000–20,000. Compare the results with the predictions of the correlation of Gnielinski.

Problem 7.11. In Problem 7.10, repeat the calculations for a 1.0-mm-diameter tube by applying the eddy diffusivity model of Reichardt (1951) [see Eqs. (7.2.20a) and (7.2.20b)] but assuming that

(a) $k = 0.48$ and $y_n^+ = 11.0$,
(b) $k = 0.40$ and $y_n^+ = 8.5$.

Compare the results with predictions using the original constants in Reichardt's model and discuss or interpret the differences.

Problem 7.12. A circular pipe with 5-cm diameter carries a hydrodynamic fully developed flow of air. The air temperature is uniform at 300 K. Starting at a location designated with axial coordinate $x = 0$, where pressure is equal to 2 bars, a uniform wall temperature of 400 K is imposed.

Using the solution of Notter and Sleicher (1972), calculate the local heat transfer coefficient at x = 16 cm. Compare the results with the predictions of the thermally developed correlation of Petukhov (1970) [Eqs. (7.3.33)–(7.3.35)]. Assume, for simplicity, that the Reynolds number remains constant at $\mathrm{Re}_D = 2 \times 10^4$.

Problem 7.13. A circular pipe with 1-cm diameter carries a hydrodynamic fully developed flow. The fluid properties are as follows:

$$\rho = 1000\,\mathrm{kg/m^3},\ \mu = 0.001\,\mathrm{kg/m\,s},\ C_P = 1.0\,\mathrm{kJ/kg\,K}.$$

The fluid temperature is uniform at 300 K. Starting at a location designated with axial coordinate $x = 0$, a uniform wall temperature of 350 K is imposed.

(a) Assuming $\mathrm{Re}_D = 2 \times 10^5$ and $\mathrm{Pr} = 0.1$, calculate and tabulate the mean temperature T_m as a function of x for $x \le 40$ cm. Plot $\theta_m = \frac{T_m - T_s}{T_{in} - T_s}$ as a function of $x^* = \frac{x}{R_0 \mathrm{Re}_D \mathrm{Pr}}$.
(b) Repeat part (a), this time for $\mathrm{Re}_D = 2 \times 10^4$ and $\mathrm{Pr} = 0.72$.

Problem 7.14. A circular pipe with 1-cm diameter carries a hydrodynamic fully developed flow. The fluid properties are as follows:

$$\rho = 1000\,\mathrm{kg/m^3},\ \mu = 0.001\,\mathrm{kg/m\,s},\ C_P = 1.0\,\mathrm{kJ/kg\,K}.$$

The fluid temperature is uniform at 300 K. Starting at a location designated with axial coordinate $x = 0$, a uniform wall heat flux of $q_s'' = 6.25 \times 10^6\ \mathrm{W/m^2}$ is imposed.

(a) Assuming that $\mathrm{Re}_D = 1.0 \times 10^5$ and $\mathrm{Pr} = 0.1$, calculate and tabulate the wall temperature T_s as a function of x for $x \leq 40$ cm. Plot $\theta_m = \frac{T_s - T_{\mathrm{in}}}{T_{m,\mathrm{out}} - T_{\mathrm{in}}}$ as a function of $x^* = \frac{x}{R_0 \mathrm{Re}_D \mathrm{Pr}}$.

(b) Repeat part (a), this time for $\mathrm{Re}_D = 1.0 \times 10^4$ and $\mathrm{Pr} = 0.72$, and $q_s'' = 6.25 \times 10^5\ \mathrm{W/m^2}$.

8 Effect of Transpiration on Friction, Heat, and Mass Transfer

When mass flows through a wall into a flow field, it modifies the velocity, temperature, and concentration profiles in the boundary layer, and thereby modifies the frictional, thermal, and mass transfer resistances in the boundary layer.

The effect of transpiration in numerical simulations, when the boundary layer is resolved, can be easily accounted for by application of the conservation principles to the wall surface. Consider the system shown in Fig. 8.1. Assume that the diffusion of the transferred species (species 1) follows Fick's law. Neglecting the contribution of the interdiffusion of species to the energy transport in the fluid [see the discussion around Eqs. (1.1.54) and (1.1.55)], the boundary conditions for the flow field at $y = 0$ will then be

$$\tau_s = \mu \left.\frac{\partial \overline{u}}{\partial y}\right|_{y=0}, \tag{8.1}$$

$$q_s'' = n_s \left(\boldsymbol{h}_s^* - \boldsymbol{h}_b^*\right) - k \left.\frac{\partial \overline{T}}{\partial y}\right|_{y=0}, \tag{8.2}$$

$$m_{1,s}'' = n_s m_{1,s} - \rho \mathcal{D}_{12} \left.\frac{\partial \overline{m}_1}{\partial y}\right|_{y=0}, \tag{8.3}$$

where n_s is the mass flux (in kilograms per square meter per seconds) through the wall and is positive for blowing, and the total (stagnation) enthalpy is defined as

$$\boldsymbol{h}^* = \overline{\boldsymbol{h}} + \frac{1}{2}|\vec{U}|^2.$$

Furthermore, $\boldsymbol{h}_b$ is the enthalpy of the incoming fluid through the boundary, $\boldsymbol{h}_s$ is the enthalpy of the fluid mixture at the wall, m_1 is the mass fraction of the transferred species (species 1), and $\mathcal{D}_{12}$ is the mass diffusivity of the transferred species with respect to the mixture (referred to as species 2). Equation (8.2) accounts for thermal and kinetic energy transfer through the interface. In practice, however, the contribution of kinetic energy is often negligible.

8.1 Couette Flow Film Model

For engineering calculations the effect of transpiration on friction, heat, or mass transfer can be accounted for by the Couette flow film model or the stagnant film

Table 8.1. *Couette flow film model predictions for transfer coefficients*

Explicit form		Implicit form	
$\frac{\dot{C}_f}{C_f} = \frac{\beta}{\exp(\beta) - 1}$	(8.7a)	$\frac{\dot{C}_f}{C_f} = \frac{\ln(1+B)}{B}$	(8.8a)
$\beta = \frac{2n_s}{\rho U_\infty C_f}$	(8.7b)	$B = \frac{2n_s}{\rho U_\infty \dot{C}_f}$	(8.8b)
$\frac{\dot{h}}{h} = \frac{\beta_{\text{th}}}{\exp(\beta_{\text{th}}) - 1}$	(8.9a)	$\frac{\dot{h}}{h} = \frac{\ln(1+B_{\text{th}})}{B_{\text{th}}}$	(8.10a)
$\beta_{\text{th}} = \frac{n_s C_P}{h}$	(8.9b)	$B_{\text{th}} = \frac{n_s C_P}{\dot{h}}$	(8.10b)
$\frac{\dot{\mathcal{K}}}{\mathcal{K}} = \frac{\beta_{\text{ma}}}{\exp(\beta_{\text{ma}}) - 1}$	(8.11a)	$\frac{\dot{\mathcal{K}}}{\mathcal{K}} = \frac{\ln(1+B_{\text{ma}})}{B_{\text{ma}}}$	(8.12a)
$\beta_{\text{ma}} = \frac{n_s}{\mathcal{K}}$	(8.11b)	$B_{\text{ma}} = \frac{m_{1,\infty} - m_{1,s}}{m_{1,s} - \frac{m''_{1,s}}{n_s}}$	(8.12b)
$\frac{\dot{\tilde{\mathcal{K}}}}{\tilde{\mathcal{K}}} = \frac{\tilde{\beta}_{\text{ma}}}{\exp(\tilde{\beta}_{\text{ma}}) - 1}$	(8.13a)	$\frac{\dot{\tilde{\mathcal{K}}}}{\tilde{\mathcal{K}}} = \frac{\ln(1+\tilde{B}_{\text{ma}})}{\tilde{B}_{\text{ma}}}$	(8.14a)
$\tilde{\beta}_{\text{ma}} = \frac{N''_s}{\tilde{\mathcal{K}}}$	(8.13b)	$\tilde{B}_{\text{ma}} = \frac{x_{1,\infty} - x_{1,s}}{x_{1,s} - \frac{N''_{1,s}}{N''_s}}$	(8.14b)

model. The two models lead essentially to the same results even though they treat the flow field somewhat differently. According to the Couette flow film model, we can write

$$\tau_s = \dot{C}_f \frac{1}{2} \rho U_\infty^2, \tag{8.4}$$

$$-k \frac{\partial T}{\partial y}\bigg|_{y=0} = \dot{h} (T_s - T_\infty), \tag{8.5}$$

$$-\rho \mathcal{D}_{12} \frac{\partial m_1}{\partial y}\bigg|_{y=0} = \dot{\mathcal{K}} (m_{1,s} - m_{1,\infty}), \tag{8.6}$$

where $\dot{C}_f, \dot{h}$, and $\dot{\mathcal{K}}$ are the coefficients for skin friction, convective heat transfer, and convective mass transfer, respectively. The dot over these parameters implies that they are affected by the mass transpiration effect.

Table 8.1 is a summary of the predictions of the Couette flow film model for these parameters. Equations (8.11a), (8.11b), (8.12a), and (8.12b) are all applicable when the mass transfer process is modeled in terms of mass flux and mass fraction, whereas Eqs. (8.13a), (8.13b), (8.14a), and (8.14b) are for the cases in which the mass transfer process is modeled in terms of molar flux and mole fraction.

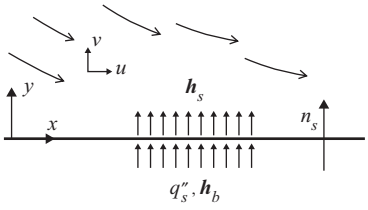

Figure 8.1. Mass transfer through an interface.

Table 8.2. *Couette flow film model predictions for Stanton numbers*

Explicit form		Implicit form	
$\frac{\dot{\mathrm{St}}}{\mathrm{St}} = \frac{\beta_{\mathrm{th}}}{\exp(\beta_{\mathrm{th}}) - 1}$	(8.15a)	$\frac{\dot{\mathrm{St}}}{\mathrm{St}} = \frac{\ln(1 + B_{\mathrm{th}})}{B_{\mathrm{th}}}$	(8.16a)
$\beta_{\mathrm{th}} = \frac{\frac{n_s}{\rho U_\infty}}{\mathrm{St}}$	(8.15b)	$B_{\mathrm{th}} = \frac{\frac{n_s}{\rho U_\infty}}{\dot{\mathrm{St}}}$	(8.16b)
$\frac{\dot{\mathrm{St}}_{\mathrm{ma}}}{\mathrm{St}_{\mathrm{ma}}} = \frac{\beta_{\mathrm{ma}}}{\exp(\beta_{\mathrm{ma}}) - 1}$	(8.17a)	$\frac{\dot{\mathrm{St}}_{\mathrm{ma}}}{\mathrm{St}_{\mathrm{ma}}} = \frac{\ln(1 + B_{\mathrm{ma}})}{B_{\mathrm{ma}}}$	(8.18)
$\beta_{\mathrm{ma}} = \frac{\frac{n_s}{\rho U_\infty}}{St_{\mathrm{ma}}}$	(8.17b)	Get B_{ma} from Eq. (8.12b)	
$\frac{\dot{\tilde{S}}t_{\mathrm{ma}}}{\tilde{\mathrm{St}}_{\mathrm{ma}}} = \frac{\tilde{\beta}_{\mathrm{ma}}}{\exp(\tilde{\beta}_{\mathrm{ma}}) - 1}$	(8.19a)	$\frac{\dot{\mathrm{St}}_{\mathrm{ma}}}{\mathrm{St}_{\mathrm{ma}}} = \frac{\ln(1 + \tilde{B}_{\mathrm{ma}})}{\tilde{B}_{\mathrm{ma}}}$	(8.20)
$\tilde{\beta}_{\mathrm{ma}} = \frac{N_s''/\boldsymbol{C}U_\infty}{St_{\mathrm{ma}}}$	(8.19b)	Get $\tilde{B}_{\mathrm{ma}}$ from Eq. (8.14b)	

The expressions listed in Table 8.1 are adequate for engineering calculations. More elaborate semiempirical expressions for $\dot{C}_f$, $\dot{h}$, and $\dot{\mathcal{K}}$ were derived, for example, for droplets evaporating in a high-temperature stream (Renksizbulut and Yuen, 1983; Renksizbulut and Haywood, 1988).

The formulas for calculating $\dot{h}$ and $\dot{\mathcal{K}}$ in Table 8.1 can all be cast in terms of Stanton numbers. These are summarized in Table 8.2, where,

$$\mathrm{St} = \frac{h}{\rho C_P U_\infty} = \frac{h}{\boldsymbol{C}\tilde{C}_P U_\infty}, \tag{8.21}$$

$$\dot{\mathrm{St}} = \frac{\dot{h}}{\rho C_P U_\infty} = \frac{\dot{h}}{\boldsymbol{C}\tilde{C}_P U_\infty}, \tag{8.22}$$

$$\mathrm{St}_{\mathrm{ma}} = \frac{\mathcal{K}}{\rho U_\infty} = \frac{\tilde{\mathcal{K}}}{\boldsymbol{C}U_\infty}, \tag{8.23}$$

$$\dot{\mathrm{St}}_{\mathrm{ma}} = \frac{\dot{\mathcal{K}}}{\rho U_\infty} = \frac{\dot{\tilde{\mathcal{K}}}}{\boldsymbol{C}U_\infty}. \tag{8.24}$$

In view of the definitions of $\dot{\mathcal{K}}$ and $\dot{\tilde{\mathcal{K}}}$, it can be shown that

$$\rho\mathcal{K} = \boldsymbol{C}\tilde{\mathcal{K}},$$
$$\rho\dot{\mathcal{K}} = \boldsymbol{C}\dot{\tilde{\mathcal{K}}}.$$

The derivation of the Couette flow model for the friction factor and the heat transfer coefficient are now demonstrated.

Wall Friction

In Fig. 8.1, let us assume that the boundary layer behaves approximately as a Couette flow field with thickness δ. Let us start from the 2D momentum boundary-layer equation for an incompressible and constant-property fluid:

$$\overline{u}\frac{\partial \overline{u}}{\partial x} + \overline{v}\frac{\partial \overline{u}}{\partial y} = -\frac{1}{\rho}\frac{d\overline{P}}{\partial x} + \frac{\partial}{\partial y}\left[(\nu + E)\frac{\partial \overline{u}}{\partial y}\right]. \tag{8.25}$$

For a Couette flow field we must have (see Section 4.1)

$$\frac{\partial \overline{u}}{\partial x} = \frac{\partial \overline{v}}{\partial y} = 0, \tag{8.26}$$

$$\overline{v} = v_s = \text{const.} \tag{8.27}$$

Equation (8.25) then becomes

$$v_s \frac{\partial \overline{u}}{\partial y} = \frac{\partial}{\partial y}\left[(\nu + E)\frac{\partial \overline{u}}{\partial y}\right]. \tag{8.28}$$

The boundary conditions for this equation are as follows. At $y = 0$,

$$\overline{u} = 0, \tag{8.29a}$$

$$(\nu + E)\frac{\partial \overline{u}}{\partial y} = \frac{\tau_s}{\rho}. \tag{8.29b}$$

At $y = \delta$,

$$\overline{u} = U_\infty. \tag{8.30}$$

We now apply $\int_0^y dy$ to both sides of Eq. (8.28) to get

$$\frac{d\overline{u}}{v_s \overline{u} + \dfrac{\tau_s}{\rho}} = \frac{dy}{\nu + E}. \tag{8.31}$$

We next apply $\int_0^\delta dy$ to both sides of Eq. (8.31) to get

$$\frac{1}{v_s} \ln\left[1 + \frac{\rho v_s U_\infty}{\tau_s}\right] = \int_0^\delta \frac{dy}{\nu + E}. \tag{8.32}$$

Let us define

$$B = \frac{\rho\, v_s U_\infty}{\tau_s} = \frac{v_s / U_\infty}{\dfrac{1}{2}\dot{C}_f}, \tag{8.33}$$

where $\dot{C}_f$ is related to the wall shear stress according to

$$\tau_s = \dot{C}_f \frac{1}{2} \rho U_\infty^2. \tag{8.34}$$

Equation (8.32) will then give

$$\frac{\dot{C}_f}{2} = \frac{\ln(1+B)}{B} \frac{1}{U_\infty}\left[\int_0^\delta \frac{dy}{\nu + E}\right]^{-1}. \tag{8.35}$$

Next, we note that when $n_s \to 0$ (which is equivalent to $B \to 0$), all parameters should reduce to their values that correspond to no transpiration conditions. Thus we must have

$$\lim_{B \to 0} \dot{C}_f = C_f. \tag{8.36}$$

Furthermore, we can write

$$\lim_{B \to 0} \frac{\ln(1+B)}{B} = 1. \tag{8.37}$$

Equations (8.35)–(8.37) imply that

$$\frac{C_f}{2} = \frac{1}{U_\infty}\left[\int_0^\delta \frac{dy}{\nu + E}\right]^{-1}. \tag{8.38}$$

More important, Eqs. (8.35) and (8.38) lead to Eq. (8.8a) in Table 8.1.

We can now easily derive Eq. (8.7a) by noting that Eq. (8.32) and (8.38) result in

$$\frac{1}{v_s}\ln(1+B) = \frac{2}{U_\infty C_f}. \tag{8.39}$$

We define

$$\beta = \frac{2v_s}{U_\infty C_f}. \tag{8.40}$$

As a result,

$$B = (\exp\beta) - 1. \tag{8.41}$$

Substitution for B from this equation into Eq. (8.8a) will result in Eq. (8.7a).

Heat Transfer Coefficient

We start with the energy equation for a Couette flow field:

$$\rho C_P v_s \frac{\partial \overline{T}}{\partial y} = \frac{\partial}{\partial y}\left[\rho C_P\left(\frac{\nu}{\mathrm{Pr}} + \frac{E}{\mathrm{Pr_{tu}}}\right)\frac{\partial \overline{T}}{\partial r}\right]. \tag{8.42}$$

The boundary conditions are as follows. At $y = 0$,

$$\overline{T} = T_s, \tag{8.43}$$

$$-\rho C_P\left(\frac{\nu}{\mathrm{Pr}} + \frac{E}{\mathrm{Pr_{tu}}}\right)\frac{\partial \overline{T}}{\partial r} = q_s''. \tag{8.44}$$

At $y = \delta$, we have $\overline{T} = T_\infty$.

By applying $\int_0^y dy$ to both sides of Eq. (8.42) and some straightforward manipulation, we get

$$\frac{d\overline{T}}{\rho C_P v_s\left(\overline{T} - T_s\right) - q_s''} = \frac{dy}{\rho C_P\left(\frac{\nu}{\mathrm{Pr}} + \frac{E}{\mathrm{Pr_{tu}}}\right)}. \tag{8.46}$$

We note that the variables were separated in this equation. We now apply $\int_0^\delta$ to both sides of Eq. (8.46) to get

$$\frac{1}{\rho C_P v_s}\ln(1 + B_{\mathrm{th}}) = \int_0^\delta \frac{dy}{\rho C_P\left(\frac{\nu}{\mathrm{Pr}} + \frac{E}{\mathrm{Pr_{tu}}}\right)}, \tag{8.47}$$

where

$$B_{\mathrm{th}} = \frac{\rho C_P v_s\left(T_s - T_\infty\right)}{q_s''} = \frac{\rho C_P v_s}{\dot{h}}. \tag{8.48}$$

Now, with some straightforward manipulations, we can cast Eq. (8.47) as

$$\dot{h} = \frac{\ln(1+B_{\text{th}})}{B_{\text{th}}} \left[\int_0^{\delta} \frac{dy}{\rho C_P \left(\frac{\nu}{\text{Pr}} + \frac{E}{\text{Pr}_{\text{tu}}} \right)} \right]^{-1}. \tag{8.49}$$

We now note that

$$\lim_{B_{\text{th}} \to 0} \frac{\ln(1+B_{\text{th}})}{B_{\text{th}}} = 1, \tag{8.50}$$

$$\lim_{B \to 0} \dot{h} = h. \tag{8.51}$$

Then, clearly,

$$h = \left[\int_0^{\delta} \frac{dy}{\rho C_P \left(\frac{\nu}{\text{Pr}} + \frac{E}{\text{Pr}_{\text{tu}}} \right)} \right]^{-1}. \tag{8.52}$$

Equations (8.49) and (8.52) then lead to Eq. (8.10a).

To derive Eq. (8.9a), let us define

$$\beta_{\text{th}} = \rho v_s (C_P/h). \tag{8.53}$$

Equations (8.47) and (8.52) then lead to

$$\rho v_s (C_P/h) = \ln(1+B_{\text{th}}).$$

As a result,

$$B_{\text{th}} = (\exp \beta_{\text{th}}) - 1. \tag{8.54}$$

Substitution for B_{th} from this equation into Eq. (8.10a) then leads to Eq. (8.9a).

Some Final Notes

The derivation of Eqs. (8.11a) and (8.12a) is also relatively straightforward (see Problem 8.5).

The derivations leading to the Couette flow model were based on the assumption that the boundary layers are at equilibrium. However, the model is known to do well under developing flow conditions as well because turbulent boundary layers approach local equilibrium quickly.

8.2 Gas–Liquid Interphase

The conditions at a liquid–gas interphase were briefly discussed in Section 1.4. We now revisit this issue and discuss high mass transfer rate situations. As discussed in Section 1.4, in most engineering problems the interfacial resistance for heat and mass transfer is negligibly small, and equilibrium at the interphase can be assumed. The interfacial transfer processes are then controlled by the thermal and mass transfer resistances between the liquid bulk and the interphase (i.e., the liquid-side resistances), and between the gas bulk and the interphase (i.e., the gas-side resistance).

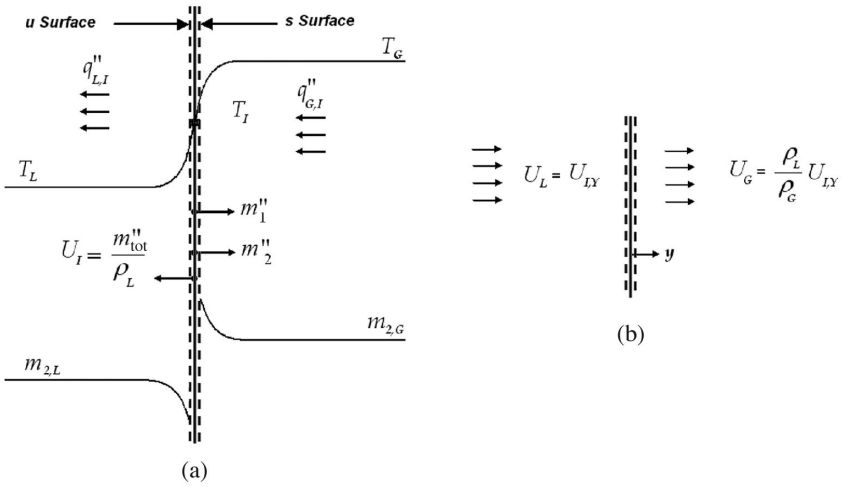

Figure 8.2. The gas–liquid interphase during evaporation and desorption of an inert species: (a) mass-fraction profiles; (b) velocities in which the coordinate is placed on the interphase.

Let us consider the situation in which a sparingly soluble substance 2 is mixed with liquid represented by species 1. If the interphase is idealized as a flat surface, the configuration for a case in which evaporation of species 1 and desorption of a dissolved species 2 occur simultaneously will be similar to Fig. 8.2(a). For simplicity, let us treat the mass flux of species 1 as known for now, and focus on the transfer of species 2. The interfacial mass fluxes will then be

$$m''_2 = (1 - m_{I,u}) m''_{\text{tot}} - \rho_{L,u} \mathcal{D}_{12,L} \left. \frac{\partial \overline{m}_2}{\partial y} \right|_u , \tag{8.55}$$

$$m''_{\text{tot}} = m''_1 + m''_2 . \tag{8.56}$$

Equation (8.55) is evidently similar to Eq. (8.3). In general, sensible and latent heat transfer take place on both sides of the interphase. When the coordinate center is fixed to the interphase, as shown in Fig. 8.2(b), there will be fluid motion in the y direction on both sides of the interphase, where

$$U_{I,y} = \frac{m''_{\text{tot}}}{\rho_L} . \tag{8.57}$$

Energy balance for the interphase gives

$$m''_1 \boldsymbol{h}_f + m''_2 \boldsymbol{h}_{2,LI} + m''_{\text{tot}} \frac{1}{2} U^2_{I,y} - q''_{LI} = m''_1 \boldsymbol{h}_g + m''_2 \boldsymbol{h}_{2,GI} + m''_{\text{tot}} \frac{1}{2} \left(\frac{\rho_L U_I}{\rho_G} \right)^2 - q''_{GI} . \tag{8.58}$$

Neglecting the kinetic energy changes, we can rewrite this equation as

$$q''_{GI} - q''_{LI} = m''_1 \boldsymbol{h}_{fg} + m''_2 \boldsymbol{h}_{2,LG} \tag{8.59}$$

where $\boldsymbol{h}_{2,LG}$ is the specific heat of desorption for species 2.

Assuming that the sensible heat conduction follows Fourier's law in both phases, the sensible heat transfer rates can be represented by convection heat transfer coefficients according to

$$q''_{GI} = k_G \frac{\partial T_G}{\partial y}\bigg|_{y=0} = \dot{h}_{GI}(T_G - T_I), \tag{8.60}$$

$$q''_{LI} = k_L \frac{\partial T}{\partial y}\bigg|_{y=0} = \dot{h}_{LI}(T_I - T_L), \tag{8.61}$$

where $\dot{h}_{GI}$ is the heat transfer coefficient between the interphase and gas bulk, and $\dot{h}_{LI}$ represents the heat transfer coefficient between the interphase and liquid bulk. The convection heat transfer coefficients must account for the distortion of the temperature profiles caused by the mass-transfer-induced fluid velocities, as described in Section 8.1.

We now discuss mass transfer. Mass transfer for species 2 can be represented by Eq. (8.55) (for the liquid side) and the following equation for the gas side:

$$m''_2 = (1 - m_{1,s})\, m''_{\text{tot}} - \rho_{G,s}\mathcal{D}_{12,G} \frac{\partial \overline{m}_2}{\partial y}\bigg|_s. \tag{8.62}$$

These equations are similar to Eq. (8.3) and include advective and diffusive terms on their right-hand sides. $\mathcal{D}_{12,G}$ and $\mathcal{D}_{12,L}$ are the mass diffusivity coefficients in the gas and liquid phases, respectively. Once again, for convenience the diffusion terms can be replaced with

$$-\rho_{G,s}\mathcal{D}_{12,G} \frac{\partial \overline{m}_2}{\partial y}\bigg|_s = \dot{\mathcal{K}}_{GI}(m_{2,s} - m_{2,G}) \tag{8.63}$$

$$-\rho_{L,u}\mathcal{D}_{12,L} \frac{\partial \overline{m}_2}{\partial y}\bigg|_u = \dot{\mathcal{K}}_{LI}(m_{2,L} - m_{2,u}), \tag{8.64}$$

where the mass transfer coefficients $\dot{\mathcal{K}}_{GI}$ and $\dot{\mathcal{K}}_{LI}$ must account for the distortion in the concentration profiles caused by the blowing effect of the mass transfer at the vicinity of the interphase.

The effect of mass-transfer-induced distortions of temperature and concentration profiles can be estimated by the Couette flow film model discussed in the previous section. Thus, in accordance with Table 8.1, the liquid- and gas-side transfer coefficients are both modified as

$$\frac{\dot{h}_{GI}}{\dot{h}_{GI}} = \frac{m''_{\text{tot}} C_{PG,t}/h_{GI}}{\exp\left(m''_{\text{tot}} C_{PG,t}/h_{GI}\right) - 1}, \tag{8.65}$$

$$\frac{\dot{h}_{LI}}{\dot{h}_{LI}} = \frac{-m''_{\text{tot}} C_{PL,t}/h_{LI}}{\exp\left(-m''_{\text{tot}} C_{PL,t}/h_{LI}\right) - 1}, \tag{8.66}$$

$$\frac{\dot{\mathcal{K}}_{GI}}{\mathcal{K}_{GI}} = \frac{m''_{\text{tot}}/\mathcal{K}_{GI}}{\exp\left(m''_{\text{tot}}/\mathcal{K}_{GI}\right) - 1}, \tag{8.67}$$

$$\frac{\dot{\mathcal{K}}_{LI}}{\mathcal{K}_{LI}} = \frac{-m''_{\text{tot}}/\mathcal{K}_{LI}}{\exp\left(-m''_{\text{tot}}/\mathcal{K}_{LI}\right) - 1}, \tag{8.68}$$

where $C_{PG,t}$ and $C_{PL,t}$ are the specific heats of the transferred species in the gaseous and liquid phases, respectively, and $h_{LI}, h_{GI}, \mathcal{K}_{LI}$ and $\mathcal{K}_{GI}$ are the convective transfer

coefficients for the limit $m''_{\text{tot}} \to 0$. When the gas–liquid system is single component (e.g., evaporation or condensation of pure liquid surrounded by its own pure vapor), then $C_{PG,t} = C_{PG}$ and $C_{PL,t} = C_{PL}$.

Equations (8.65)–(8.68) are convenient to use when mass fluxes are known. The Couette flow film model results can also be presented in the following forms, which are convenient when the species concentrations are known:

$$\frac{\dot{h}_{GI}}{h_{GI}} = \ln(1 + B_{\text{th},G})/B_{\text{th},G}, \tag{8.69}$$

$$\frac{\dot{h}_{LI}}{h_{LI}} = \ln(1 + B_{\text{th},L})/B_{\text{th},L}, \tag{8.70}$$

$$\frac{\dot{\mathcal{K}}_{GI}}{\mathcal{K}_{GI}} = \ln(1 + B_{\text{ma},G})/B_{\text{ma},G}, \tag{8.71}$$

$$\frac{\dot{\mathcal{K}}_{LI}}{\mathcal{K}_{LI}} = \ln(1 + B_{\text{ma},L})/B_{\text{ma},L}, \tag{8.72}$$

where,

$$B_{\text{th},L} = \frac{-m''_{\text{tot}} C_{PL,t}}{\dot{h}_{LI}}, \tag{8.73}$$

$$B_{\text{th},G} = \frac{m''_{\text{tot}} C_{PG,t}}{\dot{h}_{GI}}, \tag{8.74}$$

$$B_{\text{ma},G} = \frac{m_{2,G} - m_{2,s}}{m_{2,s} - m''_2/m''_{\text{tot}}}, \tag{8.75}$$

$$B_{\text{ma},L} = \frac{m_{2,L} - m_{2,u}}{m_{2,u} - m''_2/m''_{\text{tot}}}. \tag{8.76}$$

The transfer of species 1 can now be addressed. Because species 2 is only sparingly soluble, its mass flux at the interphase will be typically much smaller than the mass flux of species 1 when the phase change of species 1 is in progress. The transfer of species 1 can therefore be modeled by disregarding species 2, in accordance with Section 8.1. The following examples show how.

EXAMPLE 8.1. Water vapor at 2-bars pressure and 145 °C flows through a smooth pipe with 2.5-cm inner diameter. At a location where the steam mass flux is 6.13 kg/m^2 s, steam is injected into the pipe through a porous wall at the rate of 0.003 kg/m^2 s. The wall surface temperature is 122 °C. Calculate the friction factor and heat transfer coefficient.

SOLUTION. First, we need to find the relevant thermophysical properties. The following properties represent superheated steam at 2-bars pressure and 145 °C temperature. They are thus properties at the fluid mean temperature T_m:

$$\rho = 1.056\,\text{kg/m}^3, \quad C_P = 2062\,\text{J/kg}\,^\circ\text{C}, \quad k = 00291\,\text{W/m K},$$
$$\mu = 1.39 \times 10^{-5}\,\text{kg/m s}, \ \text{Pr} = 0.986.$$

We also calculate viscosity at the surface temperature to get

$$\mu_s = 1.303 \times 10^{-5}\,\text{kg/m s}.$$

To calculate the friction factor in the absence of transpiration we proceed by calculating the mass flux G and the Reynolds number:

$$\dot{m} = \frac{\pi}{4}D^2G = \frac{\pi}{4}(0.025\,\text{m})^2(6.14\,\text{kg/m}^2\,\text{s}) = 0.003014\,\text{kg/m}^2\,\text{s},$$
$$\text{Re}_D = GD/\mu = \left(6.14\,\text{kg/m}^2\,\text{s}\right)(0.025\,\text{m})/(1.39\times10^{-5}\,\text{kg/m}\,\text{s}) = 1.1\times10^4.$$

The flow is turbulent. The Darcy friction factor can be found from Petukhov's correlations [Eq. (7.3.36) and (7.3.40)]:

$$f_m = [1.82\log(\text{Re}_D) - 1.62]^{-2} = \left[1.82\log\left(1.1\times10^4\right) - 1.62\right]^{-2} = 0.0306,$$
$$f = f_m\left(\frac{T_s}{T_m}\right)^{-0.1} = (0.0306)\left(\frac{122+273\,\text{K}}{145+273\,\text{K}}\right)^{-0.1} = 0.0308.$$

For the heat transfer coefficient, in the absence of transpiration, we can use the correlation of Gnielinski [Eq. (7.3.41)] and correct it for the effect of property variation by using Eq. (7.3.37):

$$\text{Nu}_{D,m} = \frac{[\text{Re}_D - 1,000]\,\text{Pr}\,\frac{f_m}{8}}{1+12.7\sqrt{\frac{f_m}{8}}\left[\text{Pr}^{2/3}-1\right]} = \frac{\left[1.1\times10^4 - 1000\right](0.986)\,\frac{0.0306}{8}}{1+12.7\sqrt{\frac{0.0306}{8}}\left[(0.986)^{2/3}-1\right]} = 38.05,$$

$$\text{Nu}_D = \text{Nu}_{D,m}\,(\mu/\mu_s) = (38.05)\left(\frac{1.39\times10^{-5}\,\text{kg/m}\,\text{s}}{1.303\times10^{-5}\,\text{kg/m}\,\text{s}}\right) = 40.7,$$

$$h = \text{Nu}_D\frac{k_f}{D} = (40.7)\,\frac{0.029\,\text{W/m K}}{0.025\,\text{m}} = 47.4\,\text{W/m}^2\,\text{K}.$$

We can now correct the friction factor for the mass transfer effect:

$$\beta = \frac{2n_s}{\rho U_m C_f} = \frac{2n_s}{G\,(f/4)} = \frac{2\left(0.003\,\text{kg/m}^2\,\text{s}\right)}{(6.14\,\text{kg/m}^2\,\text{s})\,(0.0308/4)} = 0.1277,$$

$$\dot{f} = f\frac{\beta}{(\exp\beta)-1} = (0.0308)\,\frac{0.1277}{(\exp 0.1277)-1} = 0.0287.$$

For correcting the heat transfer coefficient for the effect of transpiration, we need to find C_P first. This parameter is the specific heat of steam at the surface temperature, which turns out to be

$$C_P = 2120\,\text{J/Kg K}.$$

We then proceed by writing

$$\beta_{\text{th}} = \frac{n_s C_P}{h} = \frac{\left(0.003\,\text{kg/m}^2\,\text{s}\right)(2120\,\text{J/kg K})}{47.44\,\text{W/m}^2\,\text{K}} = 0.134,$$

$$\dot{h} = h\frac{\beta_{\text{th}}}{(\exp\beta_{\text{th}})-1} = \left(47.4\,\text{W/m}^2\,\text{K}\right)\frac{0.134}{[\exp(0.134)]-1} = 44.3\,\text{W/m}^2\,\text{K}.$$

EXAMPLE 8.2. A spherical 1.5-mm-diameter pure-water droplet is in motion in dry air, with a relative velocity of 2 m/s. The air is at 25 °C. Calculate the evaporation mass flux at the surface of the droplet, assuming that at the moment of interest the droplet bulk temperature is 5 °C. For simplicity assume quasi-steady state, and for the liquid-side heat transfer coefficient (i.e., heat transfer

between the droplet surface and the droplet liquid bulk) use the correlation of Kronig and Brink (1950) for internal thermal resistance of a spherical droplet that undergoes internal recirculation according to Hill's vortex flow:

$$\mathrm{Nu}_{D,L} = \frac{h_{LI} D}{k_L} = 17.9. \tag{k}$$

SOLUTION. In view of the very low solubility of air in water, we can treat air as a completely passive component of the gas phase. The thermophysical and transport properties need to be calculated first. For simplicity, we calculate them at 25 °C:

$$C_{PL} = 4200\,\mathrm{J/kg\,K}; \quad C_{Pv} = 1887\,\mathrm{J/kg\,K}; \quad \mathcal{D}_{12} = 2.54 \times 10^{-5}\,\mathrm{m^2/s},$$
$$k_G = 0.0255\ \mathrm{W/m\,K}; \quad k_L = 0.577\ \mathrm{W/m\,K}; \quad \boldsymbol{h}_{fg} = 2.489 \times 10^6\,\mathrm{J/kg},$$
$$\mu_G = 1.848 \times 10^{-5}\,\mathrm{kg/m\,s}; \quad \rho_G = 1.185\ \mathrm{kg/m^3}; \quad \mathrm{Pr}_G = 0.728.$$

We also have $M_n = 29$ kg/kmol and $M_v = 18$ kg/kmol. We can now calculate the convective transfer coefficients. We use the Ranz and Marshall (1952) correlation for the gas side:

$$\mathrm{Re}_{D,G} = \rho_G U D/\mu_G = 192.3,$$
$$\mathrm{Sc}_G = \frac{\mu_G}{\rho_G \mathcal{D}_{12}} = 0.613,$$
$$\mathrm{Nu}_{D,G} = h_{GI} D/k_G = 2 + 0.3\mathrm{Re}_{D,G}^{0.6}\mathrm{Pr}_G^{0.333},$$
$$\Rightarrow h_{GI} = 141.7\ \mathrm{W/m^2\,K},$$
$$\mathrm{Sh}_{D,G} = \frac{\mathcal{K}_{GI} D}{\rho_G \mathcal{D}_{12,G}} = 2 + 0.3\mathrm{Re}_{D,G}^{0.6}\mathrm{Sc}^{0.333},$$
$$\Rightarrow \mathcal{K}_{GI} = 0.1604\ \mathrm{kg/m^2\,s},$$
$$\frac{h_{LI} D}{k_L} = 17.9 \Rightarrow h_{LI} = 6651\ \mathrm{W/m^2\,K}.$$

The following equations should now be solved iteratively, bearing in mind that $P = 1.013 \times 10^5\ \mathrm{N/m^2}$ and $m_{v,\infty} = 0$:

$$X_{v,s} = P_{\mathrm{sat}}(T_I)/P,$$
$$m_{v,s} = \frac{X_{v,s} M_v}{X_{v,s} M_v + (1 - X_{vs}) M_n},$$
$$B_{\mathrm{th},L} = -\frac{m'' C_{PL}}{h_{LI}},$$
$$B_{\mathrm{th},G} = \frac{m'' C_{Pv}}{h_{GI}},$$
$$B_{\mathrm{ma},G} = \frac{m_{v,\infty} - m_{v,s}}{m_{v,s} - 1},$$

$$\dot{h}_{LI} = h_{LI} \ln(1 + B_{\text{th},L})/B_{\text{th},L}, \quad \text{(a)}$$

$$\dot{h}_{GI} = h_{GI} \ln(1 + B_{\text{th},G})/B_{\text{th},G}, \quad \text{(b)}$$

$$\dot{h}_{GI}(T_G - T_I) - \dot{h}_{LI}(T_I - T_L) = m'' \boldsymbol{h}_{fg}, \quad \text{(c)}$$

$$m'' = \mathcal{K}_{GI} \ln(1 + B_{\text{ma},G}), \quad \text{(d)}$$

$$\boldsymbol{h}_{fg} = \boldsymbol{h}_{fg}|_{T_{\text{sat}}=T_I}.$$

The last equation can be dropped, noting that the interface temperature will remain close to T_G, and therefore $\boldsymbol{h}_{fg}$ will approximately correspond to T_G. It is wise to first perform a scoping analysis by neglecting the effect of mass transfer on convection heat transfer coefficients in order to get a good estimate of the solution. In that case Eqs. (a) and (b) are avoided, and Eq.(c) is replaced with

$$h_{GI}(T_G - T_I) - h_{LI}(T_I - T_L) = m'' \boldsymbol{h}_{fg}. \quad \text{(e)}$$

This scoping solution leads to $m'' = 8.595 \times 10^{-4}\,\text{kg/m}^2\,\text{s}$, $B_{\text{th},L} = -5.428 \times 10^{-4}$, and $B_{\text{th},G} = 0.01145$. Clearly, $B_{\text{th},L} \approx 0$, and there is no need to include Eq. (a) in the solution. In other words, we can comfortably write $\dot{h}_{LI} = h_{LI}$, and solve the preceding set of equations including Eq. (c). [With $B_{\text{th},L} \approx 0$, the inclusion of Eq. (a) may actually cause numerical stability problems.] The iterative solution of the aforementioned equations leads to

$$T_I = 278.1\ \text{K},$$
$$m_{v,s} = 0.00534$$
$$m'' = 8.594 \times 10^{-4}\,\text{kg/m}^2\,\text{s}.$$

The difference between the two evaporation mass fluxes is small because this is a low mass transfer process to begin with.

EXAMPLE 8.3. In Example 8.2, assume that the droplet contains dissolved CO_2 at a bulk mass fraction of 20×10^{-5}. Calculate the rate of release of CO_2 from the droplet, assuming that the concentration of CO_2 in the air stream is negligibly small. Compare the mass transfer rate of CO_2 from the same droplet if no evaporation took place.

SOLUTION. We have $M_{CO_2} = 44\,\text{kg/kmol}$. Also, $T_I \approx T_L = 5\ ^\circ\text{C}$ and $C_{\text{He}} = 7.46 \times 10^7\,\text{Pa}$. Let us use subscripts 1, 2, and 3 to refer to H_2O, air, and CO_2, respectively. We deal with a three-component mixture. However, the concentrations of CO_2 in air and water are very small. The concentration of air in water is also very small. We can therefore apply Fick's law for the diffusion of each diffusing component. From Appendix J:

$$\mathcal{D}_{31,L} = 1.84 \times 10^{-9}\,\text{m}^2/\text{s}.$$

For the diffusion of CO_2 in the gas phase, because the gas phase is predominantly composed of air, we use the mass diffusivity of the CO_2–air pair at 15 °C. As a result,

$$\mathcal{D}_{32,G} = 1.55 \times 10^{-5}\,\text{m}^2/\text{s}.$$

The forthcoming calculations then follow:

$$\begin{aligned}
\mathrm{Sc}_G &= \frac{\nu_G}{\mathcal{D}_{32,G}} = 1.01,\\
\mathrm{Sh}_{D,G} &= \frac{\mathcal{K}_{GI} D}{\rho_G \mathcal{D}_{32,G}} = 0.2 + 0.3\mathrm{Re}_{D,G}^{0.6}\mathrm{Sc}_G^{0.333},\\
\Rightarrow \mathrm{Sh}_{D,G} &= 9.06;\ \mathcal{K}_{GI} = 0.1106\ \mathrm{kg/m^2\,s},\\
\mathrm{Sh}_{D,L} &= \frac{\mathcal{K}_{LI} D}{\rho_L \mathcal{D}_{31,L}} = 17.9 \Rightarrow \mathcal{K}_{LI} = 0.022\ \mathrm{kg/m^2\,s}.
\end{aligned}$$

We must now solve the following equations simultaneously, bearing in mind that $m_{3,G} = 0$ and $m_{3,L} = 20 \times 10^{-5}$:

$$m''_{\mathrm{tot}} = m''_1 + m''_3, \tag{a}$$

$$m''_3 = m_{3,s} m''_{\mathrm{tot}} + \mathcal{K}_{GI} \frac{\ln(1 + B_{\mathrm{ma},G})}{B_{\mathrm{ma},G}} (m_{3,s} - m_{3,G}), \tag{b}$$

$$m''_3 = m_{3,u} m''_{\mathrm{tot}} + \mathcal{K}_{LI} \frac{\ln(1 + B_{\mathrm{ma},L})}{B_{\mathrm{ma},L}} (m_{3,L} - m_{3,u}), \tag{c}$$

$$X_{3,u} = \frac{P X_{3,s}}{C_{\mathrm{He}}}, \tag{d}$$

$$m_{3,s} \approx \frac{X_{3,s} M_3}{X_{3,s} M_3 + (1 - X_{3,s}) M_2}, \tag{e}$$

$$m_{3,u} = \frac{X_{3,u} M_3}{X_{3,u} M_3 + (1 - X_{3,u}) M_1}, \tag{f}$$

$$B_{\mathrm{ma},G} = \frac{m_{3,G} - m_{3,s}}{m_{3,s} - \dfrac{m''_3}{m''_{\mathrm{tot}}}}, \tag{g}$$

$$B_{\mathrm{ma},L} = \frac{m_{3,L} - m_{3,u}}{m_{3,u} - \dfrac{m''_3}{m''_{\mathrm{tot}}}}. \tag{h}$$

Note that, from Example 8.2, $m''_1 = 8.594 \times 10^{-4}\ \mathrm{kg/m^2\,s}$. The iterative solution of Eqs. (a)–(h) results in

$$\begin{aligned}
m_{3,u} &= 8.80 \times 10^{-8},\\
m_{3,s} &= 4.02 \times 10^{-5},\\
m''_3 &= 4.47 \times 10^{-6}\ \mathrm{kg/m^2\,s}.
\end{aligned}$$

When evaporation is absent, the same equation set must be solved with $m''_1 = 0$. In that case,

$$\begin{aligned}
m_{3,u} &= 8.66 \times 10^{-8},\\
m_{3,s} &= 3.96 \times 10^{-5},\\
m''_3 &= 4.38 \times 10^{-6}\ \mathrm{kg/m^2\,s}.
\end{aligned}$$

PROBLEMS

Problem 8.1. Water flows in a tube that has an inner diameter of 2.0 cm and a length of 5.25 m. The tube wall temperature is constant at 98 °C, and the water inlet temperature is 23 °C. The water mean velocity at inlet is 6.5 m/s.

1. Calculate the average water temperature at tube exit, using Gnielinski's correlation by
   (a) assuming constant fluid properties
   (b) accounting for property variations due to temperature change
2. Suppose that in part 1 a short segment of the tube at its exit is porous, and water leaks through the porous wall at the rate of 2.5 kg/m^2 s. Calculate the heat flux between the fluid and tube wall in the porous segment.

Problem 8.2. Water flows through a long tube, which has a 2-m-long heated segment. The tube inner diameter is 5 cm. The temperature and Reynolds number of water prior to entering the heated segment are 20 °C and 20,000, respectively. The flow is hydrodynamically fully developed upstream from the heated segment.

(a) The heat flux through the wall is adjusted such that the mean water temperature at the exit of the heated segment reaches 50 °C. Assuming a smooth tube wall, calculate the wall heat flux and the wall temperature at the middle and exit of the heated segment.

(b) Inspection shows that the tube surface is in fact rough, with a characteristic dimensionless surface roughness of $\varepsilon_s/D = 0.002$. Repeat the calculations in part (a).

(c) poor manufacturing, it is found out that water leaks out through the wall over a 5 cm-long central segment of the heated segment at the rate of 0.01 kg/s. Assuming that the heat flux and other conditions remain the same as in part (b), estimate the surface temperature at the middle of the heated segment. For simplicity, assume that the leakage mass flux is uniform over the 5-cm-long central segment of the heated segment.

Assume constant water properties, similar to those given for Problem 8.1.

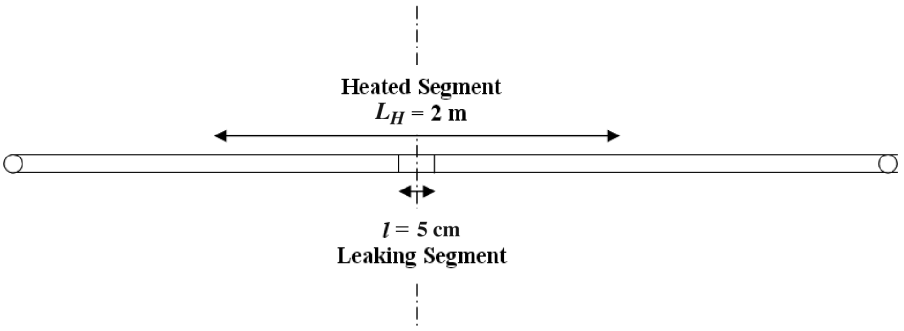

Figure P8.2

Problem 8.3. Air at 2-bars pressure and 400 K temperature flows through a smooth pipe. The inner diameter of the tube is 3.5 cm. At a location where the air mass flux is 7.0 kg/m^2 s, air is injected into the pipe through a porous wall at the rate of 0.004 kg/m^2 s. The wall surface temperature is 450 °C. Calculate the friction factor and the heat transfer coefficient.

Problem 8.4. A spherical water droplet 2 mm in diameter is moving in atmospheric air with a constant speed of 6 m/s. The air is at 20 °C

(a) Calculate the heat transfer rate between the droplet surface and air, assuming that the droplet surface is at 27 °C
(b) Repeat part (a), this time assuming that evaporation at the rate of 100 g/m^2 s is taking place at the surface of the droplet.

Combined Heat and Mass Transfer

Problem 8.5. Prove Eqs. (8.11a) and (8.12a).

Problem 8.6. The top surface of a flat, horizontal plate that is 5 cm × 5 cm in size is subject to a parallel flow of hot, atmospheric-pressure air. The air is at an ambient temperature of 100 °C and flows with a far-field velocity of $U_\infty = 5$ m/s.

(a) Calculate the rate of heat transfer from air to the surface, assuming that the surface is smooth and dry and its surface temperature is 60 °C.
(b) Assume that the surface is porous and is maintained wet by an injection of water from a small reservoir, such that the underneath of the surface remains adiabatic and the porous surface and the reservoir remain at thermal equilibrium. Find the heat transfer rate and the temperature of the surface. For simplicity, assume that the air is dry.

Hints: In part (b), there is balance between sensible heat transfer rate toward the surface and the latent heat transfer rate leaving the surface.

Problem 8.7. In Problem 8.4, assume that the droplet is in motion in air that contains water vapor at a relative humidity of 60%. Assume that the droplet is isothermal and is undergoing quasi-steady evaporation. Calculate the droplet temperature and its evaporation rate.

Problem 8.8. The surface of a 10 cm × 10 cm flat and horizontal plate is wetted by a water film. The water surface remains at 17 °C, with a liquid-side mass fraction of CO_2 of 11×10^{-6}. The concentration of CO_2 in the ambient air is negligible. The air flows parallel to the surface with a far-field velocity of $U_\infty = 10$ m/s.

(a) Calculate the mass transfer rate of CO_2 between the surface and air, assuming negligible water evaporation.
(b) Repeat part (a), this time assuming that evaporation at the rate of 0.02 kg/m^2 s takes place at the surface of the droplet.
(c) Repeat part (b), this time assuming that condensation at the rate of 0.02 kg/m^2 s takes place.

In all the calculations, assume that the transfer of CO_2 is gas-side controlled.

9 Analogy Among Momentum, Heat, and Mass Transfer

9.1 General Remarks

In the previous chapters we noted that the dimensionless boundary-layer conservation equations for momentum, thermal energy, and mass species are mathematically similar. This similarity among these dimensionless equations suggests that the mathematical solution for one equation should provide the solution of the other equations. One may argue that the empirical correlations for friction factor, heat transfer coefficient, and mass transfer coefficient represent empirical solutions to the momentum, energy, and mass-species conservation equations, respectively. Thus a correlation for friction factor of the form $f = f(\mathrm{Re})$ is the empirical solution to the momentum conservation equation for a specific system and flow configuration, whereas an empirical correlation of the form $\mathrm{Nu} = \mathrm{Nu}(\mathrm{Re}, \mathrm{Pr})$ for the same system is an empirical solution to the energy equation and an empirical correlation of the form $\mathrm{Sh} = \mathrm{Sh}(\mathrm{Re}, \mathrm{Sc})$. Thus, using the analogy arguments, knowing an empirical correlation for either of the three parameters f, Nu, or Sh for a specific system will allow us to derive empirical correlations for the remaining two parameters.

The usefulness of the analogy approach becomes clear by noting that measurement of friction factor is usually much simpler than the measurement of heat or mass transfer coefficients. Most analogy theories thus attempt to derive relations in the following generic forms that represent analogy between heat and momentum transfer:

$$\mathrm{Nu} = f_1(C_f, ..), \tag{9.1.1}$$

$$\mathrm{St} = f_2(C_f, ..). \tag{9.1.2}$$

Having such expressions, we can utilize the analogy between heat and mass transfer processes to write

$$\mathrm{Sh} = f_1(C_f, ..), \tag{9.1.3}$$

$$\mathrm{St}_{\mathrm{ma}} = f_2(C_f, ..). \tag{9.1.4}$$

For a turbulent boundary layer, when the assumptions leading to Eq. (6.7.5) are acceptable, we can use that equation for the derivation of a general analogy by writing

$$T_\infty^+ = \frac{T_s - T_\infty}{\dfrac{q_s''}{\rho C_P U_\tau}} = \int_0^{\delta_{\text{th}}^+} \frac{dy^+}{\dfrac{1}{Pr} + \dfrac{E}{\nu\,\text{Pr}_{\text{tu}}}}, \tag{9.1.5}$$

where δ_{th}^+ represents the thickness of the thermal boundary layer in wall units. Noting that $U_\tau = U_\infty\sqrt{C_f/2}$ and that $\frac{q_s''}{(T_s - T_\infty)} = h$, we find that the preceding equation gives

$$\text{Nu}_l = \frac{\text{Re}_l \text{Pr}\sqrt{C_f/2}}{\displaystyle\int_0^{\delta_{\text{th}}^+} \frac{dy^+}{\dfrac{1}{\text{Pr}} + \dfrac{E}{\nu \text{Pr}_{\text{tu}}}}}, \tag{9.1.6}$$

where l is the relevant length scale. This equation indicates that, in principle, an analogy can be formulated once an appropriate eddy diffusivity model and Pr_{tu} are applied. A large number of such analogies have been proposed, and useful summaries of these analogies were recently compiled by Thakre and Joshi (2002) and Mathpati and Joshi (2007).

These analogy arguments would apply, however, if the following conditions are met:

1. The flow field configurations are all the same (e.g., all are pipe flows or all are stagnation flow against a sphere, etc.)
2. The flow fields all have the same flow regime (either laminar or turbulent), and Re has the same order of magnitude in all of them.
3. For analogy between heat and mass transfer, Pr and Sc must have the same orders of magnitude.

In this chapter we review several important analogy theories for heat and momentum transport. Extensions to mass transfer are also discussed.

9.2 Reynolds Analogy

Consider the 2D boundary layer on a flat surface that is subject to a steady and parallel flow of an incompressible, constant-property fluid, as in Fig. 9.1. Then, near the wall,

$$\tau_{yx} = \rho\,(\nu + E)\,\frac{\partial \overline{u}}{\partial y}, \tag{9.2.1}$$

$$q_y'' = -\rho C_P \left(\frac{\nu}{\text{Pr}} + \frac{E}{\text{Pr}_{\text{tu}}}\right)\frac{\partial \overline{T}}{\partial y}. \tag{9.2.2}$$

As a result, at any location,

$$\frac{1 + E/\nu}{C_P\left(\dfrac{1}{\text{Pr}} + \dfrac{E}{\nu \text{Pr}_{\text{tu}}}\right)}\frac{d\overline{u}}{d\overline{T}} = -\frac{\tau_{yx}}{q_y''}. \tag{9.2.3}$$

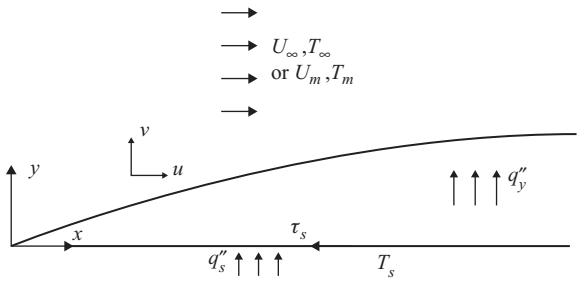

Figure 9.1. The boundary layer on a flat plate.

Let us assume that the entire flow field is turbulent, i.e., neglect the viscous and buffer zones. Furthermore, let us assume that

$$\mathrm{Pr} = \mathrm{Pr}_{\mathrm{tu}} = 1, \tag{9.2.4}$$

$$\frac{\tau_{yx}}{q''_y} = \frac{\tau_s}{q''_s} = \text{const.} \tag{9.2.5}$$

The justification for Eq. (9.2.5) is that in the boundary layer the shear stress and the normal-direction heat flux are approximately constant. With these assumptions, Eq. (9.2.3) leads to

$$d\overline{T} = -\frac{q''_s}{C_P \tau_s} d\overline{u}. \tag{9.2.6}$$

The variables have now been separated, and we can apply $\int_{T_s}^{T_m}$ to the left-hand side and $\int_0^{U_m}$ to the right-hand side to get,

$$T_m - T_s = -\frac{q''_s U_m}{C_P \tau_s}. \tag{9.2.7}$$

We now note that

$$h = \frac{q''_s}{(T_s - T_\infty)},$$

$$\tau_s = C_f \frac{1}{2} \rho U_\infty^2.$$

Equation (9.2.6) then leads to

$$\mathrm{Nu}_l = \frac{1}{2} C_f \mathrm{Re}_l. \tag{9.2.8}$$

Noting that $\mathrm{Pr} = 1$ has been assumed, we can rewrite this as

$$\mathrm{St} = C_f/2. \tag{9.2.9}$$

By using T_m and U_m as the upper limits of the integration of the two sides of Eq. (9.2.6), we implicitly assumed an internal flow, for which $l = D_H$, leading to $\mathrm{Nu} = hD_H/k$ and $\mathrm{Re} = \rho U_m D_H/\mu$; and T_m represents the temperature in the turbulent core. The analysis applies to external flow as well when T_∞ and U_∞ are used as the upper limits of the latter integrations, respectively. The analogy for external flow then leads to

$$\mathrm{Nu}_x = \frac{1}{2} \mathrm{Re}_x \, \mathrm{Pr} \, C_{f,x}, \tag{9.2.10}$$

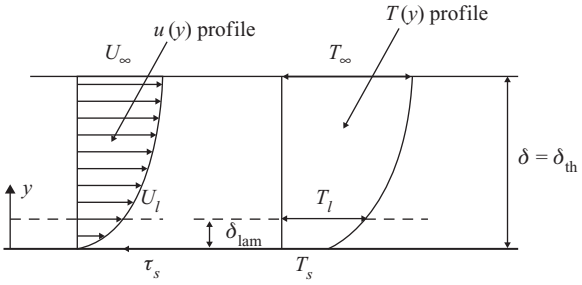

Figure 9.2. The velocity and thermal boundary layers and the definitions for the Prandtl–Taylor analogy.

$$\mathrm{St}_x = C_{f,x}/2. \tag{9.2.11}$$

where the subscript x implies a local parameter at the axial coordinate.

The Reynolds analogy is simple and easy to use and can be applied to laminar or turbulent flow. The analogy agrees with experimental data when $\mathrm{Pr} \approx 1$, which is true for common gases.

Reynolds analogy for mass transfer can be cast as

$$\mathrm{St}_{\mathrm{ma},x} = C_f/2, \tag{9.2.12}$$

$$\mathrm{Sh}_x = \frac{1}{2}\mathrm{Re}_x\mathrm{Sc}, \tag{9.2.13}$$

where

$$\mathrm{St}_{\mathrm{ma},x} = \frac{\mathcal{K}_x}{\rho U_\infty} \quad \text{and} \quad \mathrm{Sh}_x = \frac{\mathcal{K}_x x}{\rho \mathcal{D}_{12}},$$

and $\mathcal{D}_{12}$ is the mass diffusivity of transferred species with respect to the fluid mixture.

For diffusion involving inert gases, typically, $\mathrm{Sc} \approx 1$, and as a result the Reynolds analogy can be very useful.

9.3 Prandtl–Taylor Analogy

This analogy is an extension of the Reynolds analogy (Prandtl, 1910, 1928; G.I. Taylor, 1916). It maintains the basic assumptions of the Reynolds analogy, including $\mathrm{Pr} = \mathrm{Pr}_{\mathrm{tu}} = 1$, but considers two sublayers in the boundary layer. The sublayers considered are the viscous sublayer where $E = 0$ and a fully turbulent layer extending all the way to the edge of the boundary layer at which point $\overline{u} = U_\infty$ and $\overline{T} = T_\infty$ (Fig. 9.2).

Starting from Eqs. (9.2.1) and (9.2.2), we can write for the viscous sublayer

$$\frac{q''_y}{\tau_{yx}} = \frac{q''_s}{\tau_s} = -\frac{k}{\mu}\frac{\partial \overline{T}}{\partial \overline{u}}. \tag{9.3.1}$$

We can now separate the variables and integrate both sides of the resulting equation from $y = 0$ to $y = \delta_{\mathrm{lam}}$, and, assuming that $q''_y = q''_s$ and $\tau_{yx} = \tau_s$ over the entire boundary layer and assuming that at $y = \delta_{\mathrm{lam}}$, we have $\overline{T} = T_l$ and $\overline{u} = U_l$. As a result we get

$$\frac{q''_s}{\tau_s} = -\frac{k}{\mu U_\infty}\frac{T_l - T_s}{U_l/U_\infty}. \tag{9.3.2}$$

Similarly, for the remainder of the boundary layer (where the flow is turbulent), by assuming that $E \gg \nu$ and $\mathrm{Pr_{tu}} = 1$, Eqs. (9.2.1) and (9.2.2) result in

$$\frac{q_y''}{\tau_{yx}} = -C_P \frac{\partial \overline{T}}{\partial \overline{u}}.$$

This will lead to

$$\frac{q_y''}{\tau_{yx}} = \frac{q_s''}{\tau_s} = -C_P \frac{T_l - T_\infty}{U_l - U_\infty}. \tag{9.3.3}$$

We can now equate the right-hand sides of Eqs. (9.3.2) and (9.3.3) and factor out $(T_s - T_\infty)$ to get

$$\mathrm{Pr}\,(T_s - T_\infty) = -\frac{U_\infty}{U_l}\left[1 + \frac{U_l}{U_\infty}\,(\mathrm{Pr} - 1)\right](T_l - T_s)\,. \tag{9.3.4}$$

Now, because $h = \frac{q_s''}{(T_s - T_\infty)}$, this equation gives

$$h = \frac{\mathrm{Pr}}{1 + \dfrac{U_l}{U_\infty}\,(\mathrm{Pr} - 1)} \frac{(U_l/U_\infty)\,q_s''}{T_l - T_s}. \tag{9.3.5}$$

We now eliminate q_s'' from this equation by using the following expression, which itself results from Eq. (9.3.2):

$$\frac{q_s''}{(T_l - T_s)} = -\frac{k}{\mu}\frac{\tau_s}{U_l}, \tag{9.3.6}$$

and we substitute $\tau_s = C_f \frac{1}{2}\rho U_\infty^2$ into the resulting equation. The outcome will be

$$\mathrm{Nu}_x = \frac{h_x x}{k} = \frac{\dfrac{1}{2}C_f \mathrm{Re}_x \mathrm{Pr}}{1 + \dfrac{U_l}{U_\infty}\,(\mathrm{Pr} - 1)}. \tag{9.3.7}$$

This is the basic Taylor analogy. Of course U_l/U_∞ must still be specified.

One way to evaluate U_l/U_∞ is as follows. Given that for flow past a smooth surface $u^+ = \frac{u}{U_\infty\sqrt{C_f/2}}$ and assuming that δ_l corresponds to the edge of the viscous sublayer at which $y^+ = 5$, we will have

$$\frac{U_l}{U_\infty} = 5\sqrt{C_f/2}. \tag{9.3.8}$$

Substitution from this equation into Eq. (9.3.7) then gives

$$\mathrm{Nu}_x = \frac{\frac{1}{2}C_f\ \mathrm{Re}_x \mathrm{Pr}}{1 + 5\sqrt{\dfrac{C_f}{2}}\,(\mathrm{Pr} - 1)}. \tag{9.3.9}$$

For diffusive mass transfer, the analogy would give

$$\mathrm{Sh}_x = \frac{\frac{1}{2}C_f\ \mathrm{Re}_x \mathrm{Sc}}{1 + 5\sqrt{\dfrac{C_f}{2}}\,(\mathrm{Sc} - 1)}. \tag{9.3.10}$$

Equations (9.3.9) and (9.3.10) apply to pipe flow as well, by use of Re_D, Nu_D, and Sh_D for Re_x, Nu_x, and Sh_x, respectively, where $\mathrm{Nu}_D = hD/k$ and $\mathrm{Sh}_D = \frac{\mathcal{K}D}{\rho \mathcal{D}_{12}}$.

The assumption that $\delta^+_{\mathrm{lam}} = 5$, however, implies that the buffer sublayer is entirely included in the turbulent sublayer. The following alternative method can therefore be used.

Because the velocity profile in the viscous sublayer is laminar, we can write

$$U_I = \delta_{\mathrm{lam}} \frac{\tau_s}{\mu}. \tag{9.3.11}$$

Using $\tau_s = \frac{1}{2} C_f \rho U_\infty^2$, this equation can be cast as,

$$\frac{U_l}{U_\infty} = \delta^+_{\mathrm{lam}} \left[\frac{1}{2} C_f \rho U^+_\infty \right]. \tag{9.3.12}$$

We can now substitute for C_f from Eq. (5.2.38), and assuming that $\delta^+_{\mathrm{lam}} = 9$, Eq. (9.3.7) will yield,

$$\mathrm{Nu}_x = \frac{0.029 \mathrm{Re}_x^{0.8} \mathrm{Pr}}{1 + 1.525 \mathrm{Re}_x^{-0.1} (\mathrm{Pr} - 1)}, \tag{9.3.13}$$

$$\mathrm{Sh}_x = \frac{0.029 \mathrm{Re}_x^{0.8} \mathrm{Sc}}{1 + 1.525 \mathrm{Re}_x^{-0.1} (\mathrm{Sc} - 1)}. \tag{9.3.14}$$

Although the Prandtl–Taylor analogy offers a significant improvement in comparison with the simple Reynolds analogy, it deviates from experimental data for $\mathrm{Pr} \neq 1$ or $\mathrm{Sc} \neq 1$.

9.4 Von Karman Analogy

In this analogy (von Karman, 1939), all three sublayers (viscous, buffer, and the overlap sublayers) are considered. Throughout the boundary layer $q''_y = q''_s$ and $\tau_{yx} = \tau_s$ are assumed (see Fig. 9.1 for the definition of coordinates).

The derivation of this analogy has much in common with the temperature law of the wall derived earlier in Section 6.7. Recall that for flow parallel to a flat surface we have [see Eqs. (6.6.22) and (6.7.5)]

$$du^+ = \frac{dy^+}{1 + \dfrac{E}{\nu}}, \tag{9.4.1}$$

$$dT^+ = \frac{dy^+}{\dfrac{1}{\mathrm{Pr}} + \dfrac{E}{\mathrm{Pr}_{\mathrm{tu}} \nu}}. \tag{9.4.2}$$

Assume that $\mathrm{Pr}_{\mathrm{tu}} = 1$ for now. For $y^+ > 30$ we have $\frac{E}{\nu} \gg 1$ and $\frac{E}{\mathrm{Pr}_{\mathrm{tu}} \nu} \gg \frac{1}{\mathrm{Pr}}$, and these equations lead to

$$\frac{du^+}{dT^+} = 1. \tag{9.4.3}$$

This leads to

$$T^+_\infty - T^+_{|y^+=30} = U^+_\infty - u_{|y^+=30}. \tag{9.4.4}$$

Now, from Eqs. (6.5.3) and (6.7.12), respectively,

$$u^+_{|y^+=5} \approx 5 + 5\ln 6, \tag{9.4.5}$$

$$T^+_{|y^+=30} = 5\left[\mathrm{Pr} + \ln\left(1 + 5\mathrm{Pr}\right)\right]. \tag{9.4.6}$$

Equation (9.4.4) then leads to

$$T^+_\infty = 5\left\{(\mathrm{Pr} - 1) + \ln\left[\frac{5\mathrm{Pr}}{6} + \frac{1}{6}\right]\right\} + U^+_\infty. \tag{9.4.7}$$

Equations (6.7.14) and (6.7.15) can now be utilized to eliminate U^+_∞ and T^+_∞ from this equation, and that leads to

$$\mathrm{Nu}_x = \frac{\frac{1}{2}\mathrm{Re}_x\mathrm{Pr}C_f}{1 + 5\sqrt{\frac{C_f}{2}}\left\{(\mathrm{Pr} - 1) + \ln\left[1 + \frac{5}{6}(\mathrm{Pr} - 1)\right]\right\}}, \tag{9.4.8}$$

where we made use of the relation

$$\mathrm{St}_x = \frac{\mathrm{Nu}_x}{\mathrm{Re}_x\mathrm{Pr}}.$$

Equation (9.4.8) applies when $\mathrm{Pr}_{\mathrm{tu}} = 1$. When $\mathrm{Pr}_{\mathrm{tu}} \neq 1$, it can be shown that

$$\mathrm{Nu}_x = \frac{\frac{1}{2}\mathrm{Re}_x\mathrm{Pr}\mathrm{Pr}_{\mathrm{tu}}^{-1}C_f}{1 + 5\sqrt{\frac{C_f}{2}}\left\{\left(\mathrm{Pr}_{\mathrm{tu}}^{-1}\mathrm{Pr} - 1\right) + \ln\left[1 + \frac{5}{6}\left(\mathrm{Pr}_{\mathrm{tu}}^{-1}\mathrm{Pr} - 1\right)\right]\right\}}. \tag{9.4.9}$$

For diffusive mass transfer, for $\mathrm{Sc}_{\mathrm{tu}} = 1$, the analogy leads to

$$\mathrm{Sh}_x = \frac{\frac{1}{2}\mathrm{Re}_x\mathrm{Sc}C_f}{1 + 5\sqrt{\frac{C_f}{2}}\left\{(\mathrm{Sc} - 1) + \ln\left[1 + \frac{5}{6}(\mathrm{Sc} - 1)\right]\right\}}. \tag{9.4.10}$$

And, for $\mathrm{Sc}_{\mathrm{tu}} \neq 1$, it gives,

$$\mathrm{Sh}_x = \frac{\frac{1}{2}\mathrm{Re}_x\mathrm{Sc}\mathrm{Sc}_{\mathrm{tu}}^{-1}C_f}{1 + 5\sqrt{\frac{C_f}{2}}\left\{\left(\mathrm{Sc}_{\mathrm{tu}}^{-1}\mathrm{Sc} - 1\right) + \ln\left[1 + \frac{5}{6}\left(\mathrm{Sc}_{\mathrm{tu}}^{-1}\mathrm{Sc} - 1\right)\right]\right\}}. \tag{9.4.11}$$

We can also apply von Karman's analogy to internal flow by assuming that as $y^+ \to \infty$ we get $U^+ = U^+_m$ and $T^+ = T^+_m$, namely, properties representing the bulk fluid conditions. Equations (9.4.8)–(9.4.11) will then be applicable when C_f is replaced with the Fanning friction factor (or $f/4$ with f representing the Darcy friction factor) and Re_x is replaced with Re_{D_H}.

Von Karman's analogy does well for $\mathrm{Pr} \lesssim 40$ and $\mathrm{Sc} \lesssim 40$, but it becomes increasingly inaccurate as Pr and Sc increase beyond 40 (Skelland, 1974).

9.5 The Martinelli Analogy

For turbulent pipe flow, we can apply Eq. (6.7.12) to the centerline of the pipe (i.e., $y^+ = R_0^+$), noting that

$$R_0^+ = \frac{1}{2}\mathrm{Re}_D\sqrt{\frac{C_f}{2}}, \tag{9.5.1}$$

$$T_c^+ = \frac{T_s - T_c}{\dfrac{q_s''}{\rho C_P U_\tau}} = \frac{T_s - T_c}{T_s - T_m}\frac{\mathrm{Re}_D\mathrm{Pr}\sqrt{C_f/2}}{\mathrm{Nu}_D}, \tag{9.5.2}$$

where T_c represents the mean (time or ensemble averaged) temperature at the centerline. Equation (6.7.12) then leads to

$$\mathrm{Nu}_D = \frac{\dfrac{T_s - T_c}{T_s - T_m}\mathrm{Re}_D\,\mathrm{Pr}\,\mathrm{Pr}_{\mathrm{tu}}^{-1}\sqrt{\dfrac{C_f}{2}}}{5\left\{\mathrm{Pr}_{\mathrm{tu}}^{-1}\mathrm{Pr} + \ln\left[1 + 5\mathrm{Pr}_{\mathrm{tu}}^{-1}\mathrm{Pr}\right] + F\dfrac{1}{5\kappa}\ln\left[\dfrac{\mathrm{Re}_D}{60}\sqrt{C_f/2}\right]\right\}}, \tag{9.5.3}$$

where $F = 1$, in accordance with Eq. (6.7.12). This expression of course could be derived from Eq. (7.3.18) as well. With $F = 1$, however, this expression would not be adequate for liquid metals because in the derivation of Eq. (6.7.12) or (7.3.18) it was assumed that molecular thermal diffusivity is negligible in the turbulent core of the channel. When $\mathrm{Pr} \ll 1$, as in liquid metals, the contribution of molecular diffusivity to the conduction of heat in the turbulent core is no longer negligible. Martinelli (1947) removed this shortcoming by defining F as the ratio of the total thermal resistance of the turbulent core that is due to molecular and eddy diffusivities to the thermal resistance of the turbulent core that is due to eddy diffusivity alone. The parameter F is found from

$$F = \frac{\ln\left[\dfrac{5\Lambda}{5\Lambda + \dfrac{y_2^+}{R_0^+}\left(1 - \dfrac{y_2^+}{R_0^+}\right)}\right] + \dfrac{1}{\sqrt{1+20\Lambda}}\ln\left\{\dfrac{1+\sqrt{1+20\Lambda}}{1-\sqrt{1+20\Lambda}}\dfrac{\left(2\dfrac{y_2^+}{R_0^+} - 1\right) - \sqrt{1+20\Lambda}}{\left(2\dfrac{y_2^+}{R_0^+} - 1\right) + \sqrt{1+20\Lambda}}\right\}}{2\ln\left(\dfrac{\mathrm{Re}_D}{2y_2^+}\right)\sqrt{\dfrac{C_f}{2}}} \tag{9.5.4}$$

where y_2^+ is distance to the edge of the buffer zone in wall units. ($y_2^+ \approx 30$) and Λ are defined in Eq. (7.3.19a).

To use Eq. (9.5.3), we also need T_c, the temperature at the centerline, which we can find by using the temperature profiles appropriate for fluids with $\mathrm{Pr} \ll 1$ [see Eq. (7.3.19)]. The calculation of F and T_c is tedious, however. McAdams (1954) calculated and tabulated the values of these parameters, as shown in Tables 9.1 and 9.2. All properties are bulk properties in this analogy. Martinelli's analogy is known to be superior to other classical analogies for $\mathrm{Pr} \ll 1$.

9.6 The Analogy of Yu et al.

In Section 7.2, the turbulence model of Churchill for fully developed turbulent flow in circular channels was discussed [see Eqs. (7.2.28) through (7.2.35)]. Yu et al.

Table 9.1. *Values of the F factor in Martinelli's analogy (from McAdams, 1954)*

$Pe_D \downarrow$	$Re_D = 10^4$	$Re_D = 10^5$	$Re_D = 10^6$
10^2	0.18	0.098	0.052
10^3	0.55	0.45	0.29
10^4	0.92	0.83	0.65
10^5	0.99	0.985	0.980
10^6	1.00	1.00	1.00

(2001) performed a similar formulation for turbulent heat transfer by writing [see Fig. 6.4 and Eq. (7.2.28)]

$$q_y'' = -k\frac{dT}{dy} - \rho\overline{T'v'}. \tag{9.6.1}$$

Following steps similar to those summarized following Eq. (7.2.28), we can write

$$\frac{q_y''}{q_s''}\left[1 - \overline{(T'v')}^{++}\right] = \frac{dT_{\text{Ch}}^+}{dy^+}, \tag{9.6.2}$$

where the dimensionless temperature is now defined as

$$T_{\text{Ch}}^+ = \frac{k\,(T_s - T_\infty)\,U_\tau}{\nu q_s''}. \tag{9.6.3}$$

The quantity $\overline{(T'v')}^{++}$ represents the fraction of heat flux in the y direction that is due to turbulent fluctuations, namely,

$$\overline{(T'v')}^{++} = \rho C_P \overline{(T'v')}/q_y''. \tag{9.6.4}$$

Equation (9.6.2) can be integrated to derive a temperature profile, provided that $\overline{(T'v')}^{++}$ is known. Alternatively, the integration can be carried out when the turbulent Prandtl number is known, where the turbulent Prandtl number is now defined as,

$$\frac{\text{Pr}_{\text{tu}}}{\text{Pr}} = \frac{\overline{(u'v')}^{++}}{\overline{(T'v')}^{++}}\left[\frac{1 - \overline{(T'v')}^{++}}{1 - \overline{(u'v')}^{++}}\right]. \tag{9.6.5}$$

Table 9.2. *Values of the $\frac{T_s - T_m}{T_s - T_c}$ ratio in Martinelli's analogy (from McAdams, 1954)*

$\text{Pr} \downarrow$	$Re_D = 10^4$	$Re_D = 10^5$	$Re_D = 10^6$	$Re_D = 10^7$
0	0.564	0.558	0.553	0.550
10^{-4}	0.568	0.560	0.565	0.617
10^{-3}	0.570	0.572	0.627	0.728
10^{-2}	0.589	0.639	0.738	0.813
10^{-1}	0.692	0.761	0.823	0.864
1.0	0.865	0.877	0.897	0.912
10	0.958	0.962	0.963	0.966

From an extensive analysis, Yu et al. derived the following empirical correlation, which is accurate for $R_0^+ > 500$ and $\mathrm{Pr} > \mathrm{Pr_{tu}}$ for all geometries and all thermal boundary condition types:

$$\mathrm{Nu}_{D_H} = \frac{1}{\left(\frac{\mathrm{Pr_{tu}}}{\mathrm{Pr}}\right)\frac{1}{\mathrm{Nu}_{D_H,1}} + \left[1 - \left(\frac{\mathrm{Pr_{tu}}}{\mathrm{Pr}}\right)^{2/3}\right]\frac{1}{\mathrm{Nu}_{D_H,\infty}}}, \tag{9.6.6}$$

where the thermally developed Nusselt number is found from

$$\mathrm{Nu}_{D_H,\infty} = 0.07343\left(\frac{\mathrm{Pr}}{\mathrm{Pr_{tu}}}\right)^{1/3}\mathrm{Re}_{D_H}\left(\frac{C_f}{2}\right)^{1/2}. \tag{9.6.7}$$

The turbulence Prandtl number, to be used in the preceding two equations, is found from

$$\mathrm{Pr_{tu}} = 0.85 + \frac{0.015}{\mathrm{Pr}}. \tag{9.6.8}$$

The quantity $\mathrm{Nu}_{D_H,1}$ represents the Nusselt number when $\mathrm{Pr} = \mathrm{Pr_{tu}}$. For UWT boundary conditions it can be found from

$$\mathrm{Nu}_{D_H,1} = \frac{\mathrm{Re}_{D_H}\left(\frac{C_f}{2}\right)}{1 + \frac{145}{\left(U_m^+\right)^{2.5}}}. \tag{9.6.9}$$

For UHF boundary conditions, Yu et al. recommend

$$\mathrm{Nu}_{D_H,1} = \frac{\mathrm{Re}_{D_H}\left(\frac{C_f}{2}\right)}{1 + \frac{195}{\left(U_m^+\right)^{2.7}}}. \tag{9.6.10}$$

The dimensionless mean velocity U_m^+ can be calculated with Eq. (7.2.34).

9.7 Chilton–Colburn Analogy

This analogy is an empirical adjustment to Reynolds' analogy, and is meant to extend its applicability to fluids with $\mathrm{Pr} \neq 1$ or $\mathrm{Sc} \neq 1$ (Chilton and Colburn, 1934). According to this analogy, the following *j parameters* can be defined for heat and mass transfer:

$$j_{\mathrm{th}} = \mathrm{St}\ \mathrm{Pr}^{2/3} = \frac{\mathrm{Nu}_l}{\mathrm{Re}_l \mathrm{Pr}^{1/3}}, \tag{9.7.1}$$

$$j_{\mathrm{ma}} = \mathrm{St_{ma}}\mathrm{Sc}^{2/3} = \frac{\mathrm{Sh}_l}{\mathrm{Re}_l \mathrm{Sc}^{1/3}}. \tag{9.7.2}$$

The j factor, along with f or C_f, can be plotted as a function of Re_l. These plots sometimes show that the curves for the j factors are approximately parallel to the f

or C_f curves. For heat and mass transfer in turbulent flow in tubes, for example, we can use, from the Dittus and Boelter (1930) correlation,

$$\mathrm{Nu}_D = 0.023\,\mathrm{Re}_D^{0.8}\mathrm{Pr}^{1/3}, \tag{9.7.3}$$

$$\mathrm{Sh}_D = 0.023\,\mathrm{Re}_D^{0.8}\mathrm{Sc}^{1/3}. \tag{9.7.4}$$

Substitution from these equations into Eqs. (9.7.1) and (9.7.2) then gives

$$j_{\mathrm{ma}} \approx j_{\mathrm{th}} = 0.023\,\mathrm{Re}_D^{-0.2}. \tag{9.7.5}$$

This can be compared with the following correlation for turbulent pipe flow:

$$C_f = 0.046\,\mathrm{Re}_D^{-0.2}. \tag{9.7.6}$$

This comparison thus leads to

$$j_{\mathrm{ma}} \approx j_{\mathrm{th}} = C_f/2. \tag{9.7.7}$$

From there we get,

$$\mathrm{StPr}^{2/3} = C_f/2, \tag{9.7.8}$$

$$\mathrm{St}_{\mathrm{ma}}\mathrm{Sc}^{2/3} = C_f/2. \tag{9.7.9}$$

Equations (9.7.8) and (9.7.9) represent the Chilton–Colburn analogy for pipe flow. These expressions apply to other flow geometries as well, including external flow. For pipe flow the range of validity for this analogy is as follows. For heat transfer,

$$10^4 < \mathrm{Re}_D < 3 \times 10^5,$$
$$0.6 < \mathrm{Pr} < 100,$$

and for mass transfer (Skelland, 1974),

$$2000 < \mathrm{Re}_D < 3 \times 10^5,$$
$$0.6 < \mathrm{Sc} < 2500.$$

EXAMPLE 9.1. A liquid flows in a tube that has an inner diameter of 5.08 cm and a length of 1.4 m. The tube wall temperature is constant at 100 °C, and the liquid inlet temperature is 35 °C. The liquid mean velocity at the inlet is 5.1 m/s. The fluid thermophysical properties are as follows:

$$\rho = 750\,\mathrm{kg/m^3},\ C_P = 2200\,\mathrm{J/kg\,^\circ C},\ k = 0.14\,\mathrm{W/m\,K},$$
$$\mu = 1.28 \times 10^{-3}\,\mathrm{kg/m\,s}.$$

(a) Calculate the average liquid temperature at tube exit, using Gnielinski's correlation and the Chilton–Colburn analogy.
(b) Repeat the calculations with Gnielinski's correlation, assuming that the tube has an average surface roughness value of approximately 7.1×10^{-2} mm.

SOLUTION. First, let us calculate the Reynolds and Prandtl numbers and the total mass flow rate:

$$\mathrm{Pr} = \mu\, C_P/k = (1.28 \times 10^{-3}\,\mathrm{kg/m\,s})\,(2200\,\mathrm{J/kg\,K})/(0.14\,\mathrm{W/m\,K})$$

$$= 20.11$$

$$\mathrm{Re}_D = \rho U_m D/\mu = \left(750\,\mathrm{kg/m^3}\right)(5.1\,\mathrm{m/s})\,(0.0508\,\mathrm{m})/\left(1.28\times10^{-3}\,\mathrm{kg/m\,s}\right)$$
$$= 1.518\times10^5,$$

$$\dot{m} = \rho U_m \pi \frac{D^2}{4} = \left(750\,\mathrm{kg/m^3}\right)(5.1\mathrm{m/s})\,\pi\,\frac{(0.0508\,\mathrm{m})^2}{4}$$
$$= 7.753\,\mathrm{kg/s}.$$

The flow is turbulent. Because $l/D \gg 1$, we may use thermally developed heat transfer correlations.

Part (a). We now use Gnielinski's correlation. First we find friction factor from Eq. (7.3.36):

$$f = [1.82\log(\mathrm{Re}_D) - 1.62]^{-2} = [1.82\log(1.518\times10^5) - 1.62]^{-2} = 0.01648.$$

Now, using Eq. (7.3.41) we have

$$\mathrm{Nu}_{D,\mathrm{Gnielinski}} = \frac{[\mathrm{Re}_D - 1000]\,\mathrm{Pr}\,\frac{f}{8}}{1+12.7\sqrt{\frac{f}{8}}\left[\mathrm{Pr}^{2/3}-1\right]} = \frac{\left[1.518\times10^5 - 1000\right](20.11)\,\frac{0.01648}{8}}{1+12.7\sqrt{\frac{0.01648}{8}}[(20.11)^{2/3}-1]} = 1333,$$

$$h_{\mathrm{Gnielinski}} = \mathrm{Nu}_{D,\,\mathrm{Gnielinski}}\frac{k}{D} = (1333)\,\frac{0.14\,\mathrm{W/m\,K}}{0.0508\,\mathrm{m}} = 3674\,\mathrm{W/m^2\,K}.$$

We can find the mean liquid temperature by solving the following differential equation, which represents the energy conservation for the fluid, neglecting viscous dissipation:

$$\dot{m}C_P\frac{dT_m}{dx} = \pi D h\,(T_s - T_m),$$
$$T_m = T_{\mathrm{in}} \quad \text{at } x = 0.$$

The solution of this differential equation will give the temperature at $x = l$ as

$$\frac{T_m(l) - T_s}{T_{\mathrm{in}} - T_s} = \exp\left[-\frac{\pi D l h}{\dot{m}C_P}\right]. \tag{a}$$

Applying this equation, we get the mean fluid temperature:

$$T_m(l)\big|_{\mathrm{Gnielinski}} = T_s + (T_{\mathrm{in}} - T_s)\exp\left[-\frac{\pi D l h_{\mathrm{Gnielinski}}}{\dot{m}C_P}\right]$$
$$= 100\,^\circ\mathrm{C} + [(35-100)\,^\circ\mathrm{C}]$$
$$\times\exp\left[-\frac{\pi\,(0.0508\,\mathrm{m})\,(1.4\,\mathrm{m})\,(3674\,\mathrm{W/m^2\,^\circ C})}{(7.753\,\mathrm{kg/s})\,(2200\,\mathrm{J/kg\,K})}\right]$$
$$= 38.05\,^\circ\mathrm{C}.$$

Using the Chilton–Colburn analogy, we have [see Eq. (9.7.8)],

$$\mathrm{Nu}_{D,\,\mathrm{Chil-Col}} = \mathrm{Re}_D\,\mathrm{Pr}\,\mathrm{St} = \mathrm{Re}_D\,\mathrm{Pr}\left[\mathrm{Pr}^{-2/3}\left(\frac{f}{8}\right)\right] = \mathrm{Re}_D\mathrm{Pr}^{1/3}\left(\frac{f}{8}\right)$$
$$= (1.518\times10^5)(20.11)^{1/3}(0.01648/8) = 850.4.$$

The heat transfer coefficient and the liquid mean temperature at $x = l$ are found as follows.

$$h_{\text{Chil-Col}} = \text{Nu}_{D,\,\text{Chil-Col}}\frac{k}{D} = (850.4)\,\frac{0.14\,\text{W/m K}}{0.0508\,\text{m}} = 2344\,\text{W/m}^2\,\text{K},$$

$$T_m(l)\big|_{\text{Chil-Col}} = T_s + (T_{\text{in}} - T_s)\exp\left[-\frac{\pi D l h_{\text{Chil-Col}}}{\dot{m}C_P}\right]$$

$$= 100\,^\circ\text{C} + [(35-100)^\circ\,\text{C}]\exp\left[-\frac{\pi\,(0.0508\,\text{m})\,(1.4\,\text{m})\,(2344\,\text{W/m}^{2\circ}\text{C})}{(7.753\,\text{kg/s})\,(2200\,\text{J/kg K})}\right]$$

$$\approx 37\,^\circ\text{C}.$$

Part (b). We need to adjust the Nusselt number we found earlier for the effect of surface roughness. We therefore find the friction factor from the correlation of Haaland (1983) [Eq. (7.2.42)]:

$$\frac{1}{\sqrt{f}} = -1.8\log_{10}\left[\left(\frac{\varepsilon_s/D}{3.7}\right)^{1.11} + \frac{6.9}{\text{Re}_D}\right]$$

$$\Rightarrow f = \left\{-1.8\log_{10}\left[\left(\frac{7.1\times10^{-5}\,\text{m}/0.0508\,\text{m}}{3.7}\right)^{1.11} + \frac{6.9}{(1.518\times10^5)}\right]\right\}^{-2} = 0.0227.$$

We can now use the correlation of Norris (1970), Eqs. (7.1.1)–(7.1.3), whereby:

$$n = 1$$

$$\text{Nu}_{D_H}/\text{Nu}_{D_H,\text{smooth}} = \min[(C_f/C_{f,\min})^n, (4)^n]$$

$$= \min[(0.0227/0.01648), 4] = 1.377$$

$$\Rightarrow \text{Nu}_{D_H} = (1.377)(1333) = 1835.$$

This will lead to $h = 5054\ \text{W/m}^2\,\text{K}$, and Eq. (a) will then give $T_m(l)\big| = 39.16\,^\circ\text{C}$.

EXAMPLE 9.2. A 1.4-m-long tube with an inner diameter of 1.25 cm is subject to a uniform wall heat flux of $2.43\times10^4\ \text{W/m}^2$. The tube is cooled by an organic oil, with an inlet temperature of 0 °C. Using the analogy of von Karman, calculate the wall inner surface temperature at the exit for 0.11-kg/s oil mass flow rates.

The oil average properties are

$$\rho = 753\,\text{kg/m}^3, \quad C_p = 2.1\,\text{kJ/kg K}, \quad k = 0.137\,\text{W/m K}, \quad \mu = 6.6\times10^{-4}\,\text{Pa s}.$$

SOLUTION. First, let us calculate the mean velocity and the Reynolds number:

$$U_m = \frac{\dot{m}}{\rho\frac{\pi}{4}D^2} = \frac{0.11\,\text{kg/s}}{(753\,\text{kg/m}^3)\,\frac{\pi}{4}\,(0.0125\,\text{m})^2} = 1.19\,\text{m/s},$$

$$\text{Re}_D = \rho U_m D/\mu = (753\,\text{kg/m}^3)\,(1.19\,\text{m/s})\,(0.0125\,\text{m})/\left(6.6\times10^{-4}\,\text{kg/m s}\right) = 16,977.$$

The mean liquid temperature at the exit can be found from a simple energy balance on the pipe:

$$\dot{m}C_P\,[T_m(l) - T_{\text{in}}] = \pi D\,l q_s''$$

$$\Rightarrow T_m(l) = T_{\text{in}} + \frac{\pi D l q_s''}{\dot{m}C_P} = 0\,^\circ\text{C} + \frac{\pi\,(0.0125\,\text{m})\,(1.4\,\text{m})\,(2.43\times10^4\,\text{W/m}^2)}{(0.11\,\text{kg/s})\,(2,100\text{J/kg K})}$$

$$= 5.78\,^\circ\text{C}.$$

We can estimate the friction factor from Blasius' correlation:

$$C_f = \frac{0.316}{4}\mathrm{Re}_D^{-1/4} = 0.079\,(16,971)^{-1/4} = 0.00692.$$

We can now apply von Karman's analogy, assuming $\mathrm{Pr}_{\mathrm{tu}} = 1$ for simplicity:

$$\mathrm{Nu}_D = \frac{\frac{1}{2}\mathrm{Re}_D\mathrm{Pr}\ \mathrm{Pr}_{\mathrm{tu}}^{-1}C_f}{1+5\sqrt{\frac{C_f}{2}}\left\{\left(\mathrm{Pr}_{\mathrm{tu}}^{-1}\mathrm{Pr}-1\right)+\ln\left[1+\frac{5}{6}\left(\mathrm{Pr}_{\mathrm{tu}}^{-1}\mathrm{Pr}-1\right)\right]\right\}}$$

$$= \frac{\frac{1}{2}\,(16,971)\,(10.12)\,(1)^{-1}\,(0.00692)}{1+5\sqrt{\frac{(0.00692)}{2}}\left\{\left([1]^{-1}\,[10.12]-1\right)+\ln\left[1+\frac{5}{6}\left([1]^{-1}\,[10.12]-1\right)\right]\right\}} = 137.8,$$

$$h = \mathrm{Nu}_D\frac{k}{D} = (137.8)\,\frac{(0.137\,\mathrm{W/m\,^\circ C})}{0.0125\,\mathrm{m}} = 1510\,\mathrm{W/m^2\,^\circ C}.$$

We can now find the surface temperature by writing

$$T_s(l) = T_m(l) + \frac{q_s''}{h_x} = 5.78\,^\circ\mathrm{C} + \frac{(2.43\times10^4\,\mathrm{W/m^2})}{1510\,\mathrm{W/m^2\,^\circ C}} = 21.87\,^\circ\mathrm{C}.$$

EXAMPLE 9.3. The organic oil described in Example 9.2 flows in a long, hydraulically smooth and uniformly heated tube with an inner diameter of 4.5 cm. The mass flow rate is $0.45\,\mathrm{kg/m^2\,s}$. Assuming thermally developed flow, calculate the Nusselt number by using the analogy of Yu et al. (2001). Compare the result with the prediction of the correlation of Dittus and Boelter.

SOLUTION. All the relevant thermophysical properties have been calculated in Example 9.2. Let us calculate the mean velocity, and from there the Reynolds number and Fanning friction factor,

$$U_m = \frac{\dot{m}}{\rho\pi\frac{D^2}{4}} = \frac{0.45\,\mathrm{kg/s}}{(753\,\mathrm{kg/m^3})\,\pi\,\frac{(0.045\,\mathrm{m})^2}{4}} = 0.3758\,\mathrm{m/s}$$

$$\mathrm{Re}_D = \rho U_m D/\mu = \left(753\,\mathrm{kg/m^3}\right)(0.3758\,\mathrm{m/s})\,(0.045\,\mathrm{m})/\left(0.66\times10^{-3}\mathrm{kg/m\,s}\right) = 1.929\times10^4$$

$$C_f = 0.079\mathrm{Re}_D^{-0.25} = 0.0066.$$

We can now calculate the dimensionless pipe radius and the dimensionless mean velocity:

$$\tau_s = C_f\frac{1}{2}\rho U_m^2 = (0.0067)\,\frac{1}{2}\left(753\,\mathrm{kg/m^3}\right)\,(0.3758\,\mathrm{m/s})^2 = 0.3503\,\mathrm{N/m^2},$$

$$U_\tau = \sqrt{\tau_s/\rho} = \sqrt{(0.3503\,\mathrm{N/m^2})/(753\,\mathrm{kg/m^3})} = 0.02157\,\mathrm{m/s},$$

$$R_0^+ = \frac{\rho U_\tau\,(D/2)}{\mu} = \frac{\left(753\,\mathrm{kg/m^3}\right)(0.02157\,\mathrm{m/s})\,(0.045\,\mathrm{m}/2)}{(0.66\times10^{-3}\,\mathrm{kg/m\,s})} = 553.7,$$

$$U_m^+ = U_m/U_\tau = (0.3758\,\mathrm{m/s})/(0.02157\,\mathrm{m/s}) = 17.42.$$

Alternatively, we could find U_{m}^{+} from Eq. (7.2.34):

$$\begin{aligned} U_{\mathrm{m}}^{+} &= 3.2 - \frac{227}{R_0^{+}} + \left(\frac{50}{R_0^{+}}\right)^2 + \frac{1}{0.436}\ln\left(R_0^{+}\right) \\ &= 3.2 - \frac{227}{553.7} + \left(\frac{50}{553.7}\right)^2 + \frac{1}{0.436}\ln(553.7) \\ &= 17.29. \end{aligned}$$

The two values of U_{m}^{+} are evidently similar. We should now apply Eq. (9.6.6). First, we apply Eq. (9.6.8) to find the turbulent Prandtl number:

$$\mathrm{Pr}_{\mathrm{tu}} = 0.85 + \frac{0.015}{\mathrm{Pr}} = 0.85 + \frac{0.015}{10.12} = 0.8515.$$

Next, we calculate $\mathrm{Nu}_{D,\infty}$ and $\mathrm{Nu}_{D,1}$ from Eqs. (9.6.7) and (9.6.10), respectively:

$$\begin{aligned} \mathrm{Nu}_{D,\infty} &= 0.07343\left(\frac{\mathrm{Pr}}{\mathrm{Pr}_{\mathrm{tu}}}\right)^{1/3}\mathrm{Re}_D\left(\frac{C_f}{2}\right)^{1/2} \\ &= 0.07343\left(\frac{10.12}{0.8515}\right)^{1/3}(1.929\times10^4)\left(\frac{0.0066}{2}\right)^{1/2} = 186, \\ \mathrm{Nu}_{D,1} &= \frac{\mathrm{Re}_D\left(\frac{C_f}{2}\right)}{1+\frac{195}{\left(U_{\mathrm{m}}^{+}\right)^{2.7}}} = \frac{(1.929\times10^4)\left(\frac{0.0066}{2}\right)}{1+\frac{195}{(17.29)^{2.7}}} = 58.38, \\ \mathrm{Nu}_D &= \frac{1}{\left(\frac{\mathrm{Pr}_{\mathrm{tu}}}{\mathrm{Pr}}\right)\frac{1}{\mathrm{Nu}_{D,1}} + \left[1-\left(\frac{\mathrm{Pr}_{\mathrm{tu}}}{\mathrm{Pr}}\right)^{2/3}\right]\frac{1}{\mathrm{Nu}_{D,\infty}}} \\ &= \frac{1}{\left(\frac{0.8515}{10.12}\right)\frac{1}{(58.38)} + \left[1-\left(\frac{0.8515}{10.12}\right)^{2/3}\right]\frac{1}{(185.4)}} = 172.5. \end{aligned}$$

We can now compare the preceding value for the Nusselt number with the prediction of the correlation of Dittus and Boelter:

$$\mathrm{Nu}_D = 0.023\mathrm{Re}_D^{0.8}\mathrm{Pr}^{0.4} = 0.023(1.929\times10^4)^{0.8}(10.12)^{0.4} = 155.6.$$

PROBLEMS

Problem 9.1. Derive Eqs. (9.3.13) and (9.3.14). How would you modify these equations for pipe flow?

Problem 9.2. Water flows through a rectangular channel. The channel cross section is 2 cm × 4 cm. The water mean velocity and mean temperature are 7.5 m/s and 300 K, respectively. The wall temperature is 350 K. Calculate the wall heat flux by

using an appropriate empirical correlation and an appropriate correlation based on analogy between heat and momentum transfer.

Problem 9.3. Water flows at a velocity of 10 m/s parallel to a 2D smooth and flat surface. The water temperature away from the surface is 20 °C. The flat surface is heated, resulting in a heat flux of 2.5×10^5 W/m^2.

At a distance of 1.0 m downstream from the leading edge,

(a) calculate the skin-friction coefficient C_f,
(b) calculate the wall temperature based on an appropriate analogy between heat and momentum transfer,
(c) using the turbulent temperature law of the wall, calculate the water temperature 0.5 mm above the wall surface.

Assume the following constant properties for water: $\rho = 997$ kg/m^3, $C_P = 4180$ J/kg K, $\mu = 8.55 \times 10^{-4}$ kg/ms, $k = 0.62$ W/m K, Pr $= 5.2$.

Problem 9.4. Liquid sodium, at a mean temperature of 360 °C, flows through a pipe. The pipe inner diameter is 1 cm, and the flow Reynolds number is 2.5×10^5. Calculate and compare the heat transfer coefficients using Martinelli's analogy and an appropriate correlation for thermally developed flow of a low-Prandtl-number fluid in a pipe.

Problem 9.5. Consider the flow in a long, heated pipe in which the properties of an incompressible fluid can be adjusted by adding a soluble additive. The Nusslet numbers in the pipe, whose walls are hydraulically smooth, are to be calculated. For Pr $= 1.5$, 5, and 10, and for several values of Re_D in the 10^4–2×10^5 range, calculate and compare the predictions of the analogies of von Karman, Chilton–Colburn, and Yu et al., and compare them with the predictions of the empirical correlation of Gnielinski. Discuss the results.

Problem 9.6. Air at a temperature of 290 K flows into a tube that has an inner diameter of 2.5 cm and a length of 10 cm. The air average velocity is 10 m/s. The two ends of the tube are open. The tube inner wall temperature is 310 K.

(a) Estimate the average heat transfer coefficient using an appropriate correlation.
(b) Repeat part (a) using the Chilton–Colburn analogy.
(c) Discuss the potential sources of inaccuracy in your estimates, and attempt to improve your estimate.

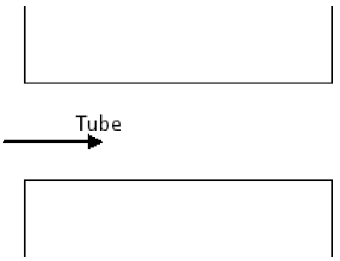

Figure P9.6

Mass Transfer

Problem 9.7. In an experiment a flat plate made from naphthalene is exposed to a parallel flow of pure air at a pressure of 1 bar. The air velocity away from the plate is 10 m/s. The air and plate are all at 300 K temperature. The experiment has been under way for 3 h.

(a) Calculate the reduction in the thickness of the naphthalene plate at 5 and 50 cm downstream from the leading edge of the plate
(b) Repeat part (a), this time assuming that the air velocity is 20 m/s.

Neglect viscous dissipation. For naphthalene vapor in air under atmospheric pressure, Sc = 2.35 at 300 K (Cho et al., 1992; Mills, 2001). Furthermore, the vapor pressure of naphthalene can be estimated from (Mills, 2001)

$$P_v(T) = 3.631 \times 10^{13} \exp(-8586/T),$$

where T is in Kelvins and P_v is in pascals.

Problem 9.8. Water flows in a tube that has an inner diameter of 2.54 cm and a length of 2.5 m. The tube wall is covered with a layer of a sparingly soluble substance (the transferred species), whose properties are similar to those of benzene. The mass fraction of the transferred species at the wall surface is equal to 0.15. The temperature of the water and the pipe is 25 °C. The water is pure at the inlet to the tube. The water mean velocity at inlet is 4.6 m/s.

1. Calculate the average mass fraction of the transferred species in water at tube exit, assuming that the surface is smooth, using
   (a) Gnielinski's correlation modified for mass transfer,
   (b) the Reynolds analogy,
   (c) the Chilton–Coulburn analogy.
2. Repeat the calculations of part 1, assuming that the tube has an average surface roughness value of approximately 4.6×10^{-2} mm.

Combined Heat and Mass Transfer

Problem 9.9. The top surface of a flat, horizontal plate that is 5 cm × 5 cm in size is subject to a parallel flow of hot, atmospheric-pressure air. The air is at an ambient temperature of 100 °C and flows with a far-field velocity of $U_\infty = 10$ m/s.

(a) Calculate the rate of heat transfer from air to the surface, assuming that the surface is smooth and dry and its surface temperature is 60 °C.
(b) Assume that the surface is porous and is maintained wet by an injection of water from a small reservoir, such that the underneath side of the surface remains adiabatic and the porous surface and the reservoir remain at thermal equilibrium. Find the temperature of the surface. For simplicity, assume that the air is dry.

Everywhere, to find heat or mass transfer coefficients, use an appropriate analogy.

Hint: In part (b), there is a balance between the sensible heat transfer rate toward the surface and the latent heat transfer rate leaving the surface.

10 Natural Convection

In free or natural convection, the macroscopic fluid motion is due to body forces and their dependence on fluid density, which itself is sensitive to the temperature or the concentration (or both) of the species that constitute the fluid.

Free convection is common in nature and has numerous applications and occurrences in industry. It is a major cause for atmospheric and oceanic recirculation and plays an increasingly important role in the passive emergency cooling systems of advanced nuclear reactors, just to name a few.

10.1 Natural-Convection Boundary Layers on Flat Surfaces

In this section we discuss the important attributes of free-convection boundary layers on flat surfaces. The simple flat-surface configuration is chosen for clarity of the discussions. The discussions of basic and phenomenological processes are much more general, however, and apply to the more complicated configurations with relatively minor modifications.

Conservation Equations

Let us focus on the 2D, steady-state boundary-layer flow of a pure, Newtonian fluid, shown in Fig. 10.1. The ambient flow is quiescent, and no phase change is taking place. The mass, momentum, and energy conservation equations for the boundary layer in x–y coordinates will then be

$$\frac{\partial}{\partial x}(\rho u) + \frac{\partial}{\partial y}(\rho v) = 0, \tag{10.1.1}$$

$$\rho u\left(\frac{\partial u}{\partial x}\right) + \rho v\left(\frac{\partial u}{\partial y}\right) = -\left(\frac{dP}{dx}\right) + \frac{\partial}{\partial y}\left(\mu\frac{\partial u}{\partial y}\right) + \rho(g_x), \tag{10.1.2}$$

$$\rho C_P\left(u\frac{\partial T}{\partial x} + v\frac{\partial T}{\partial y}\right) = \frac{\partial}{\partial y}\left(k\frac{\partial T}{\partial y}\right) + \mu\left(\frac{\partial u}{\partial y}\right)^2. \tag{10.1.3}$$

These equations are similar to those derived earlier for laminar forced-flow boundary layers over a flat surface, and can be derived by the same order-of-magnitude analysis as used in Section 2.2.

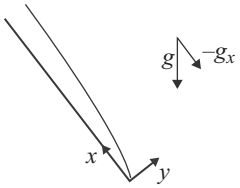

Figure 10.1. Free-convection boundary layer on a flat surface.

The last term on the right-hand side of Eq. (10.1.3) represents viscous dissipation. It is negligibly small in the majority of free-convection problems and is therefore neglected.

Away from the surface, because the fluid is stagnant,

$$-\frac{dP_\infty}{dx} + \rho_\infty g_x = 0, \tag{10.1.4}$$

$$-\frac{dP_\infty}{dx} = -\rho_\infty g_x. \tag{10.1.5}$$

Equation (10.1.2) then becomes

$$\rho u\left(\frac{\partial u}{\partial x}\right) + \rho v\left(\frac{\partial u}{\partial y}\right) = -\left(\rho_\infty - \rho\right) g_x - \left(\frac{dP}{dx} - \frac{dP_\infty}{dx}\right) + \frac{\partial}{\partial y}\left(\mu\frac{\partial u}{\partial y}\right). \tag{10.1.6}$$

A critical simplification is now made, which was originally proposed by Boussinesq. We assume that the fluid is incompressible in all aspects, except for the gravitational term in the momentum equation. We also assume that the fluid has constant properties. The assumption of incompressible fluid is reasonable because the density variations are typically quite small. However, it cannot be applied to the gravitational term because it is actually this term that causes the flow.

Furthermore, for a pure substance, we can represent the equation of state as

$$\rho = \rho\left(P, T\right). \tag{10.1.7}$$

Therefore

$$d\rho = K\left(dP\right) + \beta\left(dT\right), \tag{10.1.8}$$

where the isothermal compressibility and the coefficient of thermal expansion are defined, respectively, as

$$K = \frac{1}{\rho}\left(\frac{\partial\rho}{\partial P}\right)_T, \tag{10.1.9}$$

$$\beta = -\frac{1}{\rho}\left(\frac{\partial\rho}{\partial T}\right)_P. \tag{10.1.10}$$

In virtually all free- and mixed-convection problems, the first term on the right-hand side of Eq. (10.1.8) is much smaller than the second term; therefore we can write

$$d\rho = -\rho\,\beta\,d\,T.$$

This leads to

$$\rho_\infty - \rho = \rho\,\beta\left(T - T_\infty\right). \tag{10.1.11}$$

Thus Eqs. (10.1.1)–(10.1.3) become

$$\frac{\partial u}{\partial x} + \frac{\partial v}{\partial x} = 0, \tag{10.1.12}$$

$$u\left(\frac{\partial u}{\partial x}\right) + v\left(\frac{\partial u}{\partial y}\right) = -g_x\beta\,(T - T_\infty) - \frac{1}{\rho}\left(\frac{dP}{dx} - \frac{dP_\infty}{dx}\right) + \nu\frac{\partial^2 u}{\partial y^2}, \tag{10.1.13}$$

$$\rho C_P\left(u\frac{\partial T}{\partial x} + v\frac{\partial T}{\partial y}\right) = k\frac{\partial^2 T}{\partial y^2}. \tag{10.1.14}$$

Nondimensionalization

The main objectives of nondimensionalization are to reduce the number of parameters in the mathematical problem, derive relevant dimensionless numbers, perform order-of-magnitude comparisons among various terms, and figure out some important functional dependencies.

We need reference quantities. Let us use l as the relevant reference length. The best choice for a vertical or inclined flat plate would evidently be the plate length in the main flow direction (x direction in Fig. 10.1). With respect to velocity, in the absence of an ambient flow, a physically sensible reference velocity is

$$U_{\text{ref}} = [g\beta\, l\,(T_s - T_\infty)]^{1/2}. \tag{10.1.15}$$

We can thus define

$$x^* = x/l, \tag{10.1.16}$$

$$y^* = y/l, \tag{10.1.17}$$

$$P^* = (P - P_\infty)/\left(\rho U_{\text{ref}}^2\right), \tag{10.1.18}$$

$$\theta = (T - T_\infty)/\,(T_s - T_\infty)\,, \tag{10.1.19}$$

$$u^* = u/U_{\text{ref}}. \tag{10.1.20}$$

Equations (10.1.12)–(10.1.14) then give

$$\nabla^*\vec{U}^* = 0, \tag{10.1.21}$$

$$\vec{U}^*\,\nabla^*\,\vec{U}^* = \left(-\frac{g_x}{g}\right)\theta - \nabla^* P^* - \frac{1}{\sqrt{\text{Gr}_l}}\nabla^{*^2}\vec{U}^*, \tag{10.1.22}$$

$$\vec{U}^*\cdot\nabla^*\theta = \frac{1}{\text{Pr}\sqrt{\text{Gr}_l}}\nabla^{*^2}\theta. \tag{10.1.23}$$

The analysis thus brings out two important dimensionless parameters: the familiar Prandtl number, $\text{Pr} = \nu/\boldsymbol{\alpha}$, and the Grashof number,

$$\text{Gr}_l = \frac{g\beta\, l^3\,(T_s - T_\infty)}{\nu^2}. \tag{10.1.24}$$

The Grashof number is often interpreted as representing the ratio between inertial and viscous forces. Note that Eqs. (10.1.14) and (10.1.23) are appropriate for low-flow situations, which are typical in free-convection problems. For mixed-convection problems, a more general form for Eq. (10.1.14) is

$$\rho\, C_P\left(u\frac{\partial T}{\partial x} + v\frac{\partial T}{\partial y}\right) = k\frac{\partial^2 T}{\partial y^2} + \beta\, u\; T\frac{\partial P_\infty}{\partial x} + \mu\left(\frac{\partial u}{\partial y}\right)^2, \tag{10.1.25}$$

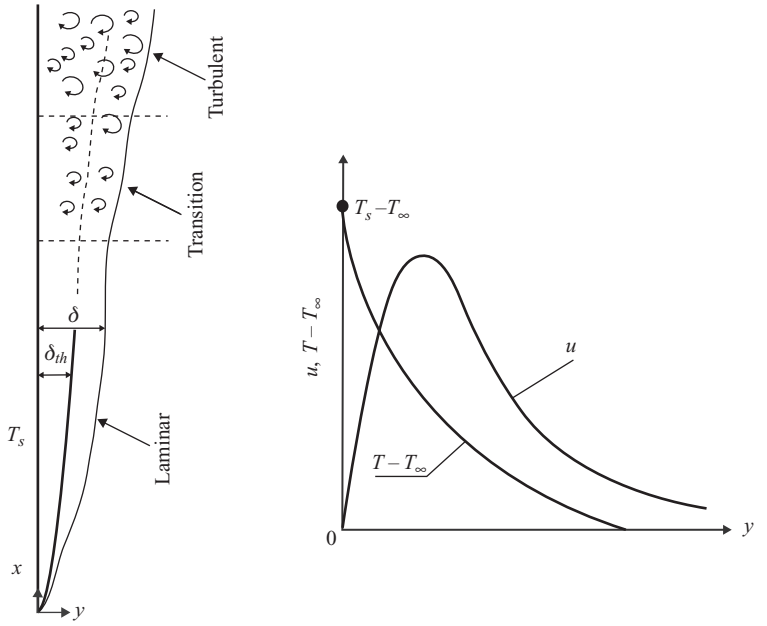

Figure 10.2. Natural-convection boundary layer on a heated vertical surface.

where the last term on the right-hand side represents the viscous dissipation. In dimensionless form, this equation gives

$$\vec{U}^* \cdot \nabla^* \theta = \frac{1}{\mathrm{Pr}\sqrt{\mathrm{Gr}_l}} \nabla^{*^2} \theta + \frac{g\beta^2 Tl}{C_P} \vec{U}^* \nabla^* P^* + \frac{g\beta l}{C_P} \frac{1}{\sqrt{\mathrm{Gr}_l}} \phi^{*^2}. \qquad (10.1.26)$$

We can see that the viscous dissipation term is negligible when $\frac{g\beta l}{C_P} \frac{1}{\sqrt{\mathrm{Gr}_l}} \ll 1$, or simply when Gr is very large. This is often the case in natural convection.

Another important dimensionless parameter, the Rayleigh number, is simply defined as

$$\mathrm{Ra}_l = \mathrm{Pr}\ \mathrm{Gr}_l = \frac{g\beta l^3 (T_s - T_\infty)}{\nu \boldsymbol{\alpha}}. \qquad (10.1.27)$$

The incentive for this definition is that in a multitude of very important free- convection problems the product of Gr_l and Pr actually shows up in the solutions or empirical correlations.

10.2 Phenomenology

The velocity and thermal boundary layers forming on a heated vertical surface that is surrounded by a quiescent fluid field are shown schematically in Fig. 10.2. The main attributes of the phenomenology that are subsequently described, with some modifications, actually apply to free convection on surfaces with other configurations. The buoyancy that results from the thermal expansion of fluid adjacent to the surface is the cause for the development of a rising boundary layer. The velocity boundary layer is thicker than the thermal boundary layer for $\mathrm{Pr} \gtrsim 1$, and the $\delta/\delta_{\mathrm{th}}$ ratio increases as Pr is increased. For $\mathrm{Pr} \ll 1$, however, the opposite can be observed, namely, $\delta_{\mathrm{th}} \lesssim \delta$.

The free-convection boundary layer is laminar near the leading edge of the heated surface, and it grows in thickness with distance from the leading edge. Eventually the laminar boundary layer becomes unstable, and transition from laminar to turbulent boundary layer starts. Farther downstream, transition to turbulent flow is eventually complete. The turbulent boundary layer is typically much thicker than the laminar boundary layer and is dominated by vortices and turbulent eddies. The turbulent boundary layer entrains mass from the surrounding fluid.

A comparison between Eqs. (10.1.1)–(10.1.3) and Eqs. (2.2.21)–(2.2.24) shows that we have assumed that the scaling analysis and the boundary-layer approximation described in Section 2.2, which lead to the latter equations, apply to free convection as well. This is true and, similar to forced flow, the boundary-layer approximations are applicable in free convection only when $\delta/x \ll 1$. For a vertical flat plate, for example, the approximations are justifiable when $\mathrm{Gr}_x \geq 10^4$ (Gebhart, 1981).

For a flat vertical plate, transition to a turbulent boundary layer occurs at

$$\mathrm{Ra}_x \approx 10^9. \tag{10.2.1}$$

A more accurate criterion for transition to turbulent boundary-layer flow for a fluid with $10^{-3} < \mathrm{Pr} < 10^3$, according to Bejan (1993), is

$$\mathrm{Gr}_x \approx 10^9. \tag{10.2.2}$$

Free convection does not occur only on vertical heated or cooled surfaces in large quiescent fluid fields. It can also occur in confined spaces with cooled or heated surfaces, and on horizontal and irregular-shaped objects. Free convection in a confined space is accompanied by the formation of one or more recirculation patterns. Figures 10.3 and 10.4 are good examples for external natural convection and show flow patterns on a heated horizontal surface and around a horizontal heated cylinder, respectively. When a horizontal, upward-facing flat surface (Fig. 10.3) is heated, the warm and buoyant gas near the surface tends to rise. Uniform rise of the entire flow field evidently would not be possible because the rising fluid must be replenished somehow. An intermittent flow field is developed instead, whereby balls of warm fluid (thermals) form and rise intermittently from the surface, while cool fluid moves downward elsewhere to replace the rising fluid.

Free convection on the surface of a blunt body leads to the formation of a boundary layer that grows in thickness with distance from the surface leading edge, and eventually leads to a rising plume. This can be observed in Fig. 10.4, where free convection on the outside of a horizontal cylinder is displayed. The boundary layer on the surface of the cylinder in this case remains laminar for $\mathrm{Ra}_D \lesssim 10^9$.

A multitude of recirculation patterns, often with significantly different time and length scales, are common in complex-shaped confined spaces. Natural-circulation flow patterns can also develop in piping and flow systems that form a closed or semi-closed loop. Thermosyphons are good examples. These are passive liquid circulation systems that are widely used in solar hot-water systems.

Numerical- and CFD-based analyses are usually possible, and are commonly applied, for complex geometries. However, certain aspects (e.g., laminar to turbulent flow regime transition criteria) need to be specified by empirical means. For

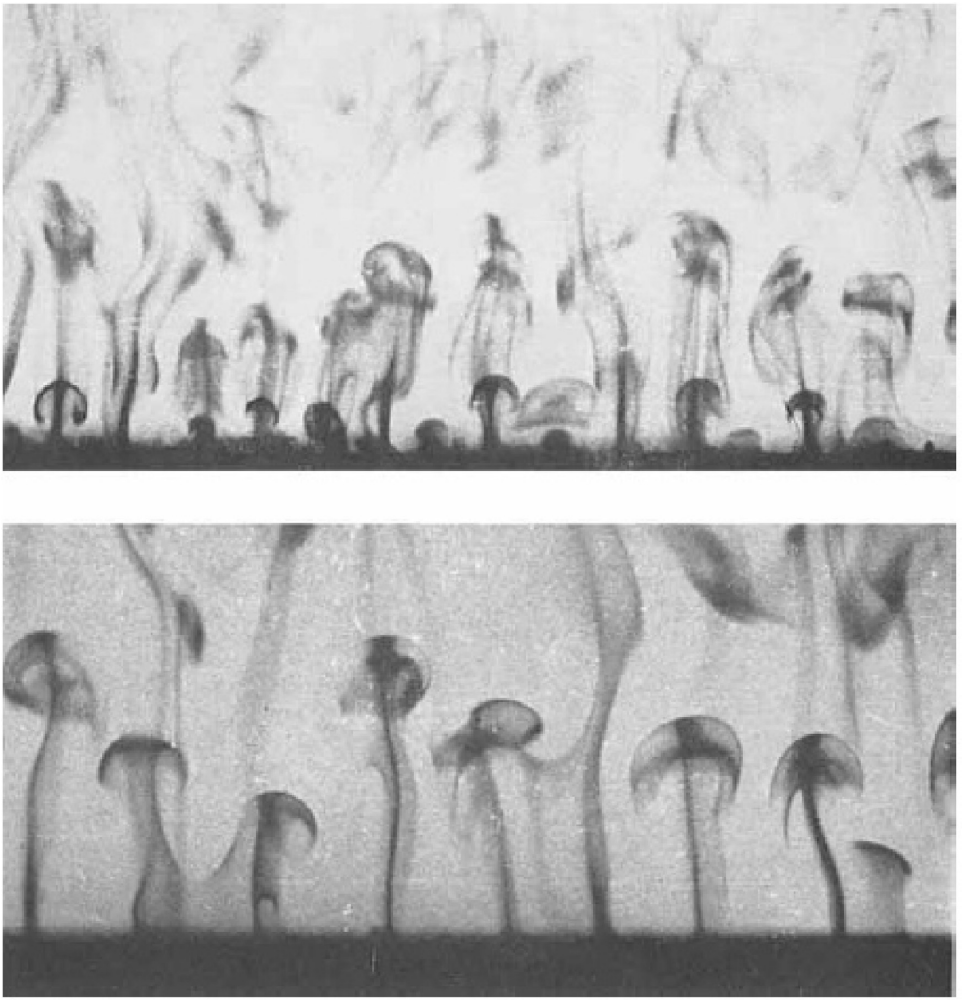

Figure 10.3. The flow field during natural convection from a horizontal, upward-facing heated surface (from Sparrow et al., 1970).

many widely occurring configurations, nevertheless, we rely on experiments and empirical correlations.

Based on the preceding brief discussion, free-convection problems can be broadly divided into three categories:

1. external (i.e., free convection on submerged bodies),
2. internal (free convection in confined space),
3. natural circulation.

In external flow free convection, the processes at the surface that support natural convection do not influence the ambient conditions in any significant manner. In internal flow the opposite is true.

10.3 Scaling Analysis of Laminar Boundary Layers

For laminar boundary-layers we can deduce very useful information about boundary-layer characteristics and the expected forms of the dimensionless heat

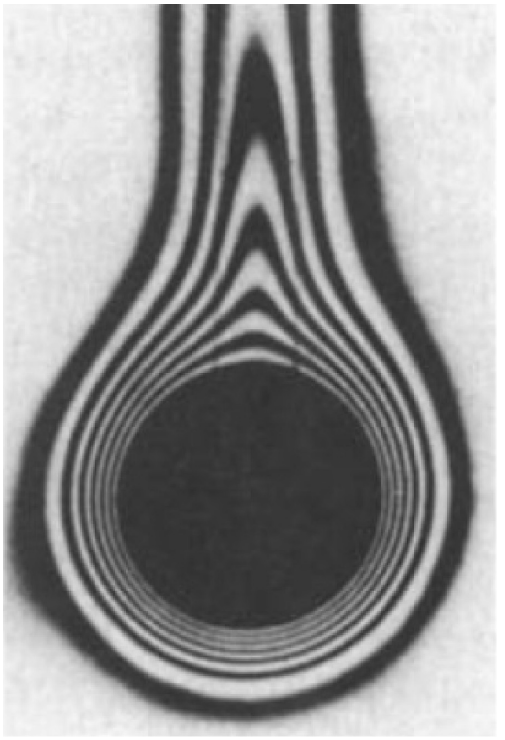

Figure 10.4. Isotherms during natural convection around a horizontal heated cylinder (courtesy of E.R.G. Eckert; from Raithby and Hollands, 1998).

transfer coefficients simply by making an order-of-magnitude assessment of the conservation equations.

Consider free convection on a heated vertical flat surface (Fig. 10.2). The conservation equations will then be

$$\frac{\partial u}{\partial x} + \frac{\partial v}{\partial y} = 0, \tag{10.3.1}$$

$$u\left(\frac{\partial u}{\partial x}\right) + v\left(\frac{\partial u}{\partial y}\right) = g\beta\,(T - T_\infty) + \nu\frac{\partial^2 u}{\partial y^2}, \tag{10.3.2}$$

$$u\frac{\partial T}{\partial x} + v\frac{\partial T}{\partial y} = \alpha\frac{\partial^2 T}{\partial y^2}. \tag{10.3.3}$$

Now assume that $\delta \approx \delta_{\text{th}}$ and $\delta/x \ll 1$ everywhere, which are reasonable assumptions for common free-convection problems. The order of magnitude of the terms in the preceding three equations become

$$\text{Eq. (10.3.1)} \Rightarrow \frac{v}{\delta_{\text{th}}} \sim \frac{u}{x}, \tag{10.3.4}$$

$$\text{Eq. (10.3.2)} \Rightarrow u\,(u/x)\,,\ v\,(u/\delta_{\text{th}}) \sim \nu\left(u/\delta_{\text{th}}^2\right),\ g\beta\,(T_s - T_\infty)\,, \tag{10.3.5}$$

$$\text{Eq. (10.3.3)} \Rightarrow \frac{u\,(T_s - T_\infty)}{x},\ \frac{v(T_s - T_\infty)}{\delta_{\text{th}}} \sim \alpha\frac{(T_s - T_\infty)}{\delta_{\text{th}}^2}. \tag{10.3.6}$$

In light of Eq. (10.3.4), the terms on the left-hand side of Eq. (10.3.5) have similar orders of magnitude. The same can be said about the terms on the left-hand side of Eq. (10.3.6). Equation (10.3.6) then gives

$$u\frac{T_s - T_\infty}{x} \sim \alpha\frac{T_s - T_\infty}{\delta_{\text{th}}^2}. \tag{10.3.7}$$

The momentum equation, Eq. (10.3.5), represents a competition among three forces:

$$\underbrace{\frac{u^2}{x}}_{\text{Inertia}} \qquad \underbrace{\nu\frac{u}{\delta_{\text{th}}^2}}_{\text{Friction}} \qquad \underbrace{g\beta\,|T_s - T_\infty|}_{\text{Buoyancy}}.$$

Two limiting conditions can be considered: when inertia is negligible and buoyancy is balanced by friction and when the effect of friction is negligible and buoyancy is balanced by inertia.

1. Buoyancy balanced by friction (negligible inertia): This occurs in fluids with $\text{Pr} > 1$. Then,

$$\nu\frac{u}{\delta_{\text{th}}^2} \sim g\beta(T_s - T_\infty). \tag{10.3.8}$$

Using the preceding expressions, we can then show that,

$$v \sim \frac{\alpha}{x}\text{Ra}_x^{1/4}, \tag{10.3.9}$$

$$u \sim \frac{\alpha}{x}\text{Ra}_x^{1/2}, \tag{10.3.10}$$

$$\frac{\delta_{\text{th}}}{x} \sim \text{Ra}_x^{-1/4}. \tag{10.3.11}$$

We can estimate the wall heat flux by writing

$$q_s'' = -k\left.\frac{\partial T}{\partial y}\right|_{y=0} \approx k\frac{T_s - T_\infty}{\delta_{\text{th}}}, \tag{10.3.12}$$

which gives

$$h_x \approx \frac{k}{\delta_{\text{th}}}, \tag{10.3.13}$$

$$\text{Nu}_x = \frac{h_x x}{k} \approx \frac{x}{\delta_{\text{th}}}. \tag{10.3.14}$$

Thus we must expect

$$\text{Nu}_x \approx \text{Ra}_x^{1/4}. \tag{10.3.15}$$

Inertia is insignificant when $(u^2/x) \ll \nu u/\delta_{\text{th}}^2$, which, by using Eqs. (10.3.10) and (10.3.11), leads to $\text{Pr} \gg 1$. A velocity boundary layer thicker than the thermal boundary layer thus develops. It can be shown that (Bejan, 2004)

$$\frac{\delta}{x} \approx \text{Ra}_x^{-1/4}\text{Pr}^{1/2}, \tag{10.3.16}$$

$$\frac{\delta}{\delta_{\text{th}}} \approx \text{Pr}^{1/2}. \tag{10.3.17}$$

2. Buoyancy balanced by inertia (insignificant friction): This occurs when $\mathrm{Pr} \ll 1$. In this case, we have

$$\frac{u^2}{x} \approx g\beta(T_s - T_\infty). \tag{10.3.18}$$

Again, using Eqs. (10.3.9), (10.3.10) and (10.3.18), we can derive

$$v \approx \frac{\alpha}{x}(\mathrm{Ra}_x \mathrm{Pr})^{1/4}, \tag{10.3.19}$$

$$u \approx \frac{\alpha}{x}(\mathrm{Ra}_x \mathrm{Pr})^{1/2}, \tag{10.3.20}$$

$$\frac{\delta_{\mathrm{th}}}{x} \sim (\mathrm{Ra}_x \mathrm{Pr})^{-1/4}, \tag{10.3.21}$$

$$\mathrm{Nu}_x \approx (\mathrm{Ra}_x Pr)^{1/4}. \tag{10.3.22}$$

The preceding expressions are valid when $\frac{u^2}{x} > \nu\frac{u}{\delta_{\mathrm{th}}^2}$, which, by using Eq. (10.3.20) and (10.3.21), implies that $\mathrm{Pr} < 1$. Furthermore, for this case we have

$$\delta \sim x\ \mathrm{Gr}_x^{1/4}.$$

It was mentioned earlier that the Grashof number is usually interpreted as a parameter representing the ratio between the buoyancy and viscous forces. The preceding scaling analysis allows us to interpret Grashof and Rayleigh numbers differently, however. Equations (10.3.11) and (10.3.21) imply (Bejan, 2004) that

$$\mathrm{Ra}_x^{1/4} = \frac{\text{surface height}}{\text{thermal boundary-layer thickness}} \quad \text{for} \quad \mathrm{Pr} > 1,$$

$$(\mathrm{Ra}_x \mathrm{Pr})^{1/4} = \frac{\text{surface height}}{\text{thermal boundary-layer thickness}} \quad \text{for} \quad \mathrm{Pr} < 1,$$

$$\mathrm{Gr}_x^{1/4} = \frac{\text{surface height}}{\text{velocity boundary-layer thickness}} \quad \text{for} \quad \mathrm{Pr} < 1.$$

Thus these dimensionless numbers, when raised to 1/4 power, can be interpreted as strictly geometric parameters that show the slenderness of the boundary layers. For $\mathrm{Pr} < 1$, for example, $\mathrm{Ra}_x^{1/4} \gg 1$ and $(\mathrm{Ra}_x \mathrm{Pr})^{1/4} \gg 1$ imply that boundary layers are very thin in comparison with the height of the surface.

Natural Convection on an Inclined Surface

The analysis thus far dealt with flow on a vertical surface. We now briefly discuss the flow over a flat, inclined surface. Let us start with an assumed 2D external flow in Cartesian coordinates (Fig. 10.5). For simplicity we assume steady state and use

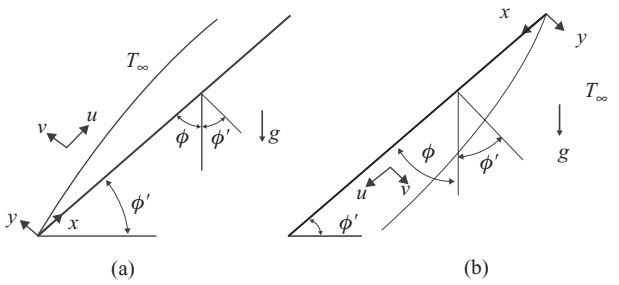

Figure 10.5. Natural-convection boundary layer on an inclined flat surface: (a) flow over the inclined surface, (b) flow under the inclined surface.

Boussinesq's approximation. Then the boundary-layer conservation equations will be [see Fig. 10.5(a)]

$$\frac{\partial u}{\partial x} + \frac{\partial v}{\partial y} = 0, \tag{10.3.23}$$

$$\rho\left(u\frac{\partial u}{\partial x} + v\frac{\partial u}{\partial y}\right) = \mu\left(\frac{\partial^2 u}{\partial x^2} + \frac{\partial^2 u}{\partial y^2}\right) - \rho g\cos\phi - \frac{\partial P}{\partial x}, \tag{10.3.24}$$

$$\rho\left(u\frac{\partial v}{\partial x} + v\frac{\partial v}{\partial y}\right) = \mu\left(\frac{\partial^2 v}{\partial x^2} + \frac{\partial^2 v}{\partial y^2}\right) - \rho g\sin\phi - \frac{\partial P}{\partial y}, \tag{10.3.25}$$

$$u\frac{\partial T}{\partial x} + v\frac{\partial T}{\partial y} = \boldsymbol{\alpha}\left(\frac{\partial^2 T}{\partial x^2} + \frac{\partial^2 T}{\partial y^2}\right). \tag{10.3.26}$$

We can now use the usual boundary-layer approximations. Away from the surface, we have hydrostatic pressure changes only; therefore

$$-\frac{\partial P_\infty}{\partial x} = \rho_\infty g\cos\phi. \tag{10.3.27}$$

Also, with boundary-layer approximations we can write from Eq. (10.3.25)

$$-\frac{\partial P}{\partial y} = \rho g\sin\phi. \tag{10.3.28}$$

Equation (10.3.28) can also be written as

$$-\frac{\partial P}{\partial y} = \rho_\infty\left[1 - \beta\left(T - T_\infty\right)\right] g\sin\phi. \tag{10.3.29}$$

Now we apply $\int_y^\infty$ to both sides of this equation to get

$$P = P_\infty + \int_y^\infty \rho_\infty g\sin\phi\left[1 - \beta\left(T - T_\infty\right)\right] dy. \tag{10.3.30}$$

Differentiating Eq. (10.3.30) with respect to x and using Eq. (10.3.27) to eliminate $\dfrac{\partial P_\infty}{\partial x}$ will give

$$-\frac{\partial P}{\partial x} = \rho_\infty g\cos\phi + \rho_\infty g\sin\phi\frac{d}{dx}\int_y^\infty \beta\left(T - T_\infty\right) dy. \tag{10.3.31}$$

(Note that $\frac{d}{dx}\int_y^\infty \rho_\infty g\sin\phi\ dy = 0$.)

Now we replace for $-\frac{\partial P}{\partial x}$ from Eq. (10.3.31) into Eq. (10.3.24) to get

$$\rho\left(u\frac{\partial u}{\partial x}+v\frac{\partial u}{\partial y}\right)=\mu\left(\frac{\partial^2 u}{\partial x^2}+\frac{\partial^2 u}{\partial y^2}\right)\pm\rho g\beta\cos\phi\,(T-T_\infty)$$
$$\pm\rho_\infty g\beta\sin\phi\frac{d}{dx}\int_y^\infty(T-T_\infty)\,dy. \tag{10.3.32}$$

For the terms that appear with $\pm$ signs, the positive signs are for the flow displayed in Fig. 10.5(a), and the negative signs apply when the flow under that surface is of interest, as shown in Fig. 10.5(b).

Scaling analysis will show that $\frac{\partial^2 u}{\partial x^2}\ll\frac{\partial^2 u}{\partial y^2}$, and therefore the term $\frac{\partial^2 u}{\partial x^2}$ can be neglected. Furthermore, it can be shown that the last term on the right-hand side of the preceding equation (the streamwise pressure gradient caused by buoyancy) is negligible when (Chen and Yuh, 1979)

$$\frac{\delta}{x}\tan\phi\ll 1. \tag{10.3.33}$$

10.4 Similarity Solutions for a Semi-Infinite Vertical Surface

Uniform Wall Temperature

The configuration of the system of interest is similar to that shown in Fig. 10.2. The conservation equations to be solved are Eqs. (10.3.1)–(10.3.3). Let us assume no blowing or suction through the wall and a constant wall temperature T_s. The boundary conditions will then be

$$u=0 \text{ at } x=0, \tag{10.4.1}$$
$$u=0, v=0, \quad T=T_s \text{ at } y=0, \tag{10.4.2}$$
$$u=0, \quad T=T_\infty \text{ at } y\to\infty. \tag{10.4.3}$$

We can obtain a similarity solution by writing for the stream function,

$$\psi=4\nu F(\eta)\left(\frac{\mathrm{Gr}_x}{4}\right)^{1/4}, \tag{10.4.4}$$

where

$$\eta=\frac{y}{x}\left(\frac{\mathrm{Gr}_x}{4}\right)^{1/4}. \tag{10.4.5}$$

$$\mathrm{Gr}_x=\frac{g\beta(T_s-T_\infty)x^3}{\nu^2}. \tag{10.4.6}$$

We can find the velocity components in the (x, y) coordinate system by writing $u=\frac{\partial\psi}{\partial y}$ and $v=-\frac{\partial\psi}{\partial x}$. However, because we are changing coordinates from (x, y) to (x, η) [see Eqs. (3.1.6)–(3.1.9)],

$$v=-\left.\frac{\partial\psi}{\partial x}\right|_\eta-\left.\frac{\partial\eta}{\partial x}\right|_y\frac{\partial\psi}{\partial\eta}, \tag{10.4.7}$$

$$u=+\left.\frac{\partial\eta}{\partial y}\right|_x\frac{\partial\psi}{\partial\eta}. \tag{10.4.8}$$

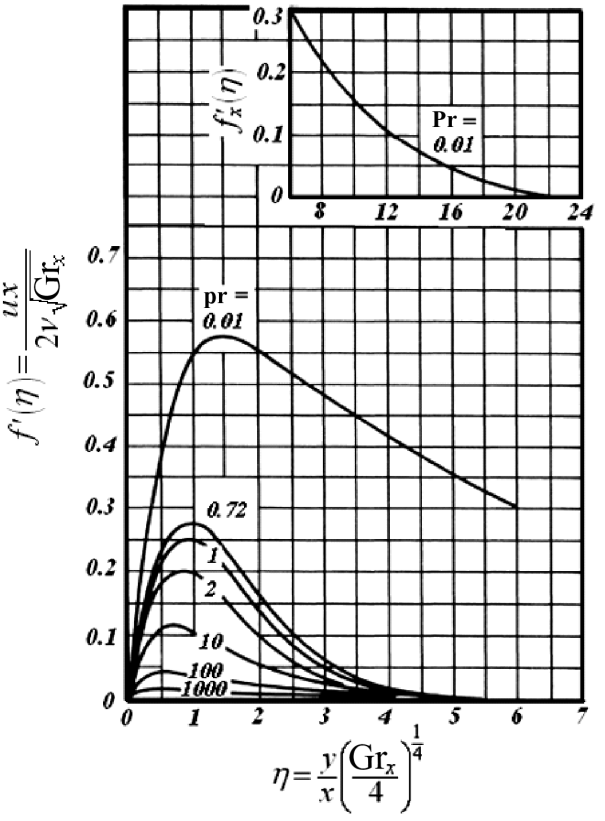

Figure 10.6. Velocity distribution across the boundary layer for natural convection over an isothermal vertical surface (from Ostrach, 1953).

We define a dimensionless temperature as

$$\theta = \frac{T - T_\infty}{T_s - T_\infty}.$$

Also, we assume that $\theta = f(\eta)$. It can then be shown that the stream function defined in Eq. (10.4.4) satisfies mass continuity represented by Eq. (10.3.1), and Eqs. (10.3.2) and (10.3.3) lead to

$$F''' + 3FF'' - 2(F')^2 + \theta = 0, \tag{10.4.9}$$

$$\frac{\theta''}{\text{Pr}} + 3F\theta' = 0. \tag{10.4.10}$$

The boundary conditions will be

$$F = 0, F' = 0, \theta = 1 \text{ at } \eta = 0, \tag{10.4.11}$$

$$F' = 0, \ \theta = 0 \text{ at } \eta \to \infty. \tag{10.4.12}$$

Ostrach (1953) numerically solved the preceding equations for the $0.01 < \text{Pr} < 1000$ range. His calculated velocity and temperature profiles are shown in Figs. 10.6 and 10.7, respectively. These figures show some useful and important features. For $\text{Pr} \gtrsim 1$, as noted, $\delta > \delta_{\text{th}}$. The velocity boundary layer is generally thicker than the thermal boundary layer in such fluids because the buoyant fluid layer causes macroscopic motion in a thicker fluid layer because of the strong viscosity. For fluids with

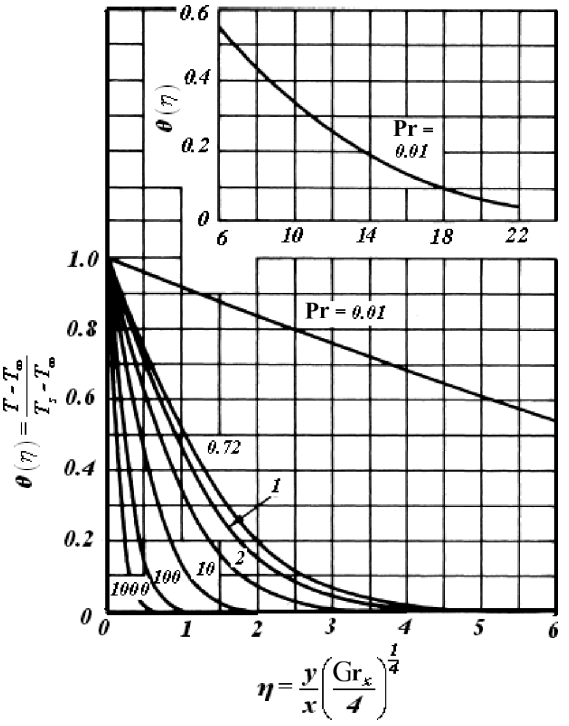

Figure 10.7. Temperature distribution across the boundary layer for natural convection over an isothermal vertical surface (from Ostrach, 1953).

$\mathrm{Pr} \ll 1$, however, the relatively low viscosity makes the effect of shear stress unimportant near the outer edge of the thermal boundary layer, and $\delta_{\mathrm{th}} \geq \delta$ becomes possible.

Now we can write

$$q_s'' = -k\left(\frac{\partial T}{\partial y}\right)_{y=0} = [-\theta'(0)]\,\frac{k\,(T_s - T_\infty)}{x}\left(\frac{\mathrm{Gr}_x}{4}\right)^{1/4}. \tag{10.4.13}$$

Noting that $\theta'(0)$ is only a function of Pr, we can cast Eq. (10.4.13) as

$$\mathrm{Nu}_x = \frac{-\theta'(0)}{\sqrt{2}}\mathrm{Gr}_x^{1/4} = \phi\,(\mathrm{Pr})\;\mathrm{Gr}_x^{1/4}, \tag{10.4.14}$$

where $\mathrm{Nu}_x = \frac{q_s''\,x}{k(T_s - T_\infty)}$. The values of function ϕ can of course be found by numerical solution of Eqs. (10.4.9) and (10.4.10). LeFevre (1956) derived the following curve fit to the numerical results:

$$\phi\,(\mathrm{Pr}) = (4)^{-1/4}\,\frac{0.75\mathrm{Pr}^{1/2}}{(0.609 + 1.221\mathrm{Pr}^{1/2} + 1.238Pr)^{1/4}}. \tag{10.4.15}$$

We can derive the average Nusselt number, defined as $\langle \mathrm{Nu}_l \rangle_l = \langle h \rangle_l\, l/k$, by noting that

$$\langle h \rangle_l = \frac{1}{l}\int_0^l h_x dx,$$

which leads to

$$\langle \mathrm{Nu}_l \rangle_l = \frac{4}{3}\mathrm{Nu}_l. \tag{10.4.16}$$

The preceding solution was based on the assumption that no blowing or suction took place through the wall and that the wall temperature was constant. It can be easily shown that a similarity solution is also possible when (see Problem 10.1)

$$T_s - T_\infty = Ax^n. \tag{10.4.17}$$

The power-law distribution in Eq. (10.4.7) can be very useful, because, in practice, surfaces that are subject to natural convection are not always isothermal. With Eq. (10.4.17), it can be shown that the similarity equations become (Sparrow and Gregg, 1958)

$$F''' + (n+3)\,FF'' - 2\,(n+1)\,(F')^2 + \theta = 0, \tag{10.4.18}$$

$$\frac{\theta''}{\mathrm{Pr}} + (n+3)\,F\theta' - 4nF'\theta = 0. \tag{10.4.19}$$

Furthermore,

$$\mathrm{Nu}_x = \frac{-\theta'(0)}{\sqrt{2}}\mathrm{Gr}_x^{1/4} = \phi\,(\mathrm{Pr}, n)\,\mathrm{Gr}_x^{1/4}. \tag{10.4.19a}$$

This is evidently similar to Eq. (10.4.14), bearing in mind that the function $\theta'(0)$ is now the solution of the preceding equations, and the function $\phi\,(\mathrm{Pr}, n)$ on the right-hand side now depends on parameter n as well. Equation (10.4.19a) shows that $q_s'' \sim x^{\frac{5n-1}{4}}$. Thus the solution with $n = 0$ corresponds to constant wall temperature (UWT boundary condition), and $n = 1/5$ corresponds to constant wall heat flux (UHF boundary conditions). Physically acceptable solutions are possible with $-3/5 < n < 1$.

The aforementioned derivations and solutions are not limited to vertical and flat surfaces. They can be applied to surfaces that are vertical but curved with respect to the horizontal plane, as long as the local radius of curvature of the surface everywhere is much larger than the thickness of the boundary layer. Thus the preceding solutions can be applied to the outside of a vertical cylinder as long as (Sparrow and Gregg, 1956a)

$$\frac{D}{l} > \frac{35}{\mathrm{Gr}_l^{1/4}}. \tag{10.4.20}$$

When this criterion is met, for $\mathrm{Pr} = 0.7$ and $\mathrm{Pr} = 1$, the application of flat-surface solutions introduces less than 5% error in comparison with a solution that explicitly accounts for surface curvature. For fluids with $\mathrm{Pr} \gtrsim 1$ the following criterion can be used (Bejan, 1993):

$$\frac{D}{l} > (\mathrm{Gr}_l\,\mathrm{Pr})^{-1/4}. \tag{10.4.21}$$

When the preceding criteria are not met, we can apply the integral method by taking into account the curvature of the surface. An analysis of this type was made by LeFevre and Ede (1956), with the following result:

$$\mathrm{Nu}_x = \left[\frac{7\,\mathrm{Ra}_x\mathrm{Pr}}{5(20+21\,\mathrm{Pr})}\right]^{1/4} + \frac{4\,(272+345\,\mathrm{Pr})\,x}{35\,(64+63\,\mathrm{Pr})\,D}, \tag{10.4.22}$$

$$\langle \mathrm{Nu}_l \rangle_l = \frac{4}{3}\left[\frac{7\mathrm{Ra}_l\mathrm{Pr}}{5(20+21\,\mathrm{Pr})}\right]^{1/4} + \frac{4\,(272+345\,\mathrm{Pr})\,l}{35\,(64+63\,\mathrm{Pr})\,D}. \tag{10.4.22a}$$

Uniform Wall Heat Flux

We now address the laminar natural convection flow parallel to a flat and vertical surface, with UHF boundary conditions. Equations (10.3.1)–(10.3.3) apply. The boundary conditions are

$$u = 0 \text{ at } x = 0, \tag{10.4.23a}$$

$$u = 0, v = 0, \quad \text{at } y = 0, \tag{10.4.23b}$$

$$u = 0, \quad T = T_\infty \text{ at } y \to \infty. \tag{10.4.23c}$$

We can derive a similarity solution for this system by defining (Sparrow and Gregg, 1956b)

$$\eta = c_1 x^{-1/5} y, \tag{10.4.24}$$

$$\theta(\eta) = \frac{c_1 (T_\infty - T)}{\left(\dfrac{q_s'' x^{1/5}}{k}\right)}, \tag{10.4.25}$$

$$\psi = c_2 x^{4/5} F(\eta), \tag{10.4.26}$$

where

$$c_1 = \left(\frac{g \beta q_s''}{5 k \nu^2}\right)^{1/5}, \tag{10.4.27}$$

$$c_2 = \left(\frac{5^4 g \beta q_s'' \nu^3}{k}\right)^{1/5}. \tag{10.4.28}$$

It can then be easily shown that the stream function of Eq. (10.4.26) satisfies the continuity equation [Eq. (10.3.1)], and Eqs. (10.3.2) and (10.3.3) lead to

$$F''' - 3(F')^2 + 4FF'' - \theta = 0, \tag{10.4.29}$$

$$\theta'' + Pr[4\theta' F - \theta F'] = 0. \tag{10.4.30}$$

It can also be shown that

$$T_s - T_\infty = -5^{1/5} \frac{q_s'' x}{k} \mathrm{Gr}_x^{*-1/5} \theta(0). \tag{10.4.31}$$

The *modified Grashof number* is defined as

$$\mathrm{Gr}_x^* = \frac{g \beta q_s'' x^4}{\nu^2 k}. \tag{10.4.32}$$

In other words, with constant wall heat flux we have $(T_s - T_\infty) \sim x^{1/5}$. We can also show from Eq. (10.4.31) that

$$\mathrm{Nu}_x = -\frac{1}{5^{1/5}} \frac{\mathrm{Gr}_x^{1/5}}{\theta(0)}. \tag{10.4.33}$$

10.5 Integral Analysis

The integral method can be applied to laminar as well as turbulent natural-convection flow on vertical surfaces. It can also be applied to inclined surfaces as

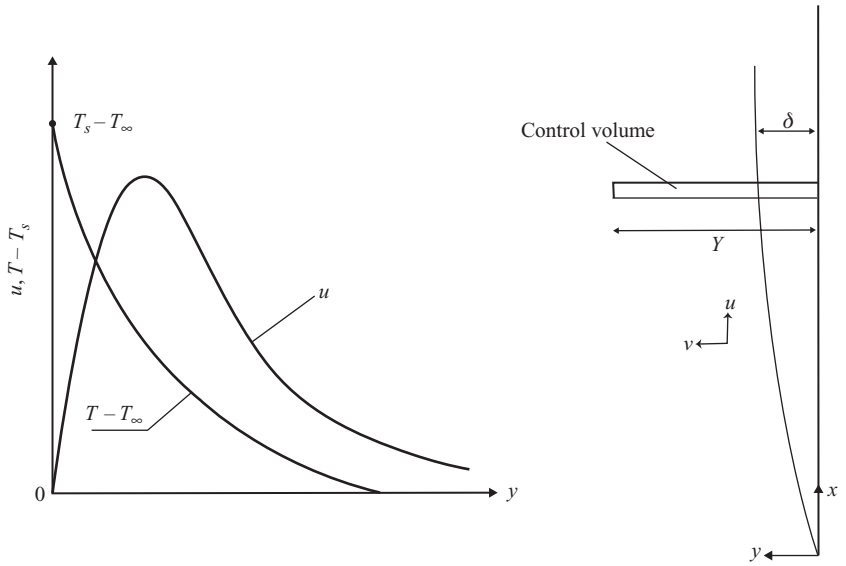

Figure 10.8. Definitions for the integral analysis for natural convection on vertical surfaces.

long as separation and dispersion of the boundary layer do not happen. The general approach is similar to the approach described in detail in Chapter 5.

Consider Fig. 10.8. Assume Pr ≈ 1, so that $\delta = \delta_{\text{th}}$. We define the control volume shown, where $Y = \text{const.}$ and is chosen so that everywhere Y$> \delta$ or δ_{th}. The governing equations are Eqs. (10.3.1)–(10.3.3). Applying $\int_0^Y dy$ to both sides of Eq. (10.3.1) gives

$$v|_Y = v_s - \frac{d}{dx}\int_0^Y u dy. \tag{10.5.1}$$

The second term in Eq. (10.3.2) can be manipulated as

$$v\frac{\partial u}{\partial y} = \frac{\partial}{\partial y}(uv) - u\frac{\partial v}{\partial y}. \tag{10.5.2}$$

Substitution of Eq. (10.5.2) into Eq. (10.3.2) and applying $\int_0^Y dy$ to all the terms in the equation gives

$$\frac{1}{2}\frac{d}{dx}\int_0^Y u^2 dy + u\,v\Big]_0^Y - \int_0^Y u\frac{\partial v}{\partial y} = \int_0^Y g\beta\,(T - T_\infty)\,dy + \left[\nu\frac{\partial u}{\partial y}\right]_0^Y. \tag{10.5.3}$$

Let us assume that $v_s = 0$, in which case the second term on the right-hand side vanishes. We now note that $\frac{\partial v}{\partial y} = -\frac{\partial u}{\partial x}$ and $\nu\frac{\partial u}{\partial y}|_{y=0} = \frac{\tau|_{y=0}}{\rho} = \frac{\tau_s}{\rho}$. Substituting from these expressions into Eq. (10.5.3) and noting that the integrand in each integral term is finite for $y < \delta$ and vanishes for $y \geq \delta$, we find that the latter equation gives

$$\frac{d}{dx}\int_0^\delta u^2 dy - g\beta\int_0^\delta (T - T_\infty)\,dy = -\frac{\tau_s}{\rho}. \tag{10.5.4}$$

We now must deal with Eq. (10.3.3). We note that

$$u\frac{\partial T}{\partial x} = \frac{\partial}{\partial x}\left[u\left(T - T_\infty\right)\right] - \left(T - T_\infty\right)\frac{\partial u}{\partial x}, \tag{10.5.5}$$

$$v\frac{\partial T}{\partial y} = \frac{\partial}{\partial y}\left[v\left(T - T_\infty\right)\right] - \left(T - T_\infty\right)\frac{\partial v}{\partial y}. \tag{10.5.6}$$

Substitution into Eq. (10.3.3) and some simple manipulation leads to

$$\rho\, C_P \frac{d}{dx}\int_0^\delta u\left(T - T_\infty\right) dy = q_s''. \tag{10.5.7}$$

We must now assume appropriate distributions for velocity and temperature. The important boundary conditions that these distributions should satisfy, starting from lowest orders, are as follows:

At $y = 0$,

$$u = 0,\ \ T = T_s \tag{10.5.8}$$

$$\beta g\left(T_s - T_\infty\right) + \nu\frac{\partial^2 u}{\partial y^2} = 0. \tag{10.5.9}$$

At $y = \delta$,

$$u = 0, \quad T = T_\infty, \tag{10.5.10}$$

$$\frac{\partial u}{\partial y} = 0, \quad \frac{\partial T}{\partial y} = 0, \tag{10.5.11}$$

$$\frac{\partial^2 u}{\partial y^2} = 0, \quad \frac{\partial^2 T}{\partial y^2} = 0. \tag{10.5.12}$$

Higher-order boundary conditions can also be included. However, not all of these conditions need to be satisfied by the assumed velocity and temperature profiles, given the approximate nature of these profiles. We can satisfy fewer boundary conditions starting from the ones with lowest orders.

Laminar Flow, Uniform Wall Temperature

Let us use a third-order polynomial for velocity and temperature distributions, namely,

$$u = a\eta^3 + b\eta^2 + c\eta + d,$$
$$T = a'\eta^2 + b'\eta + c'.$$

We now apply Eqs. (10.5.8)–(10.5.12). The results will be

$$u = U_0\eta(1 - \eta)^2, \tag{10.5.13}$$

$$\theta = (1 - \eta)^2, \tag{10.5.14}$$

where U_0 is an as-yet-unknown constant, and

$$\eta = y/\delta, \tag{10.5.15}$$

$$\theta = \frac{T - T_\infty}{T_s - T_\infty}. \tag{10.5.16}$$

Now, using these distributions in Eq. (10.5.4) and (10.5.7), we get (Goldstein et al., 1965)

$$\frac{d}{dx}\left[U_0^2\delta/105\right] = \frac{g\beta\left(T_s - T_\infty\right)}{3}\delta - U_0\frac{\nu}{\delta}, \tag{10.5.17}$$

$$\frac{d}{dx}\left[U_0\delta/30\right] = \frac{2\alpha}{\delta}. \tag{10.5.18}$$

We thus have two differential equations with two unknowns, U_0 and δ. Let us assume that (Burmeister, 1993)

$$U_0 = C_1 x^m, \tag{10.5.19a}$$

$$\delta = C_2 x^n. \tag{10.5.19b}$$

We have now added two new equations, but we have also introduced four new unknowns: C_1, C_2, m, and n. We next substitute these equations into Eqs. (10.5.17) and (10.5.18), thereby getting the following two equations:

$$(2m+1)\,C_1^2C_2^2x^{2m+2n-1} = 35\left[g\beta\left(T_s - T_\infty\right)\right]C_2^2x^{2n} - 105\nu C_1x^m, \tag{10.5.20}$$

$$(m+n)\,C_1C_2^2x^{m+2n-1} = 60\alpha. \tag{10.5.21}$$

For these equations to be satisfied, the terms involving powers of x must disappear from both sides of the equation; therefore

$$2m + 2n - 1 = 2n = m,$$

$$m + 2n - 1 = 0.$$

These two equations are satisfied with

$$m = 1/2,$$

$$n = 1/4.$$

The constants C_1 and C_2 can now be found from Eqs. (10.5.20) and (10.5.21). We eventually get

$$U_0 = 5.17\ \nu\left(\mathrm{Pr} + \frac{20}{21}\right)^{-1/2}\mathrm{Gr}_x^{1/2}x^{-1}, \tag{10.5.22}$$

$$\frac{\delta}{x} = 3.93\mathrm{Pr}^{-1/2}\left(\mathrm{Pr} + \frac{20}{21}\right)^{1/4}\mathrm{Gr}_x^{-1/4}. \tag{10.5.23}$$

We can now find an expression for Nu_x by writing,

$$q_s'' = -k\left.\frac{\partial T}{\partial y}\right|_{y=0} = -k\frac{T_s - T_\infty}{\delta}\left.\frac{\partial\theta}{\partial\eta}\right|_{\eta=0}. \tag{10.5.24}$$

This will give $\mathrm{Nu}_x = \frac{h_x x}{k} = \frac{2x}{\delta}$. Substitution from Eq. (10.5.23) then leads to

$$\mathrm{Nu}_x = 0.508\mathrm{Pr}^{1/2}\left(\mathrm{Pr} + \frac{20}{21}\right)^{-1/4}\mathrm{Gr}_x^{1/4}. \tag{10.5.25}$$

For $\mathrm{Pr} = 0.7$, the preceding equation gives $\mathrm{Nu}_x = 0.302\mathrm{Gr}_x^{1/4}$, which is only 6% higher than the prediction of the exact similarity solution (Goldstein et al., 1965).

Laminar Flow, Uniform Wall Heat Flux

The analysis in this case is similar to what was done for UWT boundary conditions. With q_s'' known, however, the assumed temperature profile must now satisfy the following condition:

$$-k\left.\frac{\partial T}{\partial y}\right|_{y=0} = q_s''. \tag{10.5.26}$$

The dimensionless temperature therefore is defined here as

$$\theta = \frac{T - T_\infty}{\dfrac{q_s''\,\delta}{2\,k}}. \tag{10.5.27}$$

Equations (10.5.13)–(10.5.15) remain unchanged. It can then be shown that, instead of Eqs. (10.5.17) and (10.5.18), we will get (Sparrow, 1955)

$$\frac{1}{105}\frac{d}{dx^*}\left[\Omega^2\Delta\right] = \frac{\Delta^2}{6} - \frac{\Omega}{\Delta}, \tag{10.5.28}$$

$$\frac{1}{30}\frac{d}{dx_*}\left[\Omega\Delta^2\right] = \frac{2}{\mathrm{Pr}}, \tag{10.5.29}$$

where $x^* = x\left(\frac{g\beta q_s''}{k\nu^2}\right)^{1/4}$, and

$$\Delta = \delta\left(\frac{g\,\beta\,q_s''}{k\,\nu^2}\right)^{1/4}, \tag{10.5.30}$$

$$\Omega = U_0\left(\frac{g\,\beta\,q_s''\;\nu^2}{k}\right)^{-1/4}. \tag{10.5.31}$$

The solution to Eqs. (10.5.28) and (10.5.29) is

$$\Omega = (6000)^{1/5}\,\mathrm{Pr}^{-1/5}\,(0.8+\mathrm{Pr})^{-2/5}\,x^{*3/5}, \tag{10.5.32}$$

$$\Delta = (360)^{1/5}\,\mathrm{Pr}^{-2/5}\,(0.8+\mathrm{Pr})^{1/5}\,x^{*1/5}. \tag{10.5.33}$$

These lead to

$$\frac{\delta}{x} = (360)^{1/5}\left[\frac{0.8+\mathrm{Pr}}{\mathrm{Pr}^2\,\mathrm{Gr}_x^*}\right]^{1/5}, \tag{10.5.34}$$

$$\mathrm{Nu}_x = \frac{q_s''\;x}{k\,(T_s - T_\infty)_x} = 0.62\left(\frac{\mathrm{Pr}^2}{0.8+\mathrm{Pr}}\right)^{1/5}\mathrm{Gr}_x^{*1/5}. \tag{10.5.35}$$

The modified Grashof number is defined as

$$\mathrm{Gr}_x^* = \frac{g\,\beta\,q_s''\;x^4}{k\;\nu^2}. \tag{10.5.36}$$

The wall temperature in this case will vary as $\sim x^{1/5}$, according to,

$$T_s - T_\infty = 1.622\frac{q_s''\,x}{k}\left[\frac{0.8+\mathrm{Pr}}{\mathrm{Pr}^2\,\mathrm{Gr}_x^*}\right]^{1/5}. \tag{10.5.37}$$

Sparrow and Gregg (1956b) compared the predictions of this analysis with the predictions of the similarity solution discussed earlier [see Eqs. (10.4.24)–(10.4.33)].

The predictions of the two methods were very similar, and very small deviations between the two methods were observed only as $\mathrm{Pr} \to \infty$.

Integral Analysis of a Turbulent Boundary Layer

The integral method can be readily applied to a turbulent natural-convection boundary layer. Equations (10.5.4) and (10.5.7), with their boundary conditions, are valid for turbulent flow as well. However, the velocity and temperature distributions must be chosen such that they would be representative of a turbulent flow. We can use, following Eckert and Jackson (1950),

$$u = U_0 \eta^{1/7} (1 - \eta)^4, \tag{10.5.38}$$

$$\theta = 1 - \eta^{1/7}. \tag{10.5.39}$$

Alternatively, we can assume that

$$u = U_0 \eta^{1/n} (1 - \eta)^2, \tag{10.5.40}$$

$$\theta = 1 - \eta^{1/n}. \tag{10.5.41}$$

A detailed derivation based on Eqs. (10.5.40) and (10.5.41) can be found in Oosthuizen and Naylor (1999), which leads to the general solution of the form

$$\mathrm{Nu}_x = f(\mathrm{Pr})\mathrm{Gr}_x^{0.4}, \tag{10.5.42}$$

$$\langle \mathrm{Nu}_l \rangle_l = \frac{1}{1.2} f(\mathrm{Pr})\mathrm{Gr}_l^{0.4}, \tag{10.5.43}$$

where $f(\mathrm{Pr})$ is a coefficient that is a function of Pr. Assuming that $n = 7$ and for $\mathrm{Pr} = 0.7$, these result in

$$\mathrm{Nu}_x = 0.0185\mathrm{Gr}_x^{0.4}, \tag{10.5.44}$$

$$\langle \mathrm{Nu}_l \rangle_l = 0.0154\mathrm{Gr}_l^{0.4}. \tag{10.5.45}$$

10.6 Some Widely Used Empirical Correlations for Flat Vertical Surfaces

For fluids with $\mathrm{Pr} \approx 1$, McAdams (1954) proposed,

$$\langle \mathrm{Nu}_l \rangle_l = 0.59\mathrm{Ra}_l^{1/4} \text{ for } 10^4 < \mathrm{Ra}_l < 10^9 \text{ (laminar flow)}, \tag{10.6.1}$$

$$\langle \mathrm{Nu}_l \rangle_l = 0.1\mathrm{Ra}_l^{1/3} \text{ for } 10^9 < \mathrm{Ra}_l < 10^{13} \text{ (turbulent flow)}. \tag{10.6.2}$$

An empirical, composite correlation that is valid over the entire Ra_l range is (Churchill and Chu, 1975a),

$$\langle \mathrm{Nu}_l \rangle_l = \left\{ 0.825 + \frac{0.387\mathrm{Ra}_l^{1/6}}{\left[1 + (0.492/\mathrm{Pr})^{9/16}\right]^{8/27}} \right\}^2. \tag{10.6.3}$$

The following correlation for a laminar boundary layer (i.e., for a $\mathrm{Ra}_l < 10^9$), also proposed by Churchill and Chu (1975a), is slightly more accurate than Eq. (10.6.3):

$$\langle \mathrm{Nu}_l \rangle_l = 0.68 + \frac{0.670\mathrm{Ra}_l^{1/4}}{\left[1 + (0.492/\mathrm{Pr})^{9/16}\right]^{4/9}}. \tag{10.6.4}$$

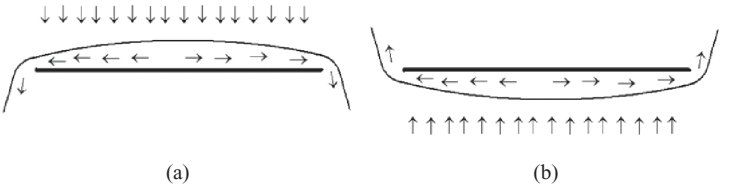

(a) (b)

Figure 10.9. Natural-convection flow field on a flat horizontal surface when gravity is stabilizing: (a) cooled, upward facing; (b) heated, downward facing.

The preceding correlations all are applicable to constant wall temperature (UWT conditions), and all properties used in these correlations can be calculated at $T_{\text{film}} = \frac{1}{2}(T_s + T_\infty)$.

For constant wall heat flux (UHF) boundary conditions, we have $(T_s - T_\infty) \sim x^{1/5}$, as shown earlier in Section 10.4 [see the discussion under Eq. (10.4.32)]. Furthermore, laminar–turbulent transition occurs at (Bejan, 2004)

$$\text{Ra}^*_{x,\,\text{cr}} \approx 10^{13}, \tag{10.6.5}$$

where

$$\text{Ra}^*_x = \text{Gr}^*_x \text{Pr} = \frac{g\beta\, q''_s\, x^4}{k\, \nu \boldsymbol{\alpha}}. \tag{10.6.6}$$

The following correlations were proposed for UHF boundary conditions by Vliet and Liu (1969), based on experiments with water (Jaluria, 2003).

For laminar flow,

$$\text{Nu}_x = 0.60\text{Ra}^{*1/5}_x \text{ for } 10^5 < \text{Ra}^*_x < 10^{13}, \tag{10.6.7}$$

$$\langle \text{Nu}_l \rangle_l = 1.25\text{Nu}_l \text{ for } 10^5 < \text{Ra}^*_l < 10^{11}. \tag{10.6.8}$$

For turbulent flow,

$$\text{Nu}_x = 0.568\text{Ra}^{*0.22}_x \text{ for } 10^{13} < \text{Ra}^*_x < 10^{16}, \tag{10.6.9}$$

$$\langle \text{Nu}_l \rangle_l = 1.136\,\text{Nu}_l \text{ for } 2 \times 10^{13} < \text{Ra}^*_x < 10^{16}. \tag{10.6.10}$$

Note that in correlations for the average Nusselt number under UHF boundary conditions, $\langle \text{Nu}_l \rangle_l$ is defined based on the average wall surface temperature, i.e.,

$$\langle \text{Nu}_l \rangle_l = \frac{q''_s\, l}{k\,(\langle T \rangle_l - T_\infty)}. \tag{10.6.11}$$

From experimental data obtained with air, Vliet and Ross (1975) derived the following correlation for the UHF boundary conditions:

$$\langle \text{Nu}_l \rangle_l = 0.55\,\text{Ra}^{*1/5}_l \text{ for laminar flow,} \tag{10.6.12}$$

$$\langle \text{Nu}_l \rangle_l = 0.17\,\text{Ra}^{*1/4}_l \text{ for turbulent flow.} \tag{10.6.13}$$

10.7 Natural Convection on Horizontal Flat Surfaces

Natural convection can occur on flat horizontal surfaces even though the gravity vector has no component parallel to these surfaces.

First, let us consider the conditions displayed in Fig. 10.9. In the case of a cooled, downward-facing surface, when $|T_s - T_\infty|$ is moderate, the fluid at the vicinity of the

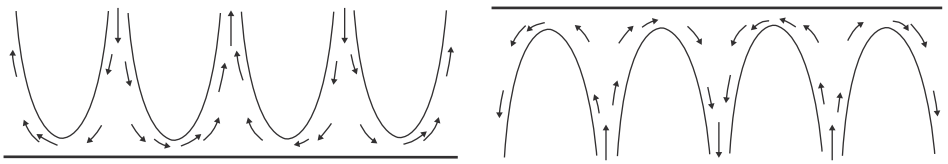

(a) (b)

Figure 10.10. Natural-convection flow field on horizontal surfaces, when gravity is destabilizing: (a) heated, upward facing; (b) cooled, downward facing.

surface cools and becomes denser than the surrounding fluid. A flow field develops that leads to the spilling or overflowing of the denser fluid at the periphery of the surface, while a downward-moving plume replenishes the denser fluid that has spilled around the surface. When $|T_s - T_\infty|$ is large, however, the flow field will consist of sinking balls of cold fluid and will be considerably more complicated. Essentially the same phenomenology will occur in the case a warm, downward-facing horizontal surface, only in the opposite direction.

The phenomenology is complicated for a heated, upward-facing flat surface, or equivalently for a cooled, downward-facing flat surface. These are shown schematically in Fig. 10.10. In the case of a heated, upward-facing surface, for example, a uniformly rising plume from the entire surface would evidently be impossible. Instead, "thermals" develop, which are essentially balls of warm fluid rising intermittently from the vicinity of the surface, only to be replaced with cool fluid that sinks toward the surface in between the thermals. The pictures shown in Fig. 10.3 display the thermals observed in an experiment. Once again, essentially the same phenomenology occurs on a cooled, downward-facing flat surface, only in the opposite direction.

Empirical correlations for natural convection on horizontal flat surfaces are often based on the characteristic length l_c, defined as,

$$l_c = A/p. \tag{10.7.1}$$

where A is the total surface area of the heated or cooled surface and p is its perimeter. Some widely applied correlations are as follows.

For cooled, upward-facing surfaces or heated, downward-facing surfaces, McAdams (1954) proposed, both with UWT boundary conditions,

$$\langle \mathrm{Nu}_{l_c} \rangle = 0.27\ \mathrm{Ra}_{l_c}^{1/4}. \tag{10.7.2}$$

The range of validity for this correlation is

$$10^5 \lesssim \mathrm{Ra}_{l_c} \lesssim 10^{10}.$$

For upward-facing heated surfaces or downward-facing cooled surfaces, with UWT boundary conditions,

$$\langle \mathrm{Nu}_{l_c} \rangle = 0.54\ \mathrm{Ra}_{l_c}^{1/4} \text{ for } 10^5 \lesssim \mathrm{Ra}_{l_c} \lesssim 10^7, \tag{10.7.3}$$

$$\langle \mathrm{Nu}_{l_c} \rangle = 0.15\ \mathrm{Ra}_{l_c}^{1/3} \text{ for } 10^7 \lesssim \mathrm{Ra}_{l_c} \lesssim 10^{11}. \tag{10.7.4}$$

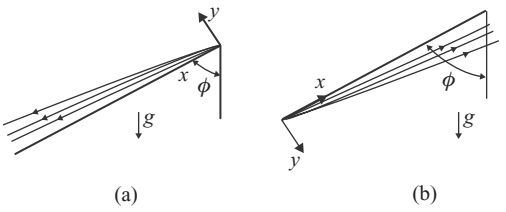

Figure 10.11. Natural-convection flow field on an inclined surface when the buoyancy force is oriented toward the surface: (a) upward-facing, cooled surface; (b) downward-facing, heated surface.

For UHF boundary conditions, instead of Eqs. (10.7.3) or (10.7.4), the following correlations can be used (Fujii and Imura, 1972):

$$\langle \mathrm{Nu}_{l_c} \rangle = 0.13\ \mathrm{Ra}_{l_c}^{1/3} \text{ for } \mathrm{Ra}_{l_c} > 5 \times 10^8, \tag{10.7.5}$$

$$\langle \mathrm{Nu}_{l_c} \rangle = 0.16\ \mathrm{Ra}_{l_c}^{1/3} \text{ for } \mathrm{Ra}_{l_c} < 2 \times 10^8. \tag{10.7.6}$$

10.8 Natural Convection on Inclined Surfaces

For natural convection on a upward-facing cooled surface or a downward-facing heated surface (Fig. 10.11), the component of gravitational body force in the boundary layer in the direction normal to the surface is oriented toward the surface. The boundary layer therefore remains coherent. The analyses and correlations for natural convection on vertical flat surfaces all are applicable to these configurations, provided that everywhere in these models and correlations g is replaced with $g \cos \phi$.

The situation is different when natural convection occurs on a heated, upward-facing or cooled, downward-facing surface, as shown in Fig. 10.12. In this case the normal component (in the y direction) of the body force acting on the fluid in the boundary layer is oriented away from the surface and tends to disrupt the boundary layer. The stability and coherence of the boundary layer will depend on the angle of inclination of the surface. When $\phi \lesssim 60^\circ$, the boundary layer remains stable and models and correlations associated with vertical surfaces can be used simply by replacing g with $g \cos \phi$. For $\phi \gtrsim 60^\circ$, however, intermittent discharging of fluid from the boundary layer takes place (Fig. 10.12). The resulting intermittent disruption and thinning of the boundary layer actually enhances heat transfer.

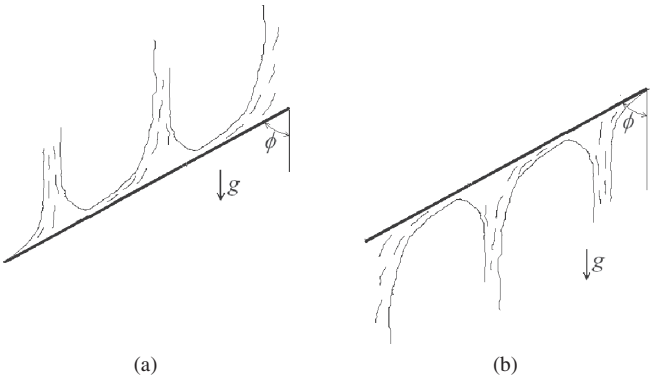

Figure 10.12. Natural-convection on an inclined surface when buoyancy causes flow intermittency: (a) upward-facing, heated surface; (b) downward-facing, cooled surface.

Table 10.1. *Laminar–turbulent transition for natural convection on flat inclined surfaces (heated and upward facing or cooled and downward facing)*

UWT surface boundary conditions (Lloyd and Sparrow, 1970)		UHF surface boundary conditions (Vliet, 1969)	
$\phi(^\circ)$	Ra_x	$\phi(^\circ)$	$\mathrm{Ra}_x{}^*$
0	8.7×10^8	0	5×10^{12}–10^{14}
20	2.5×10^8	30	3×10^{10}–10^{12}
45	1.7×10^7	60	6×10^7–6×10^9
60	7.7×10^5		

The angle of inclination has an important effect on the laminar–turbulent flow regime transition, even for conditions in which the boundary layer remains coherent. For a vertical surface, as mentioned earlier, the transition occurs at $\mathrm{Ra}_x \approx 10^9$ on a uniform surface temperature and at $\mathrm{Ra}_x^* \approx 10^{13}$ for a uniform surface heat flux. From experiments with water ($\mathrm{Pr} \approx 6.0$–6.5) Vliet (1969) and Lloyd and Sparrow (1970) reported their observations, which are summarized in Table 10.1.

Correlations are relatively scarce for conditions in whcih intermittent flow occurs, and interpolation may therefore be used for the estimation of the heat transfer coefficient. The following correlation was proposed based on the work of Fujii and Imura (1972) for intermittent-flow natural convection on an upward-facing, inclined surface subject to a constant heat flux (Jaluria, 2003);

$$\langle \mathrm{Nu}_l \rangle_l = 0.14\left[\mathrm{Ra}_l^{1/3} - \mathrm{Ra}_{\mathrm{cr}}^{1/3}\right] + 0.56\,(\mathrm{Ra}_{\mathrm{cr}} \cos\phi)^{1/4}, \tag{10.8.1}$$

where $\langle \mathrm{Nu}_l \rangle_l$ is defined based on $|T_{sl} - T_\infty|$. The ranges of parameters for this correlation are

$$10^5 < \mathrm{Ra}_l \cos\phi < 10^{11}, \tag{10.8.2}$$

$$15^\circ < \phi < 75^\circ. \tag{10.8.3}$$

The critical Rayleigh number is defined as $\mathrm{Ra}_{\mathrm{cr}} = \mathrm{Gr}_{\mathrm{cr}}\mathrm{Pr}$, and $\mathrm{Gr}_{\mathrm{cr}}$ is the Grashof number at which a deviation from laminar flow is first observed. The preceding correlation is applicable only when $\mathrm{Gr}_l > \mathrm{Gr}_{\mathrm{cr}}$, and, according to Fujii and Imura,

$$\mathrm{Gr}_{\mathrm{cr}} = \begin{cases} 5 \times 10^9 & \text{for } \phi = 15^\circ \\ 2 \times 10^9 & \text{for } \phi = 30^\circ \\ 10^8 & \text{for } \phi = 60^\circ \\ 10^6 & \text{for } \phi = 70^\circ \end{cases}. \tag{10.8.4}$$

10.9 Natural Convection on Submerged Bodies

First, let us consider the phenomenology of natural convection over a heated, horizontal cylinder, which is representative of the overall phenomenology of natural convection on other blunt bodies.

The flow field around the cylinder is schematically shown in Fig. 10.13. A boundary layer forms over the bottom surface of the cylinder and grows in thickness as it

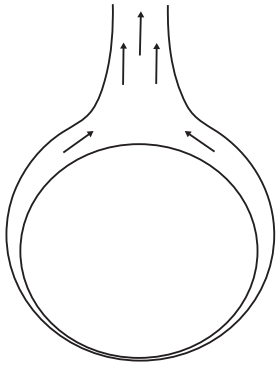

Figure 10.13. Natural-convection boundary layer on a horizontal heated cylinder.

flows upward around the cylinder. This results in a nonuniform heat transfer coefficient around the cylinder. The boundary layer eventually ends by forming a rising plume. The boundary layer can become turbulent over a portion of the cylinder. Such a transition to a turbulent boundary layer occurs on the cylinder when $\mathrm{Ra}_D \gtrsim 10^9$, where

$$\mathrm{Ra}_D = \frac{g\beta\,|T_s - T_\infty|\,D^3}{\nu\,\alpha}. \tag{10.9.1}$$

The phenomenology for natural convection over a sphere is similar to what was described for cylinders, except that the boundary layer and the flow field will now be 3D.

For laminar flow free convection on blunt bodies of various shapes, Yovanovich (1987) proposed the forthcoming simple correlation,

$$\langle \mathrm{Nu}_{l_c} \rangle = \langle \mathrm{Nu}_{l_c} \rangle_{\mathrm{Ra}_{l_c} \to 0} + \frac{0.67 G_{l_c} \mathrm{Ra}_{l_c}^{1/4}}{\left[1 + (0.492/\mathrm{Pr})^{9/16}\right]^{4/9}}, \tag{10.9.2}$$

where l_c is a characteristic length defined as

$$l_c = \sqrt{A}, \tag{10.9.3}$$

where A is the total surface area. The coefficient G_{l_c} is a geometric parameter, and $\langle \mathrm{Nu}_{l_c} \rangle_{\mathrm{Ra}_{l_c} \to 0}$ represents the average Nusselt number at the limit of $\mathrm{Ra}_{l_c} \to 0$, namely, when heat transfer is due to pure conduction. Table 10.2 is a summary of the constants in Yovanovich's correlation for various body shapes. Figure 10.14 displays the configuration and orientations of the body shapes that are listed in Table 10.2. Equation (10.9.2) is valid for laminar flow, i.e., for

$$\mathrm{Ra}_{l_c} < 10^8. \tag{10.9.4}$$

For long horizontal cylinders the following empirical correlation can be applied for $10^{-5} \le \mathrm{Ra}_D \le 10^{12}$ (Churchill and Chu, 1975b):

$$\langle \mathrm{Nu}_D \rangle = \frac{\langle h \rangle\, D}{k} = \left\{ 0.6 + \frac{0.387 \mathrm{Ra}^{1/6}}{\left[1 + \left(\frac{0.559}{\mathrm{Pr}}\right)^{9/16}\right]^{8/27}} \right\}^2. \tag{10.9.5}$$

Table 10.2. *Constants for Yovanovich's correlation (Yovanovich, 1987; Bejan, 2004)*

Body shape	$\langle \mathrm{Nu}_{l_c} \rangle_{\mathrm{Ra}_{l_c} \to 0}$	G_{l_c}
Sphere	3.545	1.023
Bisphere	3.475	0.928
Cube 1	3.388	0.951
Cube 2	3.388	0.990
Cube 3	3.388	1.014
Vertical cylinder[a]	3.444	0.967
Horizontal cylinder[a]	3.444	1.019
Cylinder[a] at 45°	3.444	1.004
Prolate spheroid ($C/B = 1.93$)	3.566	1.012
Prolate spheroid ($C/B = 0.5$)	3.529	0.973
Oblate spheroid ($C/B = 0.1$)	3.342	0.768

[a] Short cylinder with equal height and diameter.

10.10 Natural Convection in Vertical Flow Passages

Analysis of Laminar Flow Between Two Parallel Plates

One of the simplest internal natural-convection flows is the flow between two heated (or cooled) infinitely large parallel plates, shown in Fig. 10.15. The boundary condition is UWT. The channel is open to a large volume of fluid where the fluid bulk is quiescent. Natural-convection boundary layers form on both channel walls at the

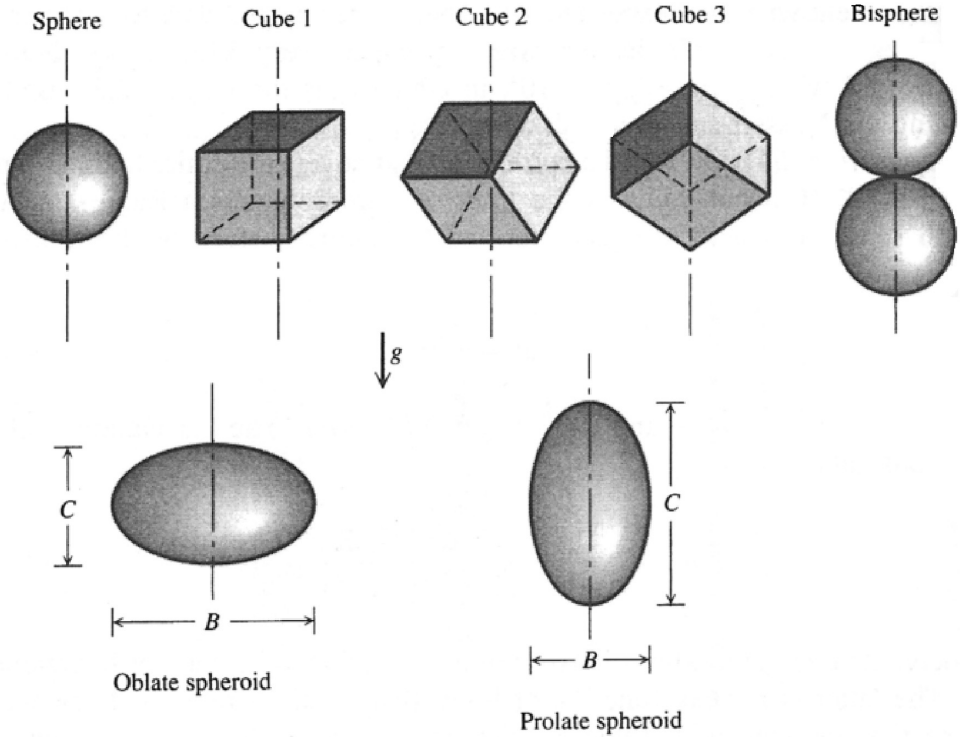

Figure 10.14. Body shapes and flow orientations referred to in Table 10.2 (after Bejan, 2004).

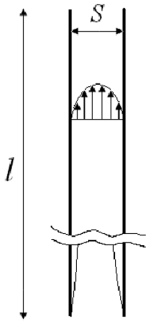

Figure 10.15. Natural convection in the space between two heated vertical parallel parallel surfaces.

inlet and grow in thickness with increasing distance from the inlet. Near the inlet, and as long as $\delta \ll S$ and $\delta_{\text{th}} \ll S$, the boundary layers are identical to the boundary layers that occur in natural convection on infinitely large vertical flat surfaces. As the boundary layers grow with distance from the inlet, however, at some point their thicknesses become comparable with S. If the channel is sufficiently long, the boundary layers on the two walls will eventually merge.

The conservation equations for steady, 2D flow (Fig. 10.15) are

$$\frac{\partial u}{\partial x} + \frac{\partial v}{\partial y} = 0, \tag{10.10.1}$$

$$u\frac{\partial u}{\partial x} + v\frac{\partial u}{\partial y} = \nu\frac{\partial^2 u}{\partial y^2} - \frac{1}{\rho}\frac{dP}{dx} - [1 - \beta\,(T - T_{\text{in}})]\,g, \tag{10.10.2}$$

$$u\frac{\partial T}{\partial x} + v\frac{\partial T}{\partial y} = \boldsymbol{\alpha}\frac{\partial^2 T}{\partial y^2}, \tag{10.10.3}$$

where Boussinesq's approximation has been used. These equations need to be solved, often numerically, noting that

$$P_{\text{in}} - P_{\text{out}} = \rho_{\text{in}} g l, \tag{10.10.4}$$

where subscripts in and out represent the channel inlet and outlet, respectively, and properties at the inlet also represent the properties of the ambient fluid outside the channel.

Two limiting conditions can be considered for which simple solutions can be derived:

1. When $\delta \ll S$ and $\delta_{\text{th}} \ll S$ everywhere (the wide-channel conditions). For fluids with $\text{Pr} \gtrsim 1$, these conditions are met when

$$(S/l) \gg \text{Ra}_l^{-1/4} \text{ or } \text{Ra}_S^{-1}. \tag{10.10.5}$$

   In this case, we can simply use the correlations for vertical, flat surfaces in infinite, quiescent fluid fields.
2. When the boundary layers on the two sides of the channel merge and the channel over most of its length is subject to essentially a boundary-layer flow. The flow field over most of the channel length in this case is similar to thermally developed internal flow in forced convection. For laminar flow it can be shown

that the thermal boundary layer engulfs the entire channel over most of its length when

$$(S/l) < \mathrm{Ra}_l^{-1/4} \text{ or } \mathrm{Ra}_S^{-1}. \tag{10.10.6}$$

This expression represents the narrow-channel limit.

In the latter case, because a thermally developed flow can be assumed, we can make a channel flow analysis by noting that Eq. (10.10.2) reduces to

$$\nu \frac{\partial^2 u}{\partial y^2} + \beta (T_s - T_{\text{in}}) g = 0, \tag{10.10.7}$$

where we have used

$$\frac{dP}{dx} = -\rho_{\text{in}} g, \tag{10.10.8}$$

$$T - T_{\text{in}} \approx T_s - T_{\text{in}}. \tag{10.10.9}$$

The justification for Eq. (10.10.9) is that because the wall–fluid heat transfer coefficient near the inlet is significantly larger than the heat transfer coefficient at locations far from the inlet, far from the channel inlet we have,

$$T_s - T_{\text{in}} \ll T_s - T. \tag{10.10.10}$$

Now we define the following two average Nusselt number definitions:

$$\langle \mathrm{Nu}_l \rangle_l = \frac{\langle q_s'' \rangle}{T_s - T_{\text{in}}} \frac{l}{k}, \tag{10.10.11a}$$

$$\langle \mathrm{Nu}_S \rangle_l = \frac{\langle q_s'' \rangle}{T_s - T_{\text{in}}} \frac{S}{k}, \tag{10.10.11b}$$

where $\langle q_s'' \rangle$ is the average heat flux over the entire heat transfer surface area. Equations (10.10.7) and (10.10.3) can now be solved. [Note that in Eq. (10.10.3), the second term on the left-hand side vanishes because $v = 0$]. The solutions of these equations then lead to

$$\langle \mathrm{Nu}_l \rangle_l = \mathrm{Ra}_S/24, \tag{10.10.12a}$$

$$\langle \mathrm{Nu}_S \rangle_l = \frac{S}{l} \frac{\mathrm{Ra}_S}{24}. \tag{10.10.12b}$$

For the case of parallel plates, when one surface is isothermal while the other surface is adiabatic, the analysis will give

$$\langle \mathrm{Nu}_l \rangle_l / \mathrm{Ra}_S = 1/12. \tag{10.10.13}$$

Thermally Developed Laminar Flow in Some Channel Geometries

A similar analysis can be carried out for other channel geometries subject to UWT boundary conditions when the narrow-channel limit applies and therefore thermally developed flow is justified, i.e., when

$$\frac{D_H}{l} > \mathrm{Ra}_{D_H}^{-1}.$$

The results of such an analysis for several channel geometries are given in Table 10.3.

Table 10.3. *Average Nusselt numbers for chimney flow in various channel geometries (Bejan, 1993)*

Cross–section geometry	$\langle \mathrm{Nu}_l \rangle_l / \mathrm{Ra}_{D_H}$
Parallel plates	1/192
Circular	1/128
Square	1/113.6
Equilateral triangle	1/106.4

Empirical Correlations for Flow Between Two Vertical Parallel Plates

For natural convection of air between two parallel plates with UWT boundary conditions, over the range $0.1 \lesssim (S/l)\mathrm{Ra}_S \lesssim 10^5$, Elenbaas (1942) proposed

$$\langle \mathrm{Nu}_S \rangle_l = \frac{\mathrm{Ra}_S}{24} \left(\frac{S}{l} \right) \left\{ 1 - \exp \left(- \frac{35}{\mathrm{Ra}_S (\frac{S}{l})} \right) \right\}^{3/4}. \tag{10.10.14}$$

This correlation is semiempirical and is an adjustment to the analytical expression in Eq. (10.10.12b).

Bar-Cohen and Rohsenow (1984) proposed the following correlations, which are meant to be applicable to all aspect ratios (all l/S ratios).

For UWT conditions,

$$\langle \mathrm{Nu}_S \rangle_l = \left[\frac{C_1}{\left(\frac{S}{l} \mathrm{Ra}_S \right)^2} + \frac{C_2}{\left(\frac{S}{l} \mathrm{Ra}_S \right)^{1/2}} \right]^{-1/2}. \tag{10.10.15}$$

For UHF conditions, let us define

$$\mathrm{Ra}_S^* = \frac{g \beta q_s'' S^4}{k \alpha \nu}, \tag{10.10.16}$$

$$\mathrm{Nu}_{S,l} = \frac{q_s''}{T_s|_{x=l} - T_{\mathrm{in}}} \frac{S}{k}. \tag{10.10.17}$$

Then,

$$\mathrm{Nu}_{S,l} = \left[\frac{C_1}{\frac{S}{l} \mathrm{Ra}_S^*} + \frac{C_2}{\left(\frac{S}{l} \mathrm{Ra}_S^* \right)^{2/5}} \right]^{-1/2}. \tag{10.10.18}$$

The constants C_1 and C_2 can be found in Table 10.4. The optimum plate spacings for maximizing the heat transfer rate from an array of parallel plates, S_{opt}, and for maximizing the heat transfer rate from each individual plate, S_{max}, are also provided in the table. The properties to be used in these correlations should be found at $(T_s + T_{\mathrm{in}})/2$ for the UWT conditions and $(T_s|_{x=l} - T_{\mathrm{in}})/2$ for UHF boundary conditions.

Table 10.4. *The coefficients and parameters in the correlation of Bar-Cohen and Rohsenow (1984)*

Surface conditions	C_1	C_2	S_{opt}	S_{max}/S_{opt}
UWT	576	2.87	$2.71\left(\mathrm{Ra}_S/S^3l\right)^{-1/4}$	1.71
UHF	48	2.51	$2.12\left(\mathrm{Ra}^*_S/S^4l\right)^{-1/5}$	4.77
One surface isothermal, one surface adiabatic	144	2.87	$2.15\left(\mathrm{Ra}_S/S^3l\right)^{-1/4}$	1.71
One surface UHF, one surface adiabatic	24	2.51	$1.69\left(\mathrm{Ra}^*_S/S^4l\right)^{-1/5}$	4.77

10.11 Natural Convection in Enclosures

Natural convection in close spaces (enclosures) is common. Some examples include solar collectors, furnaces, the space between double windows, large and small buildings, and the containment of nuclear reactors. Natural convection in enclosures is more complicated than natural convection in external flow or channel flow conditions. One or more recirculation flow patterns can form in enclosures. In large or irregular-shaped enclosures, e.g., in large buildings, a multitude of 3D recirculation loops with vastly different lengths and recirculation time scales can form. Multiple recirculation loops are also possible, even in relatively simple enclosure geometries. Figure 10.16 displays the recirculation flow in the 2D simulation of laminar natural convection around an isothermal equilateral pipe coaxially enclosed inside an

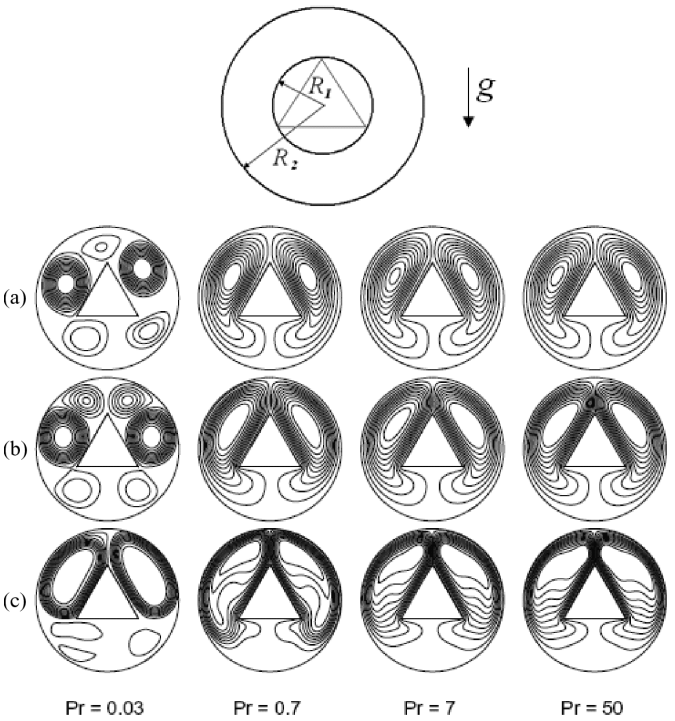

Figure 10.16. Natural circulation in the space between two concentric isothermal triangular and circular pipes, $R_2/R_1 = 2$; (a) $\mathrm{Ra}_{R_2-R_1} = 10^3$, (b) $\mathrm{Ra}_{R_2-R_1} = 10^4$, and (c) $\mathrm{Ra}_{R_2-R_1} = 10^5$ (from Yu et al., 2010).

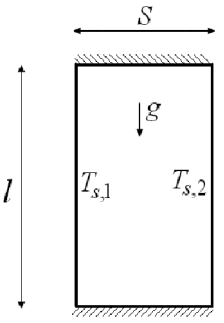

Figure 10.17. Natural convection in a 2D rectangular enclosure with isothermal sides and adiabatic top and bottom.

isothermal cylindrical pipe (Yu et al., 2010). The length scale in the definition of Rayleigh number is $R_2 - R_1$, and the aspect ratio is defined as $\alpha^* = R_2/R_1$. Multiple recirculation patterns can be noted at the lowest Prandtl number.

10.12 Natural Convection in a Two-Dimensional Rectangle With Heated Vertical Sides

This is among the most intensively studied natural convection problems. Consider the system shown in Fig. 10.17. A detailed analysis and discussion of the flow and heat transfer can be found in Bejan (2004). Analysis and experiment show that the recirculation flow characteristics depend strongly on the enclosure aspect ratio, l/S, and the Rayleigh number based on the enclosure height, Ra_l. Generally speaking, for laminar flow, four different flow and heat transfer regimes can be defined, as displayed in the flow regime map of Fig. 10.18. The flow regimes are shown schematically in Fig. 10.19.

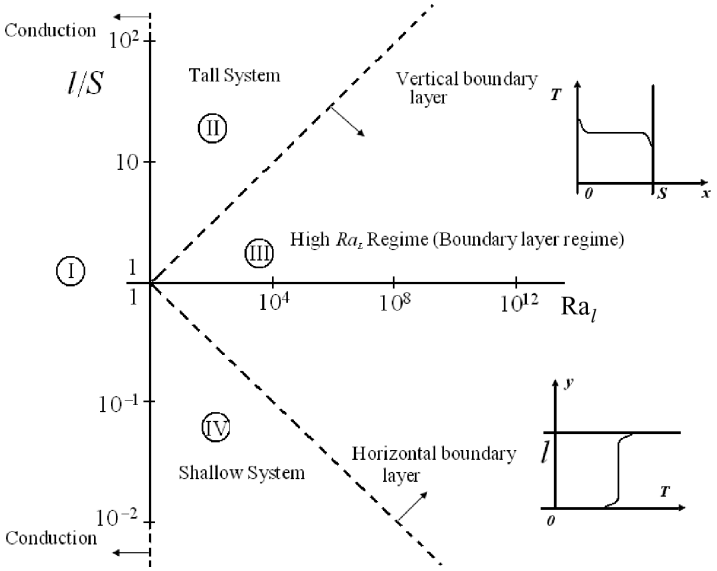

Figure 10.18. Natural-convection flow and heat transfer regimes in a vertical rectangular enclosure with isothermal vertical sides and adiabatic horizontal sides (after Bejan, 2004).

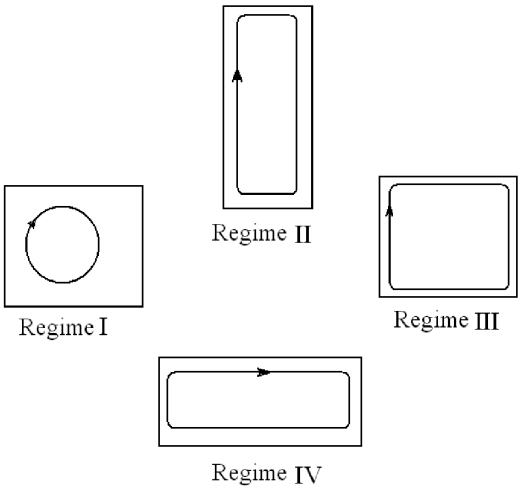

Figure 10.19. Schematic of the recirculation flow patterns associated with the flow regimes of Fig. 10.18.

When $\mathrm{Ra}_l < 1$, the buoyancy effect is too weak to cause significant convection. Thus, except for a slow-moving recirculation loop that has little effect on heat transfer, the fluid is relatively stagnant. The temperature variation in the horizontal direction is approximately linear, and the heat flux (heat transfer rate per unit surface area of the sidewall) is

$$q_s'' = k\frac{T_{\mathrm{s},1} - T_{\mathrm{s},2}}{S}. \tag{10.12.1}$$

This is equivalent to

$$\mathrm{Nu}_S = \frac{q_s''}{T_{s,1} - T_{s,2}}\frac{S}{k} = 1. \tag{10.12.2}$$

The *tall-enclosure* regime covers the range

$$\mathrm{Ra}_l > 1, \tag{10.12.3a}$$

$$l/S > \mathrm{Ra}_l^{1/4}. \tag{10.12.3b}$$

In this regime the lateral temperature profile remains linear, and $\mathrm{Nu}_S \gtrsim 1$. Distinct fluid layers can be observed neat the top and bottom horizontal boundaries.

The *boundary-layer* regime occurs over the parameter range,

$$\mathrm{Ra}_l > 1, \tag{10.12.4a}$$

$$\mathrm{Ra}_l^{-1/4} < l/S < \mathrm{Ra}_l^{1/4}. \tag{10.12.4b}$$

This is a convection-dominated regime. Distinct boundary layers form next to the vertical surfaces. The boundary layers thus constitute the recirculation flow loop while the core of the enclosure remains approximately stagnant, and the heat flux is of the order of $q_s'' \approx k(T_{s,1} - T_{s,2})/\delta_{\mathrm{th}}$.

The *shallow-enclosure* regime occurs in the parameter range

$$\mathrm{Ra}_l > 1, \tag{10.12.5a}$$

$$l/S < \mathrm{Ra}_l^{-1/4}. \tag{10.12.5b}$$

This regime is also dominated by convection. It is characterized by a counterflow pattern in the horizontal direction and thermal boundary layers on the vertical sides. The boundary layers, as well as the long horizontal core, contribute to the thermal resistance for heat transfer between the two isothermal sides.

Empirical Correlations

Empirical correlations are often in terms of Ra_S, defined as

$$\mathrm{Ra}_S = \frac{g\beta \left| T_{s,1} - T_{s,2} \right| S^3}{\nu \alpha}. \tag{10.12.6}$$

For $\mathrm{Ra}_S \lesssim 1$, the flow field in the enclosure resembles the one described earlier for a tall enclosure. A large, slowly rotating cell is observed, but heat transfer across the enclosure is essentially by conduction, leading to $\mathrm{Nu}_S \approx 1$, when Nu_S is defined in Eq. (10.12.2).

For the parameter range $2 < l/S < 10$, $\mathrm{Pr} < 10$, and $\mathrm{Ra}_S < 10^{10}$, Catton (1978) proposed

$$\langle \mathrm{Nu}_S \rangle_l = 0.22 \, (l/S)^{-1/4} \left[\frac{\mathrm{Pr}}{0.2 + \mathrm{Pr}} \mathrm{Ra}_S \right]^{0.28}. \tag{10.12.7}$$

For the parameter range $1 < l/S < 2$, $10^{-3} < \mathrm{Pr} < 10^5$, and $\frac{\mathrm{Ra}_S \mathrm{Pr}}{0.2+\mathrm{Pr}} > 10^3$, Catton (1978) recommends

$$\langle \mathrm{Nu}_S \rangle_l = 0.18 \left[\frac{\mathrm{Pr}}{0.2 + \mathrm{Pr}} \mathrm{Ra}_S \right]^{0.29}. \tag{10.12.8}$$

For the range $10 < l/S < 40$, $1 < \mathrm{Pr} < 2 \times 10^4$, and $10^4 < \mathrm{Ra}_S < 10^7$, McGregor and Emery (1969) recommend

$$\langle \mathrm{Nu}_S \rangle_l = 0.42 \mathrm{Ra}_S^{0.25} \, \mathrm{Pr}^{0.012} \, (l/S)^{-0.3}. \tag{10.12.9}$$

The same authors recommend the following correlation for the range $1 < l/S < 40$, $1 < \mathrm{Pr} < 20$, and $10^6 < \mathrm{Ra}_S < 10^9$.

$$\langle \mathrm{Nu}_S \rangle_l = 0.046 \mathrm{Ra}_S^{0.33}. \tag{10.12.10}$$

The properties in all these correlations should correspond to $(T_{s,1} + T_{s,2})/2$.

10.13 Natural Convection in Horizontal Rectangles

We now discuss natural convection in fluid layers that have small aspect ratios. Consider a fluid whose specific volume expands as a consequence of increasing temperature. When a layer of such a fluid is heated from the top, as in Fig. 10.20(a), a stable, quiescent, and thermally stratified field is developed. Heat transfer through the fluid layer will be due to conduction, and that leads to Eq. (10.12.2). When such a fluid layer is heated through its bottom surface, however, the developed temperature gradient leads to buoyancy that tends to destabilize the fluid layer while the fluid viscosity resists fluid motion. The stability of this type of fluid layers has been studied extensively. It was shown that the layer remains stable, and therefore quiescent, as long as (Pellew and Southwell, 1940)

$$\mathrm{Ra}_S \lesssim \mathrm{Ra}_{S,\mathrm{cr}} = 1708, \tag{10.13.1}$$

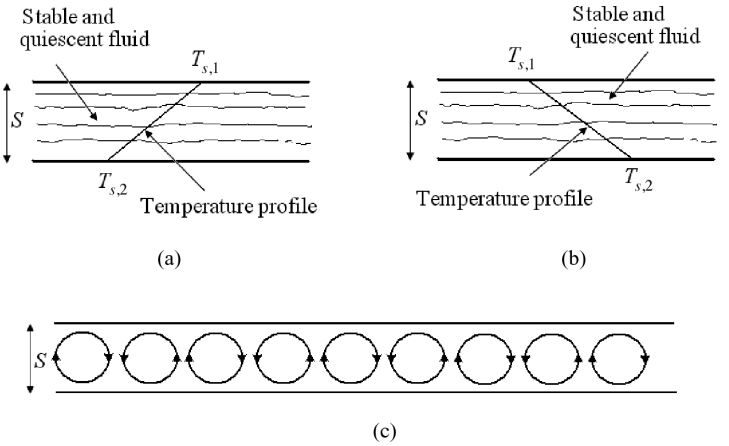

Figure 10.20. Horizontal fluid layers with small aspect ratios: (a) heated from above; (b) heated from below, $\mathrm{Ra}_S = 1708$; (c) heated from below, $\mathrm{Ra}_S = 1708$.

where Ra_S is defined in Eq. (10.12.6). At lower values of Ra_S, viscosity overwhelms buoyancy and retains the stability of the fluid layer. Above the critical Rayleigh number (also referred to as the *convection-onset Rayleigh number*) of 1708, counter-rotating recirculation cells form. This is the classical *Bénard's problem*, in honor of H. Bénard who first investigated this problem in 1900. The rotating cellules are 1D for $\mathrm{Ra}_{S,\mathrm{cr}} \leq \mathrm{Ra}_S \lesssim 5 \times 10^4$ (Fig. 10.21), but become 3D with hexagonal-shaped cells for $\mathrm{Ra}_S > 5 \times 10^4$. At much higher Ra_S values the flow eventually becomes turbulent and oscillatory.

For horizontal rectangles heated from below, the following widely applied empirical correlation is valid for the range $3 \times 10^5 \lesssim \mathrm{Ra}_S \lesssim 7 \times 10^9$ (Globe and Dropkin, 1959):

$$\langle \mathrm{Nu}_S \rangle = 0.069 \mathrm{Ra}_S^{1/3} \mathrm{Pr}^{0.074}. \tag{10.13.2}$$

Hollands et al. (1975) proposed the following correlation for air for the parameter range $1708 \lesssim \mathrm{Ra}_S \lesssim 10^8$:

$$\langle \mathrm{Nu}_S \rangle = 1 + 1.44 \left[1 - \frac{1708}{\mathrm{Ra}_S} \right]^{\bullet\bullet} + \left[\left(\frac{\mathrm{Ra}_S}{5830} \right)^{1/3} - 1 \right]^{\bullet\bullet}, \tag{10.13.3}$$

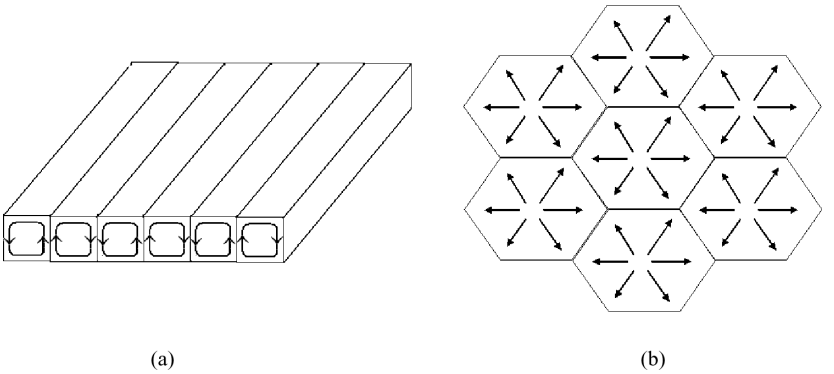

Figure 10.21. Schematic of the rotating cells in Bénard's problem: (a) 2D rolls, (b) 3D hexagonal cells.

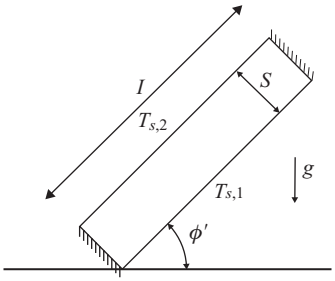

Figure 10.22. Natural convection in a tilted rectangular enclosure.

where the notation $[\ ]^{\bullet\bullet}$ implies that the bracketed quantity should be replaced with zero if it turns out to be negative. The same correlation can be applied to water, provided that a term is added to its right-hand side, leading to

$$\langle \mathrm{Nu}_S \rangle = 1 + 1.44\left[1 - \frac{1708}{\mathrm{Ra}_S}\right]^{\bullet\bullet} + \left[\left(\frac{\mathrm{Ra}_S}{5830}\right)^{1/3} - 1\right]^{\bullet\bullet} + 2.0\left[\frac{\mathrm{Ra}_S^{1/3}}{140}\right]^{C}, \qquad (10.13.4)$$

$$C = 1 - \ln\left(\mathrm{Ra}_S^{1/3}/140\right). \qquad (10.13.5)$$

Equation (10.13.4) closely matches data representing water for the range $1708 \lesssim \mathrm{Ra}_S \lesssim 3.5 \times 10^9$.

10.14 Natural Convection in Inclined Rectangular Enclosures

Interest in natural convection in tilted rectangular enclosures is primarily because of double-glazed windows and flat-plate solar panels. Figure 10.22 is a schematic of a tilted rectangular enclosure, where $T_{s,1} > T_{s,2}$ is assumed. It is noted that for $\phi' = 0$ and 180° we get the aforementioned rectangular enclosures with heating through their bottom and top surfaces, respectively, whereas $\phi' = 90°$ would lead to a high-aspect-ratio enclosure heated on one of its sides. Also, for $\phi' < 90°$, the tilted enclosure will have its heated side below its cooled surface, while the opposite is true for $90° < \phi' < 180°$. The natural-convection recirculation patterns and their resulting heat transfer rates strongly depend on the angle of inclination, as intuition would suggest. Figure 10.23 shows qualitatively the variation of $\langle \mathrm{Nu}_S \rangle$ as a function of the inclination angle, where $\langle \mathrm{Nu}_S \rangle$ is defined as

$$\langle \mathrm{Nu}_S \rangle = \frac{\langle q'' \rangle_l}{T_{s,1} - T_{s,2}} \frac{S}{k}, \qquad (10.14.1)$$

At $\phi' = 180°$, where a stable thermal stratification occurs, we obviously have $\langle \mathrm{Nu}_S \rangle = 1$. By reducing ϕ', $\langle \mathrm{Nu}_S \rangle$ increases because of recirculation, and reaches its maximum at $\phi' = 90°$. It decreases when ϕ' is reduced below 90°, until $\langle \mathrm{Nu}_S \rangle$ reaches a local minimum at an inclination angle ϕ'^*, which turns out to be a function of the aspect ratio l/S. $\langle \mathrm{Nu}_S \rangle$ increases monotonically with reducing ϕ' for $\phi' < \phi'^*$ until conditions leading to Bénard's problem are reached at $\phi' = 0$. The tilt angle at which $\langle \mathrm{Nu}_S \rangle$ hits the aforementioned relative minimum, namely ϕ'^*, depends on the aspect ratio, as shown in Table 10.5 (Arnold et al., 1976).

Table 10.5. *Variation of the tilt angle θ'^* as a function of aspect ratio (Arnold et al., 1976)*

l/s	1	3	6	12	>12
θ'^*	25°	53°	60°	67°	70°

According to Catton (1978), for aspect ratios in the range $l/S < 12$, the following correlations can be used:

For $90^\circ < \phi' < 180^\circ$,

$$\langle \mathrm{Nu}_S(\phi') \rangle = 1 + \left[\langle \mathrm{Nu}_S(90^\circ) \rangle - 1 \right] \sin\phi'. \tag{10.14.2}$$

For $\phi'^* < \phi' < 90^\circ$,

$$\langle \mathrm{Nu}_S(\phi') \rangle = \langle \mathrm{Nu}_S(90^\circ) \rangle (\sin\phi')^{1/4}. \tag{10.14.3}$$

For $0 < \phi' < \phi'^*$, when $l/S < 10$,

$$\langle \mathrm{Nu}_S(\phi') \rangle = \langle \mathrm{Nu}_S(0^\circ) \rangle \left[\frac{\langle \mathrm{Nu}_S(90^\circ) \rangle}{\langle \mathrm{Nu}_S(0^\circ) \rangle} (\sin\phi'^*)^{1/4} \right]^{\frac{\phi'}{\phi'^*}}. \tag{10.14.4}$$

For $0 < \phi' < \phi'^*$, when $l/S > 10$,

$$\langle \mathrm{Nu}_S(\phi') \rangle = 1 + 1.44 \left[1 - \frac{1708}{\mathrm{Ra}_S \cos\phi'} \right]^{\bullet\bullet} \left[1 - \frac{(\sin 1.8\phi')^{1.6}(1708)}{\mathrm{Ra}_S \cos\phi'} \right]^{\bullet\bullet} + \left\{ \left[\frac{\mathrm{Ra}_S \cos\phi'}{5830} \right]^{1/3} - 1 \right\}^{\bullet\bullet}. \tag{10.14.5}$$

This correlation actually was proposed by Hollands et al. (1976) for $l/S > 12$ and $0 < \phi' < 70^\circ$.

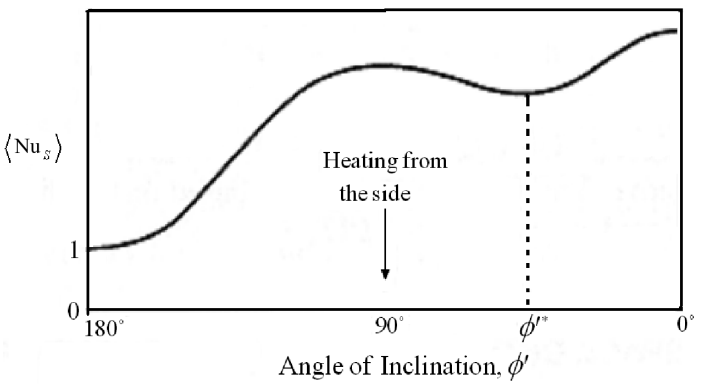

Figure 10.23. Variation of Nusselt number as a function of inclination angle (after Bejan, 2004).

10.15 Natural Convection Caused by the Combined Thermal and Mass Diffusion Effects

Mass transfer in natural convection is more complicated than in forced convection. The reason is that nonuniformity in the chemical species concentrations, which is usually the main cause of diffusive mass transfer, also contributes to nonuniformity in the fluid mixture density. The nonuniformity in the fluid density will then contribute to the buoyancy-driven flow. Thus, unlike forced convection in which the effect of diffusive mass transfer on the hydrodynamics is often negligible, mass diffusion can have a significant effect on the overall phenomenology of buoyancy-driven flows. Diffusive mass transfer in fact can cause natural convection even in adiabatic flows. Buoyancy-driven flows caused by nonuniformity of humidity in air and in buildings, and caused by nonuniformity of salinity in seawater, are some examples. When heat and mass transfer are both present, we then deal with buoyancy-driven flows caused by combined thermal and mass diffusion.

It is important to note that, unlike forced convection, the analogy between heat and mass transfer cannot be applied to derive correlations for mass transfer based on the modification of correlations for natural-convection heat transfer. The analogy-based methods for obtaining mass transfer correlation by manipulating heat transfer correlations (and vice versa) can be applied under only very restrictive, limiting conditions (see Subsection 10.15.2).

10.15.1 Conservation Equations and Scaling Analysis

Consider a two-component mixture, e.g., air–water–vapor mixture or a liquid containing a dissolved inert substance. The mixture density can thus be written, in general, as

$$\rho = \rho\left(P, T, m_1\right), \tag{10.15.1}$$

where m_1 is the mass fraction of one of the species. For convenience, let us refer to chemical species 1 as the transferred species (e.g., water vapor in an air–water-vapor mixture), and species 2 as the species (or mixture of other species) making up the remainder of the mixture. Equation (10.15.1) can be written in the following equivalent form:

$$\rho = \rho\left(P, T, \rho_1\right), \tag{10.15.2}$$

where ρ_1 is the partial density of species 1 (also often referred to as the concentration of species 1). We can expand this equation as

$$d\rho = \left(\frac{\partial \rho}{\partial T}\right)_{P,\rho_1} dT + \left(\frac{\partial \rho}{\partial \rho_1}\right)_{P,T} d\rho_1 + \left(\frac{\partial \rho}{\partial P}\right)_{T,\rho_1} dP + \left(\frac{\partial^2 \rho}{\partial T \partial \rho_1}\right)_{P} dT d\rho_1 + \cdots \tag{10.15.3}$$

The second- and higher-order terms can often be neglected because they are small in comparison with the first-order terms. Furthermore, among the first-order terms,

the third term on the right-hand side of this equation is also often negligible in comparison with the first two terms. Keeping only the first two terms on the right-hand side, we can then cast the equation as

$$d\rho = -\rho\beta dT - \rho\beta^*_{\text{ma}} d\rho_1, \tag{10.15.4}$$

where $\beta = -\frac{1}{\rho}\left(\frac{\partial\rho}{\partial T}\right)_{P,\rho_1}$ is the familiar volumetric thermal expansion coefficient and β^*_{ma} is the volumetric expansion coefficient with respect to concentration:

$$\beta^*_{\text{ma}} = -\frac{1}{\rho}\left(\frac{\partial\rho}{\partial\rho_1}\right)_{P,T}. \tag{10.15.5}$$

Neglecting the second- and higher-order terms in Eq. (10.15.3) is justified when $\beta\Delta T \ll 1$ and $\beta^*_{\text{ma}}\Delta\rho_1 \ll 1$, where ΔT and $\Delta\rho_1$ are the characteristic temperature and concentration variations in the system, respectively.

The parameter β^*_{ma} is a function of the equations of state of the chemical species constituents of the mixture, as well as their concentrations. For binary mixtures of ideal gases, a simple expression for β^*_{ma} can be easily derived as follows. The mixture density follows

$$\rho = \frac{PX_1}{\frac{R_u}{M_1}T} + \frac{P(1-X_1)}{\frac{R_u}{M_2}T}. \tag{10.15.6}$$

This leads to

$$\frac{\partial\rho}{\partial X_1} = \frac{P}{R_u T}(M_1 - M_2). \tag{10.15.7}$$

We also note that

$$\frac{\partial\rho}{\partial\rho_1} = \frac{\partial\rho}{\partial X_1}\frac{\partial X_1}{\partial\rho_1}. \tag{10.15.8}$$

The first term on the right-hand side of Eq. (10.15.6) is actually ρ_1, and from there

$$\frac{\partial\rho_1}{\partial X_1} = \frac{PM_1}{R_u T}. \tag{10.15.9}$$

Substitution from Eqs. (10.15.7) and (10.15.9) into (10.15.8) and using Eq. (10.15.5) will give

$$\beta^*_{\text{ma}} = \frac{1}{\rho}\left[\frac{M_2}{M_1} - 1\right]. \tag{10.15.10}$$

This formulation of the concentration-induced buoyancy effect was based on Eq. (10.15.2). We can start with Eq. (10.15.1), in which case we have

$$d\rho = -\rho\beta dT - \rho\beta_{\text{ma}} dm_1, \tag{10.15.11}$$

$$\beta_{\text{ma}} = -\frac{1}{\rho}\left(\frac{\partial\rho}{\partial m_1}\right)_{P,T}, \tag{10.15.12}$$

where β_{ma} is now the volumetric expansion coefficient with respect to the mass fraction. We can find the derivative on the right-hand side of this equation by writing

$$\left(\frac{\partial \rho}{\partial m_1}\right)_{P,T} = \left(\frac{\partial \rho}{\partial X_1}\right)_{P,T} \left(\frac{\partial X_1}{\partial m_1}\right).$$

The derivative $(\frac{\partial \rho}{\partial X_1})_{P,T}$ is the same as that on the right-hand side of Eq. (10.15.7), and $(\frac{\partial X_1}{\partial m_1})$ can be derived for binary mixtures of ideal gases from Eq. (1.2.8), leading to

$$\beta_{\text{ma}} = -\frac{M(M_2 - M_1)}{M_1 M_2}, \tag{10.15.13}$$

where M is the mixture molar mass [see Eqs. (1.2.9) and (1.2.10)].

We may even write

$$d\rho = -\rho\beta dT - \rho\tilde{\beta}_{\text{ma}} dX_1, \tag{10.15.14}$$

where the volumetric expansion coefficient with respect to the mole fraction is defined as

$$\tilde{\beta}_{\text{ma}} = -\frac{1}{\rho}\left(\frac{\partial \rho}{\partial X_1}\right)_{P,T}. \tag{10.15.15}$$

For a binary mixture of ideal gases, from Eq. (10.15.6), we get

$$\tilde{\beta}_{\text{ma}} = \frac{M_2 - M_1}{M}. \tag{10.15.16}$$

The parameter β^*_{ma} has the dimensions of inverse density (e.g., cubic meters per kilogram), whereas β_{ma} and $\tilde{\beta}_{\text{ma}}$ are both dimensionless. The choice among β^*_{ma}, β_{ma}, and $\tilde{\beta}_{\text{ma}}$ is of course a matter of convenience. When the species conservation equation is in terms of ρ_1, it will be easier to use β^*_{ma} and Eq. (10.15.4). Likewise, if the species conservation equation is in terms of the mass fraction or mole fraction, then it will be easier to use β_{ma} and $\tilde{\beta}_{\text{ma}}$, respectively.

Now consider the flow along the inclined flat surface shown in Fig. 10.24. The displayed flow field is similar to what was shown earlier in Fig. 10.5, except that we now deal with the combined effects of thermal and concentration-induced density variations. Assume steady state. We proceed by following Boussinesq's approximation, whereby the flow field is assumed to be incompressible everywhere in the conservation equations except in dealing with the buoyancy term in the momentum conservation equation. We also assume that Fick's law applies. We can then perform an analysis similar to that performed in Section 10.3, this time considering

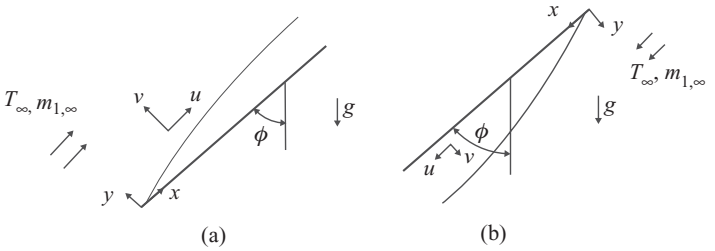

Figure 10.24. Natural convection on an inclined flat surface, caused by the combined thermal and mass diffusion effects: (a) flow over an inclined surface, (b) flow under an inclined surface.

mass diffusion as well. The conservation equations will then be

$$\nabla \cdot \vec{U} = 0 \tag{10.15.17}$$

$$\vec{U} \cdot \nabla \vec{U} = \nu \nabla^2 \vec{U} \pm g\beta \cos\phi\,(T - T_\infty) \pm g\beta^*_{\text{ma}} \cos\phi\,(\rho_1 - \rho_{I,\infty}) - \frac{1}{\rho}\nabla\,(P - P_\infty)\,, \tag{10.15.18}$$

$$\vec{U} \cdot \nabla T = \boldsymbol{\alpha} \nabla^2 T, \tag{10.15.19}$$

$$\vec{U} \cdot \nabla \rho_1 = \mathcal{D}_{I2} \nabla^2 \rho_1. \tag{10.15.20}$$

In Eq. (10.15.18), in the terms with the $\pm$ sign, the positive sign applies to the configuration shown in Fig. 10.24(a), and the negative sign applies to Fig. 10.24(b). Also, note that Eq. (10.15.20) will be the same as Eq. (1.3.18) for steady-state when $\mathcal{D}_{12}$ and the mixture density ρ are assumed to be a constant, which are often reasonable assumptions. The assumption of constant ρ is consistent with Boussinesq's approximation.

Equations (10.15.18) and (10.15.20) are convenient to use when partial density ρ_1 is used as a state variable. Alternatively, when m_1, the mass fraction of the transferred species, is used as a state variable, then these equations will be replaced, respectively, with

$$\vec{U} \cdot \nabla \vec{U} = \nu \nabla^2 \vec{U} \pm g\beta \cos\phi\,(T - T_\infty) \pm g\beta_{\text{ma}} \cos\phi\,(m_1 - m_{I,\infty}) - \frac{1}{\rho}\nabla\,(P - P_\infty)\,, \tag{10.15.21a}$$

$$\vec{U} \cdot \nabla m_1 = \mathcal{D}_{12} \nabla^2 m_1. \tag{10.15.22a}$$

When the mole fraction of the transferred species is the state variable, the equations will be replaced with

$$\vec{U} \cdot \nabla \vec{U} = \nu \nabla^2 \vec{U} \pm g\beta \cos\phi\,(T - T_\infty) \pm g\,\tilde{\beta}_{\text{ma}} \cos\phi\,(X_1 - X_\infty) - \frac{1}{\rho}\nabla\,(P - P_\infty)\,, \tag{10.15.21b}$$

$$\vec{U} \cdot \nabla X_1 = \mathcal{D}_{I2} \nabla^2 X_1, \tag{10.15.22b}$$

where $\vec{U}$ is the mole-average mixture velocity.

The set of conservation equations needs velocity, thermal, and mass transfer boundary conditions. The velocity and thermal boundary conditions (i.e., no-slip for velocity, and UWT or UHF for thermal boundary conditions at the interface

with a wall) are easy to write. The wall boundary conditions with respect to mass transfer can be any of the following:

- known concentration (UWM),

$$\rho_1 = \rho_{1,s} \tag{10.15.23}$$

or

$$m_1 = m_{1,s}. \tag{10.15.24}$$

- known flux (UMF),

$$m_1'' = m_{1,s}'' \tag{10.15.25}$$

or

$$N_1'' = N_{1,s}''. \tag{10.15.26}$$

- Equilibrium with another phase,

See the discussion in Subsection 1.4.4 for this case.

The mass flux at the boundary depends on the concentration gradient at that location according to the discussion in Section 1.4. When transferred chemical species 1 is the only contributor to the mass flux at the wall boundary,

$$m_{1,s}'' = -\frac{1}{1-m_{1,s}}\rho\mathcal{D}_{12}\left.\frac{\partial m_1}{\partial y}\right|_{y=0} = -\frac{1}{1-(\rho_{1,s}/\rho)}\mathcal{D}_{12}\left.\frac{\partial \rho_1}{\partial y}\right|_{y=0} = \mathcal{K}\ln\left(1+\mathcal{B}\_\mathrm{ma}\right), \tag{10.15.27}$$

where $\mathcal{K}$ is the mass transfer coefficient for the limit of $m_{1,s}'' \to 0$, and

$$\mathcal{B}_{\mathrm{ma}} = \frac{m_{1,\infty}-m_{1,s}}{m_{1,s}-1} = \frac{\rho_{1,\infty}-\rho_{1,s}}{\rho_{1,s}-1}. \tag{10.15.28}$$

It should also be emphasized that the velocity and mass transfer at the boundary and elsewhere are coupled. At the wall boundary, when substance 1 is the only transferred species, we can find the relation between mass flux and velocity by writing

$$m_{1,s}'' = (\rho v)_s\, m_{1,s} = \rho_{1,s} v_s. \tag{10.15.29}$$

Equations (10.15.17)–(10.15.20) can be nondimensionalized following the approach in Subsection 10.1, using $x_i^* = x_i/l$ (where x_i is the ith Cartesian coordinate), $P^* = \frac{P-P_\infty}{\rho U_{\mathrm{ref}}^2}$, $\theta = (T-T_\infty)/(T_s-T_\infty)$, $\vec{U}^* = \vec{U}/U_{\mathrm{ref}}$, with $U_{\mathrm{ref}} = [g\beta l\,(T_s-T_\infty)]^{1/2}$ [see Eq. (10.1.15)], and

$$\theta_{\mathrm{ma}} = \frac{\rho_1-\rho_{1,\infty}}{\rho_{1,s}-\rho_{1,\infty}} = \frac{m_1-m_{1,\infty}}{m_{1,s}-m_{1,\infty}}. \tag{10.15.30}$$

The dimensionless conservation equations will then be

$$\nabla^*\cdot\vec{U}^* = 0, \tag{10.15.31}$$

$$\vec{U}^*\cdot\nabla^*\vec{U}^* = -\nabla^* P^* \pm (\theta + N\theta_{\mathrm{ma}})\cos\phi + \frac{1}{\sqrt{\mathrm{Gr}_l}}\nabla^{*2}\vec{U}^*, \tag{10.15.32}$$

$$\vec{U}^* \cdot \nabla^* \theta = \frac{1}{\mathrm{Pr}\sqrt{\mathrm{Gr}_l}} \nabla^{*2} \theta, \tag{10.15.33}$$

$$\vec{U}^* \cdot \nabla^* \theta_{\mathrm{ma}} = \frac{1}{\mathrm{Sc}\sqrt{\mathrm{Gr}_l}} \nabla^{*2} \theta_{\mathrm{ma}}, \tag{10.15.34}$$

where N represents the ratio between the concentration-induced and thermally induced buoyancy terms:

$$N = \frac{\beta^*_{\mathrm{ma}} \left| \rho_{1,s} - \rho_{1,\infty} \right|}{\beta \left| T_s - T_\infty \right|} = \frac{\beta_{\mathrm{ma}} \left| m_{1,s} - m_{1,\infty} \right|}{\beta \left| T_s - T_\infty \right|} = \frac{\mathrm{Gr}_{\mathrm{ma,l}}}{\mathrm{Gr}_l}. \tag{10.15.35}$$

The concentration-based Grashof number is defined as

$$\mathrm{Gr}_{\mathrm{ma},l} = \frac{g\beta^*_{\mathrm{ma}} l^3 \left| \rho_{1,s} - \rho_{1,\infty} \right|}{\nu^2} = \frac{g\beta_{\mathrm{ma}} l^3 \left| m_{1,s} - m_{1,\infty} \right|}{\nu^2}$$
$$= \frac{g\tilde{\beta}_{\mathrm{ma}} l^3 \left| X_{1,s} - X_{1,\infty} \right|}{\nu^2}. \tag{10.15.36}$$

The preceding equations confirm the coupling among the hydrodynamic and heat and mass transfer processes. The thermal and mass transfer buoyancy effects can be in the same direction (assisting flow conditions) or in opposite directions (opposing flow conditions).

10.15.2 Heat and Mass Transfer Analogy

In the absence of mass transfer we have $N = 0$, and Eqs. (10.15.31)–(10.15.33) reduce to the pure thermally driven natural convection. The Nusselt number is then related to the temperature profile as

$$Nu = \frac{hl}{k} = -\left. \frac{\partial \theta}{\partial y^*} \right|_{y^*=0}. \tag{10.15.37}$$

Now we consider the circumstance in which there is no heat transfer, but buoyancy-driven flow is caused by mass diffusion only. Equations (10.15.17), (10.15.18), and (10.15.20) then govern the problem, and the second term on the right-hand side of Eq. (10.15.18) is dropped. We can then nondimensionalize these equations by using the following reference velocity:

$$U_{\mathrm{ref}} = \left[g l \beta^*_{\mathrm{ma}} \left| \rho_{1,s} - \rho_{1,\infty} \right| \right]^{1/2} = \left[g l \beta_{\mathrm{ma}} \left| m_{1,\mathrm{s}} - m_{1,\infty} \right| \right]^{1/2}. \tag{10.15.38}$$

We then have Eq. (11.15.31) and

$$\vec{U}^* \cdot \nabla^* \vec{U}^* = -\nabla^* P^* \pm \theta_{\mathrm{ma}} \cos\phi + \frac{1}{\sqrt{\mathrm{Gr}_{\mathrm{ma,l}}}} \nabla^{*2} \vec{U}^*, \tag{10.15.39}$$

$$\vec{U}^* \cdot \nabla^* \theta_{\mathrm{ma}} = \frac{1}{\mathrm{Sc}\sqrt{\mathrm{Gr}_{\mathrm{ma,l}}}} \nabla^{*2} \theta_{\mathrm{ma}}. \tag{10.15.40}$$

Let us also assume that we deal with very low mass transfer rates. In that case, the Sherwood number can be found from

$$\mathrm{Sh} = \frac{\mathcal{K} l}{\rho \mathcal{D}_{12}} = \frac{m''_s l}{\rho \mathcal{D}_{12} \left(m_{1,s} - m_{1,\infty} \right)} = -\left. \frac{\partial \theta_{\mathrm{ma}}}{\partial y^*} \right|_{y^*=0}. \tag{10.15.41}$$

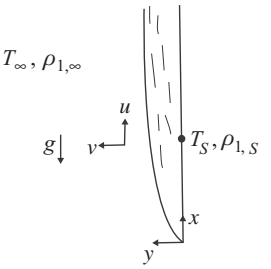

Figure 10.25. Combined natural convection on a vertical, flat surface.

Comparing the two problems (namely, pure heat transfer and pure mass transfer with low mass transfer rates), we clearly note that they are mathematically identical. The concept of heat and mass transfer analogy can then be applied. Thus, knowing correlations of the following form for heat transfer,

$$\mathrm{Nu}_l = f\left(\mathrm{Gr}_l, \mathrm{Pr}\right), \tag{10.15.42}$$

we can readily deduce correlations for mass transfer of the form

$$\mathrm{Sh}_l = f(\mathrm{Gr}_{\mathrm{ma},l}, \mathrm{Sc}). \tag{10.15.43}$$

An important point to emphasize, however, is that this deduction makes sense when Sc and Pr have similar magnitudes. Furthermore, Grashof numbers should obviously have the same range in the two problems.

10.16 Solutions for Natural Convection Caused by Combined Thermal and Mass Diffusion Effects

For laminar flow, several authors developed similarity solutions for the natural convection caused by combined thermal and mass diffusion. The published solutions are mostly for either UWT and UWM conditions (Gebhart and Pera, 1971; Chen and Yuh, 1979, 1980; Lin and Wu, 1995; Ramparasad et al., 2001) or UHF and UMF conditions (Chen and Yuh, 1979, 1980). A similarity solution for flow on an inclined flat surface with UHF and UMF boundary conditions was also derived (Lin and Wu, 1997). A common assumption in these similarity solutions is that the mass transfer rate at the wall boundary is negligibly small so that the assumption of $v_s \approx 0$ can be justified.

In the remainder of this section, some of the available similarity and numerical solutions are reviewed.

Similarity Solutions for a Vertical Flat Surface with UWT and UWM Boundary Conditions

First consider a vertical surface. The physical problem is displayed in Fig. 10.25. Let us assume (a) steady-state and stagnant ambient fluid, (b) laminar flow, (c) constant thermophysical properties, (d) that Boussinesq's approximation is applicable, (e) the velocity in the direction normal to the surface that is caused by the mass transfer at the wall boundary is negligibly small; and (f) that Fick's law is applicable.

The conservation equations, discussed earlier in Section 10.15, then give

$$\frac{\partial u}{\partial x} + \frac{\partial v}{\partial y} = 0, \tag{10.16.1}$$

$$u\frac{\partial u}{\partial x} + v\frac{\partial u}{\partial y} = g\beta\left(T - T_\infty\right) + g\beta^*_{\text{ma}}\left(\rho_1 - \rho_{1,\infty}\right) + \nu\frac{\partial^2 u}{\partial y^2}, \tag{10.16.2}$$

$$u\frac{\partial T}{\partial x} + v\frac{\partial T}{\partial y} = \boldsymbol{\alpha}\frac{\partial^2 T}{\partial y^2}, \tag{10.16.3}$$

$$u\frac{\partial \rho_1}{\partial x} + v\frac{\partial \rho_1}{\partial y} = \mathcal{D}_{12}\frac{\partial^2 \rho_1}{\partial y^2}, \tag{10.16.4}$$

The boundary conditions will be as follows. At $y = 0$,

$$u = 0,\, v = 0, \tag{10.16.5}$$

$$T = T_s,\, \rho_1 = \rho_{1,s}. \tag{10.16.6}$$

At $y \to \infty$,

$$u \to 0,\; T \to T_\infty,\; \rho_1 \to \rho_{1,\infty}. \tag{10.16.7}$$

A similarity solution can be derived by defining (Gebhart and Pera, 1971)

$$\eta = \frac{y}{x}\left[\frac{\text{Gr}_x + \text{Gr}_{\text{ma,x}}}{4}\right]^{1/4}. \tag{10.16.8}$$

The dimensionless temperature and concentration are defined, respectively, as $\theta = \left(T - T_\infty\right)/\left(T_s - T_\infty\right)$ and $\theta_{\text{ma}} = \left(\rho_1 - \rho_{1,\infty}\right)/\left(\rho_{1,s} - \rho_{1,\infty}\right)$. The stream function is assumed to follow:

$$\psi = 4\nu\left[\frac{\text{Gr}_x + \text{Gr}_{\text{ma,x}}}{4}\right]^{1/4} f\left(\eta\right). \tag{10.16.9}$$

This stream function satisfies the continuity equation. Using these definitions, we can cast Eqs. (10.16.2)–(10.16.4) and their boundary conditions as

$$f''' + 3ff'' - 2f'^2 + \frac{\theta + \boldsymbol{N}\theta_{\text{ma}}}{1 + \boldsymbol{N}} = 0, \tag{10.16.10}$$

$$\theta'' + 3\text{Pr}\;\; f\theta' = 0, \tag{10.16.11}$$

$$\theta''_{\text{ma}} + 3\text{Sc}\;\; f\theta'_{\text{ma}} = 0, \tag{10.16.12}$$

$$f'\left(0\right) = 0,\; f\left(0\right) = 0, \tag{10.16.13}$$

$$\theta\left(0\right) = 1, \theta_{\text{ma}}\left(0\right) = 1, \tag{10.16.14}$$

$$f'\left(\infty\right) = 0, \theta\left(\infty\right) = 0, \theta_{\text{ma}}\left(\infty\right) = 0. \tag{10.16.15}$$

where derivatives are all with respect to η.

The boundary condition ($v = v_s = 0$ at $y = 0$), which leads to $f\left(0\right) = 0$, obviously is not strictly correct because of mass transfer at the wall boundary. It will be a reasonable approximation when v_s, the velocity normal to the wall, is negligibly

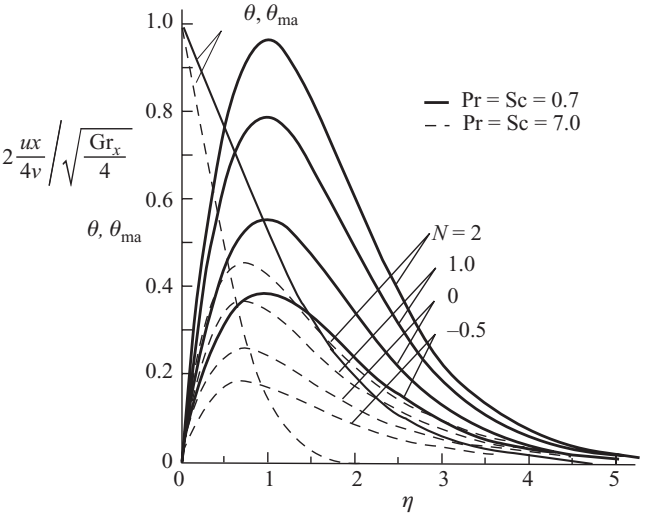

Figure 10.26. Similarity solution results for combined natural convection over a flat, vertical surface with UWT and UWM conditions (Gebhart and Pera, 1971).

small. We can derive the conditions under which $v_s \approx 0$ is justifiable by applying Eq. (10.16.2) to points at $y = 0$ (after all, that equation must be applicable everywhere in the flow field); thereby we obtain

$$v_s \left.\frac{\partial u}{\partial y}\right|_{y=0} = g\beta\,(T_s - T_\infty) + g\beta^*_{\text{ma}}\,(\rho_{1,s} - \rho_{1,\infty}) + \nu\frac{\partial^2 u}{\partial\, y^2}. \qquad (10.16.16)$$

We now require that

$$v_s \left.\frac{\partial u}{\partial y}\right|_{y=0} \ll g\beta\,(T_s - T_\infty)\,. \qquad (10.16.17)$$

For simplicity, to derive an order-of-magnitude relation, let us consider the case in which natural convection is due to thermal effects only. In that case $\text{Gr}_{\text{ma,x}} \approx 0$. In terms of the aforementioned similarity parameters, Eq. (10.16.17) will then give

$$v_s\frac{x}{\nu} \ll \frac{1}{f''(0)}\left(\frac{\text{Gr}_x}{4}\right)^{1/4}. \qquad (10.16.18)$$

In terms of orders of magnitude, this can be represented as

$$v_s\frac{x}{\nu} \ll \text{Gr}_x^{1/4}. \qquad (10.16.19)$$

This relation justifies the application of $f(0) = 0$ as the boundary condition (Gebhart and Pera, 1971).

Equations (10.16.10)–(10.16.15) are closed. They were numerically solved by Gebhart and Pera (1971). Figure 10.26 displays some of their results, where the dimensionless velocity distribution for $\text{Pr} = Sc = 0.7$ and $\text{Pr} = Sc = 7$ are shown. The displayed profiles also show assisting ($N > 0$) and opposing ($N < 0$) flow conditions.

In accordance with the assumption of a small mass flow rate through the wall boundary, we can write

$$\mathrm{Nu}_x = \frac{x}{k\,(T_s - T_\infty)}\left(-k\frac{\partial T}{\partial y}\right)_{y=0} = -\frac{1}{\sqrt{2}}\left[\mathrm{Gr}_x + \mathrm{Gr}_{\mathrm{ma},x}\right]^{1/4}\theta'(0)\,, \quad (10.16.20)$$

$$Sh_x = \frac{x}{\mathcal{D}_{12}\,(\rho_{1,s} - \rho_{1,\infty})}\left(-\mathcal{D}_{12}\frac{\partial \rho_1}{\partial y}\right)_{y=0} = -\frac{1}{\sqrt{2}}\left[\mathrm{Gr}_x + \mathrm{Gr}_{\mathrm{ma},x}\right]^{1/4}\theta'_{\mathrm{ma}}(0)\,. \quad (10.16.21)$$

Pera and Gebhart (1972) derived a similarity solution for UWT and UWM boundary conditions over a flat, 2D horizontal surface. This solution is based on the assumption that a single plume forms on the entire surface. Sripada and Angirasa (2001) conducted a numerical-analysis-based investigation of combined natural convection on a finite, 2D surface, and pointed out the shortcomings of the aforementioned similarity solution of Pera and Gebhart (1972).

Similarity Solutions for an Inclined Surface with UHF and UMF Boundary Conditions

Similarity solutions for UHF and UMF boundary conditions on an inclined flat surface were derived by Chen and Yuh (1979), and for UHF and UWM on a vertical flat surface by Lin and Wu (1997). In both cases, the coordinate transformation leading to the derivation of the similarity solutions is based on the assumption that mass transport at the boundary is negligibly small, so that the heat and mass transfer rates follow:

$$q''_s = -k\left.\frac{\partial T}{\partial y}\right|_{y=0}, \quad (10.16.22)$$

$$m''_1 = -\rho\mathcal{D}_{12}\left.\frac{\partial m_1}{\partial y}\right|_{y=0} \quad (10.16.23)$$

The formulation for an inclined surface with UHF and UMF boundary conditions is now described, as an example.

The conservation equations include Eqs. (10.16.1), (10.16.3), and (10.16.4), and the following momentum equation:

$$u\frac{\partial u}{\partial x} + v\frac{\partial u}{\partial y} = g\beta\cos\phi\,(T - T_\infty) + g\beta_{\mathrm{ma}}\cos\phi\,(m_1 - m_{1,\infty}) + \nu\frac{\partial^2 u}{\partial y^2}. \quad (10.16.24)$$

The boundary conditions include Eqs. (10.16.22) and (10.16.23) and the following equations:

$$u = 0, v = 0 \text{ at } y = 0, \quad (10.16.25)$$

$$u = 0, v = 0 \text{ at } y \to \infty, \quad (10.16.26)$$

$$T = T_\infty, m_1 = m_{1,\infty} \text{ at } y \to \infty. \quad (10.16.27)$$

We can derive a similarity solution by defining (Chen and Yuh, 1979)

$$\eta^* = \frac{y}{x}\left[\mathrm{Gr}_x^* \frac{\cos\phi}{5}\right]^{1/5}, \tag{10.16.28}$$

$$\psi = 5\,\nu\left[\mathrm{Gr}_x^* \frac{\cos\phi}{5}\right]^{1/5} F(\eta^*), \tag{10.16.29}$$

$$\theta^*(\eta^*) = \left[\mathrm{Gr}_x^* \frac{\cos\phi}{5}\right]^{1/5} \frac{T - T_\infty}{\dfrac{q_s'' x}{k}}, \tag{10.16.30}$$

$$\theta_{\mathrm{ma}}^*(\eta^*) = \left[\mathrm{Gr}_x^* \frac{\cos\phi}{5}\right]^{1/5} \frac{m_1 - m_{1,\infty}}{\dfrac{m_{1,s}'' x}{\rho \mathcal{D}_{12}}}, \tag{10.16.31}$$

where

$$\mathrm{Gr}_x^* = \frac{g\,\beta\,q_s''\,x^4}{k\,\nu^2}. \tag{10.16.32}$$

Equation (10.16.29) satisfies the mixture mass conservation equation. The momentum, energy, and mass-species conservation equation can be cast as

$$F''' + 4FF'' - 3F'^2 + \theta^* + \boldsymbol{N}^*\theta_{\mathrm{ma}}^* = 0, \tag{10.16.33}$$

$$\frac{\theta^{*\prime\prime}}{\mathrm{Pr}} + 4F\theta^{*'} - F'\theta^* = 0, \tag{10.16.34}$$

$$\frac{\theta_{\mathrm{ma}}^{*\,''}}{\mathrm{Sc}} + 4F\theta_{\mathrm{ma}}^{*'} - F'\theta_{\mathrm{ma}}^* = 0, \tag{10.16.35}$$

where

$$N^* = \frac{\beta_{\mathrm{ma}}\, m_s''/(\rho\mathcal{D}_{12})}{\beta\, q_s''/k}. \tag{10.16.36}$$

The boundary conditions for these equations are

$$F(0) = 0, F'(0) = 0, \tag{10.16.37}$$

$$\theta^{*'}(0) = -1, \quad \theta_{\mathrm{ma}}^{*'}(0) = -1, \tag{10.16.38}$$

$$F'(\infty) = 0, \quad \theta^*(\infty) = 0, \quad \theta_{\mathrm{ma}}^*(\infty) = 0. \tag{10.16.39}$$

The results of parametric solutions of the preceding equations can be found in Chen and Yuh (1979).

Confined Spaces and Channels

Natural convection by the combined effects of thermal and mass diffusion is relatively common in buildings, where gradients in temperature and moisture content of air occur in a calm ambience. The problems representing natural convection in confined spaces often require numerical solutions of the conservation equations [Eqs. (12.15.17)–(12.15.20)].

Natural convection that is due to the combined effect of thermal and mass diffusion in channels is a simpler problem than natural convection in confined spaces. Numerical investigations were reported by Nelson and Wood (1989a, 1989b) for

flow between two vertical parallel plates and by Lee (1999) for flow in a rectangular, vertical channel. For these geometries a large variety of boundary-condition combinations (assisting versus opposing thermal and mass diffusion effects; UWT or UHF boundary conditions for either side; UWM and UMF boundary conditions for either side) is possible. Only some possible boundary-condition permutations have been investigated, however.

EXAMPLE 10.1. A rectangular plate, 11 cm in width and 52 cm in length, is surrounded by quiescent air at atmospheric pressure and 20 °C temperature. The surface is warm and expected to lose heat to the air so that its temperature will not exceed 65 °C.

(a) Calculate the maximum rate of heat that the plate can dissipate into the air if the surface is horizontal and upward facing.
(b) Suppose the surface can be tilted with respect to the vertical plane by 30°, along either its shorter side or its longer side. Calculate the rate of heat dissipation for the latter two configurations.

SOLUTION. We need to find thermophysical properties. We assume pure air and use the film temperature, $T_{\text{film}} = \frac{1}{2}(T_s + T_\infty) = 315.5$ K, for properties:

$$\rho = 1.119\,\text{kg/m}^3\,,\ C_P = 1006\ \text{J/kg}\,^\circ\text{C},\ k = 0.0268\,\text{W/m K},$$
$$\mu = 1.93 \times 10^{-5}\,\text{kg/m s}\,,\ \text{Pr} = 0.724,$$
$$\boldsymbol{\alpha} = \frac{k}{\rho C_P} = 2.38 \times 10^{-5}\,\text{m}^2/\text{s},$$
$$\beta = \frac{1}{T_{\text{film}}} = 0.00317\,\text{K}^{-1}.$$

Define l_1 and l_2 as the longer and shorter sides of the plate. Then the total surface area and perimeter will be

$$A = l_1 l_2 = (0.52\,\text{m})\,(0.11\,\text{m}) = 0.0572\,\text{m}^2,$$
$$p = 2\,(l_1 + l_2) = 1.26\,\text{m}.$$

Part (a). The surface is horizontal; therefore the characteristic length will be

$$l_c = A/p = 0.0454\,\text{m},$$
$$\text{Ra}_{l_c} = \frac{g\beta\,(T_s - T_\infty)\,l_c^3}{\nu\boldsymbol{\alpha}}$$
$$= \frac{\left(9.81\,\text{m/s}^2\right)\left(0.00317\,\text{K}^{-1}\right)\left[(338 - 293)\,\text{K}\right](0.0454\,\text{m})^3}{\left(\dfrac{1.93 \times 10^{-5}\,\text{kg/m s}}{1.119\,\text{kg/m}^3}\right)(2.38 \times 10^{-5}\,\text{m}^2/\text{s})}$$
$$= 3.19 \times 10^5.$$

We can apply Eq. (10.7.3):

$$\left\langle \text{Nu}_{l_c} \right\rangle = 0.54\text{Ra}_{l_c}^{1/4} = (0.54)\left(3.19 \times 10^5\right)^{1/4} = 12.83,$$
$$\langle h \rangle = \left\langle \text{Nu}_{l_c} \right\rangle \frac{k}{l_c} = (12.83)\,\frac{0.0268\,\text{W/m K}}{0.0454\,\text{m}} = 7.57\,\text{W/m}^2\,\text{K}.$$

We then find the total rate of heat dissipation by writing

$$\dot{Q} = A\,\langle h\rangle\,(T_s - T_\infty) = \left(0.0572\,\mathrm{m}^2\right)\left(7.57\,\mathrm{W/m}^2\ \mathrm{K}\right)\left[(338-293)\,\mathrm{K}\right] = 19.49\,\mathrm{W}.$$

Part (b). For a tilt angle of $\phi = 30^\circ$, because $\phi < 45^\circ$, the boundary layer will be stable.

First we consider the configuration where the shorter side is horizontal. Then,

$$\begin{aligned}\mathrm{Gr}_{l_1} &= \frac{g\cos\phi\,\beta\,(T_s - T_\infty)\,l_1^3}{\nu^2}\\ &= \frac{\left(8.496\,\mathrm{m/s}^2\right)\left(0.00317\,\mathrm{K}^{-1}\right)\left[(338-293)\,\mathrm{K}\right](0.52\,\mathrm{m})^3}{\left(\dfrac{1.93\times10^{-5}\,\mathrm{kg/m\,s}}{1.119\,\mathrm{kg/m}^3}\right)^2}\\ &= 5.734\times10^8.\end{aligned}$$

We can use Eq. (10.4.14) and (10.4.15) because the boundary layer remains laminar:

$$\begin{aligned}\phi(\mathrm{Pr}) &= \frac{1}{(4)^{1/4}}\frac{0.75\sqrt{\mathrm{Pr}}}{\left[0.609+1.221\sqrt{\mathrm{Pr}}+1.238\,\mathrm{Pr}\right]^{1/4}} = 0.3573,\\ \mathrm{Nu}_{l_1} &= \phi(\mathrm{Pr})\mathrm{Gr}_{l_1}^{1/4} = (0.3573)\left(5.734\times10^8\right)^{1/4} = 55.29,\\ \left\langle\mathrm{Nu}_{l_1}\right\rangle_{l_1} &= \frac{4}{3}\mathrm{Nu}_{l_1} = 73.72,\\ \langle h\rangle &= \left\langle\mathrm{Nu}_{l_1}\right\rangle_{l_1}\frac{k}{l_1} = (73.72)\,\frac{0.0268\,\mathrm{W/m\,K}}{0.52\,\mathrm{m}} = 3.8\,\mathrm{W/m}^2\,\mathrm{K},\\ \dot{Q} &= A\,\langle h\rangle\,(T_s - T_\infty) = \left(0.0572\,\mathrm{m}^2\right)\left(3.8\,\mathrm{W/m}^2\,\mathrm{K}\right)\left[(338-293)\,\mathrm{K}\right]\\ &= 9.78\,\mathrm{W}.\end{aligned}$$

Note that the character $\phi(\mathrm{Pr})$ in these equations refers to the function defined in Eq. (10.4.15).

Now let us consider the configuration in which the longer side is horizontal. Then,

$$\begin{aligned}\mathrm{Gr}_{l_2} &= \frac{g\cos\phi\,\beta\,(T_s - T_\infty)\,l_2^3}{\nu^2}\\ &= \frac{\left(8.496\,\mathrm{m/s}^2\right)\left(0.00317\,\mathrm{K}^{-1}\right)\left[(338-293)\,\mathrm{K}\right](0.11\,\mathrm{m})^3}{\left(\dfrac{1.93\times10^{-5}\,\mathrm{kg/m\,s}}{1.119\,\mathrm{kg/m}^3}\right)^2}\\ &= 5.428\times10^6.\end{aligned}$$

Again, the boundary layer remains coherent and laminar, and Eqs. (10.4.14) and (10.4.15) can be applied, leading to

$$\begin{aligned}\mathrm{Nu}_{l_2} &= \phi(\mathrm{Pr})\mathrm{Gr}_{l_2}^{1/4} = (0.3573)\left(5.428\times10^6\right)^{1/4} = 17.24,\\ \left\langle\mathrm{Nu}_{l_2}\right\rangle_{l_2} &= \frac{4}{3}\mathrm{Nu}_{l_2} = 22.99,\end{aligned}$$

$$\langle h \rangle = \langle \mathrm{Nu}_{l_2} \rangle_{l_2} \frac{k}{l_2} = (22.99) \frac{0.0268\,\mathrm{W/m\,K}}{0.11\,\mathrm{m}} = 5.6\,\mathrm{W/m^2\,K},$$
$$\dot{Q} = A \langle h \rangle (T_s - T_\infty) = \left(0.0572\,\mathrm{m^2}\right) \left(5.6\,\mathrm{W/m^2.K}\right) [(338 - 293)\,\mathrm{K}]$$
$$= 14.42\,\mathrm{W}.$$

EXAMPLE 10.2. The upward-facing surface of an inclined surface that is 1.0 m wide and 1.0 m long is subject to a UHF boundary condition with $q_s'' = 15\ \mathrm{W/m^2}$. The angle of inclination with respect to the vertical plane is $\phi = 20^\circ$. The surface is exposed to atmospheric air at an ambient temperature of 20 °C.

Calculate the distributions of heat transfer coefficient and surface temperature along the surface.

SOLUTION. Let us first calculate properties by assuming a film temperature of

$$T_{\mathrm{film}} = T_\infty + 10\,^\circ\mathrm{C} = 30\,^\circ\mathrm{C} = 303\,\mathrm{K}.$$

The relevant thermophysical properties will then be

$$\rho = 1.165\,\mathrm{kg/m^3}\,,\ C_P = 1005\,\mathrm{J/kg\,^\circ C}\,,\ k = 0.0259\,\mathrm{W/m\,K},$$
$$\mu = 1.87 \times 10^{-5}\,\mathrm{kg/m\,s}\,,\ \mathrm{Pr} = 0.727,$$
$$\alpha = \frac{k}{\rho C_P} = 2.21 \times 10^{-5}\,\mathrm{m^2/s},$$
$$\beta = \frac{1}{T_{\mathrm{film}}} = 0.0033\,\mathrm{K^{-1}}.$$

In view of the large width, we assume that the boundary layer is 2D. (In other words, we neglect the end effects and assume that the width of the plate is infinitely large.) We can now check to see whether the boundary layer remains laminar:

$$\mathrm{Gr}_l^* = \frac{(g \cos\phi)\,\beta q_s'' l^4}{k \nu^2} = \frac{(9.218\,\mathrm{m/s^2})\,(0.0033\,\mathrm{K^{-1}})\,[15\,\mathrm{W/m^2}]\,(1.0\,\mathrm{m})^4}{(0.0259\,\mathrm{W/m\,K}) \left(\dfrac{1.87 \times 10^{-5}\,\mathrm{kg/m\,s}}{1.165\,\mathrm{kg/m^3}}\right)^2}$$
$$= 6.82 \times 10^{10}.$$

Because the maximum modified Grashof number is small, we assume that the natural convection boundary layer remains laminar (see Table 10.1). We use Eqs. (10.5.35)–(10.5.37), where x is parametrically varied in the $0 < x < 1\,m$ range. The results are summarized in the following list.

x (m)	Gr_x^*	T_s (°C)
0.1	6.823×10^6	24.97
0.2	1.091×10^8	25.71
0.3	5.527×10^8	26.19
0.4	1.747×10^9	26.55
0.5	4.265×10^9	26.85
0.6	8.843×10^9	27.11
0.7	1.638×10^{10}	27.33
0.8	2.795×10^{10}	27.53
0.9	4.477×10^{10}	27.71
1.0	6.823×10^{10}	27.87

EXAMPLE 10.3. A 2D vertical rectangular chamber similar to that in Fig. 10.17, 17 cm in height and 0.5 cm in width, is filled with water. The vertical surfaces are at 353 K and 303 K each, and the top and bottom surfaces are adiabatic.

Determine the flow regime in the chamber. Calculate the rate of heat transfer, per meter depth, between the two surfaces.

SOLUTION. First, let us find the thermophysical properties at the average temperature of 328 K:

$$\rho = 985.5\,\text{kg/m}^3\,,\ C_P = 4182\,\text{J/kg}\,^\circ\text{C},\ k = 0.6358\,\text{W/m K},$$
$$\mu = 5.05 \times 10^{-4}\,\text{kg/m s},\ \text{Pr} = 3.32,$$
$$\beta = 4.89 \times 10^{-4}\ \text{K}^{-1},$$
$$\boldsymbol{\alpha} = \frac{k}{\rho C_P} = 1.54 \times 10^{-7}\,\text{m}^2/\text{s}.$$

To find the flow regime, we should use the discussion in Section 10.12. Therefore,

$$\begin{aligned}
\text{Ra}_l &= \frac{g\beta\,(T_{s,1} - T_{s,2})\,l^3}{\nu\boldsymbol{\alpha}} \\
&= \frac{\left(9.81\,\text{m/s}^2\right)\left(4.89 \times 10^{-4}\ \text{K}^{-1}\right)\left[(353 - 303)\,\text{K}\right](0.17\,\text{m})^3}{\left(\dfrac{5.05 \times 10^{-4}\,\text{kg/m s}}{985.5\,\text{kg/m}^3}\right)(1.54 \times 10^{-7}\,\text{m}^2/\text{s})}, \\
&= 1.49 \times 10^{10}, \\
\frac{l}{S} &= \frac{0.17\,\text{m}}{0.005\,\text{m}} = 34, \\
\text{Ra}_l^{1/4} &= (1.49 \times 10^{10})^{1/4} = 349.4, \\
\text{Ra}_l^{-1/4} &= 0.00286.
\end{aligned}$$

Because Eqs. (10.12.4a) and (10.12.4b) are satisfied, we are dealing with the boundary-layer regime.

To calculate the heat transfer rate, first let us calculate Ra_S:

$$\begin{aligned}
\text{Ra}_S &= \frac{g\beta\,(T_{s,1} - T_{s,2})\,S^3}{\nu\boldsymbol{\alpha}} \\
&= \frac{\left(9.81\,\text{m/s}^2\right)\left(4.89 \times 10^{-4}\ \text{K}^{-1}\right)\left[(353 - 303)\,\text{K}\right](0.005\,\text{m})^3}{\left(\dfrac{5.05 \times 10^{-4}\,\text{kg/m s}}{985.5\,\text{kg/m}^3}\right)(1.54 \times 10^{-7}\,\text{m}^2/\text{s})}, \\
&= 3.8 \times 10^5.
\end{aligned}$$

We can use the correlation of McGregor and Emery (1969), Eq. (10.12.9):

$$\begin{aligned}
\langle \text{Nu}_S \rangle_l &= 0.42\text{Ra}_S^{0.25}\,\text{Pr}^{0.012}\,(l/S)^{-0.3} = (0.42)\,(3.8 \times 10^5)^{0.25}\,(3.32)^{0.012}\,(34)^{-0.3} \\
&= 3.67, \\
\langle h \rangle &= \langle \text{Nu}_S \rangle \frac{k}{S} = (3.67)\,\frac{0.6358\,\text{W/m K}}{0.005\,\text{m}} = 467\,\text{W/m}^2\ \text{K}, \\
\dot{Q} &= \langle h \rangle\, l\,(T_{s,1} - T_{s,2}) = \left(467\,\text{W/m}^2\,\text{K}\right)(0.17\,\text{m})\left[(353 - 303)\,\text{K}\right] = 3970\,\text{W/m}.
\end{aligned}$$

The heat transfer rate is per meter depth of the 2D object.

EXAMPLE 10.4. Repeat the solution of Example 10.3, this time assuming that the chamber is horizontal.

SOLUTION. We can now use the correlation of Hollands et al. (1975), Eqs. (10.13.4) and (10.13.5):

$$C = 1 - \ln\left(\frac{\mathrm{Ra}_S^{1/3}}{140}\right) = 1 - \ln\left[\frac{\left(3.8\times10^5\right)^{1/3}}{140}\right] = 1.66,$$

$$\left[1 - \frac{1708}{\mathrm{Ra}_S}\right] = 1 - \frac{1708}{3.8\times10^5} = 0.9955,$$

$$\left[\left(\frac{\mathrm{Ra}_S}{5830}\right)^{1/3} - 1\right] = \left(\frac{3.8\times10^5}{5830}\right)^{1/3} - 1 = 3.022,$$

$$\left[\frac{\mathrm{Ra}_S^{1/3}}{140}\right]^C = \left[\frac{\left(3.8\times10^5\right)^{1/3}}{140}\right]^{1.66} = 0.3347,$$

$$\Rightarrow \langle \mathrm{Nu}_S\rangle = 6.125,$$

$$\langle h\rangle = \langle \mathrm{Nu}_S\rangle \frac{k}{S} = (6.125)\,\frac{0.6358\,\mathrm{W/m\,K}}{0.005\,\mathrm{m}} = 778.9\,\mathrm{W/m^2\,K},$$

$$\dot{Q} = \langle h\rangle\, l\,(T_{s,1} - T_{s,2}) = \left(778.9\,\mathrm{W/m^2\,K}\right)(0.17\,\mathrm{m})\,[(353-303)\,\mathrm{K}]$$

$$= 6621\,\mathrm{W/m}.$$

EXAMPLE 10.5. Repeat the solution of Example 10.3, this time assuming that the chamber is tilted so that it makes an angle of 20° with the horizontal plane (see Fig. 10.22).

SOLUTION. We have $l/S = 34 > 12$. Table 10.4 shows that $\phi'^* = 70°$; therefore $\phi' < \phi'^*$ and we can use the correlation of Catton (1978), Eq. (10.14.5):

$$\left[1 - \frac{1708}{\mathrm{Ra}_S\cos\phi'}\right] = 1 - \frac{1708}{(3.8\times10^5)\cos(20°)} = 0.9951,$$

$$\left[1 - \frac{(\sin 1.8\phi')^{1.6}\,(1708)}{\mathrm{Ra}_S\cos\phi'}\right] = 1 - \frac{(\sin 36°)^{1.6}\,(1708)}{(3.8\times10^5)\cos(20°)} = 0.9979,$$

$$\left\{\left[\frac{\mathrm{Ra}_S\cos\phi'}{5,830}\right]^{1/3} - 1\right\} = \left\{\left[\frac{\left(3.8\times10^5\right)\cos(20°)}{5830}\right]^{1/3} - 1\right\} = 2.94$$

$$\Rightarrow \langle \mathrm{Nu}_S\rangle = 5.37.$$

This will lead to

$$\langle h\rangle = \langle \mathrm{Nu}_S\rangle \frac{k}{S} = 682.9\,\mathrm{W/m^2\,K},$$

$$\dot{Q} = \langle h\rangle\, l\,(T_{s,1} - T_{s,2}) = 5804\,\mathrm{W/m}.$$

PROBLEMS

Problem 10.1. Consider natural convection on a flat vertical surface. Prove that with Eq. (10.4.17) a similarity solution represented by Eqs. (10.4.18)–(10.4.19a) can be derived.

Problem 10.2. Consider natural convection of a flat, vertical surface with uniform wall heat flux (UHF) surface condition. Derive Eqs. (10.5.28) and (10.5.29). Also, show that Eqs. (10.5.32) and (10.5.33) are solutions to the latter two differential equations.

Problem 10.3. A rectangular plate is 20 cm in width and 45 cm in length. The plate is in quiescent air at atmospheric pressure and 293 K temperature. The temperature of plate surface is 350 K.

(a) Calculate the rate of heat transfer from the plate to the air, if the surface is horizontal and upward facing.
(b) Suppose the surface can be tilted with respect to the vertical pane by 30° its longer side. Calculate the rate of heat dissipation for the latter configurations.

Problem 10.4. A very large tank containing water at 350 K is separated from air by a vertical plate that is 25 cm in width and 10 cm in height. On the outside the plate is exposed to atmospheric air at 320 K temperature.

(a) Calculate the heat transfer rate through the plate assuming that water and air are both stagnant, neglecting the effect of radiation.
(b) Repeat part (a), this time assuming that air has a velocity of 0.4 m/s in the vertical, upward direction.

For water, assume that $\beta = 7.3 \times 10^{-4}\,\mathrm{K}^{-1}$.

Problem 10.5. A circular heater plate with 80-mm diameter is placed in a tank containing liquid nitrogen at 1-MPa pressure and 80 K temperature. The upward facing side of the plate is maintained at 100 K. Find the heat transfer rate between the heater and liquid nitrogen.

For liquid nitrogen properties, you may assume that

$$\rho = 745.6\,\mathrm{kg/m^3},$$
$$C_P = 2.122\frac{\mathrm{kJ}}{\mathrm{kg\,K}},\ \mu = 104 \times 10^{-6}\,\mathrm{N}\frac{\mathrm{s}}{\mathrm{m^2}},\ k = 0.122\frac{\mathrm{W}}{\mathrm{m\,K}},$$
$$\mathrm{Pr} = 1.80,\ \beta = 0.0072\,\mathrm{K}^{-1}.$$

Problem 10.6. A vertical rectangular chamber is made of two 500 mm × 500 mm parallel plates that are separated from each other by 15 mm. The chamber is filled with helium at 152-kPa pressure. One of the two plates is at 300 K, and the other surface is at 100 K. Calculate the heat transfer rate between the two plates.

Problem 10.7. The top surface of a flat, rectangular plate is at a uniform temperature of 100 °C. The plate is in stagnant atmospheric air at a temperature of 20 °C.

(a) For inclination angles with respect to the vertical direction of 20° and 45°, find the distance from the leading edge of the plate where transition from laminar to turbulent flow would take place.

(b) Assuming a total length of 1 m and a width of 0.5 m calculate the average heat transfer coefficient for the aforementioned two angles, as well as horizontal and vertical configurations.

Problem 10.8. For natural convection of a fluid with $\mathrm{Pr} > 1$ on a flat vertical surface, where $\delta > \delta_{\mathrm{th}}$, the following approximate velocity and temperature profiles can be assumed for the velocity and thermal boundary layers:

$$u = U_0 \exp\left[-(y/\delta)\right]\left\{1 - \exp\left[-(y/\delta_{\mathrm{th}})\right]\right\},$$
$$\frac{T - T_\infty}{T_s - T_\infty} = \exp\left[-(y/\delta_{\mathrm{th}})\right].$$

Using the integral method and assuming that the $\delta/\delta_{\mathrm{th}}$ ratio is known, derive differential equations for δ and δ_{th}.

Problem 10.9. A 1-cm outer-diameter cylinder, with a total length of 20 cm and a surface temperature of 90 °C is submerged in water at 20 °C.

Calculate the total rate of heat loss from the cylinder when the cylinder is horizontal and vertical.

Problem 10.10. Consider steady-state, natural convection on the outside surface of a vertical cylinder whose surface temperature is T_s. Assume that the radius of the cylinder is relatively small, such that the transverse curvature cannot be neglected.

(a) Write the mass, momentum, and energy conservation equations for the natural-convection boundary layer and their appropriate boundary conditions.

(b) Cast the conservation equations in terms of nondimensional parameters:

$$\psi = 4\nu F(\varepsilon, \eta) R_0 \left(\frac{\mathrm{Gr}_x}{4}\right)^{1/4},$$
$$\eta = \left[\frac{g\beta(T_s - T_\infty)}{4\nu^2}\right]^{1/4}\left(\frac{r^2 - R_0^2}{2R_0 x^{1/4}}\right),$$
$$\theta = \frac{T - T_\infty}{T_s - T_\infty},$$

where Gr_x is defined as in Eq. (10.4.6), and,

$$\varepsilon = \frac{2(x/R_0)^{1/4}}{\left[g\beta(T_s - T_\infty)\dfrac{R_0^3}{4\nu^2}\right]^{1/2}}.$$

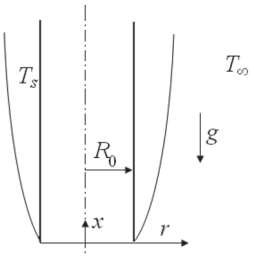

Figure P10.10

Problem 10.11. For natural convection in the annular space between two long concentric, horizontal cylinders, a correlation proposed by Raithby and Hollands (1974) is (see Table Q.6 in Appendix Q)

$$\frac{k_{\text{eff}}}{k} = 0.386 \left[\frac{\ln\left(\frac{D_o}{D_i}\right)}{(R_0 - R_i)^{3/4} \left(\frac{1}{D_i^{3/5}} + \frac{1}{D_0^{3/5}}\right)^{5/4}} \right] \left(\frac{\text{Pr}}{0.861 + \text{Pr}}\right)^{1/4} \text{Ra}_{(R_o - R_i)}^{1/4}.$$

Prove that this correlation is equivalent to

$$q' = \frac{2.425k\,(T_{s,i} - T_{s,0})}{\left[1 + \left(\frac{D_i}{D_o}\right)^{3/5}\right]^{5/4}} \left(\frac{\text{Pr}\,\text{Ra}_{D_i}}{0.861 + \text{Pr}}\right)^{1/4},$$

where $T_{s,i}$ and $T_{s,0}$ are the inner and outer surface temperatures of the annular space and q' is the heat transfer rate per unit length of the cylinders.

Problem 10.12. A 0.1-m-diameter sphere containing radioactive waste is to be maintained under deep water. The water temperature is 20 °C. To avoid boiling on the surface, it is found that the average surface temperature of the sphere must not exceed 120 °C.

(a) Calculate the total radioactive decay heat rate that the sphere can contain.
(b) Repeat the previous calculations, this time assuming that the container is replaced with a cube with the same total volume.

Problem 10.13. A vertical and rectangular surface that is 3 m high and 80 cm wide, is placed in atmospheric and quiescent air. The ambient air temperature is 20 °C. A uniform and constant heat flux of 100 W/m^2 is imposed on the surface.

(a) Calculate the heat transfer coefficient and surface temperature at the middle and at the trailing edge of the surface.
(b) Does transition to turbulence occur on the surface? If so, determine the location where the transition takes place.

Problem 10.14. The vessel shown in the figure is full to the rim with water at 90 °C. The water in the vessel is mildly stirred, so that the thermal resistance that is due

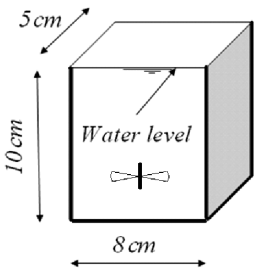

Figure P10.14

to convection on the inner surface of the walls can be neglected. The vessel wall, which is 3 mm thick, is made of aluminum. The vessel is in atmospheric air with a temperature of 20 °C. Calculate the total rate of heat loss from the vessel to air, assuming that the air is quiescent.

For simplicity, neglect heat loss from the bottom of the vessel, and neglect the effect of evaporation at the free surface of water.

Problem 10.15. A 2D vertical rectangular chamber similar to that of Fig. 10.17, 9 cm in height and 1 cm in width, is filled with atmospheric air. The vertical surfaces are at 100 °C and 20 °C temperatures, and the top and bottom surfaces are adiabatic.

(a) Determine the natural-convection heat transfer regime and calculate the rate of heat transfer, per meter depth, between the two surfaces.
(b) Repeat part (a), this time assuming that the rectangle is inclined by 25°, as in Fig. 10.22.

Problem 10.16. A double-glazed window is 1.3 m high and 0.7 m wide. The space between the glass plates making the double-glazed window, which is 2 mm thick, is filled with atmospheric air. Calculate the rate of heat loss through the window when the two glass surfaces are at 10 °C and −10 °C. Neglect the contribution of radiation heat transfer.

Problem 10.17. Two large horizontal and parallel plates are separated from each other by 3 mm of quiescent atmospheric air. The top surface is at −20 °C, and the bottom surface is at 15 °C.

(a) Calculate the heat flux that is exchanged between the two surfaces.
(b) Repeat the calculation, this time assuming that the distance between the two plates is 3 cm.

Mass Transfer and Combined Heat and Mass Transfer

Problem 10.18. In Problem 10.14, repeat the calculations this time accounting for the contribution of evaporation at the free water surface. Assume, for simplicity, that heat transfer at water surface is gas-side controlled. Assume that the ambient air has a relative humidity of 25%.

Problem 10.19. A vessel with a surface that is 10 cm × 30 cm in dimensions contains water at 40 °C. The surrounding air is at 20 °C and can be assumed to be dry. The water is agitated so that its temperature remains uniform.

(a) Calculate the evaporation rate at the surface of water, assuming that the air is stagnant. For simplicity assume that there is no wave or any other motion at the water surface. Also, for simplicity, neglect the effect of mass diffusion on natural convection.
(b) The water contains chlorine at a concentration of 25 ppm by weight. Calculate the rate of mass transfer of chlorine into the air.

Problem 10.20. The cylindrical object shown in the figure is covered by a layer of naphthalene. The surface of the cylinder is at 50 °C, and the surrounding air is at 20 °C. Calculate the heat transfer rate and the total rate of naphthalene released into the air. The air is dry and stagnant.

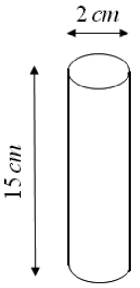

Figure P10.20

11 Mixed Convection

Mixed convection refers to conditions when forced and natural (buoyancy-driven) effects are both important and neither one can be neglected. Situations in which forced and buoyancy-driven convection terms are of similar orders of magnitude obviously fall in the mixed-convection flow category. However, in many applications we deal with either a predominantly forced convective flow in which buoyancy-driven effects are small but considerable or a predominantly buoyancy-driven flow in which a nonnegligible forced-flow contribution is also present.

Mixed convection is relatively common in nature. In more recent applications, it occurs in rotating flow loops and in the cooling minichannels in the blades of modern gas turbines. In these flow loops, Coriolis centripetal forces arise because of the rotation. When the fluid is compressible, secondary flow caused by the centripetal effect contributes to the wall–fluid heat transfer.

Mixed-convection effects are not always undesirable. In some applications we may intentionally seek buoyancy effect in order to augment heat transfer. Some recent applications of supercritical fluids are examples to this point. The very large compressibility of these fluids, which is achieved without a phase change (although a pseudo–phase change does occur for near-critical fluids) is very useful.

In situations that are predominantly forced flow, buoyancy-driven effects have four types of impact on the overall flow field:

1. They contribute (assist, resist, or do both at different parts of the flow field) to the forced-flow velocity field.
2. They cause secondary flows. The secondary flows can enhance or reduce the heat transfer rate.
3. They affect transition from laminar to turbulent flow.
4. In turbulent flow, they can modify turbulence.

11.1 Laminar Boundary-Layer Equations and Scaling Analysis

A scaling analysis can be performed for a laminar mixed-convection boundary layer, the same way that was done for natural convection in the previous chapter. This type of analysis will provide insight into the relevant dimensionless numbers and the relative magnitudes of forced and buoyancy-driven advective terms. It will also provide

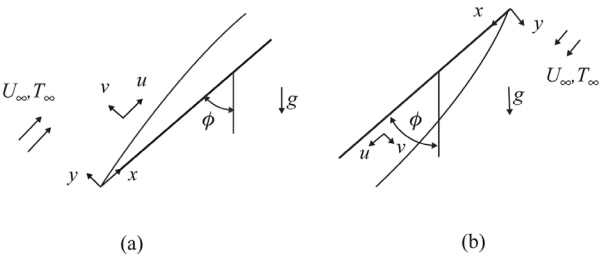

Figure 11.1. Mixed-convection flow on an inclined flat surface: (a) flow over the inclined surface, (b) flow under the inclined surface.

valuable information about the generic forms of the heat transfer correlation for laminar flow mixed convection.

Consider the 2D flow field shown in Figs. 11.1(a) and 11.1(b). Assume steady-state, and assume that Boussinesq's approximation applies. The aplication of Boussinesq's approximation is in fact justified in the vast majority of mixed-convection problems. The conservation equations for this problem were derived in Section 10.3, leading to the momentum equation in the form

$$\rho\left(u\frac{du}{dx}+v\frac{du}{dy}\right)=\mu\left(\frac{\partial^2 u}{\partial x^2}+\frac{\partial^2 u}{\partial y^2}\right)\pm\rho$$
$$g\cos\phi\beta\,(T-T_\infty)\pm\rho_\infty g\beta\sin\phi\int_y^\infty(T-T_\infty)\,dy. \qquad (10.3.32)$$

For the terms that appear with the $\pm$ sign, the positive signs are for the flow field depicted in Fig. 11.1(a) and the negative signs apply to Fig. 11.1(b). Equation (10.3.26), representing the energy conservation equation for the boundary layer when viscous dissipation is neglected, also applies. We can nondimensionalize these equations according to

$$x^*=x/l,\ y^*=y/l,\ u^*=u/U_\infty,\ v^*=v/U_\infty,\ \theta=\frac{T-T_\infty}{T_s-T_\infty}.$$

Arguments similar to those previously made for forced- and natural-convection boundary layers can be made regarding the mixed-convection boundary layer. With the exception of conditions in which a predominantly natural-convection flow field is opposed by a weak forced flow (for example, on a heated, upward-facing surface with a weak opposing downward flow) we will have $\delta \ll x$ and $\delta_{\text{th}} \ll x$ everywhere except for the immediate vicinity of the leading edge (i.e., $x \to 0$). As a result, order-of-magnitude comparisons lead to the conclusion that

$$\frac{\partial^2 u}{\partial x^2}\ll\frac{\partial^2 u}{\partial y^2},$$
$$\frac{\partial^2 T}{\partial x^2}\ll\frac{\partial^2 T}{\partial y^2}.$$

The terms $\frac{\partial^2 u}{\partial x^2}$ and $\frac{\partial^2 T}{\partial x^2}$ can thus be neglected in the boundary-layer momentum and energy equations, respectively.

For the conditions in which a predominantly natural-convection flow field adjacent to a surface is opposed by a forced flow, the fluid velocity far away from the surface is in opposite direction to the flow at the vicinity of the surface. The boundary-layer approximations will not be applicable to such cases.

When the preceding terms are neglected, the dimensionless mass, x-direction momentum, and energy equations reduce to

$$\frac{\partial u^*}{\partial x^*} + \frac{\partial u^*}{\partial y^*} = 0, \tag{11.1.1}$$

$$u^* \frac{\partial u^*}{\partial x^*} + v^* \frac{\partial u^*}{\partial y^*} = \frac{1}{\mathrm{Re}_l} \frac{\partial^2 u^*}{\partial y^{*2}} + \frac{\mathrm{Gr}_l}{\mathrm{Re}_l^2} \left[\theta \cos\phi + \sin\phi \frac{d}{dx^*} \int_{y^*}^{\infty} \theta dy^* \right], \tag{11.1.2}$$

$$u^* \frac{\partial \theta}{\partial x^*} + v^* \frac{\partial \theta}{\partial y^*} = \frac{1}{\mathrm{Re}_l \mathrm{Pr}} \frac{\partial^2 \theta}{\partial y^{*2}}. \tag{11.1.3}$$

We have thus rederived the familiar dimensionless parameters

$$\mathrm{Re}_l = \frac{U_\infty l}{\nu}, \ \mathrm{Gr}_l = \frac{g\beta (T_s - T_\infty) l^3}{\nu^2}, \ \mathrm{Pr} = \nu/\alpha. \tag{11.1.4}$$

We can also define the *Richardson number*, Ri, as

$$\mathrm{Ri} = \frac{\mathrm{Gr}_l}{\mathrm{Re}_l^2}. \tag{11.1.5}$$

The thermal boundary condition will give, as for other situations,

$$q_s'' = -k \left. \frac{\partial T}{\partial y} \right|_{y=0} = h (T_s - T_\infty).$$

From there we get

$$\mathrm{Nu}_l = hl/k = -\left(\frac{\partial \theta}{\partial y^*} \right)_{y^*=0} \tag{11.1.6}$$

The bracketed term on the right-hand side of Eq. (11.1.2) represents the contribution of natural convection. Based on the relative orders of magnitude of the terms in Eq. (11.1.2), the following criteria for the flow and heat transfer regimes can be derived,

- Pure forced convection (negligible natural convection effects):

$$\mathrm{Ri} \ll 1. \tag{11.1.7}$$

- Pure natural convection (negligible forced-convection effects):

$$\mathrm{Ri} \gg 1. \tag{11.1.8}$$

- Mixed convection:

$$\mathrm{Ri} \approx 1. \tag{11.1.9}$$

The preceding analysis also shows that the correlations for heat transfer coefficient in mixed convection should follow the generic form

$$\mathrm{Nu}_l = f (\mathrm{Re}_l, \mathrm{Pr}, \mathrm{Gr}_l, \phi). \tag{11.1.10}$$

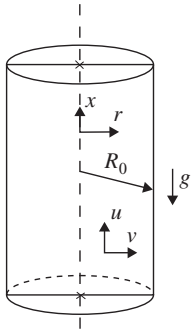

Figure 11.2. Mixed convection in a vertical pipe.

The preceding analysis and its resulting criteria dealt with external flow. We now review internal flow. Consider laminar and axisymmetric flow in a vertical circular channel (Fig. 11.2). For simplicity, let us assume steady state. Using Boussinesq's approximation (which, as mentioned before, is justified for the vast majority of mixed convection problems), we find that the conservation equations become

$$\frac{1}{r}\frac{\partial}{\partial r}(rv) + \frac{\partial u}{\partial x} = 0, \tag{11.1.11}$$

$$\rho\left(v\frac{\partial u}{\partial r} + u\frac{\partial u}{\partial x}\right) = -\frac{dP}{dx} \mp \rho g + \frac{\mu}{r}\frac{\partial}{\partial r}\left(r\frac{\partial u}{\partial r}\right), \tag{11.1.12}$$

$$\rho C_P\left(v\frac{\partial T}{\partial r} + u\frac{\partial T}{\partial x}\right) = \frac{k}{r}\frac{\partial}{\partial r}\left(r\frac{\partial T}{\partial r}\right), \tag{11.1.13}$$

where $\mp$ means upward and downward flow, respectively. (The negative sign represents upward flow, and coordinate x represents the flow direction.)

In the absence of heat transfer and forced flow, only hydrostatic pressure changes are important, and in that case Eq. (11.1.12) would give

$$\frac{dP_1}{dx} = \mp\rho_{\text{in}} g, \tag{11.1.14}$$

where the subscript in represents conditions at the inlet to the channel and P_1 is the local pressure in the absence of heat transfer and forced flow. Subtracting Eq. (11.1.14) from (11.1.12), we get

$$\rho\left(v\frac{\partial u}{\partial r} + u\frac{\partial u}{\partial x}\right) = -\frac{d}{dx}(P - P_1) \mp (\rho - \rho_{\text{in}})\, g + \frac{\mu}{r}\frac{\partial}{\partial r}\left(r\frac{\partial u}{\partial r}\right). \tag{11.1.15}$$

We can now write

$$\rho - \rho_{\text{in}} \approx -\rho\beta\,(T - T_{\text{in}})\,. \tag{11.1.16}$$

We now nondimensionalize Eqs. (11.1.11)–(11.1.13) by defining

$$u^* = \frac{u}{U_m}, \quad v^* = \frac{v}{U_m}\text{Re}_{\text{D}}\text{Pr}, \quad r^* = \frac{r}{R_0},$$

$$x^* = \frac{x/R_0}{\text{Re}_D\text{Pr}}, \quad P^* = \frac{P - P_1}{\rho U_m^2\text{Pr}}, \quad \theta = \frac{T - T_s}{T_{\text{in}} - T_s},$$

where $\mathrm{Re}_D = \rho U_m (2R_0)/\mu$, and U_m represents the mean velocity. The conservation equations then become

$$\frac{1}{r^*}\frac{\partial}{\partial r^*}(r^* v^*) + \frac{\partial u^*}{\partial x^*} = 0, \tag{11.1.17}$$

$$\frac{1}{\mathrm{Pr}}\left(v^*\frac{\partial u^*}{\partial r^*} + u^*\frac{\partial u^*}{\partial x^*}\right) = -\frac{dP^*}{dx^*} + \frac{1}{r^*}\frac{\partial}{\partial r^*}\left(r^*\frac{\partial u^*}{\partial r}\right) \pm \frac{\mathrm{Gr}_D}{\mathrm{Re}_D}\theta, \tag{11.1.18}$$

$$v^*\frac{\partial \theta}{\partial r^*} + u^*\frac{\partial \theta}{\partial x^*} = \frac{\partial}{\partial r^*}\left(r^*\frac{\partial \theta}{\partial r^*}\right), \tag{11.1.19}$$

where

$$\mathrm{Gr}_D = \frac{g\beta (T_s - T_{\mathrm{in}}) D^3}{\nu^2}. \tag{11.1.20}$$

Note that $\pm$ now implies upward flow (for a positive sign) and downward flow (for a negative sign), respectively. The following crude criteria can thus be derived.

- Pure forced convection (negligible natural-convection effects):

$$\frac{\mathrm{Gr}_D}{\mathrm{Re}_D} \ll 1. \tag{11.1.21}$$

- Pure natural convection (negligible forced-convection effects):

$$\frac{\mathrm{Gr}_D}{\mathrm{Re}_D} \gg 1. \tag{11.1.22}$$

- Mixed convection:

$$\frac{\mathrm{Gr}_D}{\mathrm{Re}_D} \approx 1. \tag{11.1.23}$$

We can also specify the expected form of heat transfer correlations by noting that

$$q_s'' = -k\left.\frac{\partial T}{\partial y}\right|_{r=R_0} = h_x (T_s - T_m), \tag{11.1.24}$$

where T_m is the bulk temperature that is defined as

$$T_m = \frac{1}{\dot{m}}\int_0^{R_0} 2\pi r \rho u T dr. \tag{11.1.25}$$

Clearly the definition of bulk temperature is identical to the mean temperature that is used for internal forced convection. We thus get

$$\mathrm{Nu}_D = \frac{hD}{k} = \frac{\mathrm{D}q_s''}{k(T_s - T_m)} = -\frac{2}{\theta_m}\left(\frac{\partial \theta}{\partial r^*}\right)_{r^*=1}. \tag{11.1.26}$$

This equation implies that for local Nusselt numbers we should expect

$$\mathrm{Nu}_{D.x} = f\left(x/R_0, \mathrm{Pr}, \frac{\mathrm{Gr}_D}{\mathrm{Re}_D}\right). \tag{11.1.27}$$

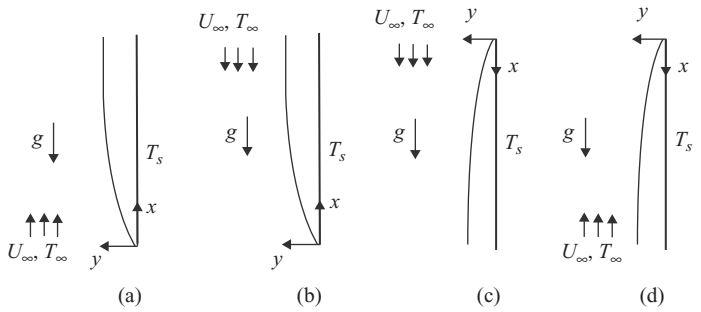

Figure 11.3. Mixed convection on a heated vertical surface: (a) assisting flow for heated surface; (b) opposing flow for heated surface; (c) assisting flow for cooled surface; (d) opposing flow for cooled surface.

In analysis and discussion of mixed-convection processes, a *buoyancy number* is sometimes defined as

$$\mathrm{Bo} = \mathrm{Gr}_l/\mathrm{Re}_l^m. \tag{11.1.28}$$

When $m = 2$, this equation gives Richardson's number, which was defined earlier.

11.2 Solutions for Laminar Flow

For flow parallel to a vertical flat plate, shown in Fig. 11.3, similarity solutions were derived for conditions in which either the forced-convection mechanism or the natural-convection mechanism was dominant (Oosthuizen and Naylor, 1999). An integral-method-based solution was also successfully derived (Kobus and Wedekind, 1996). Extensive numerical investigations were also conducted, a synopsis of which can be found in Chen and Armaly (1987).

The similarity solutions for predominantly forced-convection or predominantly natural-convection conditions (Oosthuizen and Naylor, 1999) are based on a perturbation and expansion technique. Good discussions of the perturbation and expansion technique applied to heat transfer problems can be found in Aziz and Na (1984) and Aziz (1987). The similarity solution for the predominantly forced-flow conditions are subsequently briefly reviewed. It will serve as a good example for the perturbation and expansion method.

Similarity Solution for Predominantly Forced Laminar Flow on a Flat Vertical Surface

Consider the 2D flow field in Fig. 11.3. The steady-state conservation equations are

$$\frac{\partial u}{\partial x} + \frac{\partial v}{\partial x} = 0, \tag{11.2.1}$$

$$u\left(\frac{\partial u}{\partial x}\right) + v\left(\frac{\partial u}{\partial y}\right) = \nu\frac{\partial^2 u}{\partial y^2} \pm g\beta\left(T - T_\infty\right), \tag{11.2.2}$$

$$u\frac{\partial T}{\partial x} + v\frac{\partial T}{\partial y} = \alpha\frac{\partial^2 T}{\partial y^2}, \tag{11.2.3}$$

where the positive and negative signs in Eq. (11.3.2) represent assisting [Fig. 11.3(a)] and opposing [Fig. 11.3(b)] flow conditions, respectively. The boundary conditions for these equations are

$$u = 0, \quad v = 0, \quad T = T_s \quad \text{at} \quad y = 0, \tag{11.2.4}$$

$$u = U_\infty, \quad v = 0, \quad T = T_\infty \quad \text{at} \quad y \to \infty. \tag{11.2.5}$$

Because forced convection is predominant, let us recast these equations using the coordinate transformation and similarity parameters of Blasius (Section 3.1), where now

$$\psi = \sqrt{\nu x U_\infty}\mathcal{F}(\eta). \tag{11.2.6}$$

Equations (3.1.5), (3.1.11), and (3.1.12) all apply, provided that everywhere $f(\eta)$ is replaced with $\mathcal{F}(\eta)$. We also assume that

$$\frac{T - T_\infty}{T_s - T_\infty} = \varphi(\eta). \tag{11.2.7}$$

The stream function in Eq. (3.1.10) will satisfy Eq. (11.3.1). Equations (11.2.2) and (11.2.3) will give, respectively,

$$\mathcal{F}''' + \frac{1}{2}\mathcal{F}\mathcal{F}'' \pm \mathrm{Ri}\,\varphi = 0, \tag{11.2.8}$$

$$\varphi'' + \frac{1}{2}\,Pr\,\mathcal{F}\varphi' = 0, \tag{11.2.9}$$

where the Richardson number is defined as $\mathrm{Ri} = \mathrm{Gr}_x/\mathrm{Re}_x^2$.

In comparison with Eq. (3.1.13), Eq. (11.2.8) includes the term $\pm\mathrm{Ri}\,\varphi$, which represents the effect of buoyancy. Equation (11.2.9) is similar to Eq. (3.2.10). It must be emphasized, however, that the function $\mathcal{F}(\eta)$ is not the same as the function $f(\eta)$ in Blasius' solution, because Blasius' solution did not consider buoyancy. The boundary conditions for the preceding equations are

$$\mathcal{F} = 0, \quad \mathcal{F}' = 0, \quad \varphi = 1 \quad \text{at} \quad \eta = 0, \tag{11.2.10}$$

$$\mathcal{F}' = 1, \quad \varphi = 0 \quad \text{at} \quad \eta \to \infty. \tag{11.2.11}$$

The presence of Ri in Eq. (11.2.8), which depends on x, makes it clear that this transformation has not made a similarity solution possible. However, given that $\mathrm{Ri} \ll 1$ (after all, this is required for the predominance of forced convection), the solutions to Eqs. (11.2.8) and (11.2.9) are assumed to be of the form

$$\mathcal{F} = \sum_{j=0}^{\infty} \mathrm{Ri}^j \mathcal{F}^{(j)} = \mathcal{F}^{(0)} + \mathrm{Ri}\,\mathcal{F}^{(1)} + \mathrm{Ri}^2\mathcal{F}^{(2)} + \cdots + \mathrm{Ri}^{n-1}\mathcal{F}^{(n-1)} + O(\mathrm{Ri}^n), \tag{11.2.12}$$

$$\varphi = \sum_{j=0}^{\infty} \mathrm{Ri}^j \varphi^{(j)} = \varphi^{(0)} + \mathrm{Ri}\,\varphi^{(1)} + \mathrm{Ri}^2\varphi^{(2)} + \cdots + \mathrm{Ri}^{n-1}\varphi^{(n-1)} + O(\mathrm{Ri}^n), \tag{11.2.13}$$

where $O(Ri^n)$ means the order of magnitude of Ri^n. The functions $\mathcal{F}^{(0)}$ and $\varphi^{(0)}$ actually represent the limit of $Ri \to 0$, namely purely forced-convection conditions. Therefore,

$$\mathcal{F}^{(0)} = f(\eta), \tag{11.2.14}$$

$$\varphi^{(0)} = \theta(\eta), \tag{11.2.15}$$

where $f(\eta)$ is Blasius' solution and $\theta(\eta)$ is the solution discussed in Section 3.2.

We can now proceed by neglecting terms of the order of Ri^2 and higher. We then have

$$\mathcal{F} = f + Ri\, f^{(1)}, \tag{11.2.16}$$

$$\varphi = \theta + Ri\, \varphi^{(1)}. \tag{11.2.17}$$

These equations are now substituted into Eqs. (11.2.8) and (11.2.9), and that leads to

$$f''' + \frac{1}{2} f f'' + Ri\left[\mathcal{F}'''^{(1)} + \frac{f\mathcal{F}''^{(1)}}{2} + \frac{\mathcal{F}^{(1)} f''}{2} \pm \theta\right] = 0, \tag{11.2.18}$$

$$\theta'' + \frac{1}{2} Pr\, f\theta' + Ri\left[\varphi''^{(1)} + \frac{1}{2} Pr\, \mathcal{F}^{(1)}\theta' + \frac{1}{2} Pr\, f\varphi'^{(1)}\right] = 0. \tag{11.2.19}$$

For these equations to be valid, the terms multiplied by Ri^0 and those multiplied by Ri^1 should each be equal to zero. We thus get

$$f''' + \frac{1}{2} f f'' = 0, \tag{11.2.20}$$

$$\theta'' + \frac{1}{2} Pr\, f\theta' = 0, \tag{11.2.21}$$

$$\mathcal{F}'''^{(1)} + \frac{f\mathcal{F}''^{(1)}}{2} + \frac{\mathcal{F}^{(1)} f''}{2} \pm \theta = 0, \tag{11.2.22}$$

$$\varphi''^{(1)} + \frac{1}{2} Pr\, \mathcal{F}^{(1)}\theta' + \frac{1}{2} Pr\, f\varphi'^{(1)} = 0. \tag{11.2.23}$$

The boundary conditions are as follows. At $\eta = 0$,

$$f = 0,\ f' = 0,\ \mathcal{F}^{(1)} = 0, \quad \mathcal{F}'^{(1)} = 0, \tag{11.2.24a}$$

$$\theta = 1,\ \varphi^{(1)} = 0. \tag{11.2.24b}$$

At $\eta \to \infty$,

$$f' \to 1,\ \mathcal{F}'^{(1)} \to 0, \quad \varphi^{(1)} \to 0. \tag{11.2.24c}$$

Equations (11.2.20) and (11.2.21) with their boundary conditions are identical to those discussed in Sections 3.1 and 3.2, respectively. Equations (11.2.22) and (11.2.23), with their boundary conditions, now constitute a similarity problem. They

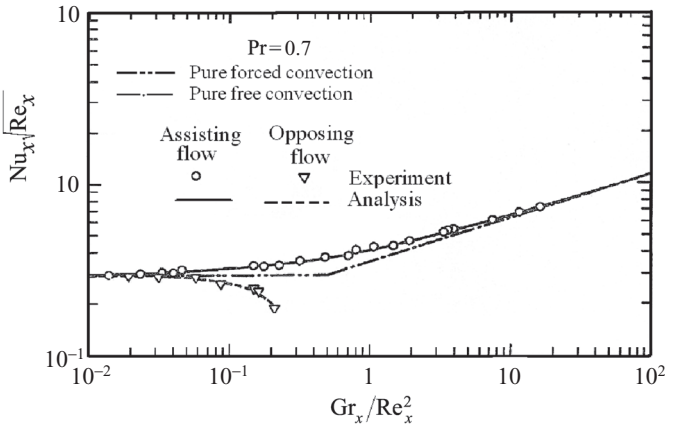

Figure 11.4. Measured and calculated local Nusselt numbers for air flow past an isothermal vertical plate (Ramachandran et al., 1985a).

are two ODEs whose solutions of course depend on Pr (Oostuizen and Naylor, 1999).

We can find the local Nusselt number by writing

$$\mathrm{Nu}_x = \frac{h_x x}{k} = \frac{x}{k}\left(-k\left.\frac{\partial T}{\partial y}\right|_{y=0}\right)\Big/(T_s - T_\infty). \tag{11.2.25}$$

This will lead to

$$\mathrm{Nu}_x = \mathrm{Nu}_{xF} - \sqrt{\mathrm{Re}_x}\mathrm{Ri}\left.\frac{\partial \varphi^{(1)}}{\partial \eta}\right|_{\eta=0}, \tag{11.2.26}$$

where the purely forced-convection Nusselt number is, from Eq. (3.2.17),

$$\mathrm{Nu}_{xF} = -\sqrt{\mathrm{Re}_x}\theta'(0). \tag{11.2.27}$$

Equation (11.2.26) can also be cast as

$$\frac{\mathrm{Nu}_x}{\mathrm{Nu}_{xF}} = 1 + \frac{\varphi^{(1)}(0)}{\theta'(0)}\mathrm{Ri}. \tag{11.2.27}$$

Numerical Studies

A numerical solution of laminar mixed convection on flat surfaces is relatively straightforward. Extensive numerical investigations were performed and successfully validated against experimental data. Figures 11.4 and 11.5 are good examples. The experimental data and numerical-solution results generally confirm that, in laminar flow, assisting mixed convection leads to a heat transfer coefficient that is larger than the heat transfer coefficients resulting from either pure forced or pure natural convection. The opposite is true for opposing-flow mixed convection, however. Thus, when forced convection is dominant, the presence of small opposing natural convection always reduces the heat transfer coefficient. Likewise, when natural convection is dominant, the presence of small opposing forced convection always

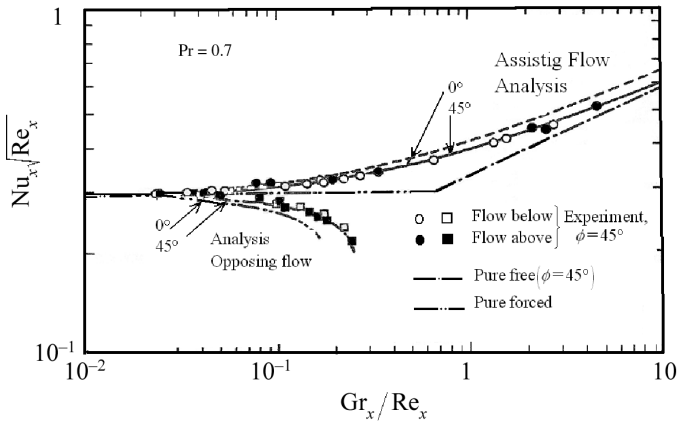

Figure 11.5. Measured and calculated local Nusselt numbers for air flow past an isothermal horizontal flat plate (Ramachandran et al., 1987).

reduces the heat transfer coefficient. These trends, it must be emphasized, are generally applicable to laminar flow. The situation for turbulent flow is more complicated because of the effect of buoyancy on turbulence as discussed later in the next section.

11.3 Stability of Laminar Flow and Laminar–Turbulent Transition

The stable laminar boundary layer can be terminated by transition to turbulent flow or by boundary-layer separation. Boundary-layer separation can occur on a heated, upward-facing surface or a cooled, downward-facing surface, and it is similar to the process that causes intermittency on horizontal surfaces in natural convection. Furthermore, on heated, upward-facing horizontal surfaces for which a counterflow of rising warm and replenishing cool fluid is required, thermals (depicted in Fig. 10.3) can form (Kudo et al., 2003). These processes are considerably more complicated than their counterparts in natural convection, however.

Because laminar–turbulent flow transition depends on forced and buoyancy flow effects both, a transition criterion of the form $f(\mathrm{Re}_{\mathrm{cr}}, \mathrm{Gr}_{\mathrm{cr}}) = 0$ or $f(\mathrm{Re}_{\mathrm{cr}}, \mathrm{Ra}_{\mathrm{cr}}) = 0$ should be expected. The criterion, furthermore, should reduce to the forced-flow laminar–turbulent transition criterion at $\mathrm{Gr}_{\mathrm{cr}} \to 0$ or $\mathrm{Ra}_{\mathrm{cr}} \to 0$ limits and to the natural-convection laminar–turbulent flow transition criterion at the $\mathrm{Re}_{\mathrm{cr}} \to 0$ limit.

For an upward-facing heated surface (or downward-facing cooled surface), laminar–turbulent flow transition can be caused by wave or vortex instability. For isothermal, flat, horizontal surfaces, experimental investigations led to (Hayashi et al., 1977; Gilpin et al., 1978)

$$\mathrm{Gr}_{l,\mathrm{cr}}/\mathrm{Re}_{l,\mathrm{cr}}^2 = 192 \quad \text{for air} \ (\mathrm{Pr} = 0.7)\,, \tag{11.3.1}$$

$$\mathrm{Gr}_{l,\mathrm{cr}}/\mathrm{Re}_{l,\mathrm{cr}}^2 \approx 78 \quad \text{for water} \ (\mathrm{Pr} = 7)\,. \tag{11.3.2}$$

However, linear vortex instability analysis suggests lower values for the right-hand side of these equations (Moutsoglu et al., 1981).

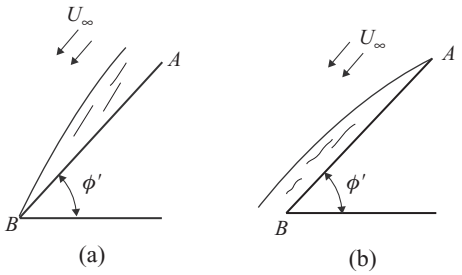

Figure 11.6. Mixed convection on an inclined heated flat surface with opposing flow: (a) predominantly natural convection, (b) predominantly forced convection.

The flow on a uniformly heated inclined surface with opposing forced flow was investigated by Misumi et al. (2007) (see Fig. 11.6) and led to the following observations. Natural convection remains predominant, and the boundary layer remains attached at very low values of free-stream velocity U_∞, as shown in Fig. 11.6(a). With increasing U_∞, boundary-layer separation will occur at the leading edge, referred to as point A in the following discussion. With further increasing U_∞, the boundary layer separation point moves downward on the surface and eventually reaches the surface's trailing edge, point B. With further increasing U_∞, the boundary layer will remain attached throughout the surface and will resemble Fig. 11.6(b). The experiments by Misumi et al. (2007) showed that, for $15 < \phi' < 75^\circ$, flow separation at the trailing and leading edges occurred, respectively, at,

$$\mathrm{Gr}^*_{l\phi'}/\mathrm{Re}_l^{2.5} = 0.35 \tag{11.3.3}$$

and

$$\mathrm{Gr}^*_{l\phi'}/\mathrm{Re}_l^{2.5} = 1.0, \tag{11.3.4}$$

where l represents the length of the surface and

$$\mathrm{Gr}^*_{l\phi'} = \frac{g \sin\phi' \beta l^4 q''_s}{\nu^2 k}. \tag{11.3.5}$$

The parameter ranges in these experiments were $7.2 \times 10^2 < \mathrm{Re}_l < 10^4$ and $5 \times 10^6 < \mathrm{Ra}^*_l < 8 \times 10^8$, where

$$\mathrm{Ra}^*_l = \frac{g\beta q''_s l^4}{k\alpha\nu}. \tag{11.3.6}$$

From the analysis of their heat transfer data, Misumi et al. also concluded that mixed convection prevails when $0.2 < (\mathrm{Gr}^*_{l\phi'}/\mathrm{Re}_l^{2.5}) < 3.0$. Pure natural convection can be assumed when $\mathrm{Gr}^*_{l\phi'}/\mathrm{Re}_l^{2.5} > 3.0$, and pure forced convection occurs when $\mathrm{Gr}^*_{l\phi'}/\mathrm{Re}_l^{2.5} < 0.2$.

For predominantly forced convection on a vertical flat surface, assisting buoyancy helps stabilize the laminar boundary layer, and therefore postpones the establishment of turbulent flow. It also dampens turbulence, leading to a reduction in the heat transfer coefficient in comparison with pure forced convection. The opposite trends are observed when opposing buoyancy effects are present. For a uniformly heated vertical surface subject to predominantly forced convection, Krishnamurthy and Gebhart (1989) derived the following criterion for transition to turbulence:

$$\mathrm{Re}_x/(0.2\mathrm{Gr}^*_x)^2 = 0.18, \tag{11.3.7}$$

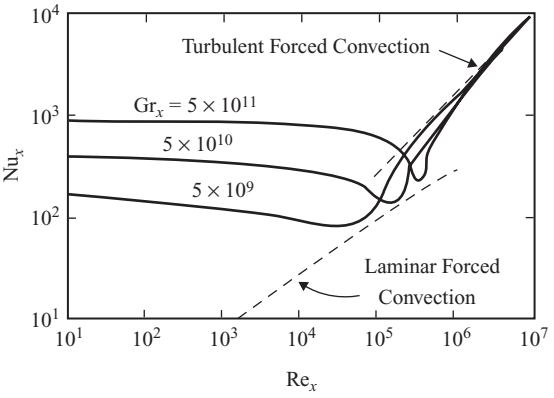

Figure 11.7. Effect of an assisting free-stream velocity on Nusselt number for a fluid with Pr = 0.7 (Patel et al., 1998).

where x is measured from the lower end of the surface (note that the forced convection flow is upward).

When the heat transfer is predominantly by turbulent natural convection, a small assisting forced flow dampens turbulence and therefore reduces the heat transfer coefficient, whereas the opposite occurs with an opposing small forced flow. These observations are evidently unlike the trends in laminar flow in which the mixed-convection heat transfer coefficient for assisting-flow conditions is consistently higher than either purely natural-convection or purely forced-convection heat transfer coefficients.

With respect to numerical simulation of turbulent mixed convection on vertical surfaces, it was found that the well-established Reynolds-averaged Navier–Stokes (RANS) type turbulence models, including the low-Reynolds-number K–ε model, do very well in predicting experimental data (Patel et al., 1996, 1998). (RANS-type turbulence models, including the K–ε model, are discussed in Chapter 12.)

Figure 11.7 displays the results of some numerical simulations by Patel et al. (1996, 1998), performed using the low-Reynolds-number K–ε model of Jones and Launder (1973). The figure clearly shows the aforementioned trends, in which a small aiding forced-flow effect in a predominantly free-convection flow actually reduces the heat transfer coefficient in comparison with purely free convective flow. These trends are confirmed by experimental data (Kitamura and Inagaki, 1987). From extensive numerical simulations, Patel et al. (1998) developed the heat transfer and flow regime map displayed in Fig. 11.8.

11.4 Correlations for Laminar External Flow

Based on a method proposed by Churchill (1977b) for laminar boundary layers, the local as well as average Nusselt numbers may be correlated as

$$\mathrm{Nu}^n = \mathrm{Nu}_F^n \pm \mathrm{Nu}_N^n, \tag{11.4.1}$$

where Nu_F and Nu_N are Nusselt numbers for purely forced and purely natural convection, respectively. The positive and negative signs represent buoyancy-assisted and buoyancy-opposed situations, respectively, and n is an empirical parameter.

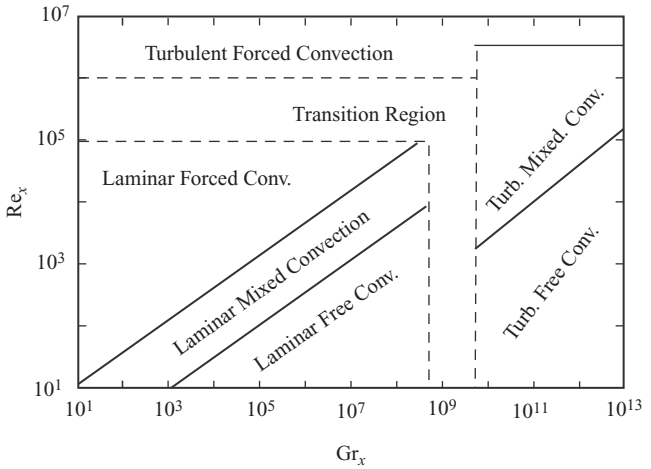

Figure 11.8. The regime map for a uniform temperature vertical flat surface with assisting mixed convection with Pr = 0.7 (Patel et al., 1998).

Eq. (11.4.1) can be presented in the following two equivalent forms:

$$\left(\frac{\mathrm{Nu}}{\mathrm{Nu}_F}\right) = \left[1 \pm \left(\frac{\mathrm{Nu}_N}{\mathrm{Nu}_F}\right)^n\right]^{1/n}, \tag{11.4.2}$$

$$\left(\frac{\mathrm{Nu}}{\mathrm{Nu}_N}\right) = \left[\left(\frac{\mathrm{Nu}_F}{\mathrm{Nu}_N}\right)^n \pm 1\right]^{1/n}. \tag{11.4.3}$$

These equations provide a useful and rather precise way for defining the thresholds for forced, free, and mixed convection. A relatively conservative way for defining the thresholds, for example, is as follows.

- Pure forced convection occurs when

$$0.99 < \left|\frac{\mathrm{Nu}}{\mathrm{Nu}_F}\right| < 1.01. \tag{11.4.4}$$

- Pure natural convection occurs when

$$0.99 < \left|\frac{\mathrm{Nu}}{\mathrm{Nu}_N}\right| < 1.01. \tag{11.4.5}$$

- Mixed convection occurs when neither of these two equations is satisfied.

For stable, laminar boundary layers, in general, we can write (Chen and Armaly, 1987),

$$\mathrm{Nu}_F = A\,(\mathrm{Pr})\,\mathrm{Re}^{1/2}, \tag{11.4.6}$$

$$\mathrm{Nu}_N = B\,(\mathrm{Pr})\,Gr^m. \tag{11.4.7}$$

These lead to

$$\frac{\mathrm{Nu}\,\mathrm{Re}^{-1/2}}{A\,(\mathrm{Pr})} = \left\{1 \pm \left[\frac{B\,(\mathrm{Pr})}{A\,(\mathrm{Pr})}Bo^m\right]^n\right\}^{1/n}. \tag{11.4.8}$$

The coefficients $A\,(\mathrm{Pr})$ and $B\,(\mathrm{Pr})$ are empirical functions, and the buoyancy number is defined here as

$$\mathrm{Bo} = \mathrm{Gr}/\mathrm{Re}^{\frac{1}{2m}}. \tag{11.4.9}$$

Correlations for Flat Surfaces

An extensive table for the preceding parameters can be found in Chen and Armaly (1987). Only a few correlations dealing with flat surfaces are reviewed here. All the properties in these correlations are to be calculated at the average film temperature. It is emphasized that these correlations are all for a laminar boundary layer, without boundary-layer separation.

- Vertical and inclined flat surface, UWT boundary condition:

  Local Nusselt number, Nu_x,

$$A\,(\mathrm{Pr}) = 0.339\,\mathrm{Pr}^{1/3}\left[1 + (0.0468/\mathrm{Pr})^{2/3}\right]^{-1/4}, \tag{11.4.10}$$

$$B\,(\mathrm{Pr}) = 0.75\mathrm{Pr}^{1/2}\left[2.5\left(1 + 2\sqrt{\mathrm{Pr}} + 2\mathrm{Pr}\right)^{2/3}\right]^{-1/4}, \tag{11.4.11}$$

$$\mathrm{Bo} = \mathrm{Gr}_x \cos\phi/\mathrm{Re}_x^2, \tag{11.4.12}$$

$$m = 1/4,\ n = 3.$$

  Range of applicability:

$$0.1 \le \mathrm{Pr} \le 100,\ 10^3 \le \mathrm{Re}_x \le 10^5,\ \mathrm{Gr}_x < 10^9,\ 0 \le \phi \le 85^\circ.$$

  Average Nusselt number, $\langle Nu_l \rangle_l$

$$A\,(\mathrm{Pr}) = [\text{right-hand side of Eq. (11.4.10)}] \times 2, \tag{11.4.13}$$

$$B\,(\mathrm{Pr}) = [\text{right-hand side of Eq. (11.4.11)}] \times \frac{4}{3}, \tag{11.4.14}$$

$$\mathrm{Bo} = \mathrm{Gr}_l \cos\phi/\mathrm{Re}_l^2, \tag{11.4.15}$$

$$m = 1/4,\ n = 3.$$

  Range of applicability:

$$0.1 \le \mathrm{Pr} \le 100,\ 10^3 \le \mathrm{Re}_l \le 10^5,\ \mathrm{Gr}_l < 10^9,\ 0 \le \phi \le 85^\circ.$$

- Horizontal flat surface, UWT boundary condition:

  Local Nusselt number, Nu_x,

$$A\,(\mathrm{Pr}) = \text{right-hand side of Eq. (11.4.10)}, \tag{11.4.16}$$

$$B\,(\mathrm{Pr}) = (\mathrm{Pr}/5)^{1/5}\,\mathrm{Pr}^{1/2}\left[0.25 + 1.6\sqrt{\mathrm{Pr}}\right]^{-1}, \tag{11.4.17}$$

$$\mathrm{Bo} = \mathrm{Gr}_x/\mathrm{Re}_x^{5/2}, \tag{11.4.18}$$

$$m = 1/5,\ n = 3.$$

  Range of applicability:

$$10^3 \le \mathrm{Re}_x \le 10^5,\ \mathrm{Gr}_x < 10^7.$$

Average Nusselt number, $\langle Nu_l \rangle_l$

$$A\,(\mathrm{Pr}) = [\text{right-hand side of Eq. (11.4.10)}] \times 2, \tag{11.4.19}$$

$$B\,(\mathrm{Pr}) = [\text{right-hand side of Eq. (11.4.17)}] \times \frac{5}{3}, \tag{11.4.20}$$

$$\mathrm{Bo} = \mathrm{Gr}_l/\mathrm{Re}_l^{5/2}, \tag{11.4.21}$$

$$m = 1/5,\ n = 3.$$

Range of applicability:

$$10^3 \le \mathrm{Re}_l \le 10^5,\ \mathrm{Gr}_l < 10^7.$$

- Vertical and inclined flat surface, UHF boundary condition:

  Local Nusselt number, Nu_x,

$$A\,(\mathrm{Pr}) = 0.464\mathrm{Pr}^{1/3}\left[1 + (0.0207/\mathrm{Pr})^{2/3}\right]^{-1/4}, \tag{11.4.22}$$

$$B\,(\mathrm{Pr}) = \mathrm{Pr}^{2/5}\left[4 + 9\sqrt{\mathrm{Pr}} + 10\mathrm{Pr}\right]^{-1/5}, \tag{11.4.23}$$

$$\mathrm{Bo} = \mathrm{Gr}_x^* \cos\phi/\mathrm{Re}_x^{5/2}, \tag{11.4.24}$$

$$\mathrm{Gr}_x^* = \frac{g\beta q_s'' x^4}{k\nu^2}, \tag{11.4.25}$$

$$m = 1/5,\ n = 3.$$

Range of applicability:

$$0.1 \le \mathrm{Pr} \le 100,\ 10^3 \le \mathrm{Re}_x \le 10^5,\ \mathrm{Gr}_x^* < 10^{11},\ 0 \le \phi \le 85^\circ.$$

Average Nusselt number, $\langle \mathrm{Nu}_l \rangle_l$,

$$A\,(\mathrm{Pr}) = [\text{right-hand side of Eq. (11.4.22]} \times 2, \tag{11.4.26}$$

$$B\,(\mathrm{Pr}) = [\text{right-hand side of Eq. (11.4.23)}] \times \frac{5}{4}, \tag{11.4.27}$$

$$\mathrm{Bo} = (\mathrm{Gr}_l^* \cos\phi)/\mathrm{Re}_l^{5/2}, \tag{11.4.28}$$

$$m = 1/5,\ n = 3.$$

Range of applicability:

$$0.1 \le \mathrm{Pr} \le 100, 10^3 \le \mathrm{Re}_l \le 10^5, \mathrm{Gr}_l^* < 10^{11}, 0 \le \phi \le 85^\circ.$$

- Horizontal flat surface, UHF boundary condition

  Local Nusselt number, Nu_x,

$$A\,(\mathrm{Pr}) = 0.464\mathrm{Pr}^{1/3}\left[1 + (0.0207/\mathrm{Pr})^{2/3}\right]^{-1/4}, \tag{11.4.29}$$

$$B\,(\mathrm{Pr}) = (\mathrm{Pr}/6)^{1/6}\sqrt{\mathrm{Pr}}\left[0.12 + 1.2\sqrt{\mathrm{Pr}}\right]^{-1}, \tag{11.4.30}$$

$$\mathrm{Bo} = \mathrm{Gr}_x^*/\mathrm{Re}_x^3, \tag{11.4.31}$$

$$m = 1/6,\ n = 3.$$

Range of applicability:

$$0.1 \le \mathrm{Pr} \le 100,\ 10^3 \le \mathrm{Re}_x \le 10^5,\ \mathrm{Gr}_x^* < 10^8.$$

Average Nusselt number, $\langle Nu_l \rangle_l$,

$$A\,(\mathrm{Pr}) = [\text{right-hand side of Eq. (11.4.29)}] \times 2, \tag{11.4.32}$$

$$B\,(\mathrm{Pr}) = [\text{right-hand side of Eq. (11.4.30)}] \times \frac{3}{2}, \tag{11.4.33}$$

$$\mathrm{Bo} = \mathrm{Gr}_l^*/\mathrm{Re}_l^3, \tag{11.4.34}$$

$$m = 1/6,\ n = 3.$$

Range of applicability:

$$0.1 \le \mathrm{Pr} \le 100,\ 10^3 \le \mathrm{Re}_l \le 10^5,\ \mathrm{Gr}_l^* < 10^8.$$

Correlations for Spheres and Cylinders

Empirical correlations for cylinders and spheres in various situations (assisting or opposing flow, longitudinal or cross flow for cylinders) are also available. According to Yuge (1960), for spheres we have the following correlations.

- Assisting flow and cross-flow,

$$\frac{\langle \mathrm{Nu}_D \rangle - 2}{\langle \mathrm{Nu}_{DF} \rangle - 2} = \left[1 + \left(\frac{\langle \mathrm{Nu}_{DN} \rangle - 2}{\langle \mathrm{Nu}_{DF} \rangle - 2} \right)^{3.5} \right]^{1/3.5}. \tag{11.4.35}$$

- Opposing flow,

$$\frac{\langle \mathrm{Nu}_D \rangle - 2}{\langle \mathrm{Nu}_{DF} \rangle - 2} = \left[1 - \left(\frac{\langle \mathrm{Nu}_{DN} \rangle - 2}{\langle \mathrm{Nu}_{DF} \rangle - 2} \right)^{3} \right]^{1/3} \quad \text{for} \quad \frac{\langle \mathrm{Nu}_D \rangle - 2}{\langle \mathrm{Nu}_{DF} \rangle - 2} < 1 \tag{11.4.36}$$

$$\frac{\langle \mathrm{Nu}_D \rangle - 2}{\langle \mathrm{Nu}_{DF} \rangle - 2} = \left[\left(\frac{\langle \mathrm{Nu}_{DN} \rangle - 2}{\langle \mathrm{Nu}_{DF} \rangle - 2} \right)^{6} - 1 \right]^{1/6} \quad \text{for} \quad \frac{\langle \mathrm{Nu}_D \rangle - 2}{\langle \mathrm{Nu}_{DF} \rangle - 2} \ge 1, \tag{11.4.37}$$

where

$$\mathrm{Nu}_{DF} = 2 + 0.493\mathrm{Re}_D^{1/2}, \tag{11.4.38}$$

$$\mathrm{Nu}_{DN} = 2 + 0.392\mathrm{Gr}_D^{1/4}. \tag{11.4.39}$$

All properties in these correlations should correspond to the film temperature. The range of validity for the correlation is

$$3.5 < \mathrm{Re}_D < 5.9 \times 10^3,\ 1 < \mathrm{Gr}_D < 10^5,\ \mathrm{Pr} = 0.7.$$

The following correlations were developed for laminar flow over a horizontal cylinder based on the analytical calculation results of Badr (1983, 1984) for the parameter range of $1 < \mathrm{Re}_D < 60$ and $0 < \mathrm{Gr}_D < 7200$ (Chen and Armaly, 1987).

- Assisting flow,

$$\frac{\langle \mathrm{Nu}_D \rangle}{\langle \mathrm{Nu}_{DF} \rangle} = 1 + 0.16\mathrm{Ri} - 0.015\mathrm{Ri}^2. \tag{11.4.40}$$

- Cross flow,

$$\frac{\langle \mathrm{Nu}_D \rangle}{\langle \mathrm{Nu}_{DF} \rangle} = 1 + 0.05\mathrm{Ri} + 0.003\mathrm{Ri}^2. \tag{11.4.41}$$

- Opposing flow,

$$\frac{\langle \mathrm{Nu}_D \rangle}{\langle \mathrm{Nu}_{DF} \rangle} = 1 - 0.37\mathrm{Ri} + 0.15\mathrm{Ri}^2. \tag{11.4.42}$$

The Richardson number is defined here according to

$$\mathrm{Ri} = \frac{\mathrm{Gr}_D}{\mathrm{Re}_D^2}.$$

11.5 Correlations for Turbulent External Flow

For an isothermal flat surface, according to Chen and Armaly (1987),

$$\frac{\mathrm{Nu}_x \mathrm{Re}_x^{-4/5}}{F(\mathrm{Pr})} = \left\{ 1 + C \left[\frac{G(\mathrm{Pr})}{F(\mathrm{Pr})} \left(\frac{\mathrm{Gr}_x}{\mathrm{Re}_x^{12/5}} \right)^{1/3} \right]^n \right\}^{1/n}, \tag{11.5.1}$$

$$\frac{\langle \mathrm{Nu}_l \rangle_l \, \mathrm{Re}_l^{-4/5}}{1.25F(\mathrm{Pr})} = \left\{ 1 + C \left[\frac{G(\mathrm{Pr})}{1.25F(\mathrm{Pr})} \left(\frac{\mathrm{Gr}_l}{\mathrm{Re}_l^{12/5}} \right)^{1/3} \right]^n \right\}^{1/n}, \tag{11.5.2}$$

where

$$F(\mathrm{Pr}) = 0.0287\,\mathrm{Pr}^{0.6},$$

$$G(\mathrm{Pr}) = 0.15\,\mathrm{Pr}^{1/3}\left[1 + (0.492/\mathrm{Pr})^{9/16}\right]^{-16/27}, \text{ for vertical} \tag{11.5.3a}$$

$$G(\mathrm{Pr}) = 0.13\,\mathrm{Pr}^{1/3} \text{ for horizontal} \tag{11.5.3b}$$

$$n = 3,$$

$$C = 0.36 \text{ for vertical, and } C = 0.006 \text{ for horizontal.}$$

The following composite correlations were recommended by Churchill (1990) for laminar and turbulent flow. They are reliable for laminar flow, but may be used for turbulent flow as an approximation. For flow over vertical plates and cylinders, as well as over spheres,

$$[\langle \mathrm{Nu}_l \rangle - \langle \mathrm{Nu}_l \rangle_0]^3 = \left| [\langle \mathrm{Nu}_l \rangle_F - \langle \mathrm{Nu}_l \rangle_0]^3 \pm [\langle \mathrm{Nu}_l \rangle_N - \langle \mathrm{Nu}_l \rangle_0]^3 \right|, \tag{11.5.4}$$

where l should be replaced with D for a cylinder or sphere, and the + and – signs stand for assisting and opposing buoyancy effect, respectively. Furthermore, $\langle \mathrm{Nu}_l \rangle_0 = 0$ for a vertical plate, $\langle \mathrm{Nu}_D \rangle_0 = 0.3$ for a vertical cylinder, and $\langle \mathrm{Nu}_D \rangle_0 = 2$ for a sphere.

For cross flow over a horizontal cylinder or sphere,

$$[\langle \mathrm{Nu}_l \rangle - \langle \mathrm{Nu}_l \rangle_0]^4 = [\langle \mathrm{Nu}_l \rangle_F - \langle \mathrm{Nu}_l \rangle_0]^4 + [\langle \mathrm{Nu}_l \rangle_N - \langle \mathrm{Nu}_l \rangle_0]^4 . \qquad (11.5.5)$$

11.6 Internal Flow

11.6.1 General Remarks

Internal flow mixed convection is significantly more complicated than internal flow natural or forced-convection. In a predominantly forced-convection flow, for example, buoyancy affects the magnitude of both hydrodynamic and thermal entrance lengths, the conditions that lead to the laminar–turbulent flow regime transition and the turbulence intensity when the flow is turbulent. Also, perhaps most important, it causes secondary flows that can enhance or reduce the fluid–wall heat transfer and can result in significant peripheral nonuniformity in the heat transfer coefficient.

The qualitative effects of natural- and forced-convection parameters on the wall heat transfer coefficients in a vertical channel can be seen in Fig. 11.9, where the Graetz number is defined as

$$\mathrm{Gz} = \mathrm{Re}_{D_H} \mathrm{Pr} \frac{D_H}{l}. \qquad (11.6.1)$$

In laminar flow, in an assisting mixed-convection flow configuration in which forced and buoyancy-induced velocities are in the same direction, the mixed-convection heat transfer coefficient is always higher than either purely forced- or purely natural-convection heat transfer coefficients. The presence of free convection in a strongly forced convection pipe flow will shorten the thermal entrance length, but will lengthen the hydrodynamic entrance length. For the opposing-flow configuration, however, the effect of natural convection in a predominantly forced-convection flow is to reduce the heat transfer coefficient. In this configuration a counterflow can actually take place in the flow passage.

In buoyancy-assisted turbulent flow, the presence of buoyancy actually deteriorates the wall–fluid heat transfer because of the partial suppression of turbulence by the buoyancy effect, leading to the reduction in Nu_x for $\mathrm{Re}_x = \text{const.}$ as $\mathrm{Gr}_x \mathrm{Pr}$ is increased. In turbulent opposing flow, on the other hand, buoyancy can slightly reduce the wall–fluid heat transfer coefficient when buoyancy effect is weak, but will enhance the wall–fluid heat transfer coefficient by enhancing turbulence when natural-convection effects are significant. Figure 11.10 displays the effect of buoyancy on Nusslet number in a uniformly heated vertical tube (Celata et al., 1998), where the buoyancy number is defined as

$$\mathrm{Bo} = (8 \times 10^4) \frac{\mathrm{Gr}_D^*}{\mathrm{Re}_D^{3.425} \mathrm{Pr}^{0.8}}. \qquad (11.6.2)$$

The effect of buoyancy on heat transfer in opposing flow (downward forced flow) is thus to enhance heat transfer. In assisting flow (upward forced flow) the effect of buoyancy is to reduce the heat transfer coefficient by the laminarization of an otherwise turbulent flow or by reducing the turbulence intensity. The

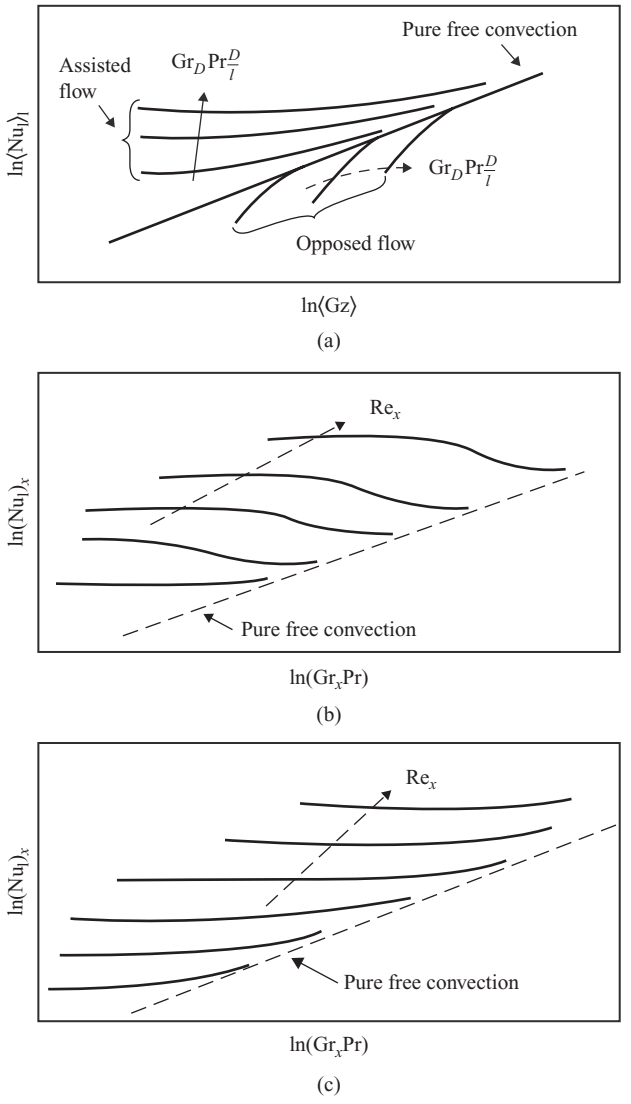

Figure 11.9. The dependence of the Nusselt number on various parameters in internal mixed convection: (a) laminar flow, (b) buoyancy-assisted turbulent flow, (c) buoyancy-opposed turbulent flow (after Aung, 1987).

$\langle Nu_D \rangle / \langle Nu_{DF} \rangle$ ratio becomes larger than one only when the natural convection effect becomes predominant.

Figure 11.11 displays the velocity profiles in a vertical, uniformly heated pipe (Tanaka et al., 1987; Celata et al., 1998). As noted, with increasing Gr_D^* while Re_D is maintained constant, first laminarization occurs and leads to a reduction in turbulent heat transfer (cases C and D). At very high Gr_D^*, however, the flow becomes turbulent and predominantly natural convection (cases E and F).

In horizontal flow passages, when forced convection is predominant, buoyancy will cause a secondary flow. Counterrotating transverse vortices develop. These secondary flows enhance the heat transfer process and result in azimuthally nonuniform heat transfer coefficients over the perimeter of the pipe.

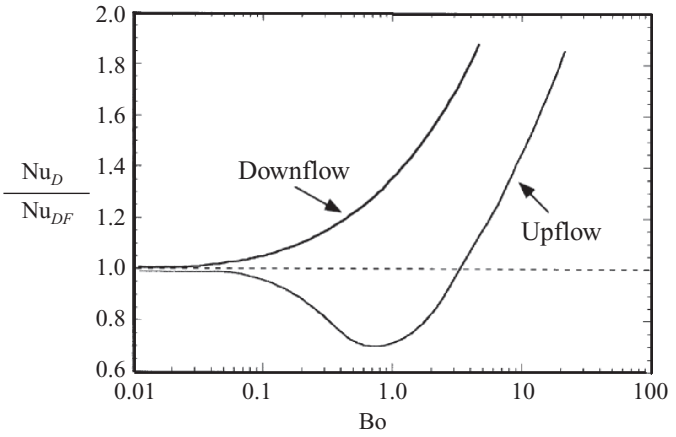

Figure 11.10. The effect of natural convection on mixed-convection heat transfer in a uniformly heated vertical pipe (after Celata et al., 1998).

11.6.2 Flow Regime Maps

For circular pipes, Metais and Eckert (1964) developed the widely applied empirical regime maps depicted in Figs. 11.12 and 11.13. The flow regime map in Fig. 11.12 is for vertical tubes and is applicable to both UWT and UHF boundary conditions, for upward and downward flows. Figure 11.13 is based on horizontal pipe data with UWT boundary conditions. The range of applicability for both figures is $10^{-2} < \mathrm{Pr}(D/l) < 1$. The regime boundaries represent 10% deviation from pure forced convection or pure natural convection.

11.7 Some Empirical Correlations for Internal Flow

Numerical simulations for internal flow mixed convection are relatively abundant and have shown good agreement with experimental data for both laminar and turbulent flow regimes. In turbulent flow it was observed that the low-Reynolds-number K–ε model of Launder and Sharma (1974) provides solutions that agree well with experimental data (Cotton and Jackson, 1990; Celata et al., 1998).

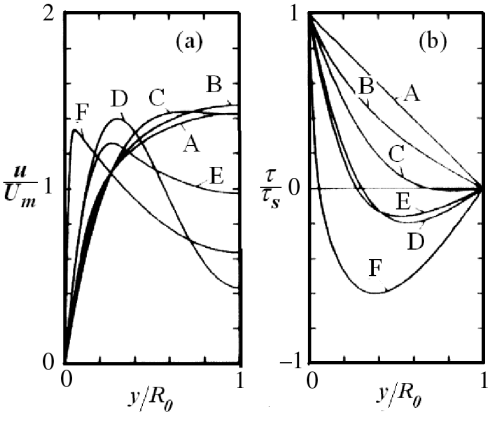

Figure 11.11. (a) Velocity and (b) shear-stress distributions in a uniformly heated vertical pipe with upward flow and $\mathrm{Re}_D = 3000$. A, $\mathrm{Gr}_D^* = 2.1 \times 10^3$, turbulent; B, $\mathrm{Gr}_D^* = 6.1 \times 10^4$, turbulent; C, $\mathrm{Gr}_D^* = 8.8 \times 10^4$, laminar; D, $\mathrm{Gr}_D^* = 2.7 \times 10^5$, laminar; E, $\mathrm{Gr}_D^* = 3.3 \times 10^5$, turbulent; F, $\mathrm{Gr}_D^* = 9.2 \times 10^6$, turbulent.

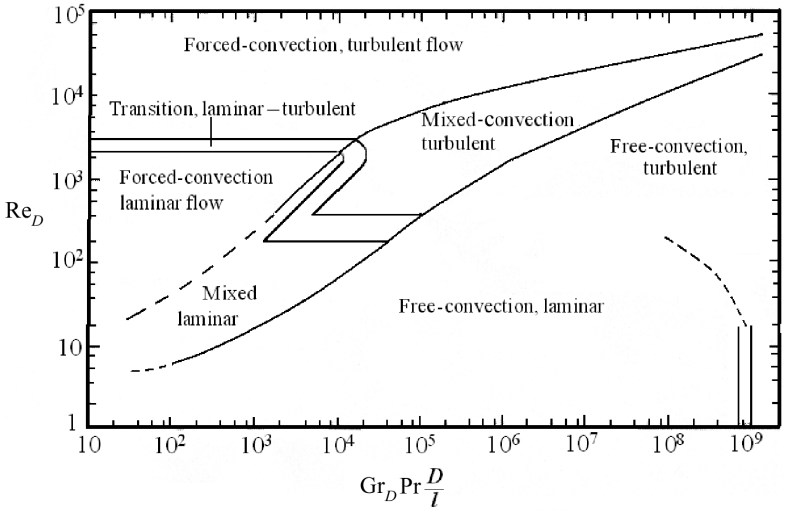

Figure 11.12. Flow and heat transfer regimes in a vertical pipe (after Metais and Eckert, 1964).

For laminar, hydrodynamically, and thermally developed flow in horizontal circular channels with UHF boundary conditions, Morcos and Bergles (1975) proposed the following empirical correlation:

$$\langle \mathrm{Nu}_D \rangle = \left\{ (4.36)^2 + \left(0.145 \left[\frac{\mathrm{Gr}_D^* \mathrm{Pr}^{1.35}}{\left(\frac{kD}{k_w t_w} \right)^{0.25}} \right]^{0.265} \right)^2 \right\}^{1/2}, \qquad (11.7.1)$$

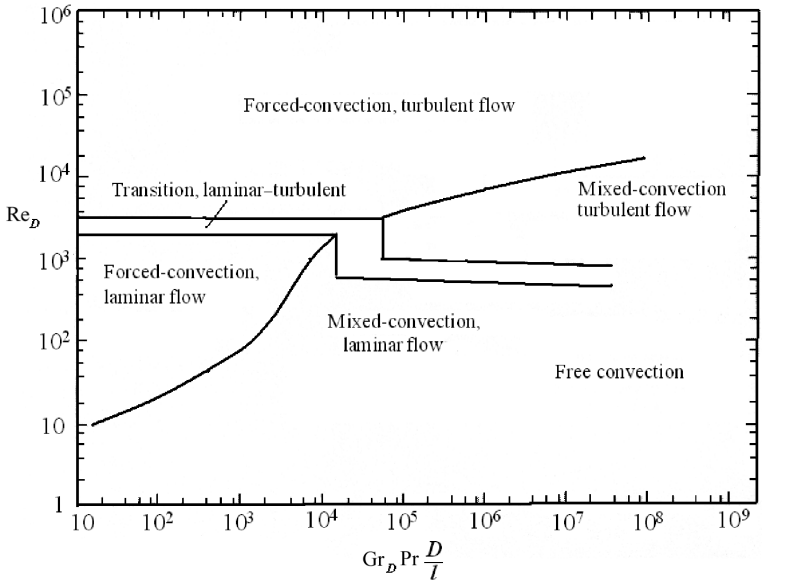

Figure 11.13. Flow and heat transfer regimes in a horizontal pipe (after Metais and Eckert, 1964).

where $\langle \mathrm{Nu}_D \rangle$ is based on circumferentially averaged heat transfer coefficient, k_w, t_w are the wall thermal conductivity and thickness, respectively, and

$$\mathrm{Gr}_D^* = \frac{g\beta q_s'' D^4}{k\nu^2}. \tag{11.7.2}$$

In the preceding correlation, all properties are to be calculated at film temperature. Its range of validity is

$$4 < \mathrm{Pr} < 175,\ 2 < \frac{hD^2}{k_w \delta_w} < 66,\ 3 \times 10^4 < \mathrm{Ra}_D = \frac{g\beta\,|\langle T_s \rangle - T_m|\, D^3}{\alpha\nu} < 10^6 \tag{11.7.3}$$

where $\langle T_s \rangle$ is the circumferentially averaged wall surface temperature and T_m is the bulk temperature. The properties are calculated at $(\langle T_s \rangle + T_m)/2$.

For the aforementioned laminar, fully developed, and thermally developed flow in a horizontal pipe with UHF boundary conditions, a simpler set of correlations are (Mori and Futagami, 1967)

$$\frac{\langle \mathrm{Nu}_D \rangle}{\mathrm{Nu}_F} = 0.04085\,(\mathrm{Re}_D \mathrm{Ra}_D^*)^{1/2} \quad \text{for Pr} = 0.7, \tag{11.7.4}$$

$$\frac{\langle \mathrm{Nu}_D \rangle}{\mathrm{Nu}_F} = 0.04823\,(\mathrm{Re}_D \mathrm{Ra}_D^*)^{1/2} \quad \text{for Pr} = 1.0, \tag{11.7.5}$$

where the modified Rayleigh number is defined here as

$$\mathrm{Ra}_D^* = \frac{g\beta\,|dT_s/dx|\, D^4}{\alpha\nu}. \tag{11.7.6}$$

The forced-convection Nusselt number in Eqs. (11.7.4) and (11.7.5) is found from $\mathrm{Nu}_F = 4.363$, and all properties are found at film average temperature. The experimentally confirmed range of validity of this correlation is

$$1.3 \times 10^6 < \mathrm{Re}_D \mathrm{Ra}_D^* < 5.6 \times 10^6.$$

For buoyancy-opposed turbulent flow in vertical tubes with UHF boundary condition, Jackson and Hall (1979) proposed

$$\frac{\langle \mathrm{Nu}_D \rangle}{\mathrm{Nu}_F} = \left[1 + 2750 \left(\frac{\overline{\mathrm{Gr}}_D}{\mathrm{Re}_D^{2.7}} \right)^{0.91} \right]^{1/3}, \tag{11.7.7}$$

where

$$\overline{\mathrm{Gr}}_D = \frac{g\,(\rho_m - \overline{\rho})\, D^3}{\overline{\rho}\nu^2} \approx \frac{g\beta\rho_m^2 (T_s - T_m) D^3}{2\mu^2},$$

$$\overline{\rho} = \frac{1}{T_s - T_m} \int_{T_m}^{T_s} \rho\,(T, P)\, dT,$$

$$\rho_m = \rho\,(T_m).$$

For vertical tubes that are subject to UWT boundary conditions, Herbert and Stern (1972) developed the following correlations.

- For buoyancy-aided flow,

$$\mathrm{Nu}_D = (8.5 \times 10^{-2})\,(\mathrm{Gr}_D \mathrm{Pr})^{1/3}, \tag{11.7.8}$$

where

$$\mathrm{Gr}_D = \frac{g\beta|T_s - \overline{T}_m|D^3}{\nu^2}, \tag{11.7.9}$$

in which $\overline{T}_m$ is the arithmetic mean of bulk temperatures at the inlet and outlet. The range of validity of the correlation is

$$4.5 \times 10^3 < \mathrm{Re}_D < 1.5 \times 10^4,\ 0.0127 \le D \le 0.0254 \text{ m},\ 0.254 \le l \le 3.30 \text{ m},$$
$$1.8 \le \mathrm{Pr} \le 2.2,\ 3 \times 10^6 \le \mathrm{Gr}_D \le 3 \times 10^7.$$

For buoyancy-opposed flow, there was no effect of buoyancy for $\mathrm{Re}_D > 1.5 \times 10^4$.

For $\mathrm{Re}_D < 1.5 \times 10^4$,

$$\mathrm{Nu}_D = 0.56\,\mathrm{Re}_D^{0.47}\,\mathrm{Pr}^{0.4}. \tag{11.7.10}$$

According to Herbert and Stern, in buoyancy-assisted forced flow the effect of buoyancy becomes negligible when

$$\mathrm{Re}_D > 3 \times 10^3 + 2.7 \times 10^{-4}\mathrm{Gr}_D\,\mathrm{Pr}. \tag{11.7.11}$$

Celata et al. (1998) developed the following empirical correlation for the average Nusselt number, based on experimental data obtained in a uniformly heated vertical tube subject to forced upflow, with $l/D = 10$–40:

$$\frac{\langle \mathrm{Nu}_D \rangle}{\langle \mathrm{Nu}_{D,\,df} \rangle} = 1 - a\,\exp\left\{-0.8\left[\log\left(\mathrm{Bo}/b\right)\right]^2\right\}, \tag{11.7.12}$$

$$a = 0.36 + 0.0065\,(l/D)\,, \tag{11.7.13}$$

$$b = 869\,(l/D)^{-2.16}\,, \tag{11.7.14}$$

where Bo is defined according to Eq. (11.6.2). The parameter $\langle \mathrm{Nu}_{D,\,df} \rangle$ here represents the downflow mean Nusselt number and should be calculated using Churchill's interpretation (Churchill, 1977b):

$$\left\langle \mathrm{Nu}_{D,\,df} \right\rangle = \left[\mathrm{Nu}_F^3 + \mathrm{Nu}_N^3\right]^{1/3} \tag{11.7.15}$$

where

$$\mathrm{Nu}_F = 0.023\,\mathrm{Re}_D^{0.8}\,\mathrm{Pr}_m^{0.4}\,(\mu_m/\mu_s)^{0.11}\,, \tag{11.7.16}$$

$$\mathrm{Nu}_N = \frac{0.15\,(\mathrm{Gr}_D \mathrm{Pr}_s)^{1/3}}{\left[1 + (0.437/\mathrm{Pr}_s)^{9/16}\right]^{16/27}}. \tag{11.7.17}$$

Subscripts m and s represent bulk and wall surface temperatures, respectively, and Gr_D is defined as in Eq. (11.7.9) except that ν is replaced with ν_s, the fluid kinematic viscosity at the wall surface temperature.

EXAMPLE 11.1. The upward-facing surface of an inclined surface that is 1.0 m wide and 80 cm long is subject to a UHF boundary condition with $q_s'' =$

20 W/m^2. The angle of inclination with respect to the vertical plane is $\phi = 10^\circ$. The surface is exposed to atmospheric air at an ambient temperature of 300 K.

Air flows parallel to the surface in the upward (assisting) direction at a velocity of 0.05 m/s. Calculate the average Nusselt number and heat transfer coefficient for the surface. Compare the result with purely free-convection and purely forced-convection Nusselt numbers.

SOLUTION. Let us first calculate properties. As an estimate, let us use $T_{\text{ref}} = T_\infty + 15 = 315$ K as the temperature for properties. We then have

$$\begin{aligned}
&\rho = 1.121\,\text{kg/m}^3\,,\ C_P = 1006\,\text{J/kg}^\circ\text{C}\,,\ k = 0.0268\,\text{W/m K},\\
&\mu = 1.93 \times 10^{-5}\,\text{kg/m s}\,,\ \text{Pr} = 0.724,\\
&\boldsymbol{\alpha} = \frac{k}{\rho C_P} = 2.37 \times 10^{-5}\,\text{m}^2/\text{s},\\
&\beta = \frac{1}{T_{\text{film}}} = 0.00317\,\text{K}^{-1}.
\end{aligned}$$

The plate is wide enough to justify neglecting the end effects and treating the boundary layer as 2D. We now calculate the modified Rayleigh and Reynolds numbers:

$$\begin{aligned}
\text{Ra}_l^* &= \frac{g\beta q_s'' l^4}{k\nu\boldsymbol{\alpha}}\\
&= \frac{\left(9.81\,\text{m/s}^2\right)\left(0.00317\,\text{K}^{-1}\right)\left[20\,\text{W/m}^2\right](0.8\,\text{m})^4}{(0.0268\,\text{W/m K})\left(\dfrac{1.93\times10^{-5}\,\text{kg/m s}}{1.121\,\text{kg/m}^3}\right)(2.37\times10^{-5}\,\text{m}^2/\text{s})} = 2.336\times10^{10},\\
\text{Re}_l &= \rho U_\infty l/\mu = \left(1.121\,\text{kg/m}^3\right)(0.05\,\text{m/s})\,(0.8\,\text{m})/1.93\times10^{-5}\,\text{kg/m s} = 2327.
\end{aligned}$$

The preceding parameter range indicates that the boundary layer remains laminar and coherent, and we can use Eqs. (11.4.26)–(11.4.28):

$$\begin{aligned}
\text{Gr}_l^* &= \frac{g\beta q_s'' l^4}{k\,\nu^2}\\
&= \frac{\left(9.81\,\text{m/s}^2\right)\left(0.00317\,\text{K}^{-1}\right)\left[20\,\text{W/m}^2\right](0.8\,\text{m})^4}{(0.0268\,\text{W/m K})\left(\dfrac{1.93\times10^{-5}\,\text{kg/m s}}{1.121\,\text{kg/m}^3}\right)^2} = 3.227\times10^{10},\\
A\,(\text{Pr}) &= 2\times0.464\text{Pr}^{1/3}\left[1+(0.0207/\text{Pr})^{2/3}\right]^{-1/4}\\
&= (0.928)\,(0.724)^{1/3}\left[1+(0.0207/0.724)^{2/3}\right]^{-1/4} = 0.815,\\
B\,(\text{Pr}) &= \frac{5}{4}\text{Pr}^{2/5}\left[4+9\sqrt{\text{Pr}}+10\text{Pr}\right]^{-1/5},\\
&= \frac{5}{4}\,(0.724)^{2/5}\left[4+9\sqrt{0.724}+(10)\,(0.724)\right]^{-1/5} = 0.6103,\\
\text{Bo} &= \text{Gr}_l^*\cos\phi/\text{Re}_l^{5/2} = \frac{\left(3.227\times10^{10}\right)\cos(10^\circ)}{(2327)^{5/2}} = 121.7,
\end{aligned}$$

$$\langle \mathrm{Nu}_l \rangle_l = A(\mathrm{Pr})\sqrt{\mathrm{Re}_l}\left[1 + \left(\frac{\mathrm{B(Pr)}}{\mathrm{A(Pr)}}\mathrm{Bo}^m\right)^n\right]^{1/n},$$

$$= (0.815)\sqrt{2327}\left[1 + \left(\frac{0.6103}{0.815}(121.7)^{1/5}\right)^3\right]^{1/3}$$

$$= 80.19,$$

$$\langle h \rangle_l = \langle \mathrm{Nu}_l \rangle_l \frac{k}{l} = (80.19)\frac{0.0268\,\mathrm{W/m\,K}}{0.8\,\mathrm{m}} = 2.68\,\mathrm{W/m^2\,K}.$$

We now calculate the average Nusselt numbers for pure forced and pure natural convection. From Table Q.1 in Appendix Q,

$$\langle \mathrm{Nu}_{l,F} \rangle_l = 2 \times 0.453\mathrm{Pr}^{1/3}\mathrm{Re}_l^{1/2} = (0.906)(0.724)^{1/3}(2,327)^{1/2} = 39.24.$$

For pure natural convection we use Eq. (10.5.35). This equation provides the local heat transfer coefficient. We note that

$$\langle h \rangle_l = \frac{1}{l}\int_0^l h_x dx.$$

This expression can be rewritten as

$$\langle \mathrm{Nu}_{l,N} \rangle_l = \frac{1}{k}\int_0^l h_x dx.$$

Using Eq. (10.5.35), we can then easily derive

$$\langle \mathrm{Nu}_{l,N} \rangle_l = \frac{5}{4}\mathrm{Nu}_{l,N} = \left(\frac{5}{4}\right)0.62\left(\frac{\mathrm{Pr}^2}{0.8 + \mathrm{Pr}}\right)^{1/5}(\mathrm{Gr}_1^* \cos\phi)^{1/5}.$$

This then gives

$$\langle \mathrm{Nu}_{l,N} \rangle_l = 78.9.$$

EXAMPLE 11.2. In an experiment, the upward-facing surface of an inclined surface that is 1.0 m wide and 12 cm long is subject to a UHF boundary condition with $q_s'' = 20\ \mathrm{W/m^2}$. The angle of inclination with respect to the vertical plane is $\phi = 35^\circ$. The surface is exposed to atmospheric air at an ambient temperature of 300 K. Air flows parallel to the surface in the downward (opposing) direction. Estimate the highest air velocity at which purely natural convection can be assumed. Also, estimate the lowest air velocity at which purely forced convection can be assumed.

SOLUTION. Let us first calculate properties. As an estimate, let us use $T_{\mathrm{ref}} = T_\infty + 15 = 315\,\mathrm{K}$ as the temperature for properties. The properties will then be similar to those calculated in Example 11.1.

We calculate the modified Rayleigh and Grashof numbers:

$$\mathrm{Ra}_l^* = \frac{g\beta q_s'' l^4}{k\nu\alpha}$$

$$= \frac{(9.81\,\mathrm{m/s^2})(0.00317\,\mathrm{K^{-1}})[20\,\mathrm{W/m^2}](0.12\,\mathrm{m})^4}{(0.0268\,\mathrm{W/m\,K})\left(\frac{1.93 \times 10^{-5}\,\mathrm{kg/m\,s}}{1.121\,\mathrm{kg/m^3}}\right)(2.37 \times 10^{-5}\,\mathrm{m^2/s})} = 1.182 \times 10^7,$$

$$\mathrm{Gr}_l^* = \frac{g\,(\cos\phi)\,\beta q_s'' l^4}{k\,\nu^2}$$
$$= \frac{\left(8.036\,\mathrm{m/s^2}\right)\left(0.00317\,\mathrm{K^{-1}}\right)\left[20\,\mathrm{W/m^2}\right](0.12\,\mathrm{m})^4}{(0.0268\,\mathrm{W/m\,K})\left(\dfrac{1.93\times10^{-5}\,\mathrm{kg/m\,s}}{1.121\,\mathrm{kg/m^3}}\right)^2} = 1.338\times10^7.$$

We use the recommendation of Misumi et al. (2007) described in Section 11.3. According to the discussion following Eq. (11.3.6),

$$\frac{\mathrm{Gr}_l^*}{\mathrm{Re}_{\mathrm{l,min}}^{2.5}} = 3 \Rightarrow \mathrm{Re}_{\mathrm{l,min}} = \left[\frac{\mathrm{Gr}_l^*}{3}\right]^{0.4} = \left[\frac{1.338\times10^7}{3}\right]^{0.4} = 457,$$
$$\frac{\mathrm{Gr}_l^*}{\mathrm{Re}_{l,\max}^{2.5}} = 0.2 \Rightarrow \mathrm{Re}_{l,\max} = \left[\frac{\mathrm{Gr}_l^*}{0.2}\right]^{0.4} = \left[\frac{1.338\times10^7}{3}\right]^{0.4} = 1350$$
$$U_{\infty,\min} = \frac{\mu\mathrm{Re}_{\mathrm{l,min}}}{\rho\, l} = \frac{\left(1.93\times10^{-5}\,\mathrm{kg/m\,s}\right)(457)}{(1.121\,\mathrm{kg/m^3})\,(0.12\,\mathrm{m})} = 0.065\,\mathrm{m/s},$$
$$U_{\infty,\max} = \frac{\mu\mathrm{Re}_{l,\max}}{\rho\, l} = \frac{\left(1.93\times10^{-5}\,\mathrm{kg/m\,s}\right)(1350)}{(1.121\,\mathrm{kg/m^3})\,(0.12\,\mathrm{m})} = 0.193\,\mathrm{m/s}.$$

Mixed convection takes place when $U_{\infty,\min} < U_\infty < U_{\infty,\max}$. $U_{\infty,\min}$ is the highest air velocity at which purely natural convection can be assumed, and $U_{\infty,\max}$ is the lowest air velocity at which purely forced convection can be assumed. In other words, pure natural convection can be assumed as long as $U_\infty < U_{\infty,\min}$. Furthermore, $U_\infty > U_{\infty,\max}$ is required for the validity of the assumption that heat transfer is by pure forced convection.

EXAMPLE 11.3. Nitrogen flows through an 88-cm long vertical pipe that is 2.5 cm in inner diameter. The pipe inner surface temperature is 100 °C. Assuming that the mean pressure and temperature of nitrogen are 2 bars and 35 °C, estimate the minimum mean velocity in the pipe that would justify neglecting the effect of natural convection.

SOLUTION. We will calculate thermophysical properties of N_2 at $T_{\mathrm{ref}} = (T_s + T_m) = 67.5$ °C temperature and 2-bars pressure:

$$\rho = 1.98\,\mathrm{kg/m^3},\ C_P = 1043\,\mathrm{J/kg\,^\circ C},\ k = 0.0289\,\mathrm{W/m\,K},$$
$$\mu = 1.97\times10^{-5}\,\mathrm{kg/m\,s},\ \mathrm{Pr} = 0.713,$$
$$\beta = \frac{1}{T_{\mathrm{film}}} = \frac{1}{(273+67.5)\,\mathrm{K}} = 0.00294\,\mathrm{K^{-1}}.$$

We may be able to use the regime map of Metais and Eckert (1964), Fig. (11.12). Therefore, let us see if we are within the parameter range of the validity of Fig. 11.12:

$$\mathrm{Pr}\frac{D}{l} = (0.713)\,\frac{0.025\,\mathrm{m}}{0.88\,\mathrm{m}} = 0.0202,$$
$$\mathrm{Gr}_D = \frac{g\beta D^3\,(T_s - T_\infty)}{\nu^2}$$

$$= \frac{(9.81\,\text{m/s}^2)\,(0.00294\,\text{K}^{-1})\,(0.025\,\text{m})^3\,(100-35)\,\text{K}}{\left(\dfrac{1.97\times10^{-5}\,\text{kg/m s}}{1.98\,\text{kg/m}^3}\right)^2} = 2.94\times10^5,$$

$$\text{Gr}_D\text{Pr}\frac{D}{l} = (0.0202)\,(2.94\times10^5) = 5959.$$

The problem parameters are clearly within the range of validity of Fig. 11.12. From the figure, for $\text{Gr}_D\text{Pr}(D/l) \approx 6000$, the minimum Reynolds number for the validity of pure forced convection assumption is $\text{Re}_D \approx 1600$. Therefore the minimum velocity for the validity of the assumption can be found as

$$U_{\text{m,min}} = \frac{\mu\,\text{Re}_D}{\rho D} = \frac{(1.97\times10^{-5}\,\text{kg/m s})\,(1600)}{(1.98\,\text{kg/m}^3)\,(0.025\,\text{m})} \approx 0.64\,\text{m}.$$

PROBLEMS

Problem 11.1. An isothermal vertical plate that is 50 cm high is suspended in atmospheric air.

(a) Assume that air, which is at 20 °C temperature, flows in the vertical, downward direction at a velocity of 0.4 m/s parallel to the plate. Determine the lowest surface average temperature at which natural convection becomes significant.

(b) Repeat part (a), this time assuming that the air flow is in the upward direction.

Problem 11.2. In Problem 10.13 assume that the warm side of the double-pane window faces a room in which air is at a temperature of 25 °C.

(a) Calculate the heat transfer coefficient between room air and the glass surface.

(b) Determine the heat transfer regime. (Natural convection, mixed convection, or forced convection?)

Problem 11.3. The mug shown in the figure is full to the rim with hot water at 90 °C. The mug's wall is 5 mm in thickness and has a thermal conductivity of 0.15 W/m K. The vessel is in atmospheric air with a temperature of 20 °C.

(a) Calculate the total rate of heat loss from the mug to air, assuming that the air is quiescent.

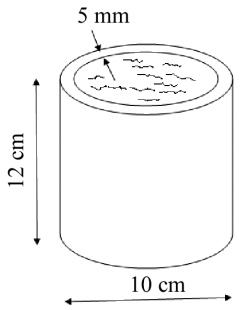

Figure P11.3.

(b) Repeat part (a), this time assuming that a breeze causes air to flow across the mug at a velocity of $U_\infty = 10$ cm/s.

For simplicity, neglect heat loss from the bottom of the mug and neglect the effect of evaporation at the free surface of water.

Problem 11.4. All correlations for the external flow Nusselt number representing average heat transfer coefficients for spheres have a constant of 2 on their right-hand sides: Why? Prove your argument.

Problem 11.5. A 0.5-m-wide and 2.5-m-high flat, vertical surface is subject to a UWT boundary condition with $T_s = 70\ ^\circ$C. The surface is exposed to air at an ambient temperature of 20 °C.

(a) Calculate the distributions of the heat transfer coefficient along the surface.
(b) Assume that air is flowing upward and parallel to the surface with a velocity of 0.05 m/s. Calculate the average heat transfer coefficient for the surface. Does laminar–turbulent transition take place? If so, specify the approximate location of the transition.

Problem 11.6. Repeat Problem 11.5, this time assuming that the surface is at an angle of 30° from horizontal plane, and is submerged in water that has a temperature of 20 °C.

Problem 11.7. An isothermal, 100 cm × 100 cm square plate is exposed to air. The air temperature is 25 °C, and the surface temperature is 45 °C.

1. Assuming pure natural convection, calculate the average heat transfer coefficients for three configurations:
   (a) vertical;
   (b) inclined at 60° to the vertical, with heated surface downward;
   (c) horizontal, upward facing.
2. Repeat part 1(a), this time assuming that the ambient air is flowing upward at a velocity of 0.1 m/s.

Problem 11.8. Consider the plate in Problem 11.1 and assume that the plate is at a uniform temperature of 70 °C. For both upward and downward flows of air, determine the range of air velocity at which mixed convection occurs.

Problem 11.9. For flow along a vertical flat plate, Raithby and Hollands (1998) developed the flow regime map depicted in Fig. P11.9.

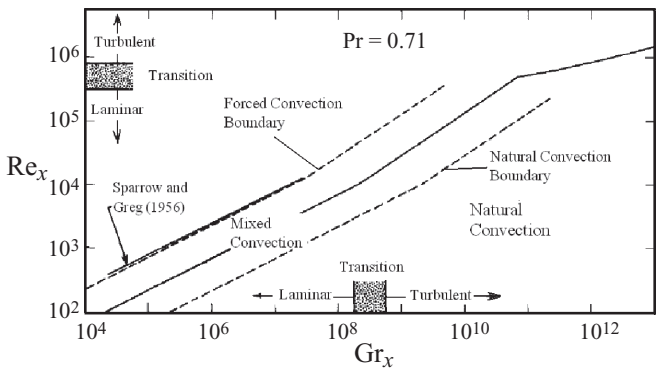

Figure P11.9.

Consider a vertical metallic tank 1 m in outer diameter and 2.34 m high. The tank is inside a building in which there is atmospheric air with 20 °C temperature. The surface of the tank is at 80 °C. Assume that a forced flow of air can be imposed on the surface of the tank in the vertical upward direction. For the points at the midheight of the tank, calculate the range of air velocities that would imply mixed convection. Compare the results with predictions of the method described in Section 11.4.

Problem 11.10. A 1-m-long heated vertical tube with 5-cm inner diameter carries an upward fully developed flow of air. The air pressure and average temperature are 1 bar and $T_{\text{in}} = 300$ K, respectively. The Reynolds number is $\text{Re}_D = 5000$.

(a) Calculate the minimum tube wall temperature, $T_{s,\min}$, that would cause the heat transfer regime to become mixed convection.
(b) Assuming that the wall temperature is at $T_{s,2}$, so that $T_{s,2} - T_{\text{in}} = 1.2(T_{s,\min} - T_{\text{in}})$, calculate the wall heat flux.

Problem 11.11. A pipe, with an inner diameter of 25 cm and a length of 7 m, carries nitrogen. The nitrogen average pressure is 10 bars and its mean temperature is 70 °C. The inner surface of the pipe can be assumed to be at 25 °C.

(a) Assume the pipe is horizontal. Estimate the minimum nitrogen mean velocity for the natural-convection effect to be unimportant.
(b) Assume the pipe is vertical. Estimate the minimum nitrogen mean velocity for the natural convection effect to be unimportant. Also, estimate the maximum nitrogen mean velocity for the forced-convection effect to be unimportant.

Problem 11.12. Water, at 1-bar pressure and a mean temperature of 40 °C flows in a horizontal pipe that is 5 cm in diameter. The mean velocity is such that $\text{Re}_D = 2.1 \times 10^3$. The flow is thermally developed. The pipe is subject to UHF boundary conditions, such that $\text{Gr}_D^* = 3 \times 10^6$. The pipe is made of stainless steel and is 3.5 mm thick.

Calculate the wall surface temperature, T_s, using the correlation of Morcos and Bergles (1975). Examine whether the application of this correlation is justified.

Problem 11.13. A horizontal pipeline carries methane gas at 100-bars pressure. The pipeline is made of carbon steel, is 15 cm in diameter, and has a thickness of the pipe wall of 6 mm. At a time of low gas consumption, natural gas flows through the pipeline at a Reynolds number of $\text{Re}_D = 2100$. Indirect solar radiation delivers a circumferentially averaged heat flux of 200 W/m^2 to the gas in the pipeline.

(a) Calculate the pipeline inner surface temperature at a location where the bulk gas temperature is 22 °C. Is the contribution of natural convection significant?
(b) Repeat part (a), this time assuming the flow rate is reduced by half.

Problem 11.14. A vertical duct that is 7 m in length and 5 cm in diameter is surrounded by atmospheric air. The duct is subject to the flow of near-atmospheric air. The air temperature at inlet is 25 °C. The duct is subject to a uniform wall heat flux of 130 W/m^2.

(a) We would like for the exit bulk temperature to be 60 °C, by imposing a forced-flow component. What should the mass flow rate be if purely forced convection is assumed?
(b) Is the assumption of negligible effect of natural convection justified?

Problem 11.15. According to Buhr (1967), free convection becomes important in a predominantly forced-convective flow in a pipe when (Reed, 1987)

$$\frac{\mathrm{Ra}_{D_H}}{\mathrm{Re}_m}\frac{D_H}{l} > 20 \times 10^{-4},$$

where the Rayleigh number is defined here as $\mathrm{Ra}_{D_H} = \frac{D_H^3 \beta g}{\nu \alpha}\left(\frac{dT_m}{dx} D_H\right)$, and all properties are to be calculated in mean bulk temperature. The preceding approximate criterion applies to vertical and horizontal pipes.

Using this criterion, determine whether natural convection effects are significant in Problem 4.20.

Problem 11.16. Use the criterion of Buhr (1967) discussed in the previous problem, determine whether natural-convection effects are significant in Problem 4.24. With the same inlet and boundary conditions, how long would the tube need to be in order for the natural-convection effect to become important?

Mass Transfer

Problem 11.17. In Problem 11.3, repeat the solution of part (b), this time accounting for evaporation at the free surface of the hot water. The relative humidity of air is 30%. For simplicity, neglect the contribution of mass diffusion to natural convection at the water surface and assume that heat transfer at the water surface is gas-side controlled.

Problem 11.18. In Problem 10.19, solve the problem, this time assuming that air flows with a velocity of 10 cm/s parallel to the water surface.

Problem 11.19. Solve Problem 10.20, this time assuming that air flows across the cylinder at a velocity of $U_\infty = 8$ cm/s.

12 Turbulence Models

In Chapter 6 we discussed the fundamentals of turbulence and reviewed the mixing length and eddy diffusivity models. As was mentioned there, these classical models do not treat turbulence as a transported property, and as a result they are best applicable to equilibrium turbulent fields. In an equilibrium turbulent field at any particular location there is a balance among the generation, dissipation, and transported turbulent energy for the entire eddy size spectrum, and as a result turbulence characteristics at each point only depend on the local parameters at that point.

Our daily experience, however, shows that turbulence is in general a transported property, and turbulence generated at one location in a flow field affects the flow field downstream from that location. One can see this by simply disturbing the surface of a stream and noting that the vortices resulting from the disturbance move downstream.

In this chapter, turbulence models that treat turbulence as a transported property are discussed. Turbulence models based on Reynolds–averaged Navier–Stokes [(RANS)-type] models are first discussed. These models, as their title suggests, avoid the difficulty of dealing with turbulent fluctuations entirely. We then discuss two methods that actually attempt to resolve these turbulent fluctuations, either over the entire range of eddy sizes [direct numerical simulation (DNS) method] or over the range of eddies that are large enough to have nonuniversal behavior [large-eddy simulation (LES) method].

12.1 Reynolds-Averaged Conservation Equations and the Eddy Diffusivity Concept

The 2D boundary layer Reynolds-averaged conservation equations for a fluid with constant properties when eddy diffusivities are used were derived in Section 6.4 [see Eqs. (6.4.12)–(6.4.16)]. These equations led to the definition of the following turbulent fluxes and properties:

$$\tau_{\text{tu}} = \mu_{\text{tu}} \frac{\partial \overline{u}}{\partial y} = \rho E \frac{\partial \overline{u}}{\partial y} = -\rho \overline{u'v'}, \tag{12.1.1}$$

$$q''_{y,\text{tu}} = -k_{\text{tu}} \frac{\partial \overline{T}}{\partial y} = -\rho C_P E_{\text{th}} \frac{\partial \overline{T}}{\partial y} = -\rho C_P \frac{E}{\text{Pr}_{\text{tu}}} \frac{\partial \overline{T}}{\partial y} = \rho C_P \overline{v'T'}, \tag{12.1.2}$$

$$j_{1,y,\mathrm{tu}} = -\rho\,\mathcal{D}_{12,\mathrm{tu}}\frac{\partial \overline{m_1}}{\partial y} = -\rho\frac{E}{Sc_{\mathrm{tu}}}\frac{\partial \overline{m_1}}{\partial y} = \rho\overline{v'm'}, \tag{12.1.3}$$

where overbars mean time or ensemble average. These expressions indicate that we need to specify E (or equivalently $\mu_{\mathrm{tu}} = \rho E$), $\mathrm{Pr}_{\mathrm{tu}}$, and $\mathrm{Sc}_{\mathrm{tu}}$ to fully characterize the turbulent flow field.

In a 3D flow field with near-isotropic turbulence, knowing E, we can find the total diffusive fluxes from the following expressions:

$$\tau_{ij} = \rho\,(\nu + E)\left(\frac{\partial \overline{u}_i}{\partial x_j} + \frac{\partial \overline{u}_j}{\partial x_i}\right), \tag{12.1.4}$$

$$q''_j = -\rho C_P\left(\frac{\nu}{\mathrm{Pr}} + \frac{E}{\mathrm{Pr}_{\mathrm{tu}}}\right)\frac{\partial \overline{T}}{\partial x_j}, \tag{12.1.5}$$

$$j_{1,\,j} = -\rho\left(\frac{\nu}{\mathrm{Sc}} + \frac{E}{\mathrm{Sc}_{\mathrm{tu}}}\right)\frac{\partial \overline{m}_1}{\partial x_j}. \tag{12.1.6}$$

The Reynolds-averaged conservation equations in Cartesian coordinates for an incompressible fluid are (note that Einstein's summation rule is used)

$$\frac{\partial \overline{u}_i}{\partial x_i} = 0, \tag{12.1.7}$$

$$\rho\frac{D\overline{u}_i}{dt} = -\frac{\partial P}{dx_i} + \frac{\partial \tau_{ij,\mathrm{lam}}}{\partial x_j} + \frac{\partial \tau_{ij,\mathrm{tu}}}{\partial x_j} + \rho g_i, \tag{12.1.8}$$

$$\rho C_P\frac{D\overline{T}}{Dt} = \tau_{ij}\frac{\partial \overline{u}_i}{\partial x_j} - \frac{\partial q''_{i,\mathrm{lam}}}{\partial x_i} - \frac{\partial q''_{i,\mathrm{tu}}}{\partial x_i} + \Phi_{\mathrm{tu}}, \tag{12.1.9}$$

$$\rho\frac{D\overline{m}_1}{Dt} = \frac{\partial}{\partial x_i}\left(-j_{1,i,\mathrm{lam}} - j_{1,i,\mathrm{tu}}\right). \tag{12.1.10}$$

Note that in Eq. (12.1.10) it is assumed that there is no volumetric generation or disappearance of species 1. Note also that, for the convenience of this discussion, all fluxes have been broken down into laminar (molecular) and turbulent components. For Newtonian a fluid that follows Fourier's law of conduction heat transfer and Fick's law for mass species diffusion, these fluxes can be expressed as

$$q''_{j,\mathrm{lam}} = -k\frac{\partial \overline{T}}{\partial x_j}, \tag{12.1.11}$$

$$q''_{j,\mathrm{tu}} = \rho\,C_P\overline{u'_j T'}, \tag{12.1.12}$$

$$\Phi_{\mathrm{tu}} = \overline{\tau'_{ij}\frac{\partial u_i}{\partial x_j}}, \tag{12.1.13}$$

$$\tau_{ij,\mathrm{lam}} = \mu\left(\frac{\partial \overline{u}_i}{\partial x_j} + \frac{\partial \overline{u}_j}{\partial x_i}\right), \tag{12.1.14}$$

$$\tau_{ij,\mathrm{tu}} = -\rho\,\overline{u'_i u'_j}, \tag{12.1.15}$$

$$\tau'_{ij} = \mu\left(\frac{\partial u'_i}{\partial x_j} + \frac{\partial u'_j}{\partial x_i}\right), \tag{12.1.16}$$

$$j_{1,j,\text{lam}} = -\rho\, \mathcal{D}_{12} \frac{\partial \overline{m}_1}{\partial x_j}, \tag{12.1.17}$$

$$j_{1,j,\text{tu}} = \rho \overline{u'_j m'_1}. \tag{12.1.18}$$

In the mixing-length model, based on an analogy with the predictions of the gas-kinetic theory (GKT) [Eq. (6.6.2)], it was assumed that the turbulent viscosity is the product of a characteristic length scale, a velocity scale, and the fluid density, namely,

$$\mu_{\text{tu}} = \rho\, l_{\text{tu}}\, U_{\text{tu}}, \tag{12.1.19}$$

This expression can in fact be considered the basis of most RANS-type turbulence models in which U_{tu}, l_{tu}, or both are treated as transported properties.

The simple eddy diffusivity (or mixing-length) models, some of which were discussed in Chapter 6, are sometimes referred to as zero-equation turbulence models, because they do not involve any turbulence transport equation. The mixing length model is simple in terms of numerical implementation, and inexpensive with respect to computation. It has the following serious disadvantages, however,

1. The mixing-length model (and indeed all zero-equation models) treats turbulence as a local phenomenon, implying equilibrium, whereby turbulence generated at one location will not be transported elsewhere.
2. The mixing-length model predicts that μ_{tu}, E, E_{th}, and E_{ma} all vanish as the velocity gradient vanishes. This is of course not true.
3. There is no general "theory" for calculating the mixing length. As a result, the mixing length needs to be derived empirically for each specific flow configuration.

12.2 One-Equation Turbulence Models

These models only use one transport equation for turbulence.

Starting from Eq. (12.1.19), let us treat U_{tu} as a transported property, with l_{tu} be found from some algebraic empirical correlation. The most obvious choice for U_{tu} is the mean turbulence fluctuation velocity, namely,

$$U_{\text{tu}} = \sqrt{K}, \tag{12.2.1}$$

where

$$K = \frac{1}{2}(\overline{u'^2} + \overline{v'^2} + \overline{w'^2}). \tag{12.2.2}$$

Clearly, instead of U_{tu}, we might as well use K as a transported property. The idea of treating the turbulence kinetic energy as a transported quantity is attributed to Prandtl (1945) and Kolmogorov (1942), among others. The transport equation for K can be derived in Cartesian coordinates by the following tedious but straightforward procedure.

1. Write the Navier–Stokes equations for all three coordinates.
2. Multiply the equation for each coordinate i by $u_i = \overline{u}_i + u'_i$
3. Perform time averaging on all the equations derived in step 2 and sum them up.

4. Multiply the time-averaged Navier–Stokes equation for each coordinate i by $\overline{u}_i$, and add the three resulting equations.
5. Subtract the outcome of step 4 from the outcome of step 3.

The result will be

$$\rho\frac{DK}{Dt} = \frac{\partial}{\partial x_l}\left(-\rho\overline{K'u_l'} - \overline{Pu_l'} + \mu\frac{\partial K}{\partial x_l}\right) - \rho\overline{u_i'u_l'}\frac{\partial \overline{u}_i}{\partial x_l} - \rho\varepsilon, \tag{12.2.3}$$

where

$$K' = u_i'u_i'/2, \tag{12.2.4}$$

$$\varepsilon = \nu\overline{\frac{\partial u_i'}{\partial x_l}\frac{\partial u_i'}{\partial x_l}}. \tag{12.2.5}$$

Let us, for clarity of discussion, examine this equation for a 2D flow in Cartesian coordinates, where (u, v) are velocity components corresponding to coordinates (x, y):

$$\rho\underbrace{\left(\frac{\partial K}{\partial t} + \overline{u}\frac{\partial K}{\partial x} + \overline{v}\frac{\partial K}{\partial y}\right)}_{\text{Convection}} = \underbrace{-\frac{\partial}{\partial y}[\rho\overline{v'(u'u' + v'v')} + \overline{v'P'}]}_{\text{Diffusion}} + \underbrace{\left(\mu\frac{\partial \overline{u}}{\partial y} - \rho\overline{u'v'}\right)\frac{\partial \overline{u}}{\partial y}}_{\text{Production}}$$
$$\underbrace{-\mu\left[\overline{\left(\frac{\partial u'}{\partial x}\right)^2} + \overline{\left(\frac{\partial u'}{\partial y}\right)^2} + \overline{\left(\frac{\partial v'}{\partial x}\right)^2} + \overline{\left(\frac{\partial v'}{\partial y}\right)^2}\right]}_{\text{Dissipation}}. \tag{12.2.6}$$

The bracketted material in the first term on the right-hand side of this equation is sometimes shown as $\rho\overline{v'K'} + \overline{v'P'}$.

Equations (12.2.3) or (12.2.6) are complicated and include averages of second- and third-order fluctuation terms. However, the terms on the right-hand side can be interpreted as representing specific processes with respect to the transport of K. This was of course done with intuition and mathematical and physical insight. Once the roles of these terms are figured out, then each term can be modeled by simpler and tractable model expressions, once again relying on physical and mathematical insight.

Thus the first term on the right-hand side of Eq. (12.2.6) can be interpreted as representing the diffusion of K. The second term represents the interaction of turbulent fluctuations with the mean flow velocity gradient and represents the production rate of turbulent kinetic energy. (This term actually appears with a negative sign in the mechanical energy transport equation for the mean flow.) Finally, the last term clearly represents the dissipation of turbulent kinetic energy. Thus the terms following the equal sign of Eq. (12.2.6) were approximated (modeled) by Prandtl, Kolmogorov, and others, as follows.

The diffusion is modeled as

$$\rho\overline{v'\,(u'u' + v'v')} + \overline{v'P'} \approx -\rho K^{1/2} l_{\text{tu}}\frac{\partial K}{\partial y}.$$

This can be rewritten as

$$\rho\overline{v'\,(u'u' + v'v')} + \overline{v'P'} = -\frac{\mu_{\text{tu}}}{\sigma_K}\frac{\partial K}{\partial y}, \tag{12.2.7}$$

where σ_K is called the effective Prandtl number for the diffusion of turbulence kinetic energy; the turbulent viscosity is to be found from

$$\mu_{\text{tu}} \approx \rho l_{\text{tu}} K^{1/2}. \tag{12.2.8}$$

We can derive the model production term by noting that $-\rho\overline{u'v'} = \tau_{xy,\text{tu}} = \mu_{\text{tu}} \frac{\partial \overline{u}}{\partial y}$, and therefore

$$\left(\mu \frac{\partial \overline{u}}{\partial y} - \rho\overline{u'v'}\right) \frac{\partial \overline{u}}{\partial y} = (\mu + \mu_{\text{tu}}) \left[\frac{\partial \overline{u}}{\partial y}\right]^2. \tag{12.2.9}$$

Often $\mu_{\text{tu}} \gg \mu$, and as a result μ is sometimes dropped from this equation.

Bearing in mind the physics of turbulent flows, we can argue that the dissipation term is controlled by the cascade process in which energy is transferred from large eddies to smaller eddies. This process can depend on only ρ, K, and l_{tu}, and based on dimensional analysis this leads to

$$-\mu \sum_{i,j} \overline{\left(\frac{\partial u_i'}{\partial x_j}\right)^2} = -\rho\varepsilon = -C_D \rho \frac{K^{3/2}}{l_{\text{tu}}}, \tag{12.2.10}$$

where C_D is a proportionality constant to be specified empirically.

Thus the transport equation for K becomes

$$\rho \frac{DK}{Dt} = \frac{\partial}{\partial y}\left(\mu + \frac{\mu_{\text{tu}}}{\sigma_K} \frac{\partial K}{\partial y}\right) + \mu_{\text{tu}} \left(\frac{\partial \overline{u}}{\partial y}\right)^2 - C_D \frac{\rho K^{3/2}}{l_{\text{tu}}}. \tag{12.2.11}$$

To apply this equation, we need to know C_D and l_{tu}. For boundary-layer flow near a wall, $\sigma_K \approx 1$ and (Launder and Spalding, 1972)

$$C_D = 0.08, \tag{12.2.12}$$

$$l_{\text{tu}} = \sqrt{C_D}\kappa y. \tag{12.2.13}$$

For the viscous sublayer as well as the buffer and overlap zones in the wall-bound turbulent flow, Wolfshtein (1969) proposed separate length scales for turbulent viscosity and dissipation:

$$\mu_{\text{tu}} = C_\mu \rho K^{1/2} l_\mu, \tag{12.2.14}$$

$$\varepsilon = C_D \frac{K^{3/2}}{l_\varepsilon}, \tag{12.2.15}$$

$$l_\mu = y\left[1 - \exp\left(-0.016\text{Re}_y\right)\right], \tag{12.2.16}$$

$$l_\varepsilon = y\left[1 - \exp\left(-0.263\text{Re}_y\right)\right], \tag{12.2.17}$$

where y is the normal distance from the wall and

$$\text{Re}_y = \rho K^{1/2} y/\mu. \tag{12.2.18}$$

Other coefficients in the Prandtl–Kolmogorov K transport equation, according to Wolfshtein, are

$$C_\mu = 0.220, \quad C_D = 0.416, \quad \sigma_K = 1.53.$$

The Prandtl–Kolmogorov one-equation model, which is based on the transport of K, thus recognizes that turbulence is a transported property. However, in practice it offers only a small advantage over the mixing-length model because it does not model the transport of the turbulence length scale. The length scale has thus to be provided empirically. The turbulence length scale depends on the flow field, however. As a result, this one-equation method is rarely applied to problems involving heat or mass transfer. Two-equation models, discussed in the forthcoming section, are instead applied.

The one-equation turbulent modeling method is of particular interest for the analysis of boundary-layer processes in aerospace applications, however, because the analysis of the flow around large flying objects is often computationally expensive. A one-equation turbulent model, proposed by Spalart and Allmaras (1992, 1994), has been remarkably successful and suitable for external flow boundary layers. The model is rarely used for heat transfer processes, however. This model is discussed in Appendix M.1.

12.3 Near-Wall Turbulence Modeling and Wall Functions

Most RANS-type turbulence models need to be modified at close proximity to a wall. The main reasons are as follows:

1. The assumption of locally isotropic turbulent dissipation and diffusion, which is made in many of these models, becomes unacceptable near a wall.
2. Turbulence becomes very complex because of the wall effect, and viscosity plays an increasingly important role as a wall is approached.

Furthermore, the intensity of turbulence transport processes drops very rapidly as a wall is approached and gradients of velocity, temperature, and concentration become very large. As a result, in numerical simulations, often very fine nodalization is required in the vicinity of a wall.

The most widely used methods for handling near-wall turbulence are the wall functions and the low-Reynolds-number turbulence models. In the wall-functions method, the universal velocity, temperature, and concentration profiles for turbulent boundary layers, which were discussed earlier in Sections 6.5 and 6.7, are utilized in order to impose the wall boundary conditions on the conservation equations. The wall-functions method can be applied with various turbulence models.

In the low-Reynolds-number models, the transport equations for turbulence properties are modified when they are applied near the wall to include the anisotropy and damping that are caused by the wall. The low-Reynolds-number models are discussed along with each specific turbulence model in the forthcoming sections.

A third method for the treatment of near-wall turbulence is often referred to as the two-layer model. In this method in the close vicinity of a wall, the turbulence modeling method is changed to the one-equation model described in the previous section. This method is also discussed along with specific turbulence models later.

The remainder of this section is devoted to the discussion of wall functions. In the wall-functions method, functions representing the (universal) distributions of

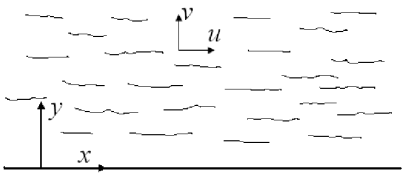

Figure 12.1. Schematic of turbulent flow past a flat surface.

fluid velocity, temperature, mass fraction, etc., are applied to the nodes closest to a wall.

Consider the flow field near a wall and assume that it is simulated as a steady-state, incompressible 2D boundary-layer flow on a smooth flat surface with x representing the main flow direction, as shown in Fig. 12.1. The universal velocity profile [see Eqs. (6.5.1)–(6.5.3)] will then apply. For simplicity, however, in near-wall turbulence modeling, the buffer zone is often not included, and instead the viscous sublayer and the overlap zone are assumed to merge at a y_u^+ normal distance from the wall; therefore,

$$u^+ = y^+ \quad \text{for } y^+ < y_u^+, \tag{12.3.1}$$

$$u^+ = \frac{1}{\kappa}\ln y^+ + B = \frac{1}{\kappa}\ln \boldsymbol{E} y^+ \quad \text{for } y^+ > y_u^+, \tag{12.3.2}$$

where κ (the Karman constant) and B are the same constants as those used in Eqs. (6.5.1)–(6.5.3), and

$$\boldsymbol{E} = \exp(\kappa B). \tag{12.3.3}$$

It is often assumed that $y_u^+ = 9$.

A similar argument can be used to derive the following wall functions for temperature, and thereby,

$$T^+ = \mathrm{Pr} y^+ \quad \text{for } y^+ < y_T^+. \tag{12.3.4}$$

For $y^+ > y_T^+$, we note that

$$\frac{\partial T^+}{\partial y^+} = \frac{1}{\dfrac{1}{\mathrm{Pr}} + \dfrac{E}{\nu \mathrm{Pr}_{\mathrm{tu}}}} \approx \frac{\mathrm{Pr}_{\mathrm{tu}}\nu}{E}, \tag{12.3.5}$$

where $T^+ = \frac{T_s - \overline{T}}{\frac{q_s''}{\rho C_P U_\tau}}$. Also, we showed earlier [Eq. (6.6.22)] that in the overlap zone we have

$$\frac{du^+}{dy^+} \approx \frac{\nu}{E}. \tag{12.3.6}$$

Using this equation and Eq. (12.3.5), we gets

$$dT^+ = \mathrm{Pr}_{\mathrm{tu}} du^+. \tag{12.3.7}$$

Integration of this equation then leads to

$$T^+ = \mathrm{Pr}_{\mathrm{tu}}(u^+ + \boldsymbol{P}). \tag{12.3.8}$$

The function $\boldsymbol{P}$ is meant to provide for transition from the viscous to the logarithmic temperature profiles:

$$\boldsymbol{P} = -\left(1 - \frac{Pr}{Pr_{\text{tu}}}\right) y_T^+. \tag{12.3.9}$$

A more elaborate analysis based on the Couette flow model at the limit of vanishingly small mass flux through the wall and van Driest's eddy diffusivity model lead to (Launder and Spalding, 1972),

$$\boldsymbol{P} = -\frac{\pi/4}{\sin(\pi/4)} (A/\kappa)^{1/2} \left(1 - \frac{\text{Pr}}{\text{Pr}_{\text{tu}}}\right) (\text{Pr}_{\text{tu}}/\text{Pr})^{1/4}, \tag{12.3.10}$$

where $A = 26$ is the constant in van Driest's eddy diffusivity model (see Section 6.6).

The parameter y_T^+ represents the distance from the wall where the values of T^+ predicted by Eqs. (12.3.4) and (12.3.8) match. It thus depends on Pr. It is easy to calculate y_T^+ in numerical simulations, however.

The following expression for the function $\boldsymbol{P}$ (Jayatilleke, 1969) is also used in some CFD codes:

$$\boldsymbol{P} = 9.24 \left[\left(\frac{\text{Pr}}{\text{Pr}_{\text{tu}}}\right)^{3/4} - 1\right] \left[1 + 0.28 \exp\left(-\frac{0.007\,\text{Pr}}{\text{Pr}_{\text{tu}}}\right)\right]. \tag{12.3.11}$$

The formulation thus far dealt with a smooth wall. We can introduce the effect of wall surface roughness by modifying the universal velocity and temperature profiles (see Section 6.5). The following expressions for the turbulent velocity are slight expansions of the expressions proposed by Cebeci and Bradshaw (1977) (CD-ADAPCO, 2008):

$$u^+ = \frac{1}{\kappa} \ln\left(\frac{\boldsymbol{E}}{f_\varepsilon} y^+\right), \tag{12.3.12}$$

where $\boldsymbol{E} = 9$ and the function f_ε is defined as

$$f_\varepsilon = \begin{cases} 1 & \text{(smooth surface)} \\ \left[B\left(\dfrac{\varepsilon_s^+ - \varepsilon_{s,\text{smooth}}^+}{\varepsilon_{s,\text{rough}}^+ - \varepsilon_{s,\text{smooth}}^+}\right) + C\varepsilon_s^+\right]^a & \text{(rough surface)}, \\ B + C\varepsilon_s^+ & \text{(fully rough surface)} \end{cases} \tag{12.3.13}$$

where

$$\varepsilon_s^+ < \varepsilon_{s,\text{smooth}}^+ \qquad \text{(smooth surface)}, \tag{12.3.14}$$

$$\varepsilon_{s,\text{smooth}}^+ < \varepsilon_s^+ < \varepsilon_{s,\text{rough}}^+ \qquad \text{(rough surface)} \tag{12.3.15}$$

$$\varepsilon_s^+ > \varepsilon_{s,\text{rough}}^+ \qquad \text{(fully rough surface)} \tag{12.3.16}$$

The default values of the coefficients in these expressions are, according to CD-ADAPCO (2008),

$$\varepsilon_{s,\text{smooth}}^+ = 2.5,$$
$$\varepsilon_{s,\text{rough}}^+ = 90,$$
$$B = 0$$

$$C = 0.253$$

$$a = \sin\left[\frac{\pi}{2}\frac{\log\left(\dfrac{\varepsilon_s^+}{\varepsilon_{s,\text{smooth}}^+}\right)}{\log\left(\dfrac{\varepsilon_{s,\text{rough}}^+}{\varepsilon_{s,\text{smooth}}^+}\right)}\right]$$

We can also define mass transfer wall functions. The mass-fraction law of the wall was discussed earlier in Section 6.7. The wall functions used in turbulence models are slightly different than the expressions presented in Section 6.7.

First, as discussed in Section 6.7, let us consider the case in which $m''_{1,s} \approx 0$ when species 1 is the only transferred mass through the wall, and if there are other species transferred through the wall then $n_s \approx 0$. Furthermore, assume that Fick's law applies. Equations (6.7.16)–(6.7.24) all apply. We can then integrate (6.7.11) to get the mass-fraction profiles.

Thus, in the viscous sublayer (which has now been extended into part of the buffer layer) where $E = 0$, for $y^+ < y^+_{\text{ma}}$,

$$m_1^+ = \text{Sc}\, y^+, \tag{12.3.17}$$

and in the overlap zone, where $y^+ > y^+_{\text{ma}}$,

$$m_1^+ = \text{Sc}_{\text{tu}}(u^+ + \boldsymbol{M}), \tag{12.3.18}$$

where y^+_{ma} is the distance from the wall where the mass-fraction profiles representing the two layers intersect. This simple analysis leads to,

$$\boldsymbol{M} = -\left(1 - \frac{\text{Sc}}{\text{Sc}_{\text{tu}}}\right) y^+_{\text{ma}}. \tag{12.3.19}$$

We can find $\boldsymbol{M}$ from a more elaborate analysis. The Couette flow film model at the limit of vanishingly small $m''_{1,s}$, applied along with van Driest's eddy diffusivity model, leads to (Launder and Spalding, 1972)

$$\boldsymbol{M} = -\frac{\pi/4}{\sin(\pi/4)}\,(A/\kappa)^{1/2}\left(1 - \frac{\text{Sc}}{\text{Sc}_{\text{tu}}}\right)(\text{Sc}_{\text{tu}}/\text{Sc})^{1/4}. \tag{12.3.20}$$

This expression is evidently the mass transfer version of Eq. (12.3.10).

Let us now consider the situation in which $m''_{1,s}$ is no longer vanishingly small or when n_s (which represents the total mass flux through the wall boundary) is no longer negligibly small. In these cases the preceding analysis does not apply. The correct boundary condition at the wall will be

$$m''_{1,s} = \overline{m}_{1,s} n_s - \rho\, \mathcal{D}_{12}\left.\frac{\partial \overline{m}_1}{\partial y}\right|_{y=0}. \tag{12.3.21}$$

When species 1 is the only transferred species through the wall, then we have $m''_{1,s} = n_s$ and the previous equation leads to

$$m''_{1,s} = -\frac{\rho\, \mathcal{D}_{12}}{1 - \overline{m}_{1,s}}\left.\frac{\partial \overline{m}_1}{\partial y}\right|_{y=0}. \tag{12.3.22}$$

The aforementioned universal profiles (velocity, temperature, and concentration) no longer apply because they were all based on the assumption of zero velocity at the wall.

Modifications to the turbulent law of the wall to account for the effect of transpiration were proposed by Stevenson (1963) and Simpson (1968) for flow past a flat surface (White, 2006). According to Stevenson (1963), the logarithmic law of the wall should be modified to

$$\frac{2}{v_s^+}\left[(1+v_s^+u^+)^{1/2}-1\right]\approx\frac{1}{\kappa}\ln y^+ + B, \tag{12.3.23}$$

where

$$v_s^+ = \frac{n_s/\rho}{U_\tau}. \tag{12.3.24}$$

According to Simpson (1968),

$$\frac{2}{v_s^+}\left[\left(1+v_s^+u^+\right)^{1/2}-\left(1+11v_s^+\right)^{1/2}\right]\approx\frac{1}{\kappa}\ln\left(\frac{y^+}{11}\right). \tag{12.3.25}$$

The preceding two expressions are evidently in disagreement with each other, however (White, 2006).

Although simulation results appear to be somewhat sensitive to the distance between the wall and the closest mesh point to the wall, the wall-functions method is very widely used in industrial applications because of the saving it offers with respect to the computations.

12.4 The K–ε Model

The K–ε is the most widely applied two-equation turbulence model. The two-equation turbulence models themselves are the most widely applied class of turbulence models at this time.

12.4.1 General Formulation

Going back to Eq. (12.1.19), we now want to treat both U_{tu} and l_{tu} as transported properties. The former can be represented by the turbulence fluctuation kinetic energy K, and therefore its transport will be represented by Eq. (12.2.11), which can be recast in the following more general form for an incompressible fluid:

$$\rho\frac{DK}{Dt}=\frac{\partial}{\partial x_i}\left[\left(\mu+\frac{\mu_{\text{tu}}}{\sigma_K}\right)\frac{\partial K}{\partial x_i}\right]+\mu_{\text{tu}}\frac{\partial\overline{u}_i}{\partial x_j}\left(\frac{\partial\overline{u}_i}{\partial x_j}+\frac{\partial\overline{u}_j}{\partial x_i}\right)-\rho\varepsilon. \tag{12.4.1}$$

For the second transport equation, instead of l_{tu} it is more convenient to use some other property that is a function of l_{tu} and K as the transported property. Several properties were proposed in the past, leading to K–ε, the $K-\tau$ (Johnson and King, 1985), and K–ω (Wilcox, 1993) models. The K–ε model is most widely applied, however. In Eqs. (12.2.14) and (12.2.15), let us use $C_D = 1$, and bear in mind that

$l_K = l_\varepsilon = l_{\text{tu}}$ away from the wall. Then, eliminating l_{tu} between the two equations will lead to,

$$\mu_{\text{tu}} = C_\mu \rho \frac{K^2}{\varepsilon}, \tag{12.4.2}$$

where C_μ is a constant to be specified empirically.

A transport equation for ε can also be derived. The procedure, which is tedious but straightforward, can be summarized as

$$2\nu \overline{\frac{\partial u_i'}{\partial x_j} \frac{\partial}{\partial x_j} [\text{NS}(u_i) - \overline{\text{NS}(u_i)}]} = 0 \tag{12.4.3}$$

where NS (u_i) is the Navier–Stokes equation for the x_i coordinate. The result will be

$$\begin{aligned} \frac{D\varepsilon}{Dt} = & \underbrace{\frac{\partial}{\partial x_l} \left(-\overline{\varepsilon' u_l'} - \frac{2\nu}{\rho} \overline{\frac{\partial u_l'}{\partial x_j} \frac{\partial \text{P}'}{\partial x_j}} - \nu \frac{\partial \varepsilon}{\partial x_l} \right)}_{\text{Diffusion}} \\ & \underbrace{- 2\nu \overline{\text{u}_l' \frac{\partial u_i'}{\partial x_j}} \frac{\partial^2 \overline{u}_i}{\partial x_l \partial x_j} - 2\nu \frac{\partial \overline{u}_i}{\partial x_j} \left(\overline{\frac{\partial u_l'}{\partial x_i} \frac{\partial u_l'}{\partial x_j}} + \overline{\frac{\partial u_i'}{\partial x_l} \frac{\partial u_j'}{\partial x_l}} \right)}_{\text{Production}} \\ & \underbrace{- 2\nu \overline{\frac{\partial u_i'}{\partial x_j} \frac{\partial u_i'}{\partial x_l} \frac{\partial u_j'}{\partial x_l}} - 2 \overline{\left(\nu \frac{\partial^2 u_i'}{\partial x_l \partial x_j} \right)^2}}_{\text{Destruction}}, \end{aligned} \tag{12.4.4}$$

where ε is defined in Eq. (12.2.5) and

$$\varepsilon' = \nu \frac{\partial u_i'}{\partial x_j} \frac{\partial u_i'}{\partial x_j}. \tag{12.4.5}$$

Equation (12.4.4) is evidently complicated and includes third-order terms. However, the terms after the equal sign of that equation can be attributed to specific processes, as displayed in Eq. (12.4.4), and modeled accordingly. The general model form of Eq. (12.4.4) is

$$\frac{D\varepsilon}{Dt} = \frac{1}{\rho} \frac{\partial}{\partial x_j} \left[\left(C_\varepsilon \rho \frac{K^2}{\varepsilon} + \mu \right) \frac{\partial \varepsilon}{\partial x_j} \right] + C_{\varepsilon 1} \frac{\varepsilon}{K} \frac{\mu_{\text{tu}}}{\rho} \left(\frac{\partial \overline{u}_i}{\partial x_j} + \frac{\partial \overline{u}_j}{\partial x_i} \right) \frac{\partial \overline{u}_i}{\partial x_j} - C_{\varepsilon 2} \frac{\varepsilon^2}{K}, \tag{12.4.6}$$

where

$$C_\varepsilon = C_\mu / \sigma_\varepsilon \tag{12.4.7}$$

and σ_ε is the Prandtl number for ε.

Using Eq. (12.4.7), we can replace $C_\varepsilon \rho (K^2/\varepsilon)$ in the first term on the right-side of Eq. (12.4.6) with the right-hand side of

$$C_\varepsilon \rho \frac{\text{K}^2}{\varepsilon} = \frac{\mu_{\text{tu}}}{\sigma_\varepsilon}. \tag{12.4.8}$$

Furthermore, because usually $\mu \ll C_\varepsilon \rho(K^2/\varepsilon)$, μ is often neglected in the first term on the right-hand side of Eq. (12.4.6).

The ε transport equation for a 2D boundary layer, in Cartesian coordinates, is

$$\frac{D\varepsilon}{Dt} = \frac{1}{\rho}\frac{\partial}{\partial y}\left(\mu + \frac{\mu_{\text{tu}}}{\sigma_\varepsilon}\frac{\partial \varepsilon}{\partial y}\right) + C_{\varepsilon 1}\frac{\varepsilon}{K}\frac{\mu_{\text{tu}}}{\rho}\left(\frac{\partial \overline{u}}{\partial y}\right)^2 - C_{\varepsilon 2}\frac{\varepsilon^2}{K}. \tag{12.4.9}$$

The coefficients σ_K, σ_ε, $C_{\varepsilon 1}$, $C_{\varepsilon 2}$, and C_μ should of course be specified empirically. Their values, however, turn out to be "universal" and need not be adjusted on a case-by-case basis. A widely used set of values, often referred to as the standard K–ε model, is (Launder and Sharma, 1974)

$$C_\mu = 0.09,\ C_{\varepsilon 1} = 1.44,\ C_{\varepsilon 2} = 1.92,\ \sigma_K = 1,\ \sigma_\varepsilon = 1.3. \tag{12.4.10}$$

The K–ε model has been modified to include the effect of various other parameters on turbulence. For example, the following equations are used in some CFD codes [Fluent 6.3 (2006), CD-ADAPCO (2008)]:

$$\rho\frac{DK}{Dt} = \frac{\partial}{\partial x_i}\left[\left(\mu + \frac{\mu_{\text{tu}}}{\sigma_K}\right)\frac{\partial K}{\partial x_i}\right] + \mu_{\text{tu}}\frac{\partial \overline{u}_i}{\partial x_j}\left(\frac{\partial \overline{u}_i}{\partial x_j} + \frac{\partial \overline{u}_j}{\partial x_i}\right) - \rho\varepsilon + G - Y, \tag{12.4.11}$$

$$\rho\frac{D\varepsilon}{Dt} = \frac{\partial}{\partial x_i}\left[\left(\mu + \frac{\mu_{\text{tu}}}{\sigma_\varepsilon}\right)\frac{\partial \varepsilon}{\partial x_i}\right] + C_{\varepsilon 1}\frac{\varepsilon}{K}\left[\mu_{\text{tu}}\left(\frac{\partial \overline{u}_i}{\partial x_j} + \frac{\partial \overline{u}_j}{\partial x_i}\right)\frac{\partial \overline{u}_i}{\partial x_j} + C_3 G\right] - C_{\varepsilon 2}\rho\frac{\varepsilon^2}{K}. \tag{12.4.12}$$

The constants σ_K, σ_ε, $C_{\varepsilon 1}$, $C_{\varepsilon 2}$, and C_μ have the same values as those given previously. The term G represents the production of turbulence kinetic energy and is given by

$$G = \beta\frac{\mu_{\text{tu}}}{\text{Pr}_{\text{tu}}} g_i \left(\frac{\partial \overline{T}}{\partial x_i}\right), \tag{12.4.13}$$

where β is the volumetric thermal expansion coefficient and g_i is the component of the gravitational vector $\vec{g}$ in the i direction. The term Y represents the effect of fluid compressibility and can be found from (Sarkar and Balakrishnan, 1990)

$$Y = 2\rho\varepsilon K/a^2, \tag{12.4.14}$$

where a is the speed of sound in the fluid. The coefficient C_3 is to be found from

$$C_3 = \tanh\left(\frac{U_{gp}}{U_{gn}}\right), \tag{12.4.15}$$

in which U_{gp} and U_{gn} are the velocity components parallel and normal to $\vec{g}$, respectively.

Thus far we discussed the hydrodynamics aspects of the K–ε model. However, knowing μ_{tu}, we can easily calculate the eddy diffusivities for heat and mass transfer by writing

$$E_{\text{th}} = E/\text{Pr}_{\text{tu}} = \frac{1}{\text{Pr}_{\text{tu}}}\frac{C_\mu K^2}{\varepsilon}, \tag{12.4.16}$$

$$E_{\text{ma}} = E/\text{Sc}_{\text{tu}} = \frac{1}{\text{Sc}_{\text{tu}}}\frac{C_\mu K^2}{\varepsilon}. \tag{12.4.17}$$

Two important points about the K–ε model should now be made.

1. In the derivation of the transport equations for K and ε up to this point, we have implicitly assumed local isotropy in the turbulent field. This assumption allowed us to treat μ_{tu} and E as scalar quantities. The assumption of local isotropy evidently becomes invalid close to walls where the damping effect of the wall on turbulent eddies becomes important. As a result, the aforementioned K and ε transport equations are not applicable all the way to the walls. The near-wall zone in a flow field thus needs special treatment. This issue is addressed later in the next section.
2. The K–ε model, as well as other models that assume that the deviatoric Reynolds stresses are linearly related to the local mean strain rate, are known to perform poorly when the mean flow streamlines have strong curvature. They are also incapable of correctly predicting the turbulence-induced secondary flows and the flow phenomena when there is rotation. Among the two-equation turbulence models, the nonlinear K–ε, briefly described in Appendix M.3, alleviates these difficulties.

12.4.2 Near-Wall Treatment

Application of Wall Functions

Near-wall turbulence in the K–ε model can be treated by using the wall functions described in Section 12.3. As mentioned earlier with respect to computational cost, the wall-functions method is the least expensive among the near-wall turbulence treatment methods. However, when wall functions are used, parts of the boundary layer (the viscous sublayer and often a significant part of the buffer or even the logarithmic zone) are not resolved. Detailed information about the unresolved layer is thus lost.

In numerical simulations, Eq. (12.3.8) and (12.3.9) and Eq. (12.3.1) or (12.3.2), whichever may be applicable, are used for the nodes closest to the wall. For those nodes, furthermore, the following boundary conditions are applied for K and ε:

$$K = \frac{U_\tau^2}{\sqrt{C_\mu}}, \tag{12.4.18}$$

$$\varepsilon = \frac{U_\tau^3}{\kappa\, y}. \tag{12.4.19}$$

Low-Re K–ε Models

Low-Re turbulence models are turbulent transport equations that are applicable throughout the boundary layer, including the buffer and viscous sublayers. When these models are used, the nodalization should be sufficiently fine to resolve the boundary layer, including the viscous sublayer. The viscous sublayer should typically be covered by five or more grids. In comparison with the wall functions, the low-Re methods have the advantage of resolving the boundary-layer details, but this advantage comes at the expense of significantly more computations.

Low-Re K–ε models are basically modifications to the K–ε models to make them applicable to near-wall conditions. The K and ε transport equations can be written as

$$\rho\frac{DK}{Dt} = \frac{\partial}{\partial x_i}\left[\left(\mu + \frac{\mu_{\mathrm{tu}}}{\sigma_K}\right)\frac{\partial K}{\partial x_i}\right] + \mu_{\mathrm{tu}}\frac{\partial \overline{u}_i}{\partial x_j}\left(\frac{\partial \overline{u}_i}{\partial x_j} + \frac{\partial \overline{u}_j}{\partial x_i}\right) - \rho\varepsilon - \rho\,\mathrm{D_T}, \tag{12.4.20}$$

$$\rho\frac{\mathrm{D}\varepsilon}{\mathrm{Dt}} = \frac{\partial}{\partial x_i}\left[\left(\mu + \frac{\mu_{\mathrm{tu}}}{\sigma_\varepsilon}\right)\frac{\partial \varepsilon}{\partial x_i}\right] + C_{\varepsilon 1}\frac{\varepsilon}{K}\mu_{\mathrm{tu}}\left(\frac{\partial \overline{u}_i}{\partial x_j} + \frac{\partial \overline{u}_j}{\partial x_i}\right)\frac{\partial \overline{u}_i}{\partial x_j} - C_{\varepsilon 2}\rho\frac{\varepsilon^2}{K} + \rho E_T. \tag{12.4.21}$$

Compared with Eqs. (12.4.1) and (12.4.6), the terms $\mathrm{D_T}$ and $\mathrm{E_T}$ have been added to Eqs. (12.4.20) and (12.4.21), respectively. Furthermore, coefficients C_μ and $\mathrm{C}_{\varepsilon 2}$ are now treated as functions of the distance from the wall, y. Several models were proposed in the past (for a brief review see Cho and Goldstein, 1994). The model by Jones and Launder (1973) is widely used, according to whom

$$D_T = 2\nu\left(\frac{\partial}{\partial y}K^{1/2}\right)^2, \tag{12.4.22}$$

$$E_T = 2\nu\left(\frac{\mu_{\mathrm{tu}}}{\rho}\right)\left(\frac{\partial^2 \overline{u}}{\partial y^2}\right)^2, \tag{12.4.23}$$

$$C_\mu = C_{\mu,\infty}\exp\left[-\frac{2.5}{1 + (\mathrm{Re_{tu}}/50)}\right], \tag{12.4.24}$$

$$C_{\varepsilon 2} = C_{\varepsilon 2,\infty}\exp\left[1.0 - 0.3\exp\left(-\mathrm{Re_{tu}^2}\right)\right], \tag{12.4.25}$$

where $\overline{u}$ in Eq. (12.4.23) represents the velocity parallel to the wall, $C_{\mu,\infty} = 0.09$, and $C_{\varepsilon 2,\infty} = 1.92$. Other model constants have the values given in Eq. (12.4.10). A slightly different form, proposed by Launder and Sharma (1974), is

$$C_\mu = C_{\mu,\infty}\exp\left[-\frac{3.4}{1 + (\mathrm{Re_{tu}}/50)}\right]. \tag{12.4.26}$$

For a 2D boundary layer, the low-Re K–ε model of Jones and Launder gives

$$\frac{\rho DK}{Dt} = \frac{\partial}{\partial y}\left[\left(\mu + \frac{\mu_{\mathrm{tu}}}{\sigma_K}\right)\frac{\partial K}{\partial y}\right] + \mu_{\mathrm{tu}}\left(\partial K/\partial y\right)^2 - \rho\varepsilon - 2\mu\left(\frac{\partial K^{1/2}}{\partial y}\right)^2, \tag{12.4.27}$$

$$\rho\frac{D\varepsilon}{Dt} = \frac{\partial}{\partial y}\left[\left(\mu + \frac{\mu_{\mathrm{tu}}}{\sigma_\varepsilon}\right)\frac{\partial \varepsilon}{\partial y}\right] + C_{\varepsilon 1}\frac{\varepsilon}{K}\mu_{\mathrm{tu}}\left(\frac{\partial \overline{u}}{\partial y}\right)^2 - C_{\varepsilon 2}\rho\frac{\varepsilon^2}{K} + 2\nu\mu_{\mathrm{tu}}\left(\frac{\partial^2 \overline{u}}{\partial y^2}\right)^2. \tag{12.4.28}$$

Two-Layer Models

In this approach, the original K–ε transport equations are solved away from the walls. Near the walls, however, the two-equation model is blended with the Prandtl–Kolmogorov one-equation model discussed in Section 12.2. Nodes in the near-wall region are thus resolved with a single equation for K, and the turbulent length scale is found from some correlation. The argument is that in the near-wall region the flow behavior is fairly universal, and so are correlations that provide for the turbulent

length scales. The model of Wolfshtein, displayed in Eqs. (12.2.14)–(12.2.18), are widely used.

12.4.3 Turbulent Heat and Mass Fluxes

Knowing the turbulent viscosity from Eq. (12.4.2), we can find the total diffusive heat and species mass fluxes from Eqs. (12.1.5) and (12.1.6) by noting that

$$\mu_{\text{tu}} = \rho E. \tag{12.4.29}$$

This would of course lead to Eqs. (12.4.16) and (12.4.17). Thus, in Eqs. (6.3.18) and (6.3.19), which represent the energy and mass-species conservation equations that need to be solved numerically along with the momentum conservation equations and the transport equations for K and ε, we use

$$\overline{\rho u_j' T'} = -\frac{\mu_{\text{tu}}}{\text{Pr}_{\text{tu}}} \frac{\partial \overline{T}}{\partial x_j}, \tag{12.4.30}$$

$$\overline{\rho u_j' m_1'} = -\frac{\mu_{\text{tu}}}{\text{Sc}_{\text{tu}}} \frac{\partial \overline{m}_1}{\partial x_j}. \tag{12.4.31}$$

12.5 Other Two-Equation Turbulence Models

Several other two-equation models are in widespread use, many of them modifications and expansions of the K–ε model. A brief description of some of these models follows. More details can be found in Appendices M.2, M.3, and M.4.

The K–ω Model

Next to the standard K–ε model, the K–ω model is probably the second most widely applied two-equation model (Wilcox, 1988, 1993, 1994). The model has been demonstrated to outperform the K–ε model for many situations, including turbulent boundary layers with zero or adverse pressure gradients and even near-separation conditions. The model is based on transport equations for K and ω, where ω is defined as

$$\omega = \frac{1}{\beta^*} \frac{\varepsilon}{K}, \tag{12.5.1}$$

and β^* is a model constant.

The K–ε Nonlinear Reynolds Stress Model

This is a two-equation model that solves for K and ε by using differential transport equations, but obtains the Reynolds stresses from nonlinear equations that are based on a generalized eddy viscosity model. The rationale is as follows. Consider the Boussinesq-based eddy diffusivity model, whereby

$$-\overline{u_i' u_j'} = \nu_{\text{tu}} \left(\frac{\partial \overline{u}_i}{\partial x_j} + \frac{\partial \overline{u}_j}{\partial x_i} \right) - \frac{2}{3} \delta_{ij} K. \tag{12.5.2}$$

This model has proven adequate for 2D flows without swirl, in which only one stress component provides the predominant influence on flow development. In flows with swirl or 3D flows to predict the experimental data well, it turns out that for each active stress component a different eddy viscosity needs to be defined. In other words, there is need for an anisotropic model for turbulent viscosity. This need can be satisfied by either of the following approaches:

1. development of separate equations for individual Reynolds stresses,
2. development of a nonlinear Reynolds stress model (RSM) to provide for the directional dependence of transport coefficients.

The K–ε nonlinear RSM is based on the latter approach (Speziale, 1987).

The Renormalized Group K–ε Model

The renormalized group (RNG) theory refers to a mathematical technique whose aim is to actually *derive* the turbulence models (in this case the K–ε model) and their coefficients (Yakhot and Orszag, 1986; Yakhot and Smith, 1992). The rationale is as follows. Consider the K–ε model. The specification of the model coefficients in traditional K–ε models is rather ad hoc. The coefficients are determined empirically, with little theoretical basis, and are assigned different values by different researchers. Unlike the K–ε and other common turbulence models that use a single length scale for the calculation of eddy viscosity, the RNG technique accounts for the subgrid eddy scales in its derivation. However, the RNG K–ε model appears to be only slightly superior to the traditional, ad hoc K–ε model.

12.6 The Reynolds Stress Transport Models

The one- and two-equation models discussed thus far avoided dealing with Reynolds stresses and turbulent heat and fluxes by using the concept of turbulent viscosity, μ_{tu}, and turbulent heat and mass diffusivities. Their derivation was based on the assumption of local isotropy, and near-wall modifications were meant to remedy this deficiency.

It is possible to derive transport equations for Reynolds stresses and turbulent fluxes of heat and mass, however. The resulting transport equations in their original forms will contain third-order terms and therefore cannot be solved. However, those terms can be modeled. The RSMs are based on this approach.

12.6.1 General Formulation

Consider an incompressible, constant-property flow. We can derive a transport equation for $\overline{u_i' u_j'}$ by the following tedious but straightforward procedure:

$$\overline{\{u_j'[\text{NS}(u_i) - \overline{\text{NS}(u_i)}] + u_i'[\text{NS}(u_j) - \overline{\text{NS}(u_j)}]\}} = 0, \tag{12.6.1}$$

where $\mathrm{NS}(u_i)$ represents the Navier–Stokes equation in the i direction. The result will be

$$\frac{D}{Dt}\overline{u_i'u_j'} = \frac{\partial}{\partial x_l}\left(-\overline{u_i'u_j'u_l'} - \underbrace{\overline{\frac{P'}{\rho}(\delta_{jl}u_i' + \delta_{il}u_j')}}_{\text{Diffusion}} + \nu\overline{\frac{\partial u_i'u_j'}{\partial x_l}}\right) - \underbrace{\left(\overline{u_i'u_l'}\frac{\partial \overline{u}_j}{\partial x_l} + \overline{u_j'u_l'}\frac{\partial \overline{u}_i}{\partial x_l}\right)}_{\text{Production}}$$

$$\underbrace{-2\nu\overline{\frac{\partial u_i'}{\partial x_l}\frac{\partial u_j'}{\partial x_l}}}_{\substack{\text{Viscous dissipation}\\ \text{of Reynolds stresses}}} + \underbrace{\overline{\frac{P'}{\rho}\left(\frac{\partial u_i'}{\partial x_j} + \frac{\partial u_j'}{\partial x_i}\right)}}_{\substack{\text{Pressure strain}\\ \text{(tends to restore isotropy)}}}. \tag{12.6.2}$$

We can likewise derive a transport equation for $\overline{u_i'T'}$ by the following procedure:

$$\overline{\{T'[\mathrm{NS}(u_i) - \overline{\mathrm{NS}(u_i)}] + u_i'[\mathrm{EE}(T) - \overline{\mathrm{EE}(T)}]\}} = 0. \tag{12.6.3}$$

where $\mathrm{EE}(T)$ represents the energy conservation equation. The result, when the effects of buoyancy on turbulence generation are neglected, is

$$\frac{D\overline{u_i'T'}}{Dt} = \frac{\partial}{\partial x_l}\left(-\overline{u_i'u_l'T'} - \delta_{il}\underbrace{\frac{\overline{P'T'}}{\rho}}_{\text{Diffusion}} + \boldsymbol{\alpha}\overline{u_i'\frac{\partial T'}{\partial x_l}} + \nu\overline{T'\frac{\partial u_i'}{\partial x_l}}\right) - \underbrace{\left(\overline{u_i'u_l'}\frac{\partial \overline{T}}{\partial x_l} + \overline{u_l'T'}\frac{\partial \overline{u}_i}{\partial x_l}\right)}_{\text{Production}}$$

$$\underbrace{-(\boldsymbol{\alpha}+\nu)\overline{\frac{\partial u_i'}{\partial x_l}\frac{\partial T'}{\partial x_l}}}_{\text{Dissipation}} + \underbrace{\overline{\frac{P'}{\rho}\frac{\partial T'}{\partial x_i}}}_{\substack{\text{Pressure–}\\ \text{temperature term}}} + \underbrace{\overline{\Phi' u_i'}}_{\text{Frictional heating}} \tag{12.6.4}$$

where

$$\Phi' = \frac{\mu}{\rho C_P}\left(\frac{\partial u_i'}{\partial x_j} + \frac{\partial u_j'}{\partial x_i}\right)\frac{\partial u_i'}{\partial x_j}. \tag{12.6.5}$$

We can also follow the previously described procedures for deriving transport equations for K and ε. It is more convenient to cast these transport equations in the following forms, however, which are compatible with the fact that we now solve for second-order terms and therefore can keep such terms in the transport equations:

$$\frac{DK}{Dt} = \frac{\partial}{\partial x_l}\left(\underbrace{-\frac{1}{2}\overline{u_i'u_j'u_l'} - \overline{\frac{P'u_l'}{\rho}}}_{\text{Diffusion}} + \underbrace{\nu\frac{\partial K}{\partial x_l}}_{\substack{\text{Molecular}\\ \text{diffusion}}}\right) - \underbrace{\overline{u_i'u_l'}\frac{\partial \overline{u}_i}{\partial x_l}}_{\text{Production}} - \underbrace{\varepsilon}_{\substack{\text{Viscous}\\ \text{dissipation}}} \tag{12.6.6}$$

$$\frac{D\varepsilon}{Dt} = \frac{\partial}{\partial x_l}\left(\underbrace{-\nu\overline{\frac{\partial u_i'}{\partial x_l}\frac{\partial u_i'}{\partial x_l}u_l'} - \frac{2\nu}{\rho}\overline{\frac{\partial u_l'}{\partial x_j}\frac{\partial P'}{\partial x_j}} + \nu\frac{\partial \varepsilon}{\partial x_l}}_{\text{Diffusion}}\right)$$

$$-2\nu u_l'\overline{\frac{\partial u_i'}{\partial x_j}\frac{\partial^2 \overline{u}_i}{\partial x_l \partial x_j}} - \underbrace{2\nu\frac{\partial \overline{u}_i}{\partial x_j}\left(\overline{\frac{\partial u_l'}{\partial x_i}\frac{\partial u_l'}{\partial x_j}} + \overline{\frac{\partial u_i'}{\partial x_l}\frac{\partial u_j'}{\partial x_l}}\right)}_{\text{Production}}$$

$$\underbrace{-2\nu\overline{\frac{\partial u_i'}{\partial x_j}\frac{\partial u_i'}{\partial x_l}\frac{\partial u_j'}{\partial x_l}} - 2\overline{\left(\nu\frac{\partial^2 u_i'}{\partial x_l \partial x_l}\right)^2}}_{\text{Destruction of the dissipation rate}}. \tag{12.6.7}$$

The preceding equations are obviously not closed because they contain third-order terms after the equal sign. However, as was done for the one- and two-equation models, we can attribute physical interpretations to all the terms after the equal sign of these equations and model them accordingly. These physical interpretations are displayed in the preceding equations. A useful discussion can be found in Chen and Jaw (1998). A simple and widely accepted set of model equations is as follows,

$$\frac{D}{Dt}\overline{u_i' u'}_j = \underbrace{\frac{\partial}{\partial x_l}\left[\left(C_K\frac{K^2}{\varepsilon}+\nu\right)\frac{\partial \overline{u_i' u_j'}}{\partial x_l}\right]}_{\text{Diffusion}} - \underbrace{\left(\overline{u_i' u_l'}\frac{\partial \overline{u}_j}{\partial x_l}+\overline{u_j' u_l'}\frac{\partial \overline{u}_i}{\partial x_l}\right)}_{\text{Stress production}} - \underbrace{\frac{2}{3}\delta_{ij}\varepsilon}_{\text{Viscous dissipation}}$$
$$\underbrace{-C_1\frac{\varepsilon}{K}\left(\overline{u_i' u'}_j-\frac{2}{3}\delta_{ij}K\right)+C_2\left(\overline{u_i' u_l'}\frac{\partial \overline{u}_j}{\partial x_l}+\overline{u_j' u_l'}\frac{\partial \overline{u}_i}{\partial x_l}-\frac{2}{3}\delta_{ij}\overline{u_n' u_m'}\frac{\partial \overline{u}_n}{\partial x_m}\right)}_{\text{Pressure–strain term}}, \tag{12.6.8}$$

$$C_K = 0.09\text{–}0.11, \quad C_1 = 2.30, \quad C_2 = 0.40,$$

$$\frac{DK}{Dt} = \frac{\partial}{\partial x_l}\left(C_k\frac{K^2}{\varepsilon}\frac{\partial K}{\partial x_l}+\nu\frac{\partial K}{\partial x_l}\right) - \overline{u_i' u_l'}\frac{\partial \overline{u}_i}{\partial x_l} - \varepsilon, \tag{12.6.9}$$

$$\frac{D\varepsilon}{Dt} = \frac{\partial}{\partial x_l}\left[\left(C_\varepsilon\frac{K^2}{\varepsilon}+\nu\right)\frac{\partial \varepsilon}{\partial x_l}\right] - C_{\varepsilon 1}\frac{\varepsilon}{K}\overline{u_i' u'}_l\frac{\partial \overline{u}_i}{\partial x_l} - C_{\varepsilon 2}\frac{\varepsilon^2}{K},$$

$$C_\varepsilon = 0.07, \quad C_{\varepsilon 1} = 1.45, \quad C_{\varepsilon 2} = 1.92, \tag{12.6.10}$$

$$\frac{D\overline{u_i' T'}}{Dt} = \underbrace{\frac{\partial}{\partial x_l}\left[\left(C_T\frac{K^2}{\varepsilon}+\boldsymbol{\alpha}\right)\frac{\partial \overline{u_i' T'}}{\partial x_l}\right]}_{\text{Diffusion}} - \underbrace{\left(\overline{u_i' u_l'}\frac{\partial \overline{T}}{\partial x_l}+\overline{u_l' T'}\frac{\partial \overline{u}_i}{\partial x_l}\right)}_{\text{Mean Flow Production}}$$
$$- C_{T1}\frac{\varepsilon}{K}\overline{u_i' T'} + C_{T2}\overline{u_m' T'}\frac{\partial \overline{u}_i}{\partial x_m}, \tag{12.6.11}$$
$$C_T = 0.07, \quad C_{T1} = 3.2, \quad C_{T2} = 0.5.$$

A model mass-species transfer equation can be written as

$$\frac{D\overline{u_i' m_1'}}{Dt} = \frac{\partial}{\partial x_l}\left[\left(C_m\frac{K^2}{\varepsilon}+\mathcal{D}_{12}\right)\frac{\partial \overline{u_i' m_1'}}{\partial x_l}\right] - \left(\overline{u_i' u_l'}\frac{\partial \overline{m}_1}{\partial x_l}+\overline{u_l' m_1'}\frac{\partial \overline{u}_i}{\partial x_l}\right)$$
$$- C_{m1}\frac{\varepsilon}{K}\overline{u_i' m_1'} + C_{m2}\overline{u_n' m_1'}\frac{\partial \overline{u}_i}{\partial x_n}. \tag{12.6.12}$$

If it is assumed that the turbulent diffusions of heat and mass species are similar (i.e., when $\mathrm{Pr_{tu}} \approx \mathrm{Sc_{tu}}$), then

$$C_m \approx C_T,$$
$$C_{m1} \approx C_{T1},$$
$$C_{m2} \approx C_{T2}.$$

12.6.2 Simplification for Heat and Mass Transfer

As noted, Eqs (12.6.11) and (12.6.12) each actually represent three separate partial differential equations in a 3D flow field. Their solution thus adds to the computational cost significantly. We often avoid these equations by making the simplifying assumption that the turbulent diffusion of enthalpy and mass species follows:

$$\rho C_P \overline{u_i' T'} = -\frac{\mu_{\text{tu}} C_P}{\text{Pr}_{\text{tu}}} \frac{\partial \overline{T}}{\partial x_i}, \tag{12.6.13}$$

$$\rho \overline{u_i' m_1'} = -\frac{\mu_{\text{tu}}}{\text{Sc}_{\text{tu}}} \frac{\partial \overline{m}_1}{\partial x_i}, \tag{12.6.14}$$

where

$$\mu_{\text{tu}} = C_\mu \rho \frac{K^2}{\varepsilon} \tag{12.6.15}$$

and $C_\mu = 0.09$.

Equations (12.6.13) and (12.6.14) are widely applied. However, they imply isotropic turbulent diffusion of heat and mass, which is evidently invalid near walls [Daly and Harlow, 1970; Launder, 1988]. Models that are meant to account for the anisotropic turbulence diffusion were proposed in the past. A model by Daly and Harlow (1970), also referred to as the generalized gradient hypothesis, can be represented as

$$\rho\, C_P \overline{u_i' T'} = -\rho\, C_P C_t \frac{K}{\varepsilon} \left(\overline{u_i' u_l'} \frac{\partial \overline{T}}{\partial x_l} \right), \tag{12.6.16}$$

where $C_t = 0.3$ (Rokni and Sunden, 2003). This equation for diffusion of mass can be written as

$$\rho \overline{u_i' m_1'} = -\rho\, C_t \frac{K}{\varepsilon} \left(\overline{u_i' u_l'} \frac{\partial \overline{m}_1}{\partial x_l} \right). \tag{12.6.17}$$

12.6.3 Near-Wall Treatment of Turbulence

The RSM equations discussed thus far did not consider the damping effect of a wall on turbulence and must therefore be modified for near-wall regions. The wall effect can be accounted for by wall functions or by use of a low-Re RSM.

Wall Functions

The wall functions for velocity, temperature, and mass fraction, described earlier in Section 12.3, all apply. Furthermore, for $y^+ > 10$, it can be shown that, for flow past a flat surface,

$$-\overline{u_t' u_n'} = U_\tau^2 = \tau_s / \rho, \tag{12.6.18}$$

$$K = U_\tau^2 \Big/ \sqrt{C_\mu}, \tag{12.6.19}$$

$$\varepsilon = U_\tau^3 / (\kappa y), \tag{12.6.20}$$

$$\overline{u_t'^2} = 5.1\, U_\tau^2, \tag{12.6.21}$$

$$\overline{u_n'^2} = U_\tau^2, \tag{12.6.22}$$

$$\overline{u_b'^2} = 2.3U_\tau^2, \tag{12.6.23}$$

where u_t', u_n', and u_b' are velocity fluctuations tangent to the surface and in the direction of the main flow, normal to the surface, and in the binormal direction, respectively.

Low-Reynolds-Number Models

Low-Re RSM models were proposed by several investigators (Hanjalic and Launder, 1976; Shima, 1988; Launder and Shima, 1989; Lai and So, 1990).

For a 2D boundary layer on a flat surface Eqs. (12.6.8)–(12.6.10) can be used with (Chen and Jaw, 1998)

$$C_K = 0.064, \quad C_\varepsilon = 0.065, \tag{12.6.24}$$

$$C_{\varepsilon 1} = 1.45, \quad C_{\varepsilon 2} = 1.90\text{–}2.0, \tag{12.6.25}$$

$$C_1 = C_{1,\infty} + 0.125\,\frac{K^{3/2}}{\varepsilon y}, \tag{12.6.26}$$

$$C_2 = C_{2,\infty} + 0.05\,\frac{K^{3/2}}{\varepsilon y}, \tag{12.6.27}$$

where y is the normal distance from the wall and

$$C_{1,\infty} = 1.5, \quad C_{2,\infty} = 0.4\text{–}0.6.$$

Launder and Shima (1989) proposed a widely applied near-wall RSM. The details of their model are provided in Appendix M.5.

12.6.4 Summary of Equations and Unknowns

The model transport partial differential equations for a 3D flow field are

Eq. (12.6.8) (six equations),
Eq. (12.6.9) (one equation),
Eq. (12.6.10) (one equation),
Eq. (12.6.11) (three equations),
Eq. (12.6.12) (three equations for each transferred species).

The unknowns in these partial differential equations are K, ε, $\overline{u_i'u_j'}$ (six of them), $\overline{u_i'T_j'}$ (three of them), and $\overline{u_i'm_l'}$ (three of them for each transferred species; l is meant to represent the transferred species). Compared with two-equation models, clearly the RSM model is computationally considerably more expensive.

12.7 Algebraic Stress Models

The Reynolds stress transport model can be simplified, and its computational cost reduced considerably, when the advection and diffusion terms in the Reynolds stress

transport equations can justifiably be dropped. The idea was first proposed by Rodi (1976).

Consider the RSM method discussed in the previous section. When advection and diffusion of Reynolds stresses are both small (e.g., in high-shear flow) or when advection and diffusion approximately cancel each other out (e.g., in local near-equilibrium), then the advection and diffusion terms in the transport equations for the Reynolds stresses can be dropped. When this is done to Eq. (12.6.8), for example, we are left with,

$$-\left(\overline{u_i'u_l'}\frac{\partial \overline{u}_j}{\partial x_l}+\overline{u_j'u_l'}\frac{\partial \overline{u}_i}{\partial x_l}\right)-\frac{2}{3}\delta_{ij}\varepsilon \quad -C_1\frac{\varepsilon}{K}\left(\overline{u_i'u_j'}-\frac{2}{3}\delta_{ij}K\right)$$
$$+C_2\left(\overline{u_i'u_l'}\frac{\partial \overline{u}_j}{\partial x_j}+\overline{u_j'u_l'}\frac{\partial \overline{u}_i}{\partial x_l}-\frac{2}{3}\delta_{ij}\overline{u_n'u_m'}\frac{\partial \overline{u}_n}{\partial x_m}\right)=0. \tag{12.7.1}$$

Likewise, in a high-shear and high-temperature-gradient flow, or when turbulence is in local near-equilibrium, the diffusion and advection terms in Eq. (12.6.11) can be dropped , leading to

$$-\left(\overline{u_i'u_j'}\frac{\partial \overline{T}}{\partial x_j}+\overline{u_j'T'}\frac{\partial \overline{u}_i}{\partial x_j}\right)-C_{T1}\frac{\varepsilon}{K}\overline{u_i'T'}+C_{T2}\overline{u_m'T'}\frac{\partial \overline{u}_i}{\partial x_m}=0. \tag{12.7.2}$$

Similarly, when the diffusion and advection terms can be justifiably dropped, Eq. (12.6.12) leads to

$$-\left(\overline{u_i'u_j'}\frac{\partial \overline{m}_l}{\partial x_j}+\overline{u_j'm_l'}\frac{\partial \overline{u}_i}{\partial x_j}\right)-C_{m1}\frac{\varepsilon}{K}\overline{u_i'm_l'}+C_{m2}\overline{u_n'm_l'}\frac{\partial \overline{u}_i}{\partial x_n}=0. \tag{12.7.3}$$

In a 3D flow, Eq. (12.7.1) actually gives six algebraic equations for $\overline{u_i'u_j'}$ terms. Likewise, Eq. (12.7.2) gives three algebraic equations in terms of $\overline{u_i'T_j'}$, and (12.7.3) gives three algebraic equations in terms of $\overline{u_i'm_l'}$ for each transferred species.

When the set of algebraic equations is solved along with the transport equations for K and ε [Eqs. (12.6.9) and (12.6.10)], the modeling approach is sometimes referred to as the K–ε–A (K–ε–algebraic) model.

For simplicity, however, the algebraic expressions for $\overline{u_i'T_j'}$ and $\overline{u_i'm_l'}$ are sometimes replaced with

$$\overline{u_i'T'}=-\frac{C_\mu}{\mathrm{Pr_{tu}}}\frac{K^2}{\varepsilon}\frac{\partial \overline{T}}{\partial x_i}, \tag{12.7.4}$$

$$\overline{u_i'm_1'}=-\frac{C_\mu}{\mathrm{Sc_{tu}}}\frac{K^2}{\varepsilon}\frac{\partial \overline{m}_1}{\partial x_i}. \tag{12.7.5}$$

In this case the model is sometimes referred to as the K–ε–E (K–ε–eddy diffusivity) model.

12.8 Turbulent Models for Buoyant Flows

Our discussion of turbulence models thus far dealt with forced-flow-dominated conditions, in which the effect of buoyancy on turbulence is negligible. In natural or mixed convection, however, buoyancy affects turbulence, as discussed in

Chapters 10 and 11. This section shows how the aforementioned RANS-type turbulence models can be modified to include the effect of buoyancy.

Conservation Equations

Consider a buoyancy-influenced flow for which Boussinesq's approximation applies, i.e., except for the gravity term in the momentum equation, everywhere else the fluid is essentially incompressible. The instantaneous conservation equations in Cartesian coordinates are then

$$\frac{d\,u_i}{d\,x_i} = 0, \tag{12.8.1}$$

$$\rho \frac{Du_i}{Dt} = -\frac{\partial P}{\partial x_i} + \nu \frac{\partial^2 u_i}{\partial x_j \partial x_j} + \rho g_i, \tag{12.8.2}$$

$$\frac{DT}{Dt} = \alpha \frac{\partial^2 T}{\partial x_j \partial x_j} + \tau_{ij} \frac{\partial u_i}{\partial x_j}, \tag{12.8.3}$$

where g_i is the component of $\vec{g}$ in i direction. An analysis similar to the one leading to Eq. (10.1.13) can now be performed, in which we now define P_∞, T_∞, and ρ_∞ as parameters representing the local properties under no-flow and no-heat-transfer conditions. The analysis then leads to

$$\frac{Du_i}{Dt} = -\frac{1}{\rho} \frac{\partial \left(P - P_\infty\right)}{\partial x_i} + \nu \frac{\partial^2 u_i}{\partial x_j \partial x_j} - g_i \beta \left(T - T_\infty\right). \tag{12.8.4}$$

The Reynolds-averaged conservation equations can now be derived. They lead to Eqs. (12.1.7)–(12.1.10), except that in Eq. (12.1.8) P should be replaced with $P - P_\infty$, and the following term should replace the last term on the right-hand side of that equation,

$$-\rho g_i \beta \left(T - T_\infty\right). \tag{12.8.5}$$

As a result, the following changes need to be incorporated in the turbulence transport equations:

- Add the following term to the right-hand side of Eq. (12.2.3):

$$-g_i \beta \overline{u_i' T'}. \tag{12.8.6}$$

- Add to the right-hand side of Eq. (12.4.4):

$$-2 g_i \beta \nu \overline{\frac{\partial u_i'}{\partial x_j} \frac{\partial T'}{\partial x_j}}. \tag{12.8.7}$$

- Add to the right-hand side of Eq. (12.6.2):

$$-\beta \left(g_i \overline{u_j' T'} + g_j \overline{u_i' T'} \right). \tag{12.8.8}$$

- Add to the right-hand side of Eq. (12.6.4):

$$-g_i \beta \overline{T'^2}. \tag{12.8.9}$$

The preceding expression introduces $\overline{T'^2}$ as a new transported property for which a transport equation is derived. The derivation of this transport equation introduces yet another transported property, $\varepsilon_{T'}$, for which another transport equation is also derived (Chen and Jaw, 1998):

$$\varepsilon_{T'} = 2\alpha \overline{\frac{\partial T'}{\partial x_i} \frac{\partial T'}{\partial x_i}}. \tag{12.8.10}$$

Model Transport Equations

The K–ε model transport equations for buoyant flow were presented in Section 12.4 [see Eqs. (12.4.11) and (12.4.12). The model transport equations for the RSM can be obtained as follows:

- Add Eq. (12.8.6) to the right-hand side of Eq. (12.6.9). When the eddy diffusivity approximation of Eq. (12.6.13) is used, add the following term to the right-hand side of Eq. (12.6.9):

$$\beta \frac{\mu_{\text{tu}}}{\text{Pr}_{\text{tu}}} g_i \frac{\partial \overline{T}}{\partial x_i}. \tag{12.8.11}$$

- Add to the right-hand side of Eq. (12.6.10):

$$-C_{\varepsilon 3} \frac{\varepsilon}{K} \beta g_i \overline{u_i' T'}. \tag{12.8.12}$$

- Add to the right-hand side of Eq. (12.6.8):

$$-(1 - C_3)\, \beta \left(g_i \overline{u_j' T'} + g_j \overline{u_i' T'} \right) - \frac{2}{3} C_3 \delta_{ij} \beta g_i \overline{u_i' T'}. \tag{12.8.13}$$

- Add to the right-hand side of Eq. (12.6.11):

$$-(1 + C_{T3})\, \beta g_i \overline{T'^2}. \tag{12.8.14}$$

The model transport equations for $\overline{T'^2}$ and $\varepsilon_{T'}$, furthermore, are

$$\frac{D\overline{T'^2}}{Dt} = \frac{\partial}{\partial x_i} \left[\left(C_{T'} \frac{K^2}{\varepsilon} + \nu \right) \frac{\partial \overline{T'^2}}{\partial x_i} \right] - 2\overline{u_i' T'} \frac{\partial \overline{T}}{\partial x_i} - 2\varepsilon_{T'}, \tag{12.8.15}$$

$$\frac{D\varepsilon_{T'}}{Dt} = \frac{\partial}{\partial x_i} \left[\left(C_{\varepsilon'} \frac{K^2}{\varepsilon} + \nu \right) \frac{\partial \varepsilon_{T'}}{\partial x_i} \right] - C_{\varepsilon' 1} \frac{\varepsilon}{K} \overline{u_i' T'} \frac{\partial \overline{T}}{\partial x_i} - C_{\varepsilon' 2} \frac{\varepsilon}{K} \varepsilon_{T'}. \tag{12.8.16}$$

Chen and Jaw (1998) listed the following values for the model constants:

$$\begin{aligned}
&C_K = 0.09, \quad C_\varepsilon = 0.07, \quad C_{T'} = 0.13, \quad C_1 = 1.8\text{–}2.8,\\
&C_{\varepsilon 1} = 1.42, \quad C_{\varepsilon'} = 0.1, \quad C_{T1} = 3.2, \quad C_2 = 0.4\text{–}0.6,\\
&C_{\varepsilon 2} = 1.92, \quad C_{\varepsilon' 1} = 2.5, \quad C_{T2} = 0.5, \quad C_3 = 0.3\text{–}0.5,\\
&C_{\varepsilon 3} = 1.44\text{–}1.92, \quad C_{\varepsilon' 2} = 2.5, \quad C_{T3} = 0.5, \quad C_T = 0.07.
\end{aligned}$$

12.9 Direct Numerical Simulation

The RANS-type turbulence models discussed thus far are all based on time or ensemble averaging, so that turbulent flow fluctuations are completely smoothed out. In these models we completely avoid the resolution of eddies. As a result of Reynolds averaging, information about details is lost in return for simplicity and fast computation. Reynolds averaging of course introduces Reynolds fluxes that need to be modeled.

With massive computer power, however, it is now possible to actually resolve turbulent eddies, at least for some problems. The possibility of resolving turbulent eddies makes it possible to simulate turbulent flows without any arbitrary assumption, and even without modeling. In this respect, the following two important methods are available:

1. Direct numerical simulation (DNS). In this method we attempt to resolve eddies of all important sizes, starting from viscous eddies all the way to the largest energy-containing eddies.
2. Large-eddy simulation (LES): In this method only large eddies are resolved, and small, isotropic eddies are modeled assuming that they have universal behavior.

In this section we briefly review the DNS method. The LES method is discussed in the next section.

The DNS technique is based on the discretization and numerical solution of basic local and instantaneous conservation equations, using grid spacing and time steps small enough to capture local random fluctuations, thus resolving both large and small turbulent eddies. Furthermore, the solution domain should be large enough to capture the behavior of largest eddies. DNS is now a well-proven and powerful analytical method that can provide accurate predictions of turbulent flow phenomena, with excellent agreement with measurements where available. It can thus be considered an alternative to high-quality experiments for many other flow processes. The method provides details about the flow field that are often impossible to directly measure.

DNS is computationally very expensive, however. It requires transient, 3D solutions of conservation equations, using time and spatial discretization that is fine enough to capture the smallest eddies over a physical domain that is large enough to capture the behavior of largest eddies and over a time period that is long enough to make the statistical analysis of the results meaningful. The 3D analysis is always required because eddies move in three dimensions. As a result, with current computer power it is used for research purposes only.

As an example, consider an incompressible, constant-property, fully developed pipe flow with an isoflux (constant wall heat flux) boundary condition. We note that we should have (See Section 4.2.3)

$$\frac{\partial \overline{T}}{\partial x} = \frac{\partial \overline{T}_m}{\partial x} = \frac{\partial \langle \overline{T}_s \rangle}{\partial x} = \text{const.}, \tag{12.9.1}$$

where $\langle \overline{T}_s \rangle$ is the wall temperature averaged over time and circumference, x is the axial coordinate, and the overbar notation represents ensemble averaging.

The nondimensional steady-state, 3D incompressible continuity, momentum, and energy equations can then be cast as (see Problem 12.12)

$$\nabla^+ \cdot \vec{U}^+ = 0, \tag{12.9.2}$$

$$\frac{\partial \vec{U}^+}{\partial t^+} + (\vec{U}^+ \cdot \nabla^+)\vec{U}^+ = -\nabla^+ P^+ + \nabla^{+2} \cdot \vec{U}^+ - \frac{4}{\mathrm{Re}_\tau}, \tag{12.9.3}$$

$$\frac{\partial \theta}{\partial t^+} + (\vec{U}^+ \cdot \nabla^+)\theta = \frac{1}{\mathrm{Pr}} \nabla^{+2}\theta + 4\frac{u_x^+}{\mathrm{Re}_\tau}, \tag{12.9.4}$$

where

$$U_\tau = \sqrt{\frac{\tau_s}{\rho}}, \quad \vec{U}^+ = \frac{\vec{U}}{U_\tau}, \quad P^+ = \frac{P - \overline{P}}{\rho U_\tau^2}, \tag{12.9.5}$$

$$\nabla^+ = \frac{\mu}{\rho U_\tau} \nabla, \quad t^+ = \frac{t \rho U_\tau^2}{\mu}, \quad \theta = \frac{\left(T_m - \overline{T}\right)}{q_s''/(\rho C_P U_\tau)}, \tag{12.9.6}$$

$$\mathrm{Re}_\tau = \rho U_\tau D/\mu, \quad x^+ = \rho U_\tau x/\mu, \quad r^+ = \rho U_\tau r/\mu. \tag{12.9.7}$$

In these equations T_m and $\overline{P}$ are the local mean temperature and pressure, respectively. The last term in Eq. (12.9.3) represents the linear dependence of $\overline{P}$ on x. The last term on the right-hand side of Eq. (12.9.4) results from Eq. (12.9.1). The velocity vector is the local instantaneous velocity, and $P - \overline{P}$ is in fact the fluctuating component of pressure if it is assumed that the mean pressure is uniform across the flow cross section. These local, instantaneous equations need to be numerically solved.

There are two widely used methods for the numerical solution of these equations.

1. Spectral techniques: These methods are based on Fourier and Chebyshev polynomial expansions. They provide better estimates of the spatial derivatives, but are difficult to apply to complex geometries.
2. Finite difference and finite volume: These techniques are flexible with respect to complex geometries.

To determine the necessary time and spatial discretization, we need to address the turbulent eddies. Let us first discuss the hydrodynamics. As mentioned in Section 6.8, eddies in a turbulent field cover a wide range of sizes. The largest eddies are comparable in size to the characteristics dimension of the turbulence-generating feature of the system (the pipe radius in pipe flow). The large eddies do not respond to viscosity and therefore do not undergo viscous dissipation. However, they lose their kinetic energy to smaller eddies, and so on, until viscous eddies are reached. Viscous eddies are small enough to be under the influence of viscosity. They are responsible for viscous dissipation. As noted in Section 6.8, in an isotropic turbulent flow field the characteristic size and time for viscous eddies are

$$l_D = \left(\frac{\nu^3}{\varepsilon}\right)^{1/4} \quad \text{(Kolmogorov's micro scale)}, \tag{12.9.8}$$

$$t_{c,D} = (\nu/\varepsilon)^{1/2}, \tag{12.9.9}$$

where ε is the turbulent dissipation rate and can be estimated in pipe flow from

$$\varepsilon \approx -\frac{4U_m\nu}{D}\left.\frac{\partial U}{\partial r}\right|_{r=R_0}. \tag{12.9.10}$$

DNS must evidently resolve the behavior of viscous eddies. It turns out that, to ensure the resolution of small and large eddies, we must use at least three nodes in the viscous sublayer (Grotzbach, 1983). Thus, for uniform mesh size, we have

$$\Delta r^+ \leq 1.88. \tag{12.9.11}$$

The axial and azimuthal dimensions of the cells, furthermore, should not be larger than πl_D, i.e.,

$$\Delta z \leq \pi l_D, \tag{12.9.12}$$

$$(D\Delta\theta) \leq \pi l_D, \tag{12.9.13}$$

where θ is the azimuthal angle. For time steps, furthermore, we must have $\Delta t \leq t_{c,D}$.

The length of the simulated channel segment, l, must be long enough to ensure that velocity fluctuations are uncorrelated at axial locations that are l apart. We can do this by choosing $l = 5D$ (Eggels et al., 1994). Once it is ensured that the fluctuations at the inlet and outlet to the physical domain are uncorrelated, then periodic boundary conditions can be imposed on the simulated channel segment in axial and azimuthal directions, whereby, for example, at any instant,

$$\vec{U}(r,\theta)_{x=0} = \vec{U}(r,\theta)_{x=l}, \tag{12.9.14}$$

$$P(r,\theta)_{x=0} = P(r,\theta)_{x=l}, \tag{12.9.15}$$

$$T^+(r,\theta)_{x=0} = T^+(r,\theta)_{x=l}, \tag{12.9.16}$$

where $\vec{U}$, P and T^+ are local and instantaneous properties.

The numerical simulation must start from some assumed turbulent characteristics. For pipe flow, as well as other self-sustaining turbulent flow fields, the assumed initial condition of course must not affect the outcome of the simulation. In other words, even if we start from an unrealistic initial guess, the flow field characteristics must be eventually correct once the DNS analysis reaches fully developed conditions. Nevertheless, we would expect the simulation to take less computation if the initial guess is reasonably close to the expected conditions. We can estimate the initial conditions, for example, by using the statistical characteristics of pipe flow. The numerical simulation should continue until the statistical properties of turbulent flow at any location become independent of time. With a reasonably accurate initial condition (borrowed from experimental fully developed turbulence characteristics, for example), for fully developed pipe flow the simulation needs to continue up to

$$t \approx 15D/U_\tau. \tag{12.9.17}$$

The preceding expression clearly shows that with increasing Re the required number of nodes increases while the time step decreases. As a result the computational cost will depend strongly on the flow Reynolds number. If it is assumed that

Table 12.1. *The required total number of nodes for a marginally sufficient resolution in fully developed pipe flow*

Re_D	l_D/D	Total number of nodes	Total number of time steps
5×10^3	0.00454	3.51×10^6	2121
10^4	0.00282	1.67×10^7	3000
5×10^4	0.000933	6.247×10^8	6708
10^5	0.000579	2.971×10^9	9487
5×10^5	0.000192	1.11×10^{11}	21,213

Blasius' friction-factor correlation applies, it can be easily shown that

$$R^+ = \frac{1}{2}\sqrt{\frac{0.316}{8}}\mathrm{Re}_D^{7/8}, \tag{12.9.18}$$

$$l_D = 1.586D\mathrm{Re}_D^{-11/16}, \tag{12.9.19}$$

$$t_{c,D} = 2.516\frac{D}{U_m}\mathrm{Re}_D^{-3/8}, \tag{12.9.20}$$

$$t = 75.47\frac{D}{U_m}\mathrm{Re}_D^{-1/8}, \tag{12.9.21}$$

For $\mathrm{Re}_D = 5000$, when one quarter of the cross section ($0 \le \theta \le \pi/2$) is simulated, we thus get $R^+ = 141$, and we can obtain a marginally sufficient resolution by using $350 \times 91 \times 110 \approx 3.5 \times 10^6$ nodes, and the total number of time steps will be about 2120.

Table 12.1 displays the minimum requirements for a marginally sufficient resolution for a fully developed pipe flow for several Reynolds numbers. The table makes it clear that, even for a flow as simple as fully developed pipe flow, DNS is currently feasible only for low Reynolds numbers.

The discussion of discretization thus far dealt with hydrodynamics only. When heat transfer is considered, for example, clearly the discretization must ensure that the thermal boundary layer is also properly resolved. As noted in Section 2.3, for a laminar boundary layer we have $\delta_{\mathrm{th}}/\delta \approx \mathrm{Pr}^{-1/3}$ for $\mathrm{Pr} \gtrsim 1$ and $\delta_{\mathrm{th}}/\delta \approx \mathrm{Pr}^{-1/2}$ for $\mathrm{Pr} \ll 1$. For diffusive mass transfer of an inert species, likewise, we have $\delta_{\mathrm{ma}}/\delta \approx \mathrm{Sc}^{-1/3}$ for $\mathrm{Sc} \gtrsim 1$, and $\delta_{\mathrm{ma}}/\delta \approx \mathrm{Sc}^{-1/2}$ for $\mathrm{Sc} \ll 1$. The previous criteria regarding the discretization requirement evidently apply as long as $\mathrm{Pr} < 1$ or $\mathrm{Sc} < 1$. Finer discreitization is required when $\mathrm{Pr} > 1$ or $\mathrm{Sc} > 1$. The total number of nodes for these cases will be of the order of $\mathrm{Pr}^3\mathrm{Re}^{9/4}$ or $\mathrm{Sc}^3\mathrm{Re}^{9/4}$. As a result, DNS analysis of scalar transport is practical only for Pr or Sc smaller than, equal to or slightly larger than one only; otherwise the required number of cells in the computational domain becomes prohibitively large. An alternative method has been applied for some cases in which $\mathrm{Pr} > 1$ or $\mathrm{Sc} > 1$, however (Lyons et al., 1991a, 1991b; Papavassiliou and Hanratty, 1997; Na and Hanratty, 2000), in which the path of a large number of scalar markers (i.e., neutral particles with random Brownian motion that corresponds to the diffusivity of the transported scalar) is followed in a flow field whose hydrodynamics is solved for by the DNS method.

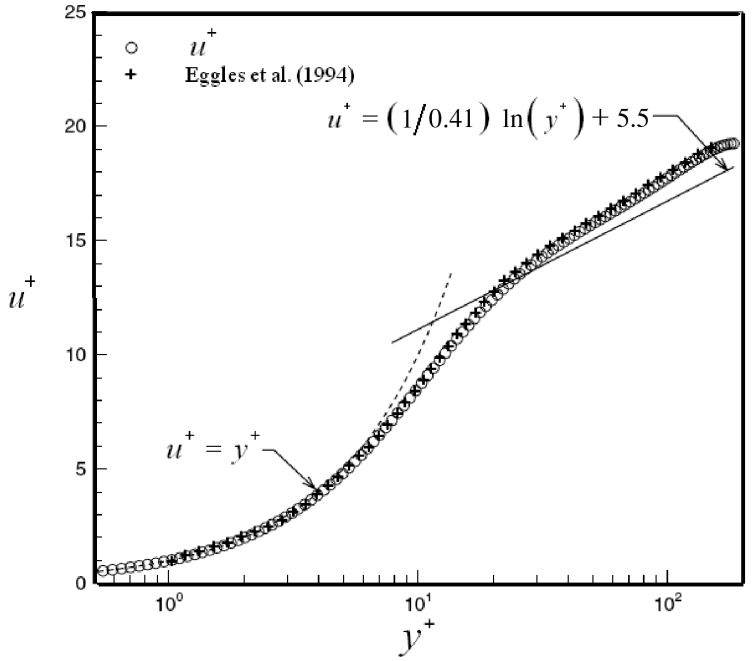

Figure 12.2. The near-wall mean velocity profile in a pipe flow (after Redjem-Saad et al., 2007).

Figures 12.2–12.4, all borrowed from Redjem-Saad et al. (2007), represent DNS predictions for fully developed turbulent pipe flow. Figure 12.4 depicts the variation of the turbulent Prandtl number in the near-wall zone for various Pr values. It confirms, as mentioned in Chapter 6, that $\mathrm{Pr_{tu}} \approx 1$ as long as $\mathrm{Pr} \approx 1$, and it deviates from unity for fluids with $\mathrm{Pr} \ll 1$.

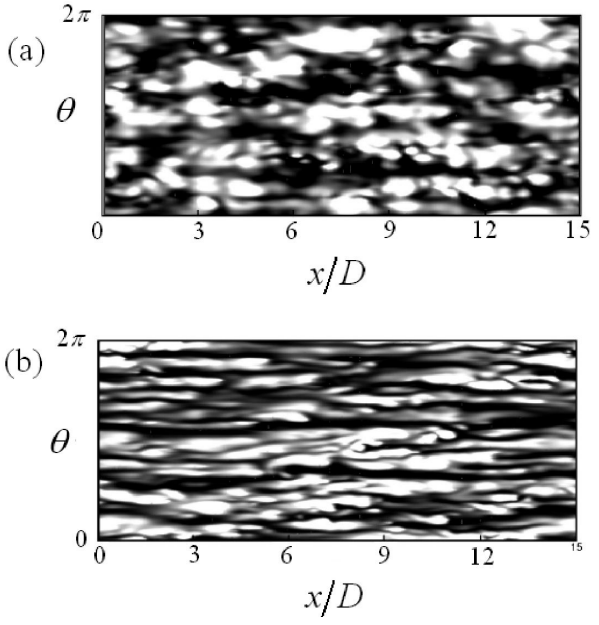

Figure 12.3. Instantaneous temperature fluctuations at $y^+ \approx 5$ in a turbulent pipe flow with $\mathrm{Re}_D = 5500$: (a) $\mathrm{Pr} = 0.026$, (b) $\mathrm{Pr} = 0.71$ (after Redjem-Saad et al., 2007).

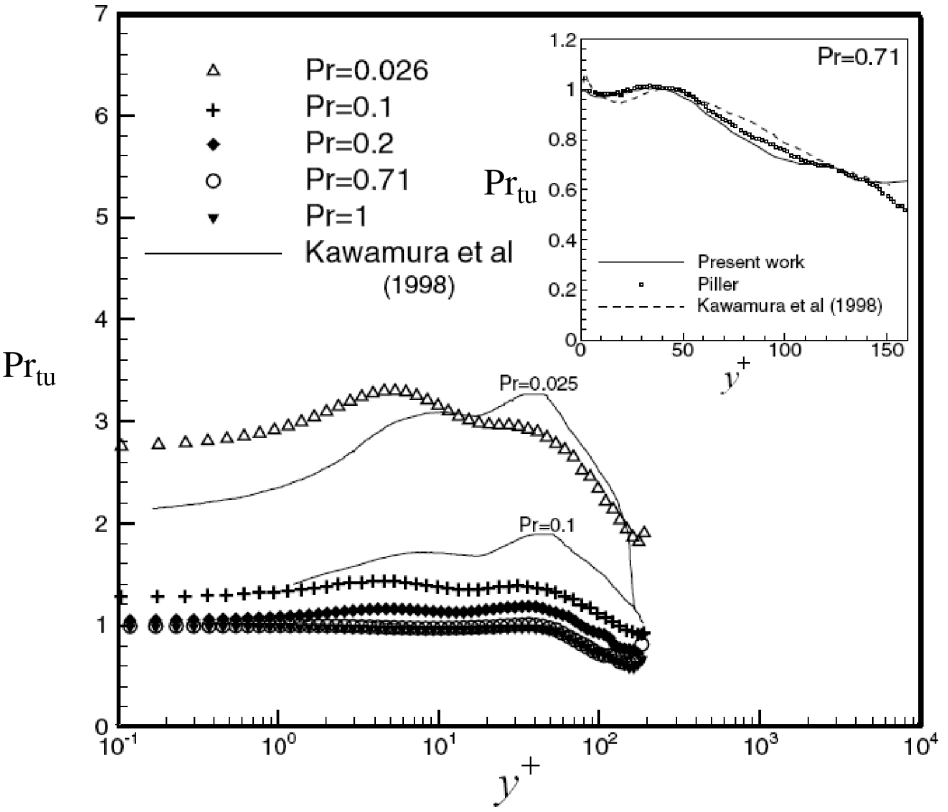

Figure 12.4. Turbulent Prandtl number in a pipe flow (after Redjem-Saad et al., 2007).

12.10 Large Eddy Simulation

LES is a method that falls between DNS and RANS-type techniques. RANS-type models completely average out the fluctuations. DNS is on the other extreme, and aims to capture and resolve all important fluctuations. The LES method attempts to resolve "large" eddies (coherent turbulent structures) while modeling very small eddies. LES is thus useful for situations for which RANS-type methods are insufficient. It is also useful for flow situations in which the frequency of mean flow fluctuations is comparable to the frequency of turbulent fluctuations.

Any high-Reynolds-number turbulent flow is characterized by large eddies that depend on the flow geometry and are responsible for most of momentum, heat, and mass transfer. The behavior of these large eddies is system and case specific. They need to be resolved because models do not apply to them. Smaller, self-similar eddies (in the sense of Kolmogorov's hypothesis), on the other hand, are relatively insensitive to the macroscopic flow geometry and behave approximately the same way, irrespective of the macroscopic geometric features. They thus do not need to be resolved and can instead be modeled. Furthermore, the modeling of small eddies does not need to be very accurate, because these eddies typically carry only a small fraction of the total turbulent kinetic energy, meaning that inaccuracies in modeling their behavior will not have a significant impact on the overall accuracy of the solution. The LES method thus is based on resolving large eddies, while the impact

of the small eddies on the behavior of a large eddy is taken into account by models. The modeling of the behavior of the small eddies, rather than resolving them, will of course come at the expense of losing small-eddy-level details. In comparison with RANS methods, however, LES provides valuable details about the flow and makes it possible to model flow and transport phenomena caused by local turbulent fluctuations. (Note that the RANS methods completely average all the fluctuations.) A good example is the possibility of combustion in a turbulent air–fuel mixture in which, in terms of the average mixture, the concentration of the fuel is lower than the threshold needed for combustion. Turbulent fluctuations in such a flow field can cause the local concentration to exceed the threshold.

LES methods allow for time steps and grid sizes an order of magnitude larger than those of DNS. They are still much more demanding than RANS-type models, however. The LES was formulated in the 1960s and was applied for modeling atmospheric flow phenomena in the 1970s and beyond. It gained increasing popularity in various engineering disciplines in the subsequent decades. It is now a widely used simulation technique.

Filtering of Conservation Equations

Consider the flow of an incompressible fluid, for which the local, instantaneous conservation equations will be

$$\frac{\partial \rho}{\partial t} + \frac{\partial}{\partial x_i}(\rho U_i) = 0, \tag{12.10.1}$$

$$\frac{\partial}{\partial t}(\rho U_i) + \frac{\partial}{\partial x_j}(\rho U_j U_i) = -\frac{\partial P}{\partial x_i} + \frac{\partial}{\partial x_j}\left(\mu \frac{\partial U_i}{\partial x_j}\right). \tag{12.10.2}$$

We would like to cast these equations such that the effect of small eddies are masked out. This can be done by "filtering" the equation, in order to filter out fluctuations with high frequencies (short wavelengths, small eddies), but leave large fluctuations (large eddies).

Filtering can be performed on a function $\phi(\vec{x})$ according to

$$\overline{\phi}(\vec{x}) = \int_{\psi} G(\vec{x}, \vec{x}')\phi(\vec{x}')\, dx', \tag{12.10.3}$$

where ψ represents the entire flow domain and $G(\vec{x}, \vec{x}')$ is the filter kernel (filter function). The function $G(\vec{x}, \vec{x}')$ must be a localized function that depends on $\vec{x} - \vec{x}'$ and becomes very large only when x and x' are close to each other. The simplest and most widely used method, very convenient for finite-difference and finite-volume methods, is to use volume averaging based on the volume of a computational cell, whereby

$$G(\vec{x}, \vec{x}') = \begin{cases} 1/V & \text{for } \vec{x}' \text{ representing a point in V} \\ 0 & \text{for } \vec{x}' \text{ representing a point outside V} \end{cases}. \tag{12.10.4}$$

This essentially filters out eddies smaller in size than $\sim V^{1/3}$. The filtered equations are now

$$\frac{\partial \rho}{\partial t} + \frac{\partial}{\partial x_i}\left(\rho \overline{U}_i\right) = 0, \tag{12.10.5}$$

$$\frac{\partial}{\partial t}\left(\rho \overline{U}_i\right) + \frac{\partial}{\partial x_j}\left(\overline{U}_j \overline{U}_i\right) = -\frac{\partial \overline{P}}{\partial x_i} + \frac{\partial}{\partial x_j}\left(\mu \frac{\partial \overline{U}_i}{\partial x_j}\right) - \frac{\partial}{\partial x_j}(\rho \overline{U_i U}_j - \rho \overline{U}_i \overline{U}_j). \tag{12.10.6}$$

We can introduce the definition

$$\tau_{ij} = \overline{U_i U}_j - \overline{U}_i \overline{U}_j. \tag{12.10.7}$$

The momentum equation then becomes

$$\frac{\partial}{\partial t}\left(\rho \overline{U}_i\right) + \frac{\partial}{\partial x_j}\left(\overline{U}_j \overline{U}_i\right) = -\frac{\partial \overline{P}}{\partial x_i} + \frac{\partial}{\partial x_j}\left(\mu \frac{\partial \overline{U}_i}{\partial x_j}\right) - \frac{\partial \tau_{ij}}{\partial x_j}. \tag{12.10.8}$$

In this equation τ_{ij} appears to play a similar role to Reynolds stress and needs to be modeled [subgrid scale (SGS) modeling]. However, it represents a much different physics than the Reynolds stress. Here τ_{ij} is associated with the turbulent energy contained in small eddies. This energy, as noted earlier, is small compared with the total turbulent energy. The accuracy of its model is not as crucial as the Reynolds stress in RANS models.

Subgrid Scale Modeling

The most commonly applied SGS model is due to Smagorinsky (1963), according to which

$$\tau_{ij} - \frac{1}{3}\tau_{kk}\delta_{ij} = -\rho \nu_T \left(\frac{\partial \overline{U}_i}{\partial x_j} + \frac{\partial \overline{U}_j}{\partial x_i}\right) = -2\rho \nu_T \overline{S}_{ij}, \tag{12.10.9}$$

where

$$\mu_T = \rho \nu_T = \text{SGS turbulence (eddy) viscosity}, \tag{12.10.10}$$

$$\overline{S}_{ij} = \text{resolved scale rate-of-strain tensor}. \tag{12.10.11}$$

The form of SGS eddy viscosity can be derived by dimensional analysis to be (Ferziger and Peric, 1996),

$$\mu_T \approx V^{2/3} |\overline{S}|.$$

A widely used form is

$$\mu_T = \rho \left(C_{s0} V^{1/3}\right)^2 \left|\overline{S}\right|, \tag{12.10.12}$$

$$\left|\overline{S}\right| = \sqrt{2\overline{S}_{ij}\overline{S}_{ij}}, \tag{12.10.13}$$

$$C_{s0} \approx 0.1\text{–}0.2. \tag{12.10.14}$$

In practice, the parameter C_{s0} is not a constant. A recommended value away from any wall is 0.1, but it needs to be reduced near a wall to account for the damping of the eddies that is caused by the wall.

Near-Wall Boundary Conditions

The SGS eddy viscosity should be reduced near a wall to account for the damping of the eddies that is caused by the wall, as just mentioned. Some commonly applied methods are as follows.

The van Driest-type damping, in accordance with the eddy diffusivity model of van Driest (see Section 6.6), results in

$$C_s = C_{s0}[1 - \exp(-y^+/A^+)]. \tag{12.10.15}$$

According to some CFD codes (Fluent, Inc., 2006; CD-ADAPCO, 2008),

$$\mu_T = \rho L_s^2 \left|\overline{S}\right|, \tag{12.10.16}$$

where κ is von Karman's constant. The length scale L_s can be found from

$$L_s = \min([1 - \exp(-y^+/A^+)]\kappa y,\ C_s V^{1/3}). \tag{12.10.17}$$

Finally, wall functions can be used, whereby

$$\frac{\overline{U}}{U_\tau} = y^+ \quad \text{for } y^+ < 10, \tag{12.10.18}$$

$$\frac{\overline{U}}{U_\tau} = \frac{1}{\kappa}\ln\left(\boldsymbol{E}y^+\right),\ \boldsymbol{E} = 9.79 \quad \text{for } y^+ > 10. \tag{12.10.19}$$

In LES analysis the velocity inlet conditions for the simulated system must account for the stochastic component of the flow at that location. We can do this by writing, at the inlet,

$$\overline{U}_i = \langle \overline{U}_i \rangle + C\,\psi\,|\left\langle \overline{U}_i \right\rangle|, \tag{12.10.20}$$

where C is the fluctuation intensity and ψ is the Gaussain random number with zero average and a variance of 1.0.

Transport of Scalar Parameters

When heat or mass transfer is also solved for, the number of the required mesh points will depends on Pr (for heat transfer) and Sc (for mass transfer). According to Dong et al. (2002),

$$N \approx \mathrm{Pr}^3\mathrm{Re}^{9/4} \text{ (for heat transfer)}, \tag{12.10.21}$$

$$N \approx \mathrm{Sc}^3\mathrm{Re}^{9/4} \text{ (for mass transfer)}. \tag{12.10.22}$$

The filtered thermal energy and mass species conservation equations, neglecting dissipation and assuming constant properties, and mass-species conservation equation, assuming that Fick's law applies, are:

$$\rho C_P\left[\frac{\partial}{\partial t}(\overline{T}) + \frac{\partial}{\partial x_j}(\overline{U}_j\overline{T})\right] = k\frac{\partial^2\overline{T}}{\partial x_j\partial x_j} - \frac{\partial q_j}{\partial x_j}, \tag{12.10.23}$$

$$\rho\left[\frac{\partial}{\partial t}(\overline{m}_1)+\frac{\partial}{\partial x_j}(\overline{U}_j\overline{m}_1)\right]=\mathcal{D}_{12}\frac{\partial^2\overline{m}_1}{\partial x_j\partial x_j}-\frac{\partial j_j}{\partial x_j}, \tag{12.10.24}$$

where m_1 is the mass fraction of the transferred species and $\mathcal{D}_{12}$ is the mass diffusivity of species 1 with respect to the mixture. The SGS fluxes can be modeled as

$$q_j=\rho C_P\left(\overline{U_jT}-\overline{U}_j\overline{T}\right)=-\rho C_P\frac{\nu_T}{\mathrm{Pr}_{\mathrm{SGS}}}\frac{\partial\overline{T}}{\partial x_j}, \tag{12.10.25}$$

$$J_j=\rho\left(\overline{U_jm_1}-\overline{U}_j\overline{m}_1\right)=-\rho\frac{\nu_T}{\mathrm{Sc}_{\mathrm{SGS}}}\frac{\partial\overline{m}_1}{\partial x_j}, \tag{12.10.26}$$

where $\mathrm{Pr}_{\mathrm{SGS}}$ is the SGS Prandtl number [≈ 0.6 (Métais and Lesieur, 1992)] and $\mathrm{Sc}_{\mathrm{SGS}}$ is the SGS Schmidt number.

12.11 Computational Fluid Dynamics

The turbulence models discussed in the previous sections are obviously useful only in numerical simulations in which flow conservation equations, along with the relevant turbulence transport equations, are numerically solved. Such numerical simulations are performed with CFD tools.

CFD refers to the field of thermal-fluid science in which the Navier–Stokes equations, the energy conservation equation, and sometimes along with the transport equations for mass species and particles, are discretized in time and space and numerically solved. These numerical solutions are performed with minimal simplifications to the transport equations or their closure relations and are therefore often computationally intensive. Because conservation and transport equations and closure relations are applied without system-specific assumptions, CFD methods can address complex flow configurations, with results that are often reasonably accurate in comparison with experimental data. The computational solution of flow equations has been the subject of intense study for several decades, resulting in the development of powerful and robust numerical algorithms for the numerical solution of flow conservation equations. Until about a decade and a half ago, CFD methods were tools of research because of their complexity and high computational cost. The rapid growth of computational power, the development of turbulence models, the evolution of powerful numerical algorithms, and the introduction of easy-to-use academic and commercial software have now turned CFD methods into tools for common engineering design and analysis. Powerful commercial CFD packages are now widely available (Fluent, Inc., 2006; CD-ADAPCO, 2008).

CFD modeling typically includes three phases. In the *preprocessing* phase the following tasks are performed:

1. Definition of geometry and physical bounds (computational domain): The computational domain is the region where the flow and transport phenomena are modeled. The defined domain evidently has inlet(s), and outlet(s) and boundaries. These could be inlets, outlets, and boundaries in a physical sense or they could be imaginary boundaries.
2. Discrete representation of the computational domain: The computational domain is divided into smaller units by defining a mesh or grid. The

discretization method of course depends on the numerical-solution method (finite difference, finite volume, finite element, etc.). The finite-volume method appears to be the most popular numerical method applied in CFD codes. In the finite-volume method, as the name suggests, the computational domain is discretized into small volumes. The conservation principles are applied to each volume (i.e., each discretized volume is treated as a control volume) in which the transport processes through the surfaces surrounding the small volumes (control surfaces). Algorithms and software for developing structured and nonstructured mesh are available (Thompson et al., 1999; Gambit, Fluent, Inc., 2006).

3. Physical and numerical modeling: Details of what needs to be solved for and the details of numerical solution techniques are specified. The selection of an appropriate turbulence model, for example, is done.

In the *simulation* phase, the discretized conservation and transport equations are numerically solved in the computational domain. Finally, in the *postprocessing* phase, the numerical-simulation results are processed, plotted, and interpreted.

Numerous books and monographs on CFD and related issues are available. Among them are the books by Roache (1998) and Blazek (2005), which are useful discussions of the basics of CFD. The book *Numerical Recipes* (Press et al., 1992, 1997) describes a multitude of algorithms and subroutines, in FORTRAN 77 and C, for their implementation. A recent book by Durbin and Medic (2007) is a useful and brief description of the computational aspects of fluid dynamics.

Some of the forthcoming problems of this chapter are to be solved with a CFD tool that you may have available and by applying a grid generation tool of your own choice.

PROBLEMS

Problem 2.1. Cast Eqs. (12.4.20) and (12.4.21) for an axisymmetric, incompressible flow in a pipe.

Problem 2.2. Cast Eqs. (12.6.8)–(12.6.11) for a 2D (x, y) boundary layer, with u and v as the velocity components in the x and y directions, respectively.

Problem 12.3 Cast Eqs. (12.6.8) and (12.6.11) for an axisymmetric, incompressible flow in a pipe.

Problem 12.4 Prove Eqs. (12.6.18)–(12.6.20) for a 2D (x, y) boundary layer.

Problem 12.5 Consider the entrance-region, steady-state, and laminar flow of an incompressible liquid ($\rho = 1000\,\text{kg/m}^3$, $\mu = 10^{-3}\,\text{Pa s}$) into a smooth pipe that is 1 mm in diameter. Using a CFD tool of your choice, solve the flow field for $\text{Re}_D = 100$ and $\text{Re}_D = 2000$, and calculate and plot $C_{f,\text{app},x}Re_D$ as a function of x^*. Compare your calculation results with the predictions of the correlation of Shah and London (1978), Eq. (4.2.13).

Problem 12.6 Consider the entrance-region, steady-state, and laminar flow of an incompressible liquid ($\rho = 1000\,\text{kg/m}^3$, $\mu = 10^{-3}\,\text{Pa s}$) into a smooth square duct with 2-mm hydraulic diameter. For $\text{Re}_{D_H} = 200$ and $\text{Re}_{D_H} = 2000$, solve the flow field using a CFD tool of your own choice, over lengths of 42 mm and 42 cm, respectively. Calculate and plot $C_{f,\text{app},x}\text{Re}_{D_H}$ as a function of x^* and compare the

results with the tabulated results of Shah and London (1978) and Muzychka and Yovanovich (2004), Eq. (4.2.17). (*Note*: For tabulated results of Shah and London, 1978, you can use the table in Problem 4.26).

Problem 12.8 Using a CFD tool of your choice, solve Problem 4.27 and compare your results with the solution obtained with the solution to Graetz's problem (Subsection 4.5.1).

Problem 12.9 Using a CFD tool of your choice, solve Problem 4.28 and compare your results with the solution obtained with the solution to the extended Graetz's problem (Subsection 4.5.3).

Problem 12.10 Using a CFD tool of your choice, solve Problem 7.13, this time using the standard K–ε model and another turbulence model of your choice.

Problem 12.11 Using a CFD tool of your choice, solve Problem 7.14, this time using the standard K–ε model and another turbulence model of your choice.

Problem 12.12 Starting from the conservation equations for an incompressible, constant-property fluid, derive Eqs. (12.9.2)–(12.9.4).

Problem 12.13 Repeat Problem 12.12, this time defining the dimensionless temperature as

$$\theta = \frac{(\langle \overline{T}_s \rangle - T)}{q_s''/(\rho C_P U_\tau)}.$$

Problem 12.14 Derive Eqs. (12.9.18)–(12.9.21).

Problem 12.15 Using a CFD tool of your choice, numerically solve Problem 7.9. Plot the temperature contous in the flow field in the bottom one-half meter of the flow channel. Repeat the calculations, this time assuming that the mass flow rate is reduced by a factor of five.

13 Flow and Heat Transfer in Miniature Flow Passages

Miniature flow passages, defined here as passages with hydraulic diameters smaller than about 1 mm, have numerous applications. Some current applications include monolith chemical reactors, inkjet print-heads, bioengineering and biochemistry (lab-on-the-chip; drug delivery with ultrathin needles, etc.), microflow devices (micropumps, micro heat exchangers, etc.), and cooling systems for microelectronic and high-power magnets, to name a few. Miniature flow passages are an essential part of *microfluidic devices*, in which can be broadly defined as devices in which minute quantities of fluid are applied. Cooling systems based on microchannels can provide very large volumetric heat disposal rates that are unfeasible with virtually any other cooling technology. Their widespread future applications may in fact revolutionize some branches of medicine and industry.

The serious study of flow in capillaries (tubes with $D \approx 1\,\text{mm}$) goes back to at least the 1960s. The application of microchannels for cooling of high-power systems is relatively new, however (Tuckerman and Pease, 1981). The literature dealing with flow in microtubes is extensive. Useful reviews include those of Papautsky et al. (2001), Morini (2004), Krishnamoorthy et al. (2007), and Fan and Luo (2008). The field of flow in miniature channels, in particular with respect to very small channels (microfluidics and nanofluidics) is a rapidly developing one. In this chapter we review the flow regimes and size-based miniature flow passage categories, and we discuss the limitations of the classical convection heat and mass transfer theory with respect to its application to miniature flow passages.

13.1 Size Classification of Miniature Flow Passages

Miniature channels cover a wide range of sizes and can be as small as a few micrometers in hydraulic diameter. Some classification of the size ranges is evidently needed.

There is no universally agreed-on size-classification convention. The following is a popular size classification.

For flow channels,

$$D_H = 10\text{–}100\,\mu\text{m, microchannels,}$$
$$D_H = 100\,\mu\text{m–}1\text{ mm, minichannels,}$$
$$D_H = 1\text{–}3\text{ mm, macrochannels,}$$
$$D_H > 6\text{ mm, conventional channels.}$$

For heat exchangers,

$$D_H = 1\text{–}100\ \mu\text{m},\ \text{micro heat exchangers},$$
$$D_H = 100\ \mu\text{m–}1\ \text{mm},\ \text{meso heat exchangers},$$
$$D_H = 1\text{–}6\ \text{mm},\ \text{compact heat exchangers},$$
$$D_H > 6\ \text{mm},\ \text{conventional heat exchangers}.$$

This size classification is far from perfect because it does not consider the fluid properties. The microchannel size range and the micro heat exchanger size range both include flow passages in which significant velocity slip and temperature jump may occur.

The classical convection theory is based on modeling the fluids as continua throughout the flow field. Because fluids are made of molecules, the applicability of the continuum-based treatment of fluids is the most obvious issue with respect to the classification of miniature flow passages. The complete or partial breakdown of the continuum behavior of fluids is thus a very important size threshold.

In an internal flow field, the fluid molecules collide with other molecules as well as with the walls. Furthermore, at any time instant on average there is a finite distance between adjacent molecules. The behavior of the fluid depends strongly on the relative significance of molecule–molecule interactions as opposed to molecule–wall interactions.

A fluid can be treated as continuum with thermophysical properties that are intrinsic to the fluid when the following two conditions are satisfied:

1. There are sufficient molecules present to make the assumption of molecular chaos and therefore the definition of equilibrium properties meaningful, and
2. the molecule–molecule interactions are much more frequent than molecule–wall interactions such that the behavior of the molecules is dictated by random, intermolecular collisions or interactions.

Molecular chaos requires the presence of at least $\sim$100 molecules when the smallest dimension of a device is crossed. As a result, condition 1 is typically met even in very small vessels, when gases at moderate pressures are encountered. When the breakdown of molecular chaos is not an issue, as the flow passage size is reduced, complications with respect to the application of conventional convection theory occur when the molecular mean free path (in cases in which the fluid is a gas) or the intermolecular distance (in the case of liquids) becomes significant in comparison with the characteristic dimension of the flow passage. With further reduction of the flow passage size, partial breakdown of the continuum-based behavior occurs when the frequency of molecule–wall interactions becomes significant compared with random intermolecular interactions. A complete breakdown of the continuum-based behavior is encountered when the molecule–wall interactions predominate over intermolecular collisions.

An unambiguous and rather precise specification of the aforementioned thresholds is relatively easy for gases. The kinetic theory of gases, according to which gas molecules are in continuous motion and undergo random collisions with other molecules as well as with vessel walls, provides good estimates of what is needed for the determination of the regime thresholds. The important length scale for gases is

the mean free path of molecules. The comparison between this length scale and the smallest feature of the flow passage determines whether continuum-based methods can be applied.

For liquids there is no reliable molecular theory, and the specification of the regime transition thresholds is not straightforward. Liquid molecules are in a continuous state of collision with their neighbors, and for them the intermolecular distance is the length scale that determines the applicability of the continuum-based models to a specific system. However, the breakdown of continuum is hardly an issue for liquids for the vast majority of applications, given that the intermolecular distances in liquids are extremely short (about 10^{-6} mm.) Useful discussions of microscale liquid flow can be found in Gad-el-Hak (1999, 2006). However, for liquids, what renders many microchannel flows different from large channels with respect to the applicability of classical theory is the predominance of liquid–surface forces (e.g., electrokinetic forces) in the former. These forces are often negligible in large channels, but can become significant in microfluidics because of their very large surface-area-to-volume ratios. Even when these forces become predominant, however, the classical continuum-based fluid mechanics theory is to be applied, only with modifications to include the effect of the latter forces. Useful discussions about these forces can be found in Probstein (2003) and Li (2004).

13.2 Regimes in Gas-Carrying Vessels

The molecular mean free path (MMFP) is defined as the average distance a molecule moves before it collides with another molecule. Clearly the MMFP is meaningful when the gas behaves as a continuum.

As mentioned earlier in Section 1.5, the simple gas-kinetic theory (GKT) models the gas molecules as rigid and elastic spheres (no internal degree of freedom) that influence one another only when they approach each other to within distances much smaller than their typical separation distances. Each molecule has a very small sphere of influence, and the motion of a molecule follows the laws of classical mechanics when the molecule is outside the sphere of influence of other molecules. Equations (1.5.9) or (1.5.10) show the prediction of the GKT for MMFP. The Knudsen number, which compares the MMFP with the characteristic length scale of the flow field, is defined in Eq. (1.6.1).

Figure 13.1 depicts the various regimes in a gas-containing vessel (Bird, 1994, Gad-el-Hak, 1999, 2003). These regimes depend on the ratio between the characteristic dimension of the vessel (characteristic dimension of the cross section, in case a flow is under way) l_c and two important length scales associated with the gas molecules: the molecular mean free path, λ_{mol}, and the average intermolecular distance, δ. The general coordinates are thus l_c/σ and δ/σ. For the purpose of clarity, however, the figure also depicts numerical values for air on the bottom and left-hand coordinates, where the subscript zero represent atmospheric air at 288 K, ρ represents the density, and n represents the number density of molecules. For air, $\sigma \approx 4 \times 10^{-10}$ m.

Referring to Fig. 13.1, in Region IV, we deal with *dense gas*. This term refers to high-density gas in which the assumption that molecules feel each other's presence only during a collision is no longer accurate. Furthermore, it is not appropriate to

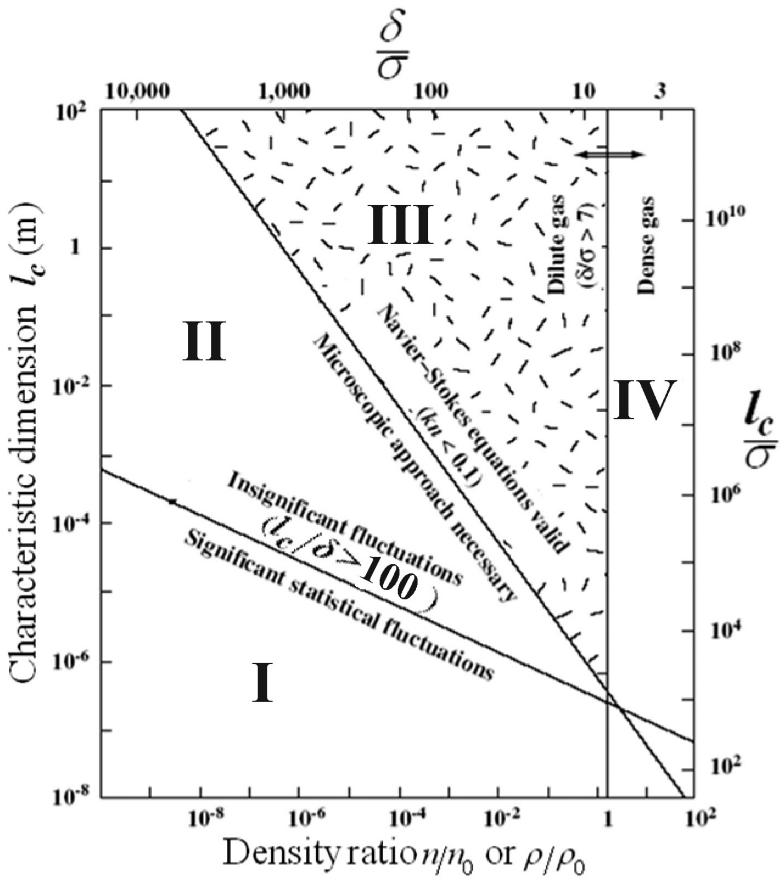

Figure 13.1. Effective limits of fluid behavior (after Bird, 1994; Gad-el-Hak, 2003).

assume that intermolecular collisions are overwhelmingly binary because ternary collisions are now significant in their frequency of occurrence. As a result, the ideal-gas law as well as the simple GKT will no longer be accurate in this regime.

In Region I, where the depth of the flow field is less than about 100 molecules, the continuum approximation fails because there are not sufficient molecules to make averaging of properties meaningful, and as a result fluctuations associated with the nonuniform distribution of molecular kinetic energy cannot be smoothed by averaging.

In Region II, the continuum approximation is invalid, even though the condition $l_c/\sigma \gg 100$ may hold, because $\mathrm{Kn}_{l_c} > 0.1$. The latter condition implies that for a typical molecule the frequency of molecule–wall interactions is at least comparable with the frequency of molecule–molecule interactions.

In Region III both continuum and quasi-equilibrium apply, and the classical continuum-based fluid mechanics and convection heat transfer analytical methods can be applied.

This region itself can be divided into two parts. For $\mathrm{Kn}_{l_c} \lesssim 0.001$, there is no need to be concerned with the partial breakdown of equilibrium right next to the wall. In the $0.001 \lesssim \mathrm{Kn}_{l_c} \lesssim 0.1$ range, however, the particulate nature of the fluid should be considered for modeling the wall–fluid interactions.

Table 1.2 displays the mean free path for dry air at several pressures and two temperatures. Clearly, when gas flow in moderate pressures and temperatures is of interest (for example, air at pressures higher than about 0.1 bar), flow passages with hydraulic diameters of about 50 μm or larger can be analyzed exactly the same way as larger flow passages are analyzed.

In light of the preceding discussion, we can define the following regimes for a gas-carrying flow passage and summarize their characteristics as follows:

- Continuum: $\mathrm{Kn}_{l_c} \lesssim 10^{-3}$. Intermolecular collisions determine the behavior of the gas, continuum models are valid, and Navier–Stokes equations with no-slip and temperature equilibrium conditions at the gas–solid interface apply.
- Temperature and velocity jump (the slip flow regime): $10^{-3} \lesssim \mathrm{Kn}_{l_c} \lesssim 10^{-1}$. Intermolecular collisions still predominate the behavior of the fluid bulk, Navier–Stokes equations apply, and corrections to near-wall phenomena are needed.
- Transition: $10^{-1} \lesssim \mathrm{Kn}_{l_c} \lesssim 10$. Intermolecular and molecule–wall interactions are both important, and Navier–Stokes equations do not apply.
- Free molecular flow: $\mathrm{Kn}_{l_c} \lesssim 10$. Molecules move ballistically and intermolecular collisions are insignificant.

We can also make the following observations on flow regimes:

1. Excluding low-pressure situations (i.e., rarefied gases), continuum methods are fine for gas-carrying microchannels with diameters larger than about 50 μm.
2. Predictive methods are available for slip flow and even free-molecular-flow regimes. Analytical models are available for regular and well-defined geometries (e.g., pipe flow and flow between two parallel plates) when rarefaction is important but the compressibility effect is insignificant.
3. Numerical methods [e.g., the direct simulation Monte Carlo (DSMC method)] can be used for complex geometries in the slip flow regime.

For flow situations, the Knudsen number can be cast in another useful form. For spherical molecules, the Chapman–Enskog approximate solution for the Boltzmann equation (see the discussion in Subsection 1.5.2) gives (Eckert and Drake, 1959)

$$\nu = 0.499\lambda_{\mathrm{mol}} \langle U_{\mathrm{mol}} \rangle, \tag{13.2.1}$$

where the mean molecular speed $\langle U_{\mathrm{mol}} \rangle$ can be found from Eq. (1.5.6):

$$\langle U_{\mathrm{mol}} \rangle = \sqrt{\frac{8\kappa_B T}{\pi m_{\mathrm{mol}}}} = \sqrt{\frac{8R_u T}{\pi M}}, \tag{13.2.2}$$

where m_{mol} is the mass of a single molecule. Furthermore,

$$Ma = \frac{U_m}{a} = \frac{U_m}{\sqrt{\gamma \dfrac{R_u}{M} T}} \tag{13.2.3}$$

where $\gamma = C_P/C_v$, U_m is the average (macroscopic) gas speed, a is the speed of sound, and M is the gas molar mass. Combining these equations, we can show that

$$\mathrm{Kn}_{l_c} = \sqrt{\frac{\pi\gamma}{2}}\frac{Ma}{\mathrm{Re}_{l_c}}, \tag{13.2.4}$$

where

$$\mathrm{Re}_{l_c} = U_m l_c/\nu. \tag{13.2.5}$$

Another important and useful point is that, for an isothermal ideal gas,

$$P\,\mathrm{Kn}_{l_c} = \frac{1}{l_c}P\nu\left(\frac{\pi M}{2R_uT}\right)^{1/2} = \frac{1}{l_c}\mu\left(\frac{\pi R_uT}{2M}\right)^{1/2} = \text{const.} \tag{13.2.6}$$

We can derive this expression by using the ideal-gas law and noting that, for gases, the dynamic viscosity is, to a good approximation, only a function of temperature.

13.3 The Slip Flow and Temperature-Jump Regime

This regime is encountered in gas-carrying microchannels or larger channels subject to the flow of a rarefied gas. It is also encountered in external flow of a mildly rarefied gas past objects and is thus common for reentry space vehicles. However, we are primarily interested in the former application, namely, the flow in microflow passages.

Among the issues that distinguish the microflow passages that operate in the slip flow regime from commonly applied large channels, the following three are particularly important:

1. The role of viscous forces: These forces are often significant in microchannels because of their large surface-to-volume ratios.
2. Compressibility: Density variations along a microchanel can be quite significant. Pressure and temperature variations both contribute to the changing density; however, in adiabatic or moderately heated channel flows the role of pressure variations is more important.
3. Axial heat conduction in the fluid: It is common practice to neglect the axial conduction for fluid flows in large channels. This is justified when $\mathrm{Pe}_{D_H} \gtrsim 100$. This limit is not always met in microchannel applications, however. The neglect of axial heat conduction in the fluid can then lead to significant errors in and misinterpretation of experimental data.

The common practice in modeling conventional flow systems is to assume no-slip, as well as thermal equilibrium conditions at a solid–fluid interface. This is not strictly correct, however. Because of the molecular nature of the gas, in a gas-carrying flow path there is nonequilibrium between the gas and wall. This nonequilibrium is typically negligible compared with the temperature and velocity variations in conventional flow systems. However, the nonequilibrium can be significant in rarefied-gas flows, and in microchannels operating in the slip flow regime. However, the boundary conditions for the continuum-based equations for these microchannels need to be modified.

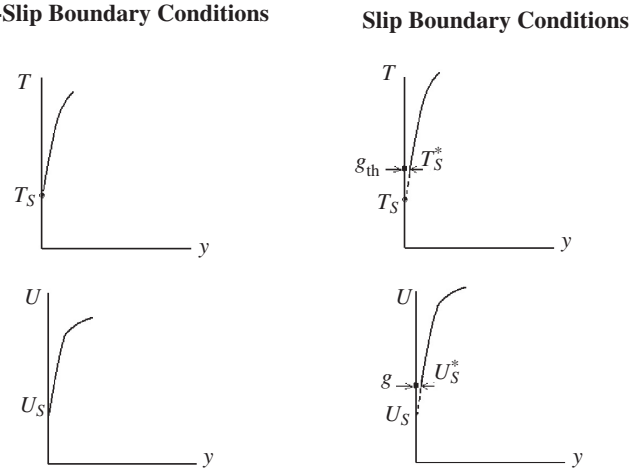

Figure 13.2. The velocity and temperature boundary conditions at a gas–solid interface.

Figure 13.2 displays the velocity and temperature conditions at a gas–solid interface. The solid surface is assumed to be at temperature T_s and to move in the tangential direction with velocity U_s. These are used as boundary conditions when slip and thermal nonequilibrium are neglected, as shown in the two plots on the left of Fig. 13.2. However, the correct boundary conditions should be as follows: At a distance g from the wall we have $T = T_s^*$ and $U = U_s^*$. According to the GKT (Deissler, 1964; Schaaf and Chambré, 1961),

$$g_{\text{th}} \approx \frac{2-\alpha_{\text{th}}}{\alpha_{\text{th}}}\frac{2\gamma}{\gamma+1}\frac{\lambda_{\text{mol}}}{\text{Pr}}, \tag{13.3.1}$$

$$g \approx \frac{2-\alpha}{\alpha}\lambda_{\text{mol}}, \tag{13.3.2}$$

$$\begin{aligned} U_s^* - U_s = {} & \frac{2-\alpha}{\alpha}\lambda_{\text{mol}}\left(\frac{\partial u}{\partial y}\right)_{y=0} + \frac{3}{4}\frac{\mu}{\rho T_s}\left(\frac{\partial T}{\partial x}\right)_{y=0} \\ & - C_1\lambda_{\text{mol}}^2\left[\left(\frac{\partial^2 u}{\partial y^2}\right) + \frac{1}{2}\left(\frac{\partial^2 u}{\partial x^2}\right) + \frac{1}{2}\left(\frac{\partial^2 u}{\partial z^2}\right)\right]_{y=0}, \end{aligned} \tag{13.3.3}$$

$$\begin{aligned} T_s^* - T_s = {} & \frac{2-\alpha_{\text{th}}}{\alpha_{\text{th}}}\left(\frac{2\gamma}{\gamma+1}\right)\frac{\lambda_{\text{mol}}}{\text{Pr}}\left(\frac{\partial T}{\partial y}\right)_{y=0} \\ & - C_2\lambda_{\text{mol}}^2\left[\left(\frac{\partial^2 T}{\partial y^2}\right) + \frac{1}{2}\left(\frac{\partial^2 T}{\partial x^2}\right) + \frac{1}{2}\left(\frac{\partial^2 T}{\partial z^2}\right)\right]_{y=0}, \end{aligned} \tag{13.3.4}$$

where y is the normal distance from the wall, α represents the tangential momentum accommodation coefficient (also referred to as the specular reflection coefficient), α_{th} is the thermal (energy) accommodation coefficient, and

$$C_1 = 9/8,$$

$$C_2 = \frac{9}{128}\frac{177\gamma - 145}{\gamma+1}.$$

Table 13.1. *Momentum accommodation coefficients: (A) common gases and surfaces (Springer, 1971); (B) gases with a silica surface (Ewart et al., 2007)*

Gas	Surface	α
(A)		
Air	Machined brass	1.0
Air	Oil	0.9
Air	Glass	0.9
N_2	Glass	0.95
CO_2	Machined brass	1.00
CO_2	Oil	0.92
H_2	Oil	0.93
He	Oil	0.87
(B)		
Nitrogen		0.908 ± 0.041
Argon		0.871 ± 0.017
Helium		0.914 ± 0.009

In Eq. (13.3.3), the second term on the right-hand side is referred to as the thermal creep. The second-order terms in the preceding equations are typically small in moderately rarefied-gas conditions and are often neglected, leaving

$$U_s^* - U_s = \frac{2-\alpha}{\alpha}\lambda_{\text{mol}}\left(\frac{\partial u}{\partial y}\right)_{y=0} + \frac{3}{4}\frac{\nu}{T_s}\left(\frac{\partial T}{\partial s}\right)_{G,y=0},$$

$$= \frac{2-\alpha}{\alpha}\lambda_{\text{mol}}\left(\frac{\partial u}{\partial y}\right)_{y=0} + 3\left(\frac{R_u T}{8\pi}\right)^{1/2}\frac{\lambda_{\text{mol}}}{T}\left(\frac{\partial T}{\partial s}\right)_{y=0}, \tag{13.3.5}$$

$$T_s^* - T_s = \frac{2-\alpha_{\text{th}}}{\alpha_{\text{th}}}\left(\frac{2\gamma}{\gamma+1}\right)\frac{\lambda_{\text{mol}}}{\text{Pr}}\left(\frac{\partial T}{\partial y}\right)_{y=0}, \tag{13.3.6}$$

where s represents the fluid motion path, and $\left(\frac{\partial T}{\partial s}\right)_{G,y=0}$ is the tangential gas temperature gradient adjacent to the wall.

The accommodation coefficients are defined as follows:

$$\alpha = \frac{\Omega_{\text{refl}} - \Omega_{\text{in}}}{\Omega_s - \Omega_{\text{in}}}, \tag{13.3.7}$$

$$\alpha_{\text{th}} = \frac{E_{\text{refl}} - E_{\text{in}}}{E_s - E_{\text{in}}}, \tag{13.3.8}$$

where Ω and E represent the momentum and energy fluxes associated with the gas molecules, the subscript in stands for incident, refl represents reflected, and the subscript s represents reflected if gas molecules reach equilibrium (i.e., thermal equilibrium and equilibrium with respect to velocity) with the flow passage wall.

Tables 13.1 and 13.2 show the momentum and thermal accommodation coefficients for several gas–solid combinations. As noted, the accommodation coefficients for many gas–solid pairs are close to one. For air, it is often assumed that $\alpha = \alpha_{\text{th}} \approx 1$.

Table 13.2. *Thermal accommodation coefficients for some gas–solid surface combinations*[a]

Gas	Solid surface	Pressure (mm Hg)	Temperature (K)	Thermal accommodation coefficient
Argon	Aluminum	0.010	295	0.832
		0.200	418	0.870
			483	0.950
	Copper	0.002	77	0.990
		1.0×10^{-6}	673	0.690
	Glass	0.001	286	0.920
			384	0.856
CO_2	Glass	–	81	0.975
		–	194	0.945
		760	300	0.450
			500	0.150
			700	0.050
	Gold	0.002	318	0.350
	Nickel	–	152	0.991
		–	279	0.933
Helium	Aluminum	0.02	418	0.073
			483	0.074
	Copper	0.004	77	0.564
			243	0.407
	Glass	0.04	70	0.383
		0.001	341	0.365
	Graphite	0.015	773	0.150
	Nickel	0.3	323	0.385
Hydrogen	Glass	0.04	70	0.800
		–	273	0.358
	Graphite	0.015–0.12	77	0.820
			195	0.380
			273	0.350
	Iron	0.025	120	0.550
			260	0.350
			450	0.310
Neon	Aluminum	0.02	418	0.159
			483	0.163
	Beryllium	0.05–0.1	305	0.090
	Glass	0.04–0.18	70	0.555
		0.0001–0.001	286	0.685
			384	0.650
Nitrogen	Copper	0.004	77	0.799
			243	0.760
	Glass	0.04–0.18	273	0.855
		0.0001–0.001	286	0.825
			384	0.753
	Gold	0.0001	850	0.400

[a] Data extracted from Saxena and Joshi (1989).

Song and Yovanovich (1987) proposed the following empirical correlation for the thermal accommodation coefficient for metallic surfaces for the temperature range 273–1250 K (Demirel and Saxena, 1996):

$$\alpha_{\text{th}} = F\left(\frac{M_G}{6.8 + M_G}\right) + (1 - F)\,\frac{2.4\xi}{(1+\xi)^2}, \tag{13.3.9}$$

where

$$\xi = M_G/M_{\text{solid}}, \tag{13.3.10}$$

$$F = \exp\left[-0.57\frac{T_s - 273}{273}\right]. \tag{13.3.11}$$

The temperatures everywhere in these expressions are in Kelvins.

In imposing the boundary conditions depicted in Fig. 13.2, noting that typically $g/l_c \ll 1$ and $g_{\text{th}}/l_c \ll 1$ in the slip flow regime, the boundary conditions that are often imposed on the flow are

$$U = U_s^* \quad \text{at } y = 0, \tag{13.3.12}$$

$$T = T_s^* \quad \text{at } y = 0. \tag{13.3.13}$$

We can shorten the algebra in analytical treatments by making the following two convenient definitions:

$$\beta_v = \frac{2 - \alpha}{\alpha}, \tag{13.3.14}$$

$$\beta_T = \frac{2 - \alpha_{\text{th}}}{\alpha_{\text{th}}}\left(\frac{2\gamma}{\gamma + 1}\right)\frac{1}{\text{Pr}}. \tag{13.3.15}$$

The boundary conditions represented by Eqs. (13.3.5) and (13.3.6) can then be recast as

$$U_s^* - U_s = \beta_v \lambda_{\text{mol}}\left(\frac{\partial u}{\partial y}\right)_s + 3\left(\frac{R_u T}{8\pi}\right)^{1/2}\frac{\lambda_{\text{mol}}}{T}\left(\frac{\partial T}{\partial s}\right)_s, \tag{13.3.16}$$

$$T_s^* - T_s = \beta_T \lambda_{\text{mol}}\left(\frac{\partial T}{\partial y}\right)_s. \tag{13.3.17}$$

The slip flow regime in small channels is virtually always laminar. As a result, analytical solutions are possible for many geometric configurations and wall boundary conditions. Some important solutions are now reviewed.

13.4 Slip Couette Flow

The Couette flow model for flow without velocity slip and temperature jump was discussed in Section 4.1. In general, when $Ma\,\text{Kn}_{l_c} \ll 1$ for internal flow, all streamwise derivatives are negligible with the exception of the pressure gradient (Zohar, 2006). Thus, with the exception of the boundary conditions, all the assumptions and arguments in Section 4.1 apply when $Ma\,\text{Kn}_{l_c} \ll 1$. For convenience, let us use the

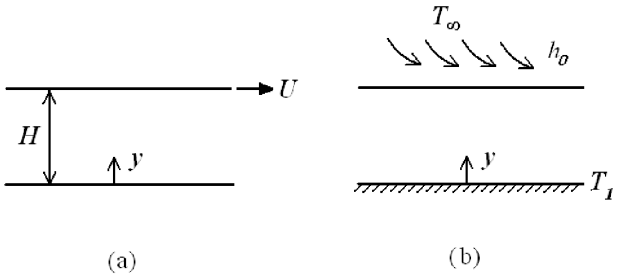

Figure 13.3. Definitions for slip Couette flow: (a) hydrodynamics, (b) heat transfer.

definitions in Fig. 13.3(a). Equations (4.1.4) and (4.1.5), along with the following boundary conditions, apply:

$$u = \beta_v \lambda_{\text{mol}} \left(\frac{\partial u}{\partial y} \right)_{y=0} \quad \text{at } y = 0, \tag{13.4.1}$$

$$u = U - \beta_v \lambda_{\text{mol}} \left(\frac{\partial u}{\partial y} \right)_{y=H} \quad \text{at } y = H. \tag{13.4.2}$$

The solution to Eq. (4.1.4) will then be

$$\frac{u}{U} = \frac{1}{1 + 2\beta_v \text{Kn}_H} \left(\frac{y}{H} + \beta_v \text{Kn}_H \right), \tag{13.4.3}$$

where $\text{Kn}_H = \lambda_{\text{mol}}/H$. The velocity profile is thus linear and appears as shown in Fig. 13.4. With slip, the velocity gradient is smaller. However, the total volumetric flow rate, per unit depth, follows

$$Q = \int_0^H u dy = HU/2, \tag{13.4.4}$$

which is identical to the no-slip case.

We can define a skin-friction coefficient (Fanning friction factor) for the lower plate by writing

$$C_f = \frac{\tau_{y=0}}{\frac{1}{2}\rho U^2}, \tag{13.4.5}$$

where $\tau_{y=0} = \mu \left(du/dy \right)_{y=0}$, and that leads to

$$C_f = \frac{2}{\text{Re}_H \left[1 + 2\beta_v \text{Kn}_H \right]} = \frac{2}{\text{Re}_H \left[1 + 2\sqrt{\frac{\pi \gamma}{2}} \beta_v \frac{Ma}{\text{Re}_H} \right]}, \tag{13.4.6}$$

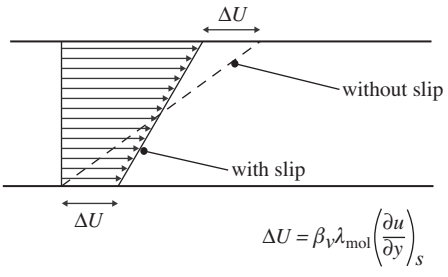

Figure 13.4. Velocity profile in slip Couette flow.

where $\mathrm{Re}_H = UH/\nu$. We can now compare the preceding result with Eq. (4.1.21) and from there write

$$\frac{\mathrm{Po}_{\text{slip}}}{\mathrm{Po}_{\text{no-slip}}} = \frac{1}{[1+2\beta_v \mathrm{Kn}_H]} = \frac{1}{\left[1+2\sqrt{\frac{\pi\gamma}{2}}\beta_v \frac{Ma}{\mathrm{Re}_H}\right]}. \tag{13.4.7}$$

where the Poiseuille number can be written as

$$\mathrm{Po} = C_f \mathrm{Re}_{D_H} = 2C_f \mathrm{Re}_H. \tag{13.4.8}$$

Clearly, the velocity slip reduces the wall friction.

Let us now consider heat transfer for the system depicted in Fig. 13.3(b), where Couette flow occurs between two parallel plates, one (the bottom plate in the figure) stationary and adiabatic, the other (the top plate) moving at a constant velocity U and subject to convective heat transfer at its outer surface. Let us assume, for simplicity, that $\alpha = \alpha_T$. Equation (4.1.5), with the following boundary conditions, applies:

$$\frac{dT}{dy} = 0 \quad \text{at } y = 0, \tag{13.4.9}$$

$$-k\frac{dT}{dy} = h_0 (T - T_\infty) \quad \text{at } y = H. \tag{13.4.10}$$

Using the velocity profile previously derived, we get

$$\varphi = \frac{\mu}{k}\left(\frac{du}{dy}\right)^2 = \frac{\mu}{k}\left[\frac{U}{H(1+2\beta_v \mathrm{Kn}_H)}\right]^2. \tag{13.4.11}$$

where the parameter φ is related to the viscous dissipation term Φ according to [see Eq. (1.1.53)]:

$$\varphi = \mu\Phi/k.$$

Equation (13.4.11) can now be substituted into Eq. (4.1.5). The solution of the latter equation will then lead to

$$T = -\frac{1}{2}\varphi y^2 + \frac{kH\varphi}{h_0} + \frac{H^2\varphi}{2} + \beta_T \mathrm{Kn}_H H^2 \varphi + T_\infty. \tag{13.4.12}$$

13.5 Slip Flow in a Flat Channel

Figure 13.5 displays the system configuration and the definition of the coordinate system.

13.5.1 Hydrodynamics of Fully Developed Flow

We now deal with Poiseuille flow in a 2D channel in the slip flow regime. Let us assume incompressible and constant-property flow (as required by the fully

Figure 13.5. Flow in a flat channel.

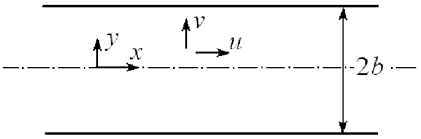

developed flow assumption). Also, let us neglect the thermal creep. The momentum equation and boundary conditions are then

$$\mu \frac{d^2u}{dy^2} - \frac{dP}{dx} = 0, \tag{13.5.1}$$

$$\frac{du}{dy} = 0 \quad \text{at } y = 0, \tag{13.5.2}$$

$$u = -\beta_v \lambda_{\text{mol}} \left(\frac{du}{dy}\right) \quad \text{at } y = b. \tag{13.5.3}$$

The solution is

$$u(y) = \frac{b^2}{2\mu}\left(-\frac{dP}{dx}\right)\left[1 - \left(\frac{y}{b}\right)^2 + 4\beta_v \text{Kn}_{2b}\right], \tag{13.5.4}$$

where $\text{Kn}_{2b} = \lambda_{\text{mol}}/(2b)$. The average velocity then follows:

$$U_m = \frac{b^2}{3\mu}\left(-\frac{dP}{dx}\right)\left[1 + 6\beta_v \text{Kn}_{2b}\right]. \tag{13.5.5}$$

The dimensionless velocity profile is

$$\frac{u}{U_m} = \frac{3}{2}\frac{1 - (y/b)^2 + 4\beta_v \text{Kn}_{2b}}{1 + 6\beta_v \text{Kn}_{2b}}. \tag{13.5.6}$$

Using Eq. (13.5.5), we can easily show that

$$\frac{\text{Po}}{\text{Po}|_{\text{Kn}\to 0}} = \frac{C_f \text{Re}_{2\text{b}}}{(C_f \text{Re}_{2\text{b}})|_{\text{Kn}\to 0}} = \frac{1}{1 + 6\beta_v \text{Kn}_{2b}}, \tag{13.5.7}$$

where, because $C_f \text{Re}_{D_H}|_{\text{Kn}\to 0} = 24$ [see Eq. (4.3.13)], then $(C_f \text{Re}_{2b})|_{\text{Kn}\to 0} = 12$.

It can also be shown that

$$\frac{U_s^*}{U_m} = \frac{u|_{y=\pm b}}{U_m} = \frac{6\beta_v \text{Kn}_{2b}}{1 + 6\beta_v \text{Kn}_{2b}}. \tag{13.5.8}$$

We now consider the flow rate in a microchannel with a finite length. For a channel with finite length, the relation between the mass flow rate and pressure drop is needed. For fully developed incompressible flow, the latter relation can be derived easily, because the pressure gradient will be a constant and the density as well as velocity will be invariant with respect to the axial position. Equation (13.5.5) can then be directly used for calculating the flow rate when the pressure drop over the channel length is known. However, as mentioned earlier, the assumption of incompressible flow is not always reasonable in microchannels subject to gas flow, for which pressure drop can be significant.

An analysis can be performed for a system such as the one shown in Fig. 13.6 when density variations are assumed to result from changes in pressure, but not

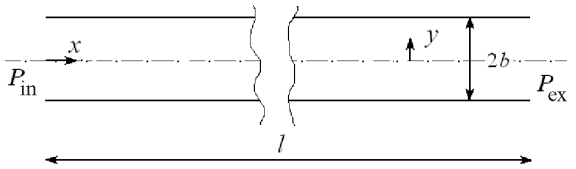

Figure 13.6. Definitions for slip flow in a flat channel with finite length.

from changes in temperature. The velocity profile is assumed to follow Eq. (13.5.4) at each location, however. The analysis will thus apply to isothermal conditions, but will also be a good approximation even when heat transfer is involved because in microchannels the density variations caused by pressure are often significantly larger than those resulting from temperature variations. Assuming that $\alpha = \alpha_T = 1$, the analysis then leads to (Arkilic et al., 1997; Zohar, 2006)

$$\frac{P(x)}{P_{ex}} = -6\mathrm{Kn}_{2b,ex} + \left\{ \left(6\mathrm{Kn}_{2b,ex} + \frac{P_{in}}{P_{ex}} \right)^2 + \left[\left(1 - \frac{P_{in}^2}{P_{ex}^2} \right) + 12\mathrm{Kn}_{2b,ex} \left(1 - \frac{P_{in}}{P_{ex}} \right) \right] \frac{x}{l} \right\}^{1/2}, \tag{13.5.9}$$

where $\mathrm{Kn}_{2b,ex}$ is based on the pressure at the exit. It can also be shown that the total mass flow rate through the flow passage is

$$\dot{m} = \dot{m}|_{\mathrm{Kn}\to 0} \left[1 + \frac{12\mathrm{Kn}_{2b,ex}}{\frac{P_{in}}{P_{ex}} + 1} \right], \tag{13.5.10}$$

where the mass flow rate without velocity slip follows:

$$\dot{m}|_{\mathrm{Kn}\to 0} = \frac{1}{3} \frac{b^3 P_{ex}^2 W}{\mu l \, (R_u/M) \, T_{ex}} \left[\left(\frac{P_{in}}{P_{ex}} \right)^2 - 1 \right], \tag{13.5.11}$$

where W is the channel width.

Equation (13.5.9)–(13.5.11) are for $\alpha = 1$. These equations can be made more general by replacing $\mathrm{Kn}_{2b,ex}$ with $\beta_v \, \mathrm{Kn}_{2b,ex}$ everywhere, with β_v defined in Eq. (13.3.14).

Figure 13.7 compares the predictions of Eq. (13.5.9) with experimental data. Close agreement between this theory and experimental data was demonstrated by other investigators as well (Jiang et al., 1999; Li et al., 2000), proving the validity of the first-order wall slip flow model.

13.5.2 Thermally Developed Heat Transfer, UHF

Symmetric Boundary Conditions

We would like to analyze a system similar to the one displayed in Fig. 4.10(c), where flow between two parallel plates with symmetric UHF boundary conditions is underway. The wall heat flux is imposed at $x = 0$. All of the assumptions underlying the

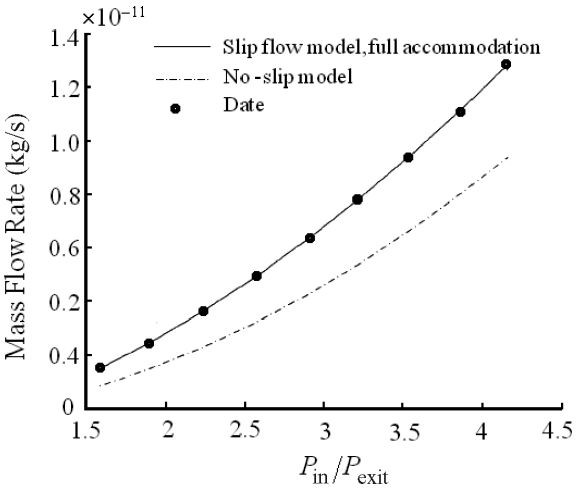

Figure 13.7. Helium mass flow rate in a microchannel at 300 K, exhausting to the atmosphere ($2b = 1.33\,\mu$m, $W = 52.2\,\mu$m, $l = 7500\,\mu$m). The solid curve is based on Eq. (13.5.10) (from Arkilic et al., 1997).

thermally developed flow apply at location x. The energy equation and boundary conditions are

$$\rho\, C_P u \frac{\partial T}{\partial x} = k \frac{\partial^2 T}{\partial y^2}, \tag{13.5.12}$$

$$\frac{\partial T}{\partial y} = 0 \quad \text{at } y = 0, \tag{13.5.13}$$

$$k \frac{\partial T}{\partial y} = -q_s'' \quad \text{at } y = \pm\, b. \tag{13.5.14}$$

We can nondimensionalize these equations similarly to what we did in Subsection 4.4.2, but for convenience we use different reference length scales for the x and y directions:

$$\eta = y/b \tag{13.5.15}$$

$$\zeta = x/(2b) \tag{13.5.16}$$

$$\theta = \frac{T - T_{\text{in}}}{\dfrac{q_s'' b}{k}}. \tag{13.5.17}$$

We also note that, consistent with the thermally developed flow assumption,

$$\frac{\partial T}{\partial x} = \frac{\partial T_m}{\partial x} = \frac{q_s''}{\rho\, U_m C_P b}. \tag{13.5.18}$$

Equations (13.5.12)–(13.5.14) then give,

$$\Psi\, f(\eta) \frac{\partial \theta}{\partial \zeta} = \frac{\partial^2 \theta}{\partial \eta^2}, \tag{13.5.19}$$

where,

$$\Psi = \text{Re}_{2b}\,\text{Pr}/4, \tag{13.5.20}$$

$$\text{Re}_{2b} = U_m\,(2b)/\nu, \tag{13.5.21}$$

$$f(\eta) = \frac{u\,(\eta)}{U_m} = \frac{3}{2} \frac{1 - \eta^2 + 4\beta_v \text{Kn}_{2b}}{1 + 6\beta_v \text{Kn}_{2b}}, \tag{13.5.22}$$

where we used Eq. (13.5.6) to derive the last equation. Equation (13.5.18), in dimensionless form, gives

$$\frac{\partial\theta}{\partial\zeta} = \frac{\partial\theta_m}{\partial\zeta} = \frac{4}{\mathrm{Re}_{2b}\mathrm{Pr}}, \tag{13.5.23}$$

where θ_m is the nondimensionalized mean temperature. This equation leads to

$$\theta_m = \frac{4\zeta}{\mathrm{Re}_{2b}\mathrm{Pr}}. \tag{13.5.24}$$

Now that the variation of the mean dimensionless temperature with ζ is known, we can represent the local θ at (ζ, η) as the summation of the mean local dimensionless temperature and a function that depends on only η:

$$\theta(\zeta, \eta) = \frac{4\zeta}{\mathrm{Re}_{2b}\mathrm{Pr}} + G(\eta). \tag{13.5.25}$$

We then get

$$\frac{d^2G}{d\eta^2} = f(\eta), \tag{13.5.26}$$

$$dG/d\eta = 0 \quad \text{at } \eta = 0. \tag{13.5.27}$$

The function $G(\eta)$ should satisfy,

$$\int_{-1}^{+1} G(\eta)\, f(\eta)\, d\eta = 0. \tag{13.5.28}$$

The solution to the preceding three equations is (Inman, 1964b)

$$G(\eta) = \left[\frac{3}{4}\eta^2 - \frac{1}{8}\eta^4 - \frac{39}{280}\right] + \left[-\frac{1}{4}\eta^2 + \frac{1}{8}\eta^4 - \frac{13}{280}\right]\left(\frac{U_s^*}{U_m}\right) + \frac{2}{105}\left(\frac{U_s^*}{U_m}\right)^2, \tag{13.5.29}$$

where U_s^*/U_m represents the nondimensionalized velocity slip at the channel wall and is given in Eq. (13.5.8).

The temperature jump at the wall, using Eq. (13.3.6), gives (note that the direction of y is now different than what was used for the derivation of the latter equation)

$$T_s^* - T_s = -\frac{2-\alpha_T}{\alpha_T}\left(\frac{2\gamma}{\gamma+1}\right)\frac{\lambda_{\mathrm{mol}}}{\mathrm{Pr}}\left(\frac{\partial T}{\partial y}\right)_{y=b} = -2\beta_T \mathrm{Kn}_{2b}\frac{q_s'' b}{k}. \tag{13.5.30}$$

The solution represented by Eqs. (13.5.25) and (13.5.29) must also satisfy

$$\theta(1) = \frac{T_s^* - T_{\mathrm{in}}}{(q_s'' b)/k} = \frac{(T_s^* - T_s) + (T_s - T_{\mathrm{in}})}{(q_s'' b)/k}. \tag{13.5.31}$$

This leads to

$$\frac{T_s - T_{\mathrm{in}}}{(q_s'' b)/k} = \theta_m + G(1) + 2\beta_T \mathrm{Kn}_{2b}. \tag{13.5.32}$$

or

$$\frac{T_s - T_m}{(q_s'' b)/k} = G(1) + 2\beta_T \mathrm{Kn}_{2b}. \tag{13.5.33}$$

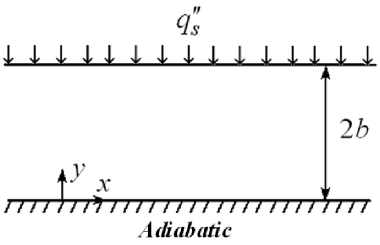

Figure 13.8. A flat channel with uniform heat flux on one surface and adiabatic on the other surface.

We can now define a Nusselt number as

$$\mathrm{Nu}_{D_H,\mathrm{UHF}} = \frac{q_s'' D_H}{k\,(T_s - T_m)} = \frac{4}{G\,(1) + 2\beta_T \mathrm{Kn}_{2b}}. \tag{13.5.34}$$

The previous two equations lead to

$$\mathrm{Nu}_{D_H,\mathrm{UHF}} = \frac{140/17}{1 - \left(\frac{6}{17}\right)\left(\frac{U_s^*}{U_m}\right) + \left(\frac{2}{51}\right)\left(\frac{U_s^*}{U_m}\right)^2 + \left(\frac{70}{17}\right)\beta_T \mathrm{Kn}_{2b}}. \tag{13.5.35}$$

This solution gives $\mathrm{Nu}_{D_H,\mathrm{UHF}}|_{\mathrm{Kn}\to 0} = 140/17$ and is thus consistent with the solution previously derived in Section 4.4.

Asymmetric Boundary Conditions

We now address the conditions in Fig. 13.8, in which one wall is subject to a constant wall heat flux, q_s'', and the other one is insulated. This is equivalent to the boundary conditions in Fig. 4.10(d), in which one of the walls is adiabatic. For this case, defining the Nusselt number according to $\mathrm{Nu}_{D_H,\mathrm{UHF}} = \frac{q_s'' D_H}{k(T_s - T_m)}$ for the heated surface, we can prove that (see Problem 13.4)

$$\mathrm{Nu}_{D_H,\mathrm{UHF}} = \frac{140/13}{1 - \left(\frac{3}{26}\right)\left(\frac{U_s^*}{U_m}\right) + \left(\frac{1}{78}\right)\left(\frac{U_s^*}{U_m}\right)^2 + \left(\frac{35}{13}\right)\beta_T \mathrm{Kn}_{2b}}. \tag{13.5.36}$$

13.5.3 Thermally Developed Heat Transfer, UWT

It was shown in Subsection 4.4.2 that, for UWT boundary conditions [see Eq. (4.4.53)]

$$(\mathrm{Nu}_{D_H})_{\text{no-slip}} = (\mathrm{Nu}_{D_H})_{\mathrm{Kn}\to 0} = 7.5407.$$

The energy conservation equation and boundary conditions, in dimensionless form, are,

$$\Psi\ f(\eta)\frac{\partial \theta}{\partial \zeta} = \frac{\partial^2 \theta}{\partial \eta^2} + \frac{1}{4}\frac{\partial^2 \theta}{\partial \zeta^2}, \tag{13.5.37}$$

where Ψ is defined in Eq. (13.5.20), η and ζ were defined in Eqs. (13.5.15) and (13.5.16), respectively, $f(\eta)$ is defined in Eq. (13.5.22), and

$$\theta = \frac{T - T_s}{T_{\text{in}} - T_s}. \tag{13.5.38}$$

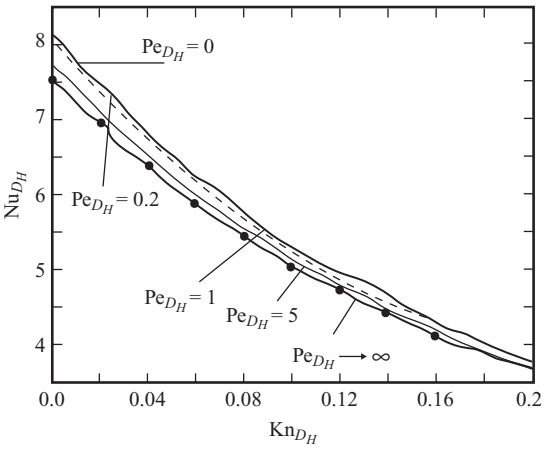

Figure 13.9. Variation of thermally developed Nu_{D_H} with Kn_{D_H} and Pe_{D_H} for air in a 2D channel with UWT boundary conditions (from Hadjiconstantinou and Simek, 2002).

Note that Eq. (13.5.37) includes axial conduction in the fluid, represented by the second term on the right-hand side. Axial conduction will be negligible when $\mathrm{Pe}_{D_H} = \mathrm{Re}_{D_H}\mathrm{Pr} > 100$.

The boundary conditions for Eq. (13.5.37) are

$$\theta = 1 \quad \text{at } \zeta \leq 0, \tag{13.5.39}$$

$$\theta = 0 \quad \text{at } \zeta \to \infty, \tag{13.5.40}$$

$$\partial\theta/\partial\eta = 0 \quad \text{at } \eta = 0, \tag{13.5.41}$$

$$\theta = -2\beta_T \mathrm{Kn}_{2b} \frac{\partial\theta}{\partial\eta} \quad \text{at } \eta = 1. \tag{13.5.42}$$

The preceding is an entrance-region problem whose solution for $\theta\,(\zeta, \eta)$ will provide for the calculation of Nusselt number from

$$\mathrm{Nu}_{D_H} = -\frac{4}{\theta_m} \left.\frac{\partial\theta}{\partial\eta}\right|_{\eta=1}. \tag{13.5.43}$$

When axial conduction is neglected, we have Graetz's problem for slip flow in a 2D channel. (Graetz's problem for a flat channel, without velocity slip, was discussed in Subsection 4.5.6.) Inman (1964a) solved this problem by the method of eigenfunctions expansion. Hadjiconstantinou and Simek (2002) numerically solved the problem, and their solution can be interpreted to represent $\alpha = \alpha_T = 1$.

Figure 13.9 depicts the dependence of Nu_{D_H} on Kn_{D_H} (Hadjiconstantinou and Simek, 2002), in which the effect of axial conduction in the fluid has been included in the analysis. As noted, Nu_{D_H} is reduced with increasing Kn_{D_H}. Also, as expected, $(\mathrm{Nu}_{D_H}) \to (\mathrm{Nu}_{D_H})_{\text{no-slip}}$ in the limit of $\mathrm{Pe}_{D_H} \to \infty$ and $\mathrm{Kn}_{D_H} \to 0$. The $\mathrm{Pe}_{D_H} \to \infty$ limit implies complete vanishing of the axial conduction effect.

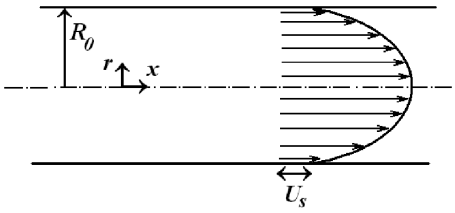

Figure 13.10. Fully-developed laminar flow with slip in a circular tube.

13.6 Slip Flow in Circular Microtubes

13.6.1 Hydrodynamics of Fully Developed Flow

The momentum conservation equation and its boundary conditions for this problem are (see Fig. 13.10)

$$-\frac{dP}{dx}+\mu\frac{1}{r}\frac{\partial}{\partial r}\left(r\frac{\partial u}{\partial r}\right)=0, \tag{13.6.1}$$

$$\frac{\partial u}{\partial r}=0 \quad \text{at } r=0, \tag{13.6.2}$$

$$u=-\beta_v\lambda_{\text{mol}}\left(\frac{\partial u}{\partial r}\right)_{r=R_0} \qquad \text{at } r=R_0. \tag{13.6.3}$$

The solution to this system is

$$u=\frac{R_0^2}{4\mu}\left(-\frac{dP}{dx}\right)\left[1-\left(\frac{r}{R_0}\right)^2+4\beta_v\text{Kn}_D\right], \tag{13.6.4}$$

where $\text{Kn}_D=\lambda_{\text{mol}}/D$. Equation (13.6.4) leads to

$$U_m=\frac{1}{R_0^2}\int_0^{R_0}2ru(r)dr=\frac{R_0^2}{8\mu}\left(-\frac{dP}{dx}\right)\left[1+8\beta_v\text{Kn}_D\right]. \tag{13.6.5}$$

Comparison between this equation and Eq. (4.3.4) indicates that, with the same pressure gradient, the velocity slip at the wall results in a higher mean flow rate. We can also show that

$$\frac{u}{U_m}=2\frac{1-\left(\frac{r}{R_0}\right)^2+4\beta_v\text{Kn}_D}{1+8\beta_v\text{Kn}_D}, \tag{13.6.6}$$

$$\frac{U_s^*}{U_m}=\frac{1}{1+\frac{1}{8\beta_v\text{Kn}_D}}. \tag{13.6.7}$$

We can now derive an expression for the friction factor, using the same method we applied for pipe flow without slip (see Subsection 4.3). Thus we start with

$$\left(-\frac{dP}{dx}\right)=\frac{2\tau_s}{R_0}=\frac{2}{R_0}\left[-\mu\left(\frac{du}{dr}\right)_{r=R_0}\right]. \tag{13.6.8}$$

We can find $\left(\frac{du}{dr}\right)_{r=R_0}$ from Eq. (13.6.6) and substitute into Eq. (13.6.8), and then we use the definition $\tau_s = C_f \frac{1}{2}\rho U_m^2$ to get

$$C_f \mathrm{Re}_D = \frac{16}{1 + 8\beta_v \mathrm{Kn}_D}. \tag{13.6.9}$$

Through a comparison with the no-slip relation [Eq. (4.3.9)], we have thus shown that

$$\frac{\mathrm{Po}}{\mathrm{Po}|_{\mathrm{Kn}\to 0}} = \frac{C_f \mathrm{Re}_D}{(C_f \mathrm{Re}_D)|_{\mathrm{Kn}\to 0}} = \frac{1}{1 + 8\beta_v \mathrm{Kn}_D}. \tag{13.6.10}$$

13.6.2 Thermally Developed Flow Heat Transfer, UHF

The system configuration is similar to the one shown in Fig. 13.10, except that now the heat flux q_s'' is imposed on the wall (the heat flux is oriented inward). Let us first consider an incompressible flow. The arguments of thermally developed flow in UHF conditions that were presented in Chapter 4 all apply here. With axial conduction in the fluid neglected, the energy conservation equation and its boundary conditions are

$$u\frac{\partial T}{\partial x} = \frac{\alpha}{r}\frac{\partial}{\partial r}\left(r\frac{\partial T}{\partial r}\right), \tag{13.6.11}$$

$$\frac{\partial T}{\partial r} = 0 \quad \text{at } r = 0, \tag{13.6.12}$$

$$T = T_s^* = T_s - \beta_T \lambda_{\mathrm{mol}} \left(\frac{\partial T}{\partial r}\right)_{r=R_0} \quad \text{at } r = R_0. \tag{13.6.13}$$

Obviously the following condition must also be satisfied:

$$k\left(\frac{\partial T}{\partial r}\right)_{r=R_0} = q_s'' \quad \text{at } r = R_0. \tag{13.6.14}$$

The thermally developed conditions also require that

$$\frac{\partial T}{\partial x} = \frac{\partial T_m}{\partial x} = \frac{2q_s''}{\rho C_P U_m R_0}. \tag{13.6.15}$$

Let us define the following dimensionless parameters:

$$\eta = r/R_0, \tag{13.6.16}$$

$$\theta = \frac{T - T_s}{\frac{q_s'' R_0}{k}}. \tag{13.6.17}$$

Equations (13.6.11)–(13.6.13) can then be cast as

$$2\frac{1 - \eta^2 + 4\beta_v \mathrm{Kn}_D}{1 + 8\beta_v \mathrm{Kn}_D} = \frac{1}{\eta}\frac{\partial}{\partial \eta}\left(\eta\frac{\partial \theta}{\partial \eta}\right), \tag{13.6.18}$$

$$\frac{\partial \theta}{\partial \eta} = 0 \quad \text{at } \eta = 0, \tag{13.6.19}$$

$$\theta = +2\beta_T \mathrm{Kn}_D \quad \text{at } \eta = 1. \tag{13.6.20}$$

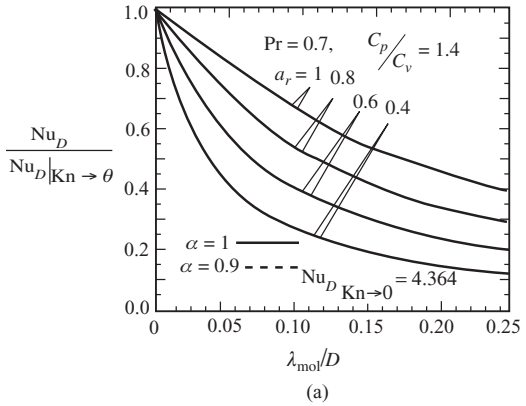

Figure 13.11. Thermally developed heat transfer coefficient in a tube: (a) UHF, (b) UWT (from Sparrow and Lin, 1962).

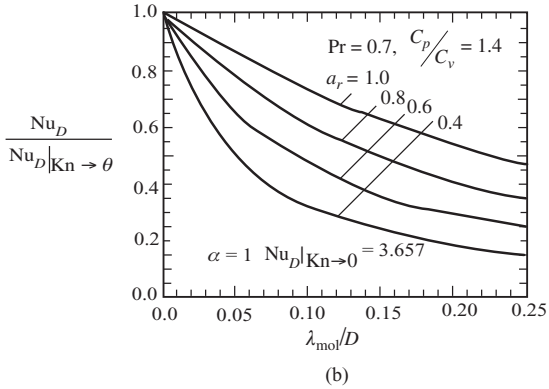

The solution to Eq. (13.6.18) is

$$\theta = \left[\frac{3}{4} - \eta^2 + \frac{1}{4}\eta^4\right] + \left[-\frac{1}{4} + \frac{1}{2}\eta^2 - \frac{1}{4}\eta^4\right]\left(\frac{U_s^*}{U_m}\right) + 2\beta_T \mathrm{Kn}_D. \quad (13.6.21)$$

We can now find the average dimensionless temperature from

$$\theta_m = \int_0^1 2\pi\,\eta\,\frac{u}{U_m}(\eta)\theta(\eta)\,d\eta \Big/ \int_0^1 2\pi\,\eta\,\frac{u}{U_m}(\eta)\,d\eta \quad (13.6.22)$$

$$\Rightarrow \theta_m = \frac{T_s - T_m}{\frac{q_s'' R_0}{k}} = \frac{11}{24} - \frac{1}{4}\left(\frac{U_s^*}{U_m}\right) + \frac{1}{24}\left(\frac{U_s^*}{U_m}\right)^2 + 2\beta_T \mathrm{Kn}_D. \quad (13.6.23)$$

We note that

$$\mathrm{Nu}_D = \frac{q_s'' D}{k(T_s - T_m)} = \frac{2}{\theta_m}. \quad (13.6.24)$$

The analysis thus leads to

$$\mathrm{Nu}_D = \frac{48/11}{1 - \frac{6}{11}\left(\frac{U_s^*}{U_m}\right) + \frac{1}{11}\left(\frac{U_s^*}{U_m}\right)^2 + \frac{48}{11}(\beta_T \mathrm{Kn}_D)}. \quad (13.6.25)$$

Figure 13.11(a) shows some calculation results (Sparrow and Lin, 1962) for a fluid with Pr = 0.7. As expected, Nu_D is reduced monotonically with increasing Kn_D.

The Effect of Compressibility

The preceding derivations assumed incompressible flow and negligible axial derivatives of all properties except pressure, which is reasonable when $Ma\,\mathrm{Kn}_D \ll 1$.

Because in microchannels density variations resulting from pressure drop are more significant than the density variations resulting from temperature change, we can modify the previous analysis, assuming that local properties can be calculated at the local pressure but at the average temperature, $T_{m,\mathrm{avg}}$. In that case, assuming $\alpha = \alpha_T = 1$ and bearing in mind that $P\mathrm{Kn} = \text{const.}$, we can show that (Jiji, 2006)

$$T_s - T_m = \frac{4\gamma}{\gamma+1}\frac{q_s'' R_0}{k\,\mathrm{Pr}}\mathrm{Kn}_D + \frac{4q_s'' R_0}{k\,(1+8\mathrm{Kn}_D)}\left(\mathrm{Kn}_D + \frac{3}{16}\right) - \frac{q_s'' R_0}{k\,(1+8\mathrm{Kn}_D)^2}\left(16\,(\mathrm{Kn}_D)^2 + \frac{14}{3}\mathrm{Kn}_D + \frac{7}{24}\right). \tag{13.6.26}$$

This equation, along with Eq. (13.6.23), then gives

$$\mathrm{Nu}_D = \frac{2}{\frac{4}{1+8\mathrm{Kn}_D}\left(\mathrm{Kn}_D + \frac{3}{16}\right) - \frac{1}{(1+8\mathrm{Kn}_D)^2}\left[16\,(\mathrm{Kn}_D)^2 + \frac{14}{3}\mathrm{Kn}_D + \frac{7}{24}\right] + \frac{4\gamma}{\gamma+1}\frac{1}{Pr}\mathrm{Kn}_D}. \tag{13.6.27}$$

It should be emphasized that Kn_D in the preceding two equations must be based on $T_{m,\mathrm{avg}}$.

13.6.3 Thermally Developed Flow Heat Transfer, UWT

For this case, as shown in Section 4.4 [see Eq. (4.4.22)],

$$\mathrm{Nu}_{\mathrm{Kn}\to 0} = 3.6568.$$

The entrance-region problem was solved by the method of eigenfunction expansion (Sparrow and Lin, 1962; Inman, 1964a) and more recently by a numerical method (Hadjiconstantinou and Simek, 2002). The solution of the former authors is for incompressible flow, without axial conduction, in which the energy conservation equation and boundary conditions can be cast as

$$2\frac{1-\eta^2+4\beta_v\mathrm{Kn}_D}{1+8\beta_v\mathrm{Kn}_D}\frac{\partial\theta}{\partial\zeta} = \frac{1}{\eta}\frac{\partial}{\partial\eta}\left(\eta\frac{\partial\theta}{\partial\eta}\right), \tag{13.6.28}$$

$$\theta = 0 \quad \text{at } \zeta = 0, \tag{13.6.29}$$

$$\frac{\partial\theta}{\partial\eta} = 0 \quad \text{at } \eta = 0, \tag{13.6.30}$$

$$\theta = -2\beta_T\mathrm{Kn}_D\left(\frac{\partial\theta}{\partial\eta}\right)_{\eta=1} \quad \text{at } \eta = 1, \tag{13.6.31}$$

where $\theta = \frac{T-T_s}{T_{\mathrm{in}}-T_s}$, $\eta = r/R_0$, and

$$\zeta = \frac{4x}{R_0\,\mathrm{Re}_D\,\mathrm{Pr}}. \tag{13.6.32}$$

Table 13.3. *Thermally developed flow Nusselt numbers for a tube with UWT boundary condition in the slip flow regime (Pr = 0.7) (from Sparrow and Lin, 1962)*

$\beta_v \mathrm{Kn}_D = 0.02$		$\beta_v \mathrm{Kn}_D = 0.05$		$\beta_v \mathrm{Kn}_D = 0.1$		$\beta_v \mathrm{Kn}_D = 0.15$		$\beta_v \mathrm{Kn}_D = 0.25$	
$\beta_T \mathrm{Kn}_D$	Nu_D	$\beta_T \mathrm{Kn}_D$	Nu_D	$\beta_T \mathrm{Kn}_D$	Nu_D	$\beta_T \mathrm{Kn}_D$	Nu_D	$\beta_T \mathrm{Kn}_D$	Nu_D
0.01849	3.645	0.08070	3.213	0.1606	2.738	0.2448	2.311	0.4094	1.730
0.03366	3.485	0.09073	3.125	0.1746	2.645	0.3001	2.06	0.5176	1.462
0.04987	3.326	0.1213	2.88	0.2501	2.228	0.3750	1.794	0.6575	1.217
0.07218	3.125	0.1553	2.645	0.3038	2.000	0.5384	1.394	0.8435	0.994
0.08717	3.001	0.1933	2.42	0.3895	1.716	0.6555	1.201	0.9725	0.882
0.1195	2.761	0.2362	2.205	0.4773	1.496	0.8026	1.022	1.2521	0.708
0.1370	2.645	0.2903	1.980	0.6126	1.248	0.9914	0.858	1.6550	0.551
0.1555	2.531	0.3338	1.829	0.6677	1.169	1.047	0.819	1.8413	0.500

The properties of the thermally developed flow can evidently be found from the solution of this system for $\zeta \to \infty$. The problem was solved by Sparrow and Lin (1962), who used the method of eigenfunction expansion. At the limit of $\zeta \to \infty$, the solution leads to $\mathrm{Nu}_D = \lambda_1^2/2$, with λ_1 representing the first eigenvalue. The solution also shows that λ_1 and equivalently Nu_D are functions of both $\beta_v \mathrm{Kn}_D$ and $\beta_T \mathrm{Kn}_D$. Table 13.3 is a summary of their results. Figure 13.11(b) depicts some calculation results from Sparrow and Lin (1962) for a gas with $\mathrm{Pr} = 0.7$. Nu_D diminishes monotonically with increasing Kn_D.

The preceding formulation and Fig. 13.11(b) are based on the assumption that axial conduction in the fluid is negligible (i.e., $\mathrm{Pe}_D \gtrsim 100$). Hadjiconstantinou and Simek (2002) numerically solved the same problem, with axial conduction considered. Their solution for fully accommodated conditions ($\alpha = \alpha_T = 1$) led to Fig. 13.12, where variations of Nu_D as a function of Kn_D and Pe_D are displayed. As can be noted, $(\mathrm{Nu}_D) \to (\mathrm{Nu}_D)_{\text{no-slip}}$ in the limit of $\mathrm{Pe}_D \to \infty$ and $\mathrm{Kn}_D \to 0$, where, at the limit of $\mathrm{Pe}_D \to \infty$, the axial conduction effect vanishes.

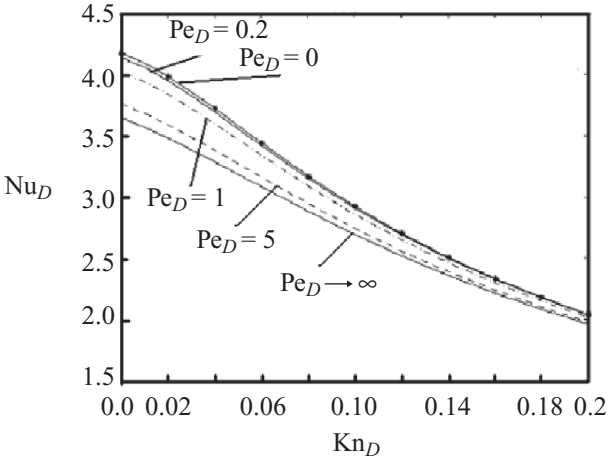

Figure 13.12. Variation of Nu_D as a function of Kn_D and Pe_D for slip flow in a microtube with constant wall temperature (from Hadjiconstantinou and Simek, 2002).

13.6.4 Thermally Developing Flow

Thermally developing flow of an incompressible gas in the slip or temperature-jump regime in circular channels was investigated by several authors. Earlier investigations include those of Sparrow and Lin (1962) and Inman (1964a) for UWT boundary conditions (Graetz's problem in the slip flow regime) and Inman (1964b) for UHF boundary conditions (extended Graetz's problem in slip flow regime). More recently, Graetz's problem in the slip flow regime was solved by Barron et al. (1997). These investigations were all based on neglecting the axial conduction as well as the viscous dissipation in the fluid. Tunc and Bayazitoglu (2001) and Aydin and Avci (2006) solved the thermally developing slip flow problem with both UWT and UHF boundary conditions, accounting for viscous dissipation. Jeong and Jeong (2006) solved the same problem for UHF boundary conditions, accounting for axial conduction as well as viscous dissipation in the fluid.

In the solution of Tunc and Bayazitoglu (2001) for UWT boundary conditions (the slip flow Graetz's problem), the energy equation and boundary conditions are the same as Eqs. (13.6.11)–(13.6.13), except that the term $+\frac{\nu}{C_P}\left(\frac{du}{dr}\right)^2$ is added to the right-hand side of Eq. (13.6.11). The initial condition, furthermore, is

$$T = T_{\text{in}} \quad \text{at} \quad x \leq 0. \tag{13.6.33}$$

It is then assumed that $\alpha = \alpha_{\text{th}} = 1$, and the following dimensionless parameters are defined: $\eta = r/R_0$; $\zeta = x/l_{\text{heat}}$, where l_{heat} is the heated length, and $\theta = \frac{T-T_s^*}{T_{\text{in}}-T_s^*}$. The preceding equations in dimensionless form then become

$$\frac{\text{Gz}\left(1-\eta^2+4\text{Kn}_D\right)}{2\left(1+8\text{Kn}_D\right)}\frac{\partial\theta}{\partial\zeta} = \frac{1}{\eta}\frac{\partial}{\partial\eta}\left(\eta\frac{\partial\theta}{\partial\eta}\right) + \frac{16\,\text{Br}}{\left(1+8\text{Kn}_D\right)^2}\eta^2, \tag{13.6.34}$$

$$\theta = 1 \quad \text{at} \quad \zeta = 0, \tag{13.6.35}$$

$$\frac{\partial\theta}{\partial\eta} = 0 \quad \text{at} \quad \eta = 0, \tag{13.6.36}$$

$$\theta = 1 \quad \text{at} \quad \eta = 1, \tag{13.6.37}$$

where Gz, the Graetz number, and Br, the Brinkman number, are defined respectively as

$$\text{Gz} = \frac{\text{Re}_D\text{Pr}\,D}{l_{\text{heat}}}, \tag{13.6.38}$$

$$\text{Br} = \frac{\mu\ U_m^2}{k\left(T_{\text{in}} - T_s^*\right)}. \tag{13.6.39}$$

Tunc and Bayazitoglu (2001) solved the preceding system by using the integral transform technique (Bayazitoglu and Ozisik, 1980). With $\theta(\zeta, \eta)$ known, the local Nusselt number can then be found from

$$\text{Nu}_{D,x} = -\frac{2\left.\dfrac{\partial\theta}{\partial\eta}\right|_{\eta=1}}{\theta_m - \dfrac{4\gamma}{\gamma+1}\dfrac{\text{Kn}_D}{\text{Pr}}\left.\dfrac{\partial\theta}{\partial\eta}\right|_{\eta=1}}. \tag{13.6.40}$$

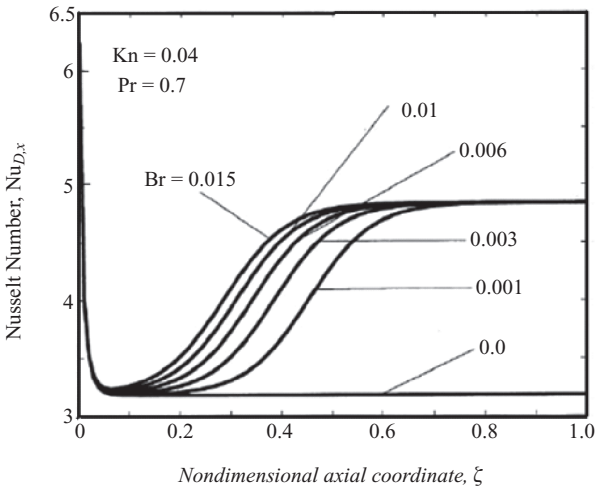

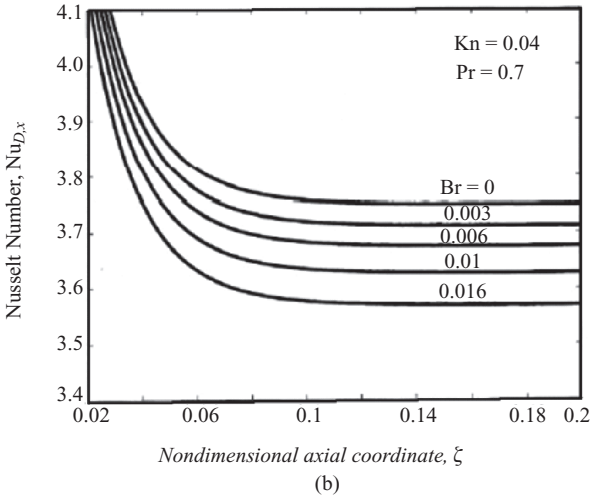

Figure 13.13. The effects of viscous dissipation and Knudsen number on the local Nusselt number in the entrance region of a microtube: (a) UWT boundary condition, (b) UHF boundary condition (Tunc and Bayazitoglu, 2001).

Figures 13.13(a) and 13.13(b) show the effect of viscous dissipation and Knudsen number on the Nusselt number in the entrance region of a microtube with UWT and UHF wall conditions, respectively. These figures show the importance of viscous dissipation in microtubes. The calculations of Tunc and Bayazitoglu also show that, for UWT and UHF conditions both, the thermally developed Nusslet number is reduced when the Knudsen number is increased.

Empirical Correlations

For short tubes with length l, subject to an isothermal flow of a rarefied, incompressible gas, Hanks and Weissberg (1964) proposed the following semiempirical correlation:

$$\mathcal{W} = \mathcal{W}_s + B\,\overline{\mathrm{Kn}}_{R_0}, \tag{13.6.41}$$

where $\overline{\mathrm{Kn}}_{R_0} = \lambda_{\mathrm{mol}}/R_0$, with the gas molecular mean free path found based on $\overline{P}$, the average pressure in the tube, and

$$B = \frac{\pi}{8} \Big/ [(l/R_0) + (3\pi/8)], \tag{13.6.42}$$

$$\mathcal{W} = \frac{\overline{P}\dot{m}/\rho}{\frac{\pi}{4}R_0^2 \Delta P \left[\frac{8R_u T}{\pi M}\right]^{1/2}}, \tag{13.6.43}$$

$$\mathcal{W}_S = 9B^2 \left[(\pi/4) + \left(\frac{128}{27\pi}(l/R_0)\right)\right], \tag{13.6.44}$$

where ΔP is the pressure drop over the length of the tube and M represents the molecular mass of the gas. Equation (13.6.41) can be cast in the following, equivalent form (Shinagawa et al., 2002):

$$C_F = D^2 \left[\frac{8R_u T}{\pi M}\right]^{1/2} \left(\frac{9}{64}\pi^2 + \frac{16}{3}\frac{l}{D}\right) \left[(\pi/8) \Big/ \left(2\frac{l}{D} + \frac{3}{8}\pi\right)\right]^2 + \frac{D^3}{8}\overline{P}\left[(\pi/8) \Big/ \left(2\frac{l}{D} + \frac{3}{8}\pi\right)\right], \tag{13.6.45}$$

where C_F, the flow conductance, is defined as

$$C_F = \frac{\dot{m}/\rho}{\Delta P}. \tag{13.6.46}$$

Shinagawa et al. (2002) investigated the flow of N_2 in microtubes and noted that the preceding correlation deviated from their data and numerical solution results primarily because the effect of inertia at high flow rates and low l/D ratios. They developed the following empirical correlation:

$$\frac{(C_{F,\mathrm{HW}} - C_F)/C_F}{\mathrm{Re}\,(D/l)} = c_1 \ln (P_{\mathrm{in}}/P_{\mathrm{ex}}) + c_2, \tag{13.6.47}$$

where $C_{F,\mathrm{HW}}$ represents the flow conductance according to the correlation of Hank and Weissberg [Eq. (13.6.45)], and

$$c_1 = -8.8 \times 10^{-3} \ln (D/l) + 1.76 \times 10^{-2},$$

$$c_2 = -6.8 \times 10^{-3} \ln (D/l) + 1.48 \times 10^{-2}.$$

Shinagawa et al. (2002) recommend this correlation for the continuum, as well as for the upper limit of the transition regime.

13.7 Slip Flow in Rectangular Channels

13.7.1 Hydrodynamics of Fully Developed Flow

Rectangular channels are common in microsystems because of their relatively simple manufacturing. They have therefore been investigated rather extensively. Ebert and Sparrow (1965) and more recently Yu and Ameel (2001) solved the fully developed flow of a compressible gas in rectangular channels.

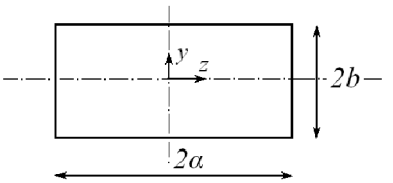

Figure 13.14. Cross section of a rectangular channel.

Consider the channel whose cross section is depicted in Fig. 13.14 and define the aspect ratio according to $\alpha^* = b/a$. Also, define dimensionless coordinates as

$$\zeta = z/a. \tag{13.7.1}$$

$$\eta = y/b. \tag{13.7.2}$$

The fully developed momentum equation, assuming incompressible and constant-property flow, is then

$$\alpha^{*2}\frac{\partial^2 u}{\partial \zeta^2} + \frac{\partial^2 u}{\partial \eta^2} - \frac{b^2}{\mu}\left(-\frac{dP}{dx}\right) = 0, \tag{13.7.3}$$

$$u = -2\beta_v \mathrm{Kn}_{2b}\frac{\partial u}{\partial \eta} \quad \text{at } \eta = 1, \tag{13.7.4}$$

$$u = -2\alpha^*\beta_v \mathrm{Kn}_{2b}\frac{\partial u}{\partial \zeta} \quad \text{at } \zeta = 1, \tag{13.7.5}$$

$$\frac{\partial u}{\partial \eta} = 0 \quad \text{at } \eta = 0, \tag{13.7.6}$$

$$\frac{\partial u}{\partial \zeta} = 0 \quad \text{at } \zeta = 0. \tag{13.7.7}$$

The solution, which can be derived by the separation-of-variables technique, is

$$\frac{u(\zeta,\eta)}{\dfrac{b^2}{\mu}\left(-\dfrac{dP}{dx}\right)} = 2\sum_{\mathrm{i}=1}^{\infty}\left\{\frac{\cos\omega_i\eta}{\omega_i^3}\left(\frac{\sin\omega_i}{1+2\beta_v\mathrm{Kn}_{2b}\sin^2\omega_i}\right)\left(1-\frac{\cosh\dfrac{\omega_i}{\alpha^*}\zeta}{\cosh\dfrac{\omega_i}{\alpha^*}+2\beta_v\mathrm{Kn}_{2b}\omega_i\sinh\dfrac{\omega_i}{\alpha^*}}\right)\right\}, \tag{13.7.9}$$

where the eigenvalues ω_i are found from

$$\omega_i \tan\omega_i = \frac{1}{2\beta_v \mathrm{Kn}_{2b}}. \tag{13.7.10}$$

The mean velocity can be found from

$$U_m = \frac{1}{ab}\int_0^a\int_0^b u(x,y)dxdy \tag{13.7.11}$$

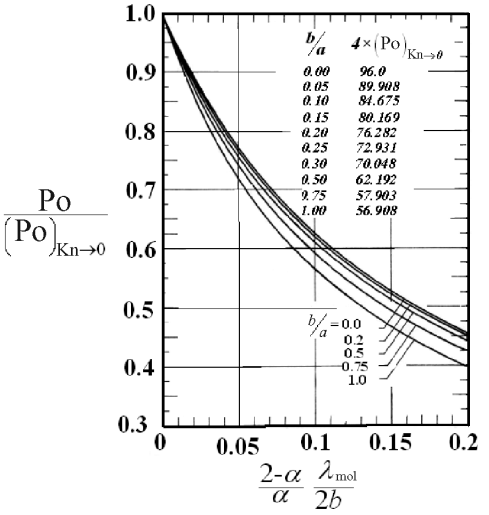

Figure 13.15. The effect of $\beta_v \mathrm{Kn}_{2b}$ on $\mathrm{Po}/\mathrm{Po}|_{\mathrm{Kn}\to 0}$ in rectangular microchannels (Ebert and Sparrow, 1965).

$$\Rightarrow \frac{U_m}{\frac{b^2}{\mu}\left(-\frac{dP}{dx}\right)} = 2\sum_{\mathrm{i}=1}^{\infty}\left\{\frac{\alpha^*}{\omega_i^5}\left(\frac{\sin^2\omega_i}{1+2\beta_v \mathrm{Kn}_{2b}\sin^2\omega_i}\right)\left(\frac{\omega_i}{\alpha^*}-\frac{\tanh\frac{\omega_i}{\alpha^*}}{1+2\beta_v \mathrm{Kn}_{2b}\omega_i\tanh\frac{\omega_i}{\alpha^*}}\right)\right\}. \tag{13.7.12}$$

We thus get

$$\frac{u(\zeta,\eta)}{U_m} = \frac{\text{right-hand side of Eq. (13.7.9)}}{\text{right-hand side of Eq. (13.7.12)}}. \tag{13.7.13}$$

Now we can derive an expression for C_f by noting that $C_f = \tau_s \big/ \left(\frac{1}{2}\rho U_m^2\right)$ and

$$\tau_s = \frac{ab}{a+b}\left(-\frac{dP}{dx}\right). \tag{13.7.14}$$

The result will be

$$C_f \mathrm{Re}_{D_H} = \frac{8}{(1+\alpha^*)^2\,[\text{right-hand side of Eq. (13.7.12)}]}. \tag{13.7.15}$$

An expression for $(C_f \mathrm{Re}_{D_H})_{\mathrm{Kn}\to 0}$ was depicted earlier in Section 4.3 [see Eq. (4.3.17)]. Figure 13.15 displays plots of $\mathrm{Po}/(\mathrm{Po})_{\mathrm{Kn}\to 0}$ or, equivalently, $C_f \mathrm{Re}_{D_H}/(C_f \mathrm{Re}_{D_H})_{\mathrm{Kn}\to 0}$. Clearly $\mathrm{Po}/(\mathrm{Po})_{\mathrm{Kn}\to 0}$ is a strong function of $\beta_v \mathrm{Kn}_{2b}$ and decreases monotonically as the latter parameter increases.

13.7.2 Heat Transfer

Yu and Ameel (2001, 2002) analytically solved the thermally developing flow of an incompressible and constant-property gas in rectangular channels with UWT and

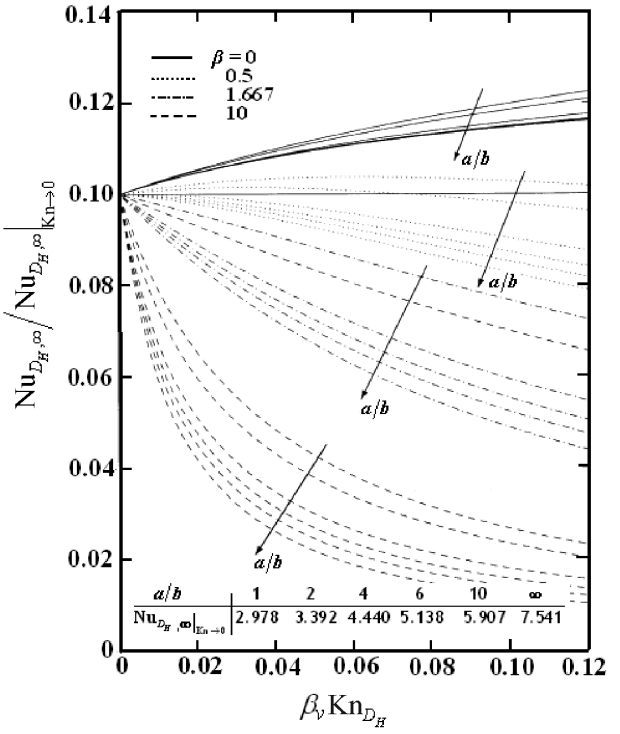

Figure 13.16. Parametric dependencies for thermally-developed slip flow in a rectangular channels with UWT boundary conditions (Yu and Ameel, 2001).

UHF boundary conditions. They assumed fully developed hydrodynamics, negligible viscous dissipation, and negligible axial conduction in the fluid.

For a UWT boundary, Yu and Ameel (2001) modified a solution method that had been derived earlier (Aparecido and Cotta, 1990; Cotta, 1993). Figure 13.16 displays the normalized thermally developed Nusslet number, $\mathrm{Nu}_{D_H,\infty}/\mathrm{Nu}_{D_H,\infty}|_{\mathrm{Kn}\to 0}$, as a function of various parameters. As noted, the normalized thermally developed Nusselt number is a strong function of the aspect ratio as well as of the Knudsen number. An interesting observation was that, for both UWT and UHF conditions (the latter to be discussed shortly), and for all aspect ratios, right at the inlet to the heated segment of the tube, the heat transfer coefficient and therefore the Nusselt number are finite because of slip at the wall and can be found from (remember that the flow is hydraulically fully developed)

$$\mathrm{Nu}_{D_H}|_{x=0} = \frac{1}{\beta_T \mathrm{Kn}_{D_H}}. \tag{13.7.16}$$

For the entrance-dominated region with UWT boundary conditions, the parametric results of Yu and Ameel (2001) indicated that the local Nusselt number, $\mathrm{Nu}_{D_H,x}$, depends on $\beta_v \mathrm{Kn}_{D_H}$ in a rather complex manner. For small β, where $\beta = \beta_T/\beta_v$, $\mathrm{Nu}_{D_H,x}$ increased with increasing $\beta_v \mathrm{Kn}_{D_H}$ (up to 20%). Above a critical value, β_{cr}, which also depended on the aspect ratio, the trend was reversed. At β_{cr}, in fact, $\mathrm{Nu}_{D_H,\infty}/\mathrm{Nu}_{D_H,\infty}|_{\mathrm{Kn}\to 0} = 1$. The magnitude of β_{cr} increased monotonically with the aspect ratio; $\beta_{\mathrm{cr}} = 0.29,\ 0.5,\ 0.67$ for $\alpha^* = 0.2,\ 0.5,\ 1$, respectively.

The parametric results of Yu and Ameel thus show that the entrance length is sensitive to the aspect ratio.

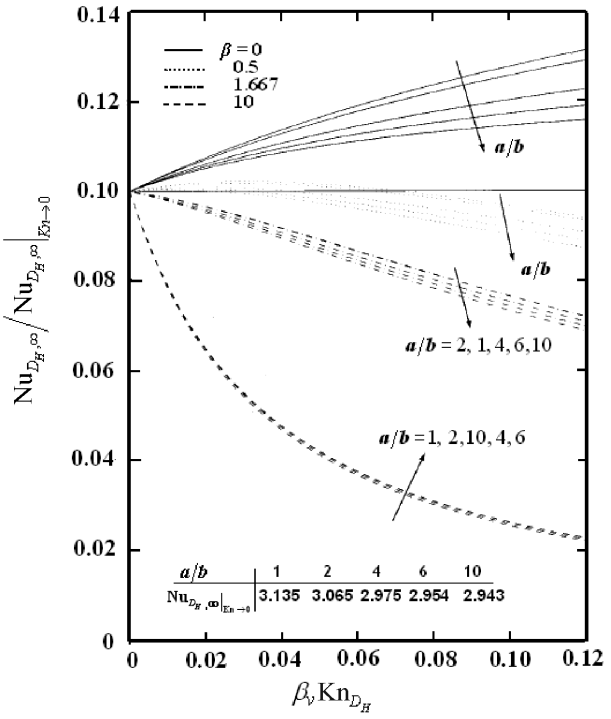

Figure 13.17. Parametric dependencies for thermally developed slip flow in a rectangular channel with UHF boundary conditions (Yu and Ameel, 2002).

We now discuss UHF boundary conditions. Figure 13.17 shows the normalized thermally developed Nusslet number, $\mathrm{Nu}_{D_H,\infty}/\mathrm{Nu}_{D_H,\infty}|_{\mathrm{Kn}\to 0}$, as a function of various parameters (Yu and Ameel, 2002). As in the case of UWT, the heat transfer coefficient at $x = 0$ (the inlet to the heated segment of the tube) is finite because of slip and can be found from Eq. (13.7.16). For the entrance-dominated region, their parametric results indicated that the local Nusselt number $\mathrm{Nu}_{D_H,x}$ depends on $\beta_v \mathrm{Kn}_{D_H}$ in a manner that is qualitatively similar to the UWT case. For small β, $\mathrm{Nu}_{D_H,x}$ increased significantly with increasing $\beta_v \mathrm{Kn}_{D_H}$ (up to 70%). Above a critical value, β_{cr}, the trend was reversed. The magnitude of β_{cr} increased monotonically with the aspect ratio; $\beta_{\mathrm{cr}} = 0.67,\ 0.8,\ 0.81$ for $\alpha^* = 0.2,\ 0.5,\ 1$, respectively.

For very large $\beta_v \mathrm{Kn}_{D_H}$, furthermore, the entrance effect disappears over a short distance and the local Nusselt number can be simply found from

$$\mathrm{Nu}_{D_H,x}(x > 0) \approx \frac{1}{\beta_T \mathrm{Kn}_{D_H}}. \tag{13.7.17}$$

13.8 Slip Flow in Other Noncircular Channels

Duan and Muzychka (2007a) proposed a useful method for estimating the friction factor in microchannels with arbitrary cross-sectional geometry.

The fully developed hydrodynamics of rectangular channels subject to slip flow were discussed in Subsection 13.7.1. From a curve fit to numerical calculations with the solution summarized in Subsection 13.7.1, Duan and Muzychka developed the following empirical correlation:

$$C = 11.97 - 10.59\alpha^* + 8.49\alpha^{*2} - 2.11\alpha^{*3}, \tag{13.8.1}$$

Table 13.4. *Definition of aspect ratio for the correlation of Duan and Muzychka (2007a)*

Geometry	Aspect Ratio, α^*	Definitions
Regular polygons	1	
Rectangle	b/a	a = half the longer side; b = half the shorter side
Trapezoid and double trapezoid	$\dfrac{2b}{a+c}$	a = half the longer base; c = half the shorter base b = half the height
Annular sector	$\dfrac{1-(R_i/R_0)}{[1+(R_i/R_0)]\phi}$	R_i = inner radius; R_0 = outer radius ϕ = half angle (in radians)
Circular annulus	$\dfrac{1-(R_i/R_0)}{[1+(R_i/R_0)]\pi}$	R_i = inner radius; R_0 = outer radius

where α^* is the aspect ratio and C is a constant to be used in

$$\frac{\mathrm{Po}}{\mathrm{Po}|_{\mathrm{Kn}\to 0}} = \frac{C_f \mathrm{Re}_{D_H}}{(C_f \mathrm{Re}_{D_H})|_{\mathrm{Kn}\to 0}} = \frac{1}{1 + C\beta_v \mathrm{Kn}_{D_H}}. \tag{13.8.2}$$

This equation is similar to Eqs. (13.5.7) and (13.6.10), in which obviously $C = 8$ for a circular channel and $C = 12$ for a flat channel (flow between two parallel plates). Using a similar approach, Duan and Muzychka derived the following expression for slip flow in an elliptic channel:

$$C = 12.53 - 9.41\alpha^* + 4.87\alpha^{*2}, \tag{13.8.3}$$

where α^* is now the ratio between the shorter and longer axes. This expression can be used as an approximation for several other channel cross sections provided that α^* is found from Table 13.4.

As discussed earlier in Section 4.6, for common, no-slip flows, Muzychka and Yovanovich (2004) proposed using the square root of the cross-sectional area of channels as the length scale in developing empirical correlations that would be applicable to channels with arbitrary cross-sectional geometry. Following the same concept, we can write for slip flow (Duan and Muzychka, 2007a)

$$\frac{C_f \mathrm{Re}_{\sqrt{A}}}{(C_f \mathrm{Re}_{\sqrt{A}})|_{\mathrm{Kn}\to 0}} = \frac{1}{1 + C\beta_v \mathrm{Kn}_{D_H}}, \tag{13.8.4}$$

which is similar to Eq. (13.8.2), except for the length scale in the definition of the Reynolds number. The constant C is found from Eq. (13.8.1) and the aspect ratio α^* should be found from Table 13.4. The calculations of Duan and Muzychka showed that their proposed method has a maximum deviation from exact solutions that is less than 10%.

13.9 Compressible Flow in Microchannels with Negligible Rarefaction

13.9.1 General Remarks

Compressibility can play an important role in gas flow in microchannels, as noted earlier. Density variations can result from variations in pressure, temperature, or both. The contribution of pressure can in particular be quite significant.

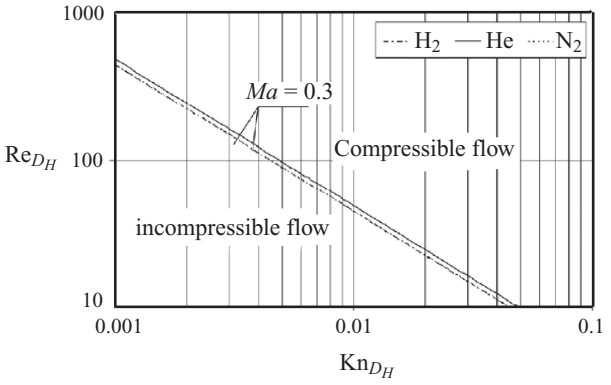

Figure 13.18. The threshold of the validity of the incompressible assumption for ideal-gas flow in channels (Morini et al., 2004).

As mentioned earlier (see Section 13.2), the velocity slip and temperature jump can be neglected with $\mathrm{Kn}_{D_H} \lesssim 10^{-3}$. For microchannel applications with moderate and high gas pressures, this criterion implies that channels with $D_H \gtrsim 40$ μm can be comfortably treated by neglecting velocity slip and temperature jump. For this type of gas flow, density variations that are due to pressure and temperature are both important. We can then model these flows by using the compressible, 1D gas flow theory.

Let us recast Eq. (13.2.4) as

$$\mathrm{Re}_{D_H} = \sqrt{\frac{\pi\gamma}{2}}\frac{Ma}{\mathrm{Kn}_{D_H}}, \tag{13.9.1}$$

where $\mathrm{Re} = \rho U_m D_H/\mu$. This equation provides a relatively simple way for determining the conditions in which compressibility is important. If we use the common practice of assuming that the effect of compressibility is negligible when $Ma < 0.3$, then Fig. 13.18 can be plotted (Morini et al., 2004), in which the curves representing $Ma = 0.3$ divide the entire diagram into compressible and incompressible flow zones. Clearly the validity of the assumption of incompressible flow depends on Kn_{D_H} and Re_{D_H} both. With increasing Kn_{D_H}, the threshold of Re_{D_H} above which compressibility becomes significant decreases. Thus for microchannels the incompressible flow assumption is valid at only very low Reynolds numbers.

In the forthcoming section we discuss microchannel flows for which compressibility is important and velocity slip is negligible.

13.9.2 One-Dimensional Compressible Flow of an Ideal Gas in a Constant-Cross-Section Channel

Consider 1D, steady flow along a channel of uniform cross section (Fig. 13.19). Furthermore, assume that heat conduction in the fluid in the axial direction is

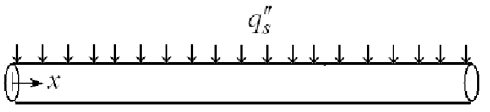

Figure 13.19. Steady 1D flow in a uniform cross-section channel.

negligible. The mass, momentum, and energy conservation equations can then be written as

$$\rho U_m = G = \text{const.}, \tag{13.9.2}$$

$$\rho U_m \frac{dU_m}{dx} = -\frac{dP}{dx} - \frac{p_f}{A}\tau_s + \rho g_x, \tag{13.9.3}$$

$$\rho C_P U_m \frac{dT}{dx} = U_m \frac{dP}{dx} + \frac{p_f}{A}\tau_s U_m + \frac{p_f}{A} q_s'', \tag{13.9.4}$$

where $\tau_s = C_f \frac{1}{2}\rho U_m^2$ and p_f represents the flow-passage wetted perimeter. The wetted perimeter is assumed to be equal to the heated perimeter here. Because $\rho = \rho\,(P, T)$, then Eq. (13.9.2) can be recast as

$$\rho \frac{dU_m}{dx} + U_m \left[\left(\frac{\partial \rho}{\partial P} \right)_T \frac{dP}{dx} + \left(\frac{\partial \rho}{\partial T} \right)_P \frac{dT}{dx} \right] = 0. \tag{13.9.5}$$

Equations (13.9.5), (13.9.3), and (13.9.4) can then be cast as

$$\boldsymbol{A} \frac{d\boldsymbol{Y}}{dx} = \boldsymbol{C}, \tag{13.9.6}$$

where $\boldsymbol{Y}$ is a column vector containing the state variables:

$$\boldsymbol{Y} = (U_m,\ P,\ T)^T. \tag{13.9.7}$$

Also $\boldsymbol{C}$ is a column vector, whose elements are

$$C_1 = 0,$$

$$C_2 = -\frac{p_f}{A}\tau_s + \rho g_x,$$

$$C_3 = \frac{p_f}{A}\tau_s U_m + \frac{p_f}{A} q_s''.$$

The elements of the coefficient matrix $\boldsymbol{A}$ are

$$A_{1,1} = \rho,\ A_{1,2} = U_m \left(\frac{\partial \rho}{\partial P} \right)_T,\ A_{1,3} = U_m \left(\frac{\partial \rho}{\partial T} \right)_P,$$

$$A_{2,1} = \rho\, U_m,\ A_{2,2} = 1,\ A_{2,3} = 0,$$

$$A_{3,1} = 0,\ A_{3,2} = -\,U_m,\ A_{3,3} = \rho\, C_P U_m.$$

The system of ODEs represented by Eq. (13.9.6) needs closure relations for the friction factor and the equation of state. The set of equations can then be easily integrated by one of a number of efficient and robust integration packages, including LSODE or LSODI (Hindmarsh, 1980; Sohn et al., 1985) and *stiff* and *stifbs* algorithms in *Numerical Recipes* (Press et al., 1992).

When the fluid is an ideal gas, then the speed of sound and the Mach number will be, respectively,

$$a = \sqrt{(dP/d\rho)_s} = \sqrt{\gamma\,(R_u/M)\,T}, \tag{13.9.8}$$

$$Ma = \frac{U_m}{a} = \frac{U_m}{\sqrt{\gamma\,(R_u/M)\,T}}. \tag{13.9.9}$$

If it is also assumed that $C_P = \text{const}$; then noting that, for ideal gases, $C_P - C_V = R_u/M$, we can easily show that

$$\boldsymbol{h} = \frac{\gamma}{\gamma - 1}\,(R_u/M)\,T, \tag{13.9.10a}$$

$$Ma = \frac{U_m}{\sqrt{(\gamma - 1)\,\boldsymbol{h}_m}}. \tag{13.9.10b}$$

For adiabatic flow in a uniform cross-section channel, when the effect of gravity is neglected, the differential conservation equations in Eq. (13.9.6) can also be cast in the following form:

$$\rho dU_m + U_m d\rho = 0, \tag{13.9.11}$$

$$dP + \frac{p_f}{A}\tau_s dx + \rho U_m dU_m = 0, \tag{13.9.12}$$

$$h_m + \frac{1}{2}U_m^2 = \boldsymbol{h}_0, \tag{13.9.13}$$

where $\boldsymbol{h}_0$ is the stagnation enthalpy. [Note that Eq. (13.9.4) represents the thermal energy equation, whereas Eq. (13.9.13) represents the total energy conservation equation.] Equation (13.9.13) can be rewritten as

$$C_P dT + U_m dU_m = 0. \tag{13.9.14}$$

Equations (13.9.11), (13.9.12), and (13.9.14) define the well-known Fanno flow. Using the ideal-gas equation of state, along with the preceding equations, it can be shown that,

$$\frac{dP}{dx} = -P\gamma Ma^2 \frac{1 + (\gamma - 1)\,Ma^2}{2\,(1 - Ma^2)} \frac{p_f}{A} C_f, \tag{13.9.15}$$

$$\frac{d\rho}{dx} = -\rho \frac{\gamma Ma^2}{2\,(1 - Ma^2)} \frac{p_f}{A} C_f, \tag{13.9.16}$$

$$\frac{dT}{dx} = -T \frac{\gamma\,(\gamma - 1)\,Ma^4}{2\,(1 - Ma^2)} \frac{p_f}{A} C_f, \tag{13.9.17}$$

$$\frac{d\,Ma^2}{dx} = \gamma Ma^4 \frac{1 + \dfrac{\gamma - 1}{2} Ma^2}{1 - Ma^2} \frac{p_f}{A} C_f. \tag{13.9.18}$$

Equation (13.9.18) can also be recast as

$$\frac{(1 - Ma^2)\,d\,Ma^2}{\gamma Ma^4 \left[1 + \dfrac{\gamma - 1}{2} Ma^2\right]} = \frac{p_f}{A} C_f\,dx. \tag{13.9.19}$$

This equation shows that, for a subsonic Fanno flow ($Ma < 1$), the Mach number increases with x, and if the channel is long enough, eventually $Ma = 1$ is reached, at which point the channel will be choked. We can find the distance to the point at which choking is encountered by applying $\int_{Ma}^{1}$ to the left-hand side and $\int_0^{l^*}$ to the right-hand side of Eq. (13.9.19). The length l^* will be the distance from the point

where the Mach number is equal to Ma to the point at which a Mach number of unity is achieved. These integrations give

$$\frac{p_f}{A}\overline{C}_f l^* = \frac{1-Ma^2}{\gamma Ma^2} + \frac{\gamma+1}{2\gamma}\ln\left[\frac{(\gamma+1)\,Ma^2}{2\left(1+\frac{\gamma-1}{2}Ma^2\right)}\right], \tag{13.9.20}$$

where $\overline{C}_f$ is the mean friction factor along the channel. This equation shows that $\frac{p_f}{A}\overline{C}_f l^*$ depends on Ma and γ only. The distance l for the Mach number to vary from Ma_1 to Ma_2 can then be found from

$$\frac{p_f}{A}\overline{C}_f l = \left(\frac{p_f}{A}\overline{C}_f l^*\right)_{Ma_1} - \left(\frac{p_f}{A}\overline{C}_f l^*\right)_{Ma_2}. \tag{13.9.21}$$

Asako et al. (2003) analyzed the compressible flow in a flat channel (flow between two parallel plates) with the channel height in the range $2b = 10$–100 μm, where rarefaction was negligible, using the direct simulation Monte Carlo (DSMC) method. They noted that the velocity profile was parabolic and was essentially the same as the profile in a 2D channel carrying an incompressible fluid. The Fanning friction factor, however, conformed to the following correlation:

$$C_f \mathrm{Re}_{D_H} = 24.00 + 2.043Ma + 14.893Ma^2. \tag{13.9.22}$$

This correlation was found to agree with experimental data (Turner et al., 2004).

The effect of compressibility in the continuum and slip flow regimes was investigated (Tang et al., 2007; Fan and Luo 2008). These investigations confirm that, in comparison with macroscale models and correlations, in general, compressibility increases the friction factor, whereas rarefaction reduces it.

13.10 Continuum Flow in Miniature Flow Passages

When gas flow at moderate and high pressures is considered, channels with hydraulic diameters larger than about 100 μm conform to continuum treatment with no-slip conditions at solid surfaces. For liquid flow, as mentioned earlier, continuum treatment and no-slip conditions apply to much smaller channel sizes.

Single-phase flow and heat transfer in millimeter and submillimeter channels were studied rather extensively in the recent past. Useful recent reviews include those of Morini et al. (2004) and Bayraktar and Pidugu (2006) and the textbook by Liou and Fang (2006). Flow channels within this size range have widespread application in miniature heat exchangers, boilers, and condensers. Although for these channels there is no breakdown of continuum, and velocity slip and temperature jump are negligibly small, some of the past investigators reported that these channels behave differently from larger channels.

Some investigators reported that well-established correlations for pressure drop and heat transfer and for laminar-to-turbulent flow transition deviate from the measured data obtained with these channels, suggesting the existence of unknown scale effects. It was also noted, however, that the apparent disagreement between conventional models and correlations on one hand and microchannel data on the other hand was relatively minor, indicating that conventional methods can be used at

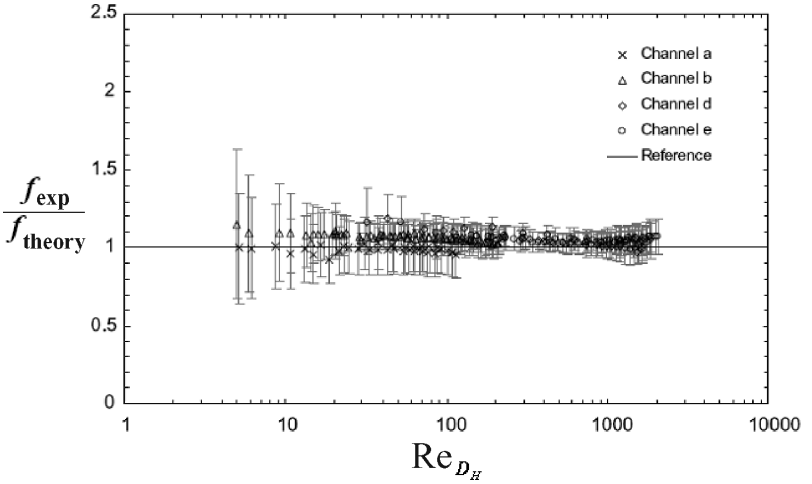

Figure 13.20. Comparison of the water data of Kohl et al. (2005) with laminar incompressible flow theory (after Kohl et al., 2005).

least for approximate microchannel analysis. Basic theory does not explain the existence of an intrinsic scale effect, however. (After all, the Navier–Stokes equations apply to these flow channels as well.) The identification of the mechanisms responsible for the reported differences between conventional channels and microchannels and the development of predictive methods for microchannels remain the foci of research.

There is now sufficient evidence that proves that in laminar flow the conventional theory agrees with microchannel data well and that the differences reported by some investigators in the past were likely due to experimental errors and misinterpretations (Herwig and Hausner, 2003; Sharp and Adrian, 2004; Tiselj et al., 2004; Kohl et al., 2005). Figures 13.20 and 13.21 depict the experimental results of Kohl et al. (2005). They measured the pressure drop, and from there the friction factor, for water and air flow in rectangular channels with $D_H = 25 \sim 100\mu$m, carefully accounting for the effects of flow development and compressibility (for experiments with air). Some experimental investigations also reported that the laminar–turbulent transition in microchannels occurred at a considerably lower Reynolds number than in conventional channels (Wu and Little, 1983; Stanley et al., 1997). The experiments by Kohl et al. (2005) clearly showed that laminar flow theory predicts their measured wall friction data very well, at least for $\mathrm{Re}_D \leq 2000$, where Re_D is the channel Reynolds number, thus supporting the standard practice in which laminar–turbulent transition is assumed to occur at $\mathrm{Re}_D \approx 2300$. Sharp and Adrian (2004) also reported that laminar to turbulent transition occurred in their experiments at $\mathrm{Re}_D \approx 1800$–$2000$.

With respect to turbulent flow, the situation is less clear. Measured heat transfer coefficients by some investigators were lower than what conventional correlations predict (Peng and Wang, 1994, 1998; Peng and Peterson, 1996), whereas an opposite trend was reported by others (Choi et al., 1991; Yu et al., 1995; Adams et al., 1997, 1999). Nevertheless, the disagreement between conventional correlations and

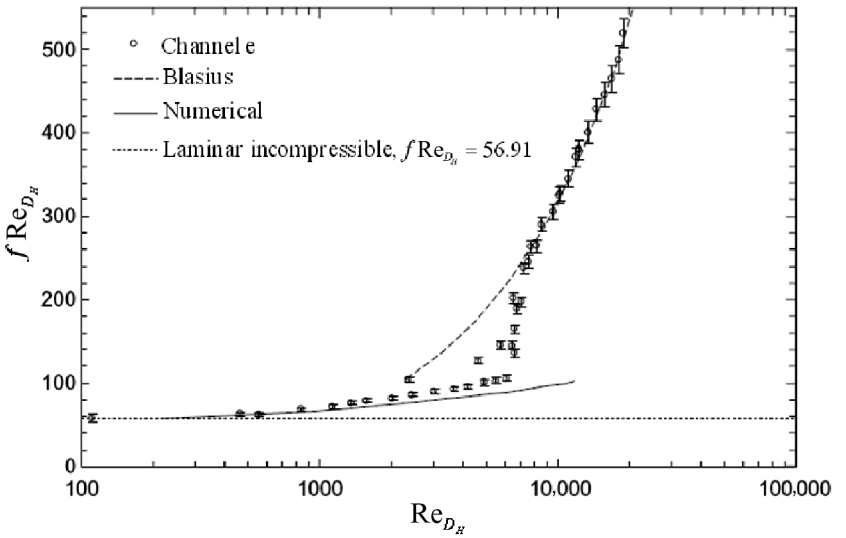

Figure 13.21. The data of Kohl et al. (2005) for air flow in a rectangular channel with $D_H = 99.8$ μm. The dotted horizontal line represents $f\,\mathrm{Re} = 56.91$, which is the incompressible analytical prediction. The solid line is based on laminar flow numerical predictions that account for compressibility (after Kohl et al., 2005).

microchannel experimental data are relatively small, and the discrepancy is typically less than a factor of 2.

The following factors should be considered when the behaviors of microchannels and conventional channels are compared.

1. Surface roughness and other configurational irregularities: The relative magnitudes of surface roughness in microchannels can be significantly larger than those of large channels. Also, at least for some manufacturing methods (e.g., electron discharge machining), the cross-sectional geometry of a microchannel may slightly vary from one point to another.
2. Surface forces: Electrokinetic forces, i.e., forces arising because of the electric double layer, can develop during the flow of a weak electrolyte (e.g., aqueous solutions with weak ionic concentrations), and these forces can modify the channel hydrodynamics and heat transfer (Yang et al., 2001; Tang et al., 2004). Detailed discussion of these forces can be found in a useful recent textbook (Liou and Fag, 2006).
3. Fouling and deposition of suspended particles: The phenomena can change surface characteristics, smooth sharp corners, and cause local partial flow blockages.
4. Compressibility: This is an issue for gas flows. Large local pressure and temperature gradients are common in microchannels. As a result, in gas flow, fully developed hydrodynamics does not occur.
5. Conjugate heat transfer effects: Axial conduction in the fluid as well as heat conduction in the solid structure surrounding the channels can be important in microchannel systems. As a result, the local heat fluxes and transfer coefficients sometimes cannot be determined without a conjugate heat transfer analysis of the entire flow field and its surrounding solid structure system. Neglecting the

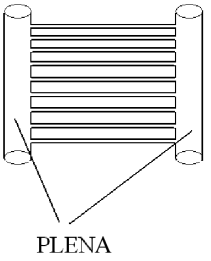

Figure 13.22. Schematic of a system composed of parallel channels connected to common plenums at their two ends.

conjugate heat transfer effects can lead to misinterpretation of experimental data (Herwig and Hausner, 2003; Tiselj et al., 2004).

6. Dissolved gases: In heat transfer experiments with liquids, unless the liquid is effectively degassed, dissolved noncondensables will be released from the liquid as a result of depressurization and heating. The released gases, although typically small in quantity (water that is saturated with atmospheric air at room temperature contains about 10 ppm of dissolved air), can affect the heat transfer by increasing the mean velocity, disrupting the liquid velocity profile, and disrupting the thermal boundary layer on the wall (Adams et al., 1999).
7. Suspended particles: Microscopic particles that are of little consequence in conventional systems can potentially affect the behavior of turbulent eddies in microchannels (Ghiaasiaan and Laker, 2001).

In addition to these issues, the subject of flow and heat transfer in parallel channels connected to common plena or headers at their two ends should be mentioned. Figure 13.22 is a schematic of such a system. Although a thermal system composed of independent single channels is in theory superior to a system similar to Fig. 13.22, in practice the majority of thermal delivery systems will be similar to the latter figure. A thermal system composed of stand-alone single channels is much more difficult to construct and assemble and, more important, may require a separate flow control for each individual channel. A thermal delivery system composed of parallel channels connected to common plena or headers, in contrast, is considerably simpler to build and requires fewer flow control devices. This convenience comes at the price of several generally unfavorable consequences, including

1. dissimilar channels, arising from variances during construction and assembly;
2. nonuniform heating;
3. nonuniformity of flow distribution among the channels; and
4. flow oscillations, which result from dynamic coupling among the channels and plena.

These issues become particularly important when phase changes (evaporation or condensation) occur in the system (Ghiaasiaan, 2008). As a result of these issues, measurements performed in a system composed of parallel channels may not always agree with the same measurements when done in a single channel. The thermal analysis of systems composed of parallel channels should thus consider these issues.

A good example in which the effects of conjugate heat transfer and axial conduction in the fluid can be very clearly seen is the study of Tiselj et al. (2004),

whose test module included 17 parallel triangular microchannels with a hydraulic diameter of 160 μm. The channels were 15 mm long. Heating was provided by a 10 mm × 10 mm thin-film electric resistor that was deposited upon the substrate. Their experimental data covered laminar water flow in the $3.2 < \mathrm{Re} < 64$ range. To analyze their data, they performed a conjugate heat transfer analysis by numerically solving the conservation equations for the coolant fluid as well as for the heat conduction in the solid structure of the test module.

Their results showed that the heat flux did not resemble UHF boundary conditions. More interesting, although near the channel inlet the heat flux was positive from the solid to the fluid, near the exit of the channels the heat transfer took place in the opposite direction. The main cause of this trend was the heat conduction in the solid structure in the axial direction.

In summary, for single-phase laminar flow in minichannels and microchannels in which the breakdown of continuum or velocity slip and temperature jump are not significant, and in which surface electrokinetic and other forces are negligible, the conventional models and correlations are adequate. Transition from laminar to turbulent flow can also be assumed to occur under conditions similar to those in conventional systems. Furthermore, conventional turbulent flow correlations may also be utilized for minichannels and microchannels provided that the uncertainty with respect to the accuracy of such correlations with respect to minichannels and microchannels is considered.

A word of caution should be made about the field of microfluidics: The field is developmental and not yet well understood. This is particularly true about liquid flow in microfluidic devices in which extremely small Reynolds numbers ($\mathrm{Re}_l \lesssim 1$) are encountered and the surface forces resulting from intermolecular forces can be very significant.

EXAMPLE 13.1. Consider a porous metallic sheet that separates a vessel containing pressurized helium from a slightly vacuumed vessel containing air. The entire system is at 300 K temperature. The pores can be idealized as cylindrical channels. For helium pressures of 100 kPa, estimate the diameter of the pores for the following thresholds:

(a) continuum with negligible slip at walls,
(b) continuum with slip at walls,
(c) free molecular flow.

SOLUTION. Let us consider the flow of helium only and the find properties of helium that will be needed. For helium at 300 K we have

$$\mu = 1.99 \times 10^{-5}\,\mathrm{kg/m\,s}.$$

Also, because the flow takes place from a vessel at near-atmospheric pressure into a slightly vacuumed vessel, an average pressure of 100 kPa for the pores is reasonable. At this pressure and 300 K temperature, we have

$$\rho = 0.160\,\mathrm{kg/m^3}\,.$$

The molecular mean free path for helium is therefore

$$\lambda_{\text{mol}} = \nu \left(\frac{\pi M}{2 R_u T} \right)^{1/2} = \frac{(1.99 \times 10^{-5} \text{kg/m s})}{(0.160 \text{ kg/m}^3)} \left[\frac{\pi \, (4 \text{ kg/kmol})}{2 \, (8314.3 \text{ J/kmol K}) \, (300 \text{ K})} \right]^{1/2}$$

$$= 1.97 \times 10^{-7} \text{ m},$$

$$= 0.197 \, \mu\text{m}.$$

The lowest pore diameter for which the assumption of continuum without velocity slip and temperature jump would be acceptable is then

$$\text{Kn}_{D,\text{continuum}} = \left(\frac{\lambda_{\text{mol}}}{D} \right)_{\text{continuum}} < 10^{-3} \Rightarrow D_{\text{min,continuum}} = \frac{\lambda_{\text{mol}}}{10^{-3}}$$

$$= 197 \, \mu\text{m} = 0.197 \text{ mm}.$$

Continnum fluid without velocity slip and temperature jump can be assumed for $D > D_{\text{min,continuum}}$.

The lower limit of the Knudsen number for the velocity slip and temperature jump is 0.1; therefore,

$$\text{Kn}_{D,\text{slip}} = \frac{\lambda_{\text{mol}}}{D_{\text{slip}}} > 10^{-1} \Rightarrow D_{\text{min,slip}} = \frac{\lambda_{\text{mol}}}{10^{-1}} = 1.97 \, \mu\text{m}.$$

A velocity slip and temperature-jump regime can thus be assumed when

$$D_{\text{min,slip}} < D < D_{\text{min,continuum}}.$$

Finally, free molecular flow can be assumed when $\text{Kn}_D > 10$; therefore,

$$\text{Kn}_{D,\text{free molecular flow}} = \frac{\lambda_{\text{mol}}}{D_{\text{free molecular flow}}} > 10 \Rightarrow D_{\text{max,free molecular flow}}$$

$$= \frac{\lambda_{\text{mol}}}{10} = 0.0197 \, \mu\text{m}.$$

We will have a free molecular flow of helium if the diameter of a pore is smaller than about 0.02 μm.

EXAMPLE 13.2. Air at a pressure of 5 bars is maintained in a vessel whose wall is made of a 2-mm-thick metallic sheet. Outside the vessel is atmospheric air at 1-bar pressure and 300 K temperature. A crack develops in the vessel wall. The crack is 2 cm long and 12 μm in width. The entire system can be assumed to be in thermal equilibrium.

(a) Determine the flow regime of the gas that leaks through the crack.
(b) Determine the leakage rate in kilograms per second.

SOLUTION. First, let us find the average properties for air, using 300 K and 3-bars pressure:

$$\rho = 3.484 \text{ kg/m}^3, \; \overline{\mu} = 1.86 \times 10^{-5} \text{ kg/m s}$$

We can now calculate the molecular mean free path and Kn_{2b}:

$$\overline{\lambda}_{\mathrm{mol}} = \overline{\nu}\left(\frac{\pi M}{2R_uT}\right)^{1/2} = \frac{(1.86\times10^{-5}\,\mathrm{kg/m\,s})}{(3.48\,\mathrm{kg/m^3})}\left[\frac{\pi\,(29\,\mathrm{kg/kmol})}{2\,(8314.3\,\mathrm{J/kmol\,K})\,(300\,\mathrm{K})}\right]^{1/2}$$

$$= 2.28\times10^{-8}\,\mathrm{m} = 0.0228\,\mu\mathrm{m},$$

$$\mathrm{Kn}_{2b} = \frac{\lambda_{\mathrm{mol}}}{2b} = \frac{(0.0228\,\mu\mathrm{m})}{(12\,\mu\mathrm{m})} = 0.0019.$$

The flow regime is thus slip flow. Because the aspect ratio of the crack cross section is extremely small ($\alpha^* = \frac{12\,\mu\mathrm{m}}{2\,\mathrm{cm}} = 6\times10^{-4}$), we idealize the flow as flow through a flat channel. We therefore use Eqs. (13.5.10) and (13.5.11). First, let us calculate the Knudsen number representing the crack's exit conditions. Because the temperature is constant, viscosity will remain constant and equal to $\overline{\mu}$. The density, however, will be $\rho_{\mathrm{ex}} = 1.161\,\mathrm{kg/m^3}$. Therefore,

$$\lambda_{\mathrm{mol,ex}} = \nu_{\mathrm{ex}}\left(\frac{\pi M}{2R_uT}\right)^{1/2} = \frac{(1.86\times10^{-5}\,\mathrm{kg/m\,s})}{(1.161\,\mathrm{kg/m^3})}\left[\frac{\pi\,(29\,\mathrm{kg/kmol})}{2\,(8314.3\,\mathrm{J/kmol\,K})\,(300\,\mathrm{K})}\right]^{1/2}$$

$$= 6.83\times10^{-8}\,\mathrm{m} = 0.0683\,\mu\mathrm{m},$$

$$\mathrm{Kn}_{2b,\mathrm{ex}} = \frac{\lambda_{\mathrm{mol,ex}}}{2b} = \frac{(0.0683\,\mu\mathrm{m})}{(12\,\mu\mathrm{m})} = 0.0057.$$

We can now use Eq. (13.5.11) to find the mass flow rate when velocity slip is neglected:

$$\dot{m}|_{\mathrm{Kn}\to0} = \frac{1}{3}\frac{b^3P_{\mathrm{ex}}^2W}{\mu l\,(R_u/M)\,T_{\mathrm{ex}}}\left(\left[\frac{P_{\mathrm{in}}}{P_{\mathrm{ex}}}\right]^2-1\right)$$

$$= \frac{1}{3}\frac{\left(6\times10^{-6}\,\mathrm{m}\right)^3\left(10^5\,\mathrm{N/m^2}\right)^2(0.02\,\mathrm{m})}{(1.86\times10^{-5}\,\mathrm{kg/m\,s})\,(2\times10^{-3}\,\mathrm{m})\left[\frac{8314.3\,\mathrm{J/kmol\,K}}{29\,\mathrm{kg/kmol}}\right](300\,\mathrm{K})}\left(\left[\frac{5\,\mathrm{bars}}{1\,\mathrm{bar}}\right]^2-1\right)$$

$$= 1.082\times10^{-4}\,\mathrm{kg/s}.$$

We can now calculate the mass flow rate from Eq. (13.5.10):

$$\dot{m} = \dot{m}|_{\mathrm{Kn}\to0}\left\{1+\frac{12\,\mathrm{Kn}_{2b,\mathrm{ex}}}{\frac{P_{\mathrm{in}}}{P_{\mathrm{ex}}}+1}\right\} = (1.082\times10^{-4}\,\mathrm{kg/s})\left\{1+\frac{(12)(0.0057)}{\frac{5\,\mathrm{bars}}{1\,\mathrm{bar}}+1}\right\}$$

$$= 1.094\times10^{-4}\,\mathrm{kg/s}.$$

EXAMPLE 13.3. For the system described in Example 13.2, assume that the air inside the container is at 298 K but the vessel wall is heated because of solar radiation. The temperature of air that flows out of the crack is 302 K. Using a constant-wall-heat-flux assumption as an approximation for the crack boundary conditions, estimate the temperature of the crack surface. Assume

that both the momentum and thermal accommodation coefficients are equal to 0.85.

SOLUTION. As an approximation, we can use the results of Example 13.2 for gas properties, given that the average pressure and temperature in the flow channel are the same in the two examples. Let us calculate the following thermophysical properties for air at 300 K:

$$C_P = 1005\,\text{J/kg K}, \quad k = 0.02565\,\text{W/m K}, \quad \text{Pr} = 0.728.$$

We will also perform an analysis similar to Example 13.2 for calculating the mass flow rate in the crack, except that everywhere $\text{Kn}_{2b,\text{exit}}$ is replaced with $\beta_v \text{Kn}_{2b,\text{exit}}$, where:

$$\beta_v = \frac{2-\alpha}{\alpha} = \frac{2-0.85}{0.85} = 1.353.$$

This analysis will then lead to

$$\dot{m} = \dot{m}|_{\text{Kn}\to 0}\left\{1 + \frac{12\,\text{Kn}_{2b,\text{exit}}\beta_v}{\frac{P_{\text{in}}}{P_{\text{exit}}}+1}\right\} = \left(1.082\times 10^{-4}\,\text{kg/s}\right)\left\{1 + \frac{(12)(0.0057)(1.353)}{\frac{5\,\text{bars}}{1\,\text{bar}}+1}\right\}$$

$$= 1.098\times 10^{-4}\,\text{kg/s}.$$

We can now calculate the wall heat flux in the flow passage by a simple energy balance.

$$\dot{m}C_P\left[T_{m,\text{ex}} - T_{\text{in}}\right] = 2(b+W)lq_s'' \Rightarrow q_s'' = \frac{\dot{m}C_P\left[T_{m,\text{ex}} - T_{\text{in}}\right]}{2\,W\,l}$$

$$= \frac{(1.098\times 10^{-4}\,\text{kg/s})(1005\,\text{J/kg K})(302-298)\text{K}}{(2)\,(0.02\,\text{m})\,(2\times 10^{-3}\,\text{m})}$$

$$= 5.5\times 10^4\,\text{W/m}^2$$

We now estimate the heat transfer coefficient by applying Eq. (13.5.35) for thermally developed flow. First, let us calculate the following two parameters based on average fluid conditions in the crack:

$$\beta\text{Kn}_{2b} = \left(\frac{2-\alpha}{\alpha}\right)\text{Kn}_{2b} = \left(\frac{2-0.85}{0.85}\right)(0.0019) = 0.00257,$$

$$\beta_T\text{Kn}_{2b} = \frac{2-\alpha_{\text{th}}}{\alpha_{\text{th}}}\left(\frac{2\gamma}{\gamma+1}\right)\frac{1}{Pr}\text{Kn}_{2b} = \frac{2-0.85}{0.85}\left(\frac{2\times 1.4}{1.4+1}\right)\frac{1}{0.728}(0.0019)$$

$$= 0.00412.$$

Thus from Eq. (13.5.8) we have

$$\frac{U_s^*}{U_m} = \frac{6\beta_v\,\text{Kn}_{2b}}{1+6\beta_v\,\text{Kn}_{2b}} = \frac{(6)\,(0.00257)}{1+(6)\,(0.00257)} = 0.001518.$$

Equation (13.5.35) then gives

$$\mathrm{Nu}_{D_H,\mathrm{UHF}} = \frac{140/17}{1-\left(\frac{6}{17}\right)\left(\frac{U_s^*}{U_m}\right)+\left(\frac{2}{51}\right)\left(\frac{U_s^*}{U_m}\right)^2+\left(\frac{70}{17}\right)\beta_T \mathrm{Kn}_{2b}}$$

$$= \frac{140/17}{1-\left(\frac{6}{17}\right)(0.01518)+\left(\frac{2}{51}\right)(0.01518)^2+\left(\frac{70}{17}\right)(0.00412)} = 8.14.$$

This value of the Nusselt number can be compared with 8.235, the Nusselt number for no-slip conditions. Velocity slip and temperature jump have obviously reduced the Nusselt number slightly. We can now calculate the heat transfer coefficient and from there the temperature difference between the fluid and the solid surface:

$$h = \mathrm{Nu}_{D_H,\mathrm{UHF}}\frac{k}{D_H} = (8.14)\frac{(0.02565\,\mathrm{W/m\,K})}{24\times10^{-6}\,\mathrm{m}} \approx 8700\,\mathrm{W/m^2\,K},$$

$$(T_s - T_m) = \frac{q_s''}{h_x} = \frac{(55000\,\mathrm{W/m^2})}{8700\,\mathrm{W/m^2\,K}} \approx 6.3\,\mathrm{K}.$$

The crack surface temperature will be approximately 306 K.
These calculations do not consider the important effect of heat conduction in the solid metal. Strong conjugate heat transfer takes place in the crack and its surrounding solid (where convection and conduction heat transfer processes are coupled). Consequently neither the UHF boundary condition assumption nor the UWT boundary condition is realistic. A useful and illustrative discussion of the errors that can result from neglecting the conjugate nature of heat transfer in this type of analysis can be found in Herwig and Hausner (2003) and Tiselj et al. (2004).

EXAMPLE 13.4. Consider the flow of helium in a long rectangular microchannel, where the accommodation coefficients are $\alpha = \alpha_T = 0.65$. The aspect ratio of the cross section of the microchannel is equal to 4, and the shorter side of the cross section is 5 μm. At a location where pressure is equal to 2 bars, the mean velocity is 20 m/s and the mean fluid temperature is equal to 320 K. Calculate the frictional pressure gradient.

SOLUTION. Let us start with the relevant thermophysical properties of helium at 320 K temperature and 2-bars pressure:

$$\mu = 2.07\times10^{-5}\,\mathrm{kg/m\,s}, \quad \rho = 0.301\,\mathrm{kg/m^3}, \quad \mathrm{Pr} = 0.687, \quad \gamma = 1.67.$$

Define a and b as half the long and short sides of the crack. Then,

$$a = 2.5\,\mu\mathrm{m}$$

$$b = \frac{a}{\alpha^*} = \frac{2.5\,\mu\mathrm{m}}{0.25} = 10\,\mu\mathrm{m},$$

$$A = 4ab = 10^{-10}\mathrm{m}^2.$$

The hydraulic diameter is then

$$D_H = \frac{p}{A} = \frac{4(a+b)}{4ab} = 8 \times 10^{-6}\,\text{m}.$$

We can now find the MMFP and the Knudsen number defined based on *2b* as the length scale:

$$\lambda_{\text{mol}} = \nu \left(\frac{\pi M}{2R_u T}\right)^{1/2} = \frac{(2.07 \times 10^{-5}\,\text{kg/m s})}{(0.301\,\text{kg/m}^3)} \left[\frac{\pi(4\,\text{kg/kmol})}{2(8314.3\,\text{J/kmol K})(320\,\text{K})}\right]^{1/2}$$

$$= 1.06 \times 10^{-7}\,\text{m} = 0.106\,\mu\text{m},$$

$$\text{Kn}_{2b} = \frac{\lambda_{\text{mol}}}{2b} = \frac{(0.106\,\mu\text{m})}{2(10\,\mu\text{m})} = 0.0053.$$

Also, we calculate $\beta_v \text{Kn}_{2b}$:

$$\beta_v \text{Kn}_{2b} = \left(\frac{2-\alpha}{\alpha}\right)\text{Kn}_{2b} = \left(\frac{2-0.65}{0.65}\right)(0.0053) = 0.01101.$$

We can now find, from Fig. 13.15 or Eq. (4.3.17), the Poiseuille number when velocity slip is neglected:

$$\text{Po}|_{\text{Kn}\to 0} = \frac{72.931}{4} = 18.23.$$

Using Fig. 13.15, we can now find the Poiseuille number when the velocity slip is considered:

$$\frac{\text{Po}}{\text{Po}|_{\text{Kn}\to 0}} = 0.915 \Rightarrow \text{Po}|_{\text{Kn}\to 0} = 16.68.$$

Knowing Po, we can now find the friction factor:

$$\text{Re}_{D_H} = \rho U_m D_H/\mu = (0.301\,\text{kg/m}^3)(20\,\text{m/s})(8 \times 10^{-6}\,\text{m})/(2.07 \times 10^{-5}\,\text{kg/m s})$$

$$= 2.32,$$

$$C_f \text{Re}_{D_H} = \text{Po} \Rightarrow C_f = \frac{16.68}{2.32} = 7.19.$$

The frictional pressure gradient can now be found:

$$\left(-\frac{dP}{dx}\right)_{\text{fr}} = 4C_f \frac{1}{D_H}\left(\frac{1}{2}\rho U_m^2\right) = (4)(7.19)\frac{1}{(8 \times 10^{-6}\,\text{m})}\left(\frac{1}{2}[0.301\,\text{kg/m}^3][20\,\text{m/s}]^2\right)$$

$$= 2.16 \times 10^8\,\text{Pa/m}.$$

EXAMPLE 13.5. Repeat the solution of Example 13.4, this time using the method of Duan and Muzychka (2007).

SOLUTION. We will use the method described in Section 13.8. First we find the speed of sound and from there the Mach number:

$$a = \sqrt{\gamma(R_u/M)T} = \sqrt{(1.67)\frac{(8314.3\,\text{J/kmol K})}{(4\,\text{kg/kmol})}(320\,\text{K})} = 1054\ \text{m/s},$$

$$Ma = U_m/a = \frac{(20\,\text{m/s})}{(1054\,\text{m/s})} = 0.019.$$

With $\alpha^* = 0.25$, we find from Eq. (13.8.1)

$$C = 11.97 - 10.59\alpha^* + 8.49\alpha^{*2} - 2.11\alpha^{*3} = 9.82.$$

We need to calculate Kn_{D_H}, the Knudsen number defined based on the hydraulic diameter and the corresponding $\beta_v \mathrm{Kn}_{D_H}$:

$$\mathrm{Kn}_{D_H} = \frac{\lambda_{\mathrm{mol}}}{D_H} = \frac{(0.106\,\mu\mathrm{m})}{(8\,\mu\mathrm{m})} = 0.01325,$$

$$\beta_v \mathrm{Kn}_{D_H} = \left(\frac{2-\alpha}{\alpha}\right) \mathrm{Kn}_{D_H} = \left(\frac{2-0.65}{0.65}\right)(0.01325) = 0.0275.$$

The Poiseuille number can now be found from Eq. (13.8.2):

$$\frac{\mathrm{Po}}{\mathrm{Po}|_{\mathrm{Kn}\to 0}} = \frac{1}{1 + C\beta_v \mathrm{Kn}_{D_H}}$$

$$\Rightarrow \mathrm{Po} = (18.23)\,\frac{1}{1 + (9.82)\,(0.0275)} = 14.35.$$

We then follow by writing

$$C_f \mathrm{Re}_{D_H} = \mathrm{Po} \;\Rightarrow C_f = \frac{14.35}{2.32} = 6.19.$$

The frictional pressure gradient can now be found:

$$\left(-\frac{dP}{dx}\right)_{\mathrm{fr}} = 4C_f \frac{1}{D_H}\left(\frac{1}{2}\rho U_m^2\right)$$

$$= (4)\,(6.19)\,\frac{1}{(8 \times 10^{-6}\,\mathrm{m})}\left(\frac{1}{2}\left[0.301\,\mathrm{kg/m^3}\right]\left[20\,\mathrm{m/s}\right]^2\right)$$

$$= 1.86 \times 10^8\,\mathrm{Pa/m}.$$

PROBLEMS

Problem 13.1. Two large parallel plates are separated from one another by 30 μm. The space between the plates is filled with stagnant helium at 0.2-bar pressure. The surface temperature of one plate is 150 °C, and the surface temperature of the other plate is 130 °C.

(a) Is rarefaction important?
(b) Find the temperature distribution in the helium layer and heat transfer rate between the two plates in kilowatts per square meter, considering the rarefaction effect. Calculate the temperature jump at each surface.
(c) Repeat part (b), this time neglecting the effect of rarefaction. Compare the results with the results of part (b).

Problem 13.2. A vertical cylinder with 100-cm outer diameter contains a cryogenic system, and its outer surface is maintained at a temperature of −150 °C. To insulate the cylinder from outside, it is placed in another coaxial cylinder with an inner diameter of 101 cm, and the annular space between the two cylinders is evacuated

to a pressure of 0.1 Pa. A leakage occurs, however, and air pressure in the annulus space reaches 10 Pa. The inner surface of the outer cylinder is 20 °C.

(a) What is the regime in the annulus space before leakage?
(b) After leakage, is rarefaction important?
(c) Assuming that air in the annular space is stagnant, calculate the heat transfer to the inner cylinder, per unit length, after leakage occurs. Calculate the temperature jump at each surface.

For simplicity, neglect the effect of thermal radiation and the effect of gravity.

Problem 13.3. Helium flows through an annular flow passage. The inner and outer diameters of the annulus are 120 and 120.7 cm, respectively. At a particular location, the pressure is 20 Pa, the helium mean temperature and velocity are −110 °C and 15 cm/s, respectively, and the heat flux at the wall surface is $-1247\ \mathrm{W/m^2}$.

Calculate the wall surface temperature, first by neglecting the rarefaction effect, and then by including the effect of rarefaction. Compare the results and discuss the difference between them.

Problem 13.4. Prove Eq. (13.5.36).

Problem 13.5. Consider slip Couette flow with the boundary conditions shown in Fig. 4.1. Derive expressions for the temperature profile and the heat fluxes at the bottom and top boundaries. Compare your results with the solution representing Couette flow without slip.

Problem 13.6. A 1.5-mm-thick plate is to be cooled by gas flow through microchannels with square cross sections. Assuming gas mean temperature and pressure of 300 K and 100 kPa, respectively, estimate the microchannel cross-section size for the following thresholds:

(a) continuum with negligible slip at walls,
(b) continuum with slip at walls,
(c) free molecular flow.

Perform these calculations for air and helium.

Problem 13.7. Atmospheric air, with a temperature of 300 K, flows through an 80-μm-thick porous membrane. The membrane's porosity (total volume fraction of pores) is 25%. The accommodation coefficients have been measured to be $\alpha = 0.79$ and $\alpha_{\mathrm{th}} = 0.24$. The superficial velocity of air through the membrane (velocity calculated based on the total membrane area) is 3.0 m/s. Assume that the pores can be idealized as smooth-walled circular flow passages 5 μm in diameter.

(a) Calculate the total pressure drop across the membrane.
(b) Neglecting heat transfer from the front and back surfaces of the membrane, calculate the thermal load that can be removed by air, in watts per square meter of the membrane, assuming that the air mean temperature reaches 301 K. Estimate the membrane temperature, assuming that the membrane remains isothermal.

Problem 13.8. Repeat the solution of Problem 13.7, this time assuming that the coolant is water and the total mass flux of water through the membrane is equal to the total mass flux of air in parts (a) and (b). Neglect electrokinetic effects.

Problem 13.9. Air, at an inlet pressure of 100 bars and an inlet temperature of 300 K, flows through a long circular-cross-section tube with a constant surface heat flux. The air velocity at the inlet is 10 m/s. Air leaves the tube at a mean temperature of 350 K.

(a) Based on inlet conditions, find the tube diameter that defines the threshold between continuum and slip flow regimes.
(b) Consider a tube whose diameter is 1/2 of the threshold diameter calculated in part (a) and that has a length-to-diameter ratio of 200. Calculate the pressure drop, the total heat transfer rate to the air, and the tube surface temperature at the exit, assuming fully developed flow and neglecting compressibility effect.
(c) Repeat part (b), this time accounting for the effect of air compressibility
(d) Repeat part (b), this time neglecting the rarefaction effect.

Assume that $\alpha = \alpha_{\text{th}} = 1.0$.

Problem 13.10. For fully developed gas flow through a circular pipe in a slip flow regime, show that the second-order velocity slip model of Deissler [Eq. (13.3.3)] leads to

$$U_s^* - U_s = \frac{2-\alpha}{\alpha}\lambda_{\text{mol}}\frac{\tau_s}{\mu} + \frac{27}{16}\lambda_{\text{mol}}^2\frac{\tau_s}{\mu R_0}.$$

Using this relation, show that

$$\frac{\tau_s R_0}{4\mu U_m} = \frac{1}{1 + 4\dfrac{2-\alpha}{\alpha}\dfrac{\lambda_{\text{mol}}}{R_0} + \dfrac{27}{4}\left(\dfrac{\lambda_{\text{mol}}}{R_0}\right)^2}.$$

Problem 13.11. Helium, at an inlet pressure of 10 bars and an inlet temperature of 220 K, flows through a rectangular channel with a very small cross-section aspect ratio and leaves with an average temperature of 245 K. The channel is assumed to be subject to a constant surface heat flux. The helium velocity at the inlet is 5 m/s.

(a) Find the size of the channel that defines the threshold between the continuum and slip flow regimes.
(b) Consider a channel whose hydraulic diameter is 1/2 of the threshold calculated in part (a) and has a length-to-hydraulic-diameter ratio of 150. Calculate the pressure drop and heat flux assuming fully developed flow and neglecting the compressibility effect.
(c) Repeat part (b), this time neglecting the rarefaction effect as well.

Assume $\alpha = \alpha_{\text{th}} = 1.0$.

Problem 13.12. A tank contains nitrogen at 300 K temperature and 1.5-bars pressure. The outside of the tank is a partially vacuumed chamber with a pressure of 3000 Pa at 300 K. The tank wall is made of 1-cm-thick metal. A crack has developed in the tank wall. Estimate the leakage rate of nitrogen assuming that the crack can be idealized as a smooth-walled rectangular channel 50 μm deep and 15 mm wide.

Problem 13.13. Consider the flow of helium in a long rectangular microchannel for which the accommodation coefficients are $\alpha = \alpha_T = 0.65$. The aspect ratio of the

cross section of the microchannel is equal to 2. The microchannel hydraulic diameter is 47 μm. At a location where pressure is equal to 1.2 bars, the Mach number representing the mean helium velocity is equal to 0.02 and the mean fluid temperature is equal to 310 K. Calculate the frictional pressure gradient.

Problem 13.14. Prove Eqs. (13.4.6).

Problem 13.15. Consider the Couette flow depicted in Fig. P13.15. The bottom plate is stationary and adiabatic, and the top plate is moving at the velocity U_1 and is cooled by an ambient fluid that is at temperature T_∞.

(a) Using first-order slip and temperature-jump conditions, and assuming that $\alpha = \alpha_T = 1$, prove that the temperature profile will be

$$T = -\frac{\varphi}{2}y^2 + \frac{kH\varphi}{h_0} + \frac{H^2\varphi}{2} + \frac{2\gamma}{\gamma+1}\frac{\mathrm{Kn}_H}{\mathrm{Pr}}H^2\varphi + T_\infty,$$

where

$$\varphi = \frac{\mu}{k}\left[\frac{U_1}{H(1+2\,\mathrm{Kn}_H)}\right]^2.$$

(b) Prove that

$$\mathrm{Nu}_H = \frac{8(1+2\,\mathrm{Kn}_H)}{1+\frac{8}{3}\mathrm{Kn}_H + \frac{8\gamma}{\gamma+1}\frac{(1+2\,\mathrm{Kn}_H)\,\mathrm{Kn}_H}{\mathrm{Pr}}},$$

where T_m is the mean (mixed-cup) temperature and

$$\mathrm{Nu}_H = \frac{2H}{k}\left(-k\left.\frac{\partial T}{\partial y}\right|_{\mathrm{y=H}}\right)\Big/(T_m - T_1).$$

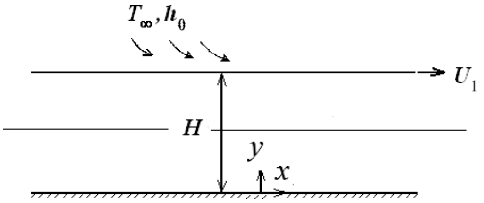

Figure P13.15

Problem 13.16. The analysis in Subsection 13.5.1 assumes symmetric boundary conditions. This assumption does not apply, for example, when the two boundary surfaces are at different temperatures. Consider Fig. P13.16 and assume that

$$u = -\beta_{v,A}\lambda_{\mathrm{mol}}\left(\frac{du}{dy}\right) \quad \text{at } y = b,$$

$$u = \beta_{v,B}\lambda_{\mathrm{mol}}\left(\frac{du}{dy}\right) \quad \text{at } y = -b,$$

where $\beta_{v,A} = \frac{2-\alpha_A}{\alpha_A}$ and $\beta_{v,B} = \frac{2-\alpha_B}{\alpha_B}$.

Derive an expression for $u(y)$. Also, assuming that $P\mathrm{Kn}_{2b} = \text{const.}$ and neglecting density variations that are due to changes in temperature, use that expression to prove that the total mass flow rate will be

$$\dot{m} = \frac{2b^3 P_{\mathrm{ex}}^2}{3\mu l\,(R_u/M)\,T_{\mathrm{ex}}} \left\{ \left(\frac{P_{\mathrm{in}}}{P_{\mathrm{ex}}}\right)^2 - 1 + 6\,(\beta_{v,A} + \beta_{v,B})\,\mathrm{Kn}_{2b,\mathrm{ex}} \left(\frac{P_{\mathrm{in}}}{P_{\mathrm{ex}}} - 1\right) \right.$$

$$\left. - 6\,(\beta_{v,A} - \beta_{v,B})^2\,\mathrm{Kn}_{2b,\mathrm{ex}}^2 \ln \frac{P_{\mathrm{in}} + (\beta_{v,A} + \beta_{v,B})\,P_{\mathrm{ex}}\mathrm{Kn}_{2b,\mathrm{ex}}}{P_{\mathrm{ex}} + (\beta_{v,A} + \beta_{v,B})\,P_{\mathrm{ex}}\mathrm{Kn}_{2b,\mathrm{ex}}} \right\}.$$

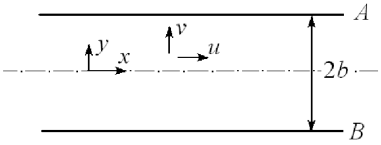

Figure P13.16. Definitions for slip flow in a flat channel with asymmetric boundary conditions.

Problem 13.17. In turbulent flow, particles that are considerably smaller in size than Kolmogorov's microscale have little effect on the turbulent characteristics of the flow, provided that their volume fraction is small. Consider an experiment in which water at room temperature is to flow in a microtube that has an inner diameter of 0.4 mm. Water should flow with a velocity in the 10–20 m/s range. Water is to pass through filters to remove troublesome suspended particles. Determine the maximum particle size that can pass through the filters.

Problem 13.18.

1. Using a programming tool of your choice, prepare a computer code that can interpolate among the data of Table 13.3 for the calculation of the Nusslet number for a thermally developed slip flow in a circular microtube with UWT boundary conditions.
2. Air, at an inlet pressure of 80 kPa and an inlet temperature of 300 K, flows through a long circular-cross-section tube with a surface temperature of 350 K. The air velocity at the inlet is 8 m/s.
   (a) Based on inlet conditions, find the tube diameter that defines the threshold between continuum and slip flow regimes.
   (b) Consider a tube whose diameter is 1/2 of the threshold diameter calculated in part (a) and has a length-to-diameter ratio of 200. Calculate the pressure drop, the total heat transfer rate to the air, and the tube surface temperature at the exit assuming fully developed flow and neglecting the compressibility effect.

Assume that $\alpha = \alpha_{\mathrm{th}} = 1.0$.

Problem 13.19. Consider a micro tube with a diameter of 4 μm, and length of 100 μm. Air, at an inlet pressure of 100 kPa and an inlet temperature of 300 K, flows through the tube. The tube has a constant surface temperature of 375 K. Air velocity at inlet is 180 m/s.

(a) Verify whether the slip flow regime applies.

(b) Plot the variation of the mean air temperature along the tube
(c) Find the distance from the inlet at which the temperature of the air becomes the same as that of the surface. Also calculate the total heat transfer rate and the pressure drop in the tube,

Assume $\alpha = \alpha_{th} = 1.0$. (*Hint:* Use interpolation routine from 13.18)

Problem 13.20. Consider the same tube as the one given in 13.19 but with a constant surface heat flux of 50 kW/m^2 and the same inlet conditions.

(a) Plot the variation of the mean air temperature along the tube
(b) Plot the variation of the surface temperature along the tube
(c) Find the mean air temperature and the tube surface temperature at the exit

For simplicity, assume fully-developed flow and neglect compressibility effects. Assume $\alpha = \alpha_{th} = 1.0$.

Problem 13.21. Repeat problem 13.19 using a computational fluid dynamic program of your choice. Show the temperature vs. length plot and the temperature contour for the center of the pipe.

Problem 13.22. Repeat problem 13.20 using a computational fluid dynamic program of your choice. Show the temperature contour for the center and the surface of the pipe. Also show the temperature vs. length plot for both the center and the surface of the pipe.

Problem 13.23. Consider a square duct with a width and height of 6 μm, and length of 100 μm. Air, at an inlet pressure of 1 bar and an inlet temperature of 300 K, flows through this tube with a constant surface heat flux of 50 kW/m^2. Air velocity at inlet is 180 m/s.

(d) Verify whether the slip flow regime applies to this problem.
(e) Find $\frac{Po}{Po_{Kn\to 0}}$ using Eq. (13.7.15) and Eq. (13.8.1). Compare the results from these equations with Fig. 13.15.
(f) Find the mean temperature of the fluid and duct surface temperature at outlet
(g) Find the heat transfer coefficient, h_{Dh}, if there is a constant surface temperature of 375 K instead of a constant surface heat flux.

Problem 13.24. Consider a rectangular duct with a width of 4 μm and height of 2 μm, and length of 80 μm. Air, at an inlet pressure of 1 bar and an inlet temperature of 300 K, flows through this tube with a constant surface heat flux of 75 kW/m^2. Air velocity at inlet is 150 m/s.

(a) Verify whether the slip flow regime applies to this problem.
(b) Find $\frac{Po}{Po_{Kn\to 0}}$ using Eq. (13.7.15) and Eq. (13.8.1). Compare the results from these equations with Fig. 13.15.
(c) Find the mean temperature of the fluid and duct surface temperature at outlet
(d) Find the heat transfer coefficient, h_{Dh}, if there is a constant surface temperature of 375 K instead of surface heat flux.

Problem 13.25. Repeat problem 13.23 using a computational fluid dynamic program of your choice. Show the temperature vs. length plot and the temperature contour for the center and surface of the duct.

Problem 13.26. Repeat problem 13.24 using a computational fluid dynamic program of your choice. Show the temperature vs. length plot and the temperature contour for the center and surface of the duct.

Problem 13.27. Consider a 10 mm long annular tube of inner radius 300 μm and outer radius 350 μm. Air, at an inlet pressure of 1 kPa and an inlet temperature of 300 K flow through this tube, with no heat transfer taking place. Find the pressure at the outlet of this tube.

APPENDIX A

Constitutive Relations in Polar Cylindrical and Spherical Coordinates

Cylindrical Coordinates (r, θ, z)

Newtonian Law of Viscosity

$$\tau_{rr} = \mu\left(2\frac{\partial u_r}{\partial r}\right) + \lambda\nabla\cdot\vec{U}, \tag{A.1}$$

$$\tau_{\theta\theta} = \mu\left[2\left(\frac{1}{r}\frac{\partial u_\theta}{\partial\theta} + \frac{u_r}{r}\right)\right] + \lambda\nabla\cdot\vec{U}, \tag{A.2}$$

$$\tau_{zz} = \mu\left(2\frac{\partial u_z}{\partial z}\right) + \lambda\nabla\cdot\vec{U}, \tag{A.3}$$

$$\tau_{r\theta} = \tau_{\theta r} = \mu\left[r\frac{\partial}{\partial r}\left(\frac{u_\theta}{r}\right) + \frac{1}{r}\frac{\partial u_r}{\partial\theta}\right], \tag{A.4}$$

$$\tau_{\theta z} = \tau_{z\theta} = \mu\left[\frac{1}{r}\frac{\partial u_z}{\partial\theta} + \frac{\partial u_\theta}{\partial z}\right], \tag{A.5}$$

$$\tau_{zr} = \tau_{rz} = \mu\left[\frac{\partial u_r}{\partial z} + \frac{\partial u_z}{\partial r}\right], \tag{A.6}$$

$$\nabla\cdot\vec{U} = \frac{1}{r}\frac{\partial}{\partial r}(r\,u_r) + \frac{1}{r}\frac{\partial u_\theta}{\partial\theta} + \frac{\partial u_z}{\partial z}. \tag{A.7}$$

Fourier's Law

$$q_r'' = -k\frac{\partial T}{\partial r}, \quad q_\theta'' = -k\frac{1}{r}\frac{\partial T}{\partial\theta}, \quad q_z'' = -k\frac{\partial T}{\partial z}. \tag{A.8}$$

Fick's Law for Binary Diffusion

$$j_{1,r} = -\rho\mathcal{D}_{12}\frac{\partial m_1}{\partial r}, \quad j_{1,\theta} = -\rho\mathcal{D}_{12}\frac{1}{r}\frac{\partial m_1}{\partial\theta}, \quad j_{1,z} = -\rho\mathcal{D}_{12}\frac{\partial m_1}{\partial z}, \tag{A.9}$$

$$J_{1,r} = -\boldsymbol{C}\mathcal{D}_{12}\frac{\partial X_1}{\partial r}, \quad J_{1,\theta} = -\boldsymbol{C}\mathcal{D}_{12}\frac{1}{r}\frac{\partial X_1}{\partial\theta}, \quad J_{1,z} = -\boldsymbol{C}\mathcal{D}_{12}\frac{\partial X_1}{\partial z}. \tag{A.10}$$

Spherical Coordinates (r, θ, $\emptyset$)

Newtonian Law of Viscosity

$$\tau_{rr} = \mu\left(2\frac{\partial u_r}{\partial r}\right) + \lambda\nabla\cdot\vec{U}, \tag{A.11}$$

$$\tau_{\theta\theta} = \mu\left[2\left(\frac{1}{r}\frac{\partial u_\theta}{\partial\theta} + \frac{u_r}{r}\right)\right] + \lambda\nabla\cdot\vec{U}, \tag{A.12}$$

$$\tau_{\phi\phi} = \mu\left[2\left(\frac{1}{r\sin\theta}\frac{\partial u_\phi}{\partial\phi} + \frac{u_r + u_\theta\cot\theta}{r}\right)\right] + \lambda\nabla\cdot\vec{U}, \tag{A.13}$$

$$\tau_{r\theta} = \tau_{\theta r} = \mu\left[r\frac{\partial}{\partial r}\left(\frac{u_\theta}{r}\right) + \frac{1}{r}\frac{\partial u_r}{\partial\theta}\right], \tag{A.14}$$

$$\tau_{\theta\phi} = \tau_{\phi\theta} = \mu\left[\frac{\sin\theta}{r}\frac{\partial}{\partial\theta}\left(\frac{u_\phi}{\sin\theta}\right) + \frac{1}{r\sin\theta}\frac{\partial u_\theta}{\partial\phi}\right], \tag{A.15}$$

$$\tau_{\phi r} = \tau_{r\phi} = \mu\left[\frac{1}{r\sin\theta}\frac{\partial u_r}{\partial\phi} + r\frac{\partial}{\partial r}\left(\frac{u_\phi}{r}\right)\right], \tag{A.16}$$

$$\nabla\cdot\vec{U} = \frac{1}{r^2}\frac{\partial}{\partial r}(r^2 u_r) + \frac{1}{r\sin\theta}\frac{\partial}{\partial\theta}(u_\theta\sin\theta) + \frac{1}{r\sin\theta}\frac{\partial u_\phi}{\partial\phi}. \tag{A.17}$$

Fourier's Law

$$q_r'' = -k\frac{\partial T}{\partial r}, \quad q_\theta'' = -k\frac{1}{r}\frac{\partial T}{\partial\theta}, \quad q_\phi'' = -k\frac{1}{r\sin\theta}\frac{\partial T}{\partial\phi}. \tag{A.18}$$

Fick's Law for Binary Diffusion

$$j_{1,r} = -\rho\mathcal{D}_{12}\frac{\partial m_1}{\partial r}, \quad j_{1,\theta} = -\rho\mathcal{D}_{12}\frac{1}{r}\frac{\partial m_1}{\partial\theta}, \quad j_{1,\phi} = -\rho\mathcal{D}_{12}\frac{1}{r\sin\theta}\frac{\partial m_1}{\partial\phi}, \tag{A.19}$$

$$J_{1,r} = -\boldsymbol{C}\mathcal{D}_{12}\frac{\partial X_1}{\partial r}, \quad J_{1,\theta} = -\boldsymbol{C}\mathcal{D}_{12}\frac{1}{r}\frac{\partial X_1}{\partial\theta}, \quad J_{1,z} = -\boldsymbol{C}\mathcal{D}_{12}\frac{1}{r\sin\theta}\frac{\partial X_1}{\partial\phi}. \tag{A.20}$$

APPENDIX B

Mass Continuity and Newtonian Incompressible Fluid Equations of Motion in Polar Cylindrical and Spherical Coordinates

Cylindrical Coordinates (r, θ, z)

Mass Continuity

$$\frac{\partial \rho}{\partial t} + \frac{1}{r}\frac{\partial}{\partial r}(\rho r u_r) + \frac{1}{r}\frac{\partial}{\partial \theta}(\rho u_\theta) + \frac{\partial}{\partial z}(\rho u_z) = 0. \tag{B.1}$$

Equations of Motion for μ = const.

$$\rho\left(\frac{\partial u_r}{\partial t} + u_r\frac{\partial u_r}{\partial r} + \frac{u_\theta}{r}\frac{\partial u_r}{\partial \theta} + u_z\frac{\partial u_r}{\partial z} - \frac{u_\theta^2}{r}\right)$$
$$= -\frac{\partial P}{\partial r} + \mu\left\{\frac{\partial}{\partial r}\left[\frac{1}{r}\frac{\partial}{\partial r}(r u_r)\right] + \frac{1}{r^2}\frac{\partial^2 u_r}{\partial \theta^2} + \frac{\partial^2 u_r}{\partial z^2} - \frac{2}{r^2}\frac{\partial u_\theta}{\partial \theta}\right\} + \rho g_r, \tag{B.2}$$

$$\rho\left(\frac{\partial u_\theta}{\partial t} + u_r\frac{\partial u_\theta}{\partial r} + \frac{u_\theta}{r}\frac{\partial u_\theta}{\partial \theta} + u_z\frac{\partial u_\theta}{\partial z} + \frac{u_r u_\theta}{r}\right)$$
$$= -\frac{1}{r}\frac{\partial P}{\partial \theta} + \mu\left\{\frac{\partial}{\partial r}\left[\frac{1}{r}\frac{\partial}{\partial r}(r u_\theta)\right] + \frac{1}{r^2}\frac{\partial^2 u_\theta}{\partial \theta^2} + \frac{\partial^2 u_\theta}{\partial z^2} + \frac{2}{r^2}\frac{\partial u_r}{\partial \theta}\right\} + \rho g_\theta, \tag{B.3}$$

$$\rho\left(\frac{\partial u_z}{\partial t} + u_r\frac{\partial u_z}{\partial r} + \frac{u_\theta}{r}\frac{\partial u_z}{\partial \theta} + u_z\frac{\partial u_z}{\partial z}\right)$$
$$= -\frac{\partial P}{\partial z} + \mu\left\{\frac{1}{r}\frac{\partial}{\partial r}\left(r\frac{\partial u_z}{\partial r}\right) + \frac{1}{r^2}\frac{\partial^2 u_z}{\partial \theta^2} + \frac{\partial^2 u_z}{\partial z^2}\right\} + \rho g_z. \tag{B.4}$$

Spherical Coordinates ($r, \theta, \emptyset$)

Mass Continuity

$$\frac{\partial \rho}{\partial t} + \frac{1}{r^2}\frac{\partial}{\partial r}(\rho r^2 u_r) + \frac{1}{r\sin\theta}\frac{\partial}{\partial \theta}(\rho u_\theta \sin\theta) + \frac{1}{r\sin\theta}\frac{\partial}{\partial \phi}(\rho u_\phi) = 0. \tag{B.5}$$

Equations of Motion for μ = const.

$$\rho\left(\frac{\partial u_r}{\partial t}+u_r\frac{\partial u_r}{\partial r}+\frac{u_\theta}{r}\frac{\partial u_r}{\partial \theta}+\frac{u_\phi}{r\sin\theta}\frac{\partial u_r}{\partial \phi}-\frac{u_\theta^2+u_\phi^2}{r}\right)$$
$$=-\frac{\partial P}{\partial r}+\mu\left\{\frac{1}{r^2}\frac{\partial^2}{\partial r^2}(r^2u_r)+\frac{1}{r^2\sin\theta}\frac{\partial}{\partial\theta}\left(\sin\theta\frac{\partial u_r}{\partial\theta}\right)+\frac{1}{r^2\sin^2\theta}\frac{\partial^2 u_r}{\partial\phi^2}\right\}+\rho g_r, \tag{B.6}$$

$$\rho\left(\frac{\partial u_\theta}{\partial t}+u_r\frac{\partial u_\theta}{\partial r}+\frac{u_\theta}{r}\frac{\partial u_\theta}{\partial \theta}+\frac{u_\phi}{r\sin\theta}\frac{\partial u_\theta}{\partial \phi}+\frac{u_r u_\theta-u_\phi^2\cot\theta}{r}\right)$$
$$=-\frac{1}{r}\frac{\partial P}{\partial\theta}+\mu\left\{\frac{1}{r^2}\frac{\partial}{\partial r}\left(r^2\frac{\partial u_\theta}{\partial r}\right)+\frac{1}{r^2}\frac{\partial}{\partial\theta}\left[\frac{1}{\sin\theta}\frac{\partial}{\partial\theta}(u_\theta\sin\theta)\right]\right.$$
$$\left.+\frac{1}{r^2\sin^2\theta}\frac{\partial^2 u_\theta}{\partial\phi^2}+\frac{2}{r^2}\frac{\partial u_r}{\partial\theta}-\frac{2\cot\theta}{r^2\sin\theta}\frac{\partial u_\phi}{\partial\phi}\right\}+\rho g_\theta. \tag{B.7}$$

$$\rho\left(\frac{\partial u_\phi}{\partial t}+u_r\frac{\partial u_\phi}{\partial r}+\frac{u_\theta}{r}\frac{\partial u_\phi}{\partial \theta}+\frac{u_\phi}{r\sin\theta}\frac{\partial u_\phi}{\partial \phi}+\frac{u_r u_\phi+u_\theta u_\phi\cot\theta}{r}\right)$$
$$=-\frac{1}{r\sin\theta}\frac{\partial P}{\partial\phi}+\mu\left\{\frac{1}{r^2}\frac{\partial}{\partial r}\left(r^2\frac{\partial u_\phi}{\partial r}\right)+\frac{1}{r^2}\frac{\partial}{\partial\theta}\left[\frac{1}{\sin\theta}\frac{\partial}{\partial\theta}(u_\phi\sin\theta)\right]\right.$$
$$\left.+\frac{1}{r^2\sin^2\theta}\frac{\partial^2 u_\phi}{\partial\phi^2}+\frac{2}{r^2\sin\theta}\frac{\partial u_r}{\partial\phi}+\frac{2\cot\theta}{r^2\sin\theta}\frac{\partial u_\theta}{\partial\phi}\right\}+\rho g_\varphi. \tag{B.8}$$

APPENDIX C

Energy Conservation Equations in Polar Cylindrical and Spherical Coordinates for Incompressible Fluids With Constant Thermal Conductivity

Cylindrical Coordinates (r, θ, z)

$$\rho C_P \left(\frac{\partial T}{\partial t} + u_r \frac{\partial T}{\partial r} + \frac{u_\theta}{r} \frac{\partial T}{\partial \theta} + u_z \frac{\partial T}{\partial z} \right) = k \left[\frac{1}{r} \frac{\partial}{\partial r} \left(r \frac{\partial T}{\partial r} \right) + \frac{1}{r^2} \frac{\partial^2 T}{\partial \theta^2} + \frac{\partial^2 T}{\partial z^2} \right] + \mu \Phi, \tag{C.1}$$

$$\begin{aligned} \Phi = 2 & \left[\left(\frac{\partial u_r}{\partial r} \right)^2 + \left(\frac{1}{r} \frac{\partial u_\theta}{\partial \theta} + \frac{u_r}{r} \right)^2 + \left(\frac{\partial u_z}{\partial z} \right)^2 \right] \\ & + \left[r \frac{\partial}{\partial r} \left(\frac{u_\theta}{r} \right) + \frac{1}{r} \frac{\partial u_r}{\partial \theta} \right]^2 + \left[\frac{1}{r} \frac{\partial u_z}{\partial \theta} + \frac{\partial u_\theta}{\partial z} \right]^2 \\ & + \left[\frac{\partial u_r}{\partial z} + \frac{\partial u_z}{\partial r} \right]^2 - \frac{2}{3} \left[\frac{1}{r} \frac{\partial}{\partial r} (r u_r) + \frac{1}{r} \frac{\partial u_\theta}{\partial \theta} + \frac{\partial u_z}{\partial z} \right]^2 . \end{aligned} \tag{C.2}$$

Spherical Coordinates (r, θ, ϕ)

$$\rho C_P \left(\frac{\partial T}{\partial t} + u_r \frac{\partial T}{\partial r} + \frac{u_\theta}{r} \frac{\partial T}{\partial \theta} + \frac{u_\phi}{r \sin\theta} \frac{\partial T}{\partial \phi} \right) = k \left[\frac{1}{r^2} \frac{\partial}{\partial r} \left(r^2 \frac{\partial T}{\partial r} \right) + \frac{1}{r^2 \sin\theta} \frac{\partial}{\partial \theta} \left(\sin\theta \frac{\partial T}{\partial \theta} \right) + \frac{1}{r^2 \sin^2\theta} \frac{\partial^2 T}{\partial \phi^2} \right] + \mu \Phi, \tag{C.3}$$

$$\begin{aligned} \Phi = 2 & \left[\left(\frac{\partial u_r}{\partial r} \right)^2 + \left(\frac{1}{r} \frac{\partial u_\theta}{\partial \theta} + \frac{u_r}{r} \right)^2 + \left(\frac{1}{r \sin\theta} \frac{\partial u_\phi}{\partial \phi} + \frac{u_r + u_\theta \cot\theta}{r} \right)^2 \right] \\ & + \left[r \frac{\partial}{\partial r} \left(\frac{u_\theta}{r} \right) + \frac{1}{r} \frac{\partial u_r}{\partial \theta} \right]^2 \\ & + \left[\frac{\sin\theta}{r} \frac{\partial}{\partial \theta} \left(\frac{u_\phi}{\sin\theta} \right) + \frac{1}{r \sin\theta} \frac{\partial u_\theta}{\partial \phi} \right]^2 + \left[\frac{1}{r \sin\theta} \frac{\partial u_r}{\partial \phi} + r \frac{\partial}{\partial r} \left(\frac{u_\phi}{r} \right) \right]^2 \\ & - \frac{2}{3} \left[\frac{1}{r^2} \frac{\partial}{\partial r} (r^2 u_r) + \frac{1}{r \sin\theta} \frac{\partial}{\partial \theta} (u_\theta \sin\theta) + \frac{1}{r \sin\theta} \frac{\partial u_\phi}{\partial \phi} \right]^2 . \end{aligned} \tag{C.4}$$

APPENDIX D

Mass-Species Conservation Equations in Polar Cylindrical and Spherical Coordinates for Incompressible Fluids

In Terms of Diffusive Fluxes

Cylindrical Coordinates (r, θ, z)

$$\rho\left(\frac{\partial m_i}{\partial t}+u_r\frac{\partial m_i}{\partial r}+\frac{u_\theta}{r}\frac{\partial m_i}{\partial \theta}+u_z\frac{\partial m_i}{\partial z}\right)=-\left[\frac{1}{r}\frac{\partial}{\partial r}\left(r j_{i,r}\right)+\frac{1}{r}\frac{\partial j_{i,\theta}}{\partial \theta}+\frac{\partial j_{i,z}}{\partial z}\right]+\dot{r}_i, \tag{D.1}$$

$$\boldsymbol{C}\left(\frac{\partial X_i}{\partial t}+\tilde{u}_r\frac{\partial X_i}{\partial r}+\frac{\tilde{u}_\theta}{r}\frac{\partial X_i}{\partial \theta}+\tilde{u}_z\frac{\partial X_i}{\partial z}\right)=-\left[\frac{1}{r}\frac{\partial}{\partial r}\left(rJ_{i,r}\right)+\frac{1}{r}\frac{\partial J_{i,\theta}}{\partial \theta}+\frac{\partial J_{i,z}}{\partial z}\right]+\dot{R}_i-X_i\sum_{l=1}^{N}\dot{R}_l. \tag{D.2}$$

Spherical Coordinates (r, θ, ϕ)

$$\rho\left(\frac{\partial m_i}{\partial t}+u_r\frac{\partial m_i}{\partial r}+\frac{u_\theta}{r}\frac{\partial m_i}{\partial \theta}+\frac{u_\phi}{r\sin\theta}\frac{\partial m_i}{\partial \phi}\right)=-\left[\frac{1}{r^2}\frac{\partial}{\partial r}\left(r^2 j_{i,r}\right)+\frac{1}{r\sin\theta}\frac{\partial}{\partial \theta}\left(\sin\theta j_{i,\theta}\right)+\frac{1}{r\sin\theta}\frac{\partial j_{i,\phi}}{\partial \phi}\right]+\dot{r}_i, \tag{D.3}$$

$$\boldsymbol{C}\left(\frac{\partial X_i}{\partial t}+\tilde{u}_r\frac{\partial X_i}{\partial r}+\frac{\tilde{u}_\theta}{r}\frac{\partial X_i}{\partial \theta}+\frac{\tilde{u}_\phi}{r\sin\theta}\frac{\partial X_i}{\partial \phi}\right)=-\left[\frac{1}{r^2}\frac{\partial}{\partial r}\left(r^2 J_{i,r}\right)+\frac{1}{r\sin\theta}\frac{\partial}{\partial \theta}\left(\sin\theta J_{i,\theta}\right)+\frac{1}{r\sin\theta}\frac{\partial J_{i,\phi}}{\partial \phi}\right]+\dot{R}_i-X_i\sum_{l=1}^{N}\dot{R}_l. \tag{D.4}$$

In a Binary Mixture with $\rho\mathcal{D}_{12} = \text{const.}$ or $C\mathcal{D}_{12} = \text{const.}$

Cylindrical Coordinates (r, θ, z)

$$\rho\left(\frac{\partial m_1}{\partial t} + u_r\frac{\partial m_1}{\partial r} + \frac{u_\theta}{r}\frac{\partial m_1}{\partial \theta} + u_z\frac{\partial m_1}{\partial z}\right)$$
$$= \rho\mathcal{D}_{12}\left[\frac{1}{r}\frac{\partial}{\partial r}\left(r\frac{\partial m_1}{\partial r}\right) + \frac{1}{r^2}\frac{\partial^2 m_1}{\partial \theta^2} + \frac{\partial^2 m_1}{\partial z^2}\right] + \dot{r}_1, \tag{D.5}$$

$$\boldsymbol{C}\left(\frac{\partial X_1}{\partial t} + \tilde{u}_r\frac{\partial X_1}{\partial r} + \frac{\tilde{u}_\theta}{r}\frac{\partial X_1}{\partial \theta} + \tilde{u}_z\frac{\partial X_1}{\partial z}\right)$$
$$= \boldsymbol{C}\mathcal{D}_{12}\left[\frac{1}{r}\frac{\partial}{\partial r}\left(r\frac{\partial X_1}{\partial r}\right) + \frac{1}{r^2}\frac{\partial^2 X_1}{\partial \theta^2} + \frac{\partial^2 X_1}{\partial z^2}\right] + X_2\dot{R}_1 - X_1\dot{R}_2. \tag{D.6}$$

Spherical Coordinates (r, θ, ϕ)

$$\rho\left(\frac{\partial m_1}{\partial t} + u_r\frac{\partial m_1}{\partial r} + \frac{u_\theta}{r}\frac{\partial m_1}{\partial \theta} + \frac{u_\phi}{r\sin\theta}\frac{\partial m_1}{\partial \phi}\right)$$
$$= \rho\mathcal{D}_{12}\left[\frac{1}{r^2}\frac{\partial}{\partial r}\left(r^2\frac{\partial m_1}{\partial r}\right) + \frac{1}{r^2\sin\theta}\frac{\partial}{\partial \theta}\left(\sin\theta\frac{\partial m_1}{\partial \theta}\right) + \frac{1}{r^2\sin^2\theta}\frac{\partial^2 m_1}{\partial \phi^2}\right] + \dot{r}_1, \tag{D.7}$$

$$\boldsymbol{C}\left(\frac{\partial X_1}{\partial t} + \tilde{u}_r\frac{\partial X_1}{\partial r} + \frac{\tilde{u}_\theta}{r}\frac{\partial X_1}{\partial \theta} + \frac{\tilde{u}_\phi}{r\sin\theta}\frac{\partial X_1}{\partial \phi}\right)$$
$$= \boldsymbol{C}\mathcal{D}_{12}\left[\frac{1}{r^2}\frac{\partial}{\partial r}\left(r^2\frac{\partial X_1}{\partial r}\right) + \frac{1}{r^2\sin\theta}\frac{\partial}{\partial \theta}\left(\sin\theta\frac{\partial X_1}{\partial \theta}\right) + \frac{1}{r^2\sin^2\theta}\frac{\partial^2 X_1}{\partial \phi^2}\right]$$
$$+ X_2\dot{R}_1 - X_1\dot{R}_2. \tag{D.8}$$

APPENDIX E

Thermodynamic Properties of Saturated Water and Steam

T (°C)	P (bars)	v_f (m^3/kg)	v_g (m^3/kg)	u_f (kJ/kg)	u_g (kJ/kg)	h_f (kJ/kg)	h_g (kJ/kg)	s_f (kJ/kg K)	s_g (kJ/kg K)
0.01	0.006117	0.00100	205.99	0.00	2374.5	0.00	2500.5	0.0000	9.1541
5	0.00873	0.00100	147.02	21.02	2381.4	21.02	2509.7	0.0763	9.0236
10	0.01228	0.00100	106.32	41.99	2388.3	41.99	2518.9	0.1510	8.8986
15	0.01706	0.00100	77.90	62.92	2395.2	62.92	2528.0	0.2242	8.7792
20	0.02339	0.00100	57.778	83.83	2402.0	83.84	2537.2	0.2962	8.6651
25	0.03169	0.00100	43.361	104.75	2408.9	104.75	2546.3	0.3670	8.556
30	0.04245	0.00100	32.90	125.67	2415.7	125.67	2555.3	0.4365	8.4513
35	0.05627	0.00100	25.222	146.58	2422.5	146.59	2564.4	0.5050	8.3511
40	0.07381	0.00100	19.529	167.50	2429.2	167.50	2573.4	0.5723	8.255
45	0.09590	0.00100	15.263	188.41	2435.9	188.42	2582.3	0.6385	8.1629
50	0.12344	0.00101	12.037	209.31	2442.6	209.33	2591.2	0.7037	8.0745
55	0.15752	0.00101	9.572	230.22	2449.2	230.24	2600.0	0.7679	7.9896
60	0.19932	0.00102	7.674	251.13	2455.8	251.15	2608.8	0.8312	7.9080
65	0.2502	0.00102	6.199	272.05	2462.4	272.08	2617.5	0.8935	7.8295
70	0.3118	0.00102	5.044	292.98	2468.8	293.01	2626.1	0.9549	7.7540
75	0.3856	0.00103	4.133	313.92	2475.2	313.96	2634.6	1.0155	7.6812
80	0.4737	0.00103	3.409	334.88	2481.6	334.93	2643.1	1.0753	7.6111
85	0.57815	0.00103	2.829	355.86	2487.9	355.92	2651.4	1.1343	7.5436
90	0.70117	0.00104	2.362	376.86	2494.0	376.93	2659.6	1.1925	7.4783
95	0.8453	0.00104	1.983	397.89	2500.1	397.98	2667.7	1.2501	7.4154
100	1.0132	0.00104	1.674	418.96	2506.1	419.06	2675.7	1.3069	7.3545
105	1.2079	0.00105	1.420	440.05	2512.1	440.18	2683.6	1.3630	7.2956
110	1.4324	0.00105	1.211	461.19	2517.9	461.34	2691.3	1.4186	7.2386
115	1.6902	0.00106	1.037	482.36	2523.5	482.54	2698.8	1.4735	7.1833
120	1.9848	0.00106	0.8922	503.57	2529.1	503.78	2706.2	1.5278	7.1297
130	2.7002	0.00107	0.6687	546.12	2539.8	546.41	2720.4	1.6346	7.0272
140	3.6119	0.00108	0.5090	588.85	2550.0	589.24	2733.8	1.7394	6.9302
150	4.7572	0.00109	0.3929	631.80	2559.5	632.32	2746.4	1.8421	6.8381
160	6.1766	0.00110	0.3071	674.97	2568.3	675.65	2758.0	1.9429	6.7503
170	7.9147	0.00111	0.2428	718.40	2576.3	719.28	2768.5	2.0421	6.6662
180	10.019	0.001127	0.1940	762.12	2583.4	763.25	2777.8	2.1397	6.5853
190	12.542	0.00114	0.1565	806.17	2589.6	807.60	2785.8	2.2358	6.5071
200	15.536	0.00116	0.1273	850.58	2594.7	852.38	2792.5	2.3308	6.4312
220	23.178	0.00119	0.08616	940.75	2601.6	943.51	2801.3	2.5175	6.2847

T (°C)	P (bars)	v_f (m^3/kg)	v_g (m^3/kg)	u_f (kJ/kg)	u_g (kJ/kg)	h_f (kJ/kg)	h_g (kJ/kg)	s_f (kJ/kg K)	s_g (kJ/kg K)
240	33.447	0.00123	0.05974	1033.12	2603.1	1037.24	2803.0	2.7013	6.1423
260	46.894	0.001276	0.04219	1128.40	2598.4	1134.38	2796.2	2.8838	6.0010
280	64.132	0.001332	0.03016	1227.53	2585.7	1236.08	2779.2	3.0669	5.8565
300	85.838	0.001404	0.02167	1332.01	2562.8	1344.05	2748.7	3.2534	5.7042
320	112.79	0.001498	0.01548	1444.36	2525.2	1461.26	2699.7	3.4476	5.5356
340	145.94	0.001637	0.01079	1569.9	2463.9	1593.8	2621.3	3.6587	5.3345
360	186.55	0.001894	0.00696	1725.6	2352.2	1761.0	2482.0	3.9153	5.0542
373.98	220.55	0.003106	0.003106	2017	2017	2086	2086	4.409	4.409

APPENDIX F

Transport Properties of Saturated Water and Steam[a]

Temperature (K)	Pressure (bars)	$v_f \times 10^3$ (m^3/kg)	$v_g \times 10^3$ (m^3/kg)	C_{pf} (kJ/kg K)	C_{pg} (kJ/kg K)	$\mu_f \times 10^6$ (kg/m s)	$\mu_g \times 10^6$ (kg/m s)	$k_f \times 10^3$ (W/m K)	$kg \times 10^3$ (W/m K)	Pr_f	Pr_g
273.15	0.00611	1.000	206.3	4.217	1.854	1750	8.02	569	18.2	12.99	0.815
275.	0.00697	1.000	181.7	4.211	1.855	1652	8.09	574	18.3	12.22	0.817
280	0.0099	1.000	130.4	4.198	1.858	1422	8.29	582	18.6	10.26	0.825
285	0.01387	1.000	99.4	4.189	1.861	1225	8.49	590	18.9	8.81	0.833
290	0.01917	1.001	69.7	4.184	1.864	1080	8.69	598	19.3	7.56	0.841
295	0.02616	1.002	51.94	4.181	1.868	959	8.89	606	19.5	6.62	0.849
300	0.03531	1.003	39.13	4.179	1.872	855	9.09	613	19.6	5.83	0.857
310	0.06221	1.007	13.98	4.178	1.882	695	9.49	628	20.4	4.62	0.873
320	0.1053	1.011	13.98	4.18	1.895	577	9.89	640	21	3.77	0.894
330	0.1719	1.016	8.82	4.184	1.895	489	10.29	650	21.7	3.15	0.908
340	0.2713	1.021	5.74	4.188	1.930	420	10.69	660	22.3	2.66	0.925
350	0.4163	1.027	3.846	4.195	1.954	365	11.09	668	23	2.29	0.942
360	0.6209	1.034	2.645	4.203	1.983	324	11.49	674	23.7	2.02	0.960
370	0.9040	1.041	1.861	4.214	2.017	289	11.89	679	24.5	1.80	0.978
373.15	1.0113	1.044	1.679	4.217	2.029	279	12.02	680	24.8	1.76	0.984
380	1.2869	1.049	1.337	4.226	2.057	260	12.29	683	25.4	1.61	0.999
390	1.794	1.058	0.98	4.239	2.104	237	12.69	686	26.3	1.47	1.013
400	2.455	1.067	0.731	4.256	2.158	217	13.05	688	27.2	1.34	1.033
420	4.37	1.088	0.425	4.302	2.291	185	13.79	688	29.8	1.16	1.075
440	7.333	1.11	0.261	4.36	2.46	162	15.4	682	31.7	1.04	1.12
460	11.71	1.137	0.167	4.44	2.68	143	15.19	673	24.6	0.95	1.17
480	17.19	1.167	0.111	4.53	2.94	129	15.88	660	38.1	0.89	1.23
500	26.40	1.203	0.0766	4.66	3.27	118	16.59	642	42.3	0.86	1.28
520	37.7	1.244	0.0525	4.84	3.70	108	7.33	621	47.5	0.84	1.35
540	52.38	1.294	0.0375	5.08	4.27	101	18.1	594	54.0	0.86	1.43
560	71.08	1.355	0.0269	5.43	5.09	94	19.1	563	63.7	0.90	1.52
580	94.51	1.433	0.0193	6.00	6.40	88	20.4	528	76.7	0.982	1.68
600	123.5	1.541	0.00137	7.00	8.75	81	22.7	497	92.9	1.14	2.15
620	159.1	1.705	0.0094	9.35	15.4	72	25.9	444	114	1.52	3.46
640	202.7	2.075	0.0057	26	42	59	32	367	155	4.2	9.6
647.3[b]	221.2	3.17	0.0032	∞	∞	45	45	238	238	∞	∞

[a] Based on Incroperra et al. (2007).
[b] Critical temperature.

APPENDIX G

Properties of Selected Ideal Gases at 1 Atmosphere

Air

Temperature T(K)	Density ρ (kg/m^3)	Specific heat, C_p (kJ/kg K)	Viscosity, μ [(kg/m s) $\times 10^7$]	Thermal conductivity, k [(W/m K) $\times 10^3$]	Prandtl number, Pr
100	3.5562	1.032	71.1	9.34	0.786
150	2.3364	1.012	103.4	13.8	0.758
200	1.7458	1.007	132.5	18.1	0.737
250	1.3947	1.006	159.6	22.3	0.72
300	1.1614	1.007	184.6	26.3	0.707
350	0.995	1.009	208.2	30.0	0.700
400	0.8711	1.014	230.1	33.8	0.690
450	0.774	1.021	250.7	37.3	0.686
500	0.6964	1.03	270.1	40.7	0.684
550	0.6329	1.04	288.4	43.9	0.683
600	0.5804	1.051	305.8	46.9	0.685
650	0.5356	1.063	322.5	49.7	0.690
700	0.4975	1.075	338.8	52.4	0.695
800	0.4354	1.099	369.8	57.3	0.709
900	0.3868	1.121	398.1	62.0	0.720
1000	0.3482	1.141	424.4	66.7	0.726
1100	0.3166	1.159	449.0	71.5	0.728
1200	0.2902	1.175	473.0	76.3	0.728
1300	0.2679	1.189	496.0	82	0.719
1400	0.2488	1.207	530	91	0.703
1500	0.2322	1.230	557	100	0.685
1600	0.2177	1.248	584	106	0.688
1700	0.2049	1.267	611	113	0.685
1800	0.1935	1.286	637	120	0.683
1900	0.1833	1.307	663	128	0.677
2000	0.1741	1.337	689	137	0.672
2100	0.1658	1.372	715	147	0.667
2200	0.1582	1.417	740	160	0.655
2300	0.1513	1.478	766	175	0.647
2400	0.1448	1.558	792	196	0.630
2500	0.1389	1.665	818	222	0.613
3000	0.1135	2.726	955	486	0.536

Nitrogen (N_2)

Temperature T(K)	Density ρ (kg/m^3)	Specific heat, C_p (kJ/kg K)	Viscosity, μ [(kg/m s) $\times 10^7$]	Thermal conductivity, k [(W/m K) $\times 10^3$]	Prandtl number, Pr
100	3.4388	1.070	68.8	9.58	0.768
150	2.2594	1.050	100.6	13.9	0.759
200	1.6883	1.043	129.2	18.3	0.736
250	1.3488	1.042	154.9	22.2	0.727
300	1.1233	1.041	178.2	25.9	0.716
350	0.9625	1.042	200.0	29.3	0.711
400	0.8425	1.045	220.4	32.7	0.704
450	0.7485	1.050	239.6	35.8	0.703
500	0.6739	1.056	257.7	38.9	0.700
550	0.6124	1.065	274.7	41.7	0.702
600	0.5615	1.075	290.8	44.6	0.701
700	0.4812	1.098	321.0	49.9	0.706
800	0.4211	1.12	349.1	54.8	0.715
900	0.3743	1.146	375.3	59.7	0.721
1000	0.3368	1.167	399.9	64.7	0.721
1100	0.3062	1.187	423.2	70.0	0.718
1200	0.2807	1.204	445.3	75.8	0.707
1300	0.2591	1.219	466.2	81.0	0.701
1400	0.2438	1.229	486	87.5	0.709
1600	0.2133	1.250	510	97	0.71

Oxygen (O_2)

Temperature T(K)	Density ρ (kg/m^3)	Specific heat, C_p (kJ/kg K)	Viscosity, μ [(kg/m s) $\times 10^7$]	Thermal conductivity, k [(W/m K) $\times 10^3$]	Prandtl number, Pr
100	3.945	0.962	76.4	9.25	0.796
150	2.585	0.921	114.8	13.8	0.766
200	1.930	0.915	147.5	18.3	0.737
250	1.542	0.915	178.6	22.6	0.723
300	1.284	0.920	207.2	26.8	0.711
350	1.100	0.929	233.5	29.6	0.733
400	0.9620	0.942	258.2	33.0	0.737
450	0.8554	0.956	281.4	36.3	0.741
500	0.7698	0.972	303.3	41.2	0.716
550	0.6998	0.988	324.0	44.1	0.726
600	0.6414	1.003	343.7	47.3	0.729
700	0.5498	1.031	380.8	52.8	0.744
800	0.4810	1.054	415.2	58.9	0.743
900	0.4275	1.074	447.2	64.9	0.740
1000	0.3848	1.090	477.0	71.0	0.733
1100	0.3498	1.103	505.5	75.8	0.736
1200	0.3206	1.115	532.5	81.9	0.725
1300	0.2960	1.125	588.4	87.1	0.721

Carbon Dioxide (CO_2)

Temperature T(K)	Density ρ (kg/m^3)	Specific heat, C_p (kJ/kg K)	Viscosity, μ [(kg/m s) $\times 10^7$]	Thermal conductivity, k [(W/m K) $\times 10^3$]	Prandtl number, Pr
220	2.4733	0.783	110.6	10.9	0.795
250	2.1657	0.804	125.7	12.95	0.780
280	1.9022	0.830	140	15.20	0.765
300	1.7730	0.851	149	16.55	0.766
320	1.6609	0.872	156	18.05	0.754
340	1.5618	0.891	165	19.70	0.746
350	1.5362	0.900	174	20.92	0.744
360	1.4743	0.908	173	21.2	0.741
380	1.3961	0.926	181	22.75	0.737
400	1.3257	0.942	190	24.3	0.737
450	1.1782	0.981	210	28.3	0.728
500	1.0594	1.02	231	32.5	0.725
550	0.9625	1.05	251	36.6	0.721
600	0.8826	1.08	270	40.7	0.717
650	0.8143	1.10	288	44.5	0.712
700	0.7564	1.13	305	48.1	0.717
750	0.7057	1.15	321	51.7	0.714
800	0.6614	1.17	337	55.1	0.716

Carbon Monoxide (CO)

Temperature T(K)	Density ρ (kg/m^3)	Specific heat, C_p (kJ/kg K)	Viscosity, μ [(kg/m s) $\times 10^7$]	Thermal conductivity, k [(W/m K) $\times 10^3$]	Prandtl number, Pr
200	1.6888	1.045	127	17.0	0.781
220	1.5341	1.044	137	19.0	0.753
240	1.4055	1.043	147	20.6	0.744
260	1.2967	1.043	157	22.1	0.741
280	1.2038	1.042	166	23.6	0.733
300	1.1233	1.043	175	25.0	0.730
320	1.0529	1.043	184	26.3	0.730
340	0.9909	1.044	193	27.8	0.725
360	0.9357	1.045	202	29.1	0.725
380	0.8864	1.047	210	30.5	0.729
400	0.8421	1.049	218	31.8	0.719
450	0.7483	1.055	237	35.0	0.714
500	0.67352	1.065	254	38.1	0.710
550	0.61226	1.076	271	41.1	0.710
600	0.56126	1.088	286	44.0	0.707
650	0.51806	1.101	301	47.0	0.705
700	0.48102	1.114	315	50.0	0.702
750	0.44899	1.127	329	52.8	0.702
800	0.42095	1.140	343	55.5	0.705
900	0.3791	1.155	371	59.0	0.705
1000	0.3412	1.165	399	61.64	0.705

Hydrogen (H_2)

Temperature T(K)	Density ρ (kg/m^3)	Specific heat, C_p (kJ/kg K)	Viscosity, μ [(kg/m s) $\times 10^7$]	Thermal conductivity, k [(W/m K) $\times 10^3$]	Prandtl number, Pr
100	0.24255	11.23	42.1	67.0	0.707
150	0.16156	12.60	56.0	101	0.699
200	0.12115	13.54	68.1	131	0.704
250	0.09693	14.06	78.9	157	0.707
300	0.08078	14.31	89.6	183	0.701
350	0.06924	14.43	98.8	204	0.700
400	0.06059	14.48	108.2	226	0.695
450	0.05386	14.50	117.2	247	0.689
500	0.04848	14.52	126.4	266	0.691
550	0.04407	14.53	134.3	285	0.685
600	0.04040	14.55	142.4	305	0.678
700	0.03463	14.61	157.8	342	0.675
800	0.03030	14.70	172.4	378	0.670
900	0.02694	14.83	186.5	412	0.671
1000	0.02424	14.99	201.3	448	0.673
1100	0.02204	15.17	213.0	488	0.662
1200	0.02020	15.37	226.2	528	0.659
1300	0.01865	15.59	238.5	568	0.655
1400	0.01732	15.81	250.7	610	0.650
1500	0.01616	16.02	262.7	655	0.643
1600	0.0152	16.28	273.7	697	0.639
1700	0.0143	16.58	284.9	742	0.637
1800	0.0135	16.96	296.1	786	0.639
1900	0.0128	17.49	307.2	835	0.643
2000	0.0121	18.25	318.2	878	0.661

Helium (He)

Temperature T(K)	Density ρ (kg/m^3)	Specific heat, C_p (kJ/kg K)	Viscosity, μ [(kg/m s) $\times 10^7$]	Thermal conductivity, k [(W/m K) $\times 10^3$]	Prandtl number, Pr
50	0.9732	5.201	60.7	47.6	0.663
100	0.4871	5.193	96.3	73.0	0.686
120	0.4060	5.193	107	81.9	0.679
140	0.3481	5.193	118	90.7	0.676
160	0.309	5.193	129	99.2	0.674
180	0.2708	5.193	139	107.2	0.673
200	0.2437	5.193	150	115.1	0.667
220	0.2216	5.193	160	123.1	0.675
240	0.205	5.193	170	130	0.678
260	0.1875	5.193	180	137	0.682
280	0.175	5.193	190	145	0.681
300	0.1625	5.193	199	152	0.680
350	0.1393	5.193	221	170	0.663
400	0.1219	5.193	243	187	0.675
450	0.1084	5.193	263	204	0.663
500	0.09754	5.193	283	220	0.668
550	0.0894	5.193	300	234	0.665
600	0.08128	5.193	320	252	0.663
650	0.0755	5.193	332	264	0.658
700	0.06969	5.193	350	278	0.654
750	0.0653	5.193	364	291	0.659
800	0.06096	5.193	382	304	0.664
900	0.05419	5.193	414	330	0.664
1000	0.04879	5.193	454	354	0.654
1100	0.04434	5.193	495	387	0.664
1200	0.04065	5.193	527	412	0.664
1300	0.03752	5.193	559	437	0.664
1400	0.03484	5.193	590	461	0.665
1500	0.03252	5.193	621	485	0.665

Water Vapor (H_2O)

Temperature T(K)	Density ρ (kg/m^3)	Specific heat, C_p (kJ/kg K)	Viscosity, μ [(kg/m s) $\times 10^7$]	Thermal conductivity, k [(W/m K) $\times 10^3$]	Prandtl number, Pr
373.15	0.5976	2.080	122.8	25.09	0.98
380	0.5863	2.060	127.1	24.6	0.98
400	0.5542	2.014	134.4	26.1	0.98
450	0.4902	1.980	152.5	29.9	0.97
500	0.4405	1.985	173	33.9	0.96
550	0.4005	1.997	188.4	37.9	0.95
600	0.3652	2.026	215	42.2	0.94
650	0.3380	2.056	236	46.4	0.93
700	0.3140	2.085	257	50.5	0.92
750	0.2931	2.119	277.5	54.9	0.91
800	0.2739	2.152	298	59.2	0.9
850	0.2579	2.186	318	63.7	0.895
873.15	0.2516	2.203	326.2	79.90	0.897
900	0.241	2.219	339	84.3	0.89
973.15	0.2257	2.273	365.5	93.38	0.888
1000	0.217	2.286	378	98.1	0.883
1073.15	0.2046	2.343	403.8	107.3	0.881
1200	0.181	2.43	448	130	0.85
1400	0.155	2.58	506	160	0.82
1600	0.135	2.73	565	210	0.74
1800	0.12	3.02	619	330	0.57
2000	0.108	3.79	670	570	0.45

APPENDIX H

Binary Diffusion Coefficients of Selected Gases in Air at 1 Atmosphere[a,b]

Substance 1	$T(K)$	$\mathcal{D}_{12}(m^2/s)$[c]
CO_2	298	0.16×10^{-4}
H_2	298	0.41×10^{-4}
He	300	0.777×10^{-4}
O_2	298	0.21×10^{-4}
H_2O	298	0.26×10^{-4}
NH_3	298	0.28×10^{-4}
CO	300	0.202×10^{-4}
NO	300	0.18×10^{-4}
SO_2	300	0.126×10^{-4}
Benzene	298	0.083×10^{-5}
Naphthalene	300	0.62×10^{-5}

[a] Based in part on Mills (2001) and Incropera et al. (2007).
[b] For ideal gases, $D_{12} \sim P^{-1} T^{3/2}$.
[c] Air is substance 2.

APPENDIX I

Henry's Constant, in bars, of Dilute Aqueous Solutions of Selected Substances at Moderate Pressures[a]

Solute	290 K	300 K	310 K	320 K	330 K	340 K
Air	62,000	74,000	84,000	92,000	99,000	104,000
N_2	76,000	89,000	101,000	110,000	118,000	124,000
O_2	38,000	45,000	52,000	57,000	61,000	65,000
CO_2	1280	1710	2170	2720	3220	–
H_2	67,000	72,000	75,000	76,000	77,000	76,000
CO	51,000	60,000	67,000	74,000	80,000	84,000

[a] Based on Edwards et al. (1979).

APPENDIX J

Diffusion Coefficients of Selected Substances in Water at Infinite Dilution at 25 °C

Solute (Substance 1)	$\mathcal{D}_{12}(10^{-9}\text{m}^2/\text{s})^a$
Argon	2.00
Air	2.00
Carbon dioxide	1.92
Carbon monoxide	2.03
Chlorine	1.25
Ethane	1.20
Ethylene	1.87
Helium	6.28
Hydrogen	4.50
Methane	1.49
Nitric oxide	2.60
Nitrogen	1.88
Oxygen	2.10
Propane	0.97
Ammonia	1.64
Benzene	1.02
Hydrogen sulfide	1.41

[a] Substance 2 is water.

APPENDIX K

Lennard–Jones Potential Model Constants for Selected Molecules[a]

	Molecule	$\tilde{\sigma}$(Å)	$\frac{\tilde{\varepsilon}}{k_B}$(K)
Ar	Argon	3.542	93.3
He	Helium	2.551	10.22
Kr	Krypton	3.655	178.9
Ne	Neon	2.820	32.8
Xe	Xenon	4.047	231.0
Air	Air	3.711	78.6
$CC1_4$	Carbon tetrachloride	5.947	322.7
CF_4	Carbon tetrafluoride	4.662	134.0
CH_4	Methane	3.758	148.6
CO	Carbon monoxide	3.690	91.7
CO_2	Carbon dioxide	3.941	195.2
C_2H_2	Acetylene	4.033	231.8
C_2H_4	Ethylene	4.163	224.7
C_2H_6	Ethane	4.443	215.7
C_6H_6	Benzene	5.349	412.3
Cl_2	Chlorine	4.217	316.0
F_2	Fluorine	3.357	112.6
HCN	Hydrogen cyanide	3.630	569.1
HC1	Hydrogen chloride	3.339	344.7
HF	Hydrogen fluoride	3.148	330
HI	Hydrogen iodide	4.211	288.7
H_2	Hydrogen	2.827	59.7
H_2O	Water	2.641	809.1
H_2S	Hydrogen sulfide	3.623	301.1
Hg	Mercury	2.969	750
I_2	Iodine	5.160	474.2
NH_3	Ammonia	2.900	558.3
NO	Nitric oxide	3.492	116.7
N_2	Nitrogen	3.798	71.4
N_2O	Nitrous oxide	3.828	232.4
O_2	Oxygen	3.467	106.7
SO_2	Sulfur dioxide	4.112	335.4
UF_6	Uranium hexafluoride	5.967	236.8

[a] Based on Hirschfelder et al. (1954).

APPENDIX L

Collision Integrals for the Lennard–Jones Potential Model[a]

$\frac{\kappa_B T}{\tilde{\varepsilon}}$	Ω_k	Ω_D	$\frac{\kappa_B T}{\tilde{\varepsilon}}$	Ω_k	Ω_D	$\frac{\kappa_B T}{\tilde{\varepsilon}}$	Ω_k	Ω_D
0.30	2.785	2.662	1.60	1.279	1.167	3.80	0.9811	0.8942
0.35	2.628	2.476	1.65	1.264	1.153	3.90	0.9755	0.8888
0.40	2.492	2.318	1.70	1.248	1.140	4.00	0.9700	0.8836
0.45	2.368	2.184	1.75	1.234	1.128	4.10	0.9649	0.8788
0.50	2.257	2.066	1.80	1.221	1.116	4.20	0.9600	0.8740
0.55	2.156	1.966	1.85	1.209	1.105	4.30	0.9553	0.8694
0.60	2.065	1.877	1.90	1.197	1.094	4.40	0.9507	0.8652
0.65	1.982	1.798	1.95	1.186	1.084	4.50	0.9464	0.8610
0.70	1.908	1.729	2.00	1.175	1.075	4.60	0.9422	0.8568
0.75	1.841	1.667	2.10	1.156	1.057	4.70	0.9382	0.8530
0.80	1.780	1.612	2.20	1.138	1.041	4.80	0.9343	0.8492
0.85	1.725	1.562	2.30	1.122	1.026	4.90	0.9305	0.8456
0.90	1.675	1.517	2.40	1.107	1.012	5.0	0.9269	0.8422
0.95	1.629	1.476	2.50	1.093	0.9996	6.0	0.8963	0.8124
1.00	1.587	1.439	2.60	1.081	0.9878	7.0	0.8727	0.7896
1.05	1.549	1.406	2.70	1.069	0.9770	8.0	0.8538	0.7712
1.10	1.514	1.375	2.80	1.058	0.9672	9.0	0.8379	0.7556
1.15	1.482	1.346	2.90	1.048	0.9576	10.0	0.8242	0.7424
1.20	1.452	1.320	3.00	1.039	0.9490	20.0	0.7432	0.6640
1.25	1.424	1.296	3.10	1.030	0.9406	30.0	0.7005	0.6232
1.30	1.399	1.273	3.20	1.022	0.9328	40.0	0.6718	0.5960
1.35	1.375	1.253	3.30	1.014	0.9256	50.0	0.6504	0.5756
1.40	1.353	1.233	3.40	1.007	0.9186	60.0	0.6335	0.5596
1.45	1.333	1.215	3.50	0.9999	0.9120	70.0	0.6194	0.5464
1.50	1.314	1.198	3.60	0.9932	0.9058	80.0	0.6076	0.5352
1.55	1.296	1.182	3.70	0.9870	0.8998	90.0	0.5973	0.5256

[a] Based on Hirschfelder et al. (1954).

APPENDIX M

Some RANS-Type Turbulence Models

M.1 The Spalart–Allmaras Model

This model (Spalart and Allmaras, 1992, 1994) is among the most widely applied one-equation turbulence models. It is an empirical model that was developed based on dimensional analysis (Blazek, 2005).

The model is based on the solution of a transport equation for the quantity $\tilde{\nu}$, which is equivalent to the turbulent eddy diffusivity, ν_{tu}, far from the wall. The standard Spalart–Allmaras model can be represented as follows. The turbulent kinematic viscosity is found from

$$\nu_{\text{tu}} = \tilde{\nu} f_{v1}, \tag{M.1.1}$$

where

$$f_{v1} = \frac{x^3}{x^3 + C_{v1}^3}, \tag{M.1.2}$$

$$x = \frac{\tilde{\nu}}{\nu}. \tag{M.1.3}$$

The transport equation for $\tilde{\nu}$ is

$$\frac{D\tilde{\nu}}{Dt} = C_{b1}(1 - f_{t2})\tilde{S}\tilde{\nu} + \frac{1}{\sigma_{\tilde{\nu}}}\left\{\nabla \cdot [(\nu + \tilde{\nu})\nabla\tilde{\nu}] + C_{b2}|\nabla\tilde{\nu}|^2\right\} - \left[C_{w1} f_w - \frac{C_{b1}}{\kappa^2} f_{t2}\right]\left(\frac{\tilde{\nu}}{y}\right)^2 + f_{t1}\|\Delta\vec{U}\|_2^2, \tag{M.1.4}$$

where,

$$\tilde{S} = S + \frac{\tilde{\nu}}{\kappa^2 y^2} f_{v2}, \tag{M.1.5}$$

$$f_{v2} = 1 - \frac{x}{1 + x f_{v1}}. \tag{M.1.6}$$

The parameter S is the absolute magnitude of vorticity,

$$S = \sqrt{2\Omega_{ij}\Omega_{ij}}, \tag{M.1.7}$$

$$\Omega_{ij} = \frac{1}{2}\left(\frac{\partial \overline{u}_i}{\partial x_j} - \frac{\partial \overline{u}_j}{\partial x_i}\right) \tag{M.1.8}$$

Also,

$$f_{t1} = g_t C_{t1} \exp\left[-C_{t2}\frac{w_t^2}{\left\|\Delta\vec{U}\right\|_2^2}\left(y^2 + g_t^2 d_t^2\right)\right] \tag{M.1.9}$$

$$f_{t2} = C_{t3}\exp[-C_{t4}x^2], \tag{M.1.10}$$

$$g_t = \min\left[0.1,\ \frac{\|\Delta\vec{U}\|_2}{w_t \Delta z_t}\right], \tag{M.1.11}$$

where d_t is the distance to the nearest tip point, Δz_t represents the spacing along the wall at the tip point, w_t is the vorticity at the wall at the tip point, and

$$f_w = g\left[\frac{1 + C_{w3}^6}{g^6 + C_{w3}^6}\right]^{1/6}, \tag{M.1.12}$$

$$g = r + C_{w2}(r^6 - r), \tag{M.1.13}$$

$$r = \frac{\tilde{\nu}}{\tilde{S}\kappa^2 y^2}, \tag{M.1.14}$$

where y is the normal distance from the wall. In Eq. (M.1.11), $\|\Delta\vec{U}\|_2$ is the two-norm of the vector $\vec{U} - \vec{U}_{\text{tip}}$, where $\vec{U}$ is the local velocity and $\vec{U}_{\text{tip}}$ is the velocity at the tip point.

The model constants are

$$\begin{aligned}
&\sigma_{\tilde{\nu}} = 2/3, \quad \kappa = 0.41,\\
&C_{b1} = 0.1355\,, \quad C_{b2} = 0.622,\\
&C_{w1} = \frac{C_{b1}}{\kappa^2} + \frac{1 + C_{b2}}{\sigma_{\tilde{\nu}}},\\
&C_{w2} = 0.3\,, \quad C_{w3} = 2\,, \quad C_{v1} = 7.11,\\
&C_{t1} = 1\,, \quad C_{t2} = 2\,, \quad C_{t3} = 1.3\,, \quad C_{t4} = 0.5.
\end{aligned} \tag{M.1.15}$$

By treating $\tilde{\nu}$, rather than the turbulent kinetic energy K, as the transported property, this model thus avoids the need for algebraic expressions for the turbulent length scale. The model is significantly less expensive computationally in comparison with the two-equation models or RSM, and is particularly useful for computationally intensive aerodynamic simulations. It is, however, rarely used for problems involving heat or mass transfer. Nevertheless, we may note that, by knowing ν_{tu} from Eq. (M.1.1), the turbulent conductivity and mass diffusivity can be found from, respectively,

$$k_{\text{tu}} = \rho\, C_P\left(\frac{\nu_{\text{tu}}}{\text{Pr}_{\text{tu}}}\right) = \rho\, C_P \frac{\tilde{\nu}\, f_{v1}}{\text{Pr}_{\text{tu}}}, \tag{M.1.16}$$

$$\mathcal{D}_{12,\text{tu}} = \frac{\nu_{\text{tu}}}{\text{Sc}_{12,\text{tu}}} = \frac{\tilde{\nu}\, f_{v1}}{\text{Sc}_{12,\text{tu}}}, \tag{M.1.17}$$

where $\mathcal{D}_{12,\text{tu}}$ denotes the turbulent diffusivity of the transferred species (species with subscript 1) with respect to the mixture. Note that, as usual in this book, Fick's

law is assumed for diffusive mass transfer. This would be the case for example if the gas is a binary mixture.

With respect to the wall boundary conditions, the standard Spalart–Allmaras model is in fact a low-Reynolds-number model and is applicable over the entire boundary layer with $\nu_{\text{tu}} = 0$ at the wall as the boundary condition. Thus, when very fine mesh is used near the wall (fine enough to resolve the viscous sublayer), there is no need to modify the model equations or apply wall functions. However, when relatively coarse mesh is used such that the viscous sublayer is not resolved, then the wall functions discussed in Section 12.3 can be applied.

The detached eddy simulation (DES) and delayed detached eddy simulation (DDES) are the recent enhancements of the Spalart–Allmars model (Travin et al., 2003; Spalart et al., 2006). These models use a RANS-type simulation method such as the Spalart–Allmaras model in the flow field, but resort to the large-eddy simulation (LES) method (discussed in Section 12.10) in parts of the flow field where unsteady flow or boundary-layer separation is expected.

M.2 The K–ω Model

The K–ω model is probably the most widely used two-equation turbulence model after the K–ε model. The model outperforms the K–ε model for some situations, including turbulent boundary layers with zero or adverse pressure gradients and can handle near-separation conditions.

The Standard K–ω Model

The standard K–ω model (Wilcox, 1988, 1993, 1994) uses K and ω as the transported properties, where ω is the specific dissipation rate, defined as

$$\omega = \frac{1}{\beta^*}\frac{\varepsilon}{K}. \tag{M.2.1}$$

The standard transport equations for K and ω are

$$\frac{D}{Dt}(\rho K) = \frac{\partial}{\partial x_j}\left[\left(\mu + \frac{\mu_{\text{tu}}}{\sigma_K}\right)\frac{\partial K}{\partial x_j}\right] + \tau_{ij,\text{tu}}\frac{\partial \overline{u}_i}{\partial x_j} - \rho\beta^*\omega K, \tag{M.2.2}$$

$$\frac{D}{Dt}(\rho \omega) = \frac{\partial}{\partial x_j}\left[\left(\mu + \frac{\mu_{\text{tu}}}{\sigma_\omega}\right)\frac{\partial \omega}{\partial x_j}\right] + \frac{\gamma\omega}{K}\tau_{ij,\text{tu}}\frac{\partial \overline{u}_i}{\partial x_j} - \rho\beta\omega^2, \tag{M.2.3}$$

where

$$\mu_{\text{tu}} = \frac{\gamma^*\rho K}{\omega}, \tag{M.2.4}$$

$$\tau_{ij,\text{tu}} = 2\mu_{\text{tu}}\left[S_{ij} - \frac{1}{3}\frac{\partial \overline{u}_k}{\partial x_k}\delta_{ij}\right] - \frac{2}{3}\delta_{ij}\rho K. \tag{M.2.5}$$

The elements of the mean strain-rate tensor are

$$S_{ij} = \frac{1}{2}\left(\frac{\partial \overline{u}_i}{\partial x_j} + \frac{\partial \overline{u}_j}{\partial x_i}\right). \tag{M.2.6}$$

According to Wilcox (1988), for high-Reynolds-number conditions,

$$\beta = \frac{3}{40}, \quad \beta^* = 0.09, \quad \gamma = \frac{5}{9},$$
$$\gamma^* = 1, \quad \sigma_K = 2, \quad \sigma_\omega = 2.$$

When wall functions are used for near-wall boundary conditions, then the following equations are to be used for the nodes that are adjacent to a smooth wall:

$$u = \frac{U_\tau}{\kappa} \ln(y^+), \tag{M.2.7}$$

$$K = \frac{U_\tau}{\sqrt{\beta^*}}, \tag{M.2.8}$$

$$\omega = \frac{U_\tau}{\sqrt{\beta^*}\kappa y}, \tag{M.2.9}$$

$$\gamma = \frac{\beta}{\beta^*} - \frac{\kappa^2}{\sigma_\omega \sqrt{\beta^*}}. \tag{M.2.10}$$

For nodes adjacent to a rough wall, however, we should use

$$\omega = \frac{U_\tau^2}{\nu} S_R, \tag{M.2.11}$$

where,

$$S_R = \begin{cases} \left(\dfrac{50}{\varepsilon_s^+}\right)^2 & \text{for } \varepsilon_s^+ < 25 \\ \dfrac{100}{\varepsilon_s^+} & \text{for } \varepsilon_s^+ > 25 \end{cases}, \tag{M.2.12}$$

where ε_s^+ is the wall roughness in wall units.

Alternatively, the near-wall conditions can be dealt with using the following low-Re parameters (Wilcox, 1993):

$$\gamma^* = \frac{\gamma_0^* + \dfrac{\mathrm{Re_{tu}}}{R_K}}{1 + \dfrac{\mathrm{Re_{tu}}}{R_K}}, \tag{M.2.13}$$

$$\gamma = \frac{5}{9} \frac{\gamma_0 + \dfrac{\mathrm{Re_{tu}}}{R_\omega}}{1 + \dfrac{\mathrm{Re_{tu}}}{R_\omega}} \gamma^{*-1}, \tag{M.2.14}$$

$$\beta^* = \frac{9}{100} \frac{\frac{5}{18} + \left(\dfrac{\mathrm{Re_{tu}}}{R_\beta}\right)^4}{1 + \left(\dfrac{\mathrm{Re_{tu}}}{R_\beta}\right)^4}, \tag{M.2.15}$$

where

$$R_K = 6, \quad R_\omega = 2.7, \quad R_\beta = 8 \quad \gamma_0 = 0.10,$$

$$\gamma_0^* = \frac{\beta}{3}, \tag{M.2.16}$$

$$\mathrm{Re}_{\mathrm{tu}} = \frac{K}{\nu\,\omega}. \tag{M.2.17}$$

The Baseline K–ω Model

The standard K–ω model just described, although very useful for the inner boundary layer, had to be abandoned in the wake region of the boundary layer in favor of the K–ε model because of its strong sensitivity to the free-stream values of ω. This difficulty was resolved by the development of baseline and shear-stress transport K–ω (SST-K–ω) models in which blending functions are defined such that the aforementioned standard K–ω model is applied near the wall, and far away from the wall the K–ω model smoothly blends into the standard K–ε model (Menter, 1994, 1996).

With some of its coefficients modified, Eq. (M2.2) applies, and Eq. (M2.3) is replaced with

$$\frac{D}{Dt}(\rho\omega) = \frac{\partial}{\partial x_j}\left[\left(\mu + \frac{\mu_{\mathrm{tu}}}{\sigma_\omega}\right)\frac{\partial\omega}{\partial x_j}\right] + \frac{\nu}{\nu_{\mathrm{tu}}}\tau_{ij,\mathrm{tu}}\frac{\partial\overline{u}_i}{\partial x_j} + 2\rho\,(1-F_1)\,\frac{1}{\sigma_{w2}\omega}\frac{\partial K}{\partial x_j}\frac{\partial\omega}{\partial x_j} - \rho\beta\omega^2, \tag{M.2.18}$$

where now

$$\mu_{\mathrm{tu}} = \frac{\rho K}{\omega} \tag{M.2.19}$$

$$\sigma_K = \left[\frac{F_1}{\sigma_{K1}} + \frac{(1-F_1)}{\sigma_{K2}}\right]^{-1}, \tag{M.2.20}$$

$$\sigma_\omega = \left[\frac{F_1}{\sigma_{\omega1}} + \frac{(1-F_1)}{\sigma_{\omega2}}\right]^{-1}. \tag{M.2.21}$$

The blending function F_1 is found from

$$F_1 = \tanh\left(\mathrm{arg}_1^4\right), \tag{M.2.22}$$

$$\mathrm{arg}_1 = \min\left\{\max\left(\frac{\sqrt{K}}{0.09\,\omega y};\ \frac{500\mu}{\rho\omega y^2}\right);\ \frac{4\rho K}{\mathrm{CD}_{K\omega}y^2\sigma_{\omega2}}\right\}. \tag{M.2.23}$$

The term $\mathrm{CD}_{K\omega}$ represents cross-diffusion, and is to be found from,

$$\mathrm{CD}_{K\omega} = \max\left\{\frac{2\rho}{\sigma_{\omega2}\omega}\frac{\partial K}{\partial x_j}\frac{\partial\omega}{\partial x_j};\ 10^{-20}\right\}. \tag{M.2.24}$$

Furthermore,

$$\beta = F_1\beta_1 + (1-F_1)\,\beta_2, \tag{M.2.25}$$

$$\gamma = F_1\gamma_1 + (1-F_1)\,\gamma_2. \tag{M.2.26}$$

The model constants are as follows:

$$\sigma_{K1} = 2.0\,, \quad \sigma_{\omega 1} = 2.0\,, \quad \beta_1 = 0.075,$$
$$\sigma_{K2} = 1.0\,, \quad \sigma_{\omega 2} = 1.168\,, \quad \beta_2 = 0.0828.$$

The subscripts 1 and 2 in these model constants represent the inner and outer regions of the boundary layer. Also, $\beta^* = 0.09$ and

$$\gamma_1 = \frac{\beta_1}{\beta^*} - \frac{\kappa^2}{\sigma_{\omega 1}\sqrt{\beta^*}}, \tag{M.2.27}$$

$$\gamma_2 = \frac{\beta_2}{\beta^*} - \frac{\kappa^2}{\sigma_{\omega 2}\sqrt{\beta^*}}. \tag{M.2.28}$$

Shear Stress Transport K–ω Model

This is an extension of the baseline K–ω model. The turbulence viscosity is defined here such that the transport of the principal turbulent shear stress is taken into account (Menter, 1994, 1996). The formulation is identical to the baseline K–ω model, except that now $\sigma_{K1} = 1.176$, and

$$\mu_{\text{tu}} = \frac{a_1 \rho K}{\max\left(a_1 \omega;\, F_2 S\right)}\,, \quad a_1 = 0.31, \tag{M.2.29}$$

where S is the absolute magnitude of vorticity [Eq. (M1.7)]. The blending function F_2 is found from

$$F_2 = \tanh\left(\arg_2^2\right), \tag{M.2.30}$$

$$\arg_2 = \min\left\{\frac{2\sqrt{K}}{0.09\,\omega y}\,;\, \frac{500\mu}{\rho\,\omega y^2}\right\}. \tag{M.2.31}$$

M.3 The K–ε Nonlinear Reynolds Stress Model

Several modification aimed at the improvement or enhancement of the K–ε model were proposed in the past. Two of the most widely used variations of the K–ε model are reviewed in this and the next sections.

The main difference between the K–ε nonlinear RSM and the standard K–ε model is that the former obtains the Reynolds stresses from nonlinear algebraic equations that are based on a generalized eddy viscosity model. The rationale is that the Boussinesq-based eddy viscosity model [see Eq. (6.4.2)] has proved adequate for 2D flow without swirl, when only one stress component provides the predominant influence on flow development. In flows with swirl, or 3D flows, to predict the data well, it appears that for each active stress a different viscosity needs to be defined. In other words, there is need for an anisotropic model for turbulent viscosity. This can be done by either developing separate equations for individual Reynolds stresses or developing a nonlinear RSM that accounts for the directional dependence of the turbulent transport coefficients. The K–ε nonlinear RSM adopts the latter approach.

Table M.1. *Coefficients for the nonlinear algebraic stress model (after Mompean et al., 1996)*

Authors(s)	C_μ	C_1	C_2	C_3
Demuren and Rodi (1984)	0.09	0.052	0.092	0.013
Rubinstein and Barton (1990)	0.0845	0.104	0.034	−0.014
Shih et al. (1993)	$0.67/(1.25+\eta)$	$-4/A$	$13/A$	$-2/A$
Gatski and Speziale (1993)	$0.680R$	$0.030R$	$0.093R$	$-0.034R$

The general form of the nonlinear Reynolds stress expression is (Speziale, 1987; Mompean et al., 1996)

$$-\overline{u_i' u_j'} = -\frac{2}{3}\delta_{ij}K + C_\mu \frac{K^2}{\varepsilon}(2S_{ij}) + C_D C_\mu^2 \frac{K^3}{\varepsilon^2}\left(S_{im}S_{mj} - \frac{1}{3}S_{mn}S_{nm}\delta_{ij}\right) + C_E C_\mu^2 \frac{K^3}{\varepsilon^2}\left(\dot{S}_{im} - \frac{1}{3}\dot{S}_{mm}\delta_{ij}\right), \tag{M.3.1}$$

where S_{ij} is defined in Eq. (M2.6) and $\dot{S}$ is the upper-convected derivative (the frame-indifferent Oldroyd derivative) of S, which is defined as,

$$\dot{S}_{ij} = \frac{\partial S_{ij}}{\partial t} + \overline{u}_k \frac{\partial S_{ij}}{\partial x_k} - \frac{\partial \overline{u}_i}{\partial x_k} S_{kj} - \frac{\partial \overline{u}_j}{\partial x_k} S_{ki}. \tag{M.3.2}$$

According to Speziale (1987),

$$C_D = 1.68, \quad C_E = 1.68, \quad C_\mu = 0.09.$$

If the advection transport term $\vec{\overline{U}} \cdot \nabla$ is neglected in Eq. (M3.1), the following nonlinear algebraic stress model is obtained,

$$-\overline{u_i' u_j'} = -\frac{2}{3}\delta_{ij}K + C_\mu \frac{K^2}{\varepsilon}(2S_{ij}) - C_1 \frac{K^3}{\varepsilon^2}\left[\frac{\partial \overline{u}_i}{\partial x_n}\frac{\partial \overline{u}_n}{\partial x_j} + \frac{\partial \overline{u}_j}{\partial x_n}\frac{\partial \overline{u}_n}{\partial x_i} - \frac{2}{3}\frac{\partial \overline{u}_m}{\partial x_n}\frac{\partial \overline{u}_n}{\partial x_m}\delta_{ij}\right] - C_2 \frac{K^3}{\varepsilon^2}\left[\frac{\partial \overline{u}_i}{\partial x_n}\frac{\partial \overline{u}_j}{\partial x_n} - \frac{1}{3}\frac{\partial \overline{u}_n}{\partial x_m}\frac{\partial \overline{u}_n}{\partial x_m}\delta_{ij}\right] - C_3 \frac{K^3}{\varepsilon^2}\left[\frac{\partial \overline{u}_n}{\partial x_i}\frac{\partial \overline{u}_n}{\partial x_j} - \frac{1}{3}\frac{\partial \overline{u}_n}{\partial x_m}\frac{\partial \overline{u}_n}{\partial x_m}\delta_{ij}\right]. \tag{M.3.3}$$

Table M.1 is a summary of the proposed values of the coefficients in the this equation. The following definitions apply for the model coefficients of Shih et al. (1993) and Gatski and Speziale (1993):

$$A = 1000 + \eta^3, \tag{M.3.4}$$

$$R = (1 + 0.0038\eta^2)/D, \tag{M.3.5}$$

$$D = 3 + 0.0038\eta^2 + 0.0008\eta^2\zeta^2 + 0.2\zeta^2, \tag{M.3.6}$$

$$\eta = \frac{K}{\varepsilon}(2S_{ij}S_{ij})^{1/2}, \tag{M.3.7}$$

$$\zeta = \frac{K}{\varepsilon}\left\{\frac{1}{4}\left(\frac{\partial \overline{u}_i}{\partial x_j} - \frac{\partial \overline{u}_j}{\partial x_i}\right)\left(\frac{\partial \overline{u}_i}{\partial x_j} - \frac{\partial \overline{u}_j}{\partial x_i}\right)\right\}^{1/2}. \tag{M.3.8}$$

Obviously a turbulent viscosity can be defined according to Eq. (12.4.2)

The K–ε nonlinear RSM is suitable for high Reynolds flow conditions. Mompean et al. (1996) noted that, although neither one of the aforementioned models agreed well with DNS data representing near-wall phenomena in a square duct flow, the model of Gatski and Speziale (1993) performed best.

The turbulent heat and mass fluxes that are needed for the solution of the turbulent energy and mass-species conservation equations can be modeled by use of the eddy diffusivity concept. The simple eddy diffusivity based on Boussinesq's hypothesis leads to Eqs. (12.4.30) and (12.4.31). The latter expressions are widely used. However, they imply isotropy and are therefore in principle inconsistent with the nonlinear stress model. Eddy diffusivity models meant to account for the anisotropic turbulent diffusion can be used instead. A model proposed by Daly and Harlow (1970), also referred to as the generalized gradient hypothesis (Rokni and Sunden, 2003), provides

$$\rho C_P \overline{u_i' T'} = -\rho C_P C_t \frac{K}{\varepsilon} \left(\overline{u_i' u_j'} \frac{\partial \overline{T}}{\partial x_j} \right), \tag{M.3.9}$$

$$\rho \overline{u_i' m_1'} = -\rho C_t \frac{K}{\varepsilon} \left(\overline{u_i' u_j'} \frac{\partial \overline{m}_1}{\partial x_j} \right), \tag{M.3.10}$$

where $C_t = 0.3$.

M.4 The RNG *K*–ε Model

The RNG theory refers to a mathematical technique whose aim is to actually derive *K*–ε and other turbulence models and their coefficients. The rationale is that the specification of the coefficient in the *K*–ε model, for example, is rather ad hoc. The coefficients are determined empirically with little theoretical basis and are assigned different values by different researchers. Unlike *K*–ε and other common turbulence models that use a single length scale for the calculation of eddy diffusivity, the RNG technique accounts for the subgrid eddy scales in its derivations.

The derivation of the RNG *K*–ε theory is rather complicated (Yakhot and Orszag, 1986; Yakhot and Smith, 1992). However, it leads to the K and ε transport equations previously described in Section 12.4 [see Eqs. (12.4.1) and (12.4.6)], with the following coefficients. The coefficient $C_{\varepsilon 2}$ is replaced with $C_{\varepsilon 2}^*$, where

$$C_{\varepsilon 2}^* = C_{\varepsilon 2} + \frac{C_\mu \eta^3 \left(1 - \dfrac{\eta}{\eta_0} \right)}{1 + \beta \eta^3}, \tag{M.4.1}$$

and

$$\eta = \Omega K / \varepsilon,$$

$$\Omega = \sqrt{2 S_{ij} S_{ij}}.$$

Other model constants are (Yakhot, 1992)

$$C_\mu = 0.0845, \ C_{\varepsilon 1} = 1.42, \ C_{\varepsilon 2} = 1.68, \ \sigma_K = 0.7194,$$
$$\sigma_\varepsilon = 0.7194, \ \ \eta_0 = 4.38, \ \ \beta = 0.012.$$

However, in terms of performance, the RNG K–ε model appears to be only slightly superior to the traditional, ad hoc K–ε model.

M.5 The Low-Re RSM of Launder and Shima

Launder and Shima (1989) proposed the following widely applied near-wall RSM model,

$$\frac{D}{Dt}\overline{u_i'u_j'} = \boldsymbol{D}_{ij} + \boldsymbol{P}_{ij} - \boldsymbol{\varepsilon}_{ij} + \boldsymbol{\Phi}_{ij} + \frac{\partial}{\partial x_k}\left[\nu\frac{\partial}{\partial x_k}\overline{u_i'u_j'}\right], \tag{M.5.1}$$

$$\frac{D\varepsilon}{Dt} = \frac{\partial}{\partial x_k}\left[\left(C_\varepsilon\frac{K}{\varepsilon}\overline{u_k'u_l'} + \nu\delta_{lk}\right)\frac{\partial\varepsilon}{\partial x_l}\right] + (C_{\varepsilon 1} + \Psi_1 + \Psi_2)\left(\frac{\varepsilon}{K}\right)\boldsymbol{P} - C_{\varepsilon 2}\left(\frac{\varepsilon\tilde{\varepsilon}}{K}\right), \tag{M.5.2}$$

$$\tilde{\varepsilon} = \varepsilon - 2\nu(\partial K^{1/2}/\partial x_j)(\partial K^{1/2}/\partial x_j). \tag{M.5.3}$$

The parameter $\boldsymbol{D}_{ij}$ represents the turbulence diffusion:

$$\boldsymbol{D}_{ij} = \frac{\partial}{\partial x_k}\left[C_s\frac{K}{\varepsilon}\overline{u_k'u_l'}\frac{\partial\overline{u_i'u_j'}}{\partial x_l}\right]. \tag{M.5.3}$$

The term P_{ij} represents the stress generation rate by mean shear:

$$\boldsymbol{P}_{ij} = \left[\overline{u_i'u_k'}\frac{\partial\overline{u}_j}{\partial x_k} - \overline{u_j'u_k'}\frac{\partial\overline{u}_i}{\partial x_k}\right]. \tag{M.5.4}$$

Also,

$$\boldsymbol{\varepsilon}_{ij} = \frac{2}{3}\delta_{ij}\varepsilon. \tag{M.5.5}$$

The term $\boldsymbol{\Phi}_{ij}$ represents the pressure strain and is assumed to be made of three components: the slow-pressure strain term (the return-to-isotropy term), $\boldsymbol{\Phi}_{ij,1}$, the rapid-pressure strain term, $\boldsymbol{\Phi}_{ij,2}$ and the wall-reflection term, $\boldsymbol{\Phi}_{ij,w}$, where,

$$\boldsymbol{\Phi}_{ij} = \boldsymbol{\Phi}_{ij,1} + \boldsymbol{\Phi}_{ij,2} + \boldsymbol{\Phi}_{ij,w}, \tag{M.5.6}$$

$$\boldsymbol{\Phi}_{ij,1} = -C_1\varepsilon a_{ij}, \tag{M.5.7}$$

$$\boldsymbol{\Phi}_{ij,2} = -C_2\left(\boldsymbol{P}_{ij} - \frac{2}{3}\delta_{ij}\boldsymbol{P}\right), \tag{M.5.8}$$

$$\boldsymbol{\Phi}_{ij,w} = \left\{C_{1w}\frac{\varepsilon}{K}\left[\overline{u_k'u_m'}n_kn_m\delta_{ij} - \left(\frac{3}{2}\right)\overline{u_k'u_i'}n_kn_j - \left(\frac{3}{2}\right)\overline{u_k'u_j'}n_kn_i\right]\right.$$
$$\left. + C_{2w}\left[\boldsymbol{\Phi}_{km,2}n_kn_m\delta_{ij} - \left(\frac{3}{2}\right)\boldsymbol{\Phi}_{ik,2}n_kn_j - \left(\frac{3}{2}\right)\boldsymbol{\Phi}_{jk,2}n_kn_i\right]\right\}\left(\frac{0.4\,K^{3/2}}{\varepsilon y}\right), \tag{M.5.9}$$

where n_k, n_m, ..., are the k and m components of the unit normal vector to the wall, y is the normal distance from the wall, and

$$\boldsymbol{P} = \frac{1}{2}\boldsymbol{P}_{kk}. \tag{M.5.10}$$

The dimensionless anisotropic part of the Reynolds stress is

$$a_{ij} = \left(\overline{u_i' u_j'} - \frac{2}{3}\delta_{ij}K\right) \Big/ K. \tag{M.5.11}$$

Also, $C_s = 0.2$, and

$$C_1 = 1 + 2.85A\,(a_{ik}a_{ki})^{1/4}\,\{1 - \exp[-(0.0067\mathrm{Re_{tu}})^2]\}, \tag{M.5.12}$$

$$C_2 = 0.75\sqrt{A}, \tag{M.5.13}$$

$$C_{1w} = -\frac{2}{3}C_1 + 1.67, \tag{M.5.14}$$

$$C_{2w} = \max\left[\left(\frac{2}{3}C_2 - \frac{1}{6}\right) \Big/ C_2,\ 0\right], \tag{M.5.15}$$

$$A = \left[1 - \frac{9}{8}\,(A_2 - A_3)\right], \tag{M.5.16}$$

$$A_2 = a_{ik}a_{ki}, \tag{M.5.17}$$

$$A_3 = a_{ik}a_{kj}a_{ji}, \tag{M.5.18}$$

$$\Psi_1 = 2.5A\left(\frac{\boldsymbol{P}}{\varepsilon} - 1\right), \tag{M.5.19}$$

$$\Psi_2 = 0.3(1 - 0.3A_2)\exp[-(0.002\,\mathrm{Re_{tu}})^2], \tag{M.5.20}$$

$$C_\varepsilon = 0.18, \quad C_{\varepsilon 1} = 1.45, \quad C_{\varepsilon 2} = 1.90,$$

$$\mathrm{Re_{tu}} = K^2/(\nu\varepsilon). \tag{M.5.21}$$

APPENDIX N

Physical Constants

Universal gas constant:

$$\begin{aligned} R_u &= 8314.3\,\text{J/kmol K} \\ &= 8.3143\ \text{kJ/kmol K} \\ &= 1545\,\text{lb}_f\text{ft/lb mol}\,^\circ\text{R} \\ &= 8.205 \times 10^{-2}\,\text{m}^3\,\text{atm/kmol K}. \end{aligned}$$

Standard atmospheric pressure:

$$\begin{aligned} P &= 101,325\ \text{N/m}^2 \\ &= 101.325\ \text{kPa} \\ &= 14.696\ \text{psi}, \end{aligned}$$

Standard gravitational acceleration:

$$\begin{aligned} g &= 9.80665\ \text{m/s}^2 \\ &= 980.665\ \text{cm/s}^2 \\ &= 32.174\ \text{ft/s}^2. \end{aligned}$$

Atomic mass unit:

$$\text{amu} = 1.66043 \times 10^{-27}\,\text{kg}.$$

Avagadro's Number:

$$\begin{aligned} N_{\text{Av}} &= 6.022136 \times 10^{26}\ \text{molecules/kmol} \\ &= 6.024 \times 10^{23}\ \text{molecules/mol}. \end{aligned}$$

Boltzmann constant:

$$\begin{aligned} \kappa_B &= 1.380658 \times 10^{-23}\,\text{J/K} \\ &= 1.380658 \times 10^{-16}\,\text{erg/K}. \end{aligned}$$

Planck's constant:

$$\begin{aligned} \boldsymbol{h} &= 6.62608 \times 10^{-34}\,\text{J s} \\ &= 6.62608 \times 10^{-27}\,\text{erg s}. \end{aligned}$$

Speed of light:

$$\begin{aligned} C &= 2.99792 \times 10^8 \text{ m/s} \\ &= 2.99792 \times 10^{10} \text{ m/s}. \end{aligned}$$

Stefan–Boltzmann constant:

$$\begin{aligned} \sigma &= 5.670 \times 10^{-8} \text{ W/m}^2 \text{ K}^4 \\ &= 1.712 \times 10^{-9} \text{ Btu/h ft}^2 \,^\circ\text{R}^4. \end{aligned}$$

APPENDIX O

Unit Conversions

Density:

$$\begin{aligned} \mathrm{kg/m^3} &= 10^{-3}\,\mathrm{g/cm^3} \\ &= 0.06243\,\mathrm{lb}_m/\mathrm{ft^3}. \end{aligned}$$

Diffusivity:

$$\mathrm{m^2/s} = 3.875 \times 10^4\,\mathrm{ft^2/h}.$$

Energy, work:

$$\begin{aligned} J &= 10^7\,\mathrm{erg} \\ &= 6.242 \times 10^{18}\,\mathrm{eV} \\ &= 0.2388\,\mathrm{cal} \\ &= 9.4782 \times 10^{-4}\,\mathrm{Btu} \\ &= 0.7376\,\mathrm{lb}_f\,\mathrm{ft}. \end{aligned}$$

Force:

$$\begin{aligned} N &= 10^5\,\mathrm{dyn} \\ &= 0.22481\,\mathrm{lb}_f. \end{aligned}$$

Heat flux:

$$\begin{aligned} \mathrm{W/m^2} &= 0.3170\,\mathrm{Btu/h\,ft^2} \\ &= 2.388 \times 10^{-5}\,\mathrm{cal/cm^2\,s}. \end{aligned}$$

Heat generation rate (Volumetric):

$$\mathrm{W/m^3} = 0.09662\,\mathrm{Btu/h\,ft^3}.$$

Heat transfer coefficient:

$$\mathrm{W/m^2\,K} = 0.17611\,\mathrm{Btu/h\,ft^2\,{}^\circ R}.$$

Length:

$$\begin{aligned} m &= 3.2808\ \text{ft} \\ &= 39.370\ \text{in} \\ &= 10^6\ \mu\text{m} \\ &= 10^{10}\ \text{Å}, \\ \text{mill} &= 10^{-3}\ \text{in}. \end{aligned}$$

Mass:

$$\begin{aligned} \text{kg} &= 10^3\ \text{g} \\ &= 2.2046\ \text{lb}_m. \end{aligned}$$

Mass flow rate:

$$\text{kg/s} = 7936.6\ \text{lb}_m/\text{h}.$$

Mass flux or mass transfer coefficient:

$$\text{kg/m}^2\text{s} = 737.3\ \text{lb}_m/\text{ft}^2\ \text{h}.$$

Power:

$$\begin{aligned} \text{W} &= 10^{-3}\ \text{kW} \\ &= 3.4121\ \text{Btu/h} \\ &= 1.341 \times 10^{-3}\ \text{hp}. \end{aligned}$$

Pressure or stress:

$$\begin{aligned} \text{N/m}^2\ (\text{Pa}) &= 10\ \text{dyn/cm}^2 \\ &= 10^{-5}\ \text{bars} \\ &= 0.020885\ \text{lb}_f/\text{ft}^2 \\ &= 1.4504 \times 10^{-4}\ \text{lb}_f/\text{in}^2\ (\text{psi}) \\ &= 4.015 \times 10^{-3}\ \text{in water} \\ &= 2.953 \times 10^{-4}\ \text{in Hg}, \\ \text{atm} &= 760\ \text{torr}. \end{aligned}$$

Specific enthalpy or internal energy:

$$\begin{aligned} \text{J/kg} &= 10^{-3}\ \text{kJ/kg} \\ &= 4.299 \times 10^{-4}\ \text{Btu/lb}_m \\ &= 2.393 \times 10^{-4}\ \text{cal/g}. \end{aligned}$$

Specific heat:

$$\begin{aligned} \text{J/kg K} &= 10^{-3}\ \text{kJ/kg K} \\ &= 0.2388\ \times 10^{-3}\ \text{Btu/lb}_m\ ^\circ\text{R} \\ &= 2.393 \times 10^{-4}\ \text{cal/g K}. \end{aligned}$$

Temperature:

$$\begin{aligned} T[\mathrm{K}] &= T[^\circ\mathrm{C}] + 273.15[\mathrm{K}], \\ T[^\circ\mathrm{R}] &= T[^\circ\mathrm{F}] + 459.67[^\circ\mathrm{R}], \\ 1\ \mathrm{K} &= 1\,^\circ\mathrm{C} = 1.8\,^\circ\mathrm{R} = 1.8\,^\circ\mathrm{F}. \end{aligned}$$

Thermal conductivity:

$$\mathrm{W/m\,K} = 0.57779\,\mathrm{Btu/h\,ft^2\,^\circ R}.$$

Velocity:

$$\begin{aligned} \mathrm{m/s} &= 3.28\ \mathrm{ft/s} \\ &= 3.600\ \mathrm{km/h}, \\ \mathrm{km/h} &= 0.6214\ \mathrm{mph}. \end{aligned}$$

Viscosity:

$$\begin{aligned} \mathrm{kg/ms} &= \mathrm{Ns/m^2} \\ &= 10\ \mathrm{poise} \\ &= 10^3\ \mathrm{cp} \\ &= 2419.1\ \mathrm{lb}_m\mathrm{/ft\,h} \\ &= 5.8015 \times 10^{-6}\,\mathrm{lb}_f\mathrm{h/ft^2} \\ &= 2.0886 \times 10^{-2}\,\mathrm{lb}_f\mathrm{s/ft^2}. \end{aligned}$$

Volume:

$$\begin{aligned} m^3 &= 10^3\,\mathrm{L} \\ &= 35.315\,\mathrm{ft^3} \\ &= 264.17\ \mathrm{gal\,(U.S.)} \end{aligned}$$

APPENDIX P

Summary of Important Dimensionless Numbers

Dimensionless Number	Definition	Interpretation
Biot number (Bi)	hl/k	Ratio of conduction resistance of a solid to the thermal resistance of a boundary layer
Brinkman number (Br)	$\dfrac{\mu U^2}{k\,\lvert\Delta T\rvert}$	Ratio of viscous dissipation to heat conduction
Buoyancy number (Bu)	$\mathrm{Gr}/\mathrm{Re}^m$	The significance of natural convection relative to forced convection
Eckert number (Ec)	$\dfrac{U_{\text{ref}}^2}{C_P\,(T_s - T_\infty)}$	Ratio of flow kinetic energy to the boundary-layer enthalpy difference
Friction factor (Darcy) (f)	$\dfrac{\left(-\dfrac{\partial P}{\partial x}\right)_{\text{fr}}}{\dfrac{1}{D_H}\dfrac{1}{2}\rho U_{\text{ref}}^2}$	Dimensionless pressure gradient for internal flow
Fanning friction factor (skin-friction coefficient) (C_f)	$\dfrac{\tau_s}{\dfrac{1}{2}\rho U_{\text{ref}}^2}$	Dimensionless surface shear stress
Fourier number (heat transfer) (Fo)	$\left(\dfrac{k}{\rho C_P}\right)\dfrac{t}{l^2}$	Dimensionless time; ratio of heat conduction to thermal storage
Fourier number (mass transfer) (Fo_{ma})	$\mathcal{D}\dfrac{t}{l^2}$	Dimensionless time; ratio of a species diffusion to that species' storage
Galileo number (Ga)	$\dfrac{\rho\,\Delta\rho\,g\,l^3}{\mu^2}$	Ratio of buoyancy to viscous force
Grashof number (Gr)	$\dfrac{g\,\beta l^3 \Delta T}{\nu^2}$	Ratio of buoyancy to viscous force
Graetz number (Gz)	$\dfrac{4Ul^2}{x}\left(\dfrac{\rho C_P}{k}\right)$	Dimensionless length important for thermally developing flow

Dimensionless Number	Definition	Interpretation
Lewis number (Le)	$\frac{\boldsymbol{\alpha}}{\mathcal{D}}$	Ratio of thermal to mass diffusivities
Nusselt number (Nu)	hl/k	Dimensionless heat transfer coefficient
Peclet number (heat transfer) (Pe)	$\mathrm{Re}_l \,\mathrm{Pr} = \frac{U\,l}{\boldsymbol{\alpha}}$	Ratio of advection to conduction heat transfer rates
Peclet number (mass transfer) ($\mathrm{Pe}_{\mathrm{ma}}$)	$\mathrm{Re}_l Sc = \frac{U\,l}{\mathcal{D}}$	Ratio of advection to diffusion mass transfer rates
Poiseuille number (Po)	$\frac{2\tau_s D_H}{\mu\, U}$	Dimensionless surface shear stress in internal flow
Prandtl number (Pr)	$\mu C_P/k$	Ratio of momentum and heat diffusivities
Rayleigh number (Ra)	$\mathrm{Gr}\,\mathrm{Pr} = \frac{g\,\beta\,l^3\Delta T}{\nu\,\boldsymbol{\alpha}}$	Product of Grashof and Prandtl numbers
Rayleigh number, modified (Ra^*)	$\frac{g\,\beta\,l^4 q''}{\nu\,\boldsymbol{\alpha}\,k}$	Rayleigh number defined for UHF boundary conditions
Reynolds number (Re)	$\rho U\,l/\mu$	Ratio of inertial to viscous forces
Reynolds number for a liquid film (Re_F)	$4\Gamma_F/\mu_L$	Ratio of inertial to viscous forces in a liquid film
Reynolds number (turbulence) (Re_y)	$\rho\, K^{1/2} y/\mu$	Reynolds number in low-Re turbulence models
Richardson number (Ri)	$\mathrm{Gr}_l/\mathrm{Re}_l^2$	The significance of natural convection relative to forced convection
Schmidt number (Sc)	$\nu/\mathcal{D}$	Ratio of momentum and mass-species diffusivities
Sherwood number (Sh)	$\frac{\mathcal{K}\,l}{\rho\mathcal{D}}$ or $\frac{\tilde{\mathcal{K}}\,l}{\boldsymbol{C}\,\mathcal{D}}$	Dimensionless mass transfer coefficient
Stanton number (for heat transfer) (St)	$\frac{h}{\rho\, C_P U} = \frac{h}{\boldsymbol{C}\,\tilde{C}_P U} = \frac{\mathrm{Nu}_l}{\mathrm{Re}_l \mathrm{Pr}}$	Dimensionless heat transfer coefficient
Stanton number for mass transfer ($\mathrm{St}_{\mathrm{ma}}$)	$\frac{\mathcal{K}}{\rho\, U} = \frac{\tilde{\mathcal{K}}}{\boldsymbol{C}\, U} = \frac{\mathrm{Sh}_l}{\mathrm{Re}_l \mathrm{Sc}}$	Dimensionless mass transfer coefficient

APPENDIX Q

Summary of Some Useful Heat Transfer and Friction-Factor Correlations

Table Q.1. *Nusselt numbers and friction factors for forced, external flow*

Geometry	Correlation	Comments	Source
Flat plate	$\delta_x = 5x\,\mathrm{Re}_x^{-1/2}$	Local laminar velocity boundary-layer thickness	Analytical
Flat plate	Eq. (3.1.30)	Local skin-friction coefficient, laminar boundary layer	Analytical
Flat plate	Eq. (3.2.32a)	Local heat transfer coefficient, laminar boundary layer, UWT, $0.5 \lesssim \mathrm{Pr} \lesssim 15$	Semianalytical
Flat plate	$\langle C_f \rangle_l = 1.328\mathrm{Re}_l^{-1/2}$	Average skin-friction coefficient, laminar boundary layer	Analytical
Flat plate	Eq. (3.2.32a)	Local heat transfer coefficient, laminar boundary layer, UWT, $0.5 \lesssim \mathrm{Pr} \lesssim 15$	Analytical
Flat plate	$\mathrm{Nu}_x = 0.453\mathrm{Re}_x^{1/2}\,\mathrm{Pr}^{1/3}$	Local heat transfer coefficient, laminar boundary layer, UHF, $0.6 \lesssim \mathrm{Pr} \lesssim 10$	Semianalytical
Flat plate	$\mathrm{Nu}_x = 0.0296\mathrm{Re}_x^{4/5}\,\mathrm{Pr}^{1/3}$	Local heat transfer coefficient, smooth- surface turbulent boundary layer, UHF, $0.6 \lesssim \mathrm{Pr} \lesssim 60$	Analogy
Flat plate	$\mathrm{Re}_{x,cr} \approx 5 \times 10^5$	Laminar–turbulent transition for a smooth plane surface	Empirical
Flat plate	$\delta_x = 0.37x\mathrm{Re}_x^{-1/5}$	Turbulent boundary-layer thickness	Empirical
Flat plate	$C_{f,x} = 0.0592\mathrm{Re}_x^{-0.2}$	Local skin-friction coefficient, smooth surface turbulent boundary layer	Empirical (Pletcher, 1987)
Flat plate	$\langle C_{f,l} \rangle_l = 0.074\mathrm{Re}_l^{-1/5} - 1742\mathrm{Re}_l^{-1}$	Average skin-friction coefficient, mixed boundary layer, smooth surface, $\mathrm{Re}_{x,cr} = 5 \times 10^5$, $5 \times 10^5 < \mathrm{Re}_l \lesssim 10^8$	Semi-empirical
Flat plate	Eq. (6.5.11)	Local skin-friction coefficient, turbulent flow, rough wall	Schlichting (1968)

Flat plate	Eq. (6.5.12)	Average skin-friction coefficient, turbulent flow, rough wall	Schlichting (1968)
Flat plate	$\mathrm{Nu}_x = \dfrac{0.3387\mathrm{Re}_x^{1/2}\,\mathrm{Pr}^{1/3}}{\left[1+(0.0468/\mathrm{Pr})^{2/3}\right]^{1/4}}$	Local heat transfer coefficient, laminar boundary layer, UWT, wide range of Pr, $\mathrm{Pe}_x \gtrsim 100$, $\mathrm{Re}_x \lesssim 5\times 10^5$	Empirical, (Churchill and Ozoe, 1973a)
Flat plate	$\langle \mathrm{Nu}_l \rangle_l = 2\left\{\dfrac{0.3387\mathrm{Re}_l^{1/2}\,\mathrm{Pr}^{1/3}}{\left[1+(0.0468/\mathrm{Pr})^{2/3}\right]^{1/4}}\right\}$	Average heat transfer coefficient, UWT, wide range of Pr, $\mathrm{Pe}_l \gtrsim 100$	Empirical, (Churchill and Ozoe, 1973a)
Long circular cylinder, cross flow	$\langle \mathrm{Nu}_D \rangle = 0.3 + \dfrac{0.62\mathrm{Re}_D^{1/2}\,\mathrm{Pr}^{1/3}}{\left[1+\left(\dfrac{0.4}{\mathrm{Pr}}\right)^{2/3}\right]^{1/4}}\left[1+\left(\dfrac{\mathrm{Re}_D}{282,000}\right)^{5/8}\right]^{4/5}$	Empirical, UWT, $\mathrm{Re}_D\,\mathrm{Pr} \gtrsim 0.2$, properties at film temperature	Churchill and Bernstein (1977)
Long noncircular cylinder, cross flow	$\langle \mathrm{Nu}_D \rangle = C\mathrm{Re}_D^m\,\mathrm{Pr}^{1/3}$	Empirical, gas flow ($\mathrm{Pr} \gtrsim 0.7$); parameters C, D, and m depend on Re_D and geometry; see the table for air	Hilpert (1933)

Geometry	Re_D	C	m
Square 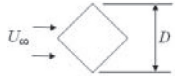	$5\times 10^3 \lesssim Re_D \lesssim 10^5$	0.246	0.588
Square 	$5\times 10^3 \lesssim Re_D \lesssim 10^5$	0.102	0.675

Table Q.1 *(continued)*

Geometry	Correlation	Comments		Source
Hexagon 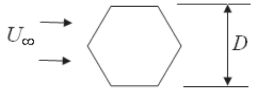	$5 \times 10^3 \lesssim \mathrm{Re}_D \lesssim 10^5$	0.153	0.638	
Hexagon 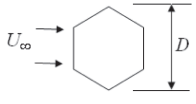	$5 \times 10^3 \lesssim \mathrm{Re}_D \lesssim 1.95 \times 10^4$ $1.95 \times 10^4 \lesssim \mathrm{Re}_D \lesssim 10^5$	0.160 0.0385	0.638 0.782	
Vertical Plate 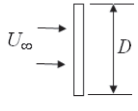	$4.0 \times 10^3 \lesssim \mathrm{Re}_D \lesssim 1.5 \times 10^4$	0.228	0.731	
Short circular cylinder, cross flow	$\langle \mathrm{Nu}_D \rangle = 0.123\mathrm{Re}_D^{0.651} + 0.00416\left(\frac{D}{l}\right)^{0.85}\mathrm{Re}_D^{0.792}$	Empirical, gas flow, $\frac{l}{D} < 4$, $7 \times 10^4 < \mathrm{Re}_D < 2.2 \times 10^5$, properties at film temperature		Zukauskas (1972)
Sphere	$\langle \mathrm{Nu}_D \rangle = 2.0 + \left(0.4\mathrm{Re}_D^{1/2} + 0.06\mathrm{Re}_D^{2/3}\right)\mathrm{Pr}^{0.4}\left(\frac{\mu}{\mu_s}\right)^{1/4}$	Empirical, $3.5 < \mathrm{Re}_D < 7.6 \times 10^4$, $0.7 \lesssim \mathrm{Pr} \lesssim 380$, properties at ambient temperature		Whitaker (1972)

Table Q.2. *Nusselt numbers and Darcy friction factors for laminar fully developed internal flow*[a]

Geometry $\left(\frac{l}{D_H} > 100\right)$	$\langle \mathrm{Nu}_{D_H,\mathrm{UHF}} \rangle$	$\langle \mathrm{Nu}_{D_H,\mathrm{UWT}} \rangle$	$f\mathrm{Re}_{D_H}$
 Equilateral triangle	1.892[b]	2.49	53.33
 Square	3.091	2.976	56.91
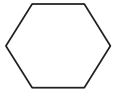 Regular hexagon	3.862	3.34	60.22
Rectangle ($\alpha^* = b/a$) 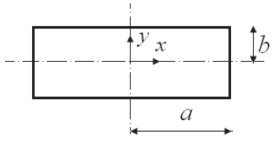	$\langle \mathrm{Nu}_{D_H,\mathrm{UHF}} \rangle = 8.235\,(1 - 10.6044\alpha^* + 61.1755\alpha^{*2} - 155.1803\alpha^{*3} + 176.9203\alpha^{*4} - 72.9236\alpha^{*5})$	$\langle \mathrm{Nu}_{D_H,\mathrm{UWT}} \rangle = 7.541\,(1 - 2.610\alpha^* + 4.970\alpha^{*2} - 5.119\alpha^{*3} + 2.702\alpha^{*4} - 0.548\alpha^{*5})$	$f\mathrm{Re}_{D_H} = 96\,(1 - 1.3553\alpha^* + 1.9467\alpha^{*2} - 1.7012\alpha^{*3} + 0.9564\alpha^{*4} - 0.2537\alpha^{*5})$
	(Shah and Bhatti, 1987)	(Shah and Bhatti, 1987)	(Shah and Bhatti, 1987)
$\alpha^* = 1.0$	3.09	2.976	56.91
$\alpha^* = 0.5$	3.017	3.391	62.19
$\alpha^* = 1/3$	2.97	3.956	68.36
$\alpha^* = 0.25$	2.94	4.439	72.93
$\alpha^* = 0.125$	2.94	5.597	82.34
$\alpha^* = 0.1$	2.95	5.858	84.68
$\alpha^* = 0$(flat channel)	8.235	7.541	96.00

Table Q.2 *(continued)*

Geometry $\left(\frac{l}{D_H} > 100\right)$	$\langle \mathrm{Nu}_{D_H,\mathrm{UHF}} \rangle$	$\langle \mathrm{Nu}_{D_H,\mathrm{UWT}} \rangle$	$f\mathrm{Re}_{D_H}$
Flat channel 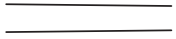	8.235	7.541	96.00
Flat channel with one side insulated 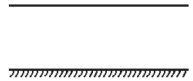	5.385[c]	4.861	96.00
Concentric annulus	Eq. (4.4.79) or (4.4.81)[a]	Eq. (4.4.78) or (4.4.80)[a]	Eq. (4.3.33)
Elliptical ($\alpha^* = b/a$) 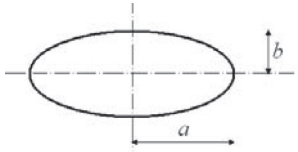			
$\alpha^* = 1.0$	4.364	3.658	64.0
$\alpha^* = 0.5$	3.802	3.742	67.29
$\alpha^* = 0.25$	2.333	3.792	72.96
$\alpha^* = 0.125$	0.9433	3.725	76.58

[a] Extracted from Shah and London (1978).
[b] For axially uniform heat flux and circumferentially uniform temperature (H1 boundary condition, see Section 1.5.4), the average Nusselt number is 3.111.
[c] This is actually for H1 boundary condition described in Section 1.4.5.

Table Q.3. *Nusselt numbers and Darcy friction factors for turbulent fully-developed internal flow*[a, b]

Geometry $\left(\frac{l}{D} \lesssim 10\right)$	Correlation	Comments	Source
Circular	$f = 0.316\mathrm{Re}_D^{-1/4}$	Smooth circular pipe, fully turbulent and $\mathrm{Re}_D \lesssim 2 \times 10^4$ [same as Eq. (7.2.38)]	Blasius (1913)
Circular	Eq. (7.2.43)	Smooth circular pipe, $2100 < \mathrm{Re}_D < 4500$	Hrycak and Andrushkiw (1974)
Circular	$f = 0.184\mathrm{Re}_D^{-0.2}$	Smooth circular pipe, fully turbulent $10^4 \lesssim \mathrm{Re}_D \lesssim 10^6$	Kays and London (1984)
Circular	Eq. (7.2.41) or (7.2.42)	Friction factor in rough circular pipe, fully turbulent $5 \leq \varepsilon_s^+ \leq 70$	Colebrook (1939), Haaland (1983),
Circular	$\frac{1}{\sqrt{C_f}} = 3.48 - 1.737 \ln\left(\frac{2\varepsilon_s}{D}\right)$	Fanning friction factor for fully rough pipes	Nikuradse (1933)
Noncircular	Eq. (7.2.47)	Effective diameter to be used in circular channel correlations for friction factor	Jones (1976)
Circular	$\mathrm{Nu}_D = 0.023\mathrm{Re}_D^{0.8}\,\mathrm{Pr}^n$ $n = 0.4$ for heating; $n = 0.3$ for cooling	Heat transfer in smooth pipes, $\mathrm{Re}_D \lesssim 10^4; 0.7 \lesssim \mathrm{Pr} \lesssim 160$	Dittus and Boelter (1930)
Circular	Eq. (7.3.33)	Heat transfer in smooth pipes, $10^4 \leq \mathrm{Re}_D \leq 5 \times 10^6$ and $0.5 \leq \mathrm{Pr} \leq 2000$	Petukhov (1970)
Circular	Eq. (7.3.41)	Heat transfer in smooth pipes, $2300 < \mathrm{Re}_D < 5 \times 10^6$ and $0.5 < \mathrm{Pr} < 2300$	Gnielinski (1976)
Circular	$\mathrm{Nu}_D = \dfrac{\mathrm{Re}_D\,\mathrm{Pr}\,(C_f/2)}{1 + \sqrt{\frac{C_f}{2}}\left[4.5\mathrm{Re}_{\varepsilon_s}^{0.2}\mathrm{Pr}^{0.5} - 8.48\right]}$, $\mathrm{Re}_{\varepsilon_s} = \varepsilon_s U_\tau / \nu$	Heat transfer in rough pipes, $0.002 < \varepsilon_s/D < 0.05$, $0.5 < \mathrm{Pr} < 10$, $\mathrm{Re}_D > 10^4$ It predicts experimental data within $\pm 5\%$, C_f represents fully rough pipe flow.	Bhatti and Shah (1987)

Table Q.3 *(continued)*

Geometry $\left(\frac{l}{D} \lesssim 10\right)$	Correlation	Comments	Source
Circular	$\mathrm{Nu}_D = \dfrac{(\mathrm{Re}_D - 1000)\, Pr\, (C_f/2)}{1 + \sqrt{\frac{C_f}{2}}\left[(17.42 - 13.77\,\mathrm{Pr}_{lu}^{0.8})\,\mathrm{Re}_{\varepsilon_s}^{0.5} - 8.48\right]}$, $\mathrm{Re}_{\varepsilon_s} = \varepsilon_s U_\tau / \nu$ $\mathrm{Pr}_{lu} = \begin{cases} 1.01 - 0.09\,\mathrm{Pr}^{0.36} & \text{for } 1 \le \mathrm{Pr} \le 145 \\ 1.01 - 0.11\ln(\mathrm{Pr}) & \text{for } 145 < \mathrm{Pr} \le 1800 \\ 0.99 - 0.29\sqrt{\ln(\mathrm{Pr})} & \text{for } 1800 < \mathrm{Pr} \le 12{,}500 \end{cases}$	Heat transfer in rough pipes, $0.001 < \varepsilon_s/D < 0.05$, $0.5 < \mathrm{Pr} < 5000$, $\mathrm{Re}_D > 2300$ It predicts experimental data within $\pm 15\%$. C_f represents fully rough pipeflow.	Bhatti and Shah (1987)
Circular	$\mathrm{Nu}_D = 5.0 + 0.025\,(\mathrm{Re}_D\,\mathrm{Pr})^{0.8}$	Liquid metal flow in smooth pipes, UWT $\mathrm{Re}_D\,\mathrm{Pr} > 100$; $l/D > 30$; $10^4 \le \mathrm{Re}_D \le 5 \times 10^6$	Seban and Shimazaki (1951)
Circular	$\mathrm{Nu}_D = 4.82 + 0.0185\,(\mathrm{Re}_D\,\mathrm{Pr})^{0.827}$	Liquid metal flow in smooth pipes, UHF $100 \lesssim \mathrm{Re}_D\,\mathrm{Pr} < 10{,}000$ $3.6 \times 10^3 \le \mathrm{Re}_D \le 9.05 \times 10^5$	Skupinski et al. (1965)
Circular	$\mathrm{Nu}_D = 3.3 + 0.02\,(\mathrm{Re}_D\,\mathrm{Pr})^{0.8}$	Liquid metal flow in smooth pipes, UWT $\mathrm{Re}_D\,\mathrm{Pr} > 100$; $l/D > 60$ All properties at mean bulk temperature	Reed (1987)

[a] Heat transfer correlations can be applied to UWT and UHF boundary conditions.
[b] Circular channel correlations can be used for estimating heat transfer coefficients for noncircular channels by replacing D with D_H.

Table Q.4. *Darcy friction factors and Nusselt numbers for laminar developing internal flow*

Geometry	Correlation	Comments	Source
Circular	Eq. (4.2.12)	Hydrodynamic entrance length, laminar flow	Chen (1973)
Circular	Eq. (4.2.13)	Apparent Fanning friction factor, laminar flow	Shah and London (1978)
Flat channel	Eq. (4.2.15)	Hydrodynamic entrance length, laminar flow	Chen (1973)
Flat channel	Eq. (4.2.16)	Apparent Fanning friction factor, laminar flow	Shah and London (1978)
Noncircular channels	Eq. (4.2.17)	Apparent Fanning friction factor, laminar flow	Muzychka and Yovanovich (2004)
Circular	Eq. (4.5.30)	Thermal entrance length, laminar flow, UWT	Analytical
Circular and noncircular	$\langle \mathrm{Nu}_{D_H} \rangle = 3.66 + \dfrac{0.0668 \mathrm{Re}_{D_H} \mathrm{Pr} \dfrac{D}{l}}{1 + 0.045 \left[\mathrm{Re}_{D_H} \mathrm{Pr} \dfrac{D}{l} \right]^{0.66}} \left(\dfrac{\mu_m}{\mu_s} \right)^{0.14}$	Thermal entrance heat transfer coefficient for hydrodynamic fully developed flow for UWT for $\mathrm{Pr} > 0.7$. It can be applied to combined entry flows for $\mathrm{Pr} \lesssim 5$. Applicable for $100 < \mathrm{Re}_D \mathrm{Pr} \dfrac{D}{l} < 1500$.	Hausen (1983)
Circular and noncircular	$\langle \mathrm{Nu}_{D_H} \rangle = 1.86 \left(\mathrm{Re}_{D_H} \mathrm{Pr} \dfrac{D}{l} \right)^{1/3} \left(\dfrac{\mu_m}{\mu_s} \right)^{0.14}$	Thermal entrance heat transfer coefficient for hydrodynamic fully developed flow for UWT. Applicable for $0.48 \lesssim \mathrm{Pr} \lesssim 16{,}700$, $0.0044 \lesssim (\mu/\mu_s) \lesssim 9.75$, and $\langle \mathrm{Nu}_{D_H} \rangle > 3.72$.	Sieder and Tate (1936)
Circular	Eqs. (4.5.73)–(4.5.75)	Thermal entrance local heat transfer coefficient for hydrodynamic fully developed flow for UHF boundary conditions	Shah and Bhatti (1987)
Flat channel	Eq. (4.5.100)	Thermal entrance length, laminar flow, UHF boundary conditions	Analytical

Table Q.4 *(continued)*

Geometry	Correlation	Comments	Source
Flat channel	Eq. (4.5.124)	Thermal entrance length, laminar flow, UWT boundary conditions	Analytical
Flat channel	Eqs. (4.5.101) and (4.5.106)	Heat transfer coefficient in thermal entrance region, laminar flow, UHF	Shah and London (1978)
Flat channels	Eqs. (4.5.128) to (4.5.132)	Heat transfer coefficient in thermal entrance region, laminar flow, UWT	Shah and London (1978)
Rectangular	Table 4.7	Heat transfer coefficient in thermal entrance region, laminar flow, UWT	Wibulswan (1966)
Circular	Eq. (4.6.1)	Heat transfer coefficient for combined entrance region, laminar flow, UHF, $0.1 \leq \text{Pr} \leq 1000$	Churchill and Ozoe (1973a)
Circular	Eq. (5.6.2)	Heat transfer coefficient for combined entrance region, laminar flow, UWT, $0.1 \leq \text{Pr} \leq 1000$	Churchill and Ozoe (1973b)
Flat channel	Eqs. (4.6.3) and (4.6.4)	Average and local transfer coefficients for combined entrance region, laminar flow, UWT	Stephan (1959) and Shah and Bhatti (1987)
Circular	Eq. (7.4.21)	Average heat transfer coefficient in thermal entrance region with UWT or UHF for turbulent flow, $\text{Pr} > 0.2$, $3500 < \text{Re}_D < 10^5$, $x/D > 3$	Al-Arabi (1982)
Circular	Eq. (7.4.23) and (7.4.24)	Local and average heat transfer coefficient in thermal entrance region with UWT or UHF for turbulent liquid metal flow, $\text{Pr} < 0.03$, $x/d > 2$ and $\text{Pe} > 500$	Chen and Chiou (1981)
Circular	Eqs. (7.5.4) and (7.5.5)	Local and average heat transfer coefficients in combined entrance region for turbulent liquid metals, $\text{Pr} < 0.03$, $2 \leq L/D \leq 3.5$ and $\text{Pe} > 500$	Chen and Chiou (1981)

Table Q.5. *Nusselt numbers for natural convection, external flow*

Geometry	Correlation	Comments	Source
Vertical flat surface	Eqs. (10.4.14)–(10.4.16)	Local and average Nusselt numbers, semianalytical, laminar boundary layer ($\mathrm{Ra}_x < 10^9$), UWT,	Ostrach (1953), LeFevre (1956)
Vertical flat surface	Eq. (10.6.4)	Average Nusselt number, empirical, laminar boundary layer ($\mathrm{Ra}_l < 10^9$), UWT	Churchill and Chu (1975a)
Vertical flat surface	Eq. (10.6.3)	Average Nusselt number, empirical, UWT, no restriction on Rayleigh number	Churchill and Chu (1975a)
Vertical flat surface	Eqs. (10.6.7) and (10.6.8)	Local and average Nusselt numbers, empirical, laminar boundary layer, UHF; $10^5 < \mathrm{Ra}_x^* < 10^{13}$ for local and $10^5 < \mathrm{Ra}_l^* < 10^{11}$ for average Nusselt number	Vliet and Liu (1969)
Vertical flat surface	Eqs. (10.6.9) and (10.6.10)	Local and average Nusselt numbers, empirical, turbulent boundary layer, UHF, $10^{13} < \mathrm{Ra}_x^* < 10^{16}$ for local and $2 \times 10^{13} < \mathrm{Ra}_x^* < 10^{16}$ for average Nusselt number	Vliet and Liu (1969)
Inclined flat surface, heated and upward facing [Fig. 10.5(a)], or cooled and downward facing [Fig. 10.5(b)]	Replace g with $\cos\phi$ in Eqs. (10.4.14)–(10.4.16)	Local and average Nusselt number, $\phi \lesssim 60^\circ$, semianalytical, laminar boundary layer ($\mathrm{Ra}_x < 10^9$), UWT, $0.01 < \mathrm{Pr} < 1000$	Based on Ostrach (1953)

Table Q.5 *(continued)*

Geometry	Correlation	Comments	Source
Inclined flat surface, heated and upward facing [Fig. 10.5(a)], or cooled and downward facing [Fig. 10.5(b)]	Replace g with $\cos\phi$ in Eq. (10.6.4)	Average Nusselt number, $\phi \lesssim 60^\circ$, empirical, no restriction	Based on Churchill and Chu (1975a)
Horizontal flat surface, heated and upward facing, or cooled and downward facing	Eqs. (10.7.3) and (10.7.4)	Empirical, UWT, $10^5 \lesssim \mathrm{Ra}_{l_c} \lesssim 10^7$	McAdams (1954)
Horizontal flat surface, heated and downward facing, or cooled and upward facing	Eq. (10.7.2)	Empirical, UHF, $10^7 \lesssim \mathrm{Ra}_{l_c} \lesssim 10^{11}$	McAdams (1954)
Horizontal flat surface, heated and upward facing, or cooled and downward facing	Eq. (10.7.5) Eq. (10.7.6)	Empirical, UHF, $\mathrm{Ra}_{l_c} > 2 \times 10^8$ Empirical, UHF, $\mathrm{Ra}_{l_c} < 2 \times 10^8$	(Fujii and Imura, 1972)
Horizontal long cylinder	Eq. (10.9.5)	Empirical, UWT, $10^{-5} \leq \mathrm{Re}_D \leq 10^{12}$	(Churchill and Chu, 1975b)
Sphere	$\langle \mathrm{Nu}_D \rangle = 2 + \dfrac{0.589\mathrm{Ra}_D^{1/4}}{\left[1 + (0.469/\mathrm{Pr})^{9/16}\right]^{4/9}}$	Empirical, $\mathrm{Pr} \gtrsim 0.7,\ \mathrm{Ra}_D \lesssim 10^{11}$	Churchill (2002)
Immersed blunt bodies of various shapes	Eq. (10.9.2) and Table 10.2	Laminar flow	Yovanovich (1987)

Table Q.6. *Nusselt numbers for natural convection in internal flow or confined spaces*

Geometry	Correlation	Comments	Source
Space enclosed between two parallel vertical plates	Eq. (10.10.15)	UWT boundary conditions, all aspect ratios	Bar-Cohen and Rohsenow (1984)
Space enclosed between two parallel vertical plates	Eq. (10.10.18)	UHF boundary conditions, all aspect ratios	Bar-Cohen and Rohsenow (1984)
Space between two parallel vertical plates	Eq. (10.12.7)	$2 < \frac{l}{S} < 10,\ \mathrm{Pr} < 10,\ \mathrm{Ra}_S < 10^{10}$	Catton (1978)
Space between two parallel vertical plates	Eq. (10.12.8)	$1 < \frac{l}{S} < 2,\ 10^{-3} < \mathrm{Pr} < 10^5,\ \frac{\mathrm{Ra}_S \mathrm{Pr}}{0.2 + \mathrm{Pr}} > 10^3$	Catton (1978)
Space between two parallel and horizontal plates with bottom surface at a higher temperature	Eq. (10.13.2)	$3 \times 10^5 \lesssim \mathrm{Ra}_S \lesssim 7 \times 10^9$	Globe and Dropkin, (1959)
Space between two parallel and horizontal plates with bottom surface at a higher temperature	Eqs. (10.13.3)–(10.13.5)	Eq. (10.13.3) is for air for $1708 \lesssim \mathrm{Ra}_S \lesssim 10^8$, Eq. (10.13.4) is for water for $1708 \lesssim \mathrm{Ra}_S \lesssim 3.5 \times 10^9$	Hollands et al. (1976)

Table Q.6 *(continued)*

Geometry	Correlation	Comments	Source
Inside a spherical cavity	$\langle \mathrm{Nu}_D \rangle = C\,(Gr_D\,\mathrm{Pr})^n$	$Gr_D\,\mathrm{Pr}$ | C | n 10^4–10^9 | 0.59 | 1/4 10^9–10^{12} | 0.13 | 1/3	Kreith (1970)
Space between long concentric horizontal cylinders	$\frac{k_{\mathrm{eff}}}{k} = 0.386 \left[\frac{\ln\left(\frac{D_0}{D_i}\right)}{(R_0 - R_i)^{3/4}\left(\frac{1}{D_i^{3/5}} + \frac{1}{D_0^{3/5}}\right)^{5/4}} \right] \left(\frac{\mathrm{Pr}}{0.861 + \mathrm{Pr}}\right)^{1/4} \mathrm{Ra}_{(R_0 - R_i)}^{1/4}$	$0.7 \le \mathrm{Pr} \le 6000$, $10 \le \left[\frac{\ln\left(\frac{D_0}{D_i}\right)}{(R_0 - R_i)^{3/4}\left(\frac{1}{D_i^{3/5}} + \frac{1}{D_0^{3/5}}\right)^{5/4}} \right]^4 \mathrm{Ra}_{(R_0 - R_i)} \le 10^7$	Raithby and Hollands (1974)
Space between concentric spheres	$\frac{k_{eff}}{k} = 0.74 \left[\frac{(R_0 - R_i)^{1/4}}{(D_0 D_i)\left(D_i^{-7/5} + D_0^{-7/5}\right)^{5/4}} \right] \left(\frac{\mathrm{Pr}}{0.861 + \mathrm{Pr}}\right)^{1/4} \mathrm{Ra}_{(R_0 - R_i)}^{1/4}$	$0.7 \le \mathrm{Pr} \le 4200$, $10 \le \frac{R_0 - R_i}{(D_0 D_i)^4\left(D_i^{-7/5} + D_0^{-7/5}\right)^5} \mathrm{Ra}_{(R_0 - R_i)} \le 10^7$	Raithby and Hollands (1974)

References

Adams, T.M., Abdel-Khalik, S.I., Jeter, S.M., and Qureshi, Z.H. (1997). An experimental investigation of single-phase forced convection in microchannels. *Int. J. Heat Mass Transfer* **41**, 851–857.

Adams, T.M., Ghiaasiaan, S.M., and Abdel-Khalik, S.I. (1999). Enhancement of liquid forced convection heat transfer in microchannels due to the release of dissolved noncondensables. *Int. J. Heat Mass Transfer* **42**, 3563–3573.

Aggarwal, A. and Gangal, M.K. (1975). Laminar flow development in triangular ducts. *Trans. Can. Soc. Mech. Eng.* **3**, 231–233.

Al-Arabi, M. (1982). Turbulent heat transfer in the entrance region of a tube. *Heat Transfer Engineering* **3**, 76–83.

Aparecido, J.B. and Cotta, R.M. (1990). Thermally developing laminar flow inside rectangular ducts. *Int. J. Heat Mass Transfer* **33**, 341–347.

Arkilic, E.B., Schmidt, M.A., and Breuer, K.S. (1997). Gaseous slip flow in long microchannels. *J. MEMS* **6**, 167–178.

Arnold, J.N., Catton, I., and Edwards, D.K. (1976). Experimental investigation of natural convection in inclined rectangular regions of differing aspect ratios. *J. Heat Transfer* **98**, 67–71.

Asako, Y., Pi, T., Turner, S., and Faghri, M. (2003). Effect of compressibility on gaseous flows in micro-channels. *Int. J. Heat Mass Transfer* **46**, 3041–3050.

Aung, W. (1987). Mixed convection in external flow. In Kakac, S., Shah, R.K., and Aung, W., eds., *Handbook of Single-Phase Convective Heat Transfer*, Chap. 15, Wiley.

Awad, M.M. (2010). *Heat transfer for laminar thermally developing flow in parallel-plates using the assymptotic method*. Third Thermal Issues in Emerging Technologies (THETA 3) Conf., Cairo, Egypt, Dec. 19–22.

Aydin, O. and Avci, M. (2006). Analysis of micro-Graetz problem in a microtube. *Nanoscale Microscale Thermophys. Eng.* **10**, 345–358.

Aziz, A. (1987). Perturbation methods. In Minkowycz, W.J., Sparrow, E.M., Schneider, G.E., and Pletcher, R.H., eds., *Handbook of Numerical Heat Transfer*, Chap. 15, Wiley.

Aziz, A. and Na, T.Y. (1984). *Perturbation Methods in Heat Transfer, Hemisphere, New York*.

Badr, H.M. (1983). A theoretical study of laminar mixed convection from a horizontal cylinder in a cross stream. *Int. J. Heat Mass Transfer* **26**, 639–653.

Badr, H.M. (1984). Laminar combined convection from a horizontal cylinder – Parallel and contra flow regimes. *Int. J. Heat Mass Transfer* **27**, 15–27.

Bar-Cohen, A. and Rohsenow, W.M. (1984). Thermally optimum spacing of vertical, natural convection cooled, parallel plates. *J. Heat Transfer* **106**, 116–123.

Barron, R.F. (1999). *Cryogenic Heat Transfer*, Taylor & Francis.

Barron, R.F., Wang, X., Ameel, T.A., and Warrington, R.O. (1997). The Graetz problem extended to slip-flow. *Int. J. Heat Mass Transfer* **40**, 1817–1823.

Batchelor, G.K. (1970). *Theory of Homogeneous Turbulence*, Cambridge University Press.

Bayraktar, T. and Pidugu, S.B. (2006). Characterization of liquid flows in microfluidic systems. *Int. J. Heat Mass Transfer* **49**, 815–824.

Bayazitoglu, Y. and Ozisik, N. (1980). On the solution of Graetz type problem with axial conduction. *Int. J. Heat Mass Transfer* **23**, 1399–1402.

Beavers, G.S., Sparrow, E.M., and Magnuson, R.A. (1970). Experiments on the breakdown of laminar flow in a parallel-plate channel. *Int. J. Heat Mass Transfer* **13**, 809–815.

Beavers, G.S., Sparrow, E.M., and Lloyd, J.R. (1971). Low Reynolds number flow in large aspect ratio rectangular ducts. *J. Basic Eng*. **93**, 296–299.

Bejan, A. (1993). *Heat Transfer*, John Wiley and Sons.

Bejan, A. (2004). *Convection Heat Transfer*, 3rd ed., Wiley.

Beskok, A. and Karniadakis, G.E. (1999). A model for flow in channels, pipes and duct in micro scale. *Microscale Thermophys. Eng*. **3**, 43–77.

Bhatti, M.S. and Shah, R.K. (1987). Turbulent and transition flow convective heat transfer in ducts. In Kacac, S., Shah, R.S., and Aung, W., eds., *Handbook of Single-Phase Convective Heat Transfer*, Chap. 4, Wiley.

Bird, G.S. (1994). *Molecular Gas Dynamics and the Direct Simulation of Gas Flows,* Clarendon.

Bird, R.B., Stewart, W.E., and Lightfoot, E.N. (2002). *Transport Phenomena*, 2nd ed., Wiley.

Blasius, H. (1908). Grenzschichten in flussigkeiten mit kleiner reibug. *Z. Math. Phys*. **56**, 1–37. (English translation in NACA TM 1256.)

Blasius, H. (1913). Das ähnlichkeitsgesetz bei reibungsvorgängeng in flüsigkeiten. *Forschg. Arb. Ing.-Wes*., No. 131, Berlin.

Blazek, J. (2005). *Computational Fluid Dynamics: Principles and Applications*, 2nd ed., Elsevier.

Boelter, L.M.K., Young, G., and Iverson, H.W. (1948). An investigation of air heaters XXXVII – Distribution of heat transfer rate in the entrance section of a circular tube. NACA TM 1451.

Bose, F., Ghiaasiaan, S.M., and Heindel, T.J. (1997). Hydrodynamics of dispersed liquid droplets in agitated synthetic fibrous slurries. *Ind. Eng. Chem. Res.* **36**, 5028–5039.

Brown, G.M. (1960). Heat or mass transfer in a fluid in laminar flow in a circular or flat conduit. *AIChE J*. **6**, 179–183.

Buhr, H.O. (1967). Heat transfer to liquid metals, with observations on the effect of superimposed free convection in turbulent flow. Ph.D. Thesis, University of Cape Town, South Africa.

Burmeister, L.C. (1993). *Convective Heat Transfer*, 2nd ed., Wiley.

Cammenga, H.K., Schulze, F.W., and Theuerl, W. (1977). Vapor pressure and evaporation coefficient of water. *J. Chem Eng. Data* **22**, 131–134.

Carlson, G.A. and Hornbeck, R.W. (1973). A numerical solution for laminar entrance flow in a square duct. *J. Applied Mech.* **40**, 25–30.

Catton, I. (1978). Natural convection in enclosures. In *Proceedings of the Sixth International Heat Transfer Conference*, Vol. 6, pp. 13–31, Hemisphere.

CD-ADAPCO (2008). User Guide, STAR-CCM+, Version 3.04.009.

Cebeci, T. and Bradshaw, P. (1977). *Momentum Transfer in Boundary Layers*, Hemisphere.

Cebeci, T. and Cousteix, J. (2005). *Modeling and Computation of Boundary-Layer Flows*, 2nd ed., Springer.

Celata, G.P., D'Annibale, F., Chiaradia, A., and Maurizio, C. (1998). Upflow turbulent mixed convection heat transfer in vertical pipes, *Int. Heat Mass Transfer* **41**, 4037–4054.

Cess, R.D. and Shaffer, E.C. (1959). Heat transfer to laminar flow between parallel plates with a prescribed wall heat flux. *Appl. Sci. Res*. **A8**, 339–344.

Chapman, S. and Cowling, T.G. (1970). *The Mathematical Theory of Non-Uniform Gases*, 3rd ed., Cambridge University Press.

Chen, R.Y. (1973). Flow in the entrance region at low Reynolds numbers. *J. Fluids Eng*. **95**, 153–158.

Chen, T.S. and Armaly, B.F. (1987). Mixed convection in external flow. In Kakac, S., Shah, R.K., and Aung, W., eds., *Handbook of Single-Phase Convective Heat Transfer*, Chap. 14, Wiley.

Chen, C.J. and Chiou, J.S. (1981). Laminar and turbulent heat transfer in the pipe entrance region for liquid metals. *Int. J. Heat Mass Transfer* **24**, 1179–1189.

Chen, C.-J. and Jaw, S.-Y. (1998). *Fundamentals of Turbulence Modeling*, Taylor & Francis.

Chen, T.S. and Yuh, C.F. (1979). Combined heat and mass transfer in natural convection on inclined surface. *Numer. Heat Transfer* **12**, 233–250.

Chen, T.S. and Yuh, C.F. (1980). Combined heat and mass transfer in natural convection along a vertical cylinder. *Int. J. Heat Mass Transfer* **23**, 451–461.

Cheng, K.C. and Wu, R.S. (1976). Viscous dissipation effects on convective instability and heat transfer in plane Poisseuille flow heated from below. *Appl. Sci. Res*. **32**, 327–346.

Chilton, T.H. and Colburn, A.P. (1934). Mass transfer (absorption) coefficients. *Ind. Eng. Chem*. **26**, 1183–1187.

Cho, C.H., Chang, K.S., and Park, K.H. (1982). Numerical simulation of natural convection in concentric and eccentric horizontal cylindrical annuli. *J. Heat Transfer* **104**, 624–630.

Cho, C., Irvine, T.F., Jr., and Karni, J. (1992). Measurement of the diffusion coefficient of naphthalene into air. *Int. J. Heat Mass Transfer* **35**, 957–966.

Cho, H.H. and Goldstein, R.J. (1994). An improved low-Reynolds-number k–ε turbulence model for recirculating flows. *Int. J. Heat Mass Transfer* **37**, 1495–1508.

Choi, S.B., Barron, R.F., and Warrington, R.O. (1991). Fluid flow and heat transfer in microtubes. In *Proceedings of the ASME 1991 Winter Annual Meeting*, DSC, Vol. **32**, pp. 123–134, American Society of Mechanical Engineers.

Churchill, S.W. (1977a). Friction-factor equation spans all fluid and flow regimes. *Chem. Eng*. **84**, 91–92.

Churchill, S.W. (1977b). A comprehensive correlation equation for laminar, assisting forced and free convection. *AIChE J*. **23**, 10–16.

Churchill, S.W. (1977c). New simplified models and formulations for turbulent flow and convection. *AIChE J*. **43**, 1125–1140.

Churchill, S.W. (1990). Combined free and forced convection around immersed bodies. In Hewitt, G.F., ed., *Hemisphere Heat Exchanger Design Handbook*, Section 2.5.9, Hemisphere.

Churchill, S.W. (2000). The prediction of turbulent flow and convection in a round tube. *Adv. Heat Transfer* **34**, 255–361.

Churchill, S.W. (2002). Free convection around immersed bodies. In Hewitt, G.F., exec. ed., *Heat Exchanger Design Handbook*, Begel House, New York.

Churchill, S.W. and Bernstein, M. (1977). Correlating equation for forced convection from gases and liquids to a circular cylinder in crossflow. *J. Heat Transfer* **99**, 300–306.

Churchill, S.W. and Chu, H.H.S. (1975a). Correlating equations for laminar and turbulent free convection from a vertical plate. *Int. J. Heat Mass Transfer* **18**, 1323–1329.

Churchill, S.W. and Chu, H.H.S. (1975b). Correlating equations for laminar and turbulent free convection from a horizontal cylinder. *Int. J. Heat Mass Transfer* **18**, 1049–1053.

Churchill, S.W. and Ozoe, H. (1973a). Correlations for laminar forced convection with uniform heating in flow over a plate and in developing and fully developed flow in a tube. *J. Heat Transfer* **95**, 78–84.

Churchill, S.W. and Ozoe, H. (1973b). Correlations for laminar forced convection in flow over an isothermal flat plate and in developing and fully developed flow in an isothermal tube. *J. Heat Transfer* **95**, 416–419.

Churchill, S.W. and Usagi, R. (1972). A general expression for the correlation of rates of transfer and other phenomena. *AIChE J*. **18**, 1121–1128.

Churchill, S.W., Yu, B., and Kawaguchi, Y. (2005). The accuracy and parametric sensitivity of algebraic models for turbulent flow and convection. *Int. J. Heat Mass Transfer* **48**, 5488–5503.

Colebrook, C.F. (1939). Turbulent flow in pipes with particular reference to the transition region between the smooth and rough pipes laws. *J. Inst. Civil. Eng*. **11**, 133–156.

Cotta, R.M. (1993). *Integral Transforms in Computational Heat and Fluid Flow*, CRC Press.

Cotton, M.A. and Jackson, J.D. (1990). Vertical tube air flows in the turbulent mixed convection regime calculated using a low Reynolds number k–ε model. *Int. J. Heat Mass Transfer* **33**, 275–286.

Coulaloglou, C.A. and Tavralides, L.L. (1977). Description of interaction processes in agitated liquid-liquid dispersions. *Chem. Eng. Science* **32**, 1289–1297.

Coutanceau, M. and Defaye, J.-R. (1991). Circular cylinder wake configurations: A flow visualization survey. *Appl. Mech. Rev*. **44**, 255–305.

Crabtree, L.F., Küchemann, D., and Sowerby, L. (1963). Three-dimensional boundary layers. In Rosenhead, L., ed., *Laminar Boundary Layers*, Dover.

Curr, R.M., Sharma, D., and Tatchell, D.G. (1972). Numerical predictions of some three-dimensional boundary layers in ducts. *Comput. Methods Appl. Mech. Eng*. **1**, 143–158.

Curtiss, C.F. and Bird, R.B. (1991). Multicomponent diffusion. *Ind. Eng. Chem. Res*. **38**, 2515–2522.

Curtiss, C.F. and Bird, R.B. (2001). Errata. *Ind. Eng. Chem. Res*. **40**, 1791.

Cussler, E.C. (2009). *Diffusion Mass Transfer in Fluid Systems*, 3rd ed., Cambridge University Press.

Daly, B.J. and Harlow, F.H. (1970). Transport equations in turbulence. *Phys. Fluids* **13**, 2634–2649.

Dacles-Mariani, J. and Zilliac, G.G. (1995). Numerical/experimental study of a wingtip vortex in the near field. *AIAA J*. **33**, 1561–1568.

Dean, R.B. (1978). Reynolds number dependence of skin friction coefficient and other bulk flow variables in two-dimensional rectangular duct flow. *J. Fluids Eng*. **100**, 215–223.

Demirel, Y. and S.C. Saxena. (1996). Heat transfer through a low-pressure gas enclosure as a thermal insulator: Design considerations. *Int. J. Energy Res*. **20**, 327–338.

Deissler, R.G. (1953). Analysis of turbulent heat transfer and flow in the entrance region of smooth passages. NACA TM 3016.

Deissler, R.G. (1955). Analysis of turbulent heat transfer, mass transfer, and friction in smooth tubes at high Prandtl and Schmidt numbers. NACA Tech. Rep. 1210.

Deissler, R.G. (1964). An analysis of second-order slip flow and temperature jump boundary conditions for rarefied gases. *Int. J. Heat Mass Transfer* **7**, 681–694.

Demuren, A.O. and Rodi, W. (1984). Calculation of turbulence-driven secondary motion in non-circular ducts. *J. Fluid Mech*. **140**, 189–xxx.

Dittus, P.W. and Boelter, L.M.K. (1930). Heat transfer in automobile radiators of the tubular type. *University of California Pub. Eng*. **2**(2), 443–461.

Dong, Y.H., Lu, X.Y., and Zhuang, L.X. (2002). An investigation of the Prandtl number effect on turbulent heat transfer in channel flows by large eddy simulation. *Acta Mech*. **159**, 39–51.

Duan, Z. and Muzychka, Y.S. (2007a). Slip flow in non-circular microchannels. *Microfluid Nanofluid* **3**, 473–484.

Duan, Z. and Muzychka, Y.S. (2007b). Compressibility effect on slip flow in non-circular microchannels. *Nanoscale Microscale Thermophys. Eng*. **11**, 259–272.

Durbin, P.A. and Medic, G. (2007). *Fluid Dynamics with a Computational Perspective*. Cambridge University Press.

Eames, I.W., Marr, N.J., and Sabir, H. (1997). The evaporation of water: A review. *Int. J. Heat Mass Transfer* **40**, 2963–2973.

Ebadian, M.A. and Dong, Z.F. (1998). Forced convection, internal flow in ducts. In Rohsenwo, W.M., Hartnett, J.P., and Cho, Y.I., eds., 3rd ed., Mc-Graw-Hill.

Ebert, W.A. and Sparrow, E.M. (1965). Slip flow in rectangular and annular ducts. *J. Basic Eng*. **87**, 1018–1024.

Eckert, E.R.G. and Drake, R.M., Jr. (1959). *Heat and Mass Transfer*, McGraw-Hill.

Eckert, E.R.G. and Drake, R.M., Jr. (1972). *Analysis of Heat and Mass Transfer*, Taylor & Francis.
Eckert, E.R.G. and Jackson, T.W. (1951). Analysis of turbulent free-convection boundary layer on flat plate. NACA Tech. Note 2207.
Edwards, D.K., Denny, V.E., and Mills, A.F. (1979). *Transfer Processes*, Hemisphere, New York.
Eggles, T.G.M., Ungar, F., Weiss, M.H., Westerweel, J., Adrian, R.J., Friedrich, R., and Nieuwstadt, F.T.M. (1994). Fully developed turbulent pipe flow: a comparison between direct numerical simulation and experiment. *J. Fluid Mech.* **268**, 175–209.
Elenbaas, W. (1942). Heat dissipation of parallel planes by free convection. *Physica* **IX**(1), 2–28.
Escudier, M.P. (1966). The distribution of mixing length in turbulent flows near walls. Heat Transfer Section Rep. TWF/TN/1, Imperial College of Science and Technoloy, London. (Cited in Launder and Spalding, 1972.)
Ewart, T., Perrier, P., Graur, I., and Meolans, J.G. (2007). Tangential momentum accommodation in microtube. *Microfluid Nanofluid* **3**, 689–695.
Falkner, V.M. and Skan, S.W. (1931). Some appropriate solutions of the boundary layer equations. *Phil. Mag*. **12**, 865–896.
Fan, Y. and Luo, L. (2008). Recent applications of advances in microchannel heat exchangers and multi-scale design optimization. *Heat Trans. Eng*. **29**, 461–474.
Ferziger, J.H. and Peric, M. (1996). *Computational Methods for Fluid Dynamics*. Springer-Verlag.
Fleming, D.P. and Sparrow, E.M. (1969). Flow in the hydrodynamic entrance region of ducts of arbitrary cross-section. *J. Heat Transfer* **91**, 345–354.
Fluent 6.3 User's Manual, 2006.
Fujii, T. and Imura, H. (1972). Natural convection from a plate with arbitrary inclination. *Int. J. Heat Mass Transfer* **15**, 755–767.
Gad-el-Hak, M. (1999). The fluid mechanics of microdevices – The Freeman Scholar Lecture. *J. Fluid Eng*. **121**, 5–33.
Gad-el-Hak, M. (2003). Comments on "critical view on new results in micro-fluid mechanics." *Int. J. Heat Mass Transfer* **46**, 3941–3945.
Gad-el-Hak, M. (2006).Gas and liquid transport at the microscale. *Heat Transfer Eng*. **27**, 13–29.
Gatski, T.B. and Speziale, C.G. (1993). On explicit algebraic stress models for complex turbulent flows. *J. Fluid Mech*. **254**, 59–78.
Gebhart, B. (1981). *Heat Transfer*, 2nd ed., McGraw-Hill.
Gebhart, B. and Pera, I. (1971). The nature of vertical natural convection flows resulting from the combined buoyancy effects of thermal and mass diffusion. *Int. J. Heat Mass Transfer* **14**, 2025–2050.
Ghiaasiaan, S.M. (2008). *Two Phase Flow, Boiling and Condensation in Conventional and Miniature Systems.* Cambridge University Press.
Ghiaasiaan, S.M. and Laker, T.S. (2001). Turbulent forced convection in microtubes. *Int. J. Heat Mass Transfer* **44**, 2777–2782.
Ghodoossi, L. and Egrican, N. (2005). Prediction of heat transfer characteristics in rectangular microchannels for slip flow regime and H1 boundary condition. *Int. J. Thermal Sci*. **44**, 513–520.
Giedt, W.H. (1949). Investigation of variation of point unit-heat-transfer coefficient around a cylinder normal to an air stream. *Trans. ASME* **71**, 375–381.
Gilpin, R.R., Imura, H., and Cheng, K.C. (1978). Experiments on the onset of longitudinal vortices in horizontal Blasius flow heated from below. *J. Heat Transfer* **100**, 71–77.
Gnielinski, V. (1976). New equations for heat and mass transfer in turbulent pipe and channel flow. *Int. Chem. Eng*. **16**, 359–368.
Globe, S. and Dropkin, D. (1959). National convection heat transfer in liquids confined by two horizontal plates and heated from below. *J. Heat Transfer* **81**, 24–28.

Goldstein, S. (1937). The similarity theory of turbulence and flow between parallel planes and through pipes. *Proc. R. Soc. London Ser. A* **159**, 473–496.
Goldstein, S., ed. (1965). *Modern Developments in Fluid Dynamics*, Vol. II, Dover.
Gombosi, T.I. (1994). *Gaskinetic Theory*. Cambridge University Press.
Graetz, L. (1885). Uber die Warmeleitungsfahigkeiten von Flussigkeiten. *Annal. Phys. Chem. Part 1*, **18**, 79–94; *Part 2*, **15**, 337–357.
Grotzbach, G. (1983). Special resolution requirement for direct numerical simulation of Rayleigh–Bénard convection. *J. Comput. Phys*. **49**, 241–264.
Haaland, S.E. (1983). Simple and explicit formulas for the friction factor in turbulent pipe flow. *J. Fluids Eng*. **105**, 89–90.
Hadjiconstantinou, N.G. (2005). Validation of a second-order slip model for dilute gas flow. *Microscale Thermophys. Eng*. **9**, 137–153.
Hadjiconstantinou, N.G. and Simek, O. (2002). Constant-wall-temperature Nusselt number in micro and nano-channels. *J. Heat Transfer* **124**, 356–364.
Hanjalic, K. and Launder, B.E. (1976). Contribution towards a Reynolds-stress closure for low-Reynolds number turbulence. *J. Fluid Mech*. **74**, 593–610.
Hanks, R.W. and Weissberg, H.L. (1964). Slow viscous flow of rarefied gases through short tubes. *J. Applied Phys.* **35**, 142–144.
Hanna, O.T. and Myers, J.E. (1962). Heat transfer in boundary-layer flows past a flat plate with a step-in wall-heat flux. *Chem. Eng. Sci*. **17**, 1053–1055.
Hartree, D.R. (1937). On an equation occurring in Falkner and Skan's approximate treatment of the boundary layer. *Proc. Cambridge Philos. Soc*. **33**, 223–239.
Hausen, H. (1983). *Heat Transfer in Counter Flow, Parallel Flow, and Cross-Flow*, McGraw-Hill.
Hayashi, Y., Takimoto, A., and Hori, K. (1977). Heat transfer in laminar mixed convection flow over a horizontal flat plate [in Japanese]. In *Proceedings of the 14th Japan Heat Transfer Symposium*, pp. 4–6.
Herbert, L.S. and Stern, U.J. (1972). Heat transfer in vertical tubes – Interaction of forced and free convection. *Chem. Eng. J*. **4**, 46–52.
Herwig, H. and Hausner, O. (2003). Critical view on new results in micro-fluid mechanics: an example. *Int. J. Heat Mass Transfer* **46**, 935–937.
Hilpert. R. (1933). Wärmeabgabe von geheizten drähten und rohren. *Forsch. Geb. Ingenieurwes*. **4**, 215.
Hindmarsh, A.C. (1980). LSODE and LSODI, two new initial value ordinary differential equation solvers. *ACM Newslett*. **15**(5), 10.
Hinze, J.O. (1975). *Turbulence*. McGraw-Hill.
Hinze, J.O. (1955). Fundamentals of the hydrodynamic mechanism of splitting in dispersion processes. *AIChE J.* **1**, 289–295.
Hirschfelder, J., Curtiss, C.F., and Bird, R.. (1954). *Molecular Theory of Gases and Liquids*, Wiley.
Hollands, K.G.T., Raithby, G.D., and Konicek, L. (1975). Correlation equations for free convection heat transfer in horizontal layers of air and water. *Int. J. Heat Mass Transfer* **18**, 879–884.
Hollands, K.G.T., Unny, T.E., Raithby, G.D., and Konicek, L. (1976). Free convection heat transfer across inclined air layers. *J. Heat Transfer* **98**, 189–193.
Howarth, L. (1938). On the solution of the laminar boundary layer equations. *Proc. R. Soc. London Ser. A*. **164**, 547.
Hrycak, P. and Andrushkiw, R. (1974). Calculation of critical Reynolds number in round pipes and infinite channels and heat transfer in transition regions. *Heat Transfer* **II**, 183–187.
Hsu, C.J. (1965). Heat transfer in a round tube with sinusoidal wall heat flux distribution. *AIChE J*. **11**, 690–695.
Inman, R.M. (1964a). Heat transfer for laminar slip flow of a rarified gas in a parallel plate channel or a circular tube with uniform wall temperature. NASA TN D-2213.

Inman, R.M. (1964b). Laminar slip flow heat transfer in a parallel plate channel or a round tube with uniform wall heating. NASA TN D-2393.

Inman, R.M. (1965). Heat transfer in thermal entrance region with laminar slip flow between parallel plates at unequal temperatures. NASA TN-D-2980.

Incropera, F.P., Dewitt, D.P., Bergman, T.L., and Lavine, A.S. (2007). *Fundamentals of Heat and Mass Transfer*, 6th ed., Wiley.

Jackson, J.D., Cotton, M.A., and Axcell, B.P. (1989). Studies of mixed convection in vertical tubes. *Int. J. Heat Fluid Flow* **10**, 2–15.

Jackson, J.D. and Hall, W.B. (1979). Influence of buoyancy on heat transfer to fluids flowing in vertical tubes under turbulent conditions. In Kakac, S. and Spalding, D.B., eds. *Turbulent Forced Convection in Channels and Bundles*, Hemisphere, pp. 613–673.

Jaluria, Y. (2003). Natural convection, in *Heat Transfer Handbook*, Bejan, A. and Kraus, A.D., eds., Chap. 7, Wiley.

Jang, J. and Werely, S. (2007). Gaseous slip flow analysis of a micromachined flow sensor for ultra small flow applications. *J. Micromech. Microeng*. **17**, 229–237.

Jayatilleke, C.L. (1969). The influence of Prandtl number and surface roughness on the resistance of the laminar sub-layer to momentum and heat transfer. *Prog. Heat Mass Transfer* **1**, 193–330.

Jeong, H.-E. and Jeong, J.-T. (2006). Extended Graetz problem including streamwise conduction and viscous dissipation in microchannel. *Int. J. Heat Mass Transfer* **49**, 2151–2157.

Jiang, L.,Wang, Y.,Wong, M., and Zohar, Y. (1999). Fabrication and characterization of a microsystem for microscale heat transfer study, *J. Micromech. Microeng*. **9**, 422–28.

Jiji, L.M. (2006). Heat Convection. Springer.

Jischa, H. and Rieke, H.B. (1979). About the prediction of turbulent Prandtl and Schmidt numbers. *Int. J. Heat Mass Transfer* **2**, 1547–1555.

Johnson, D.A. and King, L.S. (1985). Mathematically simple turbulence closure model for attached and separated turbulent boundary layers. *AIAA J.* **23**, 1684–1692.

Jones, W.P. and Launder, B.E. (1973). The prediction of laminarization with a two-equation model of turbulence. *Int. J. Heat Mass Transfer* **15**, 301–314.

Jones, C.W. and Watson, E.J. (1963). Two-dimensional boundary layers. In Rosenhead, L., ed., *Laminar Boundary Layers*, Dover.

Jones. O.C., Jr. (1976). An improvement in the calculation of turbulent friction in rectangular ducts. *J. Fluids Eng*. **98**, 173–181.

Jones, O.C., Jr. and Leung, C.M. (1981). An improvement in the calculation of turbulent friction in smooth concentric annuli. *J. Fluids Eng*. **103**, 615–623.

Kader, B.A. (1981). Temperature and concentration profiles in fully turbulent boundary layers. *Int. J. Heat Mass Transfer* **24**, 1541–1544.

Kawamura, H, Ohsake, K., Abe, H., and Yamamoto, K. (1998). DNS of turbulent heat transfer in channel flow with low to medium-high Prandtl number fluid. *Int. J. Heat Fluid Flow*, **19**, 482–481.

Kays, W.M., Crawford, M.E., and Weigand, B. (2005). *Convective Heat and Mass Transfer*, 4th ed., McGraw-Hill.

Kays, W.M. and London, A.L. (1984). *Compact Heat Exchangers*, 3rd ed., McGraw-Hill.

Kays, W.M. and Perkins, H.C. (1972). In Rohsenow, W.M. and Hartnett, J.P., eds., *Handbook of Heat Transfer*, Chap. 7, McGraw-Hill.

Khadem, M.H., Shams, M., and Hossainpour, S. (2008). Effects of rarefaction and compressibility on fluid flow at slip flow regime by direct simulation of roughness. In *Proceedings of the World Academy of Science, Engineering and Technology* **31**.

Kitamura, K. and Inagaki, T. (1987). Turbulent heat and momentum transfer of combined forced and natural convection along a vertical flat plate – Aiding flow. *Int. J. Heat Mass Transfer* **30**, 23–41.

Klebanoff, P.S. (1955). Characteristics of Turbulence in a Boundary Layer with Zero Pressure Gradient. NACA-1247.

Kobus, C.J. and Wedekind, G.L. (1996). Modeling the local and average heat transfer coefficient for an isothermal vertical flat plate with assisting and opposing combined forced and natural convection. *Int. J. Heat Mass Transfer* **39**, 2723–2733.

Kohl, M.J., Abdel-Khalik, S.I., Jeter, S.M., and Sadowski, D.L. (2005). An experimental investigation of microchannel flow with internal pressure measurements. *Int. J. Heat Mass Transfer* **48**, 1518–1533.

Kolmogorov, A.N. (1942). Equations of turbulent motion of an incompressible turbulent flow. *Izv. Akad. Nauk SSSR Ser Phys*. **4**(1–2), [Cited in Launder, B.E. and Spalding, D.B. (1972), *Mathematical Models of Turbulence*, Academic.]

Kreith, F. (1970). Thermal design of high altitude balloons and instrument packages. *J. Heat Transfer* **92**, 307–332.

Krishnamurthy, R. and Gebhart, B. (1989). Experimental study of transition to turbulence in vertical mixed convection flows. *J. Heat Transfer* **111**, 121–130.

Krishnamoorthy, C., Rao, R.P., and Ghajar, A. (2007). Single-phase heat transfer in microtubes: A critical review. In *Proceedings of the ASME-JSME Thermal Engineering Summer Heat Transfer Conference, American Society of Mechanical Engineers.*

Kronig, R. and Brink, J.C. (1950). On the theory of extraction from falling droplets, *Appl. Sci. Res*. *A* **2**, 142–154.

Kudo, K., Kato, T., Chida, H., Tagaki, S., and Tsui, N. (2003). Modeling of combined forced- and natural-convection heat transfer over upward-facing horizontal heated flat plates. *Int. J. Energy Res*. **27**, 327–335.

Labbé, O. and Sagaut, P. (2002). Large eddy simulation of heat transfer over a backward – facing step. *Numerical Heat Transfer: A*, **42**, 73–90.

Larkin, B.K. (1961). High-order eigenfunctions of the Graetz problem. *AIChE J.* **7**, 530.

Latzko, H. (1921). Der warmeubergang and einen turbulenten flussigkeitsoder gasstrom. *Z. Angew. Math. Mech. (ZAAM)* **1**, 268–290. [English translation: NACA TM 1068 (1944).]

Launder, B.E. (1988). On the computation of convective heat transfer in complex turbulent flows. *J. Heat Transfer* **110**, 1112–1128.

Lauder, B.E., Reece, G.J., and Rodi, W. (1975). Progress in the development of a reynolds-stress turbulence closure. *J. Fluid Mech*. **68**, 527–566.

Launder, B.E. and Sharma, B.I. (1974). Application of the energy dissipation model of turbulence to the calculation of flow near a spinning disc. *Lett. Heat Mass Transfer* **1**, 131–138.

Lai, Y.G. and So, R.M.C. (1990). Near-wall modeling of turbulent heat fluxes. *Int. J. Heat Mass Transfer* **33**, 1429–1440.

Launder, B.E. and Shima, N. (1989). Second-moment closure for near-wall sublayer: Development and application. *AIAA J*. **27**, 1319–1325.

Launder, B.E. and Spalding, D.B. (1972). *Lectures in Mathematical Models of Turbulence*, Academic.

Launder, B.E. and Spalding, D.B. (1974). The numerical computation of turbulent flows. *Comput. Methods Appl. Mech. Eng*. **3**, 269–289.

Lee, K.-T. (1999). Laminar natural convection heat and mass transfer in vertical rectangular ducts. *Int. J. Heat Mass Transfer* **42**, 4523–4534.

LeFevre, E.J. (1956). Laminar free convection from a vertical plane surface. *Proc. 9th Int. Congress on Applied Mech.,* Brussels, Vol. 4, p. 168.

LeFevre, E.J. and Ede, A.J. (1956). Laminar free convection from the outer surface of a vertical circular cylinder. In *Proceeding of the Ninth International Congress on Applied Mechanics*, Vol. III, pp. 175–183.

Levich, V.E. (1962). *Physicochemical Hydrodynamics.* Prentice-Hall.

Li, D. (2004). *Electrokinetics in Microfluidics,* Elsevier Academic.

Li, X., Lee, W.Y., Wong, M., and Zohar, Y. (2000). Gas flow in constriction microdevices. *Sensors Actuators A* **83**, 277–283.

Lienhard, J.H., IV (1966). Synopsis of lift, drag and vortex frequency data for rigid circular cylinders. Bulletin 300, College of Engineering Research Division, University of Washington (available at http://www.uh.edu/engines/vortexcylinders.pdf).

Lienhard, J.H., IV and Lienhard, J.H., V. (2005). *A Heat Transfer Textbook*, 3rd ed., Phlogiston Press.

Lin, H.-T. and Wu, C.-M. (1995). Combined heat and mass transfer by laminar natural convection from a vertical plate. *Heat Mass Transfer* **30**, 369–376.

Lin, H.-T. and Wu, C.-M. (1997). Combined heat and mass transfer by laminar natural convection from a vertical plate with uniform heat flux and concentration. *Heat and Mass Transfer* **32**, 293–299.

Liou, W.M. and Fang, Y. (2006). *Microfludic Mechanics*, McGraw-Hill.

Liu, J. (1974). Flow of a Bingham fluid in the entrance region of an annular tube. M.S. Thesis, University of Wisconsin-Milwaukee.

Lloyd, J.R. and Sparrow, E.M. (1970). On the instability of natural convection flow on inclined plates. *J. Fluid Mech*. **42**, 465–470.

Lundberg, R.E., McCuen, P.A., and Reynolds, W.C. (1963). Heat transfer in annular passages. Hydrodynamically developed laminar flow with arbitrary prescribed wall temperatures or heat fluxes. *Int. J. Heat Mass Transfer* **6**, 495–529.

Lyons, S.L., Hanratty, T.J., and McLaughlin, J.B. (1991a). Large-scale computer simulation of fully developed turbulent channel flow with heat transfer. *Numer. Methods Fluids* **13**, 999–1028.

Lyons, S.L., Hanratty, T.J., and McLaughlin, J.B.. (1991b). Direct numerical simulation of passive heat transfer in a turbulent channel flow. *Int. J. Heat Mass Transfer* **34**, 1149–1161.

Maa, J.R. (1967). Evaporation coefficient of liquids. *Ind. Eng. Chem. Fundamentals* **6**, 504–518.

Martinelli, R.C. (1947). Heat transfer to molten metals. *Trans. ASME* **69**, 947–959.

Mathieu, J. and Scott, J. (2000). *An Introduction to Turbulent Flow*, Cambridge University Press.

Mathpati, C.S. and Joshi, J.B. (2007). Insight into theories of heat and mass transfer at the solid – fluid interface using direct numerical simulation and large eddy simulation. *Ind. Eng. Chem. Res.* **46**, 8525–8557.

McAdams, W.H. (1954). *Heat Transmission*, 3rd ed., McGraw-Hill.

McGregor, R.K. and Emery, A.P. (1969). Free convection through vertical plane layers: Moderate and high Prandtl number fluids. *J. Heat Transfer* **91**, 391.

Menter, F.R., 1993. Zonal two-equation k–ω model for aerodynamic flows. AIAA Paper 93-2903.

Menter, F.R. (1994). Two-equation eddy viscosity turbulence models for engineering applications. *AIAA J*. **32**, 1598–1605.

Menter, F.R. (1996). A comparison of some recent eddy viscosity turbulent models. *J. Fluids Eng.* **118**, 514–519.

Metais, B. and Eckert, E.R.G. (1964). Forced mixed and free convection regimes. *J. Heat Transfer* **86**, 295–296.

Métais, O. and Lesieur, M. (1992). Spectral large-eddy simulation of isotropic and stably stratified turbulence. *J. Fluid Mech.* **239**, 157–194.

Michelsen, M.L. and Villadsen, J. (1974). The Graetz problem with axial heat conduction. *Int. J. Heat Mass Transfer* **17**, 1391–1402.

Miller, R.W. and Han, L.S. (1971). Pressure losses for laminar flow in the entrance region of ducts of rectangular and equilateral triangular cross section. *J. Appl. Mech.* **38**, 1083–1087.

Mills, A.F. (1962). Experimental investigation of turbulent heat transfer in the entrance region of a circular conduit. *J. Mech. Eng. Sci.* **4**, 63–77.

Mills, A.F. (2001). *Mass Transfer*. Prentice-Hall.

Mills, A.F. and Seban, R.A. (1967). The condensation coefficient of water. *Int. J. Heat Mass Transfer* **10**, 1815–1827.

Misumi, T., Shigemaru, S., and Kitamura, K. (2007). Fluid flow and heat transfer of opposing mixed convection adjacent to upward-facing, inclined heated plates. *Heat Transfer Asian Res.* **36**, 127–142.

Molki, M. and Sparrow, E.M. (1986). An empirical correlation for the average heat transfer coefficient in circular tubes. *J. Heat Transfer* **108**, 482–484.

Mompean, G., Gavrilakis, S., Machiels, L., and Deville, M.O. (1996). On predicting the turbulence-induced secondary flows using non-linear k–ε models. *Phys. Fluids* **8**, 1856–1868.

Moutsoglu, A., Chen, T.S., and Cheng, K.C. (1981). Vortex instability of mixed convection flow over a horizontal flat plate. *J. Heat Transfer* **103**, 257–262.

Morcos, S.M. and Bergles, A.E. (1975). Experimental investigation of combined forced and free laminar convection in horizontal tubes. *Int. J. Heat Mass Transfer* **97**, 212–219.

Mori, Y. and Futagami, K. (1967). Forced convection heat transfer in uniformly heated horizontal tubes (2nd report, theoretical study). *Int. J. Heat Mass Transfer* **10**, 1801–1813.

Morini, G.L. (2004). Single-phase convective heat transfer in microchannels: a review of experimental results. *Int. J. Thermal Sci.* **43**, 631–651.

Morini, G.L., Spiga, M., and Tartarini, P. (2004). The rarefaction effect on the friction factor of gas flow in microchannels. *Superlattices Microstructures* **35**, 587–599.

Muzychka, Y.S. and Yovanovich, M.M. (2004). Laminar forced convection heat transfer in the combined entry region of non-circular ducts. *J. Heat Transfer* **126**, 54–61.

Na, Y. and Hanratty, T.J. (2000). Limiting behavior of turbulent scalar transport close to a wall. *Int. J. Heat Mass Transfer* **43**, 1749–1758.

Nagano, Y. and Shimada, M. (1996). Development of a two-equation heat transfer model based on direct numerical simulation of turbulent flows with different Prandtl numbers. *Phys. Fluids* **8**, 3379–3402.

Narsimhan, G., Gupta, J.P., and Ramkrishna, D. (1979). A model for transitional breakage probability of droplets in agitated lean liquid-liquid dispersions. *Chem. Eng. Sci.* **34**, 257–265.

Nelson, D.J. and Wood, B.D. (1989a). Combined heat and mass transfer natural convection between vertical parallel plates. *Int. J. Heat Mass Transfer* **32**, 1779–1787.

Nelson, D.J. and Wood, B.D. (1989b). Fully-developed combined heat and mass transfer natural convection between vertical parallel plates with asymmetric boundary conditions. *Int. J. Heat Mass Transfer* **32**, 1789–1792.

Nikuradse, J. (1932). Gesetzmässigkeiten der turbulenten Strömung in glatten Rohren. *Forsch. Arb. Ing. Wes.* **356**. [English translation, NASA TT F-IO 359, 1966.]

Nikuradse, J. (1933). Strömungsgesetze in rauhen Rohnen. *Forsch. Arb. Ing.-Wes.* **361**.

Norris, R.H. (1970). Some simple approximate heat-transfer correlations for turbulent flow in ducts with rough surfaces. In *Augmentation of Convective Heat and Mass Transfer*, pp. 16–26, American Society of Mechanical Engineers.

Notter, R.H. and Sleicher, C.A. (1971a). The eddy diffusivity in turbulent boundary layer near a wall. *Chem. Eng. Sci.* **26**, 161–171.

Notter, R.H. and Sleicher, C.A. (1971b). A solution to the turbulent Graetz problem by matched asymptotic expansions-II. The case of uniform heat flux. *Chem. Eng. Sci.* **26**, 559–565.

Notter, R.H. and Sleicher, C.A. (1972). A solution to the turbulent Graetz problem -III. Fully developed and entry region heat transfer rates. *Chem. Eng. Sci.* **27**, 2073–2093.

Oosthuizen, P.H. and Hart, R. (1973). A numerical study of laminar combined convection over flat plates. *J. Heat Transfer* **96**, 60–63.

Oosthuizen, P.H. and Naylor, D. (1999). *Introduction to Convective Heat Transfer Analysis.* McGraw-Hill.

Orszag, S.A., Yakhot, V., Flannery, W.S., Boysan, F., Choudhury, D., Manizewski, J., and Patel, B. (1993). Renormalization group modeling and turbulence simulation. In So, R.M.C., Speziale, C.G., and Launder, B.E., eds., *Near Wall Turbulent Flows*, pp. 1031–1046, Elsevier.

Ostrach, S. (1953). An analysis of laminar free convection flow and heat transfer about a flat plate parallel to the direction of the generating body force. NACA Tech. Rep. 1111.

Pahor, S. and Strand, J. (1961). A note on heat transfer in laminar flow through a gap. *Appl. Sci. Res. A* **10**, 81–84.

Papautsky, I., Ameel, T., and Frazier, A.B. (2001). A review of laminar single-phase flow in microchannels. In *Proceedings of the International Mechanical Engineering Congress and Exposition*, ASME.

Papavassiliou, D. and Hanratty, T.J. (1997). Transport of a passive scalar in a turbulent channel flow. *Int. J. Heat Mass Transfer* **40**, 1303–1311.

Patel, K., Armaly, B.F., and Chen, T.S. (1996). Transition from turbulent natural to turbulent forced convection adjacent to an isothermal vertical plate. *ASME Heat Transfer Division (HTD)* **324**, 51–56.

Patel, K., Armaly, B.F., and Chen, T.S. (1998). Transition from turbulent natural to turbulent forced convection. *J. Heat Transfer* **120**, 1086–1089.

Pellew, A. and Southwell, R.V. (1940). On maintained convective motion in a fluid heated from below. *Proc. R. Soc. London Ser. A* **176**, pp. 312–343.

Peng, X.F. and Peterson, G.P. (1996). Convective heat transfer and flow friction for water flow in microchannel structures. *Int. J. Heat Mass Transfer* **39**, 2599–2608.

Peng, X.F. and Wang, B.X. (1994). Liquid flow and heat transfer in microchannels with/without phase change. In *Heat Transfer 1994, Proceedings of the Tenth International Heat Transfer Conference*, Vol. 5, pp. 159–177, Institution of Chemical Engineers.

Peng, X.F. and Wang, B.X. (1998). Forced-convection and boiling characteristics in microchannels. In *Proceedings of the 11th International Heat Transfer Conference*, pp. 371–390, Korean Society of Mechanical Engineers.

Pera, I. and Gebhart, B. (1972). Natural convection flows adjacent to horizontal surfaces resulting from the combined buoyancy effects of thermal and mass diffusion. *Int. J. Heat Mass Transfer* **15**, 269–278.

Perkins, K.R., Shade, K.W., and McEligot, D.M. (1973). Heated laminarizin gas flow in a square duct. *Int. J. Heat Mass Transfer* **16**, 897–916.

Pletecher, R.H. (1987). External flow forced convection. In Kacac, S., Shah, R.S., and Aung, W., eds., *Handbook of Single-Phase Convective Heat Transfer*, Chap. 2, Wiley.

Petukhov, B.S. (1970). Heat transfer and friction factor in turbulent pipe flow with variable physical properties. *Adv. Heat Transfer*, **6**, 503–565.

Prandtl, L. (1910). *Z. Phys*. **11**, 1072.

Prandtl, A. (1925). *Z. Angew. Math. Mech*. **5**, 136–139.

Prandtl, L. (1928). *Z. Phys.* **29**, 487.

Prandtl, L. (1933). Neuere Ergebnisse der Turbulenzforschung. *VDIZ.* (**77/5**): 105–114, 1933. [English translation *NACA TM 7320.*]

Prandtl, L. (1945). Ube rein neues formelsystem fur die ausgebildete turbulenz. *Nachr. Akad. Wiss. Gottinge Math.-Phys*. **II**, p. 6.

Press, H.W., Teukolsky, S.A., Vetterling, W.T., and Flannery, B.P. (1992). *Numerical Recipes for FORTRAN 77*, Vol. 1, Cambridge University Press.

Press, H.W., Teukolsky, S.A., Vetterling, W.T., and Flannery, B.P. (1997). *Numerical Recipes for C*, 2nd Ed., Numerical Recipe Software.

Probstein, R.F. (2003). *Physicohcemical Hydrodynamics*, 2nd ed., Wiley.

Raithby, G.D. and Hollands, K.G.T. (1974). A General Method of Obtaining Approximate Solutions to Laminar and Turbulent Free Convection Problems. In Advances Heat Transfer, Academic Press, New York.

Raithby, G.D. and Hollands, K.G.T. (1998). Natural Convection, in Rohsenow, W.M., Hartnett, J.P., and Cho, Y.I., eds, *Handbook of Heat Transfer*, 3rd Ed., Chp. 4, McGraw-Hill.

Ramachandran N., Armaly B.F., and Chen T.S. (1985). Measurement and prediction of laminar mixed convection flow adjacent to a vertical surface. *J. Heat Mass Transfer* **107**, 636–641.

Ramachandran, N., Armaly, B.F., and Chen, T.S. (1987). Measurement of laminar mixed convection from an inclined surface. *J. Heat Mass Transfer* **109**, 146–150.

Ranz, W.E. and Marshall, W.R., Jr. (1952). Evaporation from drops. Parts I and II, *Chem. Eng. Progress*, **48**, 141–146 and 173–180.

Redjem-Saad, L., Ould-Rouiss, M., and Lauriat, G. (2007). Direct Numerical Simulation of Turbulent Heat Transfer in Pipe Flows: Effect of Prandtl Number. *Int. J. Heat Mass Transfer*, **28**, 847–861.

Reed, C.B. (1987). Convective heat transfer in liquid metals. In Kakac, S., Shah, R.K., and Aung, W., eds., *Handbook of Single-Phase Convective Heat Transfer*, Chapter 8, Wiley.

Reichardt, H. (1951). Vollstandige darstellung der turbulenten geschwindigkeitsverteilung in glatten leitungen. *Z. Angew. Math. Mech*. **31**, 208–219.

Renksizbulut, M. and Yuen, M.C. (1983). Experimental study of droplet evaporation in a high-temperature air stream. *J. Heat Transfer* **105**, 384–388.

Renksizbulut, M. and Haywood, R.J. (1988). Transient droplet evaporation with variable properties and internal circulation at intermediate Reynolds numbers. *Int. J. Multiphase Flow* **14**, 189–202.

Reshotko, E. and Cohen, C.B. (1955). Heat Transfer at Forward Stagnation Point of Blunt Bodies. National Advisory Committee for Aeronautics, *Technical Note* 3513.

Reynolds, W.C., Lundberg, R.E., and McCuen, P.A. (1963). Heat transfer in annular passages. General formulation of problem for arbitrarily prescribed wall temperatures or heat fluxes. *Int. J. Heat Mass Transfer* **6**, 483–493.

Roache, P.J. (1998). *Fundamentals of Computational Fluid Dynamics*, Hermosa Publishers.

Rodi, W. (1976). New algebraic relations for calculating the Reynolds stresses. *Z. Angew. Math. Mech*. **56**, 219–221.

Rodi, W. (1982). Examples of turbulence models for incompressible flows. *AIAA J*. **20**, 872–879.

Rokni, M. and Sunden, B. (2003). Calculation of turbulent fluid flow and heat transfer in ducts by a full Reynolds stress model. *Int. J. Numer. Methods In Fluids* **42**, 147–162.

Rose, J., Uehara, H., Koyama, S., and Fujii, T. (1999). Film condensation. In *Handbook of Phase Change*, Kandlikar, S.G., Shoji, M., and Dhir, V.K., eds., pp. 523–580, Taylor & Francis.

Rowley, R.L. (1994). *Statistical Mechanics for Thermophysical Property Calculations*. Prentice Hall.

Rubinstein, R. and Barton, J.M. (1990). Nonlinear Reynolds stress models and the renormalization group. *Phys. Fluids A* **8**, 1427–1476.

Rubinstein, R. and Barton, J.M. (1992). Renormalization group analysis of the Reynolds stress transport equation. *Phys. Fluids A* **4**, 1759–1766.

Rutledge, J. and Sleicher, C.A. (1993). Direct simulation of turbulent flow and heat transfer in a channel. Part I. Smooth walls. *Int. J. Numer. Methods Fluids* **16**, 1051–1078.

Sarkar, S. and Balakrishnan, L. (1990). Application of a Reynolds-stress turbulence model to the compressible shear layer. ICASE Report 90–18, NASA CR 182002.

Saxena, S.C. and Joshi, R.K. (1989). *Thermal Accommodation and Adsorption Coefficients of Gases*. Hemisphere.

Schaaf, S.A. and Chambré, P.L. (1961). *Flow of Rarefied Gases.* Princeton University Press.

Schlichting, H. (1968). *Boundary Layer Theory*, 6th ed., McGraw-Hill.

Schrage, R.W. (1953). *A Theoretical Study of Interphase Mass Transfer*, Columbia University Press.

Schultz-Grunow, F. (1941). New frictional resistance law for smooth plates. NACA TM-986.

Schulze, H.J. (1984). *Physico-Chemical Elementary Processes in Flotation*, pp. 123–129, Elsevier.

Seban, R.A. and Shimazaki, T.T. (1951). Heat transfer to fluid flowing turbulently in a smooth pipe with walls at constant temperature. *Trans. ASME* **73**, 803–807.

Sellars, R.J., Tribus, M., and Klein, J.S. (1956), Heat transfer to laminar F in a round tube or flat conduit – Graetz problem extended. *Trans. ASME* **78**, 441–448.

Shah, R.K. and Bhatti, M.S. (1987). Laminar convective heat transfer in ducts. In Kacac, S., Shah, R.S., and Aung, W., eds., *Handbook of Single-Phase Convective Heat Transfer*, Chap. 3, Wiley.

Shah, R.K. and London, A.L. (1978). *Laminar Flow Forced Convection in Ducts*, Academic.

Sharp, K.V. and Adrian, R.J. (2004). Transition from laminar flow to turbulent flow in liquid filled microtubes. *Exp. Fluids* **36**, 741–747.
Shih, T., Zhu, J., and Lumley, J.L. (1993). A realizable Reynolds stress algebraic equation model. NASA TM-105993.
Shima, N. (1988). Reynolds stress model for near-wall and low-Reynolds-number regions. *J. Fluids Eng*. **110**, 38–44.
Shinagawa, H., Setyawan, H., Asai, T., Sugiyama, Y., and Okuyama, K. (2002). An experimental and theoretical investigation of rarefied gas flow through circular tube of finite length. *Chem. Eng. Sci.* **57**, 4027–4036.
Shinnar, R. (1961). On the behavior of liquid dispersions in mixing vessels. *J. Fluid Mech.* **10**, 259–275.
Sieder, E.N. and Tate, G.E. (1936). Heat transfer and pressure drop of liquids in tubes. *Ind. Eng. Chem.* **28**, 1429.
Siegel, R., Sparrow, E.M., and Hallman, T.M. (1958). Steady laminar heat transfer in a circular tube with prescribed wall heat flux. *Appl. Sci. Res. A* **7**, 386–392.
Simpson, R.L. (1968). The Turbulent Boundary Layer on a Porous Wall. PhD Thesis. Stanford University, Stanford, California.
Skelland, A.H.P. (1974). *Diffusional Mass Transfer*, Krieger.
Skupinski, E., Tortel, J., and Vautrey, L. (1985). Determination des coefficients de convection d'un allage sodium-potassium dans un tube circulaire. *Int. J. Heat Mass Transfer* **8**, 937–951.
Smagorinsky, J. (1963). General circulation experiments with the primitive equations I. The basic experiment. *Month. Weather Rev.* **91**(3), 99–164.
Sohn, H.Y. Johnson, S.H., and Hindmarsh, A.C. (1985). Application of the method of lines to the analysis of single fluid-solid reactions in porous media. *Chem. Eng. Sci.* **40**, 2185–2190.
Song, S. and Yovanovich, M.M. (1987). Correlation of thermal accommodation coefficient for engineering surfaces. In *Fundamentals of Conduction and Recent Developments in Contact Resistance*, M. Imber, G.P. Peterson and M.M. Yovanovich, Eds., Vol. 69, p. 107, American Society of Mechanical Engineers.
Spalart, P.R. and Allmaras, S.R. (1992). A one-equation turbulence model for aerodynamic flows. AIAA-92-0439.
Spalart, P.R. and Allmaras, S.R. (1994). A one-equation turbulence model for aerodynamic flows. Recherche Aérospatiale **1**, 5–21.
Spalart, P.R., Deck, S., Shur, M.L., Squires, K.D., Strelets. M., and Travin, A. (2006). A new version of detached eddy simulation, resistant to ambiguous grid densities. *Theor. Comput. Fluid Dyn.* **20**, 181–195.
Spalding, D.B. (1961). A single formula for the law of the wall. *J. Appl. Mech.* **28**, 455–457.
Sparrow, E.M. (1955). Laminar free convection on a vertical plate with prescribed nonuniform wall heat flux or prescribed nonuniform wall temperature. NACA TN 3508.
Sparrow, E.M. and Gregg, J.L. (1956a). Laminar free convection heat transfer from the outer surface of a vertical circular cylinder. *Trans. ASME* **78**, 1823–1829.
Sparrow, E.M. and Gregg, J.L. (1956b). Laminar free convection from a vertical plate with uniform heat flux. *Trans. ASME* **78**, 435–440.
Sparrow, E.M. and Gregg, J.L. (1956c). Buoyancy effects in forced-convection flow and heat transfer, *J. Applied Mech.* **26**, 133–134.
Sparrow, E.M. and Gregg, J.L. (1958). Similar solutions for free convection from a nonisothermal vertical plate, *J. Heat Transfer* **80**, 379–386.
Sparrow, E.M., Hallman, T.M., and Siegel, R. (1957). Turbulent heat transfer in the thermal entrance region of a pipe with uniform heat flux. *Appl. Sci. Res. Sec. A* **7**, 37–52.
Sparrow, E.M. and Lin, S.H. (1962). Laminar heat transfer in tubes under slip-flow conditions. *J. Heat Transfer* **84**, 363–369.
Sparrow, E.M., Novotny, J.L., and Lin, S.H. (1963). Laminar flow of a heat-generating fluid in a parallel-plate channel. *AIChE J.* **9**, 797–804.
Sparrow, E.M., Husar, R.B., and Goldstein, R.J. (1970). Observations and other characteristics of thermals. *J. Fluid Mech.* **41**, 793–800.

Sparrow, E.M. and Patankar, S.V. (1977). Relationships among boundary conditions and Nusselt numbers for thermally developed duct flows. *J. Heat Transfer* **99**, 483–485.

Speziale, C.G. (1987). On nonlinear K–l and K–ε models of turbulence. *J. Fluid Mech.* **178**, 459–475.

Springer, G.S. (1971). Heat transfer in rarefied gases. In Irvine, T.F. and Hartnett, J.P., eds., *Advances in Heat Transfer* Vol. 7, Academic.

Stanley, R. S., Barron, R. F., and Ameel, T. A. (1997). Two-phase flow in microchannels. In *ASME Microelectromechanical Systems*, DSC-Vol. 62/HTD-Vol. 354, pp. 143–152, American Society of Mechanical Engineers.

Sripada, R.K.L. and Angirasa, D. (2001). Simultaneous heat and mass transfer by natural convection above upward facing horizontal surfaces. *Int. J. Nonlinear Mech*. **36**, 1019–1029.

Stephan, K. (1959). Wärmeübergang und druckabfall bei nicht ausgebildeter laminarströmung in rohen und in ebenen spalten. *Chem. Ing. Tech.* **31**, 773–778.

Stevenson, T.N. (1963). A Law-of-the-Wall for Turbulent Boundary Layers with Suction or Injection. Cranfor College, Aero Report 166. (Cited in White, 2006).

Subbotin, V.I., Papovyants, A.K., Kirilov, P.L., and Ivanovskii, N.N. (1962). A study of heat transfer to molten sodium in tubes. *At. Energiya (USSR)* **13**, 380–382.

Svehla, R.A. (1962). Estimated viscosities and thermal conductivities of gases at high temperatures. NASA TR R-132.

Tanaka, H., Muruyama, S., and Hatana, S. (1987). Combined forced and natural convection heat transfer for upward flow in a uniformly heated, vertical pipe, *Int. J. Heat Mass Transfer* **30**, 165–174.

Tang, G.H., Li, Z., He, Y.L., and Tao, W.Q. (2007). Experimental study of compressibility, roughness, and rarefaction influences on microchannel flow. *Int. J. Heat Mass Transfer* **50**, 2282–2295.

Tang, G.Y., Yang, C., Chai, C.K., and Gong, H.Q. (2004). Numerical analysis of the thermal effect on electroosmotic flow, *Anal. Chim. Acta* **507**, 27–37.

Taylor, G.I. (1916). British Advisory Committee, *Aero. Rep. Mem*., **272**, (31), 423–429.

Tiselj, I., Hetsroni, G., Mavko, B., Mosyak, A., Pogrebnyak, E., and Segal, Z. (2004). Effect of axial conduction on the heat transfer in micro-channels. *Int. J. Heat Mass Transfer* **47**, 2551–2565.

Thakre, S.S. and Joshi, J.B. (2002). Momentum, mass and heat transfer in single-phase turbulent flow. *Rev. Chem. Eng.* **18**, 83–293.

Thompson, J.F., Soni, B., and Weatherill, N., eds. (1999). *Handbook of Grid Generation*, CRC Press.

Tobin, T., Muralidhar, R., Wright, H., and Ramkrishna, D. (1990). Determination of coalescence frequencies in liquid-liquid dispersions: effect of drop size dependence. *Chem. Eng. Sci.* **45**, 3491–3504.

Travin, A., Shur, M., Strelets, M., and Spalart, P.R. (2002). Physical and numerical upgrades in the detached eddy simulation of complex turbulence flows. In *Advances in LES of Complex Flows*, pp. 239–254. Kluwer Academic.

Tribus, M. and Klein, J. (1953). Forced convection from nonisothermal surfaces. In *Heat Transfer: A Symposium*, pp. 211–255, Engineering Research Institute, University of Michigan.

Tsouris, C. and Tavlarides, L.L. (1994). Breakage and coalescence models for drops in turbulent dispersions. *AIChE J.* **40**, 395–406.

Tuckerman, D.B. and Pease, R.F.W. (1981). High-performance heat sinking for VLSI. *IEEE Electron. Device Lett.* **EDL-2**, 126–129.

Tunc, G. and Bayazitoglu, Y. (2001). Heat transfer in microtubes with viscous dissipation. *Int. J. Heat Mass Transfer* **44**, 2395–2403.

Turner, S.E., Lam, L.C., Faghri, M., and Gregory, O.J. (2004). Experimental investigation of gas flow in microchannels. *J. Heat Transfer* **126**, 753–763.

Tyagi, V.P. (1966). Laminar forced convection of a dissipative fluid in a channel. *J. Heat Transfer* **88**, 161–169.

Turner, S.E., Lam, L.C., Faghri, M., and Gregory, O.J. (2004). Experimental investigation of gas flow in microchannels. *J. Heat Transfer* **126**, 753–763.

Van Driest, E.R. (1956). On turbulent flow near a wall. *J. Aerospace Sci.* **23**, 1007–1011.

Vliet, G.C. (1969). Natural convection local heat transfer on constant heat flux inclined surfaces. *J. Heat Transfer* **9**, 511–516.

Vliet, G.C. and Liu, C.K. (1969). An experimental study of turbulent natural convection boundary layers. *J. Heat Transfer* **91**, 517–531.

Vliet, G.C. and Ross, D. C. (1975). Turbulent, natural convection on upward and downward facing inclined heat flux surfaces, *J. Heat Transfer* **97**, 549–555.

von Karman, T. (1939). The analogy between fluid friction and heat transfer. *Trans. ASME* **61**, 705.

Wang, C. (1946). On the velocity distribution of turbulent flow in pipes and channels of constant cross-section. *J. Appl. Mech*. **68**, A85–A90.

Wang, Z.Q. (1982). Study on correction coefficients of laminar and turbulent entrance region effect in round pipe. *Appl. Math. Mech.* **3**, 433–446.

Weigand, B. (1996). An extract analytical solution for the extended turbulent Graetz problem with Dirichlet wall boundary conditions for pipe and channel flows. *Int. J. Heat Mass Transfer* **39**, 1625–1637.

Weigand, B., Ferguson, J.R., and Crawford, M.E. (1997). An expanded Kays and Crawford turbulent Prandtl number model. *Int. J. Heat Mass Transfer* **40**, 4191–4196.

Weigand, B., Kanzamar, M., and Beer, H. (2001). The extended Graetz problem with piecewise constant wall heat flux for pipe and channel flows. *Int. J. Heat Mass Transfer* **44**, 3941–3952.

White, F.M. (2006). *Viscous Fluid Flow*, 3rd ed., McGraw-Hill.

Whitaker, S. (1972). Forced convection heat transfer correlations for flow in pipes, past flat plates, single cylinders, spheres, and for flow in packed beds and tube bundles. *AIChE J.* **18**, 361–371.

Wibulswan, P. (1966). Laminar flow heat transfer in non-circular ducts. PhD Thesis, University of London. (Cited in Shah and Bhatti, 1987.)

Wilcox, D.C. (1988). Reassessment of scale – determining equation for advanced turbulence models. *AIAA J.* **26**, 1299–1310.

Wilcox, D.C. (1993). Comparison of two-equation turbulence models for boundary layers with pressure gradient. *AIAA J.* **31**, 1414–1421.

Wilcox, D.C. (1994). Simulation of transition with a two-equation turbulence model. *AIAA J.* **26**, 247–255.

Wilke, C.R. (1950). A viscosity equation for gas mixtures. *J. Chem. Phys.* **18**, 517–519.

Wilke, C.R. and Chang, P. (1954). Correlation of diffusion coefficients in dilute solutions, *AIChE J.* **1**, 264–270.

Wolfshtein, M. (1969). The velocity and temperature distribution in one-dimensional flow with turbulence augmentation and pressure gradient. *Int. J. Heat Mass Transfer* **12**, 301–318.

Wu, P. and Little, W.A. (1983). Measurement of friction factors for the flow of gases in very fine channels used for microminiature Joule–Thompson refrigerators. *Cryogenics* **23**, 273–277.

Yakhot, V. and Orszag, S.A. (1986). Renormalization group analysis of turbulence. I. Basic theory, *J. Sci. Comput.* **1**, 3–57.

Yakhot, V. and Smith, L.M. (1992). The renormalization group, the ε-expansion and derivation of turbulence models. *J. Sci. Comput.* **7**, 35–61.

Yang, R.J., Fu, L.M., and Hwang, C.C. (2001). Electroosmotic entry flow in a microchannel, *J. Colloid Interface Sci.* **244**, 173–179.

Yovanovich, M.M. (1987). On the effect of shape, aspect ratio and orientation upon natural convection from isothermal bodies of complex shape. *ASME Heat Transfer Division (HTD)* **82**, 121–129.

Yu, D., Warrington, R., Barron, R., and Ameal, T. (1995). An experimental and theoretical investigation of fluid flow and heat transfer in microtubes. In *Proceedings of the ASME/JSME Thermal Engineering Conference*, Vol. 1, pp. 523–530, American Society of Mechanical Engineers.

Yu, S. and Ameel, T.A. (2001). Slip flow heat transfer in rectangular microchannels. *Int. J. Heat Mass Transfer* **44**, 4225–4234.

Yu, S. and Ameel, T.A. (2002). Slip flow convection in isoflux rectangular microchannels. *J. Heat Transfer* **124**, 346–355.

Yu, Z.-T., Fan, L.-W., Hu, Y.-C., and Cen, K.-F. (2010). Prandtl number dependence of laminar natural convection heat transfer in a horizontal cylindrical enclosure with an inner coaxial triangular cylinder. *Int. J. Heat Mass Transfer* **53**, 1333–1340.

Yu, B., Ozoe, H., and Churchill, S.W. (2001). The characteristics of fully-developed turbulent convection in a round tube. *Chem. Eng. Sci.* **56**, 1781–1800.

Yuge, T. (1960). Experiments on heat transfer from spheres including combined natural and forced convection. *J. Heat Transfer* **82**, 214–220.

Zhi-qing, W. (1982). Study on correction coefficients of laminar and turbulent entrance region effects in round pipe. *Appl. Math. Mech.* **3**, 433–446.

Zohar, Y. (2006). Microchannel heat sinks. In Gad El-Hak, M., ed., *MEMS Handbook*, 2nd ed., Taylor & Francis.

Zukauskas, A.A. (1972). Heat transfer from tubes in cross flow. *Adv. Heat Transfer* **8**, 93–106.

Index